



# Assessing and control of alkaline circulation in BF operation

## (AICirc)

A large, abstract graphic in the background features swirling blue and white lines that resemble liquid or energy flow. In the upper left area, there is a faint watermark-like image of a globe with a grid pattern.

EUR 30847 EN

**Assessing and control of alkaline circulation in BF operation (AlCirc)**

European Commission

Directorate-General for Research and Innovation

Directorate C – Clean Planet

Unit C.3 — Low Emission Future Industries

Contact Andrea Gentili

E-mail [RTD-STEEL-COAL@ec.europa.eu](mailto:RTD-STEEL-COAL@ec.europa.eu)

[RTD-PUBLICATIONS@ec.europa.eu](mailto:RTD-PUBLICATIONS@ec.europa.eu)

European Commission

B-1049 Brussels

Manuscript completed in 2020.

This document has been prepared for the European Commission however it reflects the views only of the authors, and the Commission cannot be held responsible for any use which may be made of the information contained therein.

More information on the European Union is available on the internet (<http://europa.eu>).

Luxembourg: Publications Office of the European Union, 2020

PDF

ISBN 978-92-76-42016-3

ISSN 1831-9424

doi: 10.2777/929812

KI-NA-30-847-EN-N

© European Union, 2021.

Reuse is authorised provided the source is acknowledged. The reuse policy of European Commission documents is regulated by Decision 2011/833/EU (OJ L 330, 14.12.2011, p. 39).

For any use or reproduction of photos or other material that is not under the EU copyright, permission must be sought directly from the copyright holders.

All pictures, figures and graphs © VDEh-Betriebsforschungsinstitut GmbH, RFSR-CT-2015-00002 **AlCirc**

# Research Fund for Coal and Steel

## ***Assessing and control of alkaline circulation in BF operation***

**(AlCirc)**

Gerald Stubbe (BFI)  
**VDEh-Betriebsforschungsinstitut GmbH**  
Sohnstr. 65, 40237 Düsseldorf, Germany

Róbert Móger (DUNAFERR)  
**ISD DUNAFERR DUNAI VASMÚ**  
H-2400 Dunaújváros, Vasmű tér 1-3

Jenny Wikström (LKAB)  
**LKAB Group**  
Varvsgatan 45, SE-971 28 Luleå, Sweden

Bo Björkman, Hesham Ahmed, Anton Andersson (LTU)  
**Luleå University of Technology**  
SE-971 87 LULEÅ, Sweden

Lena Sundqvist, Amanda Gullberg (MEFOS)  
**SWERIM**  
Aronstorpsvägen 1, SE-974 37 Luleå, Sweden

Yousef Ahmad (SSAB)  
**SSAB EMEA AB**  
SE-61380 Oxelösund, Sweden

Hugo Stocker (VASD)  
**Voestalpine Stahl Donawitz GmbH**  
Kerpelystrasse 199, AT-8700 Leoben, Austria

Grant Agreement RFSR-CT-2015-00002

1 July 2015 to 31 December 2018

### **Final Report**



## **Table of contents**

	<b><i>Page</i></b>
Project overview table	IV
Table of deliverables	XI
1. Final Summary	1
1.1 WP1 Characterization of alkali re-circulation in the BF	1
1.1.1 Task 1.1 Alkali behaviour / balance in different industrial BF	1
1.1.2 Task 1.2 New on-line measurements	2
1.1.3 Task 1.3 Alkali impact on BF burden materials	5
1.2 WP2 Methods for alkali control in the BF	6
1.2.1 Task 2.1 Development on Online-Tool for determination of alkali-accumulation in BF	6
1.2.2 Task 2.2 Inhibition of alkali circulation	8
1.2.3 Task 2.3 Impact from slag compositions	10
1.2.4 Task 2.4 Concept for improved adaption of BF operation	11
1.3 WP3 Validation of new developed alkali control methods at operational BF	11
1.3.1 Task 3.1 Industrial trials	11
1.3.2 Task 3.2 Development of an overall concept for improved alkali control at the BF	12
1.4 WP4 Project coordination, documentation and reporting	12
1.5 Conclusions	12
2. Scientific and technical description of results	16
2.1 Objectives of the project	16
2.1.1 Introduction	16
2.1.2 State of the art	16
2.1.3 Project objectives	18
2.1.4 Methods and techniques	19
2.2 Comparison of initially planned activities and work accomplished	20
2.3 Description of activities and results	20
2.3.1 WP1 Characterization of alkali re-circulation in the BF	20
2.3.1.1 Task 1.1 Alkali behaviour / balance in different industrial BF	21
2.3.1.1.1 Determination of BF process data and alkali balance during normal operation at SSAB in Oxelösund (SSAB, SWERIM)	21
2.3.1.1.2 BF process data and alkali balance at LKAB EBF® (LKAB)	23
2.3.1.1.3 Determination of BF alkali balance during normal operation at VASD	26
2.3.1.1.4 BF alkali balances during normal operation at DUNAFERR	36

2.3.1.1.5 Comparison of alkali balances at the different blast furnaces during normal operation	47
2.3.1.1.6 Thermodynamic calculations (LTU)	48
2.3.1.1.7 Impact of alkali balance on energy consumption (SWERIM)	62
2.3.1.1.8 Heat and mass balance calculation for estimation of impact of alkali balance on energy consumption (BFI)	63
2.3.1.2 Task 1.2 New on-line measurements	70
2.3.1.2.1 Tests with new online measurements at the LKAB EBF®	70
2.3.1.2.2 Tests with new on-line measurements at SSAB BF No. 4 in Oxelösund (SWERIM, SSAB)	85
2.3.1.2.3 Laboratory trials for verification of measured alkali emissions in raceway by the optical fibre (SWERIM)	92
2.3.1.2.4 Concluding summary of measurements at EBF and BF No. 4 at SSAB in Oxelösund (Task 1.2)	95
2.3.1.2.5 On-line BF top gas measurements at VASD	96
2.3.1.2.6 BF top gas measurements at BF1 with a FTIR gas analyser at Dunafer	105
2.3.1.3 Task 1.3 Alkali impact on BF burden materials	111
2.3.1.3.1 Definition of standard coke properties at SSAB in Oxelösund (SSAB)	111
2.3.1.3.2 Investigation of alkali uptake in burden materials and the impact on their properties (LKAB, SWERIM)	111
2.3.1.3.3 Coke reactivity tests in order to assess coke attack by alkali components (LTU)	125
2.3.1.3.4 Alkali impact on coke - Chemical and physical analyses of coke after retort tests (Dunafer)	130
2.3.1.3.5 Laboratory furnace trials with two-zone inductively heated reactor (BFI)	133
2.3.2 WP2 Methods for alkali control in the BF	141
2.3.2.1 Task 2.1 Development on Online-Tool for determination of alkali-accumulation in BF	142
2.3.2.1.1 Thermodynamic calculations concerning formation of NH <sub>3</sub> and HCN coupled to alkalis (SWERIM)	142
2.3.2.1.2 Thermodynamic calculations on NH <sub>3</sub> and HCN formation (BFI)	145
2.3.2.1.3 Lab tests with the inductively heated two-zone coke bed reactor for determination of NH <sub>3</sub> and HCN formation in conjunction with alkali components (BFI)	157
2.3.2.2 Task 2.2 Inhibition of alkali circulation	164
2.3.2.2.1 Preparation of test coke (modified ash composition) to be used in laboratory tests, as basket samples and for CRI/CSR (SWERIM, LTU, LKAB)	164
2.3.2.2.2 Kinetic studies on coke with modified ash (LTU)	166
2.3.2.2.3 Investigation on basket samples in LKAB EBF® (SWERIM, LKAB)	168
2.3.2.2.4 Lab-scale trials for determination of alkali inhibiting effect by coke pre-treatment with alkali absorbing additives (BFI)	185
2.3.2.2.5 Alkali adsorbing mineral addition in basket samples (SWERIM, LKAB)	190
2.3.2.3 Task 2.3 Impact from slag compositions	192
2.3.2.3.1 Alkali gasification from slag (LTU)	192
2.3.2.3.2 Alkali evaporation from coke (SWERIM)	208
2.3.2.4 Task 2.4 Concept for improved adaption of BF operation	213
2.3.3 WP3 Validation of new developed alkali control methods at operational BF	215
2.3.3.1 Task 3.1 Industrial trials	215
2.3.3.1.1 Industrial top gas measuring campaigns with attention on NH <sub>3</sub> and HCN at VASD	215

2.3.3.1.2 Deepened evaluation of industrial measurements at the SSAB BF and the EBF® aiming in validation of the found correlations between NH <sub>3</sub> and HCN in top gas and alkali amount (SWERIM, SSAB, LKAB, LTU)	220
2.3.3.2 Task 3.2 Development of an overall concept for improved alkali control at the BF	222
2.3.4 WP4 Project coordination, documentation and reporting	222
2.4 Conclusions	223
2.5 Publications and patents	227
 List of Tables	 228
 List of Figures	 230
 List of Symbols, Indices, Acronyms and Abbreviations	 238
 List of References	 239
 Appendices	
 Technical Annex I	

## Project overview table

Sector ( <i>Coal /Steel</i> ):	Steel
Technical Group:	TGS 1
Grant Agreement No.:	RFSR-CT-2015-00002
Title:	Assessing and control of alkaline circulation in BF operation
Acronym:	ALCIRC
Beneficiaries:	BFI, MEFOS, VASD, DUNAFERR, SSAB, LKAB, LTU
Start Date:	01.07.2015
End Date:	31.12.2018
Period covered by this report:	01.07.2015 – 31.12.2018
Work Undertaken:	<ul style="list-style-type: none"> <li>• BF alkali balancing during normal operation and determination of BF process data has been performed at the BF's of Dunafer, SSAB, VASD as well as the EBF at LKAB in Task 1.1.</li> <li>• Thermodynamic calculations to simulate the reactions occurring when an alkali rich gas from the raceway is cooled while interacting with hot metal, coke, slag/slag formers or oxidic raw materials considering also halogens and zinc (LTU).</li> <li>• Impact of alkalis on energy consumption was estimated by SWERIM and BFI using thermodynamic calculations in FactSage resp. HSC Chemistry (Task 1.1).</li> <li>• New on-line measurements have been tested at LKAB EBF® and SSAB BF No.4 in Oxelösund. At both sites, top gas analysis by MS and measurements of alkali emissions in raceway by optical fibre and spectrometer were conducted (SWERIM, LKAB, SSAB; Task 1.2).</li> <li>• Extractive FTIR top gas measurements have been performed at the BF of VASD and Dunafer with the aim to measure NH<sub>3</sub> and HCN content within the BF top gas as potential indicators for alkali accumulation within the BF (Task 1.2).</li> <li>• Different further top gas measuring systems have been tested at VASD. The systems have been extractive methods as well as in-situ methods (Task 1.2)</li> <li>• Investigation of alkali uptake in burden materials (LKAB, SWERIM) from LKAB EBF has been conduct-</li> </ul>

	<p>ed in Task 1.3. Coke reactivity tests have been performed (LTU) for coke samples before and after modification and for samples collected from EBF using Thermogravimetric analyser at LTU.</p> <ul style="list-style-type: none"> <li>• Definition of standard coke properties at SSAB in Oxelösund has been conducted (Task 1.3)</li> <li>• Investigation of the alkali impact on BF coke by laboratory scale trials with a two-zone inductively heated coke bed reactor at BFI. Assessment of coke reactivities (Task 1.3).</li> <li>• Thermodynamic calculations on formation of NH<sub>3</sub> and HCN have been performed by SWERIM and BFI in Task 2.1</li> <li>• Coke with a modified ash composition have been was prepared within Task 2.2 by SWERIM and studied by basket samples in EBF and in laboratory trials for investigation on alkali impact on coke properties. Baskets containing alkali absorbing minerals in the form of olivine lumps and briquettes have also been investigated.</li> <li>• Laboratory trials for inhibition of alkali circulation by coke pre-treatment/coating with kaolin have been carried out at BFI within the inductively heated 2-zone-reactor (Task 2.2).</li> <li>• Evaporation of potassium from synthetic BF slag was studied in Task 2.3 using a two-level full factorial design of experiments. These laboratory-scale experiments were complemented by thermodynamic calculations and experiments on industrial slag samples.</li> <li>• Alkali evaporation from coke was studied in laboratory trials by SWERIM within Task 2.3</li> <li>• Industrial trials with various measuring systems have been made by VASD in order to analyse alkali behaviour (Task 3.1)</li> <li>• An overall concept for improved alkali control at the BF was developed base on the results of all previous tasks (all; Task 3.2)</li> </ul>
Main Results:	<ul style="list-style-type: none"> <li>• BF alkali balances at operational BF's and EBF indicate that slag is the dominant alkali sink. In all cases, deviations between alkali input and output have been found. (All)</li> <li>• The average K<sub>2</sub>O input was up to 1.5 kg/tHM for SSAB and Dunafer, the average Na<sub>2</sub>O input was 0.9 resp. 1.9 kg/t HM in these cases. For VASD</li> </ul>

- especially the K<sub>2</sub>O input with 7 to 8 kg/tHM is significantly higher than for the other BF's.
- For SSAB in Oxelösund (Task 1.1) a sensitivity analysis showed on the importance of accurate slag analysis, small deviations by less than 0.05% in K<sub>2</sub>O content had impact on the balance.
  - Equilibrium modelling has shown the stable compounds and phases at equilibrium when a gas from the raceway is cooled down and interacting with condensed phases. Reactions between the gas and the condensed phases coke, hot metal, slag and oxidic raw materials have been considered separately. Modelling have included all of the most important internally recirculating elements in a BF, namely K, Na, Cl, F and Zn. The totally dominating role of the slag is confirmed (Task 1.1)
  - Results of on-line measurements at LKAB EBF® and SSAB BF No.4 in Oxelösund in Task 1.2 showed that the relative change of alkali emissions in raceway could be correlated to the estimated circulating load of alkalis at BF No.4 and the indicated occasions of slips and release of scaffolds had impact on the alkali intensity in raceway at the LKAB EBF. Laboratory trials with measurements of alkali adsorption indicated that the intensity measured by the spectrometer is indirectly proportional to the formation of potassium gas by the weight loss of the sample. The NH<sub>3</sub> content in top gas at the EBF could be positively correlated to the outgoing alkalis via the dust and sludge but not the total alkali circulating load and the output via slag.
  - Extractive FTIR top gas measurements with the aim to measure NH<sub>3</sub> and HCN content at the BF of VASD were not successful due to repeated deteriorations of the optical measurement cell. As an alternative, TDLS and MS analysers resulted in more reliable NH<sub>3</sub> and HCN measurements (Task 1.2).
  - At Dunafer only low, unreliable NH<sub>3</sub> measurement values were obtained by FTIR measurements (Task 1.2). No significant correlation between measured NH<sub>3</sub> within top gas (FTIR) and operational parameters was found.
  - Reactivity test of excavated coke samples in Task 1.3 shows the alkali up-take and ash composition in general have a significant effect on coke reactivity.

	<p>The higher the alkali content the higher the reactivity of the coke. Ash components like iron, calcium and magnesium oxides were found to increase the reactivity as well.</p> <ul style="list-style-type: none"> <li>• The distribution of alkalis in the LKAB EBF® shaft for pellets and coke showed that the alkali uptake was predominantly highest in coke and at the wall positions in the lower part of the shaft (Task 1.3). The alkali uptake in pellets was higher up in the shaft when operating with acid pellets compared to olivine pellets. The decreased crushing strength of pellets in the upper shaft could be coupled to the reduction of hematite and was not due to alkalis as the uptake was low.</li> <li>• Two campaigns with different gas profiles were compared and the results showed that the overall alkali content in coke and pellets were lower for the campaign with a more pronounced central gas flow and the distribution of alkalis were more located towards the centre. Reactivity tests of excavated coke from the EBF showed that alkalis increase the coke reactivity and a linear correlation between activation energy and the alkali content was found (Task 1.3).</li> <li>• Ash and alkali content significantly affect the coke quality (CRI, CSR) and quantity of by-products (Dunafer, Task 1.3).</li> <li>• No alkali impact on BF coke in the lower temperature zone (where condensation of alkali components is expected) could be confirmed by the laboratory scale trials with a two-zone inductively heated coke bed reactor at BFI and the following analysis of coke reactivities. This is explained by unexpected condensation of alkali compounds elsewhere in the reactor (Task 1.3).</li> <li>• Thermodynamic calculations on formation of NH<sub>3</sub> and HCN by SWERIM and BFI in Task 2.1 resulted in the main conclusion that the presence of HCN and NH<sub>3</sub> at top gas conditions is not thermodynamically favoured which implies that equilibrium is not reached as both NH<sub>3</sub> and HCN were measured in ppm levels at industrial BF's. The presence of alkalis in the system only negligible effect on the formation of NH<sub>3</sub>(g), while for HCN a better correlation with alkali compounds (especially: KCN) was found by some calculations at high temperature (Task 2.1).</li> </ul>
--	--

- The results of the trials using coke with a modified ash composition by SWERIM for investigation of alkali impact on coke properties indicated in overall that the kaolin addition to coke ash or as coating seems to be beneficial for prevention of alkalis negative effects on coke. Further, all cokes prepared with kaolin, both added before cokemaking and as coating, showed lower reaction rates with CO<sub>2</sub> at all studied temperature intervals compared to the reference coke. In addition, the relative intensity of kalsilite peaks was higher for the coke with kaolin compared to the corresponding reference coke according to the XRD results, which implies that the kaolin additions favours formation of alkali bearing phases in coke ash (Task 2.2).
- The laboratory trials at BFI within the inductively heated 2-zone-reactor could not confirm the beneficial effect of coke coating with kaolin for prevention of alkalis negative effects on coke (Task 2.2).
- The laboratory-scale experiments on evaporation of potassium from synthetic BF slag complemented by thermodynamic calculations and experiments on industrial slag samples suggested that the regression model based on the full factorial design and the FactSage calculations could both predict the rate of evaporation fairly well (Task 2.3).
- Alkali evaporation from coke was studied in laboratory trials by SWERIM within Task 2.3. Here, no positive effect on alkali binding capacity by addition of kaolin could be seen based on these results. Moreover, XRD examination of the test coke containing kaolin could not identify the potassium bearing aluminosilicate phase kalsilite, despite the rather high alkali content.
- The measurements at VASD give a weak hint, that increased HCN values may correlate with increasing alkali accumulation and in this way could be an option for a qualitative long-term monitoring of the alkali state in the BF. On the other hand, the determination of the alkali circulation via NH<sub>3</sub> measurement was not possible with the above described approach. The industrial measurements at the SSAB BF and the EBF® additionally indicate that the measurement of alkali emissions in the raceway is a promis-

	<p>ing method for monitoring of the alkali state in the BF (Task 3.1).</p> <ul style="list-style-type: none"> <li>The proposed overall concept for improved alkali control at the BF involves a continuous qualitative measurement of the alkali load in the BF either by HCN measurement in the top gas or by spectrometric measurement of K or Na in the raceway. Operational means for alkali control in the BF like adjustment of the slag composition towards a lower slag basicity could be triggered when higher alkali loads are assumed e. g. based on an increased HCN concentration in the top gas or by increased detection of alkali components in the raceway (Task 2.4; 3.2)</li> </ul>
Main problems encountered:	<ul style="list-style-type: none"> <li>The chosen measurement system (FTIR) at VASD had not been suitable for BF top gas measurements due to precipitations inside the optical measuring cell of the analyser.</li> <li>Correlations between NH<sub>3</sub> or HCN values and alkali circulation resulted to be too complex for development of a simple online-tool calculation routine.</li> </ul>
Correction actions:	<ul style="list-style-type: none"> <li>Alternative measurement systems like TDLS and MS were used at VASD for BF top gas measurement campaigns</li> <li>Increased effort has been accomplished for finding correlations between NH<sub>3</sub> or HCN values and alkali circulation in the BF.</li> </ul>
Publications, patents:	<ul style="list-style-type: none"> <li>Conference paper: <ul style="list-style-type: none"> <li>Alkali in the Blast Furnace –Influence of modified ash composition in coke and charging practice, A. Gullberg et.al, ICSTI 2018, contribution ID 189.</li> </ul> </li> <li>Master thesis: <ul style="list-style-type: none"> <li>J. Carlsson, "Alkali Circulation in the Blast Furnace - Process Correlations and Counter Measures," Luleå University of Technology, 2018.</li> <li>J. Olofsson, Alkali Control in the Blast Furnace – Influence of Modified Ash Composition and Charging Practice. Master, Luleå University of Technology, 2017.</li> </ul> </li> </ul>

**BUDGET INFORMATION PER BENEFICIARY**

Based on overall costs (independently from EU financial contribution)

<b>BENEFICIARY (incl. coordinator)</b>	<b>Total amount spent to date (€) or (national currency)</b>	<b>Total allowable cost (€) as foreseen in Grant Agreement</b>
CO1 BFI	539,557 €	461,026
BEN2 SWERIM (former: MEFOS)	3,952,886 SEK; 413,170 €	664,015
BEN3 VASD	240,412 €	268,500
BEN4 DUNAFERR	104,056,695 HUF; 328,614 €	387,651
BEN5 SSAB	624,965 SEK; 61,184 €	65,275
BEN6 LKAB	908,112 SEK; 91,043 €	140,847
BEN7 LTU	312,531 €	315,399

Reasons for large deviations between total amount spent and total allowable cost

CO1 BFI	Technical problems to set up the inductively heated two-zone reactor tests
BEN2 SWERIM; BEN6 LKAB	Lower amount spent due to weak correlations between HCN and NH <sub>3</sub> to alkalis that contributed to difficulties in development of on-line tool for alkali determination.

## Table of deliverables

	<b>Description – Fulfilment of deliverable</b>
<b>D1.1</b> Alkali balance, mass balance and operational data on the investigated industrial operational BF's	Extensive alkali mass balances concerning potassium and sodium compounds have been performed in conjunction with the recording of operational data for the industrial blast furnaces of Dunafer, SSAB Oxelösund and VASD, as well for the EBF® of LKAB.
<b>D1.2</b> Determination of correlation between operational parameters and alkali balance during normal BF operation	Correlations between selected operational parameters and the alkali balance during normal BF operation have been revealed at Dunafer, SSAB, VASD and the EBF. Further, this deliverable includes thermodynamic calculations on the mechanisms of alkali circulation and on the impact on energy consumption by LTU, SWERIM and BFI.
<b>D1.3</b> Determination of ammonia concentration in BF top gas at normal operational conditions	Ammonia and additionally HCN concentration have been determined successfully during normal operational conditions at the EBF and at SSAB Oxelösund BF by mass spectrometer analysis. At Dunafer and VASD, the ammonia and HCN concentration have been measured by FTIR gas analyser. In both cases the measurements did not provide reliable results. At VASD a TDLS (tunable diode laser spectroscopy) system was tested successfully as an alternative measuring system for the ammonia concentration in the top gas. For additional determination of HCN, at VASD a mass spectrometer has further been used successfully.
<b>D1.4</b> Determination of in-furnace gas composition at EBF	The measurement of the in-furnace gas composition has been performed in form of raceway measurements with optical fibre at the EBF and additionally at the SSAB BF No. 4 in Oxelösund. Further, laboratory trials for calibrating the raceway measurements have been performed. $\text{NH}_3$ could not be detected, but the system was found to be capable to determine relative intensities of alkali components (K, Na).
<b>D1.5</b> Determination of standard coke properties for input cokes as well as especially prepared cokes with altered ash composition	Standard coke properties for input cokes as well as for especially prepared cokes with altered ash composition have been determined by Dunafer, SSAB and VASD.

<b>D1.6</b> Determination of reference state concerning coke alkali attack within the alkali cycle zone	The coke properties exposed to different alkali condensations in the alkali cycle zone have been determined by coke reactivity measurements in a thermobalance.
<b>D1.7</b> Description of alkali distribution for burden materials in the EBF	The alkali distribution within the EBF burden materials has been described in detail for different radial and vertical positions.
<b>D1.8</b> Results from thermodynamic modelling showing the impact from selected components on alkali gasification	A detailed thermodynamic model of reactions connected with alkali components at different zones of the BF has been set up. Calculations on the impact from selected components on alkali behaviour have been carried out using raw material compositions and process conditions corresponding to those at SSAB Oxelösund BF2 at normal operation.
<b>D2.1</b> Evaluation routine for determination of alkali accumulation within the BF based on online top gas composition data (e. g. ammonia), thermodynamic calculations and laboratory trials	Based on thermodynamic calculations and lab tests with a two-zone inductively heated coke bed reactor, several correlations between alkali (K) load and concentration of key compounds in the top gas (HCN and NH <sub>3</sub> ) were calculated. However, due to the large number of influencing factors, the development of a simple evaluation routine for determination of alkali accumulation within the BF was not possible. But apart from an exact quantification, a qualitative determination of the alkali accumulation within the BF by evaluation of the HCN concentration within the top gas resulted to be promising for long-term BF monitoring.
<b>D2.2</b> Determination of BF alkali accumulation at varying operational conditions	The BF alkali accumulation was determined qualitatively at varying operational conditions by deepened evaluation of gas analysis data in conjunction with alkali balances at Dunafer, SSAB, VASD and the EBF.
<b>D2.3</b> Selection of a suitable coke pre-treatment/coating procedure for best inhibition of alkali attack on coke in the BF	Coke coating with kaolin by (multiple) immersion in a kaolin suspension was selected by BFI as a promising method for inhibition of alkali attack on coke in the BF. In contrast to other trials by SWERIM and LKAB using kaolin already as additive for cokemaking, the coating procedure was investigated by lab trials with an inductively heated two-zone reactor using 20 mm industrial coke pieces, all coated with kaolin. Alkali components were only applied to the coke of the alkali evaporating zone by K <sub>2</sub> CO <sub>3</sub> solution. The coated coke from the lower-temperature zone of the two-zone reactor, which is exposed to condensing alkali components, finally was investigated for coke reactivity. However, at these trials no sufficient alkali carry-over to the condensing zone was obtained, so a beneficial effect of kaolin coating on inhibiting the alkali circulation could not be confirmed.

<b>D2.4</b> Comparative evaluation of basket samples for advice on innovative burden design	A comparative evaluation of EBF basket samples has been performed giving advice on innovative burden design in terms of addition of coke additives like kaolin.
<b>D2.5</b> Comparative results for impact of alkali on coke gasification with and without modified ash composition or coating	The impact of alkali components on coke gasification with and without modified ash composition or coating were assessed. The overall results indicated that all cokes prepared with kaolin, both added before cokemaking and as coating, at comparable alkali content showed lower reaction rates with CO <sub>2</sub> at all temperature intervals studied compared to the reference coke. Thus, kaolin addition to coke ash or as coating seems to be beneficial for prevention of alkalis negative effects on coke.
<b>D2.6</b> Preliminary results on laboratory studies on alkali capacity of slag	The alkali capacity of BF slags was studied using thermodynamic calculations and laboratory-scale experiments. The thermodynamic calculations suggested that the driving force for evaporation of potassium is lowest at low basicities and low MgO contents. These were the two compositional parameters of greatest importance. The laboratory-scale experiments confirmed the effect of basicity whereas the effect of MgO was ambiguous.
<b>D2.7</b> Result for the impact of slag composition on alkali gasification and advice on slag design for the BF	The impact of slag composition on alkali gasification was studied by thermodynamic calculations and laboratory-scale experiments. The rate of evaporation of potassium increased with increasing B2 basicities, MgO contents and temperatures of the slag. But no positive effect on alkali binding capacity by addition of kaolin could be seen based on these results. So, advice on slag design mainly refers to keep the basicity and MgO content as low as possible.
<b>D2.8</b> Concept for improved adaption of BF operation based on application of the online top gas evaluation tool and new means for alkali control	A concept for improved adaption of BF operation was worked out based on the previously obtained results. This includes the following main means for alkali control: Slag basicity, MgO content of slag, gas profile, coke with modified ash or coating by kaolin.
<b>D3.1</b> Demonstration of feasibility of the online top gas evaluation tool at industrial BF's	The feasibility of HCN and NH <sub>3</sub> measurement within BF top gas for obtaining a qualitative information on the actual alkali state of the BF was demonstrated by top gas analyses at VASD with mass spectrometer and TDLS. Further, a deepened evaluation of the industrial measurements at the SSAB BF and the EBF® within WP 1 and 2 was performed for this purpose.  A correlation between NH <sub>3</sub> in the top gas and the alkali balance does not exist during the trials, so the determination of the alkali accumulation is not possible with this approach. However, the

	measurement of HCN within the top gas might be better suited for a qualitative long-term monitoring of the alkali state in the BF. At VASD, due to the small data set feasibility of this measurement/evaluation method could not be confirmed clearly, but measurements at BF No. 4 in Oxelösund revealed that HCN and alkali emissions in raceway are positively correlated, which supports the use of HCN as indicator for the alkali state in the BF.
<b>D3.2</b> Provision of an overall alkali control concept for European BF emphasizing deteriorating raw material qualities and increased use of recycling materials	An overall alkali control concept for European BF was worked out based on alkali control e. g. by adaption of slag basicity or BF gas profile. Potentially, the use of kaolin pre-treated coke could reduce the detrimental effect of alkali components on coke especially for increasing alkali load due to deteriorating raw material qualities and increased use of recycling materials. HCN measurements in BF top gas or spectrometric measurement of K or Na in the raceway are an option for a qualitative long-term monitoring of the alkali state in the BF.
<b>D4.1</b> Written reports: Progress reports, Midterm report and Final report	Two annual reports, a mid-term-report and the final report have been prepared.
<b>D4.2</b> Presentations for coordination meetings and TGS meetings	Presentations for coordination meetings and the TGS meetings have been prepared.

## **1.      Final Summary**

### **1.1     *WP1 Characterization of alkali re-circulation in the BF***

#### **1.1.1    Task 1.1 Alkali behaviour / balance in different industrial BF**

Determination of BF process data and alkali balance during normal operation for SSAB in Oxelösund have been conducted for different periods. The average K<sub>2</sub>O input was up to 1.5 kg/tHM, while the Na<sub>2</sub>O input was 0.9 kg/tHM. Common for all periods studied was the negative accumulation of alkalis in BF No. 4 over time i.e. alkalis were drained out from the BF according to the mass balance. A sensitivity analysis with respect to slag analysis and amount revealed that the analytical accuracy for analyzing alkali in the slag is crucial as even small deviations in the range of 0.05% for K<sub>2</sub>O content in slag will impact on the mass balance significantly. In contrast to this, the alkali balancing conducted for the LKAB EBF® showed that alkalis were accumulated in the furnace for the selected period. It was also noticed that there were differences in how well the balance added up between different parts of the campaign.

A detailed alkali balancing has been done at VASD with the analysis of all relevant materials. Therefore a sampling campaign has been done with all input and output flows except hot metal. The total Na<sub>2</sub>O input was between 1.5 and 2 kg/tHM, while the K<sub>2</sub>O input was between 7 and 8 kg/tHM. In this balance the contribution of sinter to the overall input of Na<sub>2</sub>O was around 50% and of K<sub>2</sub>O around 82%. Since the mass flow of the latter one is four times higher, it is obvious that the contribution of sinter is most important for alkali balancing regarding the input flow. During the campaign more than 98% of alkali compounds have left the BF via the slag.

During the campaign the sum of the Na<sub>2</sub>O output has been higher than the sum of the input. K<sub>2</sub>O behaves different: At the end the K<sub>2</sub>O input was significantly higher (up to 15%) than the output.

The main influencing parameters on the alkali content in slags are the slag temperature and the basicity. An increase in the hot metal temperature, which simultaneously means an increase in slag temperature, has led to lower potassium content in the slag. The same behaviour has been found for the basicity. This is well known and a low slag basicity procedure is common at VASD due to the high alkali load.

Further influencing parameters have been analysed for samples with comparable slag temperature and basicity: Regarding the K<sub>2</sub>O content in slags there is a positive correlation with the flame-temperature and the content of Mn in the slag. There is a negative correlation to top gas temperature, share of pulverized coal, MgO and Al<sub>2</sub>O<sub>3</sub> in the slag. The mentioned slag components are depending on the slag condition itself, i.e. its temperature and composition – so the direct relationship between alkali content and these components does probably not exist.

For determination of BF alkali balances at DUNAFERR, several investments (e. g. automatic coke sampler; railway weighing machine for slag) have been made in order to achieve accurate measurement of quantities of input and output streams, as well as the chemical compositions thereof.

Dunaferr has determined the alkali balances at its blast furnace in three test periods and worked out correlations associated with alkali content in slag respectively alkali removal via slag. The following main results were found:

- Average K<sub>2</sub>O input: Up to 1.5 kg/tHM; average Na<sub>2</sub>O input: Up to 1.9 kg/t HM
- Balance deficits in alkali balance are significant in all three periods,
- Deficits of Na<sub>2</sub>O- and K<sub>2</sub>O-balances have reverse signs in each period (in-out: positive value for Na<sub>2</sub>O; negative for K<sub>2</sub>O)
- The composition of blast furnace charge significantly differed in each period,
- Relevant differences are detected in alkali-content of the sinter and blast furnace coke in each period.
- The basicity of slag, as well as tapping temperature have significant, non-negligible effect on alkali-content of slag, hereby also on alkali removal. Both increase of slag basicity and increase of tapping temperature result in decrease of alkali-content of slag, thereby worsening of the efficiency of alkali removal.
- The increase of sulphur removal efficiency is accompanied by the decrease of alkali removal efficiency.

Preliminary modelling of the reactions between alkali containing gases and condensed phases were carried at LTU using FACTSAGE and using data for the BF at SSAB Oxelösund without considering any recirculating load of alkalis. Results were summarized in reaction schemes as the gas is cooled down and for interaction with different condensed phases. More detailed calculations are reported in Task 1.3. The impact of the alkali circulation on energy consumption was calculated in FACTSAGE by SWERIM based on results from the thermodynamic calculations by LTU. The calculations were based on potassium only and for the assumption that 75% of the circulating amount is below the cohesive zone. The calculations resulted in an energy consumption of 29 MJ/tHM (8 kWh/tHM) for a K circulating load of 15 kg/tHM. This is corresponding to the energy consumption 0.44 kWh/tHM for a circulating load of 1 kg K<sub>2</sub>O. This value is quite in-line with the BFI calculations which resulted in 0.4 kWh per kg of K<sub>2</sub>O, but has a large uncertainty due to the unknown amount of intermediate carbonate formation in the BF, which would strongly increase the specific energy consumption.

For the assumption that the energy released from all exothermic reactions happening above the cohesive zone can be considered as lost and will only contribute to increased top gas temperature, the LTU calculations resulted in an energy consumption of 53 MJ/tHM (resp. 14.7 kWh/tHM) for a potassium circulating load of 15 kg/tHM and This is equivalent to a coke consumption of 1.3 kg/tHM based on the consumption of 1.36 kg coal per kg coke and the energy value 8.6 kWh/kg coal.

### **1.1.2 Task 1.2 New on-line measurements**

New on-line measurements were tested at LKAB EBF® for the period 2016-10-31 to 2016-11-11 (SWERIM, LKAB). These measurements include continuous top gas analyses with mass spectrometer (MS) for analysis of NH<sub>3</sub> and HCN content in top gas as well as continuous measurements of temperature- and emissions from alkali present in the raceway using a lance with optical fibre connected to a spectrometer. The MS-measurements were performed for 6 days, approximately 8 hours each day whereas the raceway measurements for alkali emissions was

performed continuously for the whole period. According to the top gas measurements, the HCN content was low, below 1 ppm whereas the NH<sub>3</sub> concentration was ranging from a few ppm up to 20 ppm. MS-measurement was also attempted on gas retrieved by a shaft probe from inside the EBF but no NH<sub>3</sub> could not be detected in these measurements. Regular measurements determining temperature and gas composition (in terms of CO, CO<sub>2</sub> and H<sub>2</sub>) on nine positions along the furnace diameter, were done on a daily basis. Material samples were also taken daily with shaft probes, characterization of these to assess alkali distribution is reported in Task 1.3.

The relative intensities of alkali emissions in raceway measured on one tuyere at the LKAB EBF® varied over the period and correlations between indicated slips/release of scaffolds to the relative intensities of alkali emissions could be seen. Also a negative correlation between raceway measurements to the alkali output via slag was indicated i.e. the intensity dropped when the alkali output via the slag was high.

A two week long campaign with on-line measurements were performed during the period 2017-1-08 to 2017-11-22 at SSAB BF No. 4 in Oxelösund ([SWERIM, SSAB](#)). This period included continuous measurements of NH<sub>3</sub> and HCN content in top gas by MS as well as continuous measurements of relative intensities of alkali emissions in raceway by similar equipment and setups as applied at the LKAB EBF®. The on-line measurements from LKAB EBF and SSAB BF No.4 were evaluated by studying trends and variations of HCN, NH<sub>3</sub> and relative intensities of alkali emissions in raceway to process- and tap data, by multivariate analyses in SIMCA and to the calculated alkali load. The results were indicating that top gas composition with respect to NH<sub>3</sub> and HCN as well as alkalis emissions in raceway can be related to alkalis in the process. Occasions of slips and release of scaffolds in conjunction with a change in alkali intensity in raceway could be identified during measurements periods at both sites. At the EBF, the alkali emission measurement responded faster than at the industrial furnace. The alkali balancing at BF No.4 showed on a negative accumulated load of alkali over time and the relative change of alkali intensity in raceway correlated well to the calculated load. Moreover, laboratory trials for calibrating the raceway measurements showed on a linear trend between the relative alkali intensity from adsorption to the mass loss from sample. This can verify the alkali emission measurements in raceway at both EBF and BF No.4 and the coupling to the alkali load. However, the optical fibre was installed at only one tuyere at both sites and a potential implementation in future will require installations at several tuyeres for a better overview. This might also explain the weak statistical model obtained for prediction of alkali intensity by process variables and tap data. For the top gas measurements with MS, the relationships found between process variables and concentrations of NH<sub>3</sub> and HCN differed somewhat between the experimental and industrial BF. First of all, no or very small levels of HCN was detected at the EBF whereas higher HCN levels than NH<sub>3</sub> were measured at the industrial BF. Common for both sites was the negative correlation of NH<sub>3</sub> to eta CO and positive correlation to moisture in top gas (H<sub>2</sub>O) and high cooling losses. Based on the EBF evaluation, NH<sub>3</sub> concentrations followed the alkali content in top gas dust and sludge with a decreasing trend over time. In contrast, the alkali balance of the EBF campaign showed on an increasing alkali circulating load from starting of the MS-measurements. Both cooling losses at tuyeres and skinflow temperatures at two levels were overall positively correlated to NH<sub>3</sub> and the skinflow temperatures showed on a similar declining trend over the campaign. Thus, the NH<sub>3</sub> concentrations in top gas can be formed from alkali reactions as it was observed to correlate to alkali in dust and sludge. However, the formation will also be affected by other factors such as gas profile, temperatures etc.

One theory is that NH<sub>3</sub> can give indications on when the output of alkali via the top is high but not the total circulating load. High outputs via the top could be favored by a warm shaft, at colder conditions the alkali cycle is instead shifted further down in the furnace and/or the extent of oxidation and condensation on walls bigger.

Extractive FTIR top gas measurements have been performed at the BF of VASD with the aim to measure NH<sub>3</sub> and HCN content within the BF top gas as potential indicators for alkali accumulation within the BF. Several attempts to measure these compounds with stepwise improvement of the gas sampling system failed due to a detrimental “coating” of the gas cell mirrors with nickel compounds and partly the formation of deposits (e. g. NH<sub>4</sub>Cl) in the pipes of the measurement system. These effects occurred after the fine filter, which means that the deposits must have formed out of the gas phase and not due to any dust in the system. The origin of the nickel compounds was not totally clarified, but it could be assumed that some corrosion of stainless steel parts might be involved in the liberation of nickel. At the end the combination of the selected measurement technique, the installed gas sampling system and the gas itself has not allowed reliable top gas measurements at the industrial BF.

In order to measure NH<sub>3</sub> reliably laser spectroscopy (tunable diode laser spectroscopy – TDLS) has been tested in two configurations: Direct laser measurement into the open gas room and a gas diffusion probe, which prevents the influence of dust to the measurement. The measured NH<sub>3</sub> (TDLS) has increased up to around 74 ppm for the direct measurement. The gas diffusion probe worked very stable, but here quite fluctuating NH<sub>3</sub> values with peaks up to 100 ppm were measured.

Furthermore, mass spectroscopy has also been tested in order to measure the concentration of HCN and NH<sub>3</sub> in the top gas. HCN was regularly lower than 8 ppm, but during normal BF operation virtually no NH<sub>3</sub> was detected.

For development of the new online measurements aiming in quantification of the BF alkali cycle, Dunaferr has carried out BF top gas measurements at BF1 with a FTIR gas analyser. The top gas sampling probe was located after dust catcher and cyclone. The sample gas preparation system is designed to avoid any water condensation e. g. by heated gas lines/pipes and rotameters placed in a heated box. A portable gas sampling unit in connection with a multicomponent FTIR gas analyser was used. The main analysed components are H<sub>2</sub>O, HCN, NH<sub>3</sub> and NO<sub>2</sub>, since they are assumed to be connected with alkali components in the BF. The measured data are evaluated in form of frequency distribution curves and checked for statistical correlations.

The NH<sub>3</sub> measurement was very sensitive to the measuring conditions, with special regard to the wetting, sludging of gas filter of the sampler. Only low, unreliable NH<sub>3</sub> measurement values were obtained.

No significant correlation was found regarding the measured HCN and NH<sub>3</sub> values, with other operational data. A weak correlation was found for the joint change in H<sub>2</sub>-content of top gas and the hot blast pressure. No significant correlation between slag, hot metal and FTIR analysis values was found.

### **1.1.3 Task 1.3 Alkali impact on BF burden materials**

Detailed modelling of the reactions occurring between an alkali rich gas and the various condensed materials within a BF were made at LTU using FACTSAGE. Interacting condensed materials were coke, hot metal, slag and oxidic raw materials. In addition to the alkalis, K and Na, also halogenes, Cl and F, as well as Zn were considered. Calculations were carried out for conditions more generally applicable to BF operations than the preliminary calculations mentioned for task 1.1, i.e. an top pressure of 2 atm and the circulating load of alkalis, halogenes and zinc were estimated based on literature data.

Modelling shows the totally dominating role of the slag phase for the removal of alkalis as well as the importance that a minimum amount of the alkali containing slag is passing through the high-temperature regions of the blast furnace, i.e. raceway and vicinity of raceway. The modelling also shows that the carbonate and cyanide cycles claimed by several authors, probably have low importance for the circulating load of alkalis in a blast furnace.

Investigations on alkali uptake in burden materials from several campaigns at the LKAB EBF® was studied by LKAB and SWERIM. The alkali uptake was generally higher in coke than in pellets and highest alkali contents were found close to wall and in the lower part of the shaft in both pellets and coke. The distribution of alkali in the shaft was affected by the gas profile, the alkali load was indicated to be lower in general when the EBF was operated with a more central gas profile compared to when the EBF was more wall working. The alkali contents in coke and pellets closer to the wall was higher and the difference to the center samples was more pronounced when the EBF was wall-working. No correlation between pellets crushing strength and the alkali content in pellets could be seen but the reduction degree followed the same pattern as the alkali uptake with increased reduction degree with increasing depth and closer distance to the wall. Increased alkali contents closer to the wall was also seen by the analyses of probe shaft samples from one of the campaigns. The potassium content was proportional to the carbon content in pellets and mixed fractions from the upper- and lower shaft probe. Generally higher alkali contents could be seen in material from the lower shaft probe. Based on examination of basket samples containing fluxed potfurnacepellets in campaign C31 and C32 (LKAB) it was seen that the highest alkali uptake in pellets take place in the cohesive zone. In undranted pellets and in pellets from the thermal reserve zone, alkali is found in ganuge and in the iron oxide matrix around decomposed gangue. In the cohesive zone, alkali is instead found in silicate slags and in build ups around the pellets. The alkali uptake is influenced by pellet basicity B2 and choice of additive, an increased basicity will decrease the extent of alkali uptake in pellets whereas additions of quartzite will increase the uptake.

Alkali up-take by descending coke in the experimental blast furnace EBF and its effect on coke reactivity were evaluated (LTU). Several coke sample after quenching and excavation were collected and their alkali content were determined. Among the excavated samples, seven samples were chosen to evaluate their reactivity. The samples (1-2 mm, ~500 mg) were subjected to slow heating under CO<sub>2</sub>. The alkali content were found to have a significant effect on coke reactivity which is attributed to their catalytic effect. Moreover, the other ash components like iron, calcium and magnesium oxides were found to also influence the coke reactivity. The activation energy of coke gasification was found to decrease as the alkali content increases and as the coke samples descend more in the EBF or in other words as it reside longer in the EBF.

Dunaferr in the form of service activity carried out 12 Carbotest retort tests (Coking tests), 116 CRI, CSR tests and 6 granulometric composition specification analyses.

The coal blends for coking were blended with around 5, 10 and 15 % alkali components ( $\text{Na}_2\text{O}$  and  $\text{K}_2\text{O}$  separately).

During coking, the  $\text{Na}_2\text{O}$ - and  $\text{K}_2\text{O}$ -content did not change. The increase in the alkali content of coal makes coke properties worse (increasing CRI and decreasing CSR-value), further the Carbotest tests showed that ash content and alkalis significantly affect the quantity of by-products like coal water and dissolved cyanides in the water.

For investigation of the alkali impact on BF coke, laboratory scale trials with a two-zone inductively heated coke bed reactor have been performed at BFI. The aim is to prepare industrial coke samples in a way that potassium is added in amounts assumed to be present within the BF at the alkali cycling zone. In order to evaluate the influence of different alkali loads, different amounts of potassium have been applied to the coke by pre-treatment (immersion) with different potassium carbonate solutions ( $\text{K}_2\text{CO}_3$ ). For the coke, a metallurgical coke sample from VASD has been used, which was crushed and sieved to an average particle size of around 20 mm. The input gas into the two-zone reactor was a simplified synthetic BF top gas (dry). For some trials, further the input  $\text{H}_2$  concentration was varied starting from the base value of 3 Vol.-%  $\text{H}_2$  to 5 Vol.-%. The temperature settings have been 1300°C at the (lower) alkali evaporation zone (zone 1) and 800°C at the (upper) zone (zone 2), where gasified alkali compounds are expected to condense again.

The impact of different alkali loads on the coke was assessed by determination of the coke reactivity by thermogravimetric analysis (TG analysis) of the coke from lower temperature zone 2, where a condensation of evaporated alkali compounds from the high temperature zone 2 as one step of an alkali cycle was expected.

The calculated activation energies as a measure of coke reactivity are quite scattered in a narrow range between 135 and 159 kJ/mol. But K analysis revealed that only a low amount of evaporated K from zone 1 reached the zone 2 within this experimental set-up, which explains that finally no clear correlation was found between activation energy and the K content (load) of zone 1. This is explained by problems with the experimental set-up like insufficient gas stream between the two temperature zones or by condensation of evaporated alkali compounds at other parts of the reactor.

## **1.2    *WP2 Methods for alkali control in the BF***

### **1.2.1    Task 2.1 Development on Online-Tool for determination of alkali-accumulation in BF**

Thermodynamic calculations on formation of  $\text{NH}_3$  and  $\text{HCN}$  in BF and how the formation of these are affected by presence of alkalis was conducted in FACTSAGE by SWERIM. The input data for the calculations was based on typical process data from SSAB BF No.4 in Oxelösund and the calculations were based on the temperature range 50 to 2400°C. The presence of alkalis in the system had no effect on the formation of  $\text{NH}_3(\text{g})$  according to the calculations but lowered the formed amount of  $\text{HCN}(\text{g})$  at temperatures above 2200°C. Moreover, also concluded from the

calculations was that the presence of HCN and NH<sub>3</sub> at top gas conditions is not thermodynamically favoured which implies that equilibrium is not reached as both NH<sub>3</sub> and HCN were measured in ppm levels at BF No. 4 in Oxelösund.

BFI has performed thermodynamic equilibrium calculations on the correlation between NH<sub>3</sub> and HCN and alkali load (in the form of KCN) in the blast furnace. The calculations are a contribution to the development of a calculation routine for determination of the amount of accumulated /circulating alkali components derived from the BF top gas analysis. The equilibrium calculations were performed with the Software FactSage® separately for seven hypothetic temperature zones in the blast furnace from 1800°C near the raceway to 200°C in the final top gas. For simplification, no gas transfer between the different zones was taken into account. The gas composition within the different temperature zones was assumed for the main components CO and CO<sub>2</sub> based on a typical course of the gas utilisation with temperature. For each temperature zone, 15 calculations were done including three varied hydrogen concentrations (1, 2, 3 Vol.-%) and 5 varied KCN input amounts (equivalent to 0, 2, 4, 6 and 8 kg K<sub>2</sub>O/t HM).

NH<sub>3</sub> was found to be stable mostly at lower temperature with a maximum at 600°C. With increasing temperature, the calculated amount of NH<sub>3</sub> decreased. At the zone of expected alkali circulation (around 1000°C), the calculated amount of NH<sub>3</sub> was only ¼ of the value at 600°C. For NH<sub>3</sub> only a low influence of the alkali (KCN) amount was found. In contrast to this, the influence of H<sub>2</sub> on NH<sub>3</sub> is significantly higher in all BF temperature zones. By far the highest amount of HCN was calculated to be formed at high temperature near the raceway (1800°C). At this zone, a very high influence of the alkali (KCN) amount on HCN was determined. For lower temperature, the calculated amount of HCN drops significantly, so that below 800°C it is negligible. The influence of the alkali amount on the amount of HCN already at 1000°C is much higher than those compared for NH<sub>3</sub>. The influence of H<sub>2</sub> on the the calculated HCN amount is still higher than the influence of alkali compounds (KCN).

Finally, NH<sub>3</sub> seems to be unsuitable as an indicator for the amount of accumulated alkali components in the BF, since the calculated increase in concentration would be too low to be measured. Further, the influence of variations in the H<sub>2</sub> concentration strongly overwhelms the influence of alkali compounds on NH<sub>3</sub> formation.

HCN seems to be better suited as an indicator for the amount of accumulated alkali components, since the calculated concentration is already higher than that of the NH<sub>3</sub> at the assumed alkali circulation zone (ca. 1000°C). Especially at high temperature (1800°C), the amount of the formed HCN is high (>> 100 ppm) with a very clear positive correlation to the alkali content. In an operational BF, a part of the formed HCN from the high temperature zone would be expected to "survive" within the final top gas, even if it would not be thermodynamically stable at these conditions. But also for HCN formation, the amount of H<sub>2</sub> must be taken into account.

In order to verify the above mentioned results from the thermodynamic calculations and to check the suitability of the HCN or NH<sub>3</sub> measurement within the top gas for determination of the alkali accumulation, gas analyses of these components have been carried out during laboratory trials with the two-zone reactor. The experimental set-up and procedure is similar as described for Task 1.3.

The measurement of NH<sub>3</sub> throughout the trials in the two-zone reactor only performed fairly

satisfactory for the first four trials. For the following trials, the measured NH<sub>3</sub> values were not reliable any more (extreme scattering), finally no NH<sub>3</sub> was detected any more. The reason might be the formation of solid precipitations from NH<sub>3</sub> (e. g. NH<sub>4</sub>Cl) within reactor or pipes, which may be formed in combination with trace compounds in the process gas (e. g. HCl).

The HCN measurements in contrast to NH<sub>3</sub> were reliable. The result is a clearly positive correlation between the measured HCN and the K content in the coke, but the coefficient of determination (linear regression) with R<sup>2</sup>=0.38 is not very high, which reflects the highly scattered values. As a final conclusion, the BFI lab tests give a clear indication, that the measurement of HCN in the BF top gas might be a promising method to deliver useful information on the actual alkali accumulation within a blast furnace. But it must be noted, that other parameters like the H<sub>2</sub> concentration may have an even larger influence on the formation of HCN than K components have (as thermodynamic calculations show). Based on the set of data investigated within this project, it was not possible to develop a simple calculation routine suitable for determination of the amount of circulating alkali components in the BF, even though some correlations with the HCN content have been found.

### **1.2.2 Task 2.2 Inhibition of alkali circulation**

Coke samples with modified ash composition were prepared in a small-scale coking test retort at DMT GmbH & Co. KG in Germany. The recipes for preparation of test coke samples were designed based on a standard coal blend used by SSAB where the ash composition was altered by additions of kaolin, bauxite, or silver sand (SWERIM, LKAB, LTU). The prepared coke samples were put in basket samples in the LKAB EBF and also investigated for their reactivity using thermogravimetric analyser at LTU from which the gasification kinetic parameters were estimated. It was obvious from the results that added minerals have marginal effect on the coke reactivity and reaction kinetics. Selected test coke samples (additions of 1-2% kaolin, 1% silver sand and 1% bauxite in coke ash) were further charged to the EBF in baskets at two campaigns. Excavated samples, from EBF, of test coke showed similar trend as above, i.e. the higher the alkali content the higher the reactivity of coke. The alkali up-take by modified ash coke was more influenced by the conditions coke was exposed to rather than the added mineral. However, examination of coke by SEM and XRD revealed that all identified aluminosilicate phases contained alkali, the main alkali phases found was kalsilite and leucite and alkali was distributed throughout the whole coke piece. During SEM/EDS analysis of coke containing Bauxite (Al<sub>2</sub>O<sub>3</sub>) and silversand (SiO<sub>2</sub>) respectively, unreacted grains of Al<sub>2</sub>O<sub>3</sub> and SiO<sub>2</sub> were found, which was also confirmed in XRD. This indicated that both minerals added to the coke ash were inactive in the adsorption of alkali.

Thus, the coke with additions of kaolin was selected for further studies in laboratory furnace for investigation of alkali adsorbing capacity and the effects on coke properties by alkali uptake. For these trials, coke with 4% and 8% kaolin in coke ash was prepared and also a coke coated with kaolin in addition to the coke studied in baskets. In the first step, coke was first exposed to potassium vapour in separate trials to achieve a potassium uptake of around 2%. In the second step, gasification of the different coke types in CO<sub>2</sub> was studied. The results indicated in overall that the kaolin addition to coke ash or as coating seems to be beneficial for prevention of alkalis negative effects on coke. All cokes treated with potassium in the Tammann furnace had K<sub>2</sub>O contents of similar level, roughly 2%. Further, all cokes prepared at DMT with kaolin, both added before cokemaking and as coating, showed lower reaction rates with CO<sub>2</sub> at all temperature intervals

studied compared to the reference coke. In additions, the relative intensity of kalsilite peaks was higher for the coke with kaolin compared to the corresponding reference coke according to the XRD results, which implies that the kaolin additions favour formation of alkali bearing phases in coke ash.

At BFI, based on previous results with reactivity tests on coated coke samples, and supported by results of thermodynamic calculations, also kaolin was selected as the most promising coke additive aiming in capturing the alkali components into high-melting K compounds like kalsilite ( $KAlSiO_4$ ), so that they can be discharged from the alkali cycle in the blast furnace.

In contrast to the previously described trials by SWERIM and LKAB, which were using kaolin mostly as additive for cokemaking, here the *coating* of near-industrial scale coke pieces with kaolin was investigated by lab trials with the inductively heated two-zone reactor (see chapter 2.3.1.3.5, Task 1.3). Industrial coke samples from VASD (crushed to 20 mm coke pieces) were used. Alkali components were only applied to the coke of the high-temperature zone (alkali evaporating zone) using  $K_2CO_3$  solution (see description in chapter 2.3.1.3.5). The applied alkali amount with a target of 2 % K (for preparation in 1014 g/l  $K_2CO_3$  solution) corresponds to the alkali load expected to be present within the alkali circulation zone of industrials BF's. For coating the coke samples with the kaolin, a slurry of 14 % kaolin in water has been prepared, in which the coke has been immersed 1x or 3x (kaolin addition: 1.5 % resp. 5 %).

In order to assess the inhibiting effect of the kaolin coating of coke on alkali evaporation or alkali attack on coke, process gas analyses for HCN were performed during the trials in the two-zone reactor. After the trial, only the coated coke from the lower-temperature zone (zone 2) of the two-zone reactor, which is exposed to condensing alkali components, was investigated for coke reactivity. The intended absorption of alkali compounds by the kaolin coating was expected to result in lower potassium evaporation from the hot zone (zone 1), and in this way in a lower HCN concentration within the process gas. Further, an effect on the coke reactivity (respectively the activation energy  $E_a$ ) in the lower temperature zone (zone 2) was expected in dependency on the K load and on the amount of kaolin coating.

Finally, it was found, that with the present experimental set-up a positive influence of kaolin coating on the capture of alkali components and thus the inhibition of alkali circulation could not be confirmed, which is explained by problems with the experimental set-up like insufficient gas stream between the two temperature zones or by condensation of evaporated alkali compounds at other parts of the reactor.

Alkali uptake in lumpy olivine and olivine briquettes made of fine grained olivine and lime was studied from basket samples in the LKAB EBF® (SWERIM, LKAB). The baskets containing olivine were excavated from different positions in the EBF and the samples were evaluated by comparing chemical analyses and by examination in SEM. The alkali content was highest in samples found at largest depth in general and seemed to be more favoured in the lumpy olivine compared to the briquettes. However, the highest uptake of alkali was less than 0.3%. According to the SEM examination, alkali was found in Si-containing phases with no or very little CaO. This could be related to the fact that  $Ca^{2+}$  and  $K^+$  are competing about the same interstitial positions in the Si-network of a slag. Some alkali could be found inside pores of olivine grains but the highest concentrations appeared to be in phases situated in mixed regions of olivine and binder. As the binder phase is surrounding the olivine grains, reaction of alkali with minerals in olivine might be hindered. Thus, CaO as binder might have a negative effect on the alkali uptake capacity, which is

supported by the lower uptake of alkali in briquettes than lumps.

### **1.2.3 Task 2.3 Impact from slag compositions**

The alkali capacity of BF slags was studied using thermodynamic calculations and laboratory-scale experiments (LTU). The thermodynamic calculations suggested that the driving force for evaporation of potassium is lowest at low basicities and low MgO contents. These were the two compositional parameters of greatest importance. The laboratory-scale experiments confirmed the effect of basicity whereas the effect of MgO was ambiguous.

The rate of potassium evaporation from synthetic BF slags was studied in laboratory-scale experiments using a full factorial design of experiments with parameters: B2 basicity, MgO content and temperature. The evaporation followed first order kinetics and the statistically significant parameters on the 95% confidence level were the B2 basicity, MgO content and temperature. The rate of evaporation of potassium increased with increasing B2 basicities, MgO contents and temperatures. FactSage calculations were used to simulate the evaporation in an open system and the results of the calculations could be linearly transformed to fit the experimental results. The same experimental setup was used to study the evaporation of potassium from industrial slag samples. The results suggested that the regression model based on the full factorial design and the FactSage calculations could both predict the rate of evaporation fairly well for slags of compositions within the compositional domain of the design of experiments.

Trials in laboratory have been conducted to study alkali evaporation from coke (SWERIM). Three different cokes were selected for the trials, all excavated from the LKAB EBF® but during different campaigns (C32, C33). One of the cokes contained 2 wt-% kaolin and approximately 1.5% alkali after being in the EBF. The other two cokes contained 0.3 and 1.5% alkali after being in the EBF respectively and were both industrially produced. The alkali evaporation trials were performed in a vertical tube furnace with inert atmosphere (Ar) and heating from room temperature up to 1600°C. The weight loss of the samples started around 1200-1250°C with highest start of reaction temperature for the coke containing kaolin. However, this sample had the highest weight loss and it was revealed by the chemical analysis that the percentage drop of alkali was 82%, which was the highest loss among the studied cokes. Thus, no positive effect on alkali binding capacity by addition of kaolin could be seen based on these results. It should be emphasized that the coke studied were collected from different EBF campaigns and the kaolin containing coke was produced in pilot scale, compared to the reference cokes which were industrially produced. Moreover, XRD examination of the test coke containing kaolin could not identify the potassium bearing aluminosilicate phase kalsilite, despite the rather high alkali content. Thus, further characterization by XRD and SEM will be needed to investigate how alkalis are present in the different cokes, if it is bound in mineral phases or as free alkalis. Studies on which conditions that are favourable for formation of i.e. kalsilite could also clarify why no kalsilite could be found in the coke after alkali treatment trials in Task 2.2.

#### **1.2.4 Task 2.4 Concept for improved adaption of BF operation**

By evaluation of the previous results concerning influences on the alkali balance and thermodynamic calculations, the main possible operational means for alkali control in the BF have been identified as follows:

- Increase the removal of alkalis by the slag, by:
  - Adjustment of the slag composition towards a lower slag basicity
  - Increasing of the slag volume
  - Replacing CaO by MgO in the added slag formers
  - Lower flame temperature
- Increase the alkali output via the top gas by a more central gas profile
- Kaolin addition to coke

These measures could be triggered when higher alkali loads are assumed e. g. based on an increased HCN concentration in the top gas or by increased detection of alkali components in the raceway.

### **1.3 *WP3 Validation of new developed alkali control methods at operational BF***

#### **1.3.1 Task 3.1 Industrial trials**

The aim of the industrial trials was the validation of the new developed online top gas evaluation tool in order to determine the actual amount of the alkali cycle in the BF. Even if many efforts have been made within the previous work packages to determine correlations between the envisaged top gas components NH<sub>3</sub> and HCN, and the alkali amount in the BF, the situation was too complex to develop a simple calculation routine for quantification of the actual alkali amount in the BF. Many other parameters have been found also to have a significant influence on formation of these gas compounds.

Nevertheless, the results of the previous work packages show, that the measured amount of HCN and (with weaker correlation) NH<sub>3</sub> could however be an option to get some qualitative information on the alkali accumulation in the BF by comparison of the measured concentration in the top gas during a longer periods with otherwise comparable operating conditions. Due to this reason, industrial top gas measuring campaigns with attention on NH<sub>3</sub> and HCN have been performed at VASD within this task. Further, a deepened evaluation of the industrial measurements at the SSAB BF and the EBF® within WP 1 and 2 was performed.

The measurements at VASD give a weak hint, that increased HCN values may correlate with increasing alkali accumulation and in this way could be an option for a qualitative long-term monitoring of the alkali state in the BF. On the other hand, the determination of the alkali circulation via NH<sub>3</sub> measurement was not possible with the above described approach.

The industrial measurements at the SSAB BF and the EBF® additionally indicate that the measurement of alkali emissions in the raceway is a promising method for monitoring of the alkali state in the BF.

### **1.3.2 Task 3.2 Development of an overall concept for improved alkali control at the BF**

The proposed overall concept for improved alkali control at the BF involves a continuous qualitative measurement of the alkali load in the BF either by HCN measurement in the top gas or by spectrometric measurement of K or Na in the raceway. For both types of measurement, the HCN measurement in the top gas (by mass spectrometer) and for the spectrometric measurement of K or Na in the raceway, the feasibility of a long-term measurement at an industrial blast furnace has been proven. The spectrometric measurement in the race way could be improved if the measurements would be done on several tuyeres for a better overview of the alkalis passing the raceway. Then the correlation of the measured amount of K and Na to the overall alkali load would be improved as well. Here, a long-term data evaluation for a specific blast furnace will be necessary to obtain usable results for the qualitative determination of the alkali state.

When an increased alkali load would be detected by the mentioned on-line measurements, one of the basic measures for alkali control in the blast furnace as described at Task 2.4 would be triggered. The most common method would be a periodic alkali removal by applying a lower slag basicity.

### **1.4 WP4 Project coordination, documentation and reporting**

The project coordination, documentation and reporting was an ongoing task throughout the whole duration of the project. 11 coordination meetings and TGS meetings have been carried out including presentations from all partners. Further, two annual reports (2015; 2017) and a Mid-term-report (end of 2016) on the ALCIRC project have been prepared for the European Commission.

### **1.5 Conclusions**

#### *Alkali balancing, distribution and impact on burden materials (WP1)*

Estimation of the alkali circulating load at SSAB BF No.4 and the LKAB EBF based on analyses and weights of in- and outgoing materials indicated that alkalis were drained from the BF in the first case and accumulated in the second. The average K<sub>2</sub>O input was up to 1.5 kg/tHM, while the Na<sub>2</sub>O input was 0.9 kg/tHM. A sensitivity analysis on K<sub>2</sub>O content in slag and slag amount revealed that even small analytical errors in the 0.05% range will have significant impact on the balance. Thus, correct alkali balances is difficult to achieve with available data and existing sampling procedures. Further, detailed alkali balancing has been done at VASD with the analysis of all relevant materials. The total Na<sub>2</sub>O input was between 1.5 and 2 kg/tHM, while the K<sub>2</sub>O input was between 7 and 8 kg/tHM. During the campaign the sum of the Na<sub>2</sub>O output has been higher than the sum of the input. K<sub>2</sub>O behaves different: At the end the K<sub>2</sub>O input was significantly higher (up to 15%) than the output.

Dunafer has determined the alkali balances at its blast furnace in three test periods and worked out correlations associated with alkali content in slag respectively alkali removal via slag. The average K<sub>2</sub>O input was up to 1.5 kg/tHM, while the average Na<sub>2</sub>O input amounted to maximum 1.9 kg/t HM. Balance deficits in alkali balance have been significant: The deficits of Na<sub>2</sub>O- and K<sub>2</sub>O-balances have reverse signs in each period (in-out: positive value for Na<sub>2</sub>O; negative for K<sub>2</sub>O). The main influencing parameters on the alkali content in slags at the investigated BF's are the slag temperature and the basicity. An increase in the hot metal temperature, which simultaneously means an increase in slag temperature, has led to lower potassium content in the slag. The same behaviour has been found for the basicity.

Detailed modelling of the reactions occurring between an alkali rich gas and the various condensed materials within a BF were made by LTU using FACTSAGE. The results showed that the slag phase is essential for alkali removal and also the importance of having a minimum amount of alkali containing slag passing through the high temperature regions of the blast furnace i.e. raceway and vicinity of raceway. The modelling also shows that the carbonate and cyanide cycles claimed by several authors, probably have low importance for the circulating load of alkalis in the BF.

The calculated energy impact of alkali compounds in the blast furnace ions resulted in an energy consumption of 29 MJ/tHM (8 kWh/tHM) for a circulating K load of 15 kg/tHM (SWERIM). This is corresponding to the energy consumption 0.44 kWh/tHM for a circulating load of 1 kg K<sub>2</sub>O, which has also roughly been confirmed by BFI calculations. In these calculations it is assumed, that the energy from the exothermic reactions occurring above the cohesive zone contributes to the concerned chemical reactions in these zones.

If it is assumed that the energy from the exothermic reactions above the cohesive zone is lost and will only contribute to an increased top gas temperature, the energy consumed will correspond to 53 MJ/tHM (14.7 kWh), which is equivalent to an additional coke consumption of 1.3 kg/tHM (1.36 kg coal per kg coke; energy value: 8.6 kWh/kg coal).

Investigations on alkali uptake in burden materials based on samples from several campaigns showed that the alkali uptake was highest in coke compared to pellets and that the alkali uptake increased with depth from charging level in general for all materials. The alkali uptake in pellets was seen to be highest in the cohesive zone with alkali present in silicate slags and build ups around the pellets. In indurated pellets and pellets from the thermal reserve zone, alkali was found in gangue and in the iron oxide matrix around the decomposed gangue. Increased basicity will decrease the alkali uptake in pellets whereas additions of quartzite will increase it. By comparing two campaigns operating with different gas profiles, one being more central working and the other more wall working, the alkali uptake in coke and pellets was higher towards the walls in the latter case. The overall alkali circulating load was also indicated to be lower in the campaign with a more central gas profile. Moreover, evaluation of coke in TGA revealed that alkali increase coke reactivity.

#### *On-line measurements and thermodynamic calculations (WP1 and WP2)*

The NH<sub>3</sub> content in top gas measured at the LKAB EBF and SSAB BF No.4 in Oxelösund was shown to increase with increasing moisture content in the top gas and decrease with increasing eta CO. At the EBF, high NH<sub>3</sub> contents was also observed at high skinflow temperatures and low burden levels. The correlations to skinflow could be linked to the gas distribution and more favorable conditions for NH<sub>3</sub> contents in top gas when the BF is wall working. This was also supported by measurements at BF1 VASD with higher NH<sub>3</sub> content in top gas when the BF was wall working and when the burden level dropped. For the alkali balancing, no correlation between alkali load and NH<sub>3</sub> could be seen at the industrial BF's or the LKAB EBF. However, the alkali content in dust and sludge was shown to be positively correlated to NH<sub>3</sub> at the EBF, implying that measurement of the NH<sub>3</sub> content in top gas can be indicative for alkali outputs via the top but not the total alkali circulating load. Moreover, thermodynamical calculations by SWERIM and BFI showed that the formation of NH<sub>3</sub> is not or only to a very small extent affected by presence of alkalis. The conclusion is thereby that

$\text{NH}_3$  content in top gas is not suitable as an indicator for the total alkali recirculating load.

$\text{HCN}$  was only detected in a very low amount in the top gas at the LKAB EBF whereas the concentration in top gas at BF No.4 in Oxelösund was higher than that of  $\text{NH}_3$  and the compounds seemed negatively correlated to each other. The same trend was observed at the MS measurements at VASD BF1 with higher concentrations of  $\text{HCN}$  compared to  $\text{NH}_3$  and also with an indicated negative correlation. By the statistical modelling of process data combined with the online measurements of top gas and alkali emissions in raceway, the  $\text{HCN}$  content in top gas was shown to be positively correlated to the relative alkali emissions in raceway and flame temperature. Thermodynamic calculations on  $\text{HCN}$  formation by BFI indicated that the amount of  $\text{HCN}$  increased with alkali load but the presence of  $\text{HCN}$  is not thermodynamically stable at top gas temperatures, implying that equilibrium is not reached and that  $\text{HCN}$  measured in top gas was formed in the lower part of the BF. Lab tests conducted by BFI for determination of  $\text{NH}_3$  and  $\text{HCN}$  formation in the presence of alkalis revealed that the content of  $\text{HCN}$  correlates positively with the alkali content and therefore could be used as an indication on alkali accumulation in the BF. Moreover, the relative intensity of alkali emissions measured in raceway was shown to be positively correlated to the relative change of estimated alkali circulating load at BF No. 4 and laboratory trials verified that the relative intensities of potassium adsorption is indirectly proportional to the potassium concentration in the gas phase. Thus, the raceway measurements on alkali emissions by a lance with optical fibre connected to a spectrometer can be used for indications on when larger amounts of alkalis are passing. However, the alkali emissions were only measured in one tuyere at BF No.4 out of twenty which also can explain the weak statistical model obtained for prediction of intensity of alkali emission by process- and tap data. The  $\text{HCN}$  content in top gas could not be coupled quantitatively to the circulating load of alkalis due to the difficulties to close up the balances by available data concluded in Task 1.1. No clear correlation was even seen when comparing the relative changes of  $\text{HCN}$  and the estimated circulating load of alkalis. In addition, the results from thermodynamic calculations and statistical analyses of process data and top gas measurements implied that the formation of  $\text{HCN}$  takes place in the high temperature zone and is proportional to the alkali load. However, as the gas ascends, other parameters will have impact on the  $\text{HCN}$  content and the final concentration measured in top gas will not directly be readable for the circulating alkali load in the BF.

#### *Inhibition of alkali circulation and impact from slag composition*

Coke with modified ash composition was studied by basket samples in the LKAB EBF and in additional laboratory trials with purpose to study if the detrimental effects by alkali on coke could be limited. Reactivity studies on untreated coke showed that the mineral additions in coke ash had only marginal effects on coke reactivity and reaction kinetics. For basket samples, no conclusions could be drawn regarding if the mineral additions had been beneficial or not due to the varying conditions each basket had been exposed to. However, kaolin was shown to be the only mineral that had been active in alkali adsorption and further studies in laboratory was therefore focusing on coke with kaolin incorporated in coke ash or as coating. Based on these trials, kaolin in coke ash or as coating was indicated to be beneficial for prevention of alkalis negative effects on coke as these showed on lower reaction rates with  $\text{CO}_2$  at all temperature intervals studied compared to the reference coke. Also, the relative intensities of peaks corresponding to the alkali bearing phase kalsilite was higher for coke with kaolin compared to the corresponding reference coke, which

implies that the kaolin additions favour formation of alkali bearing phases in coke ash.

The alkali capacity of BF slags was studied using thermodynamic calculations and laboratory scale experiments (LTU). The thermodynamic calculations suggested that the driving force for evaporation of potassium is lowest at low basicities and low MgO contents. These were the two compositional parameters of greatest importance. The laboratory-scale experiments confirmed the effect of basicity whereas the effect of MgO was ambiguous.

#### *Overall concept for improved alkali control at the BF*

Part of the concept for improved alkali control at the BF is a continuous qualitative measurement of the alkali load in the BF either by HCN measurement in the top gas and/or by spectrometric measurement of K or Na in the raceway. When an increased alkali load would be detected, the previously described measures for alkali control in the blast furnace like decreased slag basicity would be triggered.

For both types of measurement, the HCN measurement in the top gas (by mass spectrometer) and for the spectrometric measurement of K or Na in the raceway, the feasibility of a long-term measurement at an industrial blast furnace has been proven. The spectrometric measurement in the raceway could be improved if the measurements would be done on several tuyeres for a better overview of the alkalis passing the raceway. Then the correlation of the measured amount of K and Na to the overall alkali load would be improved as well. But here, a long-term data evaluation for a specific blast furnace will be necessary to obtain usable results for reliable qualitative determination of the alkali state.

#### *Recommendations for industrial implementation of online measurements*

For (semi-quantitative) online measurement/evaluation of alkali accumulation within the blast furnace, two technical options for industrial implementation are usable:

- Measurement of alkali compounds directly in the raceway by using a lance with optical fibre connected to a spectrometer. This technique was proven to be applicable at the tuyeres of an industrial blast furnace.
- Measurement of HCN in the top gas as an indirect indication on alkali accumulation in the BF. - For this task, a mass spectrometer worked reliably in industrial conditions, while a FTIR gas analyser delivered ambiguous results. While at Dunafer a FTIR system generally worked, at VASD the measurement was not reliable due to the formation of Ni containing deposits on the gas cell mirrors. Even if the origin of the disturbing Ni compounds at VASD could finally not be clarified within this research project, this cannot be regarded as a general obstacle for use of a FTIR analyser at BF top gas. However, for avoiding FTIR measurement problems with Ni compounds it is recommended to design the BF gas sampling system without using any Ni containing (e. g. stainless steel) gas tubes.

Further, the measurement of the NH<sub>3</sub> content in the top gas was shown to be indicative for alkali outputs via the top. For this measurement, TDLS gas analysers (tunable diode laser spectroscopy) have proven the industrial applicability. The big advantage of the TDLS is that it is an in-situ measuring system and therefore a gas sampling and preparation is not necessary. Two configurations for laser spectroscopy are available, one as a cross-over system with laser source and receiver opposite to each other and one with a (single) gas diffusion probe. The TDLS systems

should be installed in a way to prevent dust accumulation or water condensation before the optical windows (cross-over system) respectively the sensor head (diffusion probe), which would disturb the measurement.

#### *Recommendations for future R&D work*

Based on the outcome of this research project, the following future R&D work is recommended:

- Deeper investigation of the complex correlations between operational BF parameters, the alkali accumulation and the content of trace compounds within the top gas (e. g. HCN concentration) for further development of the online measurements for determination of alkali accumulation.
- Starting from promising initial results within this research project, more intensive investigations of different means for protecting coke from alkali attack are recommended (e. g. use of further additives and procedures).

## **2. Scientific and technical description of results**

### **2.1 Objectives of the project**

#### **2.1.1 Introduction**

The presence of alkali compounds within the blast furnace (BF) process is very detrimental to BF operation and -productivity due to several kinds of influences, which are stated below. Further, the resulting alkali cycle in the BF leads to an enhanced energy and coke consumption.

Thus, control of alkali compounds in the BF is essential. Usually this is achieved by limiting the alkali input in the BF by selection of alkali lean raw materials (coke; ferrous burden). Due to worldwide decreasing availability of high-quality primary raw materials, there is an increasing necessity to process lower quality raw materials, often resulting in higher alkali input.

The objective of the research project is to develop and establish new concepts for alkali control in the BF based on an online top gas measurement tool for determination of the state of alkali accumulation, and on the development and controlled application of new techniques for enhanced alkali removal from the BF alkali cycle. This enables a decreased reductant and energy consumption, especially when using lower quality raw materials and operating at high alkali loads. The on-line application of the new alkali control concepts shall lead to improved hot metal quality and reduced raw material and energy consumption within the BF process. Thus, this research project focuses on the integration of online process monitoring and control of steel production using mathematical methods for a multi-criteria optimisation of steel production with respect to BF productivity and resource efficiency.

#### **2.1.2 State of the art**

As mentioned above, alkali compounds are very detrimental to BF operation, since they cause enhanced coke attack by lowering the coke strength in the lower part of the BF and by shifting the gasification ( $C + CO_2 = 2 CO$ ) to lower temperature and thus increasing coke reactivity [1, 2, 5, 6, 9, 19]. Further, alkali compounds in the BF lead to increased sinter disintegration and pellet swelling, each depending strongly on sinter/pellet composition (basicity) [1, 2, 5, 19]. Another detrimental effect of alkalis is the formation of scaffolds, which affect burden descent and may reduce lining life [1, 2, 8, 19]. The main influences on BF operation are decreased BF permeability

and in result lower productivity and thermal instability [1, 2, 3].

Typically, alkali components are charged to the BF as alkali silicates in the ores, coke and fluxes [19]. Today at Steel Companies in Western Europe and Asia the typical alkali input in the BF is max. 2.5 kg/tHM (being only 1.5-1.7 kg/tHM at some plants) [3]. The alkali input is reported to originate each by around 50 % from ore, pellets and sinter on the one hand and coke and coal on the other hand [1]. Most part of the alkali components leave the BF via slag [3]. In older measurements at a small BF (300t/d foundry iron) it was revealed that on continuous operation roughly 3/4 of the alkali input leave the furnace via the slag and 1/4 via the top gas dust [12]. This is in accordance with newer BF alkali balance calculations, showing an imbalance of 20-30%, which is explained by uncontrolled alkali release via top gas, from where the alkalis are dissolved in gas cleaning water [3]. A significant part of the alkalis is present as cyanides, so generally alkali release via top gas is unwanted in order to minimize pollution of gas cleaning water.

The highest alkali enrichment in the BF is found around 2 m above tuyere level ( $T = 1000-1100^{\circ}\text{C}$ ) with  $\text{K}_2\text{O} + \text{Na}_2\text{O}$  being around 1/4 of total slag formers mass [1]. The average alkali load on coke is reported to be 2 % (20 % in coke ash) with highest values in deadman (5-7 %) [1]. The residence time of alkalis depends on slag basicity and is reported to be between 21 and 24 h [1]. Key values concerning the alkali impact on BF operation are reported in [3]: An increased alkali input by 1 kg/tHM leads to a decreased BF productivity by 4.5 % and increased total fuel consumption by 2.3 %. The main reason is the lower hearth drainage capacity [3].

State of knowledge is the existence of alkali circulation mechanisms within the BF, which to the largest extent are based on K-compounds. This alkali cycle leads to an increased alkali concentration in the lower part of the BF [19]. The K-cycle amount is estimated to be in the range of 3-4x K-input amount [1]. In literature, several alkali cycle mechanisms are postulated [10-14]. All of them include the potassium cyanide (KCN) formation as a key component. When alkali components (silicates, oxides...) reach the high-temperature zone of the BF, they are decomposed, producing K vapour and subsequently KCN by reaction with coke and tuyere gas. The produced KCN vapour ascends in the BF shaft, cools down and condenses on coke and ferrous burden, where it is oxidised to solid  $\text{K}_2\text{CO}_3$ . The  $\text{K}_2\text{CO}_3$  descends with the burden, may decompose to  $\text{K}_2\text{O}$  and reaches again the high-temperature zone, by which the K-cycle is closed. **Figure 1** illustrates this simplified alkali cycle mechanism.

KCN is known to react readily with water vapour, which usually is present in the BF. The produced ammonia may partly react further with CO to form HCN [18]. This is expressed by the following reactions:



These reactions are responsible for the generation of ammonia and HCN in the upper BF stack, of which especially  $\text{NH}_3$  is found in the BF top gas.

In literature, some references are given regarding means for alkali control in the BF respectively removal of alkalis via the slag. Most common method for alkali removal via slag is the application of a decreased BF slag basicity [1, 2, 3, 4, 5]. This may be done e. g. by a periodic "cleaner" operation with reduced flux rate, which results in lower slag basicity. A disadvantage of this method is an increased S-content in hot metal, which requires enhanced desulphurisation. Further proposed methods for alkali control are: Application of an increased slag volume - resulting in an

increased fuel rate, application of a lower Si content in hot metal, the reduction of BF flame temperature and finally central gas flow intensification [1, 2, 3, 4, 5].

For capturing of alkali compounds and fixing them in form of stable compounds at high temperature, the use of aluminosilicates has been proposed in different technical fields. For example, for alkali removal from coal derived fuels gases at high temperature (and subsequent use in gas turbines), aluminosilicates like kaolinite, activated bauxite etc. have been tested as successful retention agents to be used in a fixed bed adsorber [7]. In the ceramic industry, synthesised aluminosilicates e. g. of the type  $\text{KAlSiO}_4$  proved to be very corrosion resistant and to have a high melting point, making them interesting for high temperature applications ( $1750^\circ\text{C}$  for  $\text{KAlSiO}_4$ ) [20].

In order to reduce the detrimental effect of alkali compounds on BF operation, a modification of coke ash chemistry by addition of 2-3% silica or kaolin to the coke oven charge was proposed [4]. Also the coating of BF pellets with kaolinite was tested successfully by trials in the experimental blast furnace (EBF). Here a coating with water based kaolinite slurry (5 kg/t pellets) resulted in more stable EBF operation, higher productivity and lower reductant consumption [21, 22, 23].

### 2.1.3 Project objectives

The objective of the research project is to develop and establish new methods for online alkali control in the BF, based on a novel Online top gas measurement Tool for determination of the alkali accumulation in the operational blast furnace.

The new Online Tool will be applied at different representative BF's for monitoring of the alkali cycle amount. In **Table 1** a comparison of the main technical data of the relevant operational BF's at Dunaferr, SSAB and VASD is presented.

**Table 1** Comparison of main technical data of operational BF's at Dunaferr, SSAB and VASD

Technical data of BF	Dunaferr (BF 1 / 2)	SSAB (BF 2 / 4)	VASD (BF 1 / 4)
Hearth diameter [m]	7.2 /7.6	8.0 / 8.6	8.0 / 8.0
Working volume [ $\text{m}^3$ ]	824;960 / 892;1033	1100 / 1360	1205 / 1343
Hot metal production [t/d]	1629 / 1714	2200 / 3000	2000 / 2000
Main burden components	Sinter (60 %) Pellets (40 %)	Pellets (100 %)	Sinter (64 %) Pellets (20 %) Lump Ore (16 %)
Additional reducing agents	Natural gas	PCI	PCI

The selected BF's differ in operational modes and concerning alkali input. Monitoring of the alkali cycle amount enables the premature detection of operational states with elevated alkali load. In this way, countermeasures for alkali control may be triggered at an early stage in order to prevent operational disturbances at the BF.

For BF alkali control some promising novel measures are developed within the research project, like coke pre-treatment/coating with alkali absorbing minerals as well as a more optimised adjustment of BF slag composition.

Finally, concepts will be worked out for improved BF alkali control by combined application of the Online top gas measurement Tool with selected methods for inhibition of the alkali circulation. The concepts will consider the special restraints at the different operational BF's. Finally, the concepts

will be validated by operational trials at the different BF's in comparison with normal operational data.

#### **2.1.4 Methods and techniques**

The technological approach with methods and techniques to achieve the project objectives is divided into the following steps:

- Assessment of alkali behaviour in the BF during normal operation by conventional monitoring of operational process parameters and alkali balancing at different BF's
- Assessment of alkali impact on burden materials - Definition of reference state of coke attack at different BF's (standard coke tests). Investigation of coke attack at BF conditions with different alkali loads (laboratory furnace trials). Investigation of alkali uptake in fluxes and ferrous materials.
- New on-line measurements based on ammonia (and HCN) analysis of BF top gas via FTIR Spectrometer and mass spectrometer. This Online Tool will be developed by extensive operational top gas measurement campaigns at 4 different industrial BF's during normal operation. The evaluation routine for the Online top gas measurement Tool will be developed based on thermodynamic calculations and laboratory trials for calibration and determination of reaction rates. Theoretical background: Equations (1) and (2) are the basis for estimation of the KCN content in the BF shaft, and thus the amount of the alkali cycle.
- New methods for inhibition of the alkali circulation are investigated – Coke pre-treatment/coating procedures are developed, using alkali absorbing additives. The aim is to drain alkalis via the slag by addition of Al-silicates, which react with KCN to stable  $KAlSiO_4$ . The K-activity will be decreased in this way, in order to prevent alkali evaporation and thus prevent the K-compounds to enter again into the alkali cycle (see **Figure 1** - Simplified alkali cycle mechanism (only K) in the BF and option for draining alkalis). Here, laboratory furnace trials are performed for assessment of the inhibiting effect under different alkali loads. Further, alkali absorbing mineral addition is tested by basket samples of the EBF.
- The impact of adjusted slag compositions on alkali removal is investigated based on lab tests and EBF results
- Industrial trials are performed at different industrial BF's for validation of the previously developed alkali control concept based on the on-line top gas measurement tool. Selected operational parameters will be varied at the BF in order to validate the impact of alkali control measures on the BF alkali cycle.

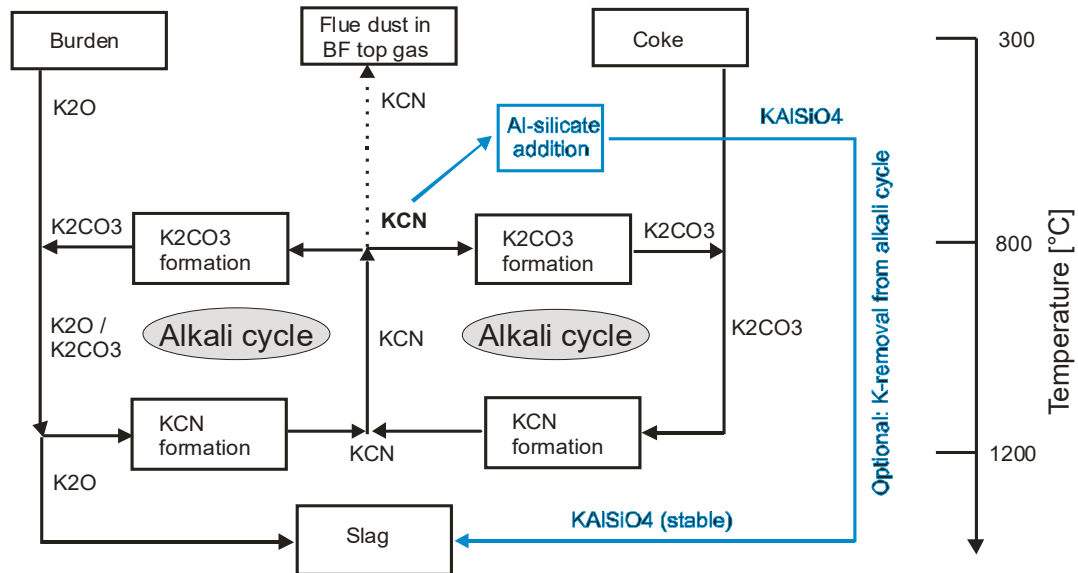


**Figure 1:** Simplified alkali cycle mechanism (only K) in the BF and option for draining alkalis via the slag

## 2.2 Comparison of initially planned activities and work accomplished

All initially planned work was done, but especially the development of the online tool for determination of alkali accumulation in the BF was faced by a tremendous complexity of results. Therefore deepened investigations with increased effort were required within WP 1 and WP 2. Finally, a simple calculation routine for determination of alkali accumulation in the BF could not be developed. So, the effort for validation of the new developed alkali control methods at an operational BF by industrial trials (WP 3) on the other hand was reduced. Here, only the validation of qualitative correlations between NH<sub>3</sub> and HCN in top gas and alkali accumulation were possible.

## 2.3 Description of activities and results

### 2.3.1 WP1 Characterization of alkali re-circulation in the BF

The main Objectives of WP1 are as follows:

- Definition of reference state concerning alkali behaviour / balance in different industrial BF and one Experimental BF and their correlation to operational parameters of the BF
- Performance of continuous NH<sub>3</sub> concentration measurements at the BF top gas during different defined normal operational conditions. NH<sub>3</sub> is analysed as a possible indicator for the amount of alkali cycle within the BF
- Estimation of alkali circulation and alkali load on coke during normal BF operation
- Definition of reference state concerning alkali impact on BF burden materials like coke, fluxes and ferrous materials (with special emphasis on the different input materials and operational conditions at the compared BF's)

### 2.3.1.1 Task 1.1 Alkali behaviour / balance in different industrial BF

#### 2.3.1.1.1 Determination of BF process data and alkali balance during normal operation at SSAB in Oxelösund (SSAB, SWERIM)

SSAB in Oxelösund has collected process data and material samples for normal production periods to be evaluated. The average alkali input to their blast furnaces was 0.75 kg Na<sub>2</sub>O and 1.18 kg K<sub>2</sub>O per tonne of hot metal respectively during 2014. Alkali balances based on process- and tap data for SSAB in Oxelösund have been conducted for two time periods in 2016, see **Table 2**. In period 1, the iron ore charged to the BF consisted of 20% acid pellets and 80% olivine pellets whereas period 2 is corresponding to a reference run with 100% olivine pellets. The K<sub>2</sub>O input to the BF was slightly higher during period 1 whereas the input of Na<sub>2</sub>O seems to be equal between the two periods. Slag volume, basicity and K<sub>2</sub>O output in slag are all higher in Period 1 whereas Al<sub>2</sub>O<sub>3</sub> and MgO are lower. However, the total alkali output seems to be equal between the different periods.

**Table 2** Alkali balance for run with 20% acid pellets (period 1) and 100% olivine pellets (period 2) at SSAB in Oxelösund

	Period 1	Period 2	
K <sub>2</sub> O input	1.5	1.2	kg/tHM
Na <sub>2</sub> O input	0.9	0.9	kg/tHM
Slag			
Slag volume	180	155	kg/tHM
Slag basicity	0.92	0.89	
K <sub>2</sub> O	0.92	0.74	Wt.-%
Al <sub>2</sub> O <sub>3</sub>	12.0	13.8	Wt.-%
MgO	12.7	15.4	Wt.-%
Alkali output	116	115	%

In **Figure 2**, the alkali output for a longer time period in 2016 can be seen. The average output for the selected time interval is 118% which means that alkalis are drained out from the BF rather than accumulated. This imbalance might be caused by incomplete raw material analyses.

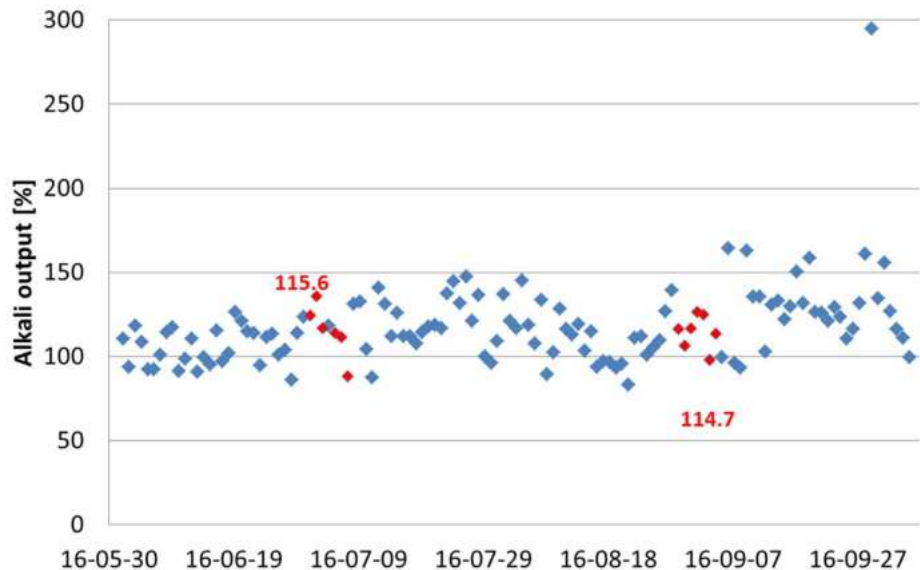


**Figure 2** Alkali output ( $K_2O$ ) in BF at SSAB in Oxelösund June–October 2016.

The  $K_2O$  slag content in relation to slag volume for the same time period is shown in **Figure 3**. It is a distinct decrease in slag volume when changing back to 100% olivine pellets around July–August.

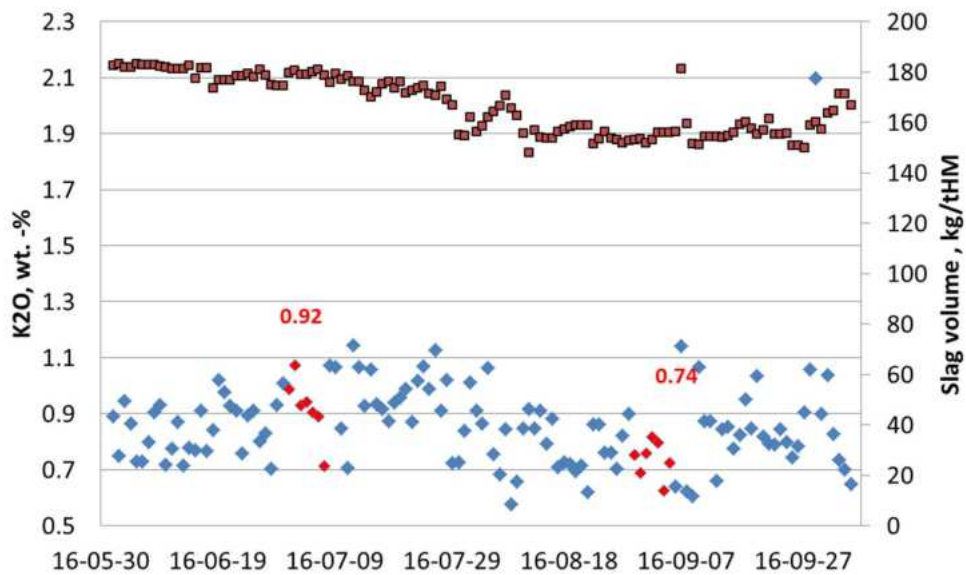


**Figure 3** Slag volume in relation to the  $K_2O$  content in slag June–October 2016.

For a period in 2017 in conjunction with top gas measurements with MS, an additional mass balance of  $K_2O$  in BF No.4 at SSAB in Oxelsöund was done. The results are seen in **Figure 4**. These data indicate that the output of potassium is higher than the input over time, the mean value being 109% for the period. The output of  $K_2O$  seems to be affected by the slag basicity, as seen by the flatter slope of the output-curve when slag basicity increases.

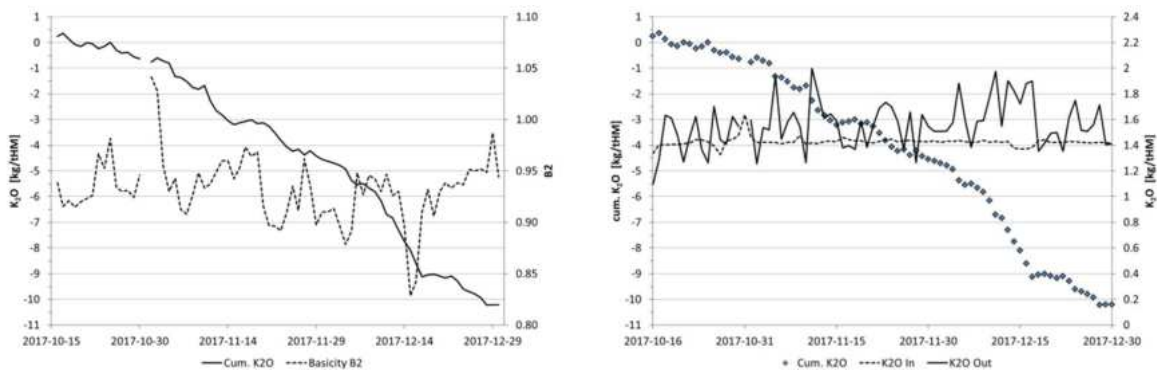


**Figure 4** K<sub>2</sub>O output and basicity from autumn 2017 at BF No.4 SSAB in Oxelösund.

A sensitivity analysis was made to study the importance of correct analyses when making a balance of K<sub>2</sub>O in the BF, see **Figure 5**. By the diagram it is shown that an analytical variation of 0.05% in the analysis of K<sub>2</sub>O in the slag will change the output by several percentages and the error will increase with slag volume. Moreover, analytical errors for compounds used to calculate the slag volume, such as Al<sub>2</sub>O<sub>3</sub>, will also by itself have impact on the K<sub>2</sub>O output even if the K<sub>2</sub>O content in slag is correct. Thus, the balancing of K<sub>2</sub>O is sensitive for the alkali content of and the amount of slag and this might partly explain why there is a negative accumulation of K<sub>2</sub>O for a period stretching over two months. The importance of the chemical composition including the moisture content of ingoing material have not been studied here but as the chemical composition of the ingoing materials is in general conducted less frequently than slag, the imbalance of K<sub>2</sub>O can probably also be partly explained by deviations in these data.

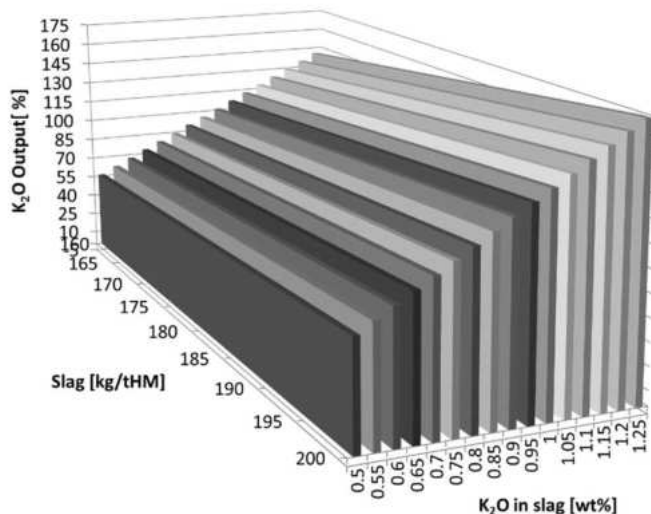


**Figure 5** Sensitivity analysis of K<sub>2</sub>O balance with respect to K<sub>2</sub>O content in slag and the slag amount.

### 2.3.1.1.2 BF process data and alkali balance at LKAB EBF® (LKAB)

LKAB has operated the experimental blast furnace (LKAB EBF) and research for conducted in connection to this for the project. It is an important tool for product development, primarily used for assessing burden performance but also in various BF process development projects. It is typically operated in campaigns of six to eight weeks. A campaign was performed from September 21 to November 11, 2016. During this operating period several Alcinc activities were performed, within different work packages and tasks. For the last few hours of operation, various research samples were added, in labelled baskets. Some of these were prepared for Alcinc and have also

been investigated within Alcirc. Operation was interrupted and the shaft flushed by nitrogen and cooled for about two weeks before the shaft was excavated, basket samples and other material samples were retrieved. A general overview of the campaign is presented in **Figure 6**, where daily (24h) averages have been calculated for some key process parameters.

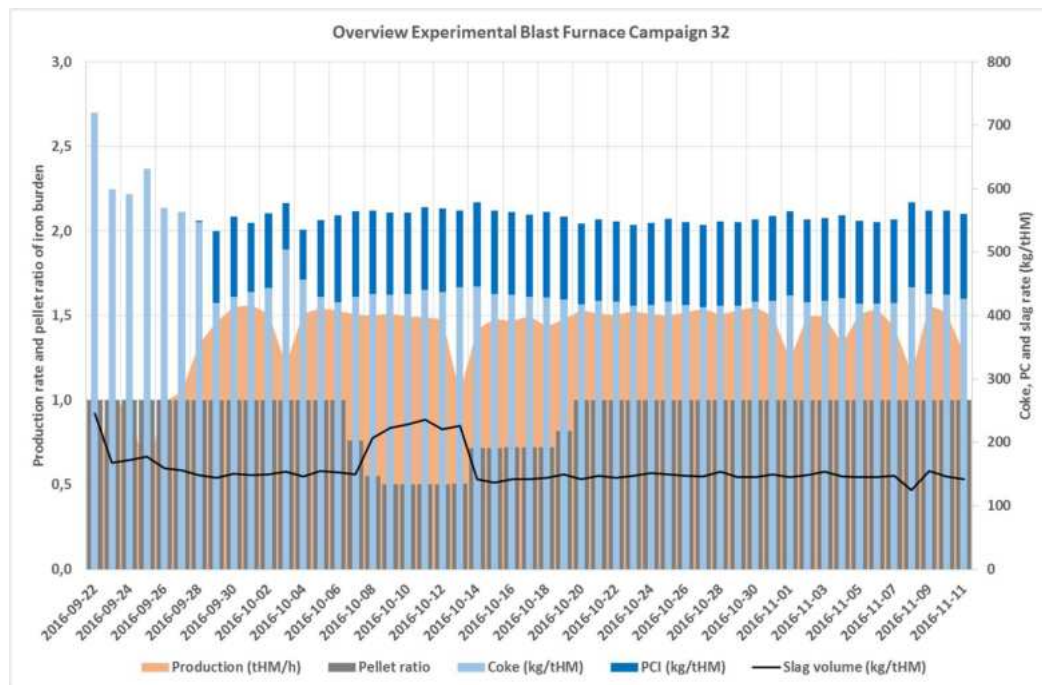


**Figure 6** Overview of campaign 32 LKAB EBF 2016

A campaign starts with a “heating up period” that requires five to seven days of operation. PCI is started towards the end of this period. During this campaign several pellet types were tested, in periods of two to three days. For some days mixed pellet and sinter burdens were operated (indicated by lower pellet ratio shown with grey bars in the diagram). Slag ratio was set at around 150 kg/tHM for most of the burdens, except for a few days when (a comparatively) high amount of sinter was used. Blast parameters were selected to reach a production rate around 1,5 tHM/h for all trial periods and lower rates are results of disturbances or planned stops in operation. PCI rate aimed at 130 kg/tHM.

As part of Task 1.1, alkali balances have been made for campaign 32, based on normal sampling and analyzing procedures, described below. Calculations were done on 24h basis, regardless of operating conditions, for the entire duration of the campaign. Preliminary results in terms of daily input and output of potassium (as K<sub>2</sub>O) and sodium (as Na<sub>2</sub>O) are displayed in **Figure 7** and **Figure 8**.

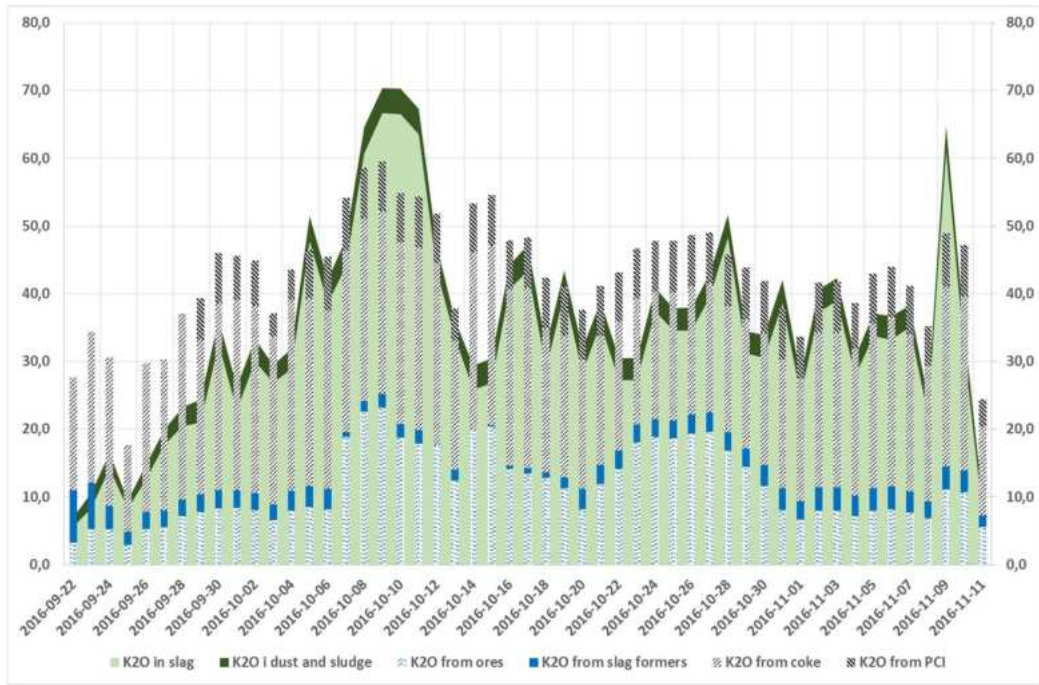


**Figure 7** Preliminary potassium balance - Campaign 32 LKAB EBF

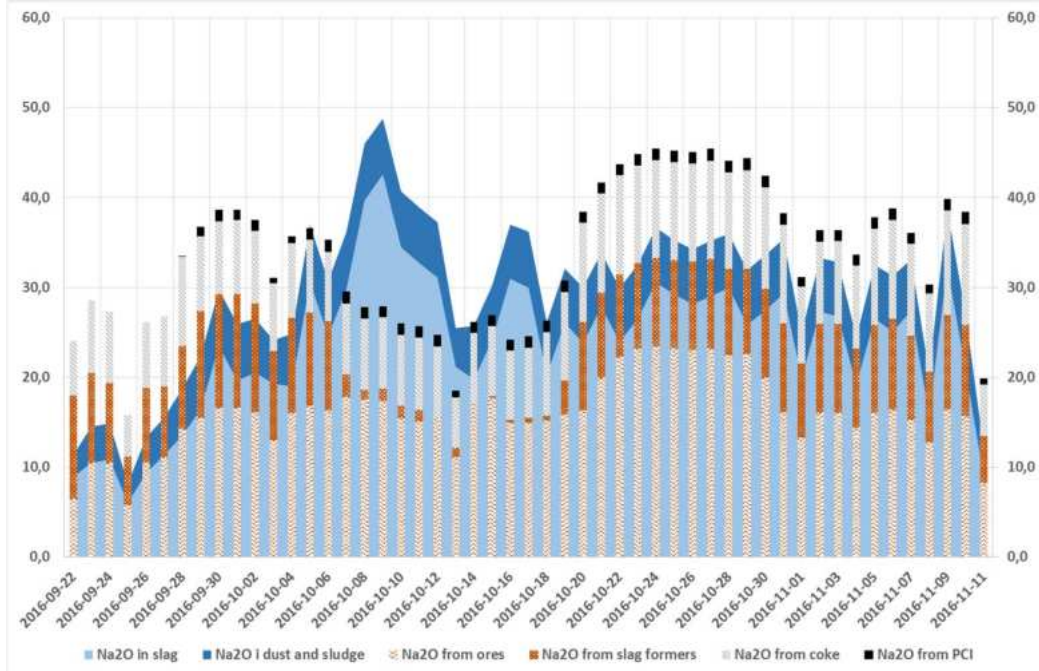


**Figure 8** Preliminary Sodium balance - Campaign 32 LKAB EBF

Bars give calculated amounts, in kg per 24h, of potassium and sodium respectively, charged and injected, with iron burden, slag formers, coke and coal. Colored areas denote the outtake, in slag and particles removed from the top gas, as dust and sludge. Alkali content in dry coarse dust is negligible. Sludge is not sampled and analyzed regularly but previous investigations indicate a substantial alkali content in the sludge. In these preliminary calculations and as an conservative estimation 4 kg of (dry) sludge is assumed, with a content of 1% K<sub>2</sub>O and 2% Na<sub>2</sub>O.

In comparison to industrial blast furnaces raw material characteristics are in most respects more stable in the EBF, as the burden is not brought directly from a producing plant on a continuous basis. All burden materials are instead handled "batchwise". A typical "pellet batch" that lasts for three to five days of EBF operation is in the range of 500 tons and can be produced in about one

hour in one of LKABs pellet plants. It is typically retrieved from production in about that time, and a sample for initial laboratory testing and analysis is prepared as the pellets are brought to a separate storage, at the production site. Close to being tested pellets are transported by truck to the EBF and an intermediate storage. It is sampled as it is brought into day bins inside the EBF plant (about 15 tons at a time or every eight hours, if used as single iron bearing material). Typically some of these samples, representing a few days of operation are mixed before being characterized again, to ensure that any inconsistency can be detected. Experience is that pellet batches in most respects are consistent (size distribution and moisture content sometimes vary but composition and other properties we can measure tend to be homogeneous). The variations in Na<sub>2</sub>O and K<sub>2</sub>O with iron burden during campaign 32 are a result of differences between the many pellet batches tested within the campaign.

A typical coke batch represents more coke than what is used within a single campaign and usually taken from production over a few days. Sometimes a change of batch is done within a campaign. In campaign 32, two batches (with quite similar characteristics) of reference coke was used, along with two batches of test coke. Regarding the preliminary evaluation of alkali behavior, all of these are regarded as comparable. Small differences in content of K<sub>2</sub>O and Na<sub>2</sub>O are however taken into account in the calculations.

From the plotted data it can be seen that there were variations in the chemical composition of charged ferrous materials. Especially for sodium , the slag formers (quartzite and steelmaking slags) had a noticeable contribution to the total input. The outtake with blast furnace slag varied significantly from day to day. These variations has been further analyzed for selected time periods, together with results of the MS measurements reported in Task 1.2.

The calculations show that the overall balance do not quite add up and that the estimated total input is higher than the total output, 84% for K<sub>2</sub>O and 87% for Na<sub>2</sub>O respectively. From the figures it can also be noticed that there are differences in how well the balance can be closed for different parts of the campaign.

### **2.3.1.1.3 Determination of BF alkali balance during normal operation at VASD**

At the beginning a rough alkali balance for a period of one month has been done at VASD in order to get an overview of the main sources and sinks. This has been done with the available data, which is gathered regularly and with its limitations like a lack of analysis frequency for some materials or even no analysis for some materials. In **Figure 9** and **Figure 10** this rough alkali balance is shown for K<sub>2</sub>O and Na<sub>2</sub>O, where the height of input and output streams represents the relative amount of the particular stream. It is obvious, that sinter and slag have been the dominant alkali source and sink respectively at VASD BF. The latter one is responsible for more than 95% of alkali output. It has to be mentioned that the ratio between output and input mass flow is around 90% for K<sub>2</sub>O and 85% for Na<sub>2</sub>O.

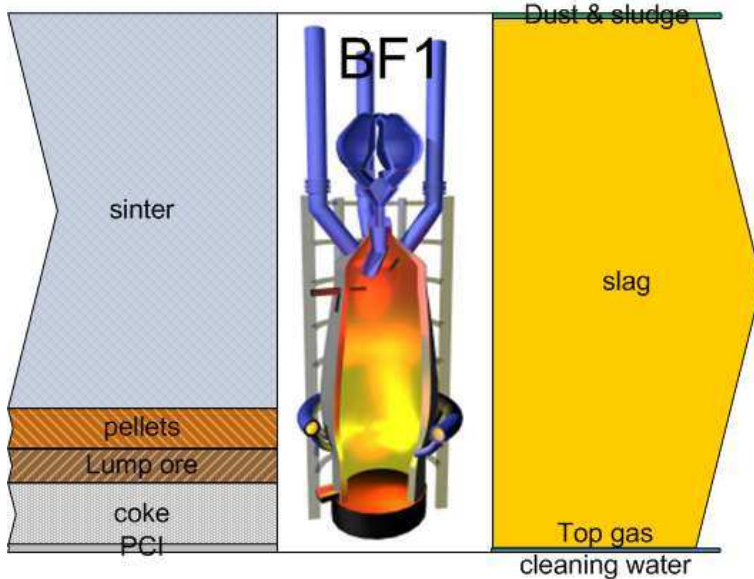


**Figure 9** Rough relative  $K_2O$  balance for BF1 at VASD

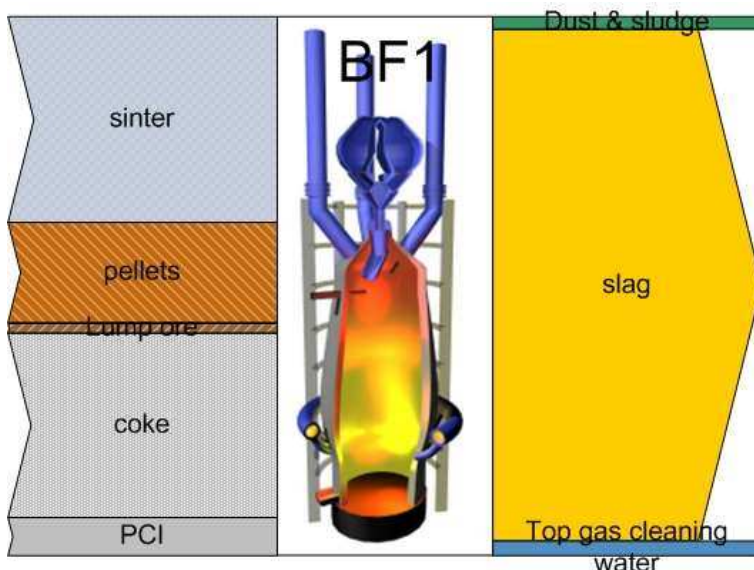


**Figure 10** Rough relative  $Na_2O$  balance for BF1 at VASD

The fact that the materials with the highest alkali amount are analysed most frequent is beneficial for further alkali balancing. For proper alkali balancing the frequency of sampling and analysing has to be more often. A more detailed alkali balancing has been done at VASD with the analysis of all relevant materials. Therefore, a sampling campaign has been done with all input and output flows except hot metal. The sampling positions for the raw materials have been next to the BF in order to get near-term information. For example, the pulverized coal has been sampled at the coal injection lines immediately before the injection lances. Top gas dust and BF sludge has been sampled in the morning and has been assigned to the day before. In a prior investigation the alkali content of hot metal had been analysed and it had not been possible to measure any alkali because the content had been below the chemical detection limit. So, as a boundary condition the alkali content of hot metal and the washing water have been set to zero. The latter one has been done because  $NaOH$  dosing for pH-control and the fact that the washing water is circulating wouldn't allow calculating the share of this flow properly. As could be seen in the rough balance the share of this flow is low in any case. During the sampling campaign only one BF has been in operation because the other one has been in intermediate repair. Hence the volume of dust and sludge could be assigned com-

pletely to one BF. The balance has been done on a daily basis. In **Table 3** the share of the input and output flow for the six days investigated in detail is shown. The input flow is dominated by the sinter, while output is dominated by the slag.

**Table 3** share of material flow in % of total mass per day

date	Input								Output			
	coke 1	coke 2	small coke	fine coke	sinter	quartz	lump ore	pellets	PC	dust	sludge	slag
<b>05.09.2016</b>	10.7	4.0	1.0	1.2	57.1	0.4	4.7	15.0	5.8	4.9	0.3	94.8
<b>06.09.2016</b>	11.1	4.2	1.0	1.2	59.1	0.4	4.7	13.2	5.0	2.2	0.3	97.4
<b>07.09.2016</b>	11.0	4.4	1.1	1.2	57.5	0.4	4.8	14.7	4.9	2.2	0.3	97.5
<b>08.09.2016</b>	10.7	4.2	1.1	1.2	57.1	0.4	4.8	15.6	4.7	2.0	0.3	97.7
<b>09.09.2016</b>	10.8	4.3	1.1	1.2	56.5	0.4	4.9	16.3	4.5	3.2	0.3	96.5
<b>10.09.2016</b>	11.0	4.1	1.3	1.0	56.1	0.4	4.8	16.8	4.4	2.4	0.3	97.2

In **Figure 11** the evolution of the relative amount of hot metal and slag is shown, the first day represents the baseline with a value of 100%. HM and slag have increased during the campaign except on the last day where production has been lower.

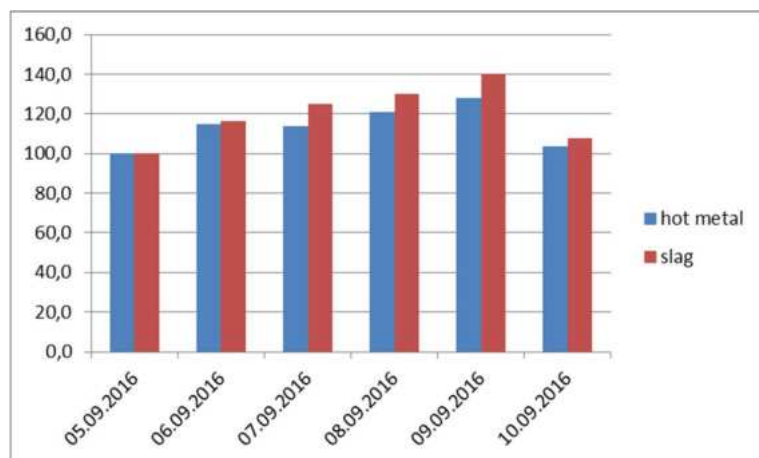


**Figure 11** Evolution of relative amount of hot metal and slag

In **Figure 12** the specific values for the input of Na<sub>2</sub>O and K<sub>2</sub>O are shown. Na<sub>2</sub>O input has been quite stable for the first three days and has decreased afterwards till the 9<sup>th</sup> of September. This has been accompanied with a decrease in the Na<sub>2</sub>O content of both lump cokes and lower reducing agents rate. Additionally, the specific sinter rate has decreased, while on the last day the specific burden rate has increased in general. The specific K<sub>2</sub>O rate has been highest on the 7<sup>th</sup> due to a higher input by the sinter. The decrease afterwards has been by reason of a decreased sinter rate. Due to the fact that we cannot measure the alkali circulation the balance between in- and outflow is adduced as a comparative value with relevance to NH<sub>3</sub> in the top gas.

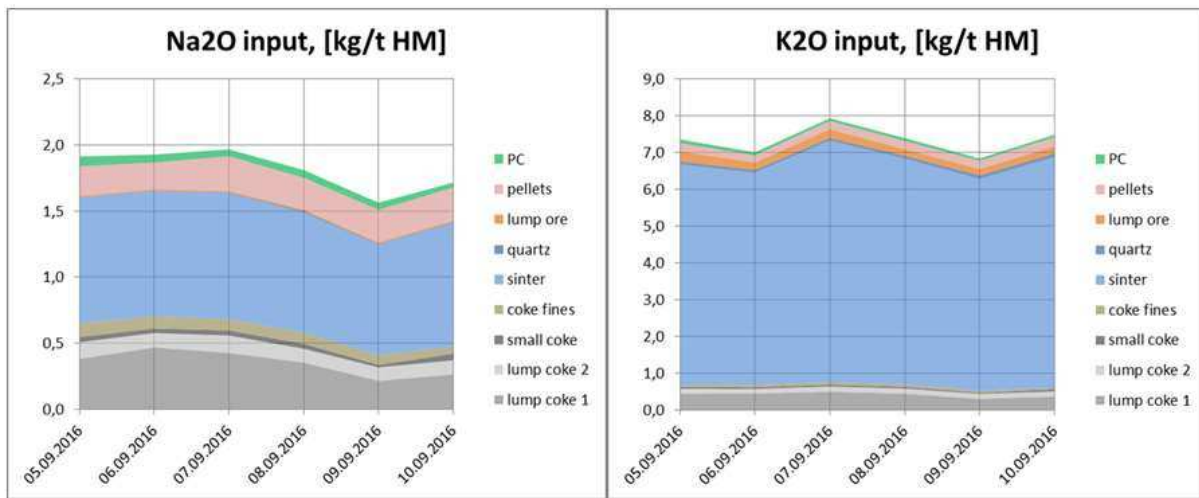


**Figure 12** Specific Na<sub>2</sub>O and K<sub>2</sub>O input

In this balance the contribution of sinter to the overall input of Na<sub>2</sub>O is around 50% and of K<sub>2</sub>O around 82%. Since the mass flow of the latter one is four times higher, it is obvious that the contribution of sinter is most important for alkali balancing regarding the input flow. In **Figure 13** the share of slag, dust and sludge regarding the output flow is shown. During the campaign more than 98% of alkali has left the BF via the slag. Sludge and BF dust has a minor role in this balance because the masses have been very low compared to the slag.

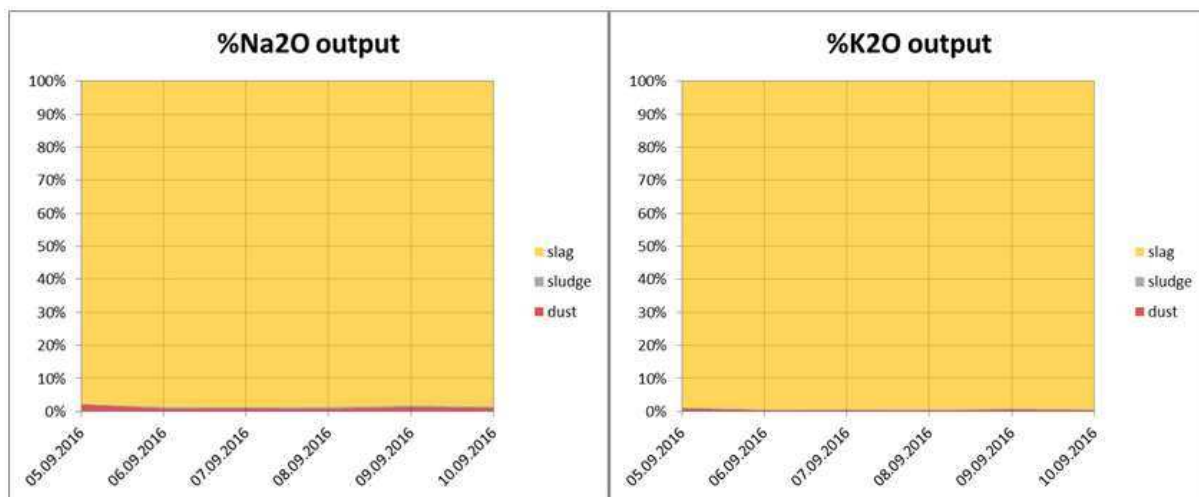


**Figure 13** Contribution of alkali output flow

Regarding the absolute amount of Na<sub>2</sub>O and K<sub>2</sub>O the daily behaviour is shown in **Figure 14**. While the output of Na<sub>2</sub>O follows the slag amount, the input is lower than the output on the 8<sup>th</sup> and 9<sup>th</sup> of September. The behaviour of the input flow has already been described before. The cumulated data have a variance of -2.3% at the end of the campaign that means that the sum of the output is higher than the sum of the input. K<sub>2</sub>O behaves different: The input is always higher than the output except on the 9<sup>th</sup> of September. This comes along with higher slag volume and higher potassium content in the slag. At the end the input is 15% higher than the output. It must be mentioned that on the 9<sup>th</sup> a change in the burden distribution has been done. This has been done for preparation of a planned stop a few days later. The distribution has been changed from a wall working to a centre working furnace. The effect on the temperature right below the stock level is shown in **Figure 15**. The temperature represents the mean daily value of eight thermocouples, which are located below

the stock level just in front of the wall. The temperature at the wall has been decreasing after changing the burden distribution and the burden descent has been erratic. Therefore, the number of slipping has been nearly four times higher on the last day compared with the first day.

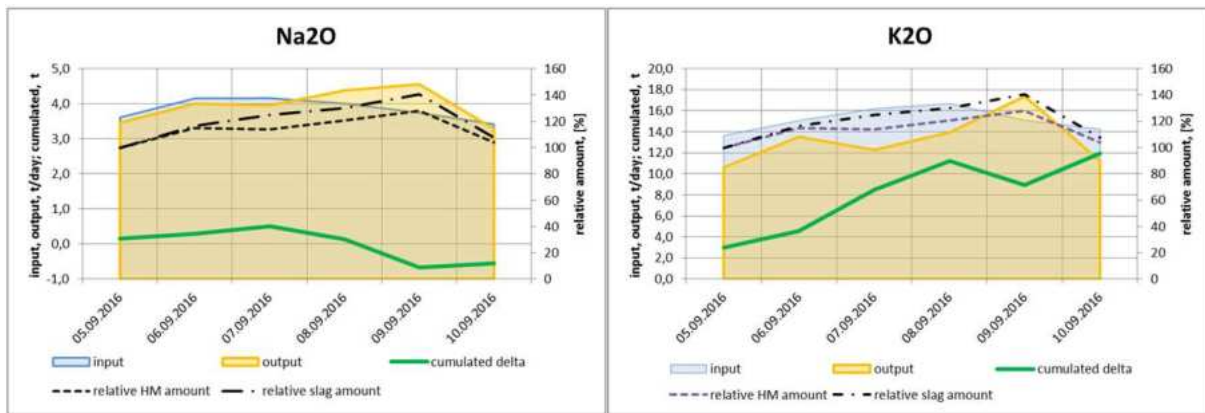


**Figure 14** Absolute alkali in- and output in t/day and cumulated data in tons and relative HM and slag amount

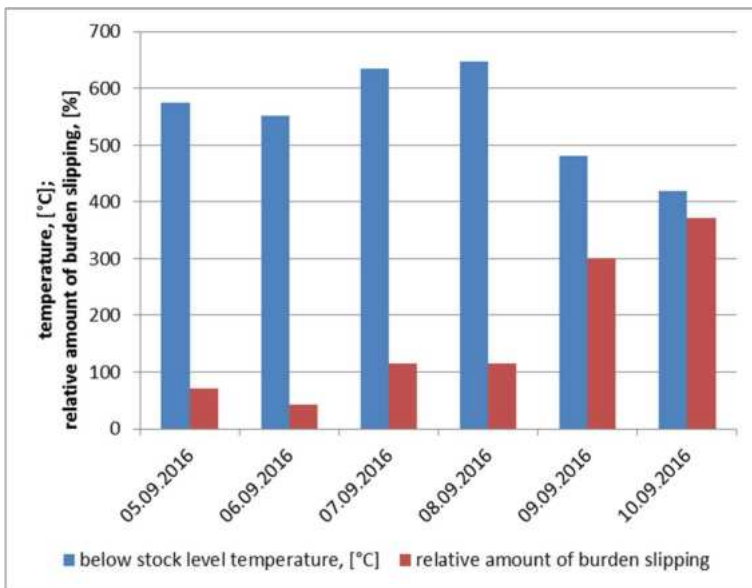


**Figure 15** Change of the mean temperature of sub-stock level temperature and increase in burden slipping

Due to the gap in the alkali balance another balance has been done for a period of one month. In this balance only the variation in the analysis of sinter and slag has been considered. The trend for the balance of Na<sub>2</sub>O and K<sub>2</sub>O has been similar to the balance with the extensive analysis of all materials. The cumulated mass difference between in- and output of Na<sub>2</sub>O is -6.8% and those for K<sub>2</sub>O 10.4% compared to the sum of output (see **Figure 16**).

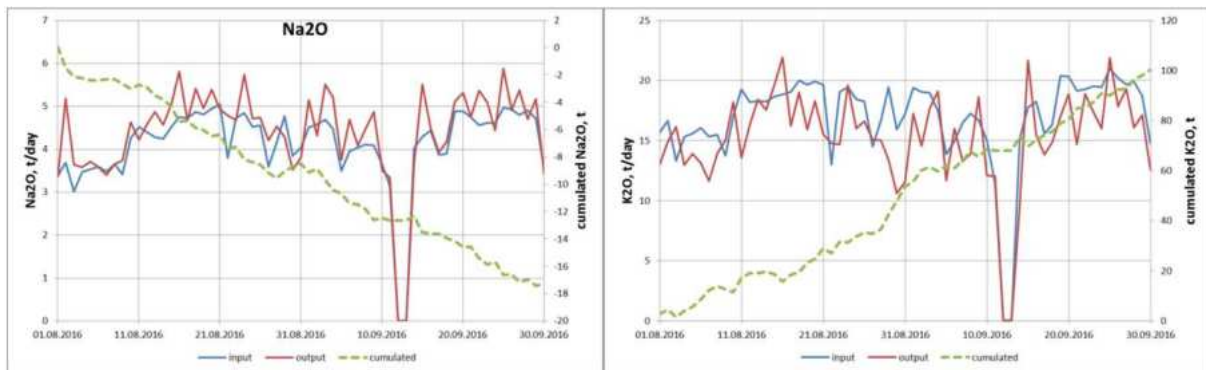


**Figure 16** Alkali balance for one month considering only variation in slag and sinter analysis

In **Figure 17** the alkali content in the slag is illustrated as a function of the hot metal temperature and the basicity for the campaign with detailed analysis. While the correlations with Na<sub>2</sub>O were low, those for K<sub>2</sub>O were notable. An increase in the hot metal temperature, which simultaneously means an increase in slag temperature, has led to lower potassium content in the slag. The same behaviour has been found for the basicity. The influence of the temperature and the basicity on the alkali content in slags is well known and a low slag basicity procedure is common at VASD due to the high alkali load.

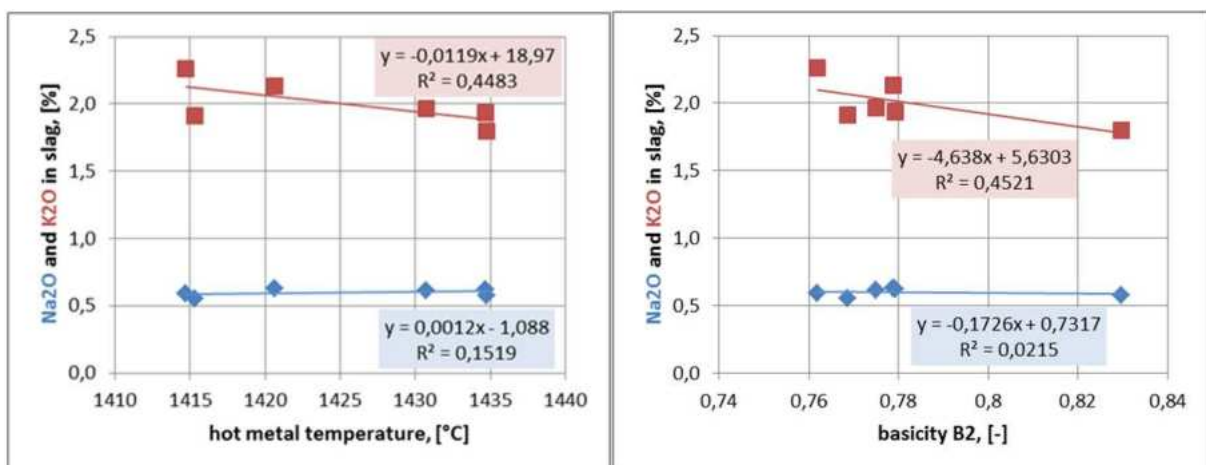


**Figure 17** Alkali content in slag depending on HM temperature and basicity

The above-mentioned gap between in- and output may be due to an insufficient analysis of slag. The operational procedure covers only one sample, which is taken at a predefined time during a tap. That means that for every tap only one sample and the corresponding analysis is known. It is expected that especially the potassium content in the slag and its temperature will change during the tapping process.

Due to this uncertainty six taps have been analysed more in-depth. Therefore, in addition to the regular slag sample further ones have been taken in defined time steps of 5 minutes. At the same time the hot metal temperature has been measured. In **Figure 18** the HM-temperature vs. the basicity B2 of these slag samples are shown. The additional number of samples is between four and six depending on the tapping time. The HM-temperature doesn't change much, the greatest difference is 12°C, in most cases it's less than 6°C. A big variation can be noticed at the basicity B2. As we know that B2 is very important for the Alkali capacity of slag, we can't neglect the time-depending influence during tapping on Alkali capacity. The variation of Alkalies for these additional slag samples can be seen in **Figure 19**.

The solid line indicates the value when the regular and the additional samples will have the same content in Na<sub>2</sub>O respectively K<sub>2</sub>O. The absolute difference for Na<sub>2</sub>O is only small, but the one for K<sub>2</sub>O is remarkable. For these six taps the divergence between the mean value of the additional samples and the regular one is 0.1%. The understanding of a varying Alkali-content through one tap leads to a recalculation of the balance above. Therefore, the K<sub>2</sub>O content in the slag has been increased for 0.1% (absolute). The cumulated difference between the input and the output mass sinks from around 100 tons to 50 t which means relatively from 10.4% to 5% (see **Figure 20**), respectively.

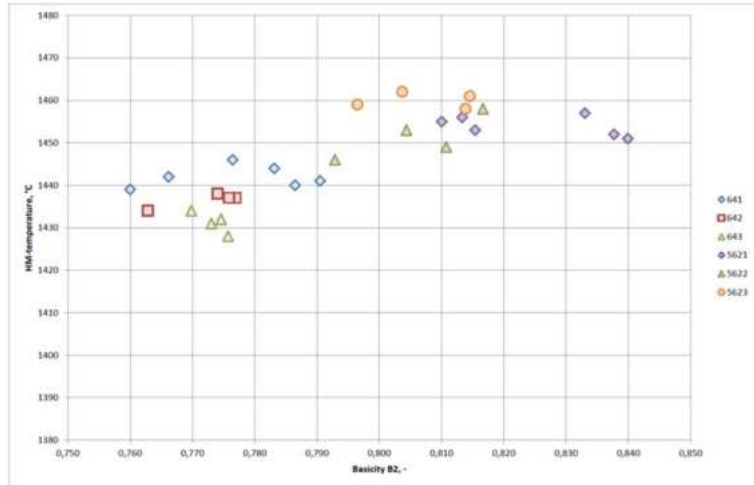


**Figure 18** In-depth analysis of slag samples (same symbols belong to same taps)

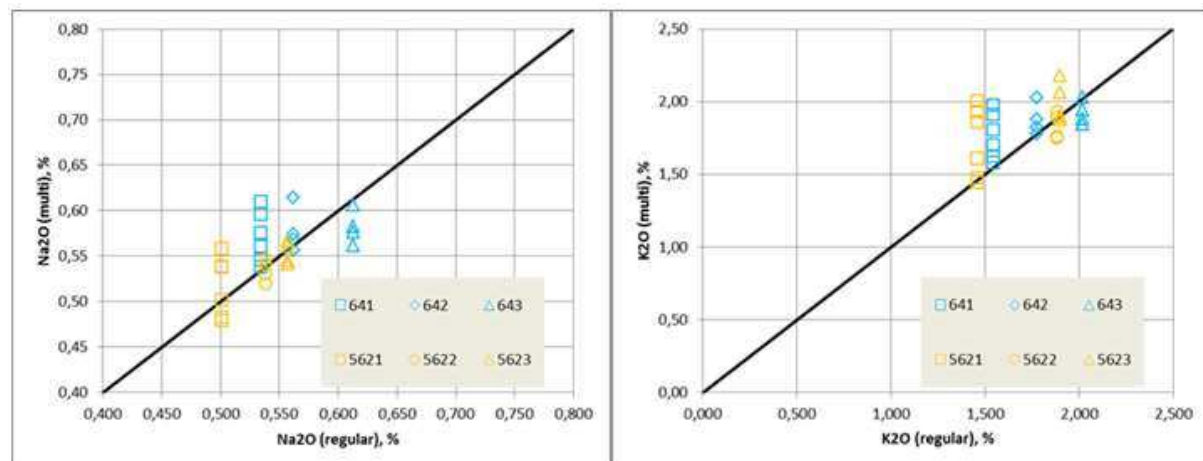


**Figure 19** Variation of the content in Na<sub>2</sub>O (left) and K<sub>2</sub>O (right) compared to the regular slag analysis

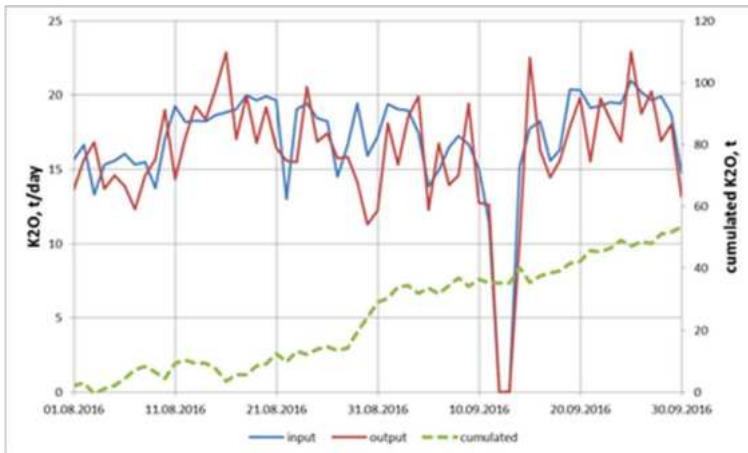


**Figure 20** Recalculation of K<sub>2</sub>O balance with corrected K<sub>2</sub>O content of the slag

While the influence of slag temperature and basicity particularly for potassium has already been shown, the influence of BF process conditions on alkali content of slag has been analysed for a large number of tap data. Therefore, more than 3000 taps and the corresponding process data have been investigated. The alkali-content of slags has been grouped in steps of 0.1% K<sub>2</sub>O and the associated process and slag data were calculated as a mean value for each group. These leads to an almost normal distributed numbers of taps (see **Figure 21**). The basicity for this basic quantity shows its important role for the potassium yield: the lower the basicity, the higher the Alkali content.

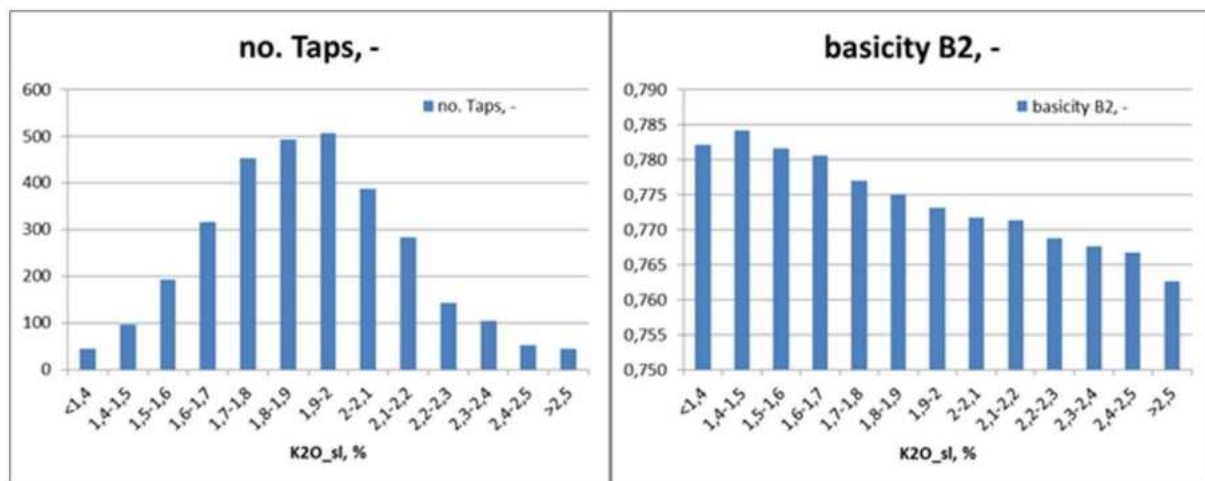


**Figure 21** Distribution of K<sub>2</sub>O content in the slag (left) and basicity B2 (right)

The dominating influence of HM temperature and particularly B2 doesn't allow finding any other potential relationships to process conditions. That's why the data has been reduced by including only taps with HM temperature between 1415 and 1425°C and basicity B4 between 0.815 and 0.825. From there the number of acceptable taps has been reduced to around 200 (see **Figure 22**); now the variation in HM temperature is very low.

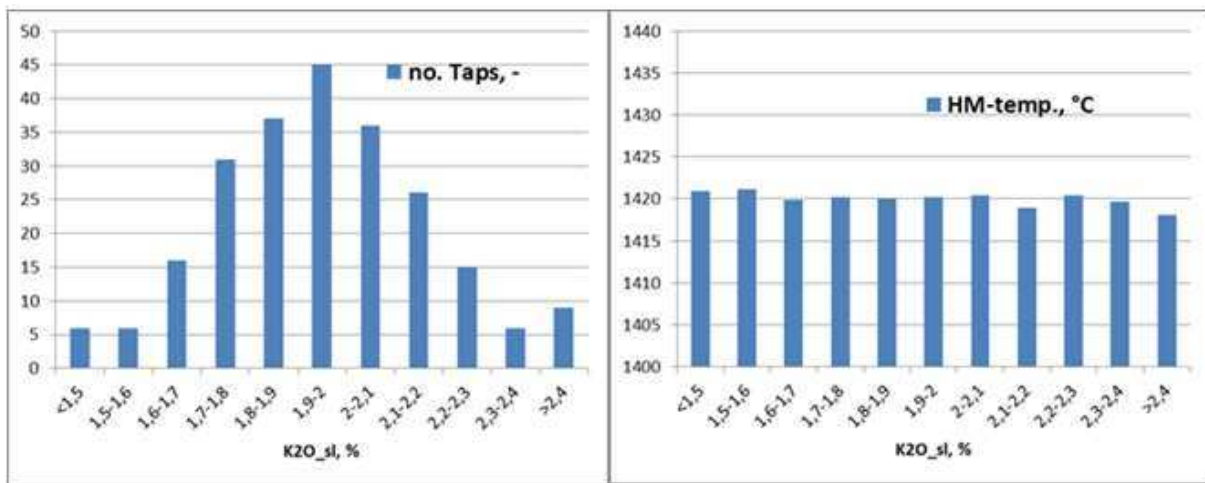


**Figure 22** Distribution of K<sub>2</sub>O after data selection (left) and HM temperature for the defined groups (right)

From **Figure 23** to **Figure 25** the correlations, which have been found, are shown. It must be considered that the first and last two bars only belong to a mean value of a few taps, so the variation can be high. Regarding the K<sub>2</sub>O content in slags there is a positive correlation with the flame-temperature and the content of Mn in the slag. There is a negative correlation to top gas temperature, share of pulverized coal, MgO and Al<sub>2</sub>O<sub>3</sub> in the slag. These mentioned slag components are depending on the slag condition itself, i.e. its temperature and composition – so the direct relationship between alkali content and these components does probably not exist. The role of physical characteristics like viscosity and wettability was not investigated and could also have an effect on the alkali capacity of slags.

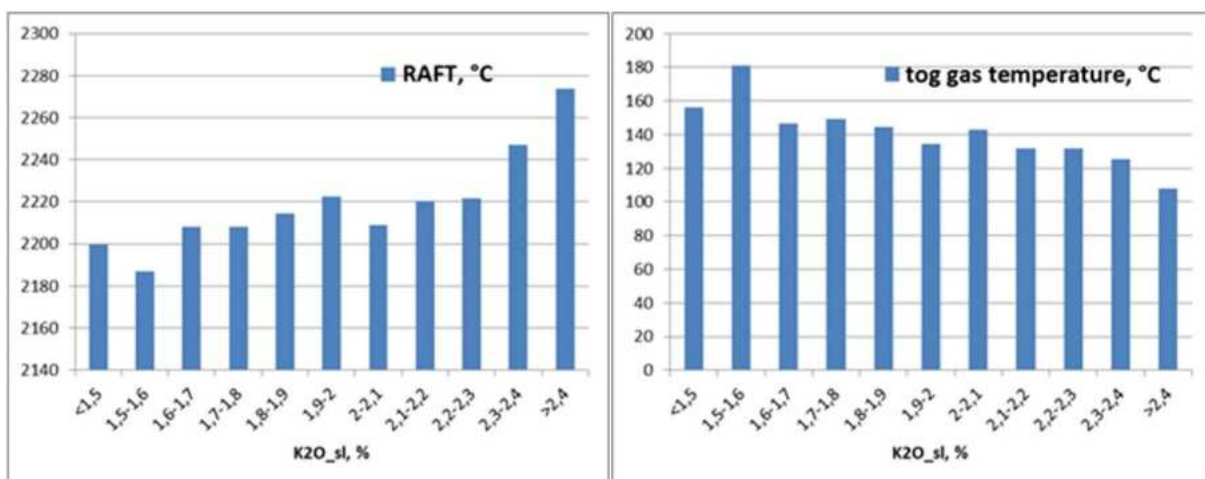


**Figure 23** Flame temperature (left) and top gas temperature (right)

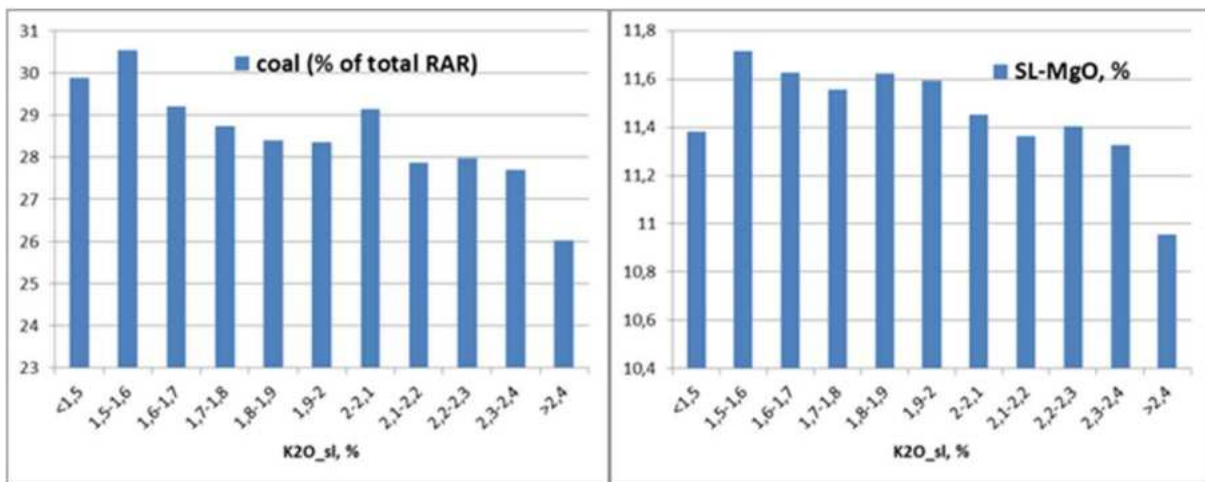


**Figure 24** share of pulverized coal in reducing rate (left) and MgO content of slag (right)

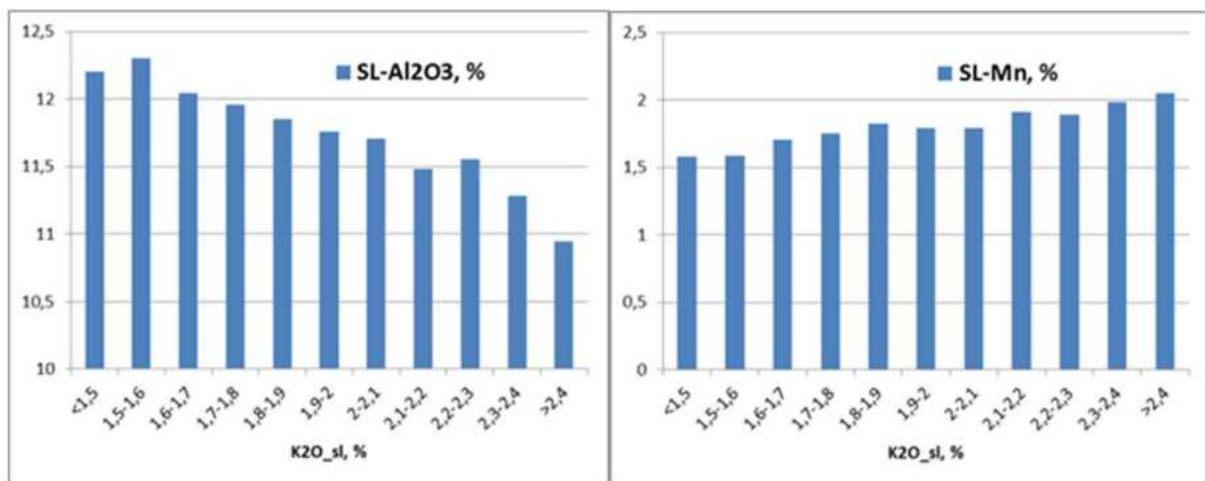


**Figure 25** Al<sub>2</sub>O<sub>3</sub> (left) and Mn (right) in slag

A very interesting event has happened during July 2017. After a planned BF stop permeability (**Figure 26** left) has got bad going along with a brief increase in burden slipping and low HM temperatures. This month has been characterized by changing HM demands and production has been therefore not stable. The heat flow in the lower stack area has been low since the planned stop and has been keeping its low level. On the other side the heat flow at the belly has been remarkable high after the 14<sup>th</sup> of July (see **Figure 26** right). This thermal state may indicate the building of accretions in the lower stack area. The K<sub>2</sub>O balance has been showing an unexpected behaviour because while the K<sub>2</sub>O input has been decreasing till the 20th due to a reduction in the sinter rate the output has kept high. So, the cumulated mass has decreased during this time whereas it has been rather stable before and afterwards. On the one hand the absolute K<sub>2</sub>O volume has decreased after the planned BF stop but on the other hand the stack temperatures have implicated the building of accretions. These inconsistent indications may be answered by the higher heat flow at the belly. Probably the decomposition of accretions in the belly has been more dominant than the building of accretions in the belly. So, there has been a change in the thermal condition of the BF probably caused by the BF stop and this has led to a shift of the accretion building and dissolution area.

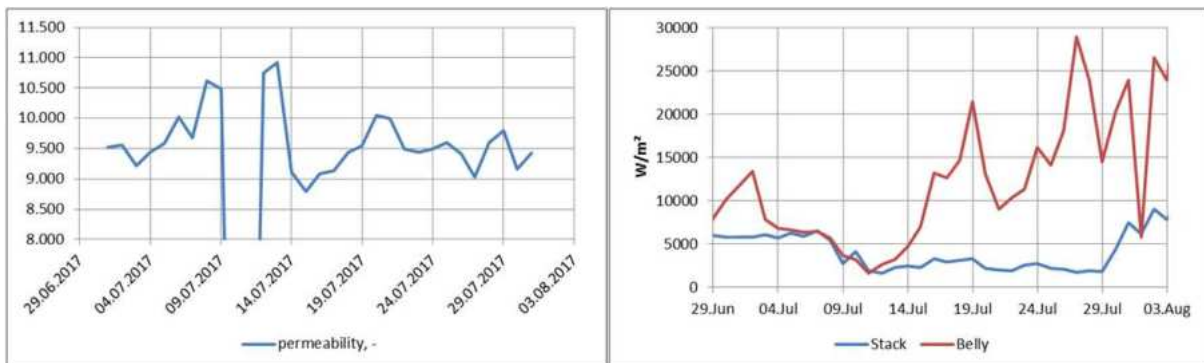


**Figure 26** permeability (left) and heat flow in the belly and lower stack (right)

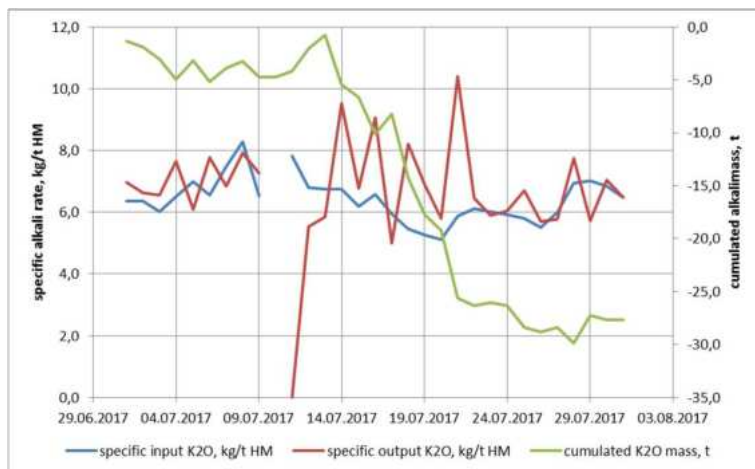


**Figure 27** specific  $K_2O$  flow and its cumulated mass

### 2.3.1.1.4 BF alkali balances during normal operation at DUNAFERR

For determination of BF alkali balances at DUNAFERR, several investments have been made in order to achieve accurate measurement of quantities of input and output streams, as well as the chemical compositions thereof. The development and investment topics required from the point of view of the project are specified as follows.

Installation of automatic sampler on the belt conveyor system used for coke given to the Ironworks Coke is supplied to the blast furnace by K7 belt conveyor. Formerly the sample was taken manually. Though this method conforms to standard, but it is time-consuming and labour-intensive, belt conveyor stoppage and re-start may be damaging and consume additional energy. The preparation of the installation of automatic sampler, which complies with the standard, started with enquiries on 27 May 2015. A second-hand, but renovated piece of equipment from Hungary was regarded as the most favourable. For installation the conveyor bridge pillar had to be reinforced, its steel structure had to be reconstructed, unnecessary pipelines on conveyor bridge top had to be demolished, sample storage tanks had to be constructed and installed.

Designing was started on 8 August 2015, and then following several modifications, improvements it was completed on 2 February 2016. Then the contractor company was chosen from the tenderers. Steel structure assembly was completed on 6 July 2015, and then the sampler was located and commissioned. Coking Plant specialists also took part in establishing the control, furthermore in coordinating the overall project. Following the test run the equipment takeover took place on 10 August 2016. **Figure 28** shows the automatic coke sampler installed on the belt conveyor system.



**Figure 28** Automatic coke sampler on the belt conveyor system

Automatic dynamic railway weighing machine required for blast furnace slag volume measurement. Significant part of alkalis is discharged from the blast furnace with the slag produced during smelting. Its chemical composition was clear based on the samples taken by tappings, but the mass was specified only by means of theoretical calculations. This indicator can be used on longer term, but it is not enough for making accurate material balance.

To solve the problem we chose railway weighing of the liquid slag while being transported to the place of processing.

We chose the technically and financially most suitable one from five tenders in August 2015. Following contracting the designing, permitting and preparing works were completed by the beginning of 2016, and hereby we could start on-site works in March. Following construction, integration and calibration of data collecting and displaying system the National Transport Authority gave the permit for putting into use in July 2016. **Figure 29** shows the installed automatic dynamic railway weighing machine for blast furnace slag.



**Figure 29** Automatic dynamic railway weighing machine for blast furnace slag

Reconstruction of material charging measurement data collecting system at the hoppers of Blast Furnace 1 in order to increase accuracy and reliability

In the former system self-developed electronics and one personal computer were installed on the scale car. A self-developed software and a lookout application ran on the computer, with Windows XP being the OS.

There were lots of failures with it: Windows XP, hardware failures, no spare for electronics, etc.

We thought the solution lies in the application of an Omron PLC. This PLC serves all the functions that the former electronics could perform, but at a greater speed and with greater reliability. We used an Omron display terminal, on which the former images were developed so that the operators can switch as smoothly as possible. Besides the PLCs on the 4 cars the system is equipped with a so-called central 5th PLC. The function of it among other things is to draw up as well as transfer the formulas to the appropriate scale car. Central PLC and PLCs on scale cars are connected by Ethernet/IP through optical and wireless media.

Functions fulfilled:

- Writing, testing of PLC programs
- Writing, testing of display terminal programs
- Reconstruction of the communication network

Experiences, advantages:

- missed data arising from computer and communication failures have been decreased to a significant degree
- function expansions requested by the plant (e.g.: monitoring of interlock bridge)
- following short-term network interruptions data can be replaced
- instead of independently developed card a commercially also available instrument was installed (spare parts available)

Dunafer has determined the alkali balances at its blast furnace in three test periods: Phase I, II, III, IV (**Table 4**).

The results of the alkali balances at Dunafer during the four test periods are presented in **Table 5**.

**Table 4** Test periods for BF alkali balancing at Dunafer

phase	period
I	2016.03.01 - 2016.03.14.
II	2016.08.08 - 2016.08.21.
III	2016.11.28 - 2016.12.11.
IV	2017.05.15 - 2017.05.28.

**Table 5** Results of alkali balances at Dunafer during four test periods

phase	alkali	sinter	pellets	slag_dpp	limestone	coke	slag	dust	dorr_sludge
I	na2o	29766,00	2311,86	0,00	144,91	12000,52	26137,05	269,93	252,97
	k2o	13439,97	243,94	0,00	504,04	13368,45	36576,79	288,72	362,84
II	na2o	17673,69	11319,15	3396,17	113,90	8055,06	20636,87	383,91	
	k2o	4580,93	9973,04	908,77	301,59	11383,69	29788,16	384,29	
III	na2o	20492,43	6248,77	1761,72	69,16	11481,33	26251,44	339,77	
	k2o	9387,50	5018,55	938,57	405,31	16429,78	46053,96	452,68	
IV	na2o	21919,87	6396,20	0,00	20,21	12753,04	27413,13	624,08	1502,20
	k2o	15385,46	11265,50	0,00	147,92	20927,56	56885,23	1139,41	2889,16

phase	alkali	input	output	in-out	(i-o)/i
I	na2o	44223,29	26659,95	17563,34	0,397
	k2o	27556,40	37228,35	-9671,94	-0,351
II	na2o	40557,97	21020,78	19537,19	0,482
	k2o	27148,02	30172,45	-3024,42	-0,111
III	na2o	40053,40	26591,21	13462,20	0,336
	k2o	32179,71	46506,63	-14326,92	-0,445
IV	na2o	41089,32	29539,41	11549,91	0,281
	k2o	47726,45	60913,80	-13187,35	-0,276

*amounts in kg*

*slag\_dpp: slag dump processing product*

phase	alkali	sinter	pellets	slag_dpp	limestone	coke	slag	dust	dorr_sludge
I	na2o	1,112	0,086	0,000	0,005	0,448	0,976	0,010	0,009
	k2o	0,502	0,009	0,000	0,019	0,499	1,366	0,011	0,014
II	na2o	0,837	0,536	0,161	0,005	0,382	0,978	0,018	
	k2o	0,217	0,472	0,043	0,014	0,539	1,411	0,018	
III	na2o	0,960	0,293	0,083	0,003	0,538	1,230	0,016	
	k2o	0,440	0,235	0,044	0,019	0,770	2,158	0,021	
IV	na2o	0,814	0,238	0,000	0,001	0,474	1,018	0,023	0,056
	k2o	0,572	0,419	0,000	0,005	0,777	2,113	0,042	0,107

phase	alkali	input	output	in-out
I	na2o	1,652	0,996	0,656
	k2o	1,029	1,390	-0,361
II	na2o	1,921	0,996	0,926
	k2o	1,286	1,429	-0,143
III	na2o	1,877	1,246	0,631
	k2o	1,508	2,179	-0,671
IV	na2o	1,526	1,097	0,429
	k2o	1,773	2,263	-0,490

*amounts in kg/tHM*

*slag\_dpp: slag dump processing product*

phase	burden, t	coke, t	slag, t	pig iron, t	burden, kg/t	coke, kg/t	slag, kg/t
I	44363,120	13262,470	8333,146	26775,500	1656,855	495,321	311,223
II	33926,020	10702,585	5325,500	21108,200	1607,244	507,034	252,295
III	34480,850	10506,618	6060,680	21343,700	1615,505	492,259	283,956
IV	42350,960	13098,097	6677,500	26917,700	1573,350	486,598	248,071

The following statements can be made:

- Balance deficits in alkali balance are significant in all three periods,
- Deficits of Na<sub>2</sub>O- and K<sub>2</sub>O-balances have reverse signs in each period,
- Arising from the above alkali-balances are not applicable to draw far-reaching conclusions, as well as to connect it with other tests/processes,
- The composition of blast furnace charge significantly differed in each period,
- Relevant differences are detected in alkali-content of the sinter and blast furnace coke in each period.

The changes in single parameters characterizing the quality of blast furnace coke are presented by the following figures, showing frequency distribution of the percentage of coke ash (**Figure 30**), S (**Figure 31**), K<sub>2</sub>O (**Figure 32**) and Na<sub>2</sub>O (**Figure 33**).

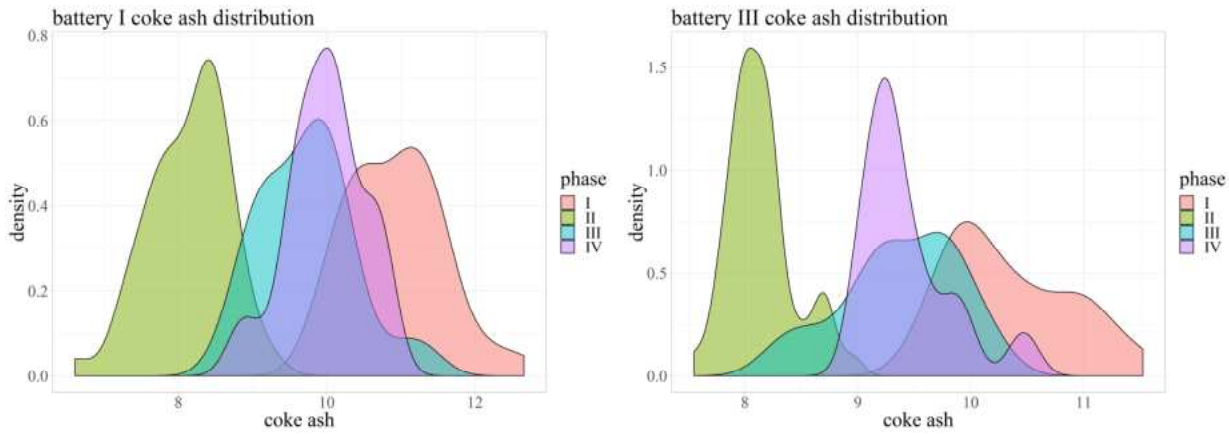


**Figure 30** Frequency distribution of coke ash percentage (battery I and III; pink: phase I, green: phase II, blue: phase III, purple: Phase IV)

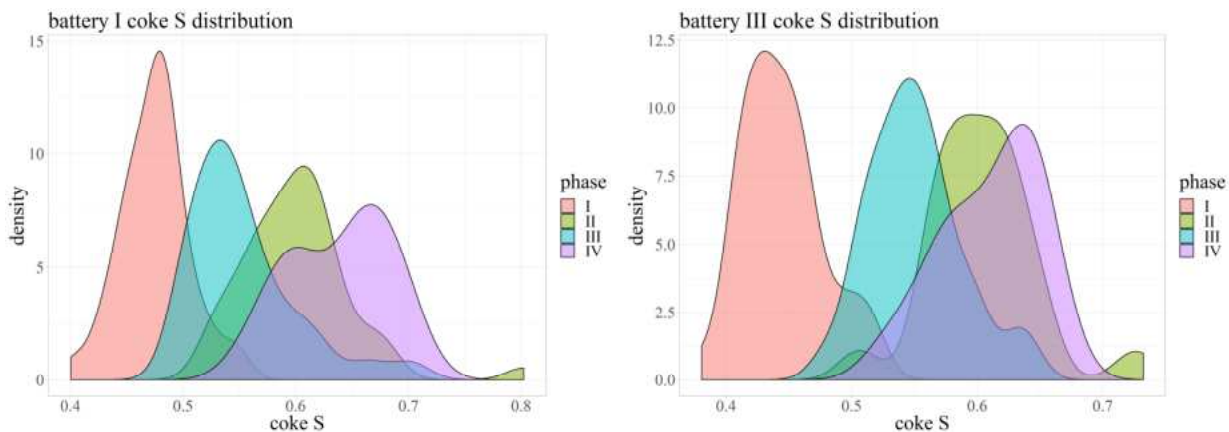


**Figure 31** Frequency distribution of coke S percentage (battery I and III; pink: phase I, green: phase II, blue: phase III, purple: Phase IV)

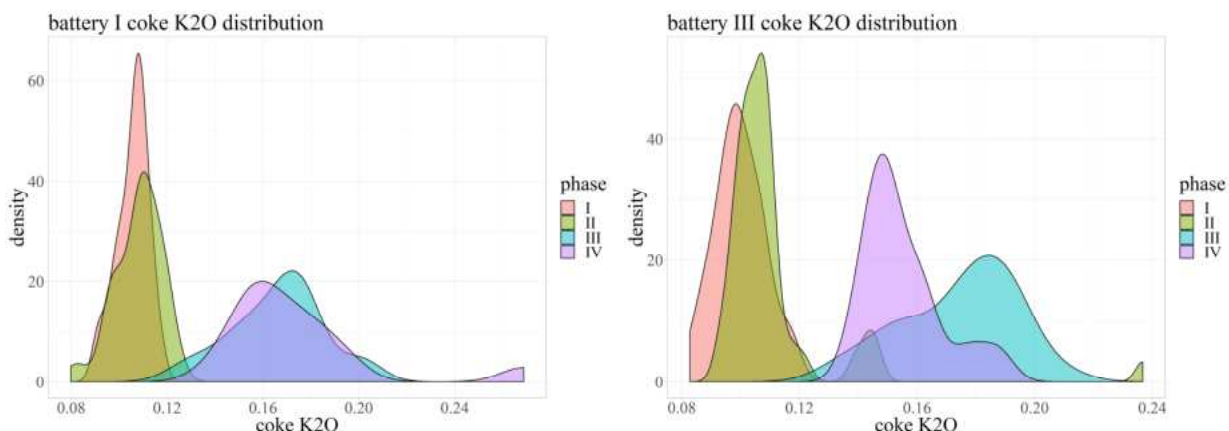


**Figure 32** Frequency distribution of coke K<sub>2</sub>O percentage (battery I and III, pink: phase I, green: phase II, blue: phase III, purple: Phase IV)

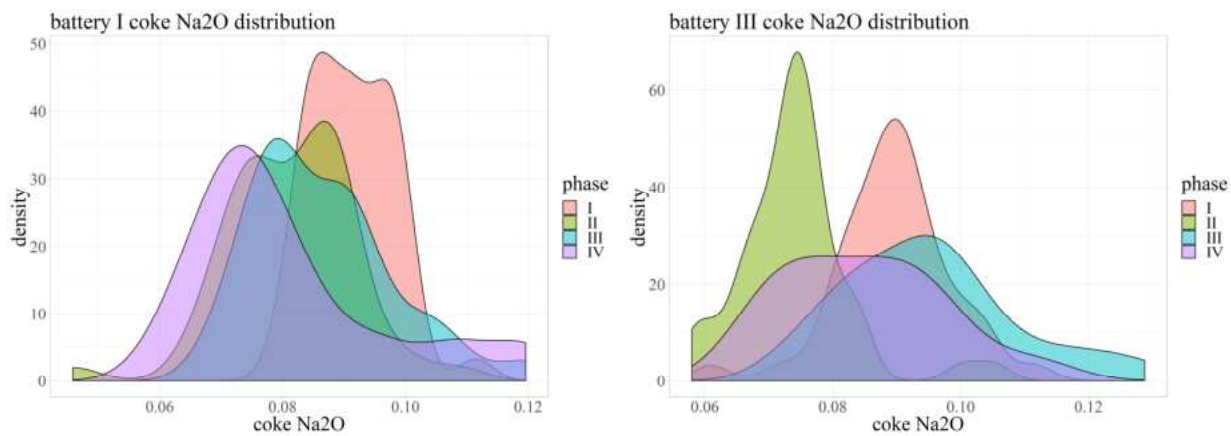


**Figure 33** Frequency distribution of coke  $\text{Na}_2\text{O}$  percentage (battery I and III, pink: phase I, green: phase II, blue: phase III, purple: Phase IV)

The BF alkali-balances were performed by the following procedure:

- all charging data - qualities and weighed quantities - were recorded in database,
- all tapping data - quantities and analysis values - were recorded in database,
- sinter analysis data - nine samples per day - were recorded in database,
- pellets and other charge materials analysis data - sample per week - were recorded in database,
- quantity data of alkali-balances were determined by summing up the products of quantity and composition data pairs of every single item (i.e. discrete charging data, tapping data)

The following statistical tests were performed to determine certain correlations of alkali removal, jointly for data of all three test periods (**Figure 34**, **Figure 35**).

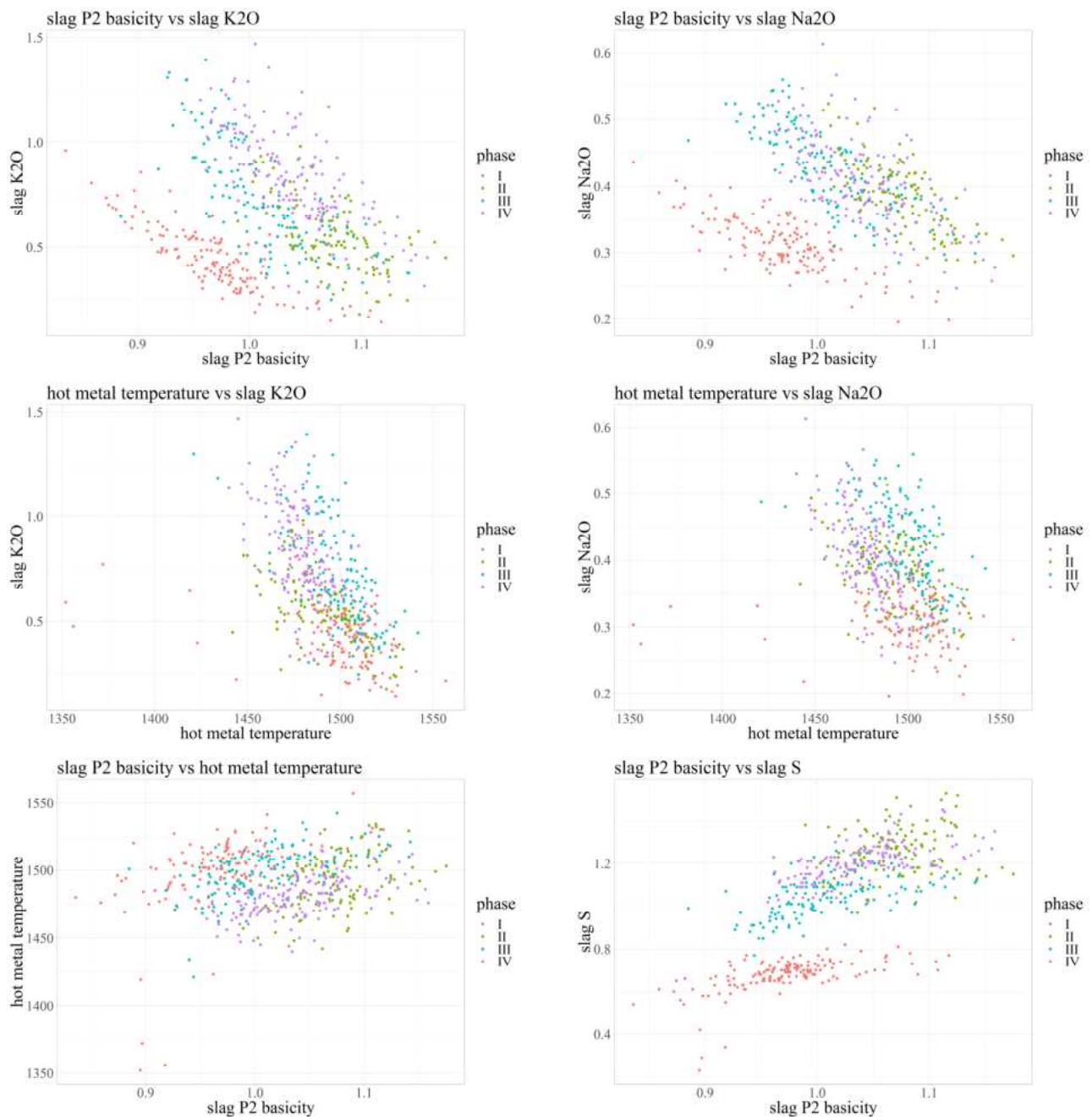


**Figure 34** Statistical tests to determine correlations of alkali removal, jointly for data of all three test periods – Part 1: slag basicity, hot metal temperature vs slag K<sub>2</sub>O, Na<sub>2</sub>O and slag S content (pink: phase I, green: phase II, blue: phase III, purple: Phase IV)

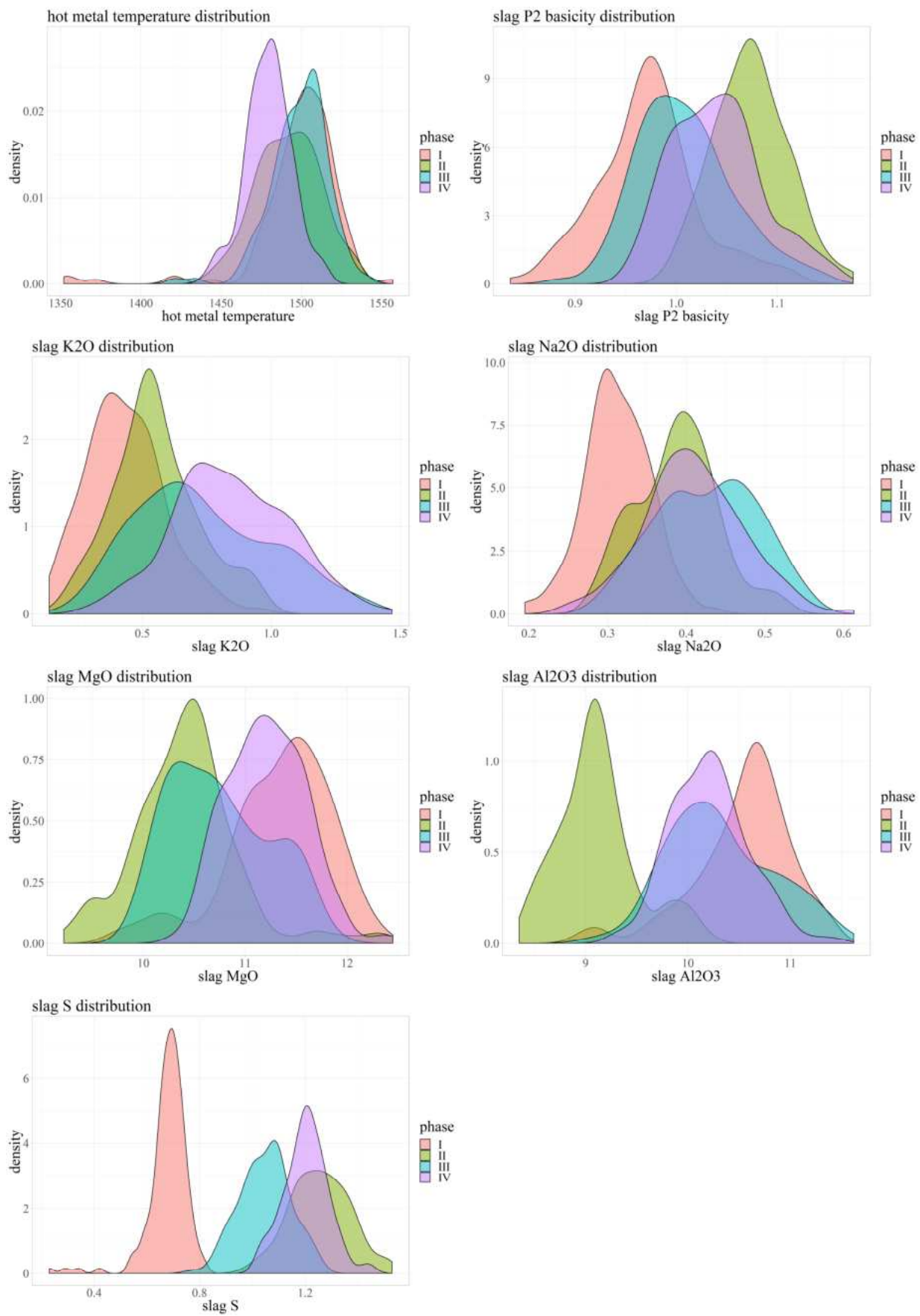


**Figure 35** Statistical tests to determine correlations of alkali removal, jointly for data of all three test periods – Part 2: Frequency distributions of hot metal temperature, slag basicity, slag K<sub>2</sub>O, slag Na<sub>2</sub>O, slag MgO, slag Al<sub>2</sub>O<sub>3</sub> and slag S content (pink: phase I, green: phase II, blue: phase III, purple: Phase IV)

The following comments can be made:

- Both in the case of K<sub>2</sub>O-, Na<sub>2</sub>O-content of slag and S-content of slag significant shift can be detected at the sets of points characterizing particular periods,
- Shifting of the sets of points is clearly explained by formerly presented change in the quality of blast furnace charge (i.e. specific slag quantity, alkali load, change of coal charge),
- The spread within the sets of points is justified by relative instability of blast furnace charge within the particular period of time.

Due to the above it is more practical to pay special attention to the analysis of the relations in a particular period of time. The information specific of the alkali-balances of the third period are presented by the following charts (**Figure 36**, **Figure 37**, **Figure 38**, **Figure 39**):

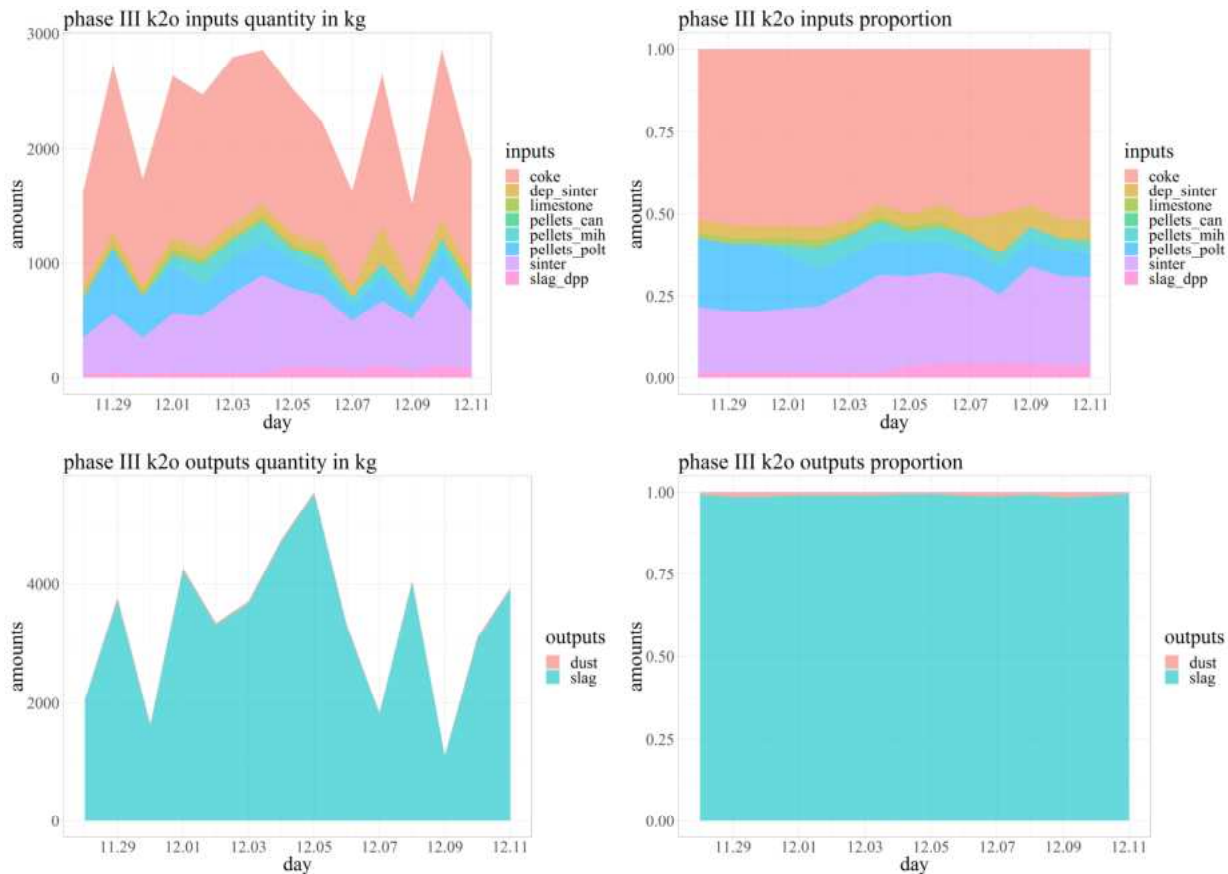


**Figure 36** K<sub>2</sub>O inputs and outputs (kg; proportion) during Phase III

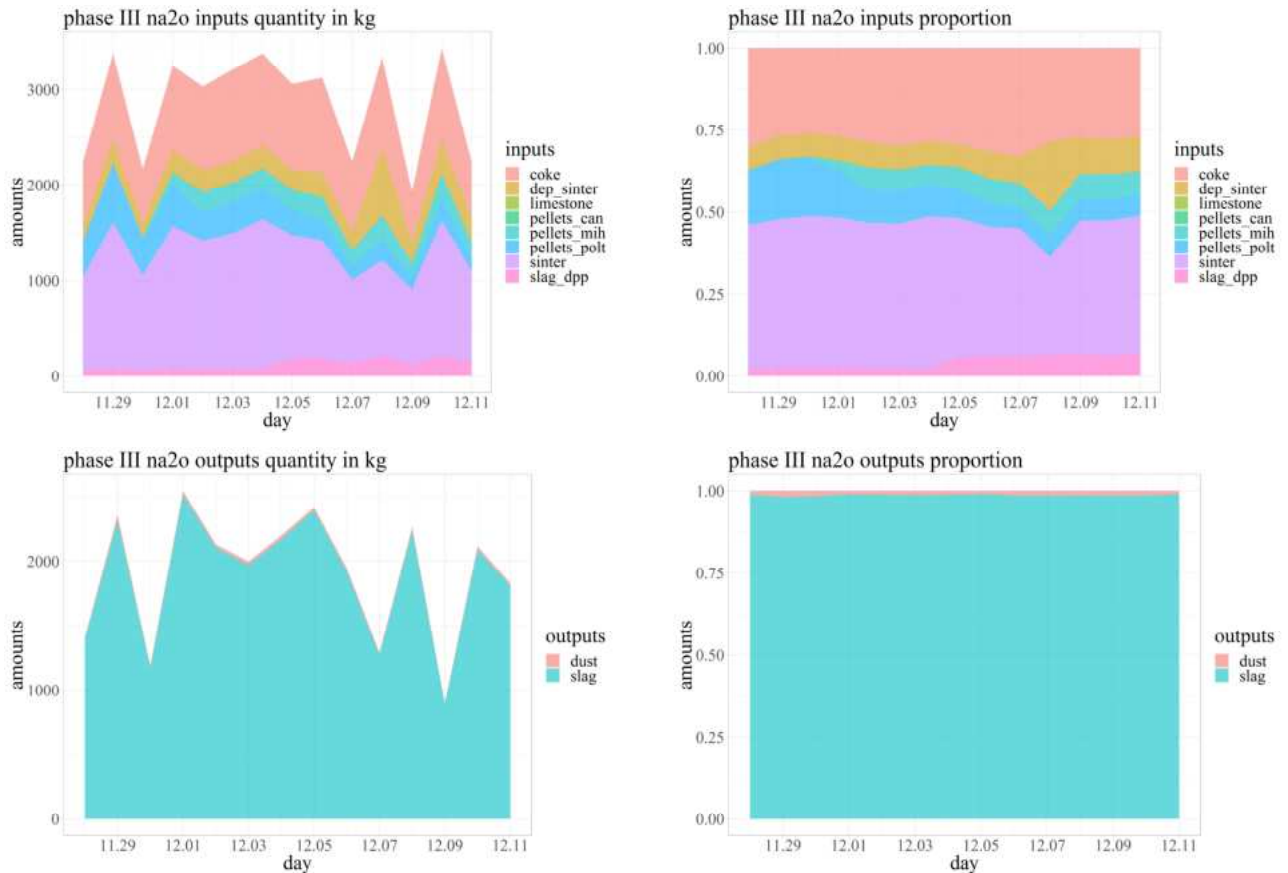
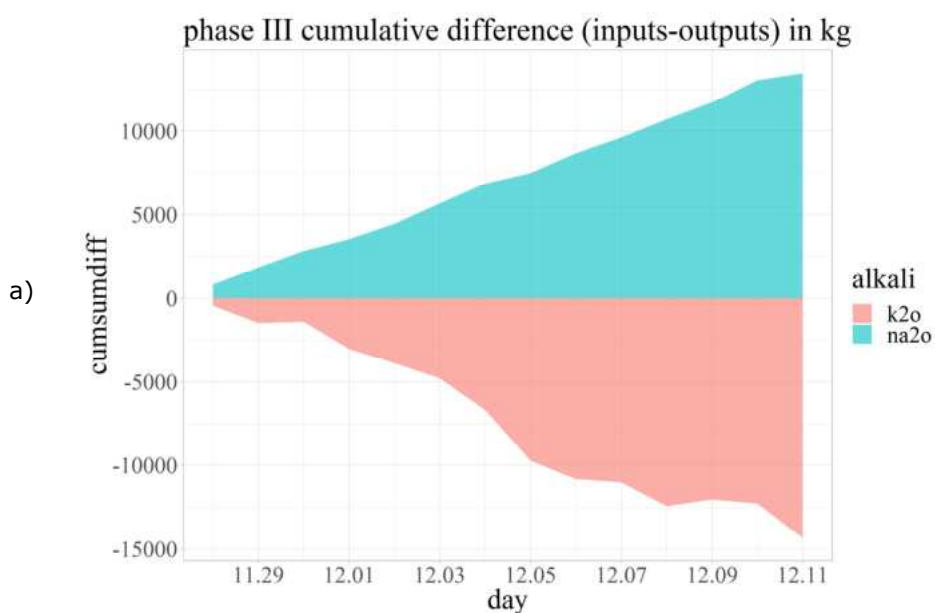


**Figure 37** Na<sub>2</sub>O inputs and outputs (kg; proportion) during Phase III



### phase III trend of slag Na<sub>2</sub>O and K<sub>2</sub>O

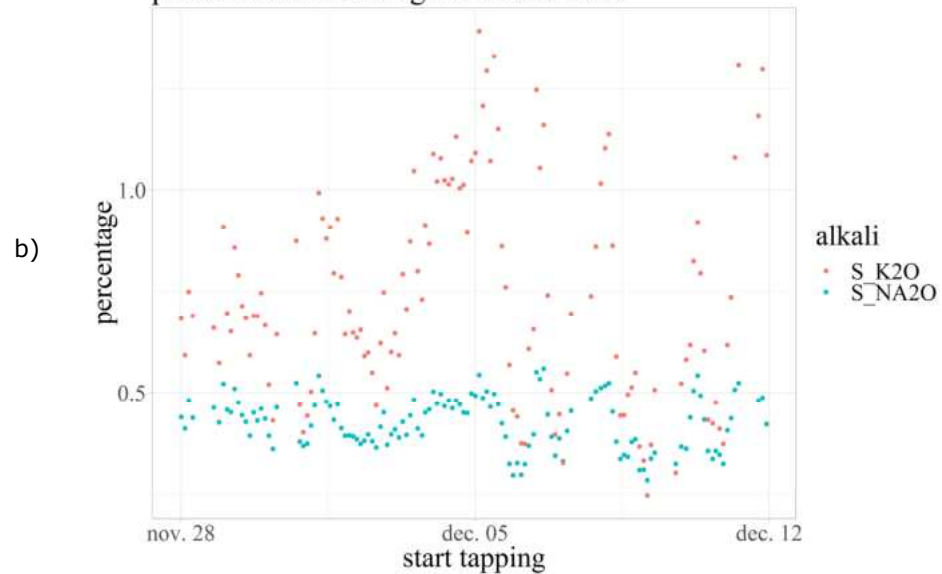


**Figure 38** a) Cumulative difference (inputs-outputs) K<sub>2</sub>O and Na<sub>2</sub>O; b) Time trend of Na<sub>2</sub>O and K<sub>2</sub>O percentage in BF slag (Phase III)

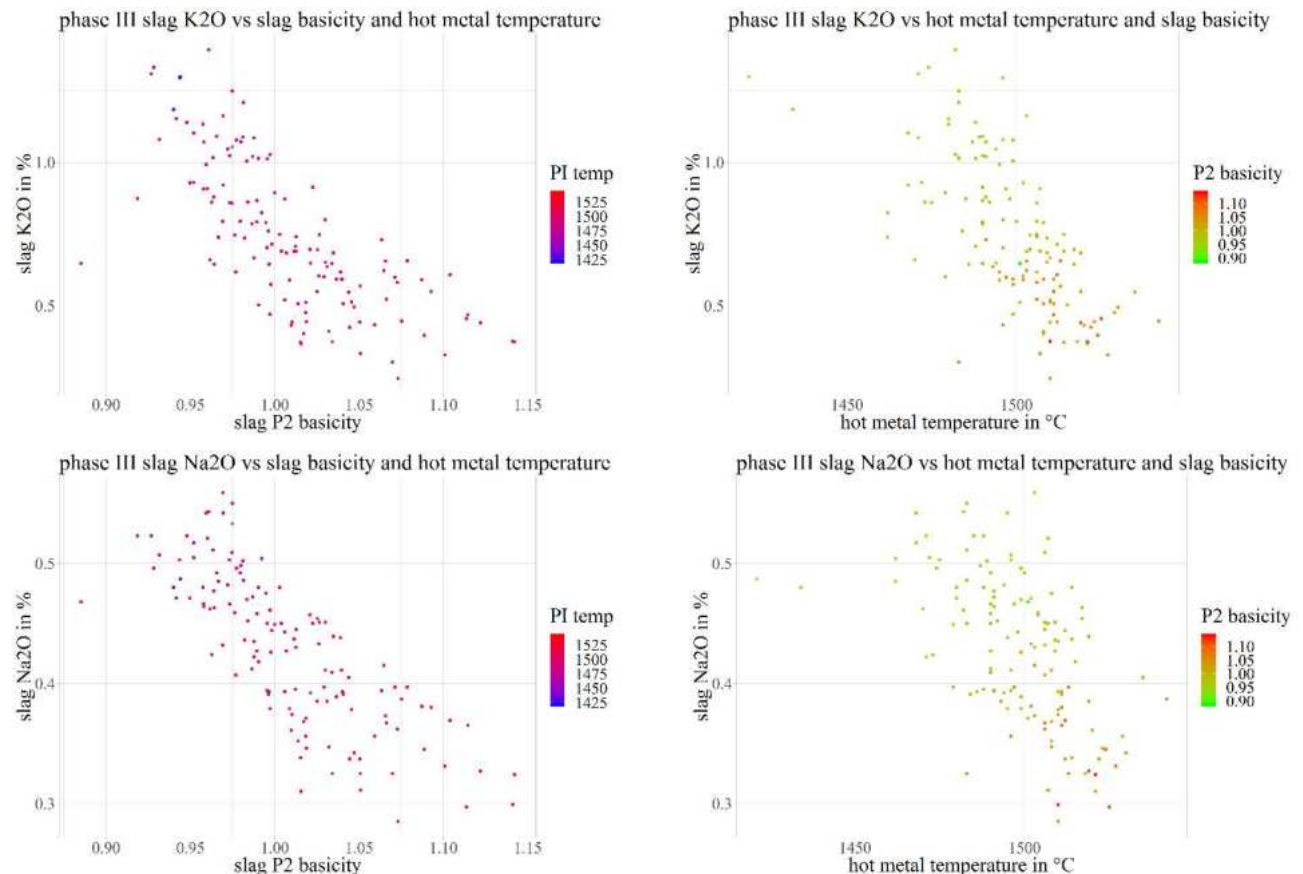


**Figure 39** Statistical evaluations to determine correlations concerning K<sub>2</sub>O and Na<sub>2</sub>O content of slag (Phase III)

Based on the results of the alkali balances during the measurement periods at Dunafer, the following main conclusions are drawn:

- Balance deficits in alkali balance are significant in each period.
- Deficits of Na<sub>2</sub>O- and K<sub>2</sub>O-balances have reverse signs in each period.
- The deviations of alkali balances are not attributable to measurement uncertainties.
- Arising from the above alkali-balances are not applicable to draw far-reaching conclusions, as well as to connect it with other tests/processes,
- The composition of blast furnace charge significantly differed in each period.
- Relevant differences are detected in alkali-content of the sinter and blast furnace coke in each period.
- The basicity of slag, as well as tapping temperature have significant, non-negligible effect on alkali-content of slag, hereby also on alkali removal.
- Both increase of slag basicity and increase of tapping temperature result in decrease of alkali-content of slag, thereby worsening of the efficiency of alkali removal.
- The increase of sulphur removal efficiency is accompanied by the decrease of alkali removal efficiency.

#### **2.3.1.1.5 Comparison of alkali balances at the different blast furnaces during normal operation**

In **Table 6** the results of the alkali balances performed at the three industrial blast furnaces as well the balance from the LKAB EBF® are summarized. The potassium input (K<sub>2</sub>O) at VASD with 6.5 to 8 kg/t HM is significantly higher (ca. 5x) than those at all other blast furnaces (Dunafer, SSAB and LKAB EBF®). The difference concerning the sodium input (Na<sub>2</sub>O) is lower between the different blast furnaces: Here the highest input is observed at Dunafer and VASD (1.5 to 2 kg/t HM), which is around 2x the value of the SSAB blast furnace and LKAB EBF®. In all cases a difference between the input and output amount of potassium and sodium as calculated from the analyses and mass data was observed. For potassium, at Dunafer and SSAB the observed output amount exceeded the input amount (up to 145 % of input; negative accumulation), while at VASD and LKAB EBF® the observed output amount was lower than the input (84 – 90 % of input; accumulation). For sodium, at SSAB and VASD the observed output amount exceeded the input amount (up to 118 % of input), while at Dunafer and LKAB EBF® the observed output amount was lower than the input (52 – 87 % of input). At SSAB a sensitivity analysis was performed with the result that balancing of K<sub>2</sub>O was very sensitive for the alkali content of slag and the amount of slag, which might partly explain the negative accumulation of K<sub>2</sub>O for a longer period.

For the operational blast furnaces, the hot metal temperature and the slag basicity (with negative correlation) were identified as the main influencing operational parameters promoting the alkali output. According the evaluation of VASD operational data, further the flame temperature, Mn in slag, top gas temperature, the share of PCI, as well as the MgO and Al<sub>2</sub>O<sub>3</sub> content may indicate conditions promoting the alkali output via the slag.

**Table 6** Alkali balances at industrial BF's – Summary of results

Aspects	Unit	Dunafer	SSAB	VASD	LKAB (EBF®)
K <sub>2</sub> O input	kg/t HM	1.0 to 1.8	1.2 to 1.5	6.5 – 8	1.3
Na <sub>2</sub> O input	kg/t HM	1.5 to 1.9	0.9	1.5 - 2	1.0
K <sub>2</sub> O output	% of input	111 to 145 %	K <sub>2</sub> O: 109 % (all alkali: max. 118%	90 %	84 %
Na <sub>2</sub> O output	% of input	52 to 72 %		107 %	87 %
Main Influences on alkali output	---	K <sub>2</sub> O and Na <sub>2</sub> O: HM temp.; slag basicity*	Slag basicity*	K <sub>2</sub> O: <u>HM-temp.</u> ; <u>slag basicity</u> *; flame temp., Mn in slag, top gas temp*, share of PCI*, MgO* and Al <sub>2</sub> O <sub>3</sub> * in slag	---
* negative correlation					

### 2.3.1.1.6 Thermodynamic calculations (LTU)

#### *Calculation procedure and assumptions*

Thermodynamic calculations to simulate the reaction occurring in a blast furnace have been carried out at LTU. It is well known that alkali circulation in a blast furnace is to some or even large extent controlled by the kinetics of the reactions. Nevertheless, calculation of the equilibrium conditions based on fundamental thermodynamic data can give an insight into the reactions that can occur. The purpose of the present calculations is to give an insight into the reactions occurring in a blast furnace with the recirculating elements, mainly alkaline but also chlorine, fluorine and zinc, at equilibrium conditions but not with any aim to be able to describe the precise quantitative relationships. The heterogeneous nature of the process is instead described by considering the different reaction systems that can exist in a blast furnace, e.g. the reaction systems gas - coke, gas - ferrous burden material etc., as further described below. Quantitative equilibrium calculations have been carried out using the simulation package FACTSAGE [24] version 7.1, using the databases FactPS, FTmisc and FToxicid.

Calculations have been carried out using raw material compositions and process conditions corresponding to those at SSAB Oxelösund BF2. Data based on the normal operation of BF2 at SSAB Oxelösund are given in **Table 7** and **Table 8**. Normal operation includes injection of blast furnace dust but the chosen data is from a period without dust injection. The blast furnace is operated at ambient pressure, resulting in a slight overpressure in the top. Preliminary calculations were carried out at the pressure 1 atm throughout the furnace. However, to be more generally applicable to European blast furnace operation some changes were introduced in the extended calculations reported here. A higher pressure has been assumed, 2.6 atm below the bosh region

and 2 atm above, temperature of bosh region estimated based on calculation of melting range for slag forming components in the raw materials. It is known that volatile elements can cause a substantial circulating load within the blast furnace. The preliminary calculations were carried out using the raw material data given in **Table 7**. To be more generally applicable all of the calculations discussed further on in this text have been carried out with content of circulating elements, K, Na, Cl, F and Zn, increased to a level that can be estimated to prevail at steady state conditions, see further text below. The data given in **Table 7** for MPBO-alkaline and Coke-alkaline are the recalculated compositions used to describe the recirculating load for alkaline.

**Table 7** Blast amount and composition as well as composition of injection coal

Material	T (°C)	Nm <sup>3</sup> /thm	Composition (Vol%)				
			O <sub>2</sub>	N <sub>2</sub>	H <sub>2</sub> O		
Blast	933	1043	22.5	76.2	1.2		
	Composition (wt%) dry basis					Moisture	
	C	H	N	O	Ash		
Inj. Coal	83.0	4.33	2.15	4.09	5.65	0.5	

**Table 8** Raw material data used in the calculations

Raw material	Amount kg/thm	Composition wt% dry basis					
		Fetot	FeO	Fe <sub>2</sub> O <sub>3</sub>	SiO <sub>2</sub>	Al <sub>2</sub> O <sub>3</sub>	CaO
MPBO	1326.8	66.8	0.5	94.94	1.8	0.32	0.45
LD-slag	59.4	18.75	24.13		11.5	1.1	41.8
Limestone	13.8	0.24	0	0.2	1.2	0.8	53
Coke	401.9	0.4	0	0.52	6.74	3.11	0.16
Inj. Coal	80.4	0.498		0.71	2.26	1.47	0.41
Briquette	85.4	57.48	73.98	0	5.48	1.02	8.82
MPBO-alkaline	1326.8	66.8	0.5	94.94	1.8	0.32	0.45
Coke-alkaline	401.9	0.4		0.52	6.74	3.11	0.16
		Composition wt% dry basis					
		MgO	MnO	TiO <sub>2</sub>	Na <sub>2</sub> O	K <sub>2</sub> O	S
MPBO	1.3			0.35	0.04	0.02	0.001
LD-slag	10.57	3.1	1.4	0.06	0.05	0.06	0
Limestone	1.2	0.03	0.02	0.04	0.02	0.06	0
Coke	0.086	0.01	0.16	0.063	0.145	0.596	86.5
Inj. Coal	0.12	0.005	0.042	0.01	0.003	0.29	83.0
Briquette	2.1	2.02	0.46	0.07	0.113	0.213	3.95
MPBO-alkaline	1.3			0.35	0.125	0.375	0.001
Coke alkaline	0.086	0.01	0.16	0.505	1.516	0.596	86.5

**Table 9** Assumed hot metal composition at temperatures above the temperature of the cohesive zone. In wt%.

Fe	Si	C	Ti	Mn	S
96.44	0.4	2.5	0.1	0.5	0.06

The level of increased content of recirculating elements is selected so as to represent what can be assumed to be normal operation of European blast furnaces based on a literature survey. The amount of alkalis recirculating in the furnace has from the excavation of Japanese blast furnaces [25-27] been estimated to be in the range 17 to 24 kg/thm. This is perhaps the most precise figure existing for the recirculating load. Normal alkali load to a blast furnace is according to Kurunov [28] in the order of 2.5 kg/tHM, i.e. pointing to a recirculating alkali load in the order of 8 times the amount in the raw materials. The data for the blast furnace operations at SSAB in Oxelösund shows an alkali load corresponding to 1.87 kg alkali/tHM, somewhat lower than the 2.5 kg [28]. The total recirculating load was therefore set to 15 kg/tHM in the present calculations. The literature survey clearly shows that the slag is the major output for alkalis but at levels above the bosh region, considerable accumulation of alkalis has been observed in the coke but also in the iron burden. At lower temperatures, according to literature data at 1200°C and below, the accumulation

of alkalis in raw material is very limited [29-33]. Therefore, two different approaches have been used: At temperatures from 1200°C and below no accumulation of alkali in the raw materials is assumed. For the calculations of reactions with a gas coming from higher temperatures, this gas will however contain increased alkali content, as obtained from the previous calculation step at 1250°C. For calculation purposes, the increased alkali load at temperatures above 1200°C has been introduced through an increased alkali content of coke and pellets in the charge. Ryösä [31] and Lundgren [32] has determined alkaline content in MPBO pellets and coke, respectively, excavated from LKAB's experimental blast furnace. The alkali content used in the raw materials MPBO-alkaline and coke alkaline, **Table 8**, is obtained so as to be in rough agreement with the data given for alkaline content by Ryösä [31] and Lundgren [32] in the region just above the cohesive zone and to totally give an alkaline load of 15 kg/tHM.

The level of chlorine is assumed to be 0.4 kg/tHM and is assumed to be introduced through the injection coal. Chlorine content in other raw materials is assumed to be neglectable. Considering the data given in [34] where chlorine output/input almost equals one, it is for the present purpose assumed that total chlorine load within the blast furnace is equal to amount present in the raw materials. Lacking other information, the amount of fluorine is assumed to be one tenth of the chlorine load, i.e. 0.04 kg/tHM.

The level of zinc load at SSAB Oxelösund BF2 is lower than what in the literature is stated to be the normal zinc load. To make the calculated results more generally applicable to blast furnace operation, the level of zinc load in raw materials has been chosen to be 250 g/tHM. Based on the data given by Esezobor and Balogun [35] the circulating load is estimated to be in the order of six times the amount in the raw materials, i.e. 1500 g/tHM. This is in the calculations adjusted by increasing the amount of zinc in the briquettes. Zinc is assumed present as Zinc oxide in the raw material.

The high temperatures prevailing in the raceway region makes almost all of the materials passing through this extremely high temperature region, except coke, to evaporate. It was therefore determined to start the modeling by calculating the conditions in the raceway region, point 1 in **Figure 40**.

Calculations in the raceway region [24] are made assuming that coke and PCI are reacting with the blast. The amount of PCI and blast is according to the proportions given in **Table 7** with one hour as the calculation base. The amount of coke reacting is calculated so as to just give an excess of coke present in the raceway.

The temperature is set to 2100°C. The gas produced in the raceway is then cooled down to 200°C in steps of 50°C without interaction with any other material, simulating channeling in the furnace.

In all calculation cases, the pressure is decreased from 2.6 atm to 2 atm at the assumed temperature of the cohesive zone.

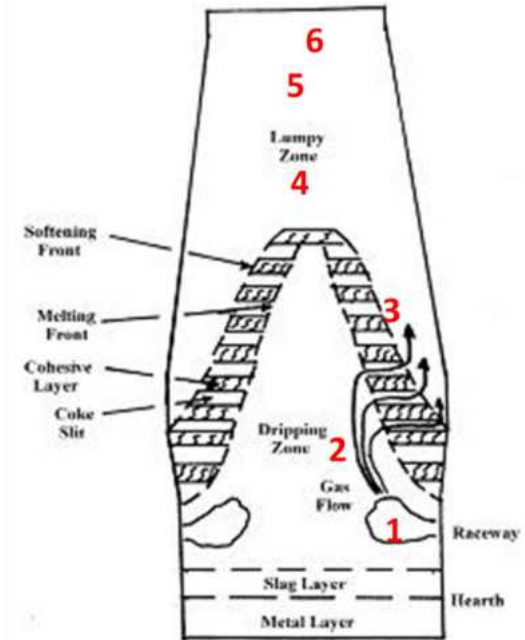


**Figure 40** Schematic illustration of calculation steps.

Interaction of the gas generated from combustion in the raceway is then calculated for four different cases:

- a/ Interaction of gas with coke.
- b/ Interaction with slag formers. Although FeO content in slag at equilibrium conditions is much lower than the real ones, at least in the vicinity of the cohesive zone, no adjustments were made for that.
- c/ interaction with hot metal down to 1350°C. Analysis of hot metal as given in **Table 9**. A carbon content of 2.5 wt% has been assumed for the hot metal to represent an average value of carbon content in the temperature range considered.
- d/ Interaction with solid iron oxide raw materials at temperature below 1350°C.

In all calculation cases involving iron-oxide bearing raw materials or coke, the analysis for MPBO-alkaline and Coke alkaline has been used at temperatures above 1200°C.

In **Table 10** the main assumptions and parameters for the thermodynamic calculations as described above are summarized.

**Table 10** Main assumptions and parameters for the thermodynamic calculations

Parameter	Assumption / Value	Comment
Raceway	Excess amount of coke; T=2100°C	Coke and PCI are reacting with the blast; Gas from combustion in raceway equilibrated with either coke, slag formers, hot metal or iron raw materials during cooling (in steps of 50°C down to 200°C)
Cohesive zone temperature	1350°C	Estimated from calculations of where 75% of slag formers are molten
Pressure	Tuyere level: 2.6 bar; above cohesive zone: 2 bar	
Average alkali load	1.87 kg alkali/tHM	Data from SSAB Oxelösund
Total recirculating alkali load	Set to 15 kg/tHM	Estimated to be approx. 8 times input, based on literature data
Accumulation of alkali in the raw materials	1/ 1200°C and below, no accumulation 2/ 1250°C and above, increased alkali load assumed to be distributed between iron oxide pellets and coke	1/ Gas coming from higher temperature may however contain increased alkali content 2/ Distribution between iron oxide raw materials and coke estimated from literature data from excavations of LKAB EBF
Chlorine input	Assumed to be 0.4 kg/tHM	Chlorine entering BF through injection coal
Fluorine load in raw materials	0.04 kg/tHM	No data available, Set to be 1/10 of chlorine input
Zinc load in raw materials	250 g/tHM	Estimated at a higher level than what is present in raw materials from SSAB Oxelösund
Total circulating zinc load	1500 g/tHM	Set to be six times input load based on literature data; assumed to be present in the residue briquette

#### Results from thermodynamic calculations

##### Preliminary calculations

Preliminary calculations on conditions corresponding to operational conditions at BF2 at SSAB Oxelösund were carried out initially. The calculations were done at a pressure of 1 atm and without considering an increased alkali load due to circulation of alkali compounds within the BF. Presence of halogens and zinc were neither considered. The main conclusions are similar as for the calculations with higher top gas pressure and when a circulating load of alkali is considered, except for course when halogen compounds are formed in appreciable amount. Reporting of thermodynamic calculations has therefor been concentrated on conditions with an increased top gas pressure and considering an increased alkaline load.

### Estimation of temperature in the cohesive zone

In the cohesive zone, a large pressure drop occurs. In order to have some assumption on at which temperature this pressure drop occur. It was assumed that all slag forming oxides both in coke and iron oxide bearing materials behaves equally. The amount of molten slag was then calculated considering all slag forming oxides present in raw materials charged from above as well as 2 or 10% of the original  $\text{Fe}_2\text{O}_3$  content still present as  $\text{FeO}$ , the rest already reduced to metallic iron. The share of molten slag was calculated in the temperature interval 1200 to 1600°C. At 1350°C, 75 and 68% of the total oxide amount was present as liquid slag with 2 and 10% of the  $\text{Fe}_2\text{O}_3$  content as  $\text{FeO}$ , respectively. This temperature, 1350°C was used as the temperature for the cohesive zone, where pressure decreases from 2.6 atm to 2 atm.

### Cooling of gas from raceway

Formed chemical compounds containing K, Na, Cl and F, when the gas from the raceway is cooled is given in **Appendix 1.1**. Only the results for phases containing K, Na, Zn, Cl and F is presented and discussed in the present text. As Zn is assumed to be present only in iron oxide raw materials, in the present case assumed to be present in the briquettes, Zn is not present in the gas coming from raceway. The calculated results for cooling of the gas from the raceway for K is given in **Figure 41** below.

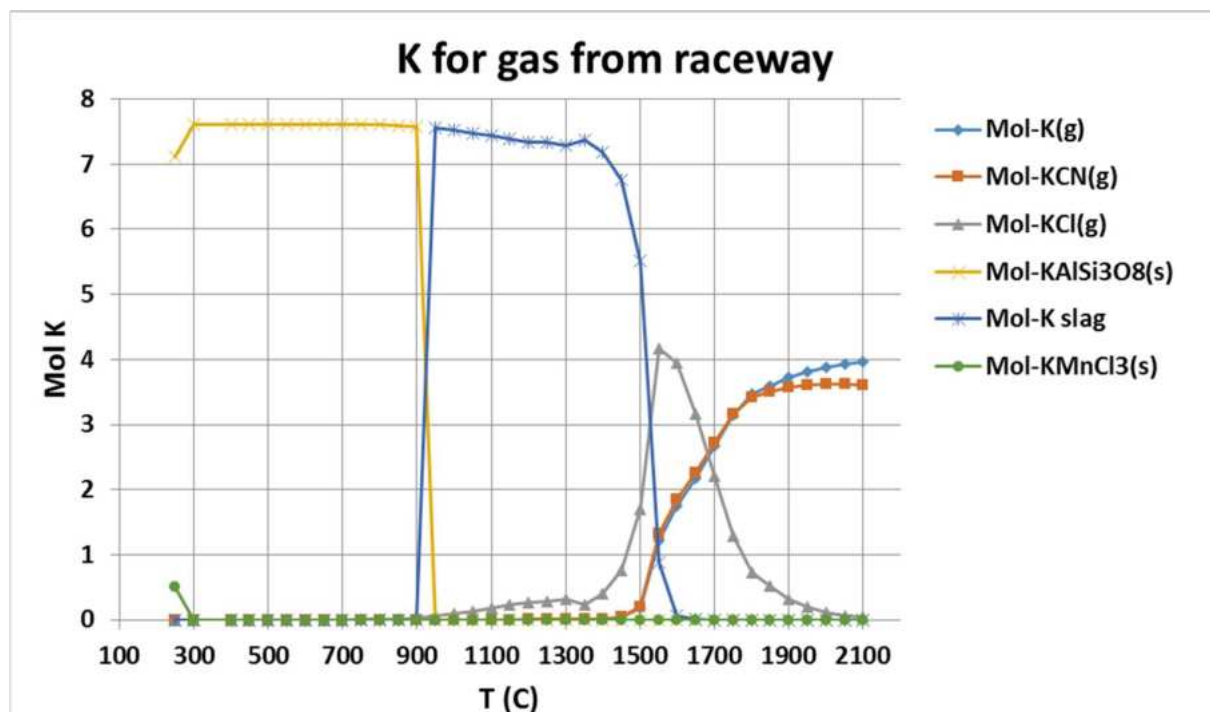


**Figure 41** Potassium containing compounds formed upon cooling of the gas coming from raceway.

At a temperature of 2100°C, all of the ash components present in the reacting coke and pulverized coal will be vaporized. Potassium is vaporized in the raceway as  $\text{K(g)}$  and  $\text{KCN(g)}$ , which also are the dominating potassium containing gas species down to 1650°C. At about 2000°C  $\text{KCl(g)}$  is starting to form in unnegelectable amount and becomes the dominating gas species at 1650°C, replaced as dominating potassium containing phase at about 1500°C by a small amount of slag phase that has started to condense from the gas. As a condensed liquid slag is formed alkalis in the vapor

start to dissolve in the slag, at increasing levels as the gas is cooled. The slag starts to form in unneglectable amount at 1600°C and is the totally dominating K-phase from 1500°C down to 950°C, at lower temperatures replaced by solid  $KAlSi_3O_8$ . The slag at low temperature is in principle a slag within the system K-Na-Al-Si. At very low temperature, 250°C, there is a thermodynamic driving force to form  $KMnCl_3(s)$ . If this phase is formed in reality at such low temperature is another question.

Sodium behaves in very much the same way as Potassium. Sodium is present in the gas at high temperatures as  $Na(g)$  and  $NaCN(g)$ . Already at high temperature  $NaCl(g)$  starts to form in the gas phase and becomes the dominating sodium containing gas compound from about 1500°C and down to 900°C. Below 900°C alkaline containing gas species can be neglected.

Sodium starts to dissolve in the slag as soon as a slag phase is formed and slag becomes the dominating sodium containing phase from 1500°C and down to 950°C. Below 950°C sodium forms  $NaAlSi_3O_8(s)$ , which then becomes the dominating sodium compound.

Chlorine and Fluorine are evaporated at high temperatures as  $AlCl(g)$  and  $AlF(g)$ , but also in minor amounts as  $HCl(g)$  and  $CaCl(g)$ . At 1550°C  $HF(g)$  has become the dominating Fluorine compound, which it continues to be down to 400°C. At intermediate temperatures, around 1500°C,  $NaCl(g)$  and  $KCl(g)$  has formed in appreciable amounts, whereas  $HCl(g)$  is the totally dominating chlorine containing compound at low temperature. It should be pointed out that the present thermodynamic model for the slag not include any solubility for halides in the slag. A small solubility of halides in the slag will of course influence the results, and possibly to a large extent responsible for the distribution of halides, at temperatures where slag is formed but also to some extent for distribution of alkalis to slag. At very low temperatures  $KMnCl_3(s)$ ,  $CaFCI(s)$  and  $MgF_2(s)$  are precipitated from the gas phase at equilibrium conditions.

#### Gas from raceway reacting with coke

In this case, gas from raceway is interacting with coke. Measurements show that the coke is enriched in alkali at temperatures higher than 1250°C (10). At temperatures above 1250°C the coke is considered to be enriched in alkaline as described above whereas at 1250°C and below the composition of the coke is assumed to be as the original analysis. The calculated potassium containing compounds are shown in **Figure 42** below.

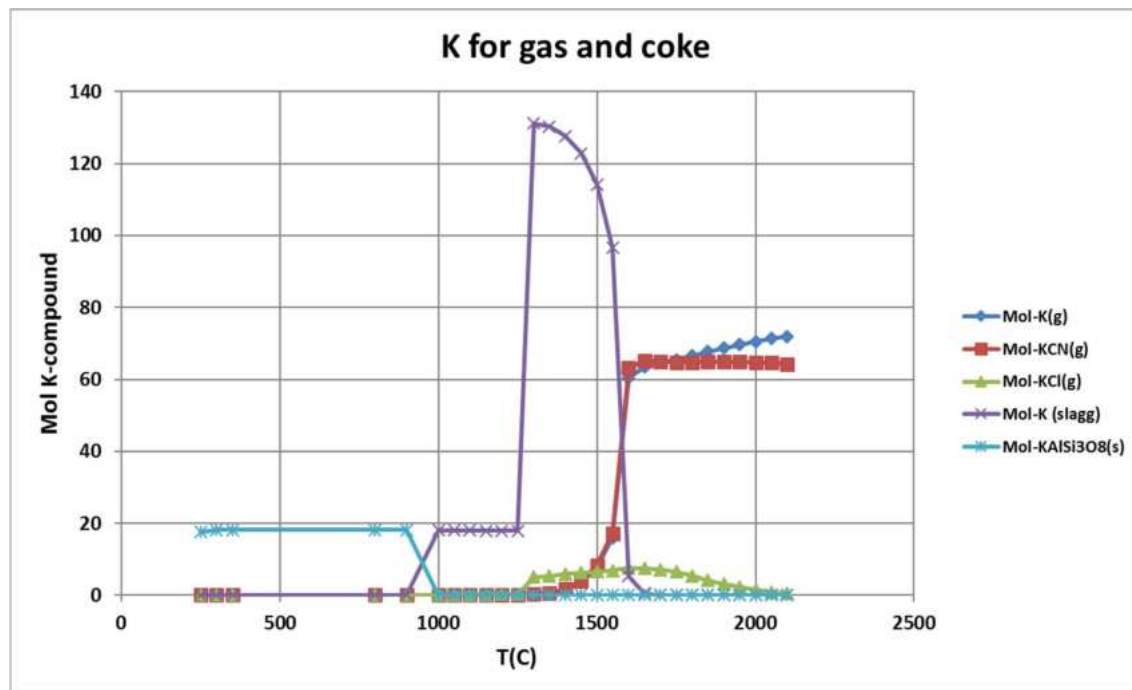


**Figure 42** Potassium containing compounds formed upon cooling of the gas coming from raceway while interacting with coke.

As in all other cases potassium is vaporized as K(g) and KCN(g) at the very high temperatures prevailing in the raceway. With decreasing temperature some of the vapor components react to form KCl(g) but the majority of potassium is as K(g) and KCN(g). At temperatures above 1750°C ash components in coke form AlN(s) or SiC(s) or are vaporized. At 1750°C a slag phase starts to form and is present in appreciable amount below 1650°C. As soon as a slag is present, alkaline starts to dissolve in the slag and the slag phase becomes the dominant alkaline containing phase from about 1550°C and down to 1000°C, below which temperature the slag phase disappears. At temperatures below 1000°C potassium will instead condense into KAISi<sub>3</sub>O<sub>8</sub>. It should be pointed out that the drastic change in total potassium content between 1300°C and 1250°C is due to the assumption of an alkaline enriched coke at temperatures from 1300°C and above.

As in all other cases, Sodium behaves very similar to Potassium, c.f. **Appendix 1.2**. Differences as compared to Potassium being small changes in the relative amount of compounds and the total level of Sodium, which is lower than for Potassium. At lower temperatures where a slag not exist, Sodium condenses into NaAlSi<sub>3</sub>O<sub>8</sub>.

Chlorine is in the high temperature gas mainly present as AlCl(g) and minor amounts as KCl(g), CaCl(g), NaCl(g) and HCl(g), c.f. **Appendix 1.2**. At moderately high temperatures KCl(g) becomes the dominant Chlorine containing gas species and at temperatures below 1250°C HCl(g) is dominating species. At very low temperatures, the calculations indicate a possibility that KMnCl<sub>3</sub>(s) and CaFCl(s) forms followed by a decrease in content of HCl in the gas. Fluorine is present in the high temperature gas as AlF(g) but with decreasing temperatures increases the amount of HF(g), which becomes the dominating gas species below 1600°C and down to 800°C. At even lower temperatures, MgF<sub>2</sub>(s) can form and at 250°C there is a thermodynamic driving force for the formation of CaFCl(s). It should once more be emphasized that the present model for the slag phase not allow for any solubility of neither Cl nor F in the slag.

### Gas from raceway reacting with slag formers

At high temperatures potassium is present in the gas as K(g) with minor amounts present as KCl(g), KOH(g) and KF(g), c.f. **Appendix 1.3**. As the temperature is decreased, more and more of the potassium is dissolved in the slag and below 1500°C the slag becomes the dominant potassium containing phase. At temperatures below 1250°C the reactions become much more complex and the calculated potassium compounds are illustrated in **Figure 43**.

K(g) is the dominating potassium compound at 1250°C and down to 1050°C, below which KCl(g) becomes dominating, in both cases together with minor amount of KOH(g) and KF(g). The amount of slag is quite low at 1250°C and below and consequently the content of potassium in slag is low. At further decreased temperatures, solid potassium containing phases start to appear. In consecutive order with lowered temperature  $\text{KAlO}_2(\text{s})$ ,  $\text{K}_2\text{Ca}(\text{CO}_3)_2(\text{s})$ ,  $\text{K}_2\text{Ca}_2(\text{CO}_3)_3(\text{s})$ ,  $\text{KCl}(\text{s})$ ,  $\text{KAlSiO}_4(\text{s})$  and finally at 300°C the calculations indicate a thermodynamic driving force for the formation of  $\text{KMg}_3\text{AlSi}_3\text{O}_{10}(\text{OH})_2$ , although the probability that such a complex compound can be formed at this low temperature is very low, if not present already in the raw materials. Several authors have claimed that alkali carbonates play an important role in the alkali cycles in the blast furnace. This is the only case calculated in this study where any alkali carbonates forms. The calculations indicate that potassium-calcium carbonates can form in appreciable amount in a quite broad temperature range from 900°C and down to 300°C.

As previous, sodium reacts in a similar manner as potassium, c.f. **Appendix 1.3**. The main difference being the solid phases formed at low temperature, namely  $\text{Na}_2\text{Ca}_8\text{Al}_6\text{O}_{18}(\text{s})$ ,  $\text{Na}_2\text{Ca}_3\text{Al}_{16}\text{O}_{28}(\text{s})$ ,  $\text{NaAlSiO}_4(\text{s})$  and at very low temperature  $\text{NaFeSi}_2\text{O}_6(\text{s})$ . The calculations for the slag phase at low temperature show a peculiar behavior in the way that the slag disappears and reappears several times. This could be due to some shortcomings in the slag model connected to the sodium component. At least the slag occurring at the lowest temperature can be questioned, built up mainly within the system  $\text{Na}_2\text{O}-\text{SiO}_2-\text{TiO}_2$  and very small and neglectable amounts of other possible slag components, including  $\text{K}_2\text{O}$ .

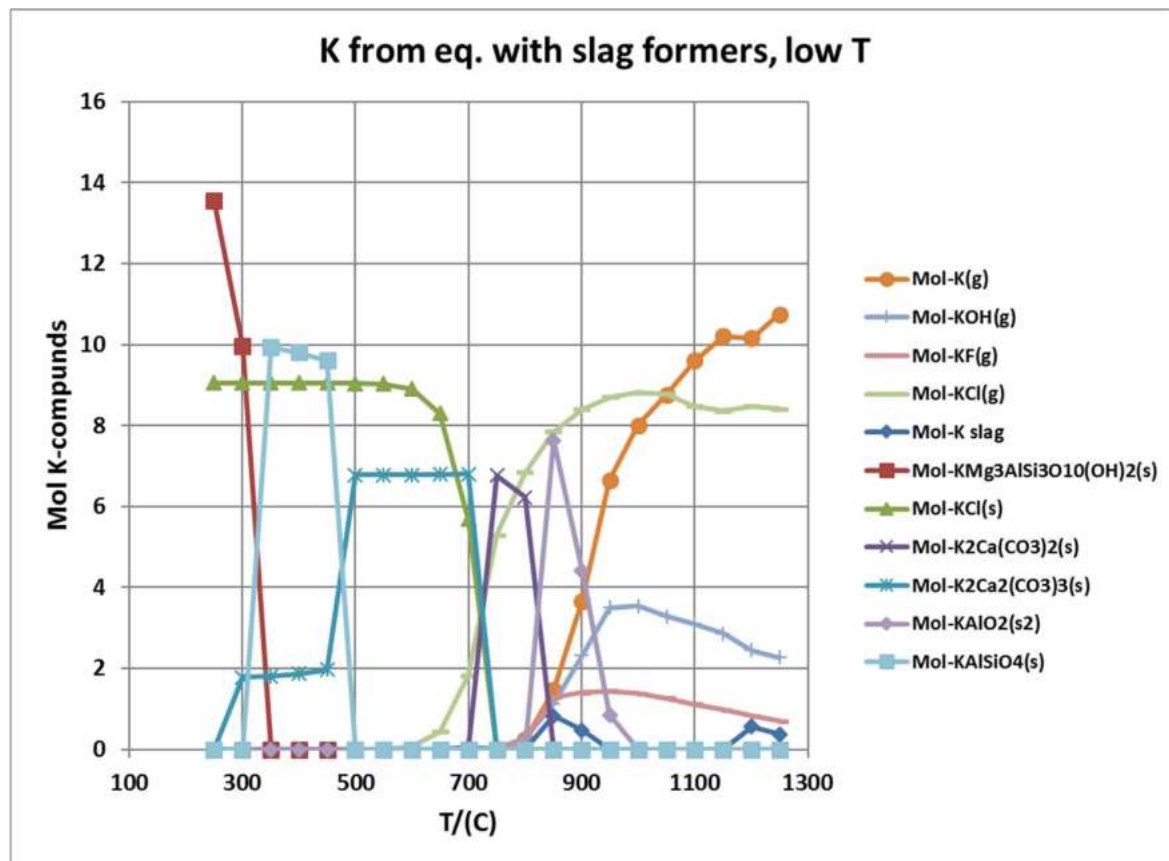


**Figure 43** Potassium containing compounds formed upon further cooling of the gas interacting with slag formers at 1300°C.

In the presence of a slag or at lower temperatures solid slag formers, chlorine is at higher temperatures mainly existing as KCl(g) together with smaller amount of NaCl(g) and HCl(g). KCl(g) is the dominating compound down to 750°C, replaced at even lower temperature by KCl(s). Fluorine is at very high temperatures mainly as HF(g) and at intermediate temperatures as KF(g). Below 800°C the partial pressure of HF(g) becomes negligible as solid phases start to form. With decreasing temperature, the solid phases with a thermodynamic driving force to form are Ca<sub>5</sub>Si<sub>2</sub>F<sub>2</sub>O<sub>8</sub>(s), CaF<sub>2</sub>(s), and at very low temperature Mg<sub>9</sub>Si<sub>4</sub>F<sub>2</sub>O<sub>16</sub>(s) and Mg<sub>5</sub>Si<sub>2</sub>F<sub>2</sub>O<sub>8</sub>(s).

At the very reducing conditions that exist when slag or slag-formers co-exist with gas generated in raceway, Zn is almost solely present as Zn(g) down to 900°C where a zinc-containing MeO-phase is formed. The MeO-phase can form a miscibility gap and here we can see that two MeO-phases with somewhat different composition co-exist. The maximum amount of zinc-containing MeO-phase occurs at 750°C. At 700°C ZnS(s) can form and is according to the calculations the dominating zinc containing phase down to the lowest temperature. The calculations also show that there is a thermodynamic driving force to form a zinc-containing spinel-phase between 550 and 450°C.

Gas from raceway reacting with hot metal and at temperatures below 1350°C with iron bearing raw materials.

The complete calculated results are given in **Appendix 1.4** and **Appendix 1.5**. The results do not show any large surprise in comparison to earlier calculations. Potassium and sodium are mainly as K(g) and Na(g) in the gas phase at higher temperatures. At temperatures between 1400 and 1800°C, KCl(g) and NaCl(g) can exist in appreciable amount but at temperatures where a slag

phase exists, the slag is the major alkaline holding phase. At temperatures where the slag disappears, the major alkaline containing phases are formed within the system alkaline oxide–alumina-silica. At very low temperatures, the calculations indicate that KCl(s) can form in appreciable amount.

Cl and F exist in the gas phase as AlCl(g), HCl(g) and AlF(g) at high temperatures. At temperatures corresponding to the cohesive zone, HCl (g) is the dominating chlorine species. As already mentioned, KCl(s) is the main condensed chlorine containing species at temperatures below 700°C. When Zn(g) starts to condense the calculations also in this case shows that it should be in the form of a zinc-containing MeO-phase and at very low temperature ZnS(s) might form.

### Discussion

The calculations verify clearly that the only condensed phase able to hold alkalis at the temperatures prevailing below the cohesive zone is the slag and the ash components still present in the coke matrix. As soon as a slag is formed there is a large driving force to extract alkalis into the slag at equilibrium conditions. To maximize the output of alkalis by the slag, it is of course beneficial to have a low basicity of the slag and thereby a high capacity of the slag to hold alkali in agreement with findings in several literature sources, e.g. van der Velde et al. [36] and Lu and Holditch [37]. The final alkali content will however also be strongly influenced by the temperature profiles in horizontal direction at different vertical levels and the gas flow in these directions. At higher temperatures alkalis present in molten slag or in slag phases in e.g. coke, will evaporate in a rate controlled by the kinetics, mainly influenced by temperature but also by slag composition. In addition to slag chemistry, another important parameter will thus be the amount of slag flowing through the central colder parts of the tuyere and hearth regions. An operation with colder central parts of the lower regions and larger amount of slag flowing through these colder regions should maximize the output of alkalis through slag. As the evaporation of alkalis from a slag percolating through the coke layer or in contact with hot metal is kinetically controlled, the residence time for the slag in the lower high temperature region will also have an impact. Conclusions regarding alkalis from the present calculations is in line with conclusions by Lin et al [34] who found that low slag basicity, control of alkali input and increased MgO and Al<sub>2</sub>O<sub>3</sub> content at constant basicity (CaO/SiO<sub>2</sub>) are the main parameters controlling output of alkalis.

Lu and Holditch [37] has in a review of the Canadian experiences and the measures taken to prevent alkali cycling in a blast furnace concluded that alkali control can be obtained in three different ways; 1/ limiting the input, 2/ ensuring an adequate thermal reserve of the furnace 3/ promoting the removal of alkalis by the slag, by lowering the basicity and flame temperature, by replacing CaO with MgO in the slag formers and by increasing the slag volume and depending on the furnace construction 4/ higher furnace pressure and 5/ increased oxygen enrichment in the blast.

Cleaning of the furnace at intermittent intervals by using more acidic fluxes was claimed to be regular operational practice in Canada. Further control strategies could be to operate on lower Si-content in hot metal and ensuring a more central gas flow.

The alkaline cycling was by Lu and Holditch [37] described as consisting of three or possibly four different cycles. Starting from the lower part of the blast furnace;

- 1/ The silicate cycle, where the potassium content in silicates from ore or carbon bearing material and in slag are reduced and disintegrated giving potassium vapor that rises up and partly condense again in approximately the bosh region in slag or at coke particles.
- 2/ The cyanide cycle, where condensed cyanides are formed in the upper part of the shaft and descends with the burden to the bosh region where they are once again evaporated.
- 3/ The carbonate cycle, where potassium carbonate is precipitated almost up in the throat, descends with the burden and is reduced and vaporized in the shaft.
- 4/ The fourth cycle is claimed to be the formation of potassium carbides on coke high up in the shaft followed by vaporization of potassium far down in the furnace.

The present calculation has not shown any driving force to form an alkali cyanide cycle nor a potassium carbide cycle. Cyanides are from equilibrium considerations expected to exist as  $\text{HCN(g)}$  in the upper stack. In only one of the calculated cases is carbonates formed, namely potassium-calcium-carbonates at temperatures below 900°C when gas from the high temperature region is reacting with slag formers.

Lilius [38] presented predominance diagrams for the systems K-C-O and K-C-N-O at 1200 K, 1400 K and 1600 K at  $p(\text{K,g}) = 10^{-4}$  atm and for the system K-C-N-O at various total pressures and  $p(\text{KCN, g}) = 10^{-4}$  to  $10^{-6}$  atm. From the diagrams it was concluded that at these conditions  $\text{K}_2\text{CO}_3(\text{l})$  will not be formed and also the formation of  $\text{KCN(l)}$  is outside the operational window for blast furnaces. Lilius [38] therefore concludes that the presence of a cyanide cycle, as proposed by Lu [37] is unlikely, and the formation of  $\text{K}_2\text{CO}_3$  at lower temperatures will only occur if the adsorption of alkalis in silicates present in ore or coke is hindered in some way. Abraham and Staffansson [39] concludes that even though the silicate is more stable, its formation may not take place to large extent and that cyanides are unstable in the low temperature region with respect to carbonates and silicates.

Averin and Khodak [40] made a thermodynamic analysis of the formation and decomposition of cyanides in a Blast Furnace. They conclude that the temperature and conditions in the BF hearth are such that alkali is transferred to the gas phase and by interaction with carbon and nitrogen forms cyanides. At the conditions in the lumpy zone they almost completely condense by interacting with wustite, forms oxides and dissolve in primary slag. Reduction of alkali silicates by solid carbon and subsequent volatilization of potassium at temperatures between 1000 and 1350°C is stated to be totally dominating over reduction through the  $\text{CO}/\text{CO}_2$  gas. They also conclude that the main part of potassium, which is reduced in the hearth and transferred to gas, form cyanides in the lumpy zone at temperatures between 1000 and 1350°C. The decomposition of cyanides by oxidation from  $\text{CO}_2$  in the gas phase is unlikely.

Chlorine and Fluorine is vaporized at high temperatures as  $\text{KCl(g)}$ ,  $\text{NaCl(g)}$  and  $\text{AlF(g)}$  and from coke also as  $\text{AlCl(g)}$ . Together with coke or when just considering a gas phase,  $\text{HCl(g)}$  and  $\text{HF(g)}$  is the dominating compound in a broad moderate temperature range. For a gas reacting with slag formers or iron-bearing raw materials  $\text{KCl(g)}$  as well as  $\text{HF(g)}$  and  $\text{KF(g)}$  is dominating down to temperatures of 700 to 800°C, followed by condensation of  $\text{KCl(s)}$ ,  $\text{CaF}_2(\text{s})$  and complex fluorinated

silicates. Considering the very short residence time for a gas at temperatures below 800°C and the low temperatures it is unreasonable that much reactions will occur. A very high level of accumulation is thus unlikely. KCl is present in the gas phase and presence of KCl(s) in the gas leaving the blast furnace is thus likely, as also found by Lin [34]. Their analysis of dust generated in blast furnaces has shown that the majority of potassium in dust was present as KCl, but also as KHCO<sub>3</sub> and KZn(CN)<sub>3</sub> or K<sub>2</sub>Zn(CN)<sub>4</sub>. Sodium in dust was shown to exist as (Na,K,Zn)HCO<sub>3</sub>, (K,Na)Cl, NaCl and Na<sub>2</sub>CO<sub>3</sub>. Formation of KHCO<sub>3</sub> was found in samples taken just above stock line as well as in shaft samples taken as far down as about the middle of the reserve zone [34]. Leimalm et al [41] found about 0.2 and 1 to 1.5 wt%, analysis calculated as K<sub>2</sub>O, in blast furnace dust and blast furnace sludge samples, respectively, obtained from the LKAB's EBF.

The model used for the slag phase does not include halogens. However, Lin et al [34] concludes from analysis of blast furnace slags that the zinc-content is very low.

Zinc is in the high temperature region volatilized as Zn(g), which is the dominating Zn-compound down to about 800°C. At equilibrium conditions condensations of zinc into ZnO (solid solution in MeO-phase), ZnS(s) and to lesser extent in a spinel phase occurs below 900°C, which according to the calculations is the cause of the circulating load. It should be pointed out that the model used for the slag phase gives very low zinc content in the slag at these conditions.

The BF is a process where chemical reactions are controlled by the kinetics of the reactions and the mass flow rate of phases through different parts. Considering all the different reactions proceeding, temperature and mass flow variations not only in vertical but also in horizontal directions, it is a very demanding task to formulate a precise model for the BF. However, thermodynamic calculations using appropriate assumptions and conditions can give an insight into which reactions that can proceed in different parts of the BF. In the present calculations it was decided to start the calculations from the combustion in raceway and then follow the reactions occurring when this gas interacts with different single materials/raw material types during the upwards flow of the gas. A choice that simplified the calculations. The results are of course an approximation of the reality in a blast furnace. Ideally, the calculations should be carried out in a repeated cycle with gases flowing upwards and condensed phases flowing downwards until a steady state is obtained. Considering the time frame for this work that was not regarded possible to do. It could however be very useful to develop a model for the BF, divided into different stages and simulating non-equilibrium conditions by controlling the flows of material/phases between the different stages, in Fact terminology a Reactor-model.

### Conclusions

Calculations have been performed showing the reactions occurring between gas coming from raceway of a blast furnace, interacting with solid and condensed material during the ascent, and cooling down. Interaction with coke, hot metal, slag formers and iron-bearing raw materials have been considered separately, as well as the reactions occurring for only the cooling of the gas phase, simulating channeling in the furnace.

- At equilibrium conditions and at the very high temperatures prevailing at or near the race-way, alkalis are reduced and evaporated, and further up oxidized, condensed and dissolved in the slag phase.
- Calculations have clearly shown the dominating role of the slag phase to remove alkalis from the blast furnace. At equilibrium conditions, practically all alkali would dissolve in the slag and only limited access to the slag or otherwise kinetic restrictions would result in condensation further up in the blast furnace.
- Measures that minimize high temperatures in the slag during the descent towards the hearth will maximize the slags capacity to eliminate alkalis from the circulation.
- Potassium not dissolved in a slag is depending on T and interacting material condensed as  $KAlSi_3O_8$  (s),  $KCl$ (s),  $KAlSiO_4$ ,  $KAIO_2$ , K-Ca carbonates or complex silicates.
- Sodium not dissolved in slag is at lower temperature condensed as either  $NaAlSi_3O_8$ ,  $NaAlSiO_4$ , Na-Ca aluminates or alumina-silicates.
- Chlorine and Fluorine is at high temperatures vaporized as  $KCl(g)$ ,  $NaCl(g)$ ,  $AlF(g)$  and  $AlCl(g)$ . Depending on conditions,  $KCl(s)$  and  $CaF_2(s)$  can condense but vapor species are dominating down to low temperatures. Major accumulation of halogens is thus unlikely.
- Zinc is in the high temperature region volatilized as  $Zn(g)$ . At equilibrium conditions condensations of Zinc into  $ZnO$  (solid solution in MeO-phase),  $ZnS(s)$  and to lesser extent in a spinel phase occurs below 900°C.

### **2.3.1.1.7 Impact of alkali balance on energy consumption (SWERIM)**

Based on results from thermodynamic calculations performed by LTU on the alkali cycle within Task 1.1, additional calculations have been conducted on the alkali cycle and its effect on energy consumption (SWERIM). The calculations have been limited to K-compounds and performed in FactSage 6.1 for a fixed potassium load of 15 kg/tHM and with the assumption that ¾ of the potassium cycle is below the lumpy zone at 1200°C. The assumed distribution of K above and below the cohesive zone is supported by the results from studies on alkali uptake in burden materials from EBF later described in task 1.3.

The distribution of K in K-containing compounds at different temperature intervals is based on LTUs calculations. At temperatures between 1650°C and 2100°C, K is present as  $K(g)$  and  $KCN(g)$  with the distribution of 50%/50%. Between 950°C and 1650°C, K is dissolved in a slag phase and from 905°C and below, K is present as  $KSi_2O_3$ . A table summarizing all reactions and reaction enthalpies is found in **Appendix A Table A1**. Reactions and a schematic description of the assumed cycle is shown in **Figure 44**. The calculations resulted in an energy consumption of 29 MJ/tHM (8 kWh/tHM) for a K circulating load of 15 kg/tHM. This is corresponding to the energy consumption 0.44 kWh/tHM for a circulating load of 1 kg  $K_2O$ . In this calculation it is assumed, that the energy from the exothermic reactions occurring above the cohesive zone contributes to the concerned chemical reactions in these zones. However, if it is assumed that the energy from the exothermic reactions happening above the cohesive zone is considered as lost and will only contribute to an increased top gas temperature, the energy consumed will correspond to 53 MJ/tHM (14.7 kWh). This is equivalent to a coke consumption of 1.3 kg/tHM based on the consumption of 1.36 kg coal per kg coke and the energy value 8.6 kWh/kg coal. It should be emphasised that these calculations are only considering the energy consumption by the chemical reactions within the alkali cycle, not

the increased coke consumption by the alkalis catalytic effect on the solution loss reaction and the degradation of coke by alkalis. Moreover, the energy consumption associated with disturbances caused by alkalis, such as release of scaffolds from walls that can lead to erratic burden descent and that cold and unreduced materials reaches raceway, is not included.

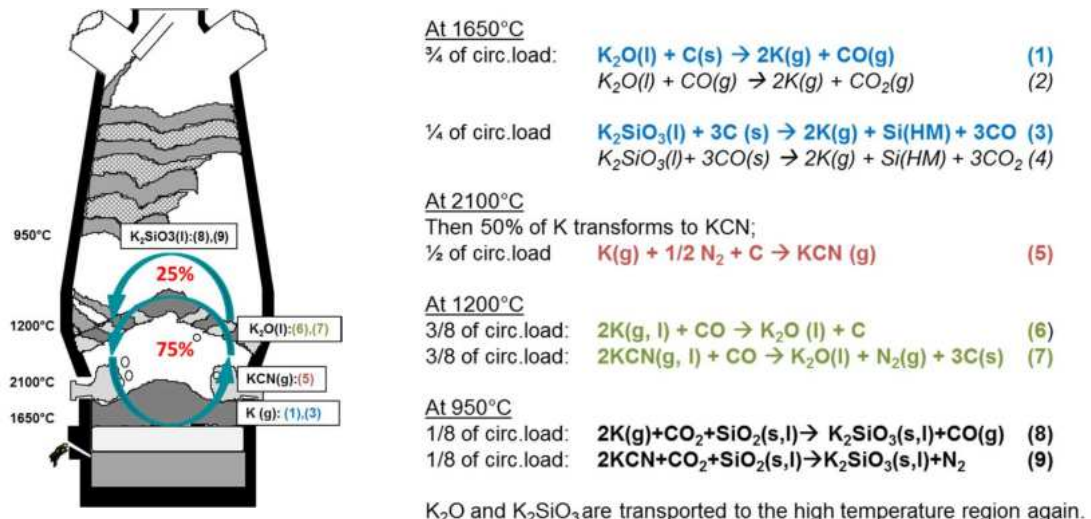


**Figure 44** Schematic description of the assumed potassium cycle (left) and reactions (right).

### 2.3.1.1.8 Heat and mass balance calculation for estimation of impact of alkali balance on energy consumption (BFI)

For revealing the mechanisms of enrichment and depletion of alkali components by thermochemical calculations, the BFI in a first step based on a literature survey has defined the main alkali components to be taken into account in the calculations (**Table 11**). Here, the selected sodium and potassium compounds are given with the corresponding melting- and boiling temperature. The chlorides are of special importance, since they may cause HCl formation, which can further react with other in-furnace gases.

**Table 11** Main alkali components to be taken into account in the thermochemical calculations

Compound / Element	Melting point in °C	Boiling point in °C	Compound / Element	Melting point in °C	Boiling point in °C
Na	98	883	KCl	771	1477
NaCl	800	1465	$K_2O$	878	881
$Na_2O$	1132	-	KOH	406	1323
NaOH	323	1388	$KNO_3$	339	-
$Na_2CO_3$	858	-	$K_2CO_3$	901	-
NaCN	562	1530	$K_2SO_4$	1074	-
$Na_2SiO_4$	1089	-	KCN	622	1625
K	63	759	$K_2SiO_4$	976	-

The selected alkali components have been used in thermodynamic calculations, in order to determine the enrichment and depletion of alkali components in the BF and the impact of alkali components on BF energy consumption.

For this purpose, a calculation model has been set-up based on the Software HSC Chemistry®. The calculation model includes different reaction zones with characteristic chemical reactions, which are based on the reaction mechanism for K compounds stated in (**Figure 45**). The reaction efficiencies (partition of the reactant to be reacted) are either estimated or partly assumed based on FactSage® calculations (element distributions).

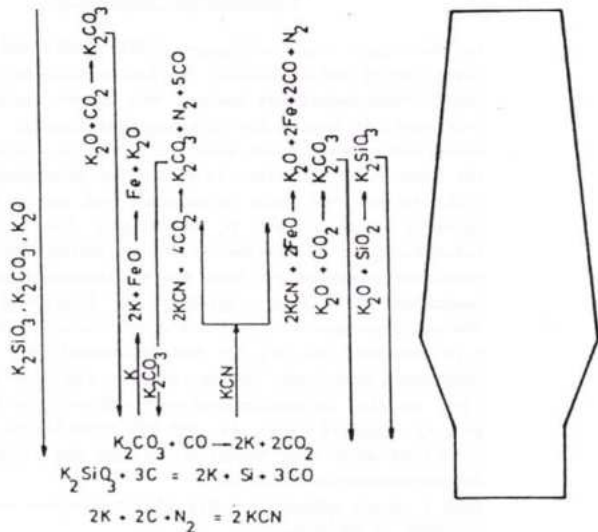


**Figure 45** Characteristic chemical reactions and reaction mechanism for potassium compounds in the blast furnace [42]

In contrast to **Figure 45**, potassium- and sodium silicates  $KAlSiO_4$  respectively  $NaAlSiO_4$  are included in the calculations according to results of previous thermochemical calculations by LTU. In those calculations also  $KAlSi_2O_6$  respectively  $NaAlSi_2O_6$  are reported to be present. But these compounds are not included in the BFI model because the corresponding reactions roughly show the same Delta H compared to  $KAlSiO_4$ . Consequently, the selection of one of the alkali-silicate compounds instead of the other one only has negligible effect on the calculated energy consumption.

The calculation model includes 5 reaction units and a final recirculation of alkali compounds. In each unit only chemical reactions with alkali components are considered. Other necessary reactants (e. g. CO, CO<sub>2</sub>, FeO, SiO<sub>2</sub>) are added only to the extent of their consumption. It clearly can be assumed that these reactants are available in excess in relation to the alkali compounds. The distribution of products to different reaction units is determined according operational experience (alkali balance) or parallel FactSage® calculations.

In **Figure 46** the Scheme of the alkali balance calculation model with reaction units and material streams is presented. The given numbers correspond to temperatures in °C. For simplification, three temperature stages are assumed: 1500°C (Hearth and combustion zone), 1100°C (Cyanide reactions; FeO Reduction) and 900°C (Carbonate and silicate formation).

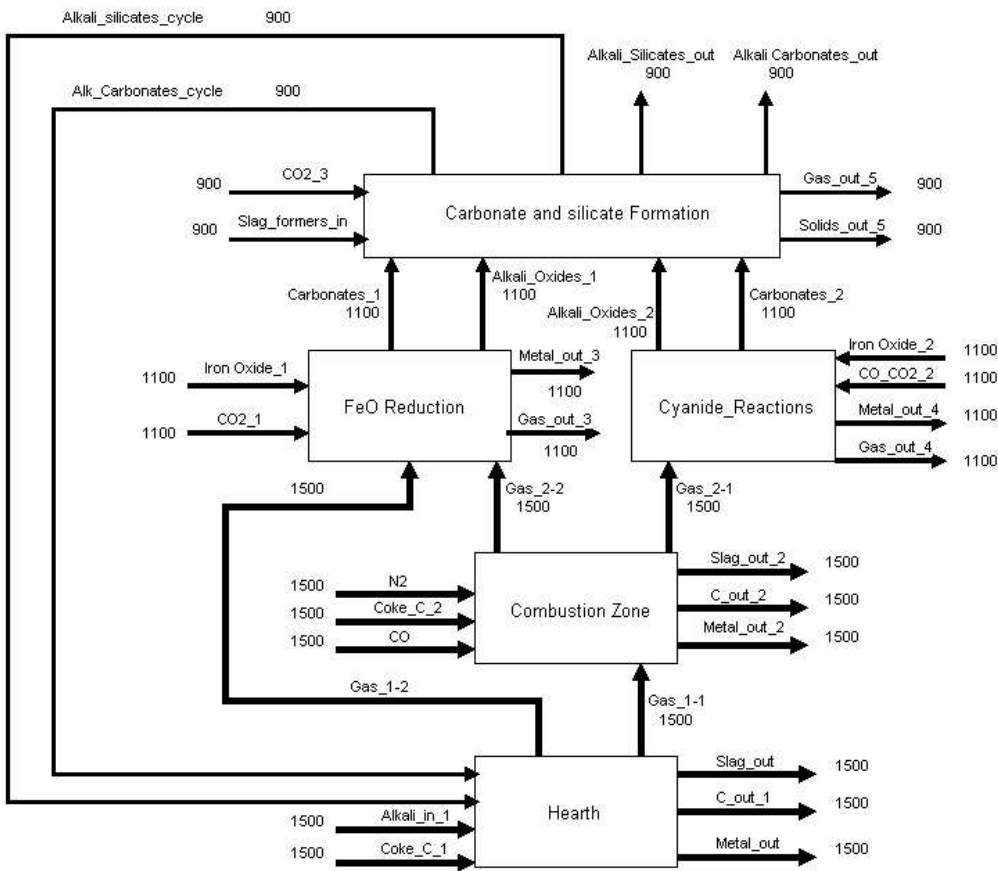
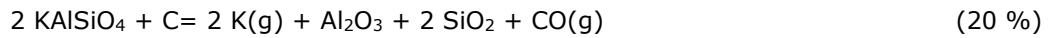


**Figure 46** Scheme of alkali balance calculation model with reaction units and material streams (given numbers: temperatures in °C)

For potassium (K) compounds the following reactions and percentages of reaction progress are defined for the given reaction units:

### Hearth



### Combustion Zone

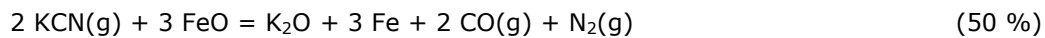


Output gas distribution 100 % to cyanide reactions unit

### FeO Reduction



### Cyanide Reactions

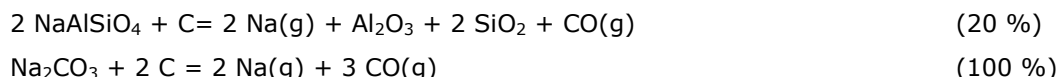


### Carbonate and silicate Formation



For sodium (Na) compounds the following reactions and percentages of reaction progress are considered for the given reaction units:

## Hearth



(20 %)

(100 %)

## Combustion Zone



(100 %)

Output gas distribution **100 %** to cyanide reaction unit (0% to FeO reduction unit)

## FeO Reduction



(0 %)

## Cyanide Reactions



(50 %)



(50 %)

## Carbonate and silicate Formation



(0 %)



(100 %)

In the Hearth unit for both alkali compounds 20 % of the alkali silicates are assumed to react with carbon. This partition is derived from the results of FactSage® calculations for a simplified BF slag composition. The FeO-Reduction unit shows a positive free enthalpy (Delta G) for K at all relevant temperatures and for Na at higher temperature above 1100°C. Due to this behaviour, for the described calculations the reaction progress is set to zero in all cases and all the output gas from the combustion zone unit is distributed to the cyanide reactions unit.

For the cyanide reactions unit, the percentage of reaction progress is assumed to be distributed equally (50:50 %) either to the reaction with FeO and to the reaction with CO<sub>2</sub>. Since the Delta H for both reactions is roughly the same, this assumption is not critical in terms of the overall calculated energy consumption.

In the initial calculations within the Carbonate and silicate Formation unit no carbonate formation is assumed. This means 100 % of the alkali oxides are assumed to react to alkali-(Al)-silicate. The assumption of carbonate formation in this unit (partly, instead of silicate formation) is part of a following sensitivity analysis in terms of energy consumption. In the Carbonate and silicate Formation unit the alkali components are distributed to the largest part (95 %) to the alkali cycle and only to 5 % to the alkali output (dust) stream.

The calculations have been performed separately for potassium and sodium with alkali input amounts equivalent to 1 kg K<sub>2</sub>O (corresponds to 3.36 kg KAISiO<sub>4</sub>) respectively 1 kg Na<sub>2</sub>O (corresponds to 4.58 kg NaAlSiO<sub>4</sub>). As result of the calculations, the amount and composition of the different materials streams has been determined. This also includes the consumption figures for burden materials like coke reacting with alkali components.

The calculation results for 1 kg K<sub>2</sub>O input (as KAISiO<sub>4</sub>) are presented in **Figure 47** (amount of material streams) and in **Figure 48** (Elemental distribution of K within the different streams), whereas the calculation result for 1 kg Na<sub>2</sub>O input (as NaAlSiO<sub>4</sub>) is presented in the same way in **Figure 49** and **Figure 50**. The total carbon consumption due to the alkali reactions for instance is 95 g C per kg K<sub>2</sub>O equivalent (Coke\_C\_1/2; **Figure 47**), respectively 143 g C per kg Na<sub>2</sub>O equivalent (Coke\_C\_1/2; **Figure 49**). Within the hearth zone around 98 – 99 % of the input K respectively Na are removed via the output slag (Slag\_out), which corresponds quite well with the previ-

ously determined alkali balances at VASD (e. g. K balance; **Figure 51**) and therefore confirms the selected distribution values within the units.

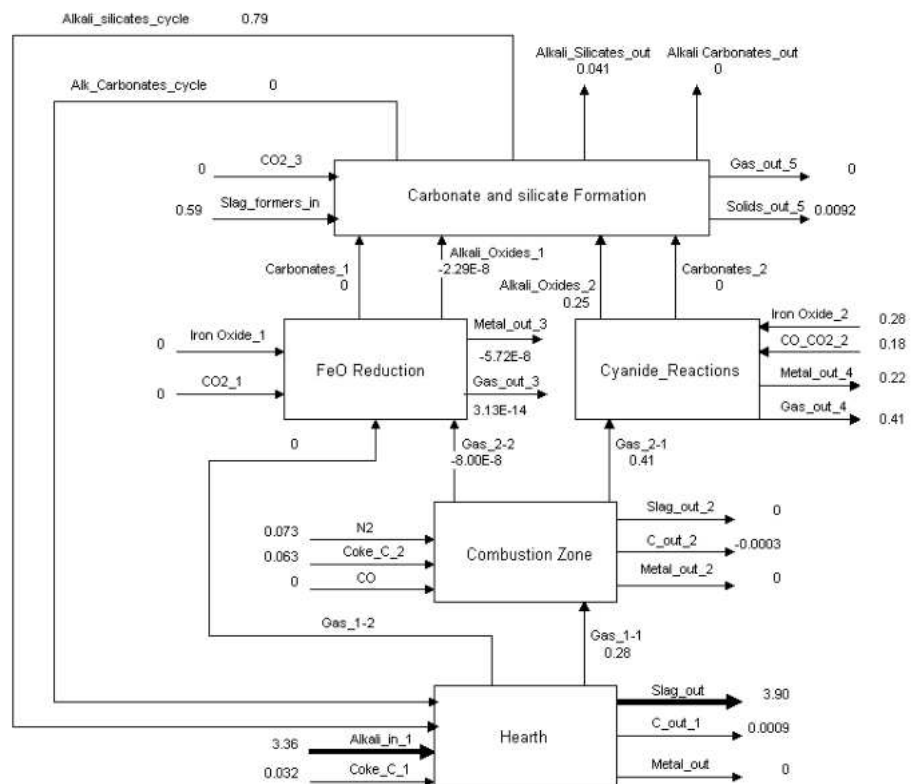


**Figure 47** Calculation result for 1 kg K<sub>2</sub>O input (as KAlSiO<sub>4</sub>) - Amount of material streams in kg

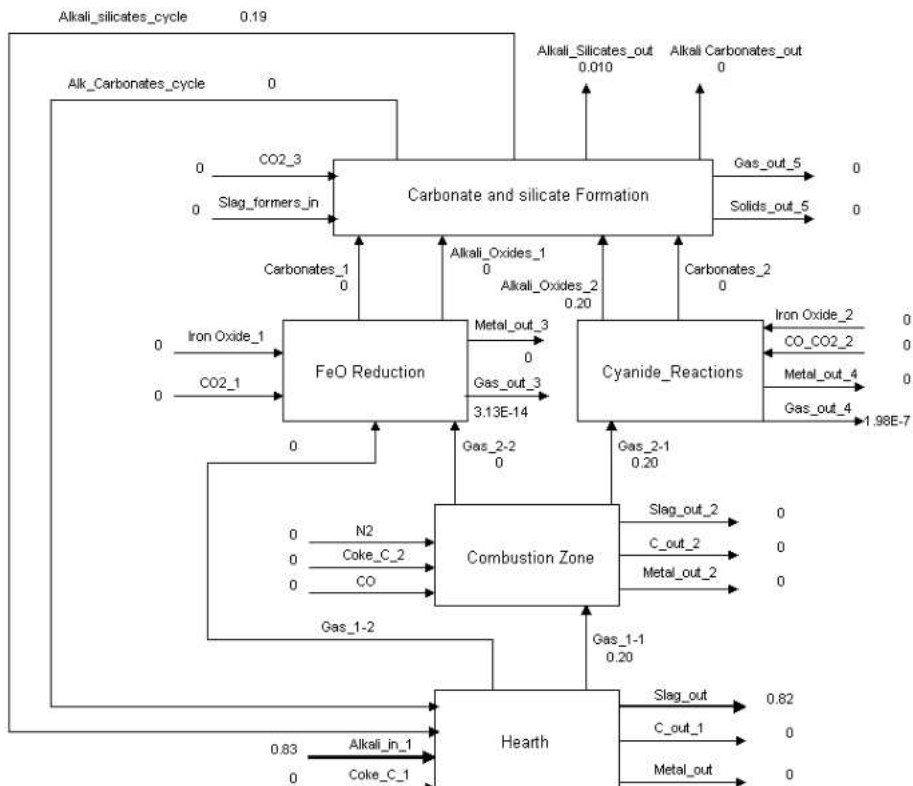


**Figure 48** Calculation result for 1 kg K<sub>2</sub>O input (as KAlSiO<sub>4</sub>): Elemental distribution of K within the different streams (in kg)

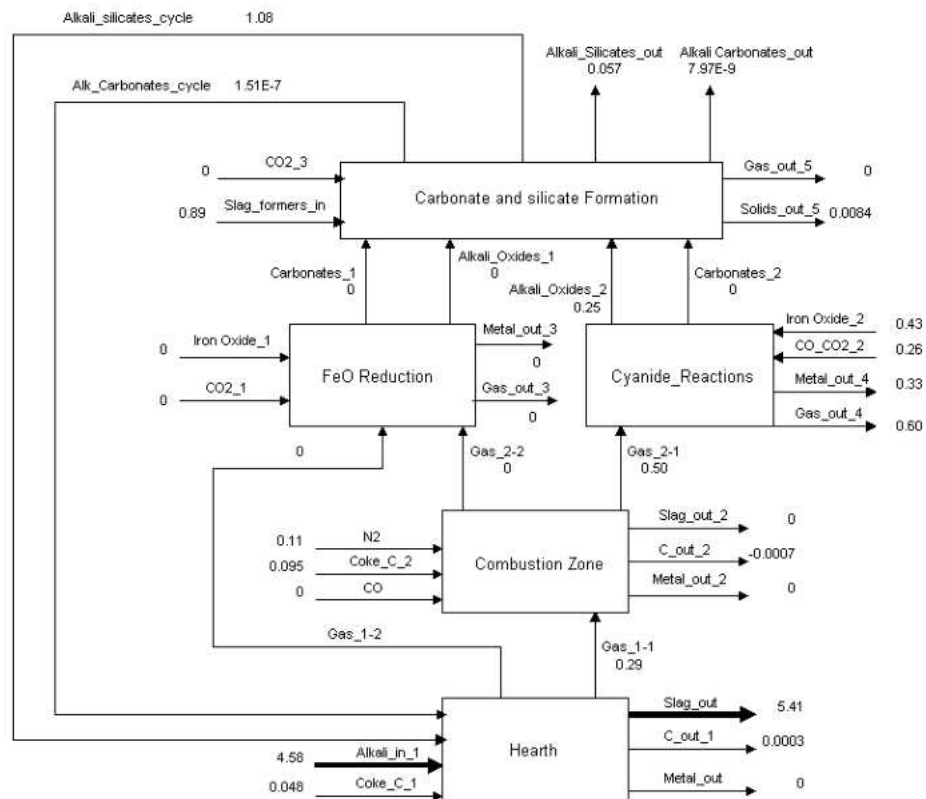


**Figure 49** Calculation result for 1 kg Na<sub>2</sub>O input (as NaAlSiO<sub>4</sub>): Amount of materials streams in kg

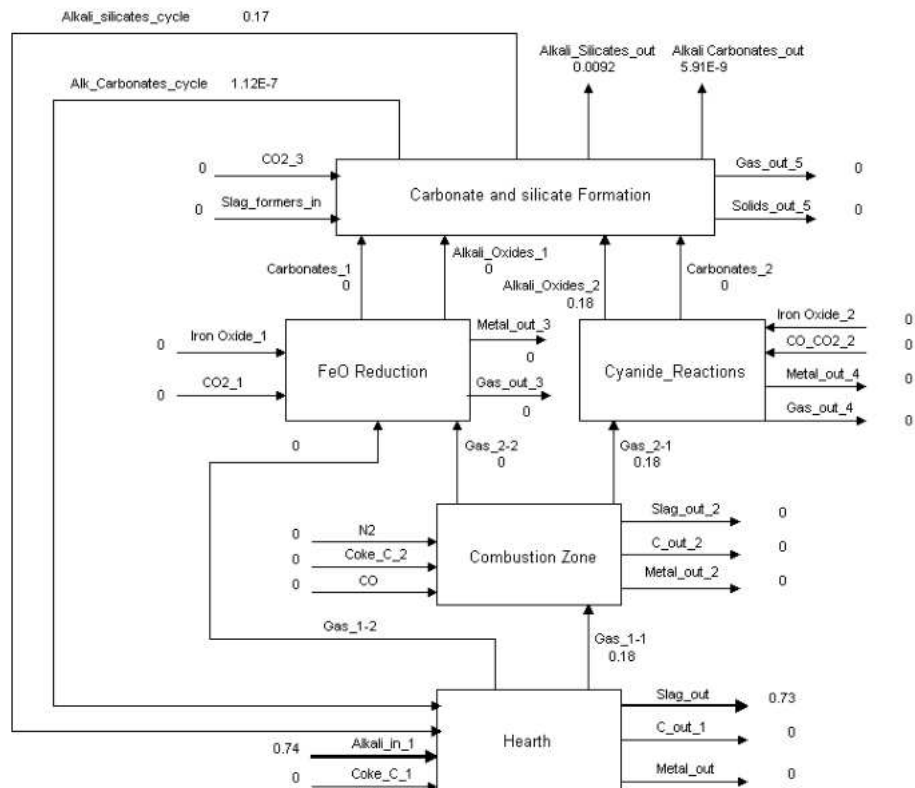


**Figure 50** Calculation result for 1 kg Na<sub>2</sub>O input (as NaAlSiO<sub>4</sub>): Elemental distribution of Na within the different streams (in kg)

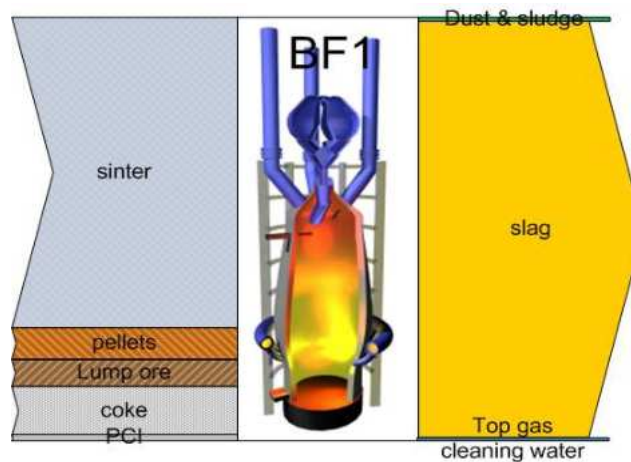


**Figure 51** K balance at VASD blast furnace

**Table 12** Energy consumption due to K input and -cycle

Unit / Reaction Zone	Total Enthalpy in kWh *
Carbonate Formation	-0.35
Cyanide_Reactions	0.04
FeO Reduction	0.00
Combustion Zone	0.00
Hearth	0.73
<b>Total</b>	<b>0.43</b>

\* Calculated for 1 kg K<sub>2</sub>O equivalent input

**Table 13** Energy consumption due to Na input and -cycle

Unit / Reaction Zone	Total Enthalpy in kWh *
Carbonate Formation	-0.36
Cyanide_Reactions	-0.04
FeO Reduction	0.00
Combustion Zone	-0.03
Hearth	1.07
<b>Total</b>	<b>0.64</b>

\* Calculated for 1 kg Alkali oxide (K<sub>2</sub>O, Na<sub>2</sub>O) equivalent input

In **Table 12** the energy consumption within all reaction units is listed for K input and -cycle, whereas the same results are listed for Na within **Table 13**. The most significant amount of energy is consumed in the hearth for alkali reduction and evaporation, while at the carbonate and silicate

formation unit a significant energy amount is released. The other units only contribute marginally to the energy balance. In total 0.43 kWh of energy are required for 1 kg K<sub>2</sub>O input, while for 1 kg Na<sub>2</sub>O 0.64 kWh of energy is needed.

A sensitivity analysis was performed for identification of the largest influences on the energy consumption. Here mainly an increasing partition of the carbonate reaction within the unit. Carbonate and silicate formation would strongly increase the amount of required energy in the hearth. For Na and 100 % carbonate reaction the total energy consumption would be 10.7 kWh per kg of Na<sub>2</sub>O, while at 100% silicate reaction the total energy consumption would only amount to the previously determined 0.64 kWh. This means that the knowledge on the amount of carbonates within the BF alkali cycle would be crucial for the energy balance.

### 2.3.1.2 Task 1.2 New on-line measurements

#### 2.3.1.2.1 Tests with new online measurements at the LKAB EBF®

Top gas analyses with mass spectrometer on NH<sub>3</sub> and HCN was conducted during daytime by *LKAB* and *MEFOS* at LKABs EBF in autumn of 2016. The instrument combines an Ion-molecule Reaction (IMR) technique with Electron impact Ionization principle (EI) and has double internal capillaries with possible dilution, which allows measurement of high and low concentrations at the same time. For the measurements at EBF, the instrument was calibrated for NH<sub>3</sub>-gas. During the measurement periods, frequent sampling of dust and sludge were performed as well as continuous measurements of alkali emissions in raceway. In addition, material samples as well as gas and temperature measurements were collected once a day by two shaft probes. The position of the gas sampling probe for the top-gas measurements was situated after the dust catcher and before the venture scrubber, the process outline and position of top gas probe is illustrated in **Figure 52** below.

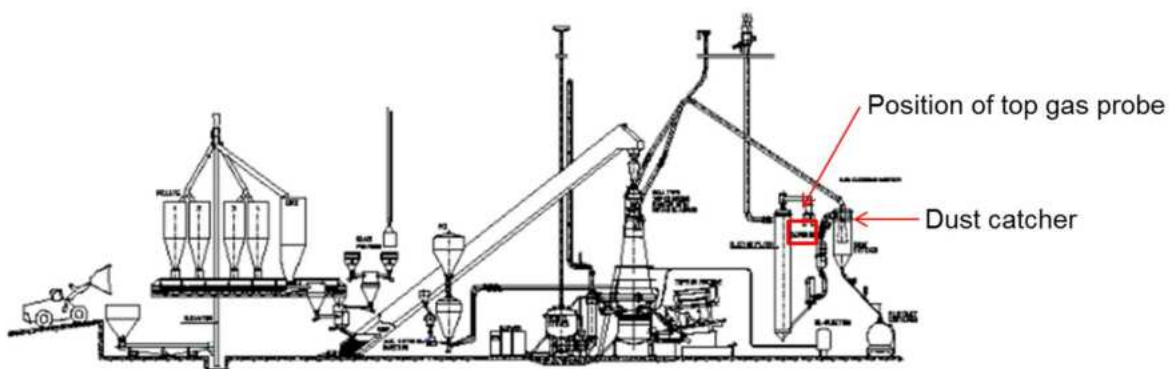


**Figure 52** Process view of LKAB EBF

The top gas was kept at a temperature of 150-180°C by a heated pipe and introduced to a cabinet for gas flow control before going into the mass spectrometer. The instrument set up was tested by measuring top gas under a couple of hours some days before the planned trials. A principle sketch of the instrument layout is seen in **Figure 53** below.

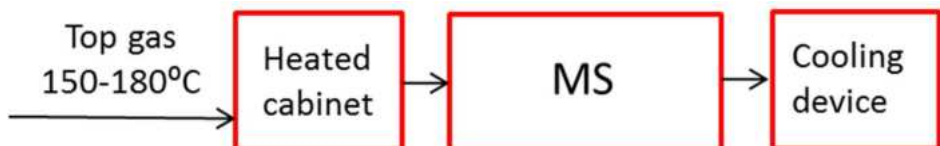


**Figure 53** Principle sketch of MS outline.

MS-measurement was attempted on gas retrieved by a shaft probe from inside the EBF. NH<sub>3</sub> could not be detected in these measurements. Regular measurements determining temperature and gas composition (in terms of CO, CO<sub>2</sub> and H<sub>2</sub>) on nine positions along the furnace diameter, were done on a daily basis. Material samples were also taken daily with shaft probes, characterization of these to assess alkali distribution is reported in Task 1.3.

For continuous measurements of temperature- and emissions from alkali present in the raceway, a lance with optical fibre connected to a spectrometer was installed at tuyere No.2, see positions of tuyeres (T) and tap hole (TH) in **Figure 54**. These measurements contribute to qualitative analyses and can give indications on when a larger amount of alkalis are passing in front of the tuyere.

The optical fibre was placed in the inner tube of a lance, protecting it from heat in the blow pipe. The design of the lance allowed nitrogen purging between the outer- and inner tube to maintain sufficient cooling of the optical fibre. By using a high temperature glue sustaining temperatures above 200°C, the optical fibre was mounted in the fixture. The fixture was designed to promote the optical fibre to collect radiation in a direction straight into the blowpipe of the blast furnace.

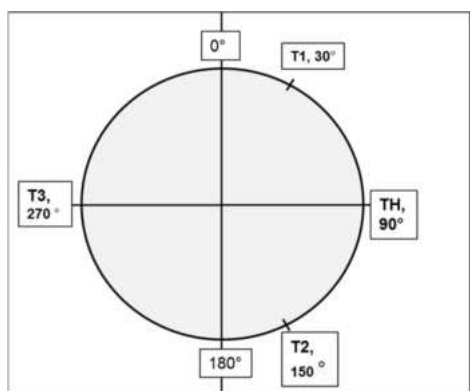


**Figure 54** Position of tuyeres T1-T3 in EBF.

Prior to the measurements, a reference spectrum was recorded at different exposure times for the sensor of the spectrometer. A reference lamp with a known heat radiation distribution was used to create a calibration file, which is needed to compensate for absorptions in the optical fibre and non-linearity in the sensor of the spectrometer. The temperature estimation was made on radiation guided from the raceway to a spectrometer by the optical fibre and thereby converted to intensities at different wavelengths of visible light. The recorded spectra were stored every 5 second and post processed in order to estimate the present temperature and radiation related to emission from alkali. A typical recorded spectrum from the raceway is shown in **Figure 55**.

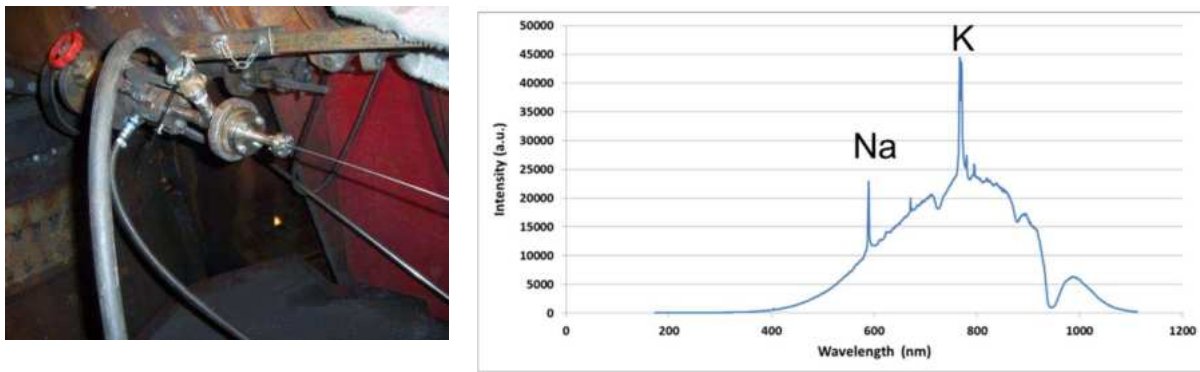


**Figure 55** Optical fibre was mounted as the PC injection lance (left). Typical spectrum from raceway (right).

For the temperature evaluation, an interval of the radiation spectrum unaffected of alkali radiation was chosen. The following equation (3) is Planck's law of heat radiation where T is temperature in °C,  $k_B$  Boltzmanns constant and  $\lambda$  the wavelength of the light. The factor A includes the emissivity and was assumed constant in these calculations. Planck's distribution law of heat radiation was used under the assumption: in a narrow interval the emission number is equal.

$$I(\lambda) = \frac{A}{\lambda^5} \frac{1}{\exp\left[\frac{hc}{\lambda k_B(T+273)}\right] - 1} \quad (3)$$

The emission of alkali was analyzed as the area between the emission line in the spectrum and the heat radiation curve divided by the area under the heat radiation curve. The wavelength interval for the area calculation was chosen as the interval between the two points, at opposite side of the emission line, where only heat radiation was recorded.

Temperature and relative intensities of alkali (Na, K) in EBF raceway from 2<sup>nd</sup> to 11<sup>th</sup> of November measured with the optical fibre is shown in **Figure 56**. Alkali emissions in raceway are indicated during the whole period but a significant intensity drop is found for alkalis from the 8<sup>th</sup> of November and forth while the calculated temperature at the same time is higher. Highest intensities of alkalis are found for the period 2<sup>nd</sup>-4<sup>th</sup> of November.

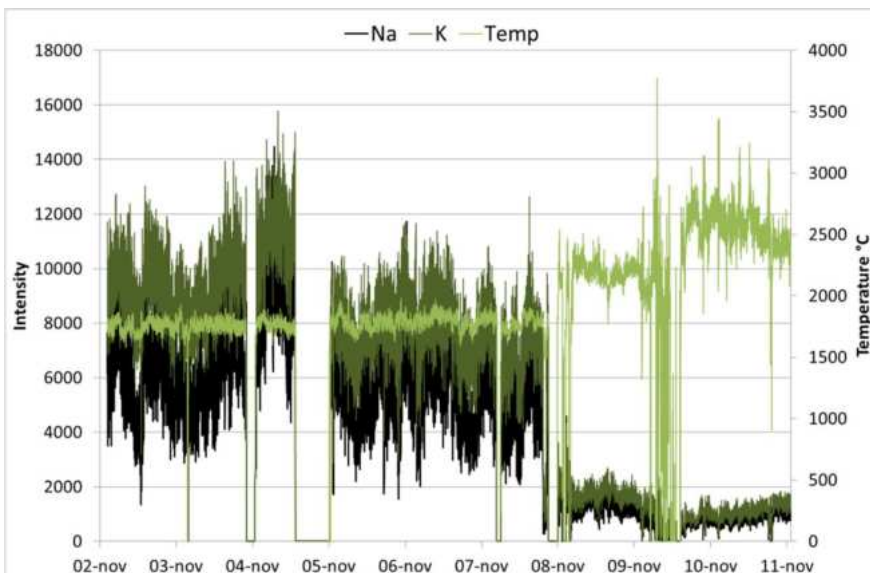


**Figure 56** Temperature and relative intensities of Na, K and in raceway measured with a spectrometer on light guided from the raceway by optical fibre during C32 in EBF.

Indicative for hanging and slipping of burden material could be a drastic drop in burden level in conjunction with elevated wall temperatures (skinflo). If cold and unreduced material is passing raceway, reduced cooling losses at tuyeres could also be expected. The trend of the skinflow temperatures are also indicative for the gas flow distribution, higher wall temperatures are expected when the BF is wall-operated i.e. more gas passing along the wall rather than centre. The lance with optical fibre was mounted in tuyere no.2 (150°) and in **Figure 57**, the measured intensity of alkali in raceway is plotted together with alkali in slag, total cool heat losses from tuyeres, skin flow temperatures above tuyere no.2 at two levels (16.8 m, 17.41 m), blast flow and burden level. The dashed vertical lines are highlighting time points of indicated slips above tuyere no.2 by drops in burden level and increased skinflow temperatures at the radial position of 150°. By studying the response on the alkali emissions in raceway, the trend of the curve is in all cases at a minimum just before the curve peaks, which is also the case for the heat losses at the tuyeres. This is supporting the occurrence of a slip, as the temperature in raceway is expected to drop if cold and unreduced materials are passing raceway. The intensity of alkalis is dependent on the temperature, which therefore should be affected by this. The peaking of alkali intensity and tuyere cooling losses after the slip might be explained by reduction and vaporization of alkalis in raceway.

By comparing the trends between alkali emissions in raceway and the alkali output via the slag (**Figure 57**), the correlation between them seems more negative than positive, meaning that higher alkali intensities in raceway were more common when the alkali output in slag was low. This is expected as the alkali dissolution in slag is favoured at colder conditions due to less silica reduction to HM and hence, lower slag basicity. At high heat level of the BF, the reduction and vaporization of alkalis in raceway is instead favoured and more alkalis will tend to recirculate. The indicated slip with high alkali output via the slag around the 10<sup>th</sup> of November shows the same trends as the other highlighted slips but the response of the alkali in raceway is less prominent here. As mentioned earlier, the intensity of alkalis was dropping around the 8<sup>th</sup> of November due to unexplained reasons. This happened in conjunction with a stoppage that might have had an impact on the signal from the optical fibre. The high alkali output occurred almost two days after the relative intensity corresponding to alkalis had dropped, which indicates that it was not the high alkali output that was causing this drop in measured relative intensity.

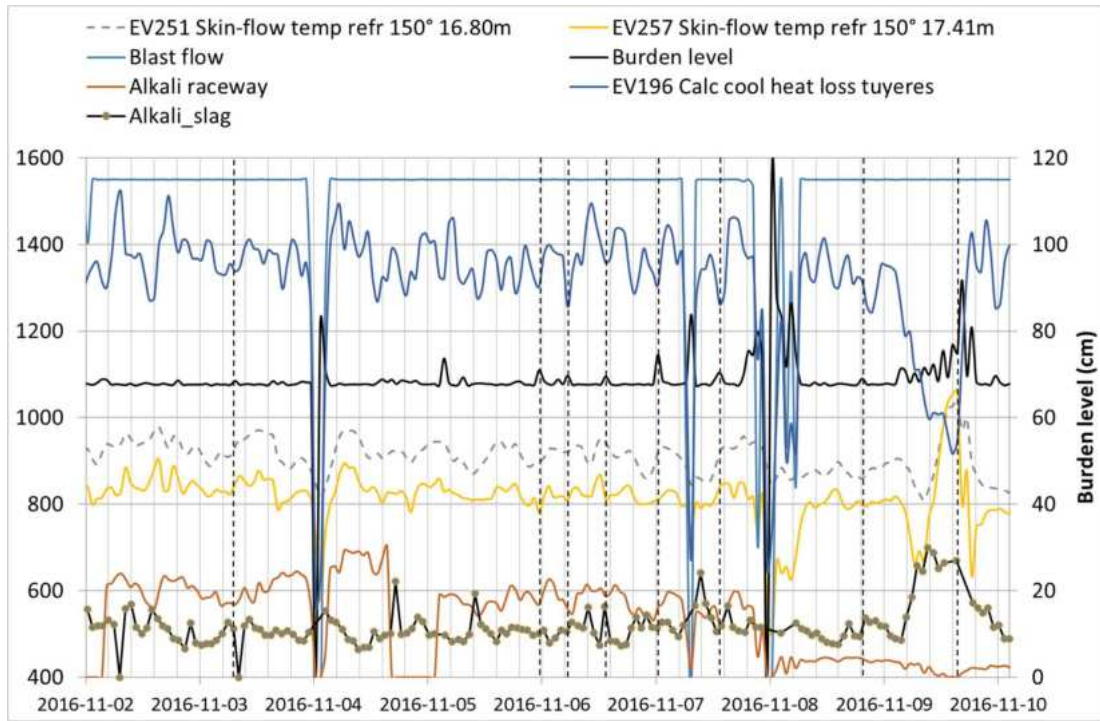


**Figure 57** Heat losses from shell, tuyeres, skinflow temperatures, burden level and alkali in raceway and slag.

MS-measurements top gas with specific focus on  $\text{NH}_3$ ,  $\text{HCN}$  and  $\text{H}_2\text{O}$  were performed for 6 days, approximately 8 hours each day. In **Figure 58**, analysed  $\text{NH}_3$ ,  $\text{H}_2\text{O}$  and  $\text{HCN}$  concentrations in top gas for one day (2 Nov) are shown together with other gas parameters such as temperature, gas utilization ( $\eta$  CO), CO and  $\text{CO}_2$  etc. In general, for all days, the concentration of  $\text{NH}_3$  shows a strong positive correlation to  $\text{H}_2\text{O}$  in the gas and both are varying in a cyclic way consistent with charging. A negative correlation to  $\eta$  CO is also indicated when comparing the trend of the  $\eta$  CO curve to the one for  $\text{NH}_3$ .  $\eta$  CO is in general increased every time when adding hematite in terms of iron ore pellets charged. At higher oxygen potential i.e. higher  $\eta$  CO, the  $\text{NH}_3$  concentration in the top gas is decreasing.

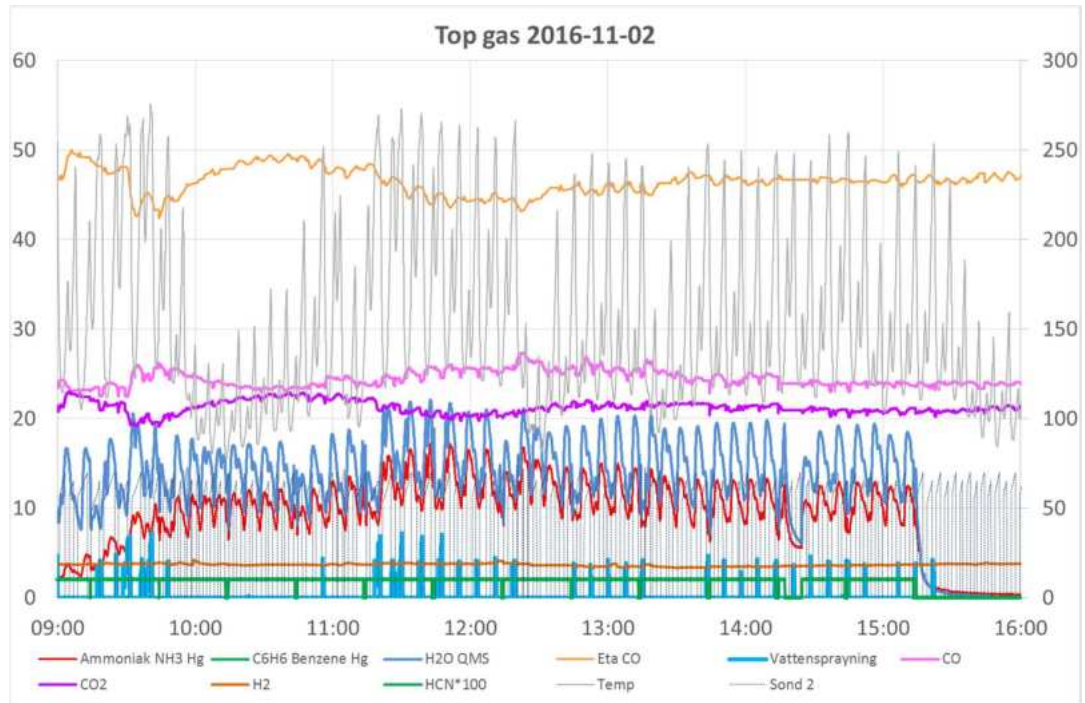


**Figure 58** MS analysis of NH<sub>3</sub>, H<sub>2</sub>O, HCN shown together with other top gas parameters.

An overview of the measuring period with mean values from MS and optical fiber in raceway is shown in **Figure 59** together with alkali in slag and the process variables eta CO, blast flow, top gas temperature and burden level. As revealed by the figure, eta CO is gradually increasing over the measuring period, the mean value being slightly higher during the latter part of the period. Some stoppages during the period occurred, as can be seen by the drastic drops in blast flow and burden level. Associated with these stoppages are also increased eta CO while the intensity of alkali in raceway is reduced. By comparing the measured NH<sub>3</sub>-levels in top gas from start to end date, it can be seen that the highest concentrations in the top gas was during the 31<sup>th</sup> of October with 10-15 ppm and lowest in the end between 9-10<sup>th</sup> of November below 5 ppm. The intensity of alkali in raceway is following the same trend with highest values in the start of the period from 2<sup>nd</sup> of November that declines overtime with the lowest levels detected for the last two days during the 9<sup>th</sup> to 10<sup>th</sup> of November.

Alkali output via the slag is also visualized in **Figure 59** by the analyzed % of alkali in tapped slag. Around the 10<sup>th</sup> of November, the alkali output seemed highest here. At the same time, the burden level drops while the top gas temperature increases and eta CO is reduced. At this period, no measurements with MS were ongoing but the intensity of alkali emission in raceway was dropping.

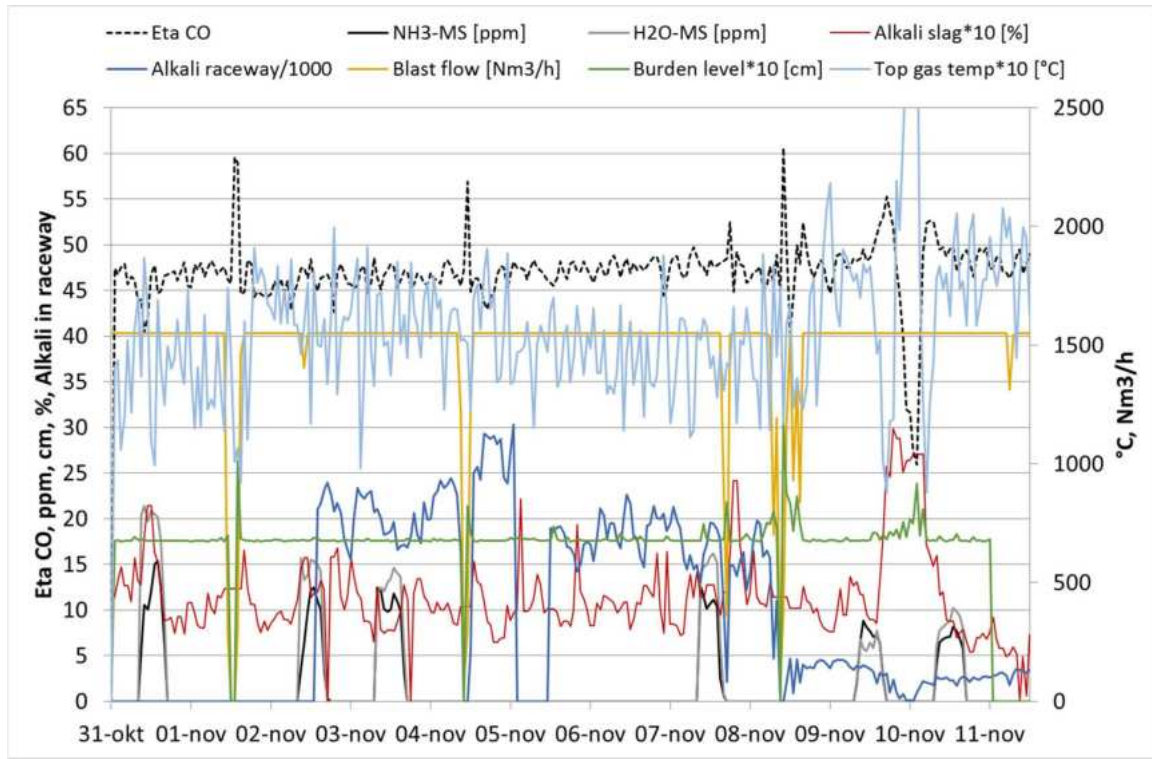


**Figure 59** Overview of some process parameters, alkali in slag together with MS and raceway measurements during EBF campaign C32.

The alkali output via sludge and dust is plotted in **Figure 60** together with mean values for  $\text{NH}_3$  and  $\text{H}_2\text{O}$  measured by the MS. According to this, a positive correlation between alkali output via the top gas dust and  $\text{NH}_3$  in top gas can be seen. As the trend for  $\text{NH}_3$  content, the alkali content in dust and sludge are highest for the early periods and declines with time being lowest in the end of the campaign. As also observed earlier, the  $\text{H}_2\text{O}$  measured by the MS is shown to be strongly correlated to  $\text{NH}_3$ .

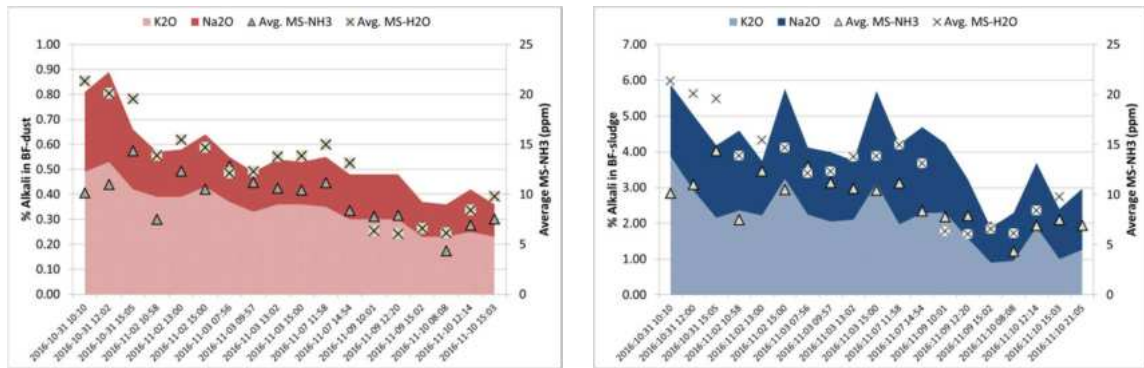


**Figure 60** Alkali in BF dust and sludge together with average MS- $\text{NH}_3$  during sampling time.

Unlike for the alkali content in the top gas dust, the correlation between top gas  $\text{H}_2\text{O}$  and  $\text{NH}_3$  to alkalis in slag is not found, see **Figure 61**. There are two occasions with high alkali outputs via the slag during MS measurements, one at the 31<sup>th</sup> of October and the second during the 10<sup>th</sup> of November. The  $\text{NH}_3$ -concentration is higher in the first case in contrast to the latter case and the trend of the curve shows in overall weak correlation to the alkali content in slag. According to the alkali balance from the same campaign described in Task 1.1 (**Figure 7** and **Figure 8**), there is a steady build-up of alkalis in the EBF from the start date of the measurements the 31<sup>th</sup> of October until the high outputs around the 8-9<sup>th</sup> of November. The  $\text{NH}_3$  concentrations in top gas and the alkali content in top gas dust and sludge are instead decreasing with time. Thus, the  $\text{NH}_3$  concen-

tration in top gas is perhaps not indicative for the total alkali circulating load but can give information about the alkali output via the top.

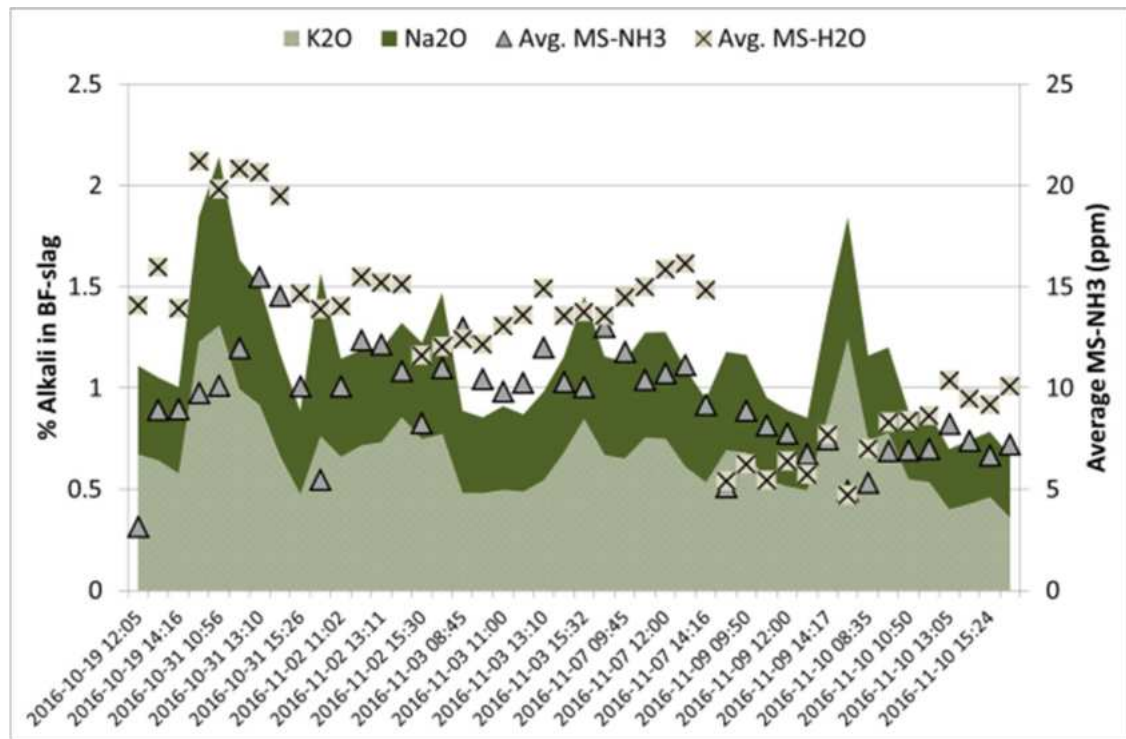


**Figure 61** Alkalies in BF-slag together with MS-H<sub>2</sub>O and MS-NH<sub>3</sub>.

Mean values of the alkali intensities in raceway between taps have been plotted together with the alkali in slag, see **Figure 62**. By studying the relative changes of the curves within separate days, a negative correlation between alkali in slag and the raceway alkali intensities can be seen. This was also noticed earlier in **Figure 57** but averaging the spectrometer data made the relationship clearer.

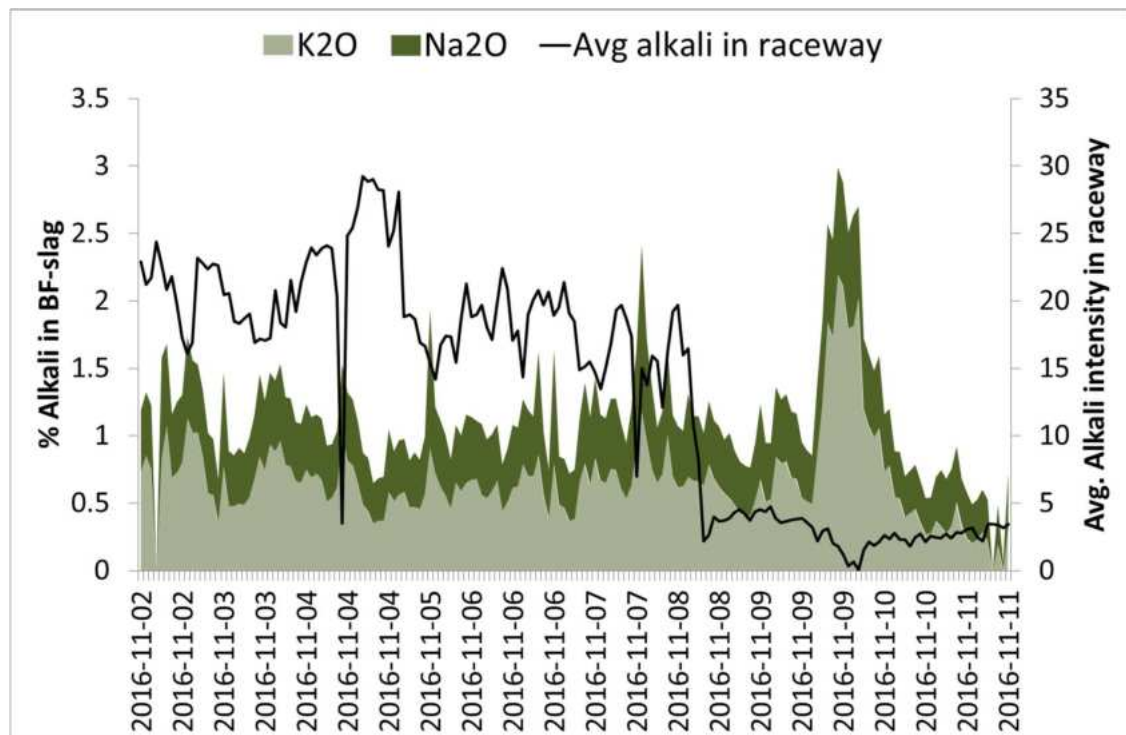


**Figure 62** Alkalies in slag together with mean values for alkali intensity in raceway.

$\text{NH}_3$  and  $\text{H}_2\text{O}$  has been plotted versus eta CO and top gas temperature, see **Figure 63–Figure 66**. Both  $\text{NH}_3$  and  $\text{H}_2\text{O}$  shows overall a negative correlation to eta CO i.e. both are decreasing with higher oxygen potential in the top gas. Eta CO was 40 and below for a period during 2016-10-31 and are found as outsiders to the linear trend in **Figure 63**. The EBF was operated with a more central gas profile in the morning the 31th of October that later shifted to have more flat gas profile, which might have impact on the correlation between Eta CO and  $\text{NH}_3$ . Moreover, there is no clear correlation to top gas temperature for neither of the gases.

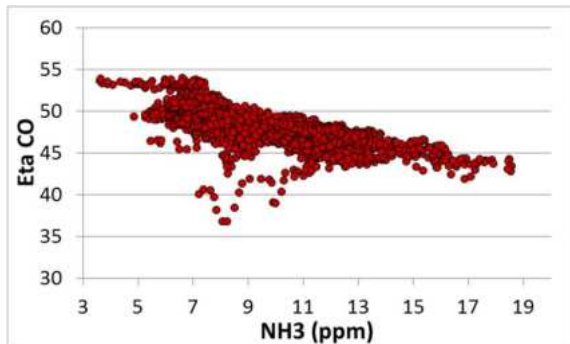


**Figure 63** MS- $\text{NH}_3$  vs. eta CO

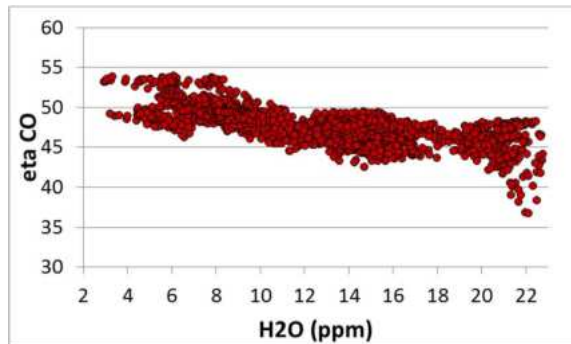


**Figure 64** MS- $\text{H}_2\text{O}$  vs. eta CO

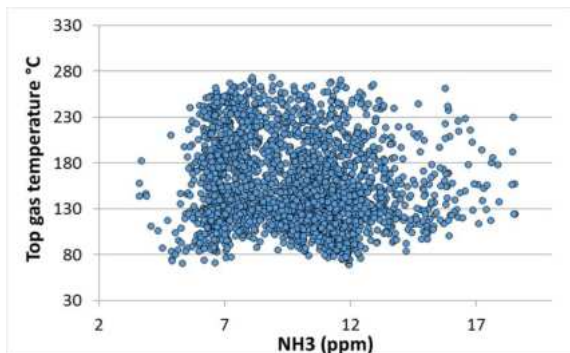


**Figure 65** MS- $\text{NH}_3$  vs. top gas temperature

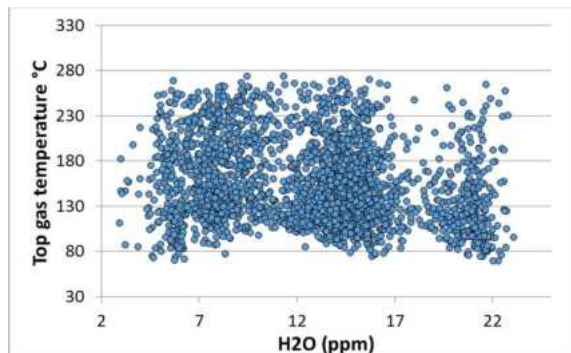


**Figure 66** MS- $\text{H}_2\text{O}$  vs. top gas temperature

By plotting  $\text{NH}_3$  versus cooling losses in tuyeres and skin flow temperatures, a positive correlation can be seen in both cases, see **Figure 67**. At  $\text{NH}_3$  concentrations above 14 ppm, the correlation to both cooling losses and skin flow temperatures becomes closer to linearity. The high skin flow temperatures could be indicating that gas is more distributed towards the walls and/or no or very small scaffold formations on the walls. For the latter case and under the assumption that  $\text{NH}_3$  is reflecting the alkali load, low  $\text{NH}_3$  concentrations at low skinflow temperatures can be explained by alkalis condensing and forming compounds that stick to the walls with less alkali drained via the top as a cause. For the same assumption, the positive correlation to cooling losses in tuyeres could be coupled to increased reduction and vaporisation of alkalis at high temperatures in raceway, which will enhance the build of alkali circulating load.

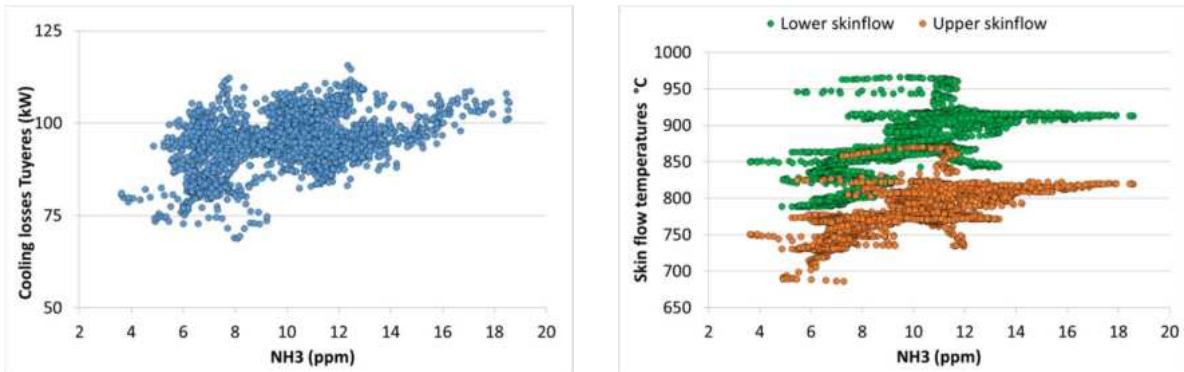


**Figure 67** Total cooling losses tuyeres (left) and skin flow temperature (right) as a function of NH<sub>3</sub> in top gas.

To further study how the formation of NH<sub>3</sub> and alkali emissions in raceway correlates to the BF process, a data set with process data, tap data, raceway- and MS data has been put together for multivariate analyses in SIMCA 14.1. The tools used for the evaluation is Principal Component Analysis (PCA) that is useful for obtaining an overview of the data set by projecting the data on a coordinate system. A second tool is Partial Least Squares Projections to Latent Structure (PLS) that work in the same way but is more useful to link several variables together to see how variables (X) can predict response (Y) variables. A third tool is OPLS. OPLS stands for orthogonal PLS with the difference that the model is separated into two different Y, one that explains Y and several orthogonal rotations that are not explained by Y. The number of rotation will vary depending on how many are deemed necessary by SIMCA to get a fitting model. The resulting degree of explanation and prediction is the same as for PLS with the benefit of OPLS giving more easily interpreted models. The data set has been computed based on average data in minute basis, see variable list in **Appendix Table A2**. The tap data has been attached to the data set without averaging which means that there is a lot of missing data for these variables.

An OPLS-model (M1) with minute-averages for the whole period with MS-measurements and with NH<sub>3</sub> as response variable (Y) had a Q<sup>2</sup> cum value of 59% and a R<sup>2</sup> cum of 68%. The score scatter plot and DmodX line plot in **Figure 68** reveals that observations from 2016-10-31, 2016-11-02 and 2016-11-09 are outside the confidence interval of the model and should thereby be regarded as outliers, see group highlighted in red.

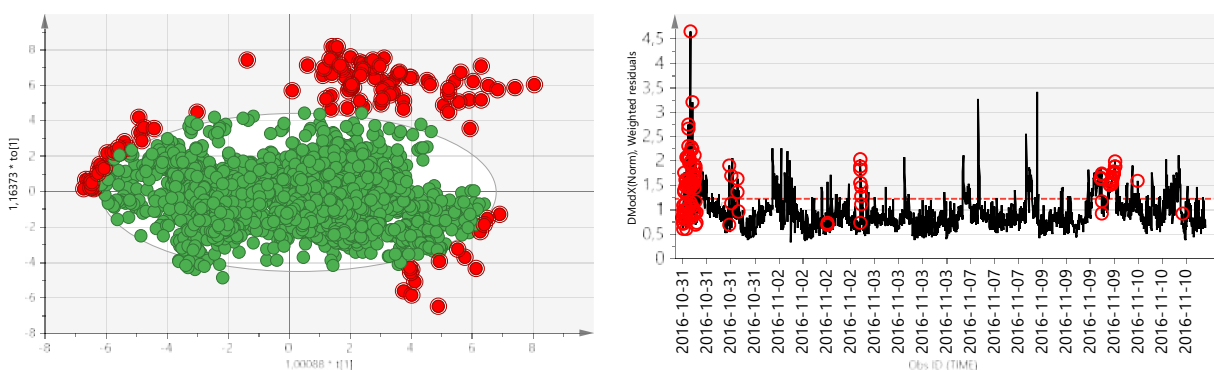


**Figure 68** Score scatter plot (left) and DmodX line plot (right) for M1 with Y=NH<sub>3</sub>.

A new model excluding the observations from 2016-10-31 resulted in an R<sup>2</sup>Ycum being 77% and Q<sup>2</sup>Y cum at 70%. A variable importance plot (VIP) of M2 (**Figure 69**) shows the most important variables to explain and predict NH<sub>3</sub> content in the topgas. Based on this, the temperature and alkali emission in raceway measured by the optical fibre has largest impact on topgas NH<sub>3</sub> followed

by MS-H<sub>2</sub>O, eta CO, skin flow temperatures and heat losses from shell and tuyeres. Skin flow temperatures are measured by thermocouples placed on two levels (upper, lower) of the shaft spread over 6 radial positions. The impact of slag and HM composition on the NH<sub>3</sub> content in the topgas is weak according to the model and was thereby not included in the VIP plot.

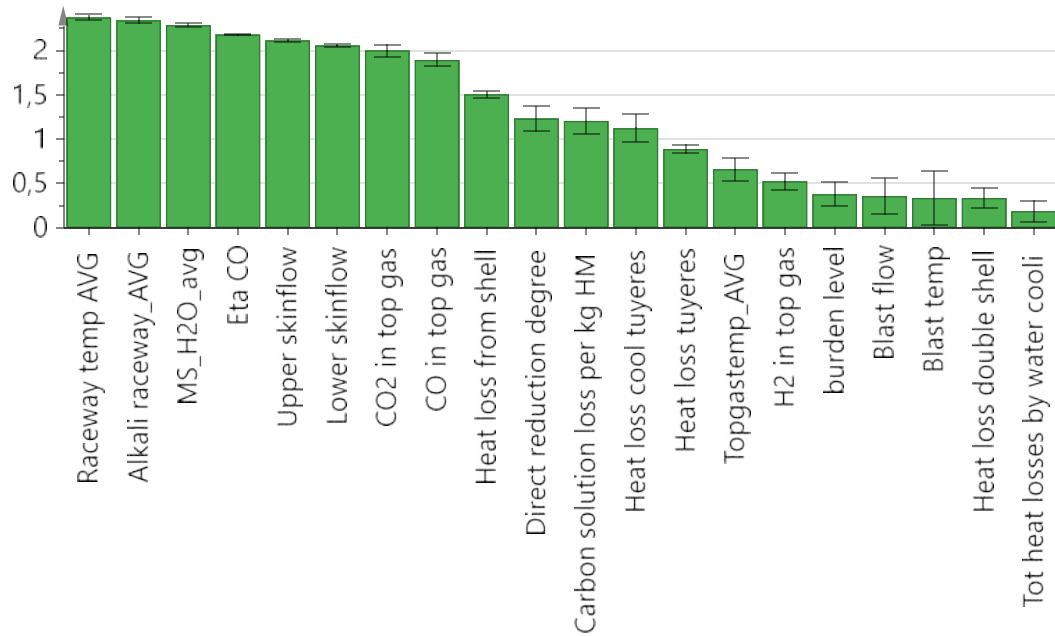


**Figure 69** VIP plot of M1 showing the most important variables to explain NH<sub>3</sub>.

A coefficient plot shows in what direction variables affects NH<sub>3</sub> i.e. if the variable has a positive or negative impact. According to coefficient plot of M2 in **Figure 70**, topgas content of NH<sub>3</sub> is positively correlated to raceway temperature and relative alkali intensity in the raceway, topgas content of H<sub>2</sub>O, skinflow temperatures, CO in top gas etc. This means that NH<sub>3</sub> concentration in top gas was high whenever these variables were high. Variables having negative impact on topgas content of NH<sub>3</sub> are eta CO, heat losses from shell, top gas temperature etc. Thus, the formation of NH<sub>3</sub> seem to be favored at low gas efficiencies and indirect reduction (low eta CO, high direct reduction degree and high carbon solution loss), at low burden levels and low heat losses in double shell. The low gas efficiency indicators together with the positive correlations to skin flow temperatures could be due to high NH<sub>3</sub> levels at periods when the EBF was wall-working i.e. higher gas distribution towards the walls. This is also supported by the negative correlation to top gas temperature.

Based on M1, the positive correlation to alkali in raceway could be coupled to the alkali cycle, more alkalis that are passing raceway is an indicator of the alkali circulating load that also can be read by the NH<sub>3</sub> concentration in top gas. However, both NH<sub>3</sub>-concentration in top gas and the alkali intensity in raceway dropped by unexplained reasons in the end of the campaign. These happenings can be correlated and related the alkali circulating load but it can also be explained by other unknown reasons. Moreover, the alkali emissions in raceway should be valued as relative and thereby compared to other variables by comparing trends in a short time perspective. The intensity drop around the 8<sup>th</sup> of November will therefore have a large impact on the model as SIMCA is treating the variable variation quantitative. It is not possible to verify that the drop of alkali emission and NH<sub>3</sub> in top gas coincided at the same time as the MS-measurements were only conducted on day time basis for some hours each time and unfortunately not during the occurrence

of the signal drop in raceway around the 8<sup>th</sup> of November, see **Figure 59**.

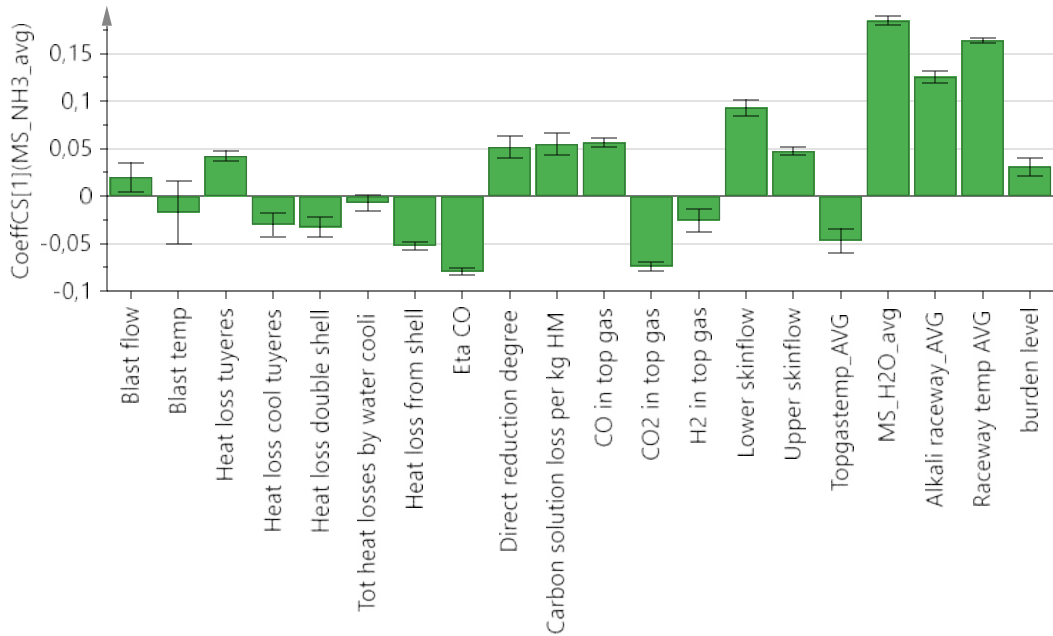


**Figure 70** Coefficient plot of M1 showing the influence (+/-) of variables on NH<sub>3</sub>.

A new model (M2) was computed with relative alkali intensity in raceway as response variable (Y) instead of top gas content of NH<sub>3</sub> with a Q2 cum of 87% and R2 cum of 91%. This model covers the period with the raceway measurements, which were started the 2<sup>nd</sup> of November. In the score scatter plot of M2 (**Figure 71**), grouping of the observations can be seen. The red group is corresponding to observations in the latter part of campaign starting from 8<sup>th</sup> of November and can be related to the drastic intensity drop of alkalis around this date in association with a process stop-page (**Figure 57**).

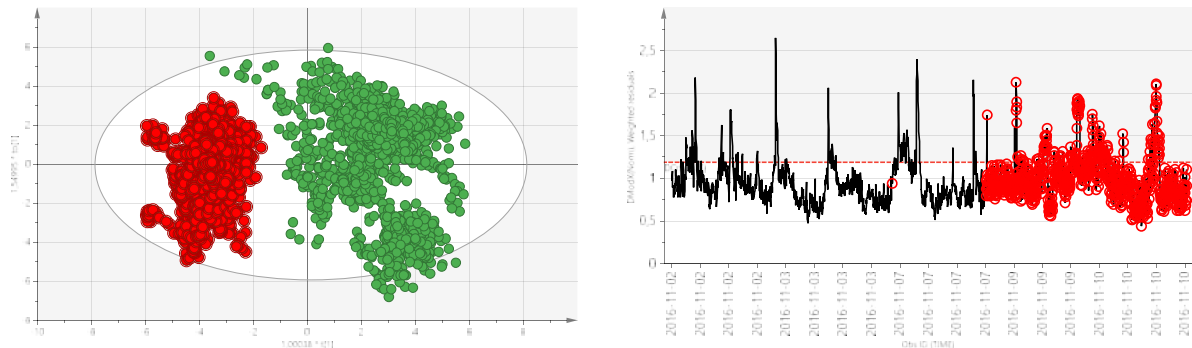


**Figure 71** Score scatter plot (left) and DModX line plot of M2 with alkali in raceway=Y.

The VIP plot of M2 indicates that Raceway Temp, skinflow temperatures (individually and mean), MS-H2O and MS-NH<sub>3</sub>, eta CO and CO in top gas and heat loss from tuyeres and shell are the most important variables to explain and predict the measured relative alkali intensity in raceway.

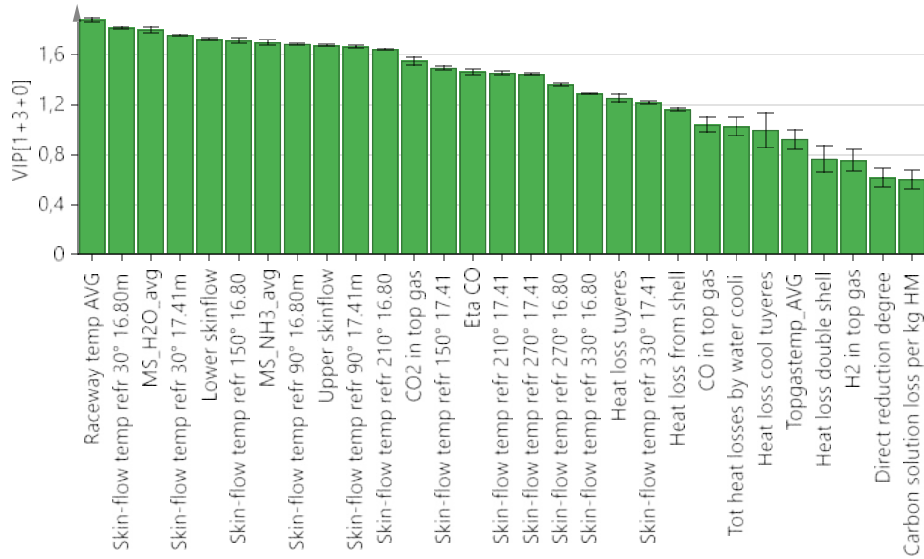


**Figure 72** VIP plot of M2 showing the variables with highest impact on Y=alkali in raceway.

According to the model, the intensity of alkalis in raceway is positively correlated to; NH<sub>3</sub> and H<sub>2</sub>O concentrations in top gas, raceway temperature, heat losses at tuyeres and shell, skin flow temperatures and K<sub>2</sub>O and Na<sub>2</sub>O in slag, see **Figure 73**. This means that the relative alkali intensity in raceway will be high whenever these variables are high. The top gas composition in terms of CO, CO<sub>2</sub> and H<sub>2</sub> seem all to have a negative influence as well as skinflow temperatures at 330° i.e. the relative intensity of alkalis in raceway will decrease whenever these are increasing. The skinflow temperatures measured directly above T2 (150°) at two levels where the optical fibre was mounted shows both on a positive correlation to alkali in raceway. This might be coupled to the occurrences of slips and release of scaffolds above T2 highlighted in **Figure 57** as the skinflow temperatures is expected to increase as well as the alkali emissions in raceway. However, a negative correlation to alkali in slag was observed when comparing curve trends in **Figure 57**, which is contradictory to the results of M2 as the alkali content in slag showed on a positive correlation. This shows on the difficulties and uncertainties of evaluating a qualitative variable with this kind of tool for a relatively large time perspective.

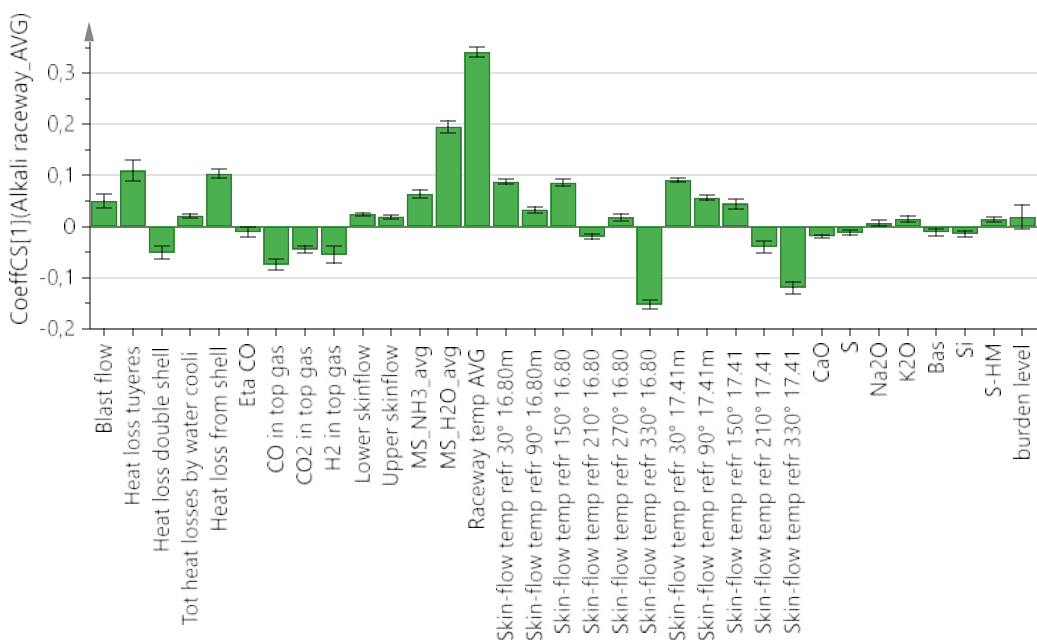


**Figure 73** Coefficient plot of M2 showing the influence (+/-) of variables on Y=alkali in raceway.

As M2 included the period with the unexplained drop in the intensity of alkalis in raceway from the 8<sup>th</sup> of November, a new model, M3, without these observations was computed to see if this would have any effect on the observed correlations. The model had a R<sup>2</sup>Y cum of 62% and a Q<sup>2</sup>Y cum of 50%, see VIP plot in **Figure 74**. The raceway temperature is still the variable with highest impact followed by the skin flow temperatures and heat losses. The main difference from M2 is that the impact of MS-NH<sub>3</sub> and MS-H<sub>2</sub>O is less when removing the observations from 8-10<sup>th</sup> of November. Also the tap variables are less important and the influence of alkali in slag is not even significant.

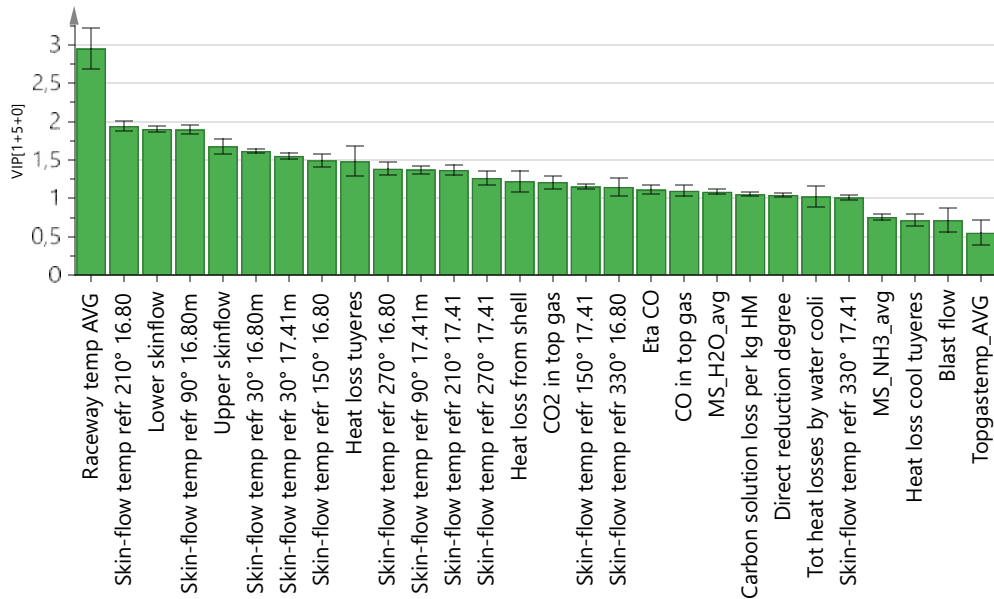


**Figure 74** VIP plot of M3

As before, both NH<sub>3</sub> and H<sub>2</sub>O in top gas are positively correlated to alkali emission in raceway, which also is the case for raceway temp and heat losses at tuyeres and shell (**Figure 75**). The overall skinflow temperatures are positively correlated as before but the individual thermocouples are different from M2. For instance, both skin flow temperatures above T2 (150°) are now negatively correlated to the alkali intensity.

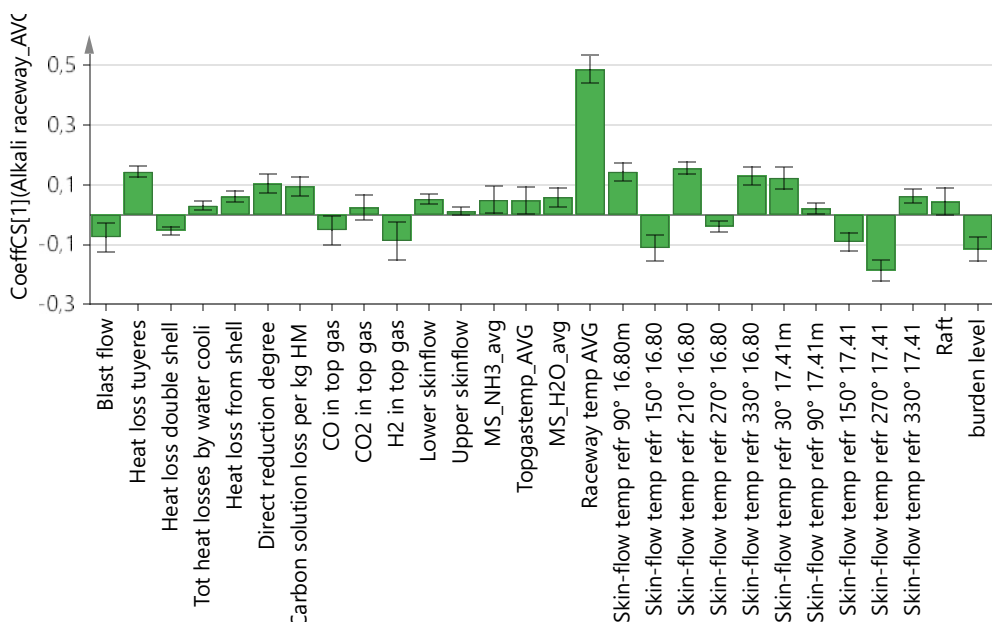


**Figure 75** Coefficient plot of M3 showing the influence (+/-) of variables on alkali emission in raceway.

To further investigate if the NH<sub>3</sub> content in top gas can be correlated to the alkali circulating load, models in SIMCA was computed for each individual day. For each model, MS-NH<sub>3</sub> was put as response variable (Y) and only observations with values of MS-NH<sub>3</sub> was included in the models. The results are summarized in **Table 14** by showing the influence (+/-) of the most important variables as well as the R<sup>2</sup> and Q<sup>2</sup> values. All models showed on high degree of explanation and prediction with R<sup>2</sup> and Q<sup>2</sup> values above 70%. However, by studying the influence of each variable on NH<sub>3</sub> it is revealed that it is not consistent within the different days for most of the variables. The only variable that has the same influence for all days is MS-H<sub>2</sub>O and it is always positively correlated to NH<sub>3</sub>. Eta CO is in all cases negatively correlated to NH<sub>3</sub> except during the 31th of October. The correlation was negative also for this model but not significant as the confidence interval crossed 0, thereby given the sign +/--. For most of the days, heat losses at tuyeres are positively correlated to NH<sub>3</sub> which implies that high heat losses at tuyeres will contribute to high NH<sub>3</sub> content in top gas. This was also seen when plotting the heat losses against NH<sub>3</sub> in **Figure 67** and could be explained by elevated alkali reduction and vaporisation at high temperatures in the raceway that favours alkali circulation.

The other variables have in some cases positive- and in other cases negative influence on NH<sub>3</sub> which implies that these variables are only indirectly associated to NH<sub>3</sub>. Skin flow temperatures showed on an overall positive correlation to the NH<sub>3</sub> content in top gas when plotting upper and lower skinflow respectively to the NH<sub>3</sub> content in **Figure 67**. The varying influence as seen by the SIMCA evaluation from day to day could resemble the different gas distributions (wall/centre) and presence or absence of scaffolds on the walls. As discussed earlier, low skinflow temperatures could be a sign of scaffold formation and more alkalis condensing and oxidizing on burden materials and walls instead of going out of the EBF via the top. This would show on a positive correlation to the NH<sub>3</sub> content, like during the 3<sup>rd</sup> and 9<sup>th</sup> of November. Both skinflow temperatures, NH<sub>3</sub> in top gas and the alkali in top gas dust were all declining over time, being lowest in the end of the campaign, even though the gas profile was more distributed towards wall than central. Formations of scaffolds on the wall could have occurred to a larger extent in the latter part of the campaign, which could explain this. This could be perhaps be confirmed by the more frequent occasions of slips as highlighted in **Figure 57**.

**Table 14** Summary of variable influence (+/-) on MS-NH<sub>3</sub> for day-models.

Date	31/10-16	2/11-16	3/11-16	7/11-16	9/11-16	10/11-16
R <sup>2</sup> Y cum (%)	89	87	75	77	74	95
Q <sup>2</sup> Y cum (%)	88	86	73	73	72	94
MS-H <sub>2</sub> O	+	+	+	+	+	+
Alkali in raceway	No value	+	+/-	-	+/-	+/-
Temperature raceway	No value	-	+	-	+/-	+/-
Upper skinflow	+	-	+	-	+	-
Lower skinflow	-	+/-	+	-	+	-
Eta CO	+/-	-	-	-	-	-
Top gas temperature	-	+/-	+/-	-	+/-	+/-
Heat loss tuyeres	+/-	+	+	-	+	+
Heat loss shell	-	-	+/-	+	+	-
Burden level	+/-	+/-	+	+/-	+/-	+/-

### **2.3.1.2.2** Tests with new on-line measurements at SSAB BF No. 4 in Oxelösund (SWERIM, SSAB)

A two week long measurement campaign stretching between 2017-11-08 and 2017-11-22 was conducted in October at BF No.4 at SSAB steel plant in Oxelösund with continuous MS analyses of NH<sub>3</sub> and HCN contents in top gas, continuous raceway measurements with optical fibre for alkali emissions as well as frequent dust and sludge sampling. In addition, isokinetic sampling of dust in the gas duct before the gas cleaning was performed during this period. The isokinetic sampling enables correlation of the dust amount to gas volume and production and the sampling position ensures that the characteristics of the dust has not been affected by the gas cleaning steps. The measurements were conducted at normal process conditions but also at periods with intended changes of top gas temperature, slag basicity and flame temperature as well as process stoppages.

The top gas analysis was conducted with a V&F Analyse und Messtechnik GmbH Airsense Compact (newer models use the name Combisense), the same kind as used at the EBF. The position of the gas sampling probe was situated into one of the four exhaust pipes, approximately at the same height as the charging system. BF No.4 is a low pressure BF operating at an overpressure of only 50-100 mbar so the gas had to be pumped into the MS. To avoid condensation, the whole system was heated including pump and gas pipes transporting the gas from sampling point to the MS one floor down. A cabinet was installed before the MS for flow control and filtering of the gas before going into the MS and the system was regularly back blown with nitrogen to avoid particles entering the MS. The back blow can be seen as the measured data dips down towards 0 each time it was performed. Raceway measurements with optical fibre had the same layout as previous measurements conducted at LKABs experimental furnace.

The collected MS-data is shown in **Figure 76** together with the blast flow of the BF. Occasions where the BF blast flow decreased to 0 indicates process stops and can be seen in the beginning around 9<sup>th</sup> of November and between 13-14<sup>th</sup> of November respectively. The mass spectrometer readings were more stable in the latter half of the campaign from 2017-11-14 to 2017-11-22 and the evaluation has therefore been focused on that period. In contrast to the EBF-measurements, HCN could be detected at BF No.4 and the concentrations of HCN were even higher than those for NH<sub>3</sub>.

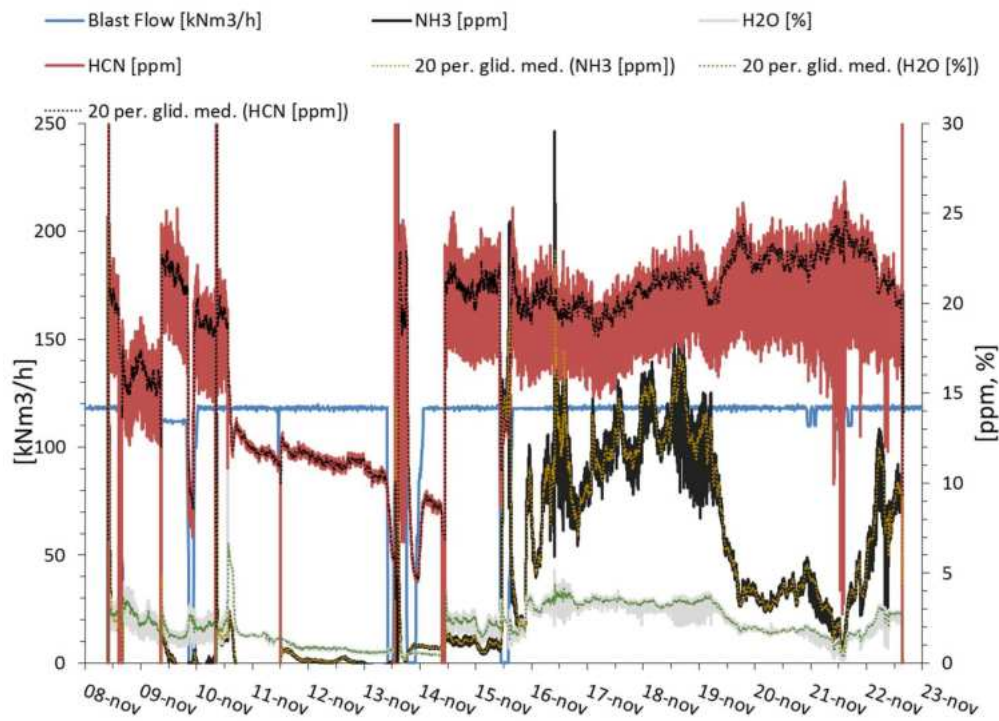


**Figure 76** Concentrations of HCN, NH<sub>3</sub> and H<sub>2</sub>O measured by MS and blast flow for the period.

During the trial period, measurements using a UV/VIS spectrometer were performed and light guided via an optical fibre from the raceway of the BF in Oxelösund (Tuyere No.9) to study the emissions related from alkalis in the raceway. As for the EBF, the relative intensity of alkali emissions were plotted together with selected process variables such as burden level and cooling losses at tuyeres to study the relative change of alkali intensity in raceway during an indicated burden slip (**Figure 77**). The dashed vertical lines in the figure are highlighting the indicated slips by a drastic drop in burden without reduced blast. At the EBF, a drastic drop in tuyere cooling losses was always present in conjunction with the indicated slip and the skinflow temperatures responded by an increase in temperature at the same time. For the measurements at the industrial BF, no such clear trends could be observed. Instead, the relative intensity of alkali emissions is peaking some hours after indicated slips at 16<sup>th</sup> and 17<sup>th</sup> of November. Longer response times are expected when changes occur in the lower- or upper part in an industrial BF compared to the EBF.

Before the drop in burden level between 24<sup>th</sup> and 25<sup>th</sup> of November, the alkali intensity is dropped rapidly while the flame temperature is increased at the same time. The explanation is probably due to reduced PCI which is occurring at the same time, see **Figure 77**.

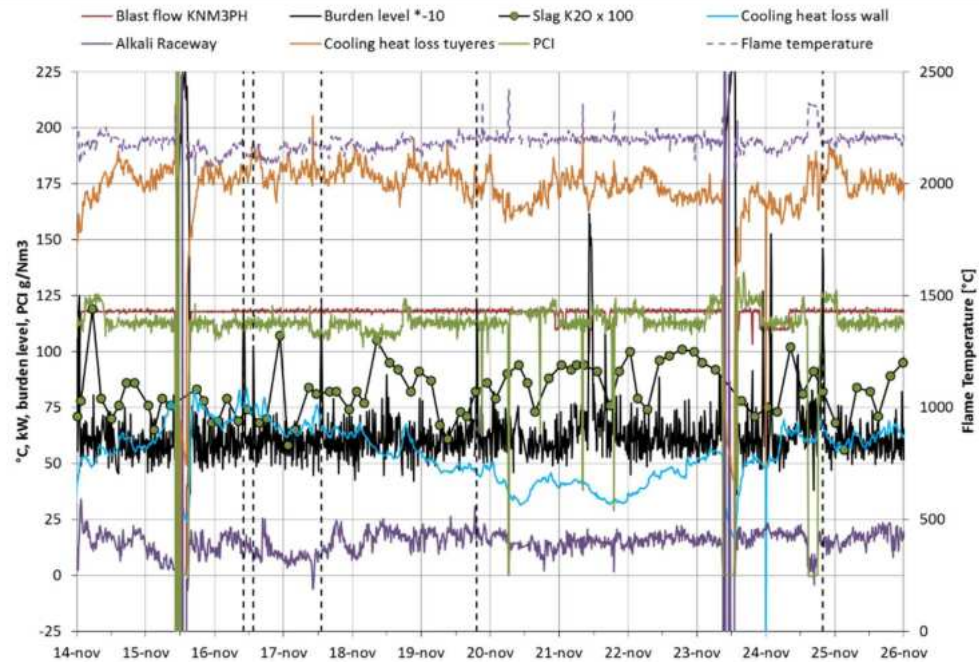


**Figure 77** Cooling losses, flame temperature, relative intensity of emissions related to alkali in raceway, burden level,  $K_2O$  in slag, blast flow and brick temperature for the period with raceway measurements at BF No.4 in Oxelösund.

The cumulative alkali amount for a longer period is plotted together with the relative intensity of alkali emissions in raceway, see **Figure 78**. By comparing the curves with respect to the relative change of each it is indicated that there is an overall positive correlation between the alkali load and relative alkali intensities in raceway. In the start of the period, the relative intensity for alkali was highest and so was also the alkali circulating load according to the mass balance. The relative change of the cumulative alkali load is negative over time, implying that alkalis are drained out from the BF and the circulating load should thereby decrease. The intensity of alkalis in raceway is also decreasing over time, being lowest in the end of the period. This is in accordance with theory as alkali emissions in raceway are expected to increase with increased circulating load.

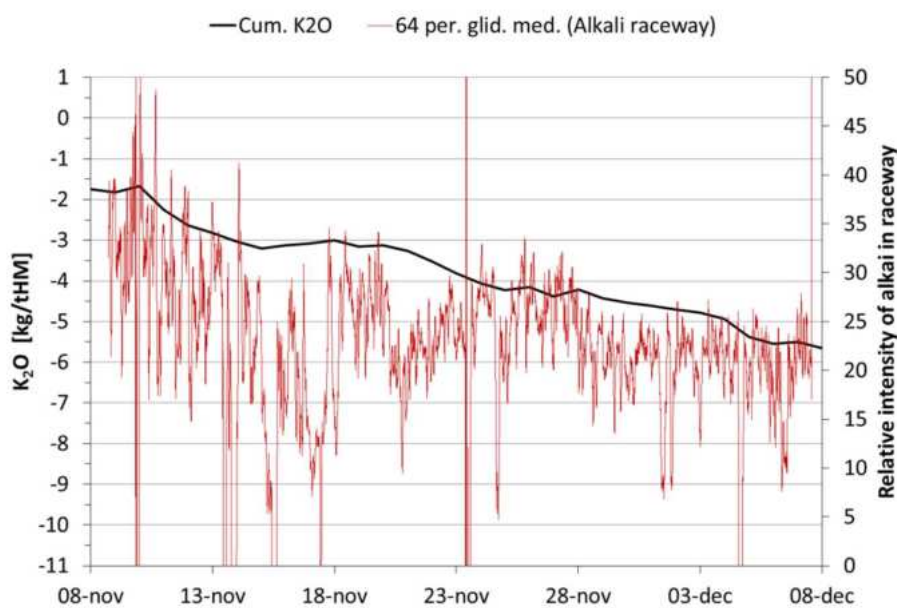


**Figure 78** Cumulative amount of  $K_2O$  and relative intensity of emissions related to alkali in raceway.

**Figure 79** show the trends of mean alkali and potassium (K) relative intensities in raceway compared to the amount of K<sub>2</sub>O in the slag. Compared to the previous figure showing the calculated alkali load relative the intensity, the comparison to the content of K<sub>2</sub>O in the slag is not as clear.

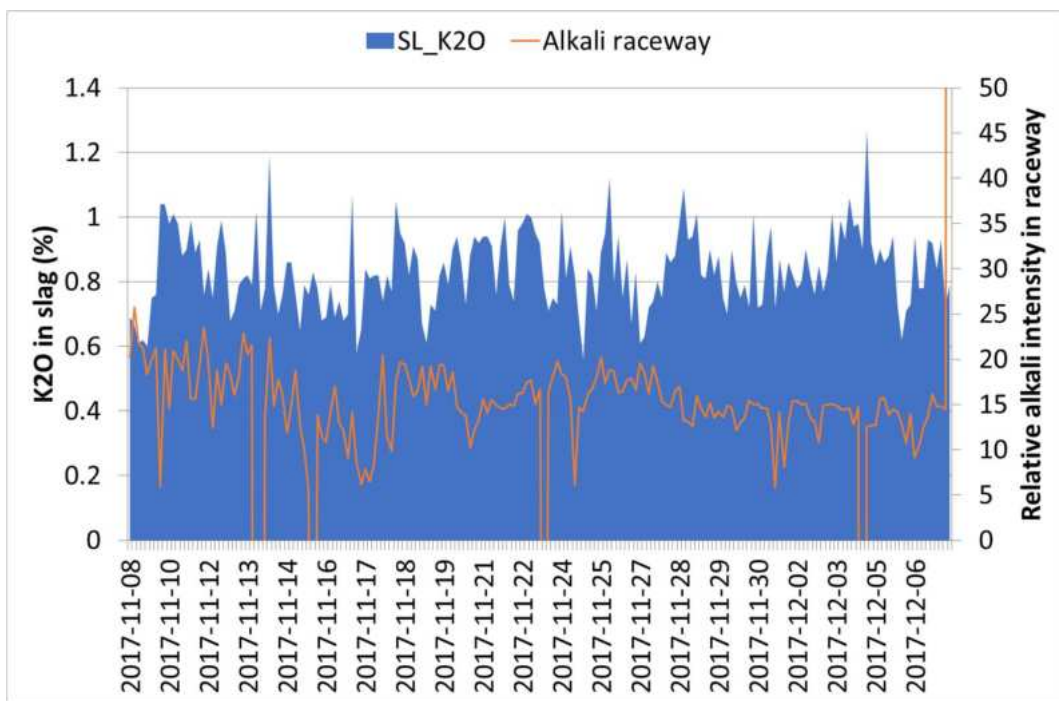


**Figure 79** Alkali measurements in the raceway compared to the K<sub>2</sub>O in slag.

The MS-NH<sub>3</sub> and MS-HCN concentrations in the top have been plotted together with alkali contents of some dust samples collected during the measurements see **Figure 80**. The dashed vertical lines are indicating occasions with lowering of burden level by purpose to study the effect on alkali and zinc levels in top gas dust. Isokinetic dust samples of BF-dust were collected from gas duct before the cyclone and can be regarded as the total off-gas dust i.e. BF-dust and sludge combined. A positive correlation between NH<sub>3</sub> and alkali content in both dust and sludge was observed for the EBF, with higher alkali and NH<sub>3</sub> in the start of the period and lowest in the end. That trend is more difficult to see for the data at the industrial BF. In the EBF the gaseous compounds formed in the high temperature regions reaches the top, although oxidized and condensed from the gas phase, while in the industrial BF there are large volumes materials as e.g. central coke bed that the gas can interact with. Therefore, the gaseous compounds formed in the high temperature region of the industrial BF will not reach the top as easily as in the EBF. The total amount of material for collected sludge samples were too small to enable individual analysis, instead two or three collected sludge samples from different occasions had to be combined. Due to the narrow time interval studied here, the analyses of sludge samples have therefore been discarded. The total alkali content in the isokinetic sample collected before the first occasion with lowered burden level around 09:30 was slightly higher than the corresponding sample collected during the first trial and also in the evening samples collected after 19:00. The alkali content in the BF-dust samples collected just before- and during the second trial with lowered burden shows on a slightly decreased alkali content in the second sample. This is indicative for a higher alkali output via the top gas. Referring to the NH<sub>3</sub> concentration, the relative change of the curve cannot be coupled to the alkali content in dust, more samples are needed to confirm this.

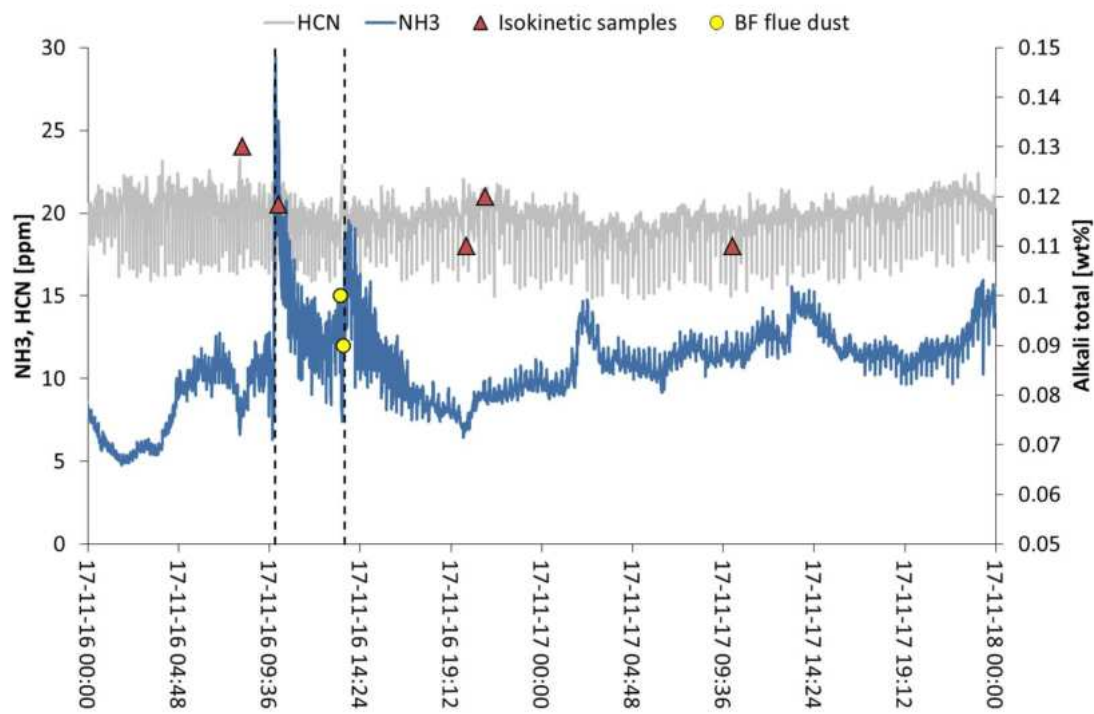


**Figure 80** MS-NH<sub>3</sub> and MS-HCN concentrations together with alkali content in dust and sludge samples. Dashed vertical lines are highlighting occasions with decreased burden level.

The MS-data was analyzed by using multivariate analysis in SIMCA 15 (1) to investigate and statistically determine any connection between NH<sub>3</sub> and HCN in top gas to process data and alkali. Only the data collected between 2017-11-14 and 2017-11-22 was used in the analysis as there had been problem to get stable readings from the MS before. The data set used in SIMCA was prepared by removing all observations where the blast flow indicated no or low production (blast flows lower than 80 kNm<sup>3</sup>/h) and points where the HCN and NH<sub>3</sub> data was negative.

The combination of MS data with process data resulted in a model named **MSP** containing 1086 observations. The PCA model had a R<sup>2</sup>X at 84% and Q<sup>2</sup>X at 46%, R<sup>2</sup>X explains how well the model fit the observations and Q<sup>2</sup>X how well it predicts variation. The observations grouped up into three different groups as seen in the PCA score plot on the left in **Figure 81**. The grouping depended on the time period for the observations. The time period differed in e.g. having a lower basicity (the blue group) or by having higher basicity (the red group). The PCA loading plot in the right part of **Figure 81** shows how the variables correlate to each other. Variables close to each other are positively correlated while negatively correlated variables are found across the diagonally. The grouping also correlates to the loading plot in the right part of the figure, meaning that the blue group was positively correlated to e.g. flame temperature and HCN(g). The red group is instead associated with high NH<sub>3</sub> and H<sub>2</sub>O, high CO in top gas and high cooling effects. As observed during evaluation of MS-measurements at the EBF, ETA CO<sub>2</sub> seem to be negatively correlated to NH<sub>3</sub>. The black group can be characterized by high top gas temperatures but low blast flow and blast temperatures.

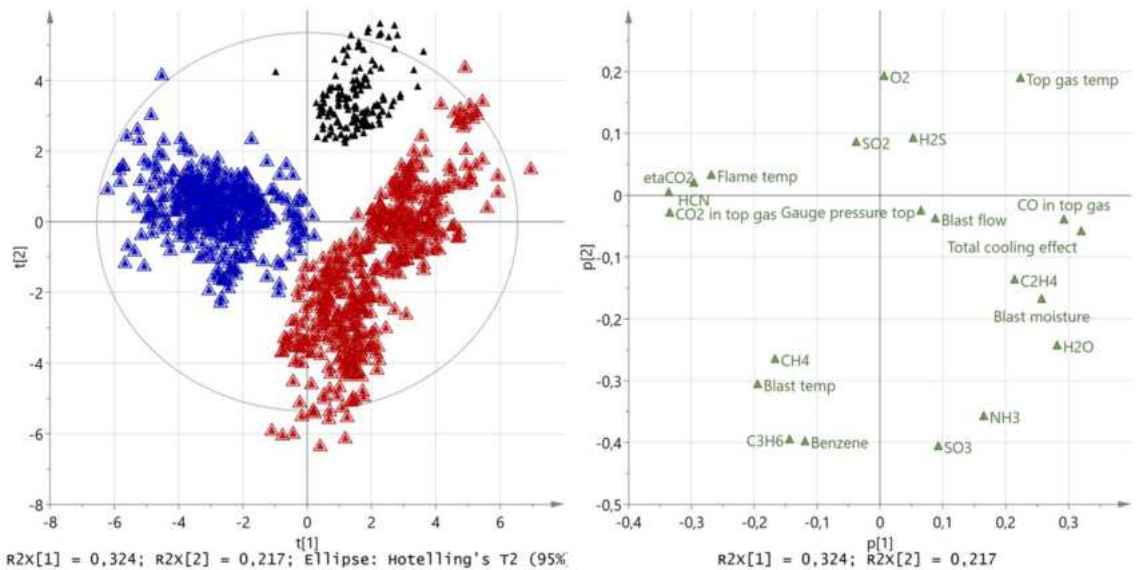


**Figure 81** (Left) Score plot over the PCA model MSP. (Right) Loading plot for the same PCA model.

The observations within the different groups are corresponding to different time periods of the campaign, the black group is from the first part, the red group from the middle part and blue group in the latter part.

An OPLS model with Y=NH<sub>3</sub> and HCN for the **MSP** data set resulted in a R<sup>2</sup>Y of 86% and a Q<sup>2</sup>Y of 86%. The VIP plot in **Figure 82** shows that H<sub>2</sub>O is the most important variable overall for the OPLS model followed by total cooling effects, SO<sub>3</sub> in top gas, CO<sub>2</sub> in top gas and eta CO<sub>2</sub>.

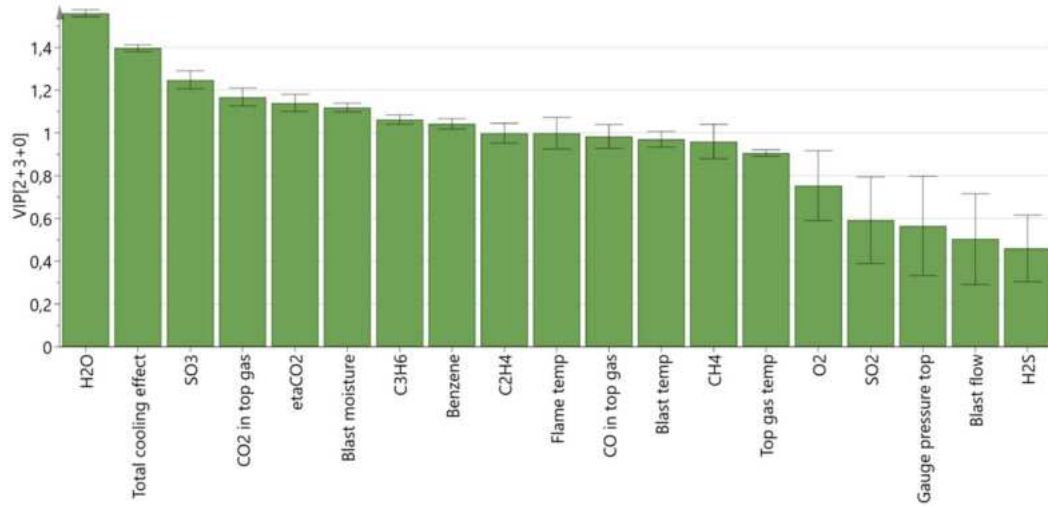


**Figure 82** VIP plot for the OPLS model where Y=HCN, NH<sub>3</sub>.

The coefficient plot shows how the variables affect one or more chosen variable Y, in this case HCN/NH<sub>3</sub>. Variables that have error bars that include zero are not statistically significant for the model. As seen in **Figure 83**, H<sub>2</sub>O is the variable that affects NH<sub>3</sub> the most and it is positively correlated to NH<sub>3</sub>. Other significant parameters for the formation of NH<sub>3</sub> are blast temperature, total cooling effects and SO<sub>3</sub>. The main similarities to the EBF are the negative correlation of NH<sub>3</sub> to eta CO<sub>2</sub> and the positive correlation to H<sub>2</sub>O in top gas. The positive correlation to total cooling losses in this case can be compared to the positive correlation between NH<sub>3</sub> and cooling losses in tuyeres for the EBF case.

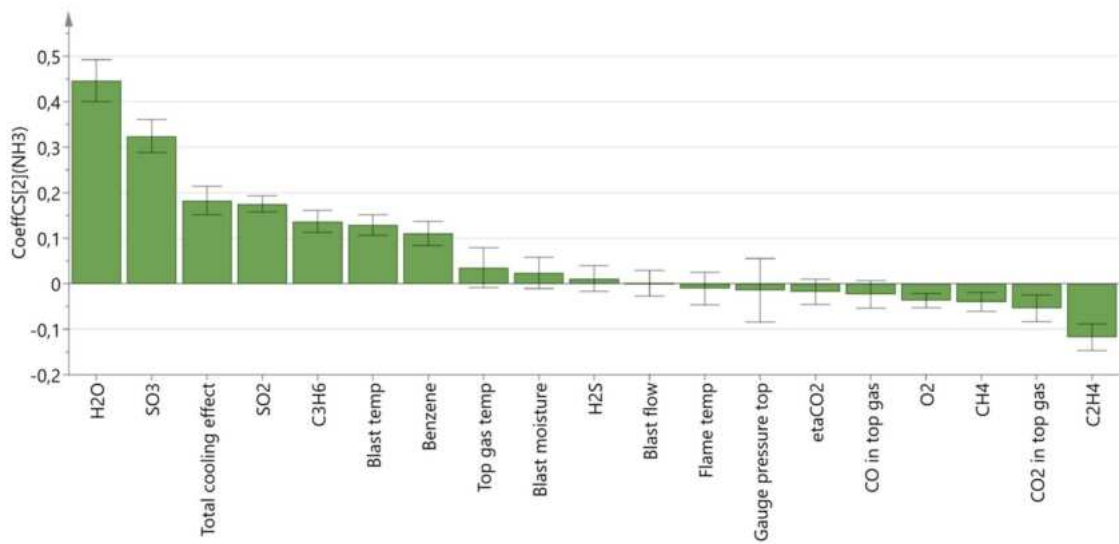


**Figure 83** Coefficient plot for the OPLS model where  $\text{Y}=\text{HCN}, \text{NH}_3$  showing the influence (+/-) of variables on  $\text{NH}_3$ .

The coefficient plot showing the influence of variables on HCN in **Figure 84** below shows that HCN is instead negatively correlated to  $\text{H}_2\text{O}$  and total cooling effects. Similar to  $\text{NH}_3$  is that  $\text{H}_2\text{O}$  is the variable with strongest impact on HCN and that both are shown to be positively correlated to top gas temperature and negative correlation to eta CO.

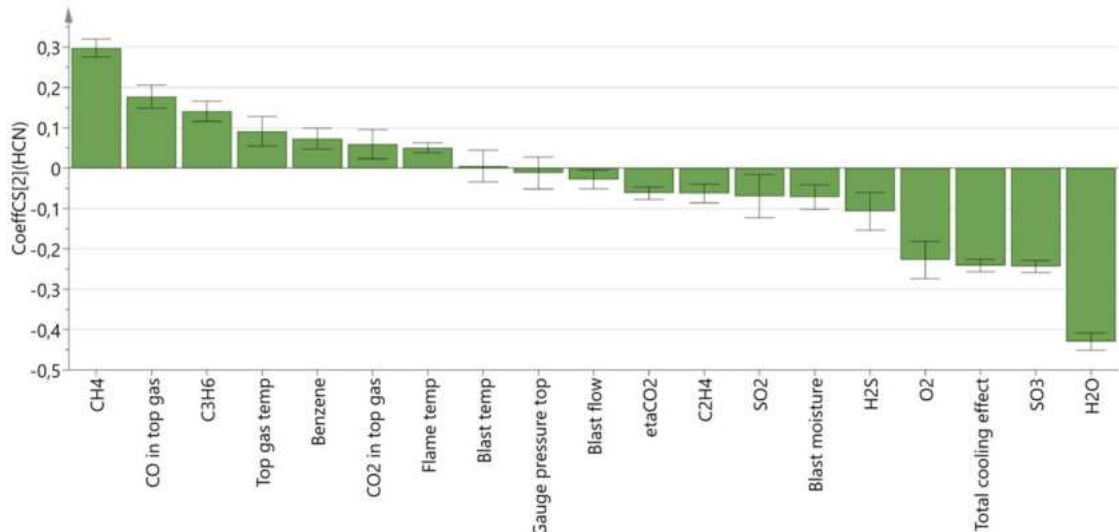


**Figure 84** Coefficient plot for the OPLS model where  $\text{Y}=\text{HCN}, \text{NH}_3$  showing the influence (+/-) of variables on HCN.

An OPLS model was created from MS and process data which included the spectroscopic raceway measurements for alkali. The dataset was averaged to every ten minute to correlate all data points to the same observation time and to remove some of the noise present in the data. The created model with  $\text{Y}=\text{alkali}$  in raceway had a weak explained variation,  $R^2\text{Y}$ , of 29% and also a weak predicted variation,  $Q^2\text{Y}$ , of 27%. The VIP plot in **Figure 85** shows the importance for each variable used in the model which highlights Top gas temperature as being the most important variable for the model as a whole followed by  $\text{C}_3\text{H}_6$  and Benzene. HCN and eta  $\text{CO}_2$  have also impact on alkalis in raceway according to this while  $\text{NH}_3$  have less impact.

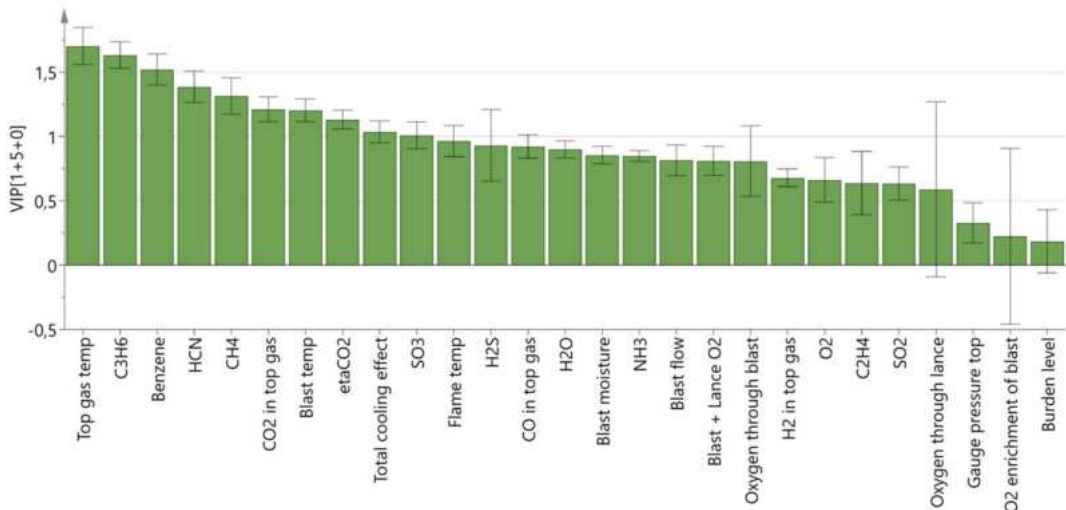


**Figure 85** VIP plot for the OPLS model with Y=Alkali raceway.

The coefficient plot in **Figure 86** below shows that HCN and C<sub>3</sub>H<sub>6</sub> was correlated positively to Y "alkali raceway" while top gas temperature and blast temperature was negatively correlated to it. Furthermore, the relative intensity of alkali emissions in raceway seem to be favored by high cooling losses and high CO<sub>2</sub> in top gas, which could be linked to high heat level and high gas efficiencies.

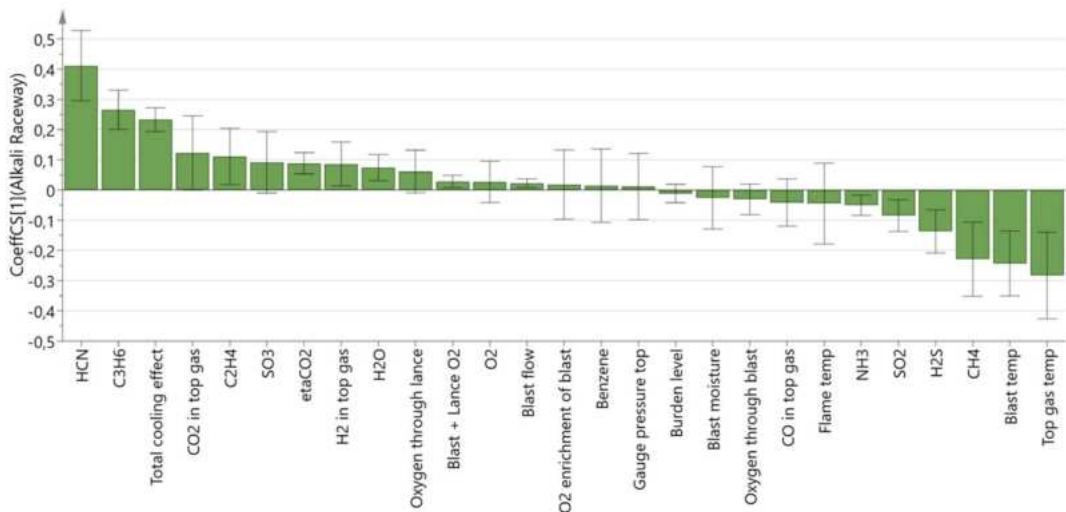


**Figure 86** Coefficient plot for the OPLS model with Y=alkali raceway.

### 2.3.1.2.3 Laboratory trials for verification of measured alkali emissions in raceway by the optical fibre (SWERIM)

To further evaluate the alkali emissions in raceway at BF No.4 and the LKAB EBF, measurements on light guided by an optical fibre to the spectrometer from the inside of a laboratory tube furnace have been conducted for study of alkali adsorption. The tube furnace, principle in **Figure 87**, has a temperature range from room temperature to 1600 °C. The temperature ramping rate was set to 2 K per minute to avoid cracking of the inner tube surrounding the crucible. 7 g of Potassium silicate (SiO<sub>2</sub>:K<sub>2</sub>O 2.5:1 wt%) was mixed with 2 g of activated charcoal (particle size  $\approx$  100  $\mu$ m) in a graphite crucible and heated from room temperature up to 1600°C. The same trial was performed twice; the first trial to monitor the weight loss relative time and temperature for the sample and the second with the spectrometer. Spectroscopic readings were compared with recorded weight

loss for the corresponding temperature, to relate the relative intensity of potassium radiation at different temperatures correlated to weight loss of the chemical sample. With the used spectrometer, light in the region from 350 to 1040 nm can be recorded, including the visible region. Evaluation of potassium content in the furnace atmosphere was made by calculating the quote between the potassium absorption line and the heat radiation in the same wavelength interval. To be noted, absorption was studied here while the measurements at EBF and the industrial furnace are looking at alkali emissions. The heat radiation under the potassium line is calculated out from a curve fit to the heat radiation curve not affected by emission from specific components in the sample and gas phase. In order to correlate the two different trials in the tube furnace the time scale was calculated as a relative time as percentage from the start (0%) to the end (100%) of the experimental time.

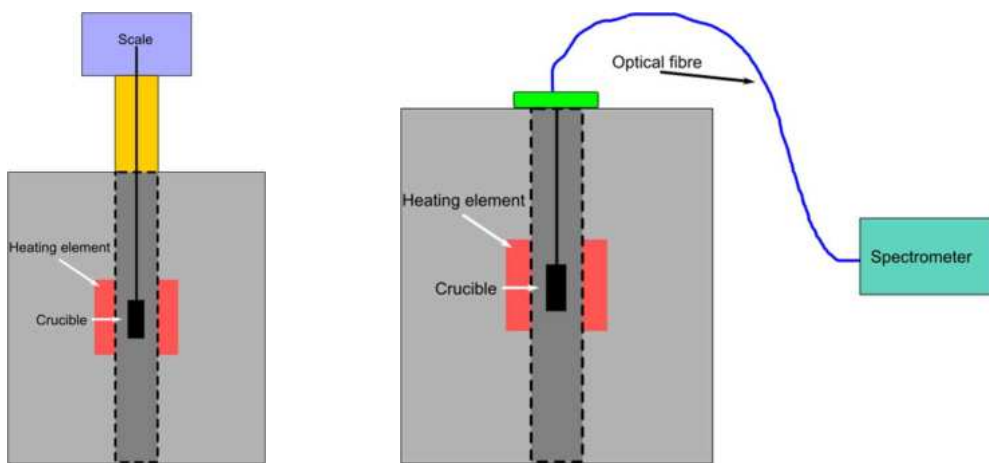


**Figure 87** Principle of the tub furnace prepared with scale (left) and spectroscopic (right) measurements. The sample was placed in a crucible and heated.

Some of the recorded spectra are plotted at different experimental times and increasing temperatures in **Figure 88** and **Figure 89**. As can be seen in **Figure 88** at experimental time 56.7% and a temperature of 1093°C, almost no light absorption from potassium was present but at 62.8% time, which is corresponding to the temperature of 1173°C, an absorption line occurs at wavelength 766 nm. The light absorption from Potassium is increased when the temperature in the tube furnace increase and the spectra from time 72.3 to 88.2% is shown in **Figure 89**. These spectra correspond to temperatures of 1297-1506°C. Also other absorption lines are present in the spectra, for instance from Sodium at 588 nm, but these absorptions lines were not evaluated here.

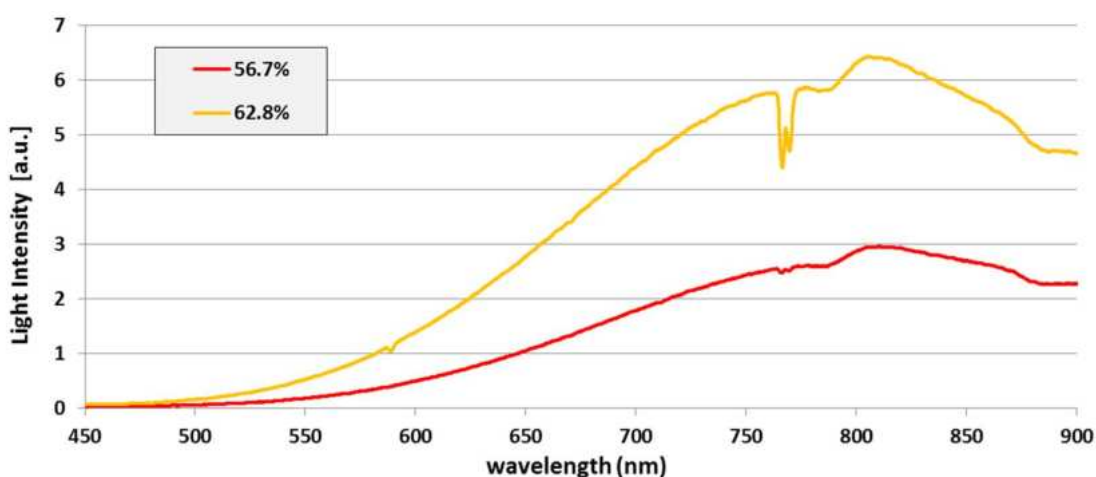


**Figure 88** Spectra recorded at experimental time 56.7 and 62.8%.

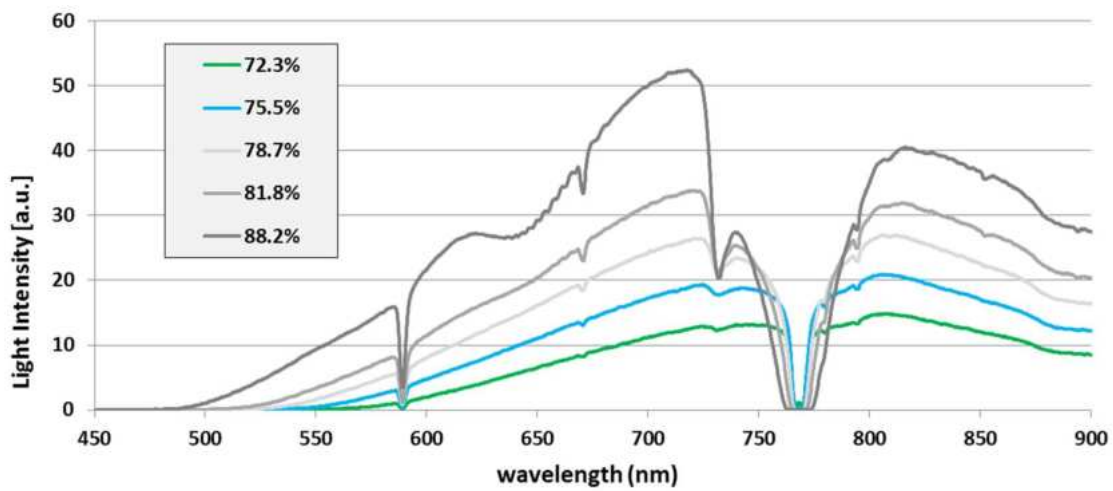


**Figure 89** Spectra recorded at experimental times 72.3 to 88.2%.

**Figure 90** shows the weight loss of the sample and the light intensity absorbed by Potassium as a function of temperature in the tube furnace. The light absorption is a negative value by definition and calculated through the light intensity at the absorption frequency for Potassium minus the heat radiation for the background divided by the intensity of the background. The sample inside of the tub furnace started to radiate light around 700°C and spectroscopic results are very noisy at experimental times lower than 30% and temperatures lower than 750°C why **Figure 90** is plotted in the scale started at 30%. The noisy evaluation is caused by too low light radiation at temperatures lower than 750°C. The integration time of the spectrometer had to be lowered during the experiment because of saturation of the detector why a region between 65 and 69% was excluded while the detector of the spectrometer was saturated. Above 90% of time the results were excluded, the resolution of the recorded spectra became unstable because of too short integration times of the spectrometer and high amount of condensate Potassium in the tube furnace.

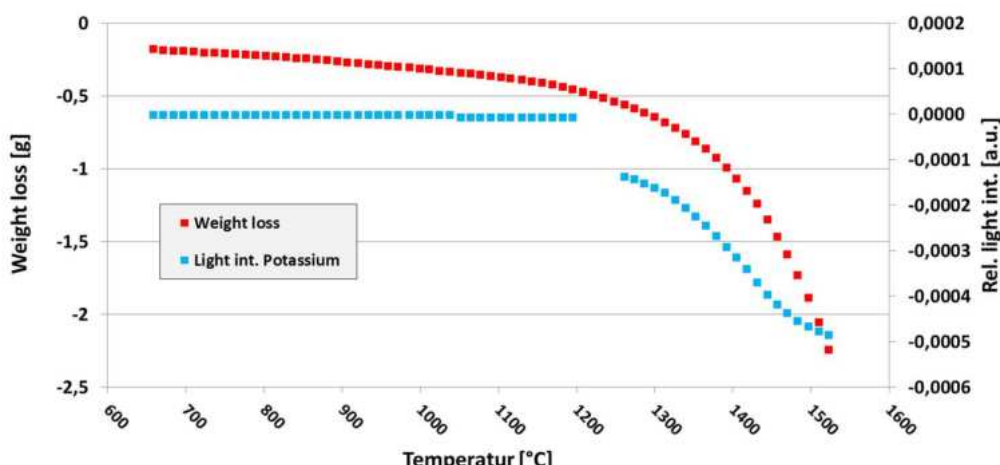


**Figure 90** The weight loss of the sample and light intensity absorbed by reduced and degassed Potassium in the tub furnace.

The derivative of the Potassium weight loss  $dm/dT$  (derivative of Potassium weight loss with respect to the temperature) is plotted as a function of the light absorption of Potassium in **Figure 91** when the temperature increased during the heating experiment. In the figure where the value of

the intensity is around -0.00015 and down to -0.00045, the graph shows a linear behavior, which indicates the amount of evaporated Potassium in the tube furnace increase linear with respect of the weight loss speed. At a point of intensity -0.00045 linearity ends and the graph gas another inclination to -0.00049.

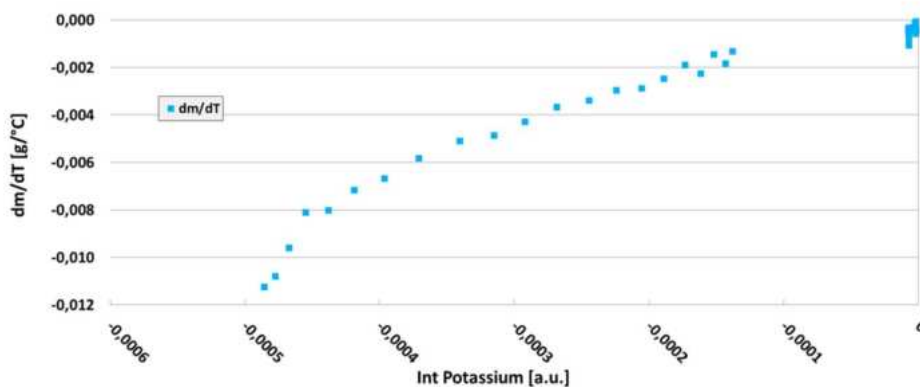


**Figure 91** The weight loss of Potassium as a function of the light intensity absorbed in the tub furnace.

The light absorption lines in the spectra from other elements than Potassium probably occurs from contaminations in the tube furnace. Ingoing chemicals in the experiments were pure. The linear behavior in **Figure 91** between -0.00045 and -0.00049 probably have another inclination because the gas phase in the furnace is saturated with Potassium and condensation of Potassium starts at colder part of the furnace, for instance the lid. The condensation of Potassium was indicated by a small explosion which occurred under the lid while the tub furnace was opened and the lid removed after finalized tube furnace trials.

#### 2.3.1.2.4 Concluding summary of measurements at EBF and BF No. 4 at SSAB in Oxelösund (Task 1.2)

The evaluation of MS-measurements and raceway measurements with optical fibre at LKABs experimental BF and BF No.4 at SSAB in Oxelösund are indicating that top gas composition with respect to  $\text{NH}_3$  and HCN as well as alkalis emissions in raceway can be related to alkalis in the process. Occasions of slips and release of scaffolds in conjunction with a change in alkali intensity in raceway could be identified during measurements periods at both sites. At the EBF, the alkali emission measurement responded faster than at the industrial furnace. The alkali balancing at BF No.4 showed on a negative accumulated load of alkali over time and the relative change of alkali intensity in raceway correlated well to the calculated load. Moreover, laboratory trials for calibrating the raceway measurements showed on a linear trend between the relative alkali intensity from adsorption and mass loss from sample. This can verify the alkali emission measurements in raceway at both EBF and BF No.4 and the coupling to the alkali load. However, the optical fiber was installed at only one tuyere at both sites and a potential implementation in future will require installations at several tuyeres for a better overview. This might also explain the weak statistical model obtained for prediction of alkali intensity by process variables and tap data.

For the top gas measurements with MS, the relationships found between process variables and concentrations of  $\text{NH}_3$  and cyanide differed somewhat between the experimental and industrial BF. First of all, no or very small levels of HCN was detected at the EBF whereas higher HCN levels than

$\text{NH}_3$  were measured at the industrial BF. Common for both sites was the negative correlation of  $\text{NH}_3$  to eta CO and positive correlation to moisture in top gas ( $\text{H}_2\text{O}$ ) and high cooling losses. Based on the EBF evaluation,  $\text{NH}_3$  concentrations followed the alkali content in top gas dust and sludge with a decreasing trend over time. In contrast, the alkali balance of the EBF campaign showed an increasing alkali circulating load from starting of the MS-measurements. Both cooling losses at tuyeres and skinflow temperatures at two levels were overall positively correlated to  $\text{NH}_3$  and the skinflow temperatures showed on a similar declining trend over the campaign. Thus, the  $\text{NH}_3$  concentrations in top gas can be formed from alkali reactions as it was observed to correlate to alkali in dust and sludge. However, the formation will also be affected by other factors such as gas profile, temperatures etc. One theory is that  $\text{NH}_3$  can give indications on when the output of alkali via the top is high but not the total circulating load. High outputs via the top could be favored by a warm shaft, at colder conditions the alkali cycle is instead shifted further down in the furnace and/or the extent of oxidation and condensation on walls bigger.

### 2.3.1.2.5 On-line BF top gas measurements at VASD

For the planned on-line BF top gas measurements at VASD, the BFI has compared available FTIR measurement systems from different suppliers and has finally selected and purchased a FTIR Spectrometer, which is capable for simultaneous and continuous analysis of 100 different gases and which is designed for industrial environment without the need for liquid  $\text{N}_2$  for detector cooling. The purchased FTIR is flexible in terms of data interface, so that it easily can be integrated in the VASD system environment.

The system integration of the FTIR spectrometer at VASD has been discussed between BFI and VASD. The resulting measurement scheme is presented in **Figure 92**.

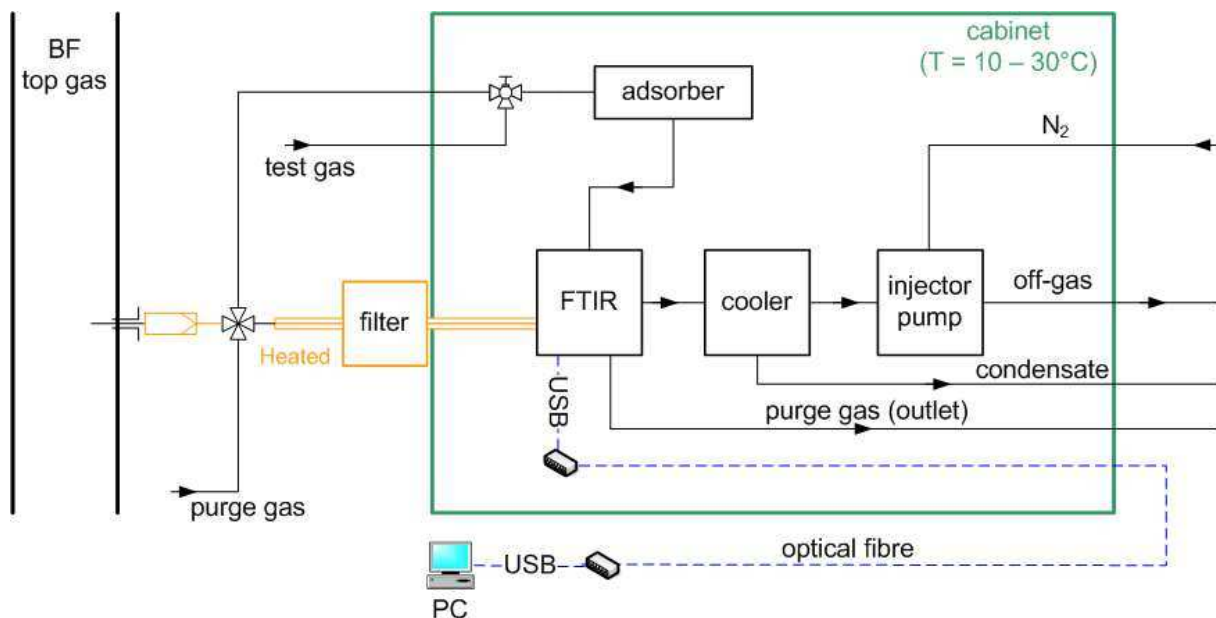


**Figure 92** BF top gas measurement scheme at VASD

The layout for a proper gas sampling system, which fulfils the requirements of the FTIR, has been intensely discussed. The FTIR needs a measuring gas temperature of around  $185^\circ\text{C}$  and an ambient temperature of  $10-40^\circ\text{C}$  itself. The former will be obtained by a heated pipe for the measuring gas, the latter by a temperature-controlled cabinet. In order to avoid the installation of a heated

pump between the FTIR and the filter, an injector pump has been attached after the FTIR. The amount of dust in the measuring gas has to be low, therefore the gas probe has a ceramic filter and an additional filter is installed before the FTIR as a back-up filter. In order to keep the filter in the probe clean it will be possible to purge it with nitrogen. The FTIR itself needs some purge gas, which will be dehumidified in an absorber upstream. Since the data interface of the FTIR is an USB-port, there is the need for an USB extender, which enables to transfer the data signal from USB to optical fibre and back to USB. The latter one is connected to a computer, which will process the measuring data.

In **Figure 93** the position of gas sampling is shown in a side view of BF1 at VASD. The gas probe has been installed on one of the existing flanges, which are on the top gas uptake-pipes. The gas sampling position is roughly ten meters above the burden height. The decision on this position is due to the accessibility and the fact that there should already be a homogenised gas composition.

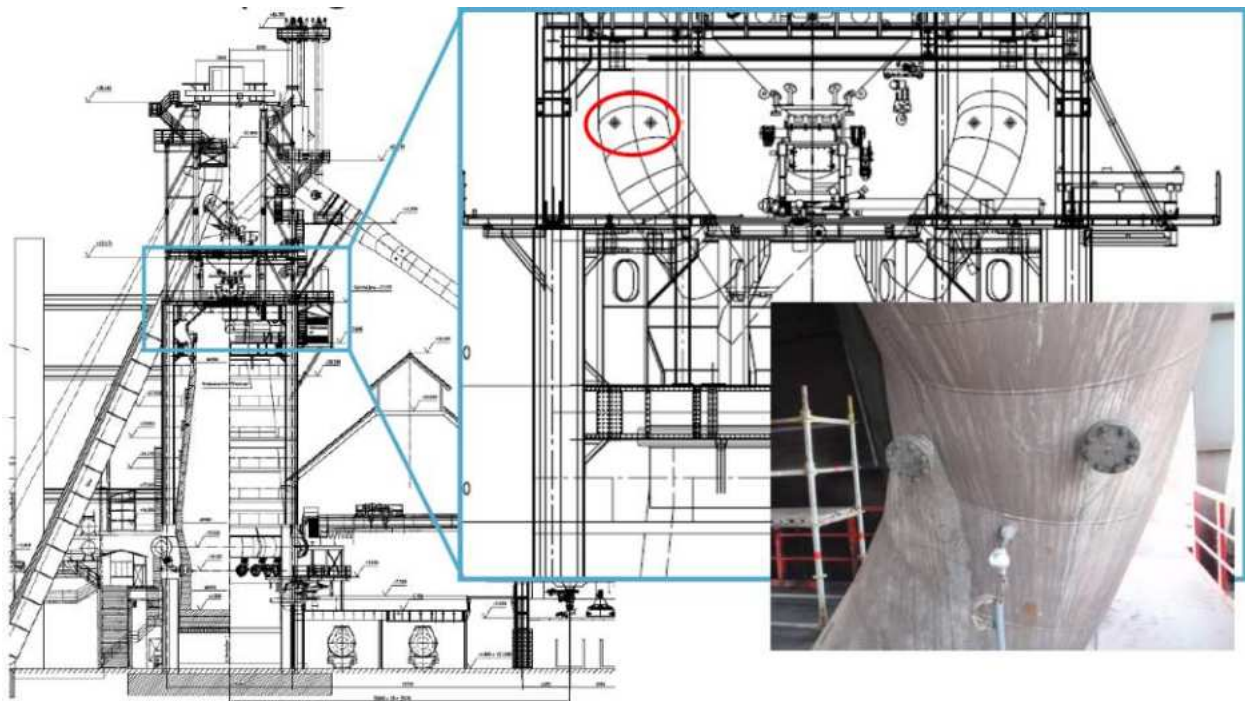


**Figure 93** Position of gas sampling at BF1 at VASD

The gas measurement system has been activated and the obtained results are shown in **Figure 94**. While the very first data points are representing the calibration of the measurement system, the period afterwards is showing stable measuring conditions. During this period no NH<sub>3</sub> is measured while the CO content is in a reasonable level. After a few hours the signals show increasing variability and they are not reasonable any more. The images in **Figure 95** are showing the change in the spectra from stable operation (left) to implausible condition (right).

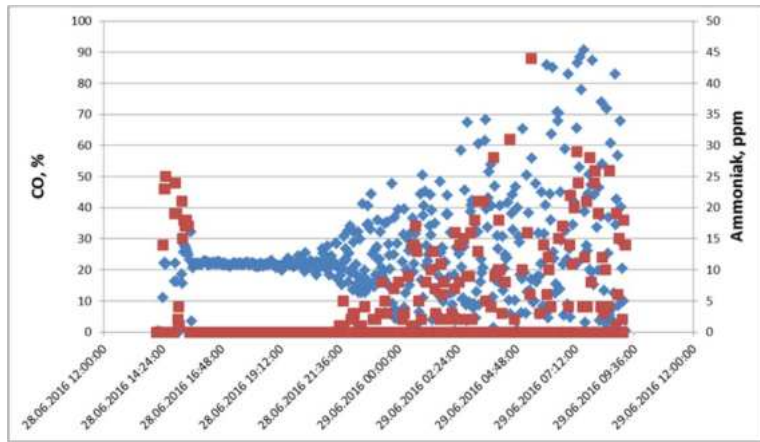


**Figure 94** Results during activation of the FTIR and after a couple of hours (blue: CO, red: NH<sub>3</sub>)

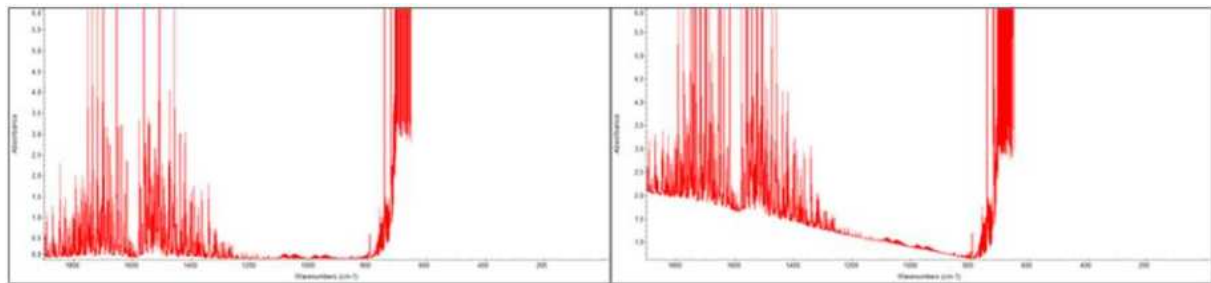


**Figure 95** FTIR spectra for stable conditions (left) and implausible conditions (right) of measurement

Due to these results the measurement system has been investigated in more detail. The mirrors of the gas cell have been disassembled and a grey, dark deposition on the surface has been detected (**Figure 96**). An EDX and Raman Analysis have been done and a composition of nickel and sulphur has been analysed. This composition has been mullerite (NiS), which has a melting point of around 800°C. At the same time the second filter has been investigated and has not shown any indications of contamination. So it has been assumed that this compound has not passed the filter, because otherwise it has to be gaseous, but the temperature level in the sampling system has been much too low. That means that the formation of this compound has happened after the second filter, but it has not been clear how NiS has been arising. Maybe several intermediate stages have been necessary. However, the source of nickel has been unknown. It has been coming from the furnace, the material of the sampling system or the gas cell itself, which is Ni-coated. In order to find the source for Ni the condensate of the gas has been collected and analysed. In a first step a bypass has been built in order to avoid gas flowing through the measurement system.



**Figure 96** Mirror of the gas cell with depositions

The condensate collected first of all has been analysed and elements, which has been found in the material of the sampling system, have been found too. At the same time this condensate has been very acid with a pH-value of 1.18. While analysing the condition of the sampling system, a deposition in a small unheated part between the heated pipe and the measurement system has been found (see **Figure 97**) and has been responsible for decreasing and finally missing gas flow. An EDX analysis of this material has shown that the main elements have been C, N, and Cl. Ni has not been found there, but the fact that chlorides are known to cause corrosion to stainless steel tubes (Cr-Ni-steel) may be an indication that the material of the sampling system could be the source for Ni. As a consequence, the isolation of the unheated parts has been improved in order to avoid a decrease in gas temperature.

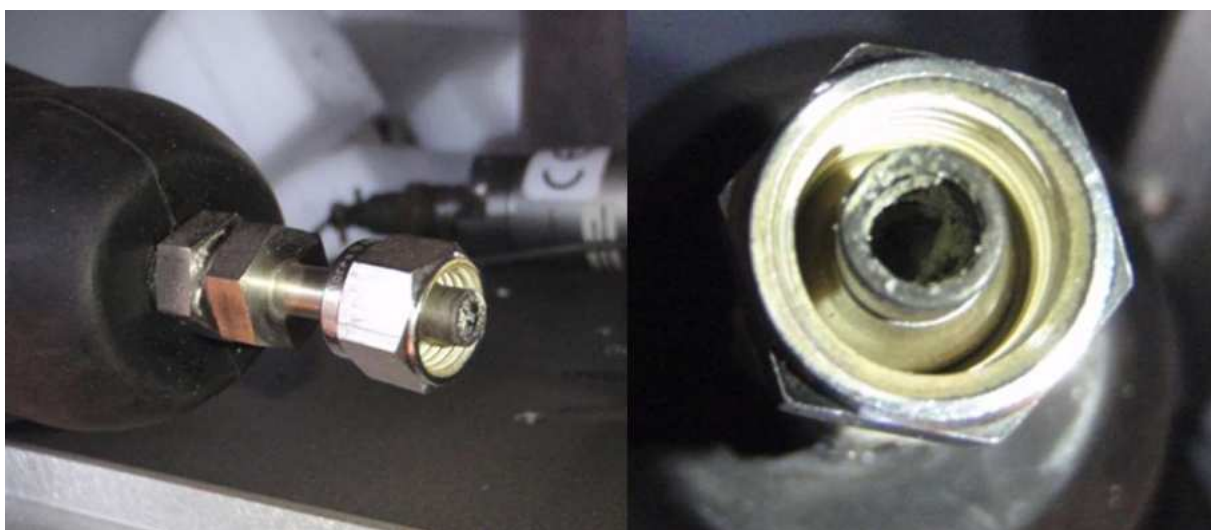


**Figure 97** Depositions in the sampling system

After improving the isolation of the gas sampling system in order to avoid gas cooling a restart of the FTIR has been done. Again, the period of reliable measurement has only been a few hours and the trial has been stopped without usable data. There has been the suspicion that  $\text{Ni}(\text{CO})_4$  may be the source for the Ni-deposition at the mirrors. Since this species is not stable at higher temperature, the part of the gas sampling system from the ceramic filter (gas sampling probe) to the back-up filter has been changed to a temperature of 240°C. The pipe from the back-up filter to the FTIR has been kept at a temperature of 185°C in order to fulfil its needs. However, the following restart has not brought any improvements. At the end the combination of the selected FTIR measurement technique, the installed gas sampling system and the gas itself has not allowed reliable measure-

ments and has not been working. It is assumed, that the degradation of the FTIR gas cell due to Ni deposition might be avoided by use of a redesigned Ni-free tubing of the gas sampling system.

The dysfunctional FTIR has been the reason why some alternatives for the FTIR have been investigated and have been installed. In order to measure NH<sub>3</sub> reliable and for an acceptable period laser spectroscopy (tunable diode laser spectroscopy – TDLS) has been tested in two configurations. Furthermore, mass spectroscopy has also been tested in order to measure the concentration of some additional species in the top gas.

Two configurations for laser spectroscopy have been tested – both are in-situ systems, one with a cross over system (see **Figure 98**) and one with a gas diffusion probe (see **Figure 99**).

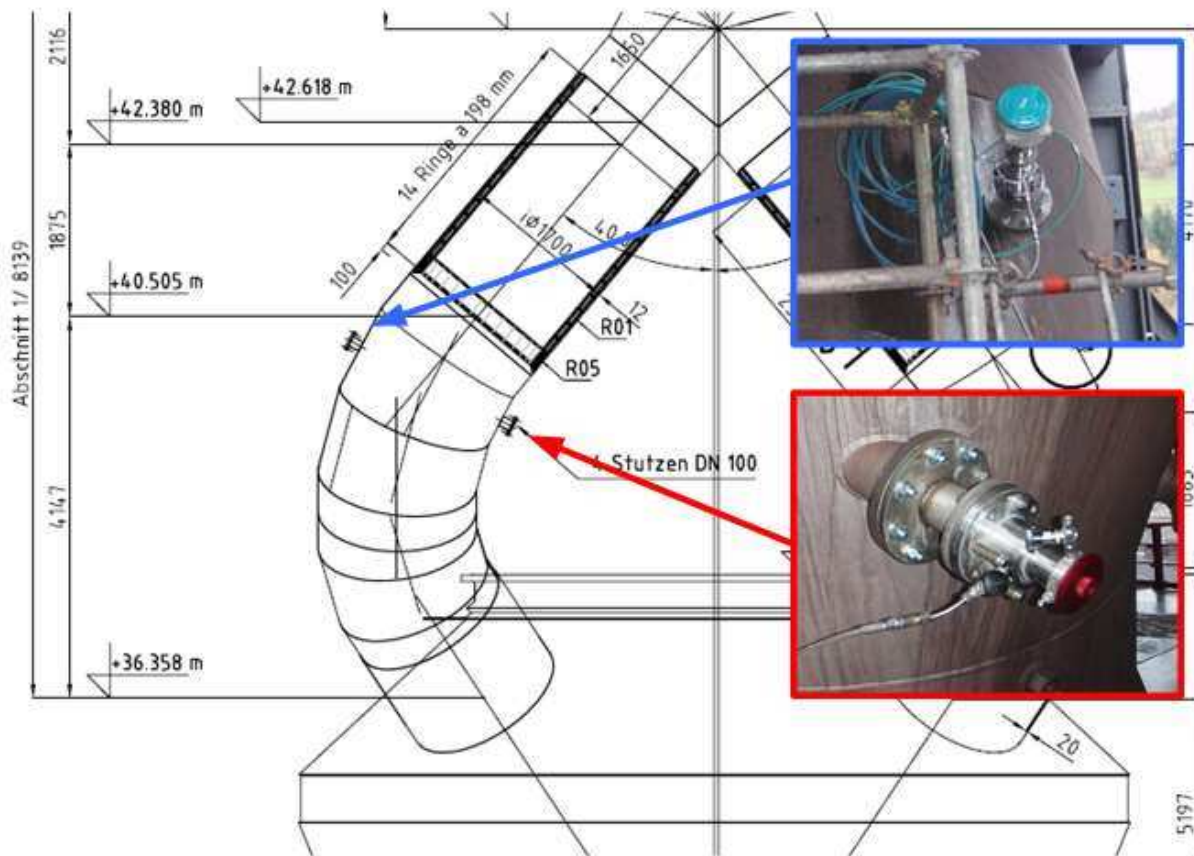


**Figure 98** Configuration of cross over TDLS (upper part: transmitter, lower part: receiver)

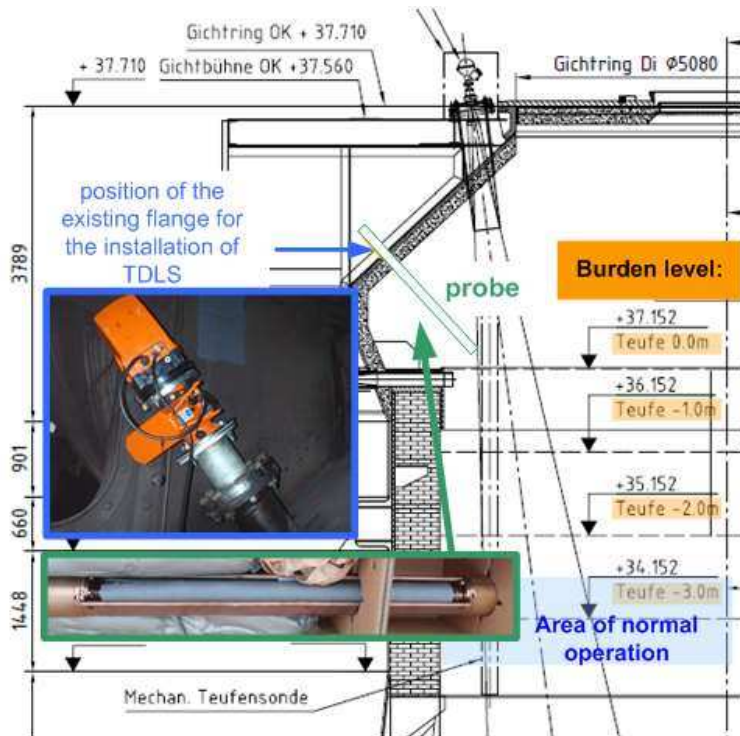


**Figure 99** configuration of the TDLS with the gas diffusion probe (analysing unit within the blue box, probe within the green box)

The big advantage of the TDLS is that it is an in-situ measuring system and therefore a gas sampling and preparation is not necessary. The existing top gas dust concentration doesn't disturb the quality of the measurement much, a compensation of temperature is necessary. Due to its high selectivity only one (or two) species in the gas can be analysed. The cross over system needs a pair of connectors which are directly opposite or else a measurement is not possible. As a consequence, only connectors at the upcoming pipes at the BF top have been accessible at VASD BFs which have been around 6 meter above the burden level. As shown the position of the connectors has not been horizontal but inclined – an installation of a new pair of connectors has not been possible without excessive effort and therefore has not been done. The results of NH<sub>3</sub> measurement with the cross over system is shown in **Figure 100**. At the beginning there has been a very low NH<sub>3</sub> content because BF has stopped and purged with nitrogen. While going back on hot blast the NH<sub>3</sub> has increased up to around 74 ppm. NH<sub>3</sub> has decreased afterwards to around 20 ppm. The quality of measurement has got worse which has been indicated by nearly constant levels of NH<sub>3</sub> at the end.

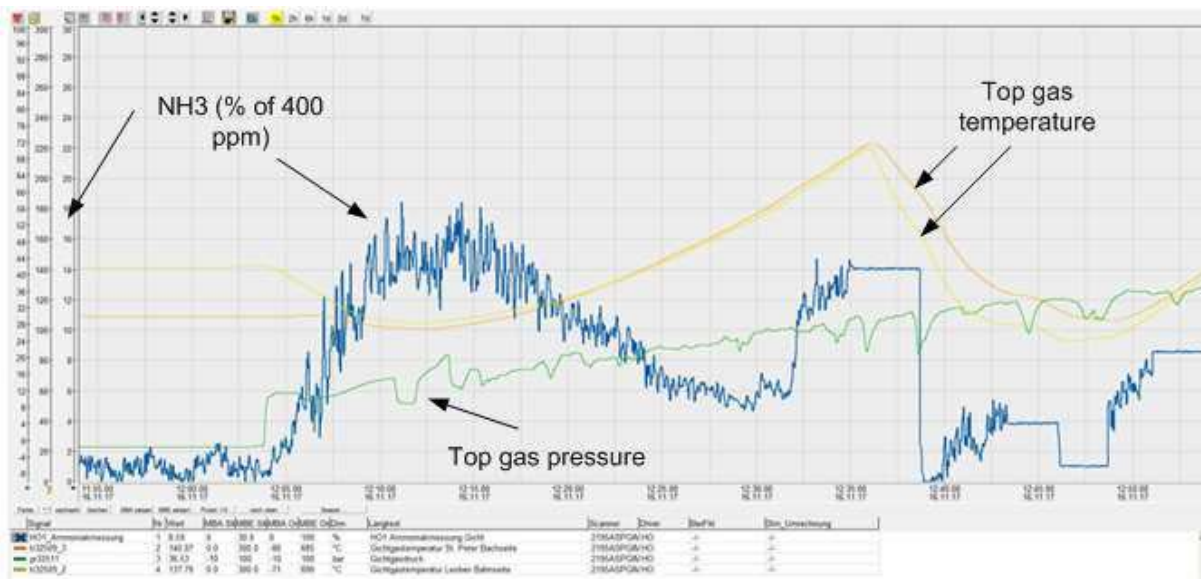


**Figure 100** Cross over results during the start-up (NH<sub>3</sub> is shown in % of 400 ppm)

As the quality of measurement has been very low a closer look has been done at the equipment. After opening the covers the reason for this has got clear: The area in front of the receiver has been blocked due to an accumulation of dust, see the left side of **Figure 101**. Although the optic window and the channel have been purged with nitrogen its amount has been obviously too low in order to keep this channel free of coarse dust particles. To make matters worse, condensation has happened and filled the lower part and purging has caused the formation of foam in front of the optic window. Although the measuring results have been reliable this system has been demounted because of the constraints.



**Figure 101** Area in front of the receiver filled with dust particles (left) and condensation (right)

The gas diffusion probe has been installed at the BF top next, although the probe has not been in an optimal position, but the existing connectors and flanges have not allowed any other positions. For best results gas has to flow rectangular to the gas diffusion probe. Nevertheless, it should also be possible to get reliable conditions in our case. The measuring unit has been in operation for more than two months and has been demounted before the BF blow down in July. In **Figure 102** the daily average of NH<sub>3</sub> in the top gas is shown. The NH<sub>3</sub> content is fluctuating very much, a deeper analysis of the results is shown in Task 3.1.

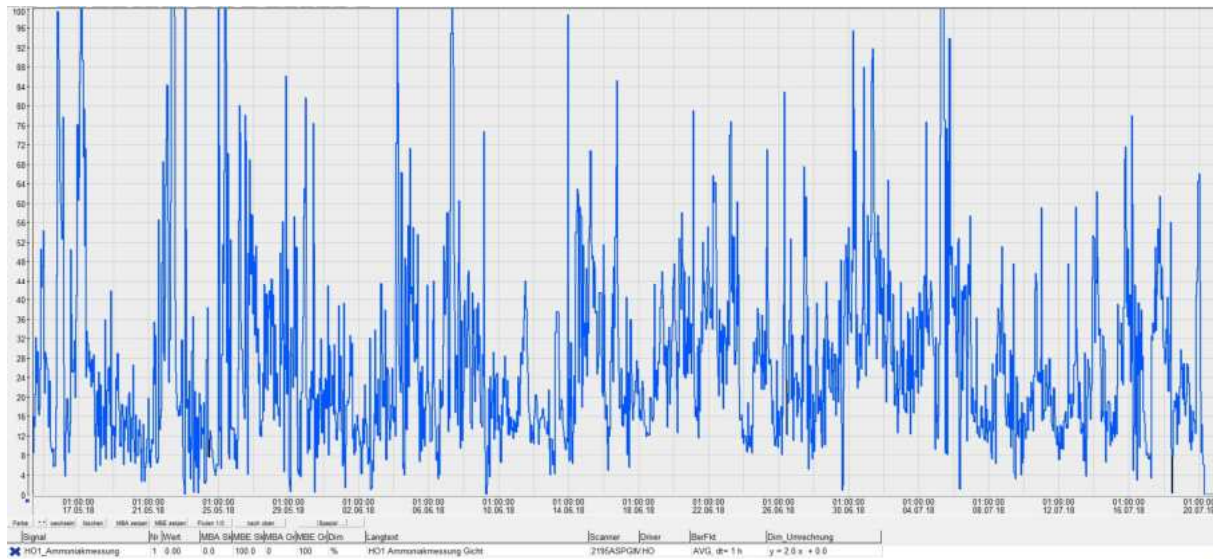


**Figure 102** Daily average of NH<sub>3</sub> in top gas in ppm from 14<sup>th</sup> of May till 20<sup>th</sup> of July

Although TDLS with the gas diffusion probe has worked very stable, the position has not been very good. Due to the required diameter for the installation no alternative position has been possible. A further disadvantage of the TDLS is the limitation in measurable species. During the progress of the ALCIRC project some partners have assumed a stronger indication by HCN in order to analyse the Alkali circulation.

Because of these restrictions a measuring campaign with a mass spectroscopy has been started. Therefore, the existing sampling system, which had already been used for the FTIR, has been utilized. The trial has been planned for four weeks but only the first two weeks brought good results. Exemplary the O<sub>2</sub> content in the top gas is shown in **Figure 103**. An unexpected high O<sub>2</sub> content in the last 10 days is indicating that there has something been wrong with the mass spectroscopy. Due to the formation of depositions in some capillary tubes a valve has to be opened and ambient air has been sucked into the MS. Before this has happened, measurements have not been possible beginning at the 29<sup>th</sup> of May. The reason has been a failure of the vacuum pump and it has been necessary to exchange this pump. Therefore, measurements have not been able for a couple of days.

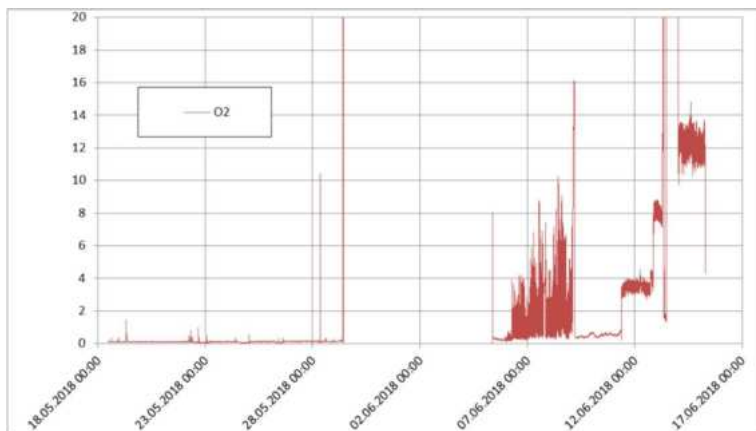


**Figure 103** O<sub>2</sub> (%) content in the top gas measured with the MS

In **Figure 104** HCN and NH<sub>3</sub> measured with the MS are shown. HCN is regularly lower than 8 ppm. During this period the BF has been stopped for several times, that can be identified by a significant decrease of HCN. During normal BF operation virtually no NH<sub>3</sub> is detected. When BF has stopped there is a significant increase of NH<sub>3</sub> in the measured gas. It bears mentioning that the results of

the TDLS show a similar behaviour - see **Figure 105**. Although the absolute value differs both are showing an increase in NH<sub>3</sub> during a BF stop and at the same time the humidity of the gas changes similarly. At first glance the results are disturbing, but a deeper look clarifies this behaviour: during BF stop the top of the BF is flooded with steam and this steam is made of water which has been chemical treated- i.e. ammonium hydroxide for reasons of corrosion control. So, during steam injection NH<sub>3</sub> is released and is measured by both measurement systems. When the top of the furnace is flooded with nitrogen instead of steam NH<sub>3</sub> doesn't increase, this can be seen at the end of the NH<sub>3</sub> trend in **Figure 105**.

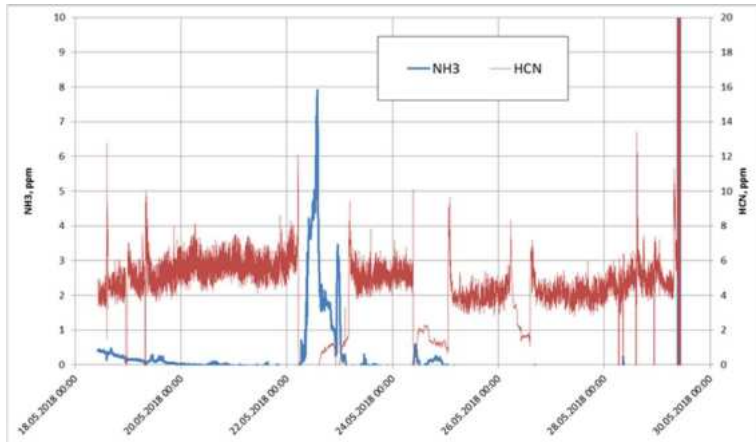


**Figure 104** Reliable measuring data of HCN and NH<sub>3</sub> in top gas during MS campaign

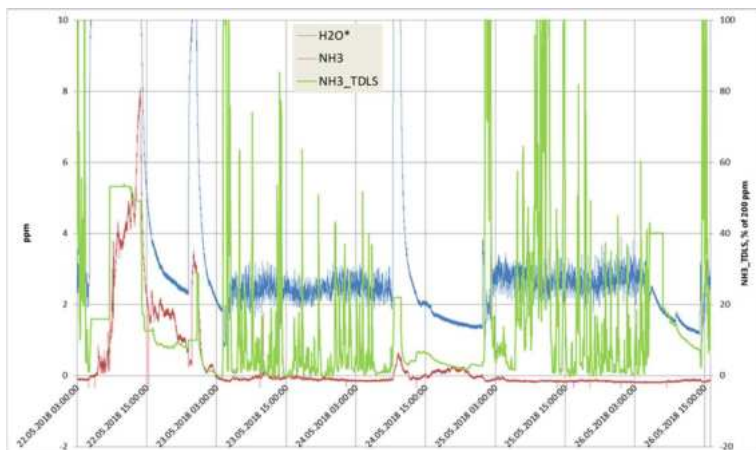


**Figure 105** Comparison of NH<sub>3</sub> measured with MS (red line) and TDLS (green line)

Comparing the different measuring systems, it is obvious that TDLS as an in-situ method is preferable over the extractive methods (FTIR, MS). The latter ones have not measured any significant NH<sub>3</sub> contents during BF operation, but at least MS has measured NH<sub>3</sub> during BF stop and steam injection. Although NH<sub>3</sub> is present in the top gas, it has not been detected with the extractive methods. The reason for this is not clear, probably there have been some chemical reactions going on with

NH<sub>3</sub> in the gas sampling system and its concentration has been very, very low before the gas could reach the measuring unit at the end.

### 2.3.1.2.6 BF top gas measurements at BF1 with a FTIR gas analyser at Dunafer

For development of the new online measurements aiming in quantification of the BF alkali cycle, Dunafer has carried out BF top gas measurements at BF1 with a FTIR gas analyser. The top gas sampling probe is located after dust catcher and cyclone. The sample gas preparation system is designed to avoid any water condensation e. g. by heated gas lines/pipes and rotameters placed in a heated box. A portable gas sampling unit in connection with a multicomponent FTIR gas analyser was used.

The main analysed components are H<sub>2</sub>O, HCN, NH<sub>3</sub> and NO<sub>2</sub>, since they are assumed to be connected with alkali components in the BF. The measured data are evaluated in form of frequency distribution curves and checked for statistical correlations. Trends and distributions of measurement data provided by FTIR are presented by the following figures for H<sub>2</sub>O (**Figure 106**), HCN (**Figure 107**), NH<sub>3</sub> (**Figure 108**) and NO<sub>2</sub> (**Figure 109**).

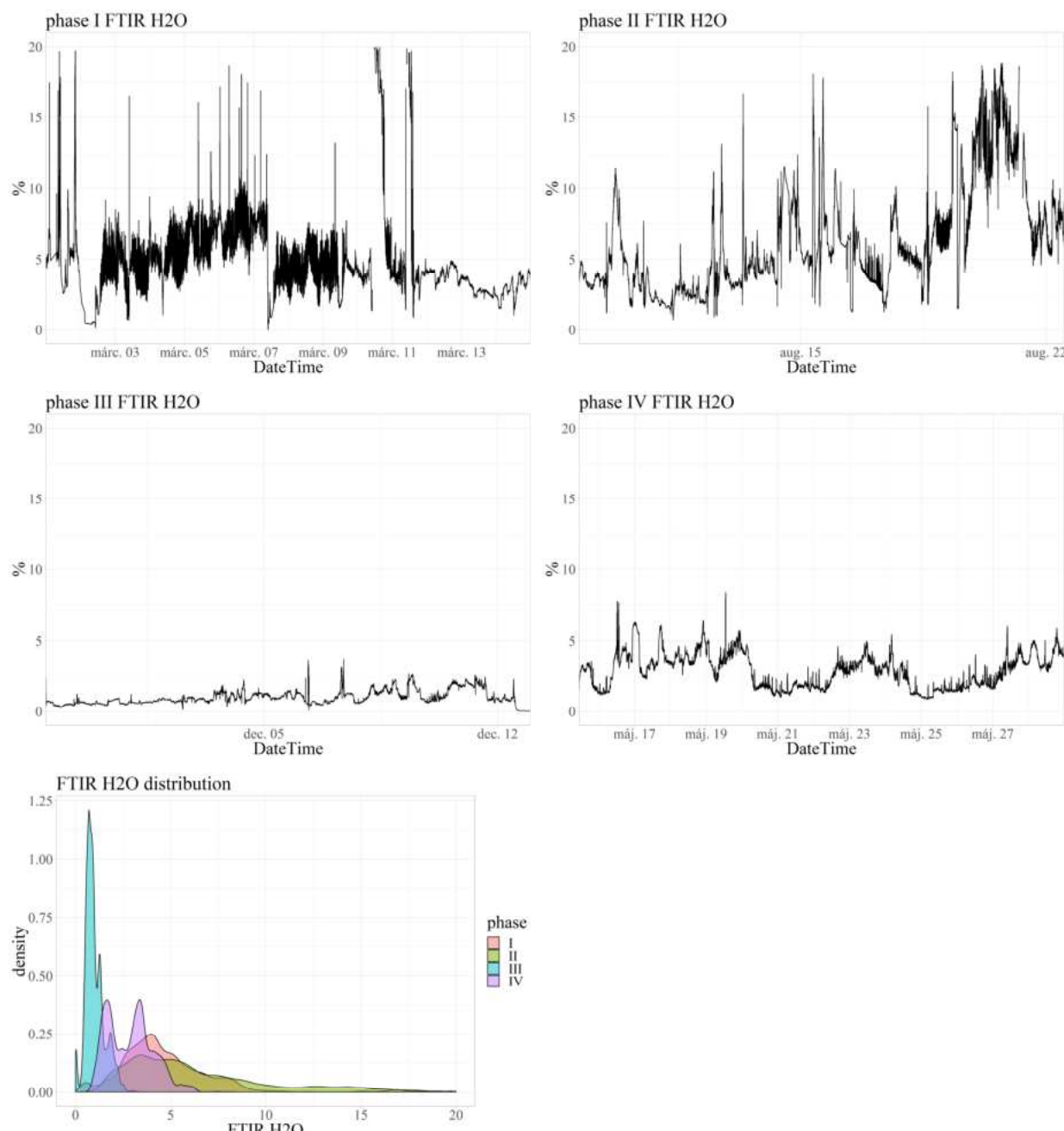


**Figure 106** Measured H<sub>2</sub>O percentage and frequency distribution (pink: phase I, green: phase II, blue: phase III, purple: phase IV)

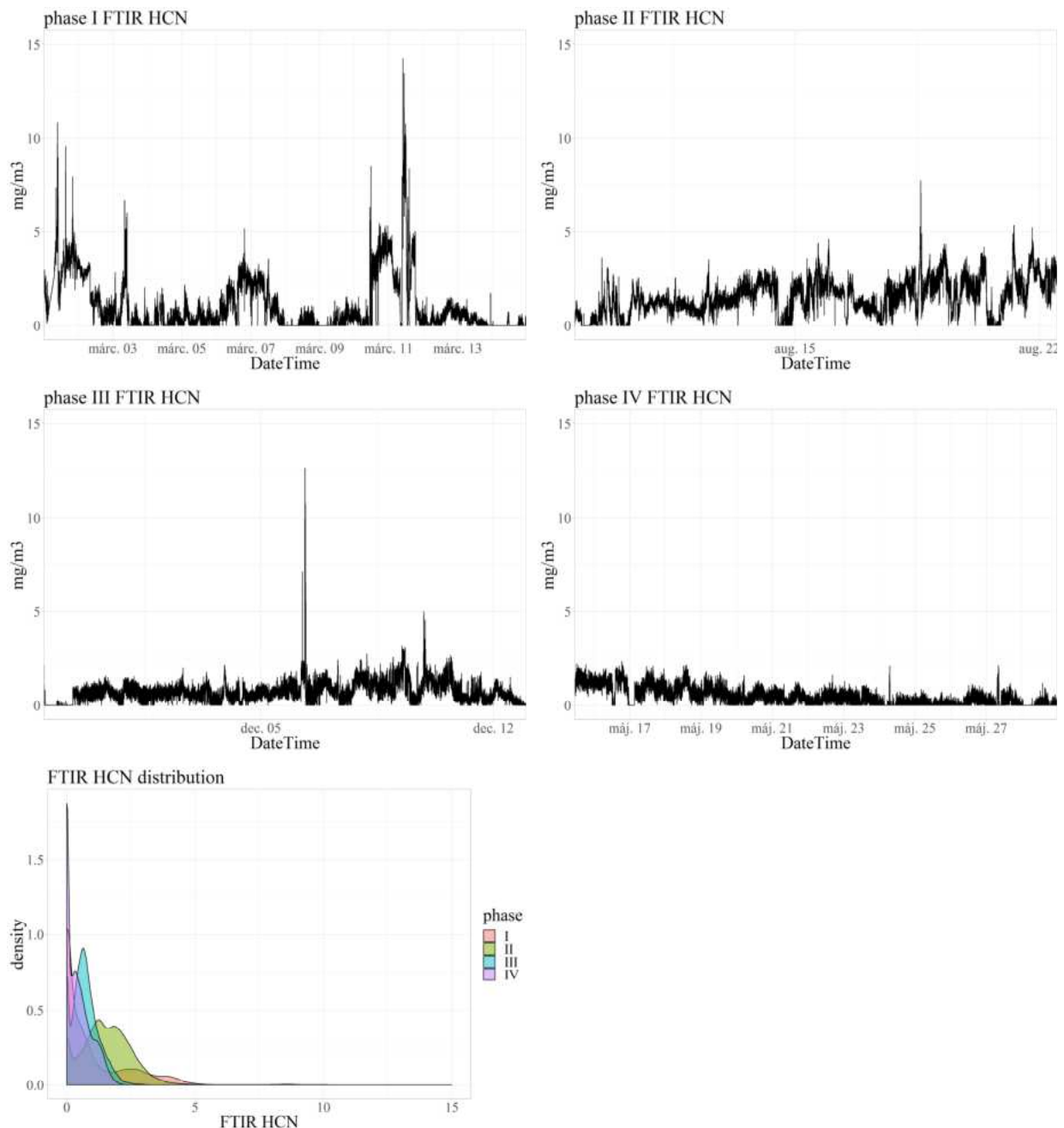


**Figure 107** Measured HCN percentage and frequency distribution (pink: phase I, green: phase II, blue: phase III, purple: phase IV)

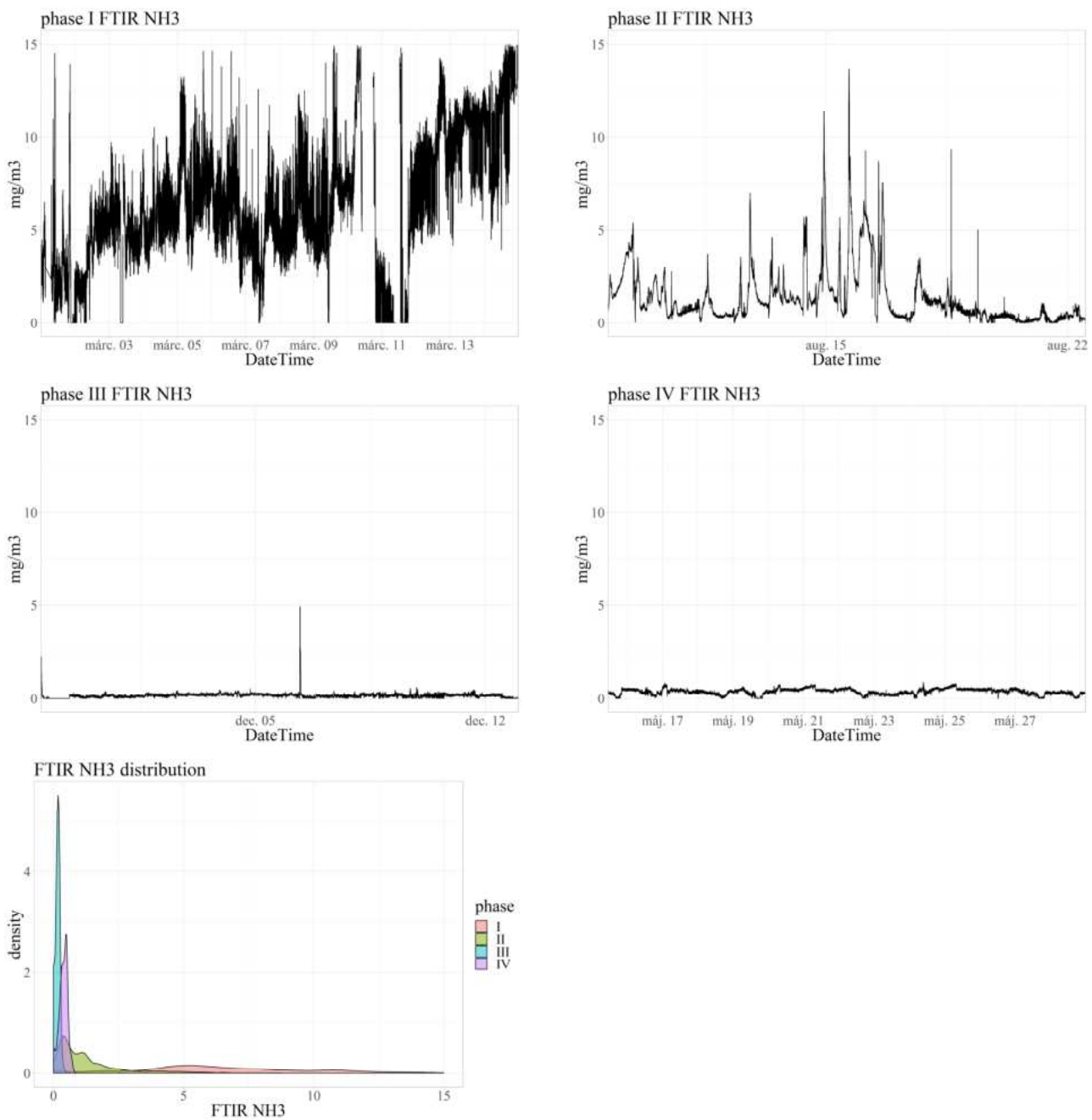


**Figure 108** Measured NH<sub>3</sub> percentage and frequency distribution (pink: phase I, green: phase II, blue: phase III, purple: phase IV)

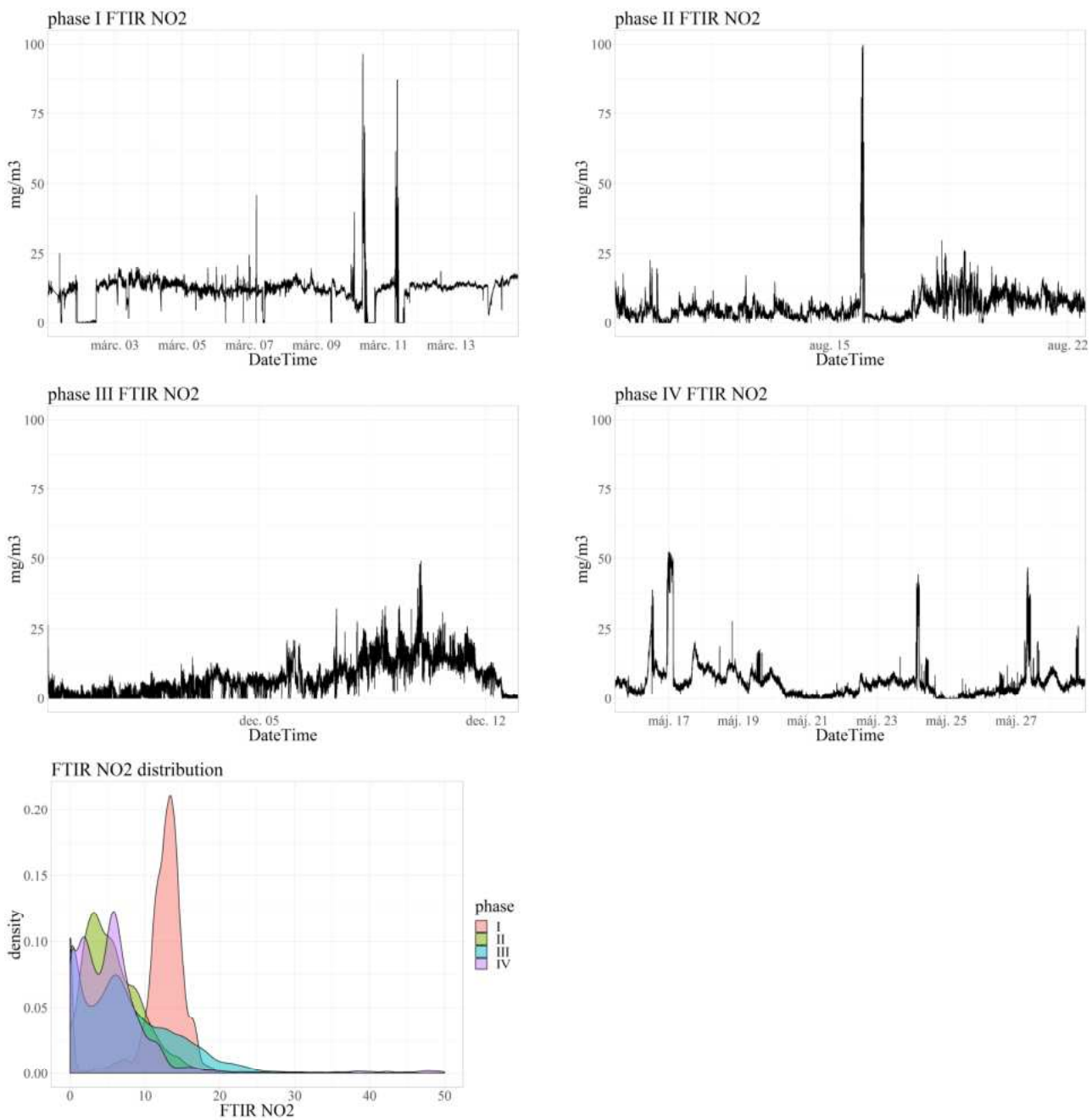


**Figure 109** Measured NO<sub>2</sub> percentage and frequency distribution (pink: phase I, green: phase II, blue: phase III, purple: phase IV)

With a view to search correlations for the FTIR top gas measurements with operational data and single blowing parameters, extensive statistical tests were performed, after having removed the values outside particular data lines (**Figure 110**).

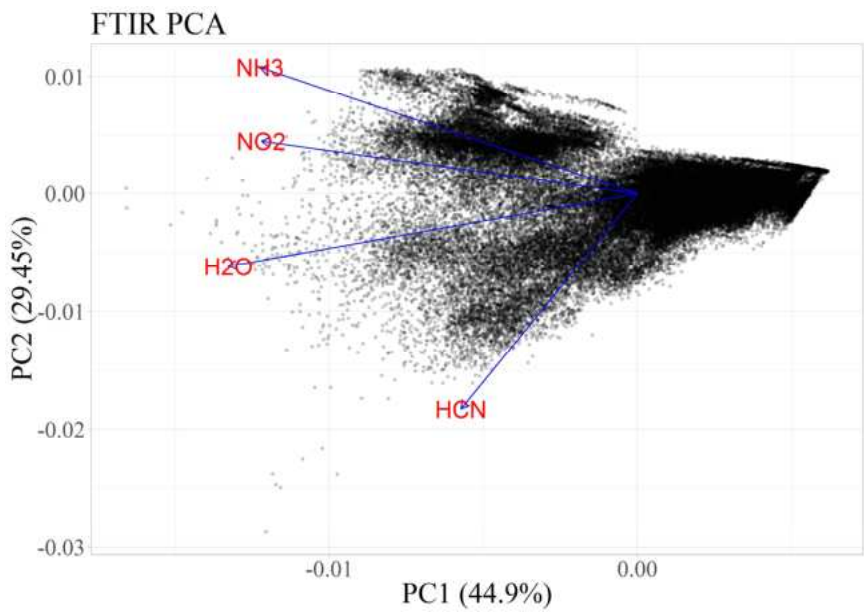


Figure 110 a)

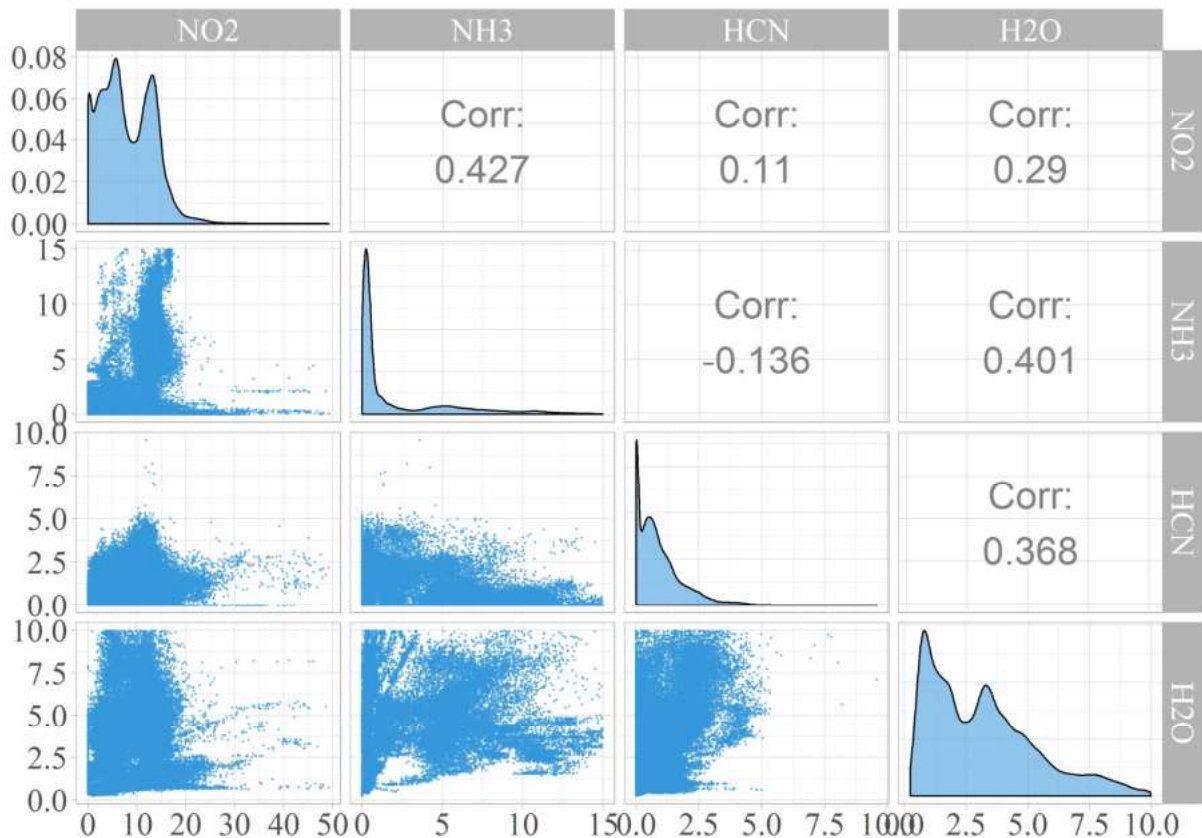
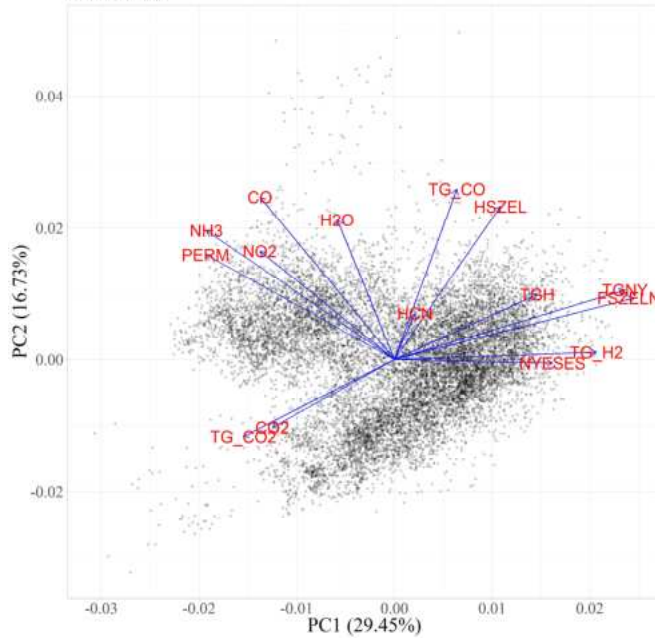
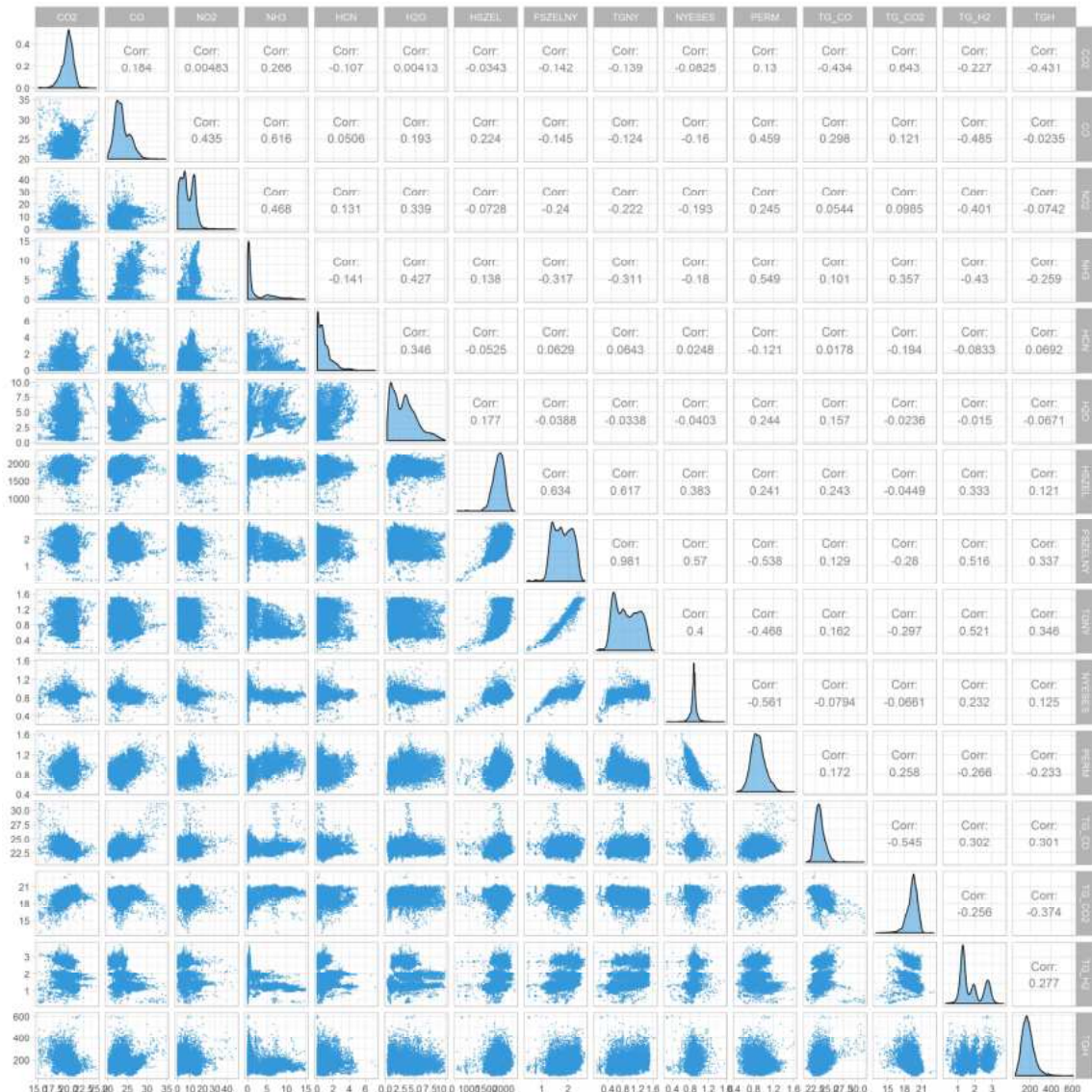


Figure 110 b)

### FULL PCA



**Figure 110 c)**



**Figure 110 d)**

**Figure 110 a)-d)** Examples of statistical tests performed to search correlations for the FTIR top gas measurements

The following statements can be made:

- NH<sub>3</sub> measurement was very sensitive to measuring conditions, with special regard to the wetting, sludging of gas filter of the sampler
- Goodness of top gas moisture content specification forecast the possibility of assessing other analysed components
- We found no significant correlation between FTIR analysis values
- CO<sub>2</sub> as well as CO values analysed by FTIR and determined by industrial top gas analyser correlated with surprisingly low value, which may even be accepted in the case of CO knowing that usual measuring range of FTIR is less than 1%
- CO<sub>2</sub> value of FTIR showed better correlation with top gas temperature than CO<sub>2</sub> value of industrial top gas analysis
- **As regards HCN, NH<sub>3</sub> values no particularly striking correlation can be found**, joint change in H<sub>2</sub>-content of top gas, hot blast pressure and HCN might be interesting
- Very clear correlation was detected between hot blast pressure and top gas pressure, which is not surprising, knowing that in accordance with the present blast furnace operation philosophy the pressure drop value is kept on almost constant level (in contrast to the common control to hot blast volume with given top gas pressure).
- No significant correlation between slag, hot metal and FTIR analysis values was found

### **2.3.1.3 Task 1.3 Alkali impact on BF burden materials**

#### **2.3.1.3.1** Definition of standard coke properties at SSAB in Oxelösund (SSAB)

SSAB Oxelösund production coke is of high quality and the properties of coke correspond to CSR (68.8-70.0%) and CRI (19.8-21.0%) as well as good mechanical strength with Micum values of M<sub>40</sub> 85.1-87.4% and M<sub>10</sub> 6.0-6.8%. The alkali in the coke is around 0.22 % (1.9 wt. % in ash), K<sub>2</sub>O 0.15 wt. % (1.3 wt. % in ash), Na<sub>2</sub>O 0.07 wt. % (0.59 wt. % in ash), S 0.69 wt. %. The ash content average 2015 is 11.7%. The coke ash has a chemical composition (wt. %) of: Fe<sub>2</sub>O<sub>3</sub> (5.2), SiO<sub>2</sub> (58.5), Al<sub>2</sub>O<sub>3</sub> (28.4), CaO (1.2) and MgO (0.7). The actual values of the coke analyses varies slightly depending on coal-mixes used.

#### **2.3.1.3.2** Investigation of alkali uptake in burden materials and the impact on their properties (LKAB, SWERIM)

Burden material samples are collected both during operation and after the quench of each EBF campaign. During operation, material samples are taken daily at the two shaft probes, **Figure 111 a).** Excavation samples are taken from each pellet layer at ten to thirteen predetermined positions **Figure 111 b).** Basket samples of ferrous burden materials and coke are charged to different layers in the EBF prior to the quench and are recoverd during the excavation.

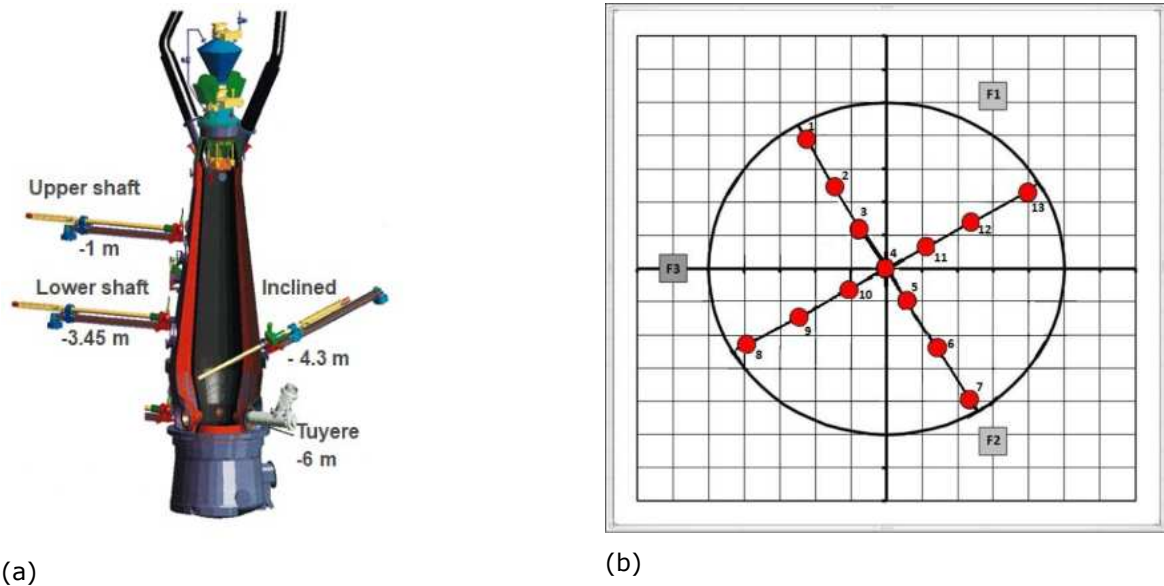


**Figure 111** Material sampling positions during operation (a) and excavation (b).

The different sample types investigated in this project are summarized in **Table 15**.

**Table 15** Samples of interest from the EBF in the Alcinc project.

Campaign	Burden	Shaft probe	Excavation		Baskets	
			Pellet	Coke	Pellet	Coke
C30	100% acid pellet		x			
C31	100% olivine pellet		x	x*	x	x*
C32	100% olivine pellet	x	x	x*	x	x*
C33	50% acid pellet/50% sinter		x			x*
	* = analysed by SWERIM					

Process conditions and charging sequence of the burden materials for the last 24h of operation of the campaigns are summarized in **Table 16** and **Table 17** respectively.

**Table 16** Process conditions prior to the quench of the EBF campaigns 30-33.

	<b>C30</b>	<b>C31</b>	<b>C32</b>	<b>C33</b>
<b>Burden material</b>	100% Acid pellet 07-mar-14	100% Olivine Pellet 23-okt-14	100 % Olivine Pellet 11-nov-16	50% Acid pellet/50% Sinter 15-dec-17
<b>Production</b>	1,6	1,5	1,49	1,45
<b>Slag</b>	150	146	142	233
<b>Coke rate</b>	421	407	425	431
<b>PCI</b>	152	148	133	136
<b>Total fuel rate</b>	573	553	558	567
<b>EtaCO</b>	46	47	48	44
<b>DRR</b>	32	27	33	34
<b>Blast</b>	1692	1518	1561	1536
<b>Blast temp</b>	1195	1198	1199	1198
<b>Blast H<sub>2</sub>O</b>	25	20	13	22
<b>O<sub>2</sub> to Lance</b>	80	74	50	60
<b>O<sub>2</sub> to Blast</b>	50	46	55	60
<b>Slag basicity</b>	1,1	0,9	0,98	0,91
<b>Si in hot metall</b>	1,9	1,49	1,8	1,77
<b>S in hot metall</b>	0,03	0,03	0,03	0,05
<b>Hot metall temp</b>	1466	1449	1452	1397

**Table 17** Charging sequence in the EBF prior to the quench. W→C wall to centre and C→W centre to wall.

		Centre							Wall	
Direction		0mm	20mm	200mm	225mm	250mm	280mm	310mm	350mm	
<b>C30</b>	W→C	Coke		40%					60%	
	C→W	Pellets+ nutcoke						100%		
<b>C31</b>	W→C	Coke		40%					60%	
	C→W	Pellets				100%				
<b>C32</b>	C→W	Coke		40%	20%				40%	
	W→C	Pellets				15%		70%		15%
<b>C33</b>	C→W	Coke		40%	20%				40%	
	W→C	Pellets			15%			50%		35%

Chemical composition of pellets (including potassium), crushing strength and reduction degree is routinely determined, for all pellet layers in the blast furnace shaft. The last four EBF excavations have been compared for alkali up-take, based on potassium content of excavated pellets compared to potassium content from indurated pellets, **Figure 112**. Temperature measurements with the vertical shaft probe is normally done prior to the quench of the EBF and the result from the temperature measurements are included in the left-hand vertical axes in each contour plot.

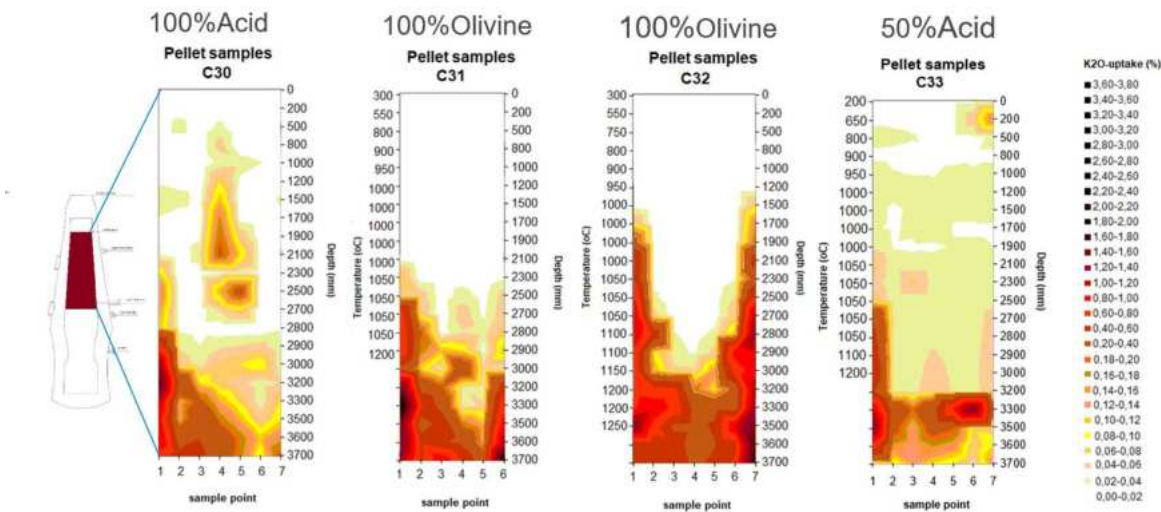


**Figure 112** Potassium up-take in excavated pellets from the last four campaigns in the EBF.

It can be concluded that high alkali up-take is found predominantly at the wall positions and in the lower part of the shaft (sample points 1 and 7 in **Figure 112**) for all four campaigns. Acid pellets, campaign 30 and 33 have alkali up-take higher up in the shaft than olivine pellets.

Coke samples from LKAB EBF have been collected from two different campaigns, C31 and C32, in assistance by SWERIM after quenching and excavation from shaft, raceway level and hearth and chemically analysed for the alkali content. Coke samples from the shaft have been collected at 5 different radial positions at 7 different levels, going from position of shaft probes towards tuyere 2, see illustration in **Figure 113**. A number of these samples located at different depths will be selected for further reactivity studies using a Thermogravimetric analyzer by LTU.

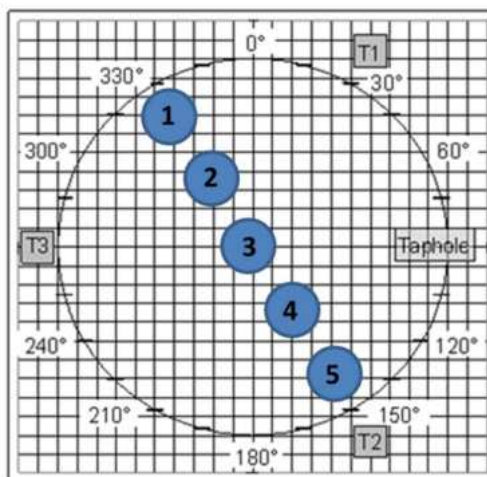


**Figure 113** Radial positions of coke samples from shaft

From C32 in 2016, coke samples excavated at different horizontal and vertical positions have been analysed with respect to the alkali content and compared to the previous campaign 31 in 2015 with a different charging practice. For both campaigns, coke was sampled according to the same sampling procedure; see radial position of samples in **Figure 113**.

As seen in **Table 17**, the charging of the coke in C31 was more located towards the middle (thicker layer in the middle) of the shaft creating a gas chimney. During campaign 32 the coke was more evenly distributed during charging.

In **Figure 114**, alkali up-take in coke samples from the excavation of Campaigns 31 and 32, described by SWERIM, is compared with alkali up-take in pellets for the same campaigns. According to this, the distribution of alkali in coke was different between C31 and C32. At the same depth, the alkali content in both coke and pellets was in general higher towards the walls during C32. For C31, the alkali content in coke was highest in center at depths between 2500 and 3000 mm from top. Compared to C32, the alkali contents in both coke and pellets was higher in the upper shaft in C31, which could be explained by a more pronounced central gas flow. Moreover, based on the comparison between C31 and C32 with respect to the alkali content in pellets and coke, the circulating load of alkalis seem to be higher during C32.

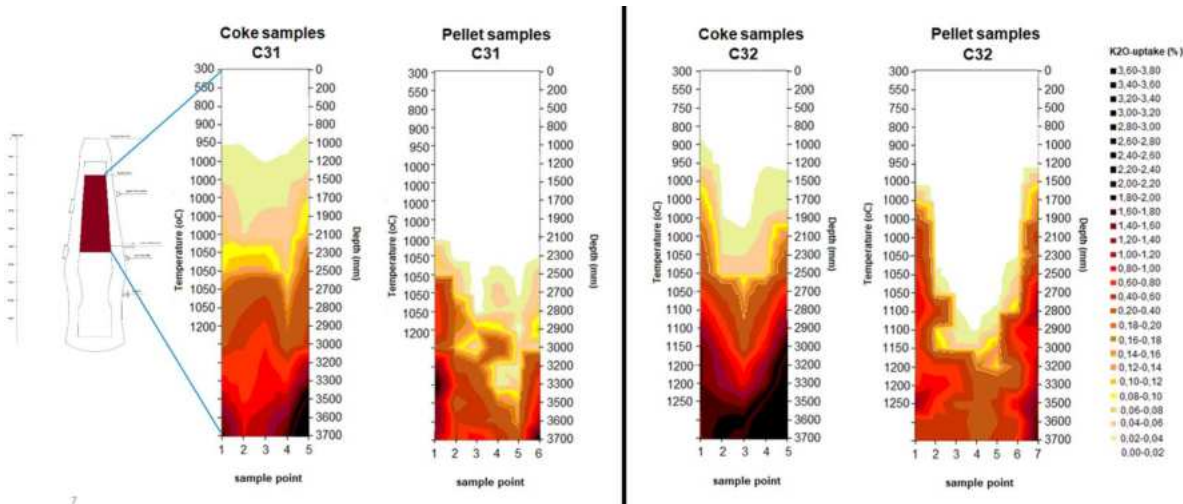


**Figure 114** Alkali (potassium) up-take in coke and pellet samples from Campaigns 31 and 32 and temperature measurement with the vertical probe.

Coke has an overall higher alkali up-take than pellets in the blast furnace shaft and have alkali up-take higher up in the shaft. The effect of alkali up-take in coke is detrimental for the coke strength. If the coke starts to disintegrate it will affect the gas permeability in the blast furnace. In pellets alkalis can cause swelling and hence also weaken the strength of the pellets. Crushing strength of non-sintered pellets from the four last excavations are presented in **Figure 115**.

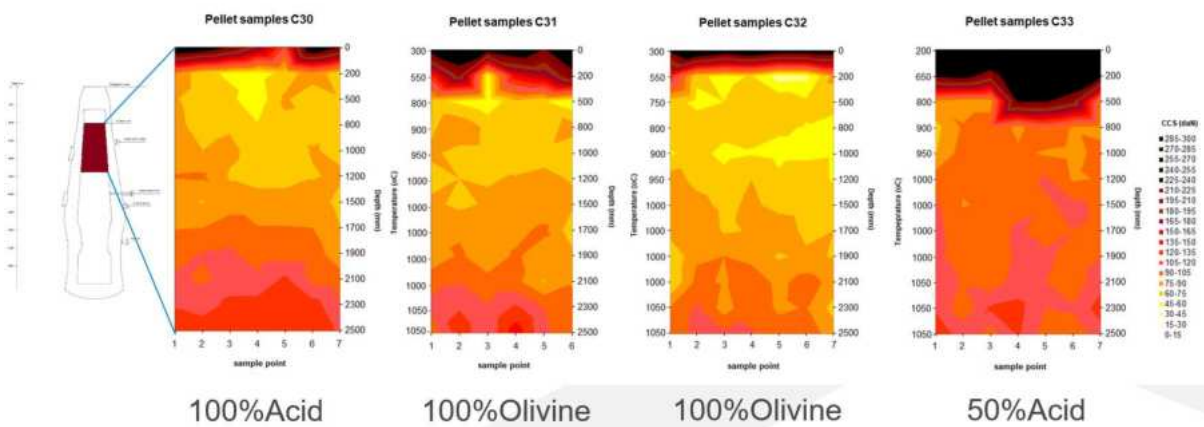


**Figure 115** Crushing strength of non-sintered pellets from EBF Campaigns 30-33.

Indurated pellets have generally a crushing strength above 220daN. As the pellet enters the blast furnace and the reduction from hematite to magnetite and wüstite starts, the crushing strength

decreases. When the pellet starts to metallise, the crushing strength start to increase again. As seen in **Figure 113**, there is almost no alkali up-take in the upper part of the blast furnace shaft where the reduction from hematite to magnetite and wüstite takes place. Therefore, the reduced crushing strength in the upper part of the shaft in **Figure 115**, is not from alkali up-take but from phase transformations due to reduction.

Reduction degree for the four campaigns in the EBF is visualised in the same way as the alkali up-take and crushing strength in **Figure 116**.

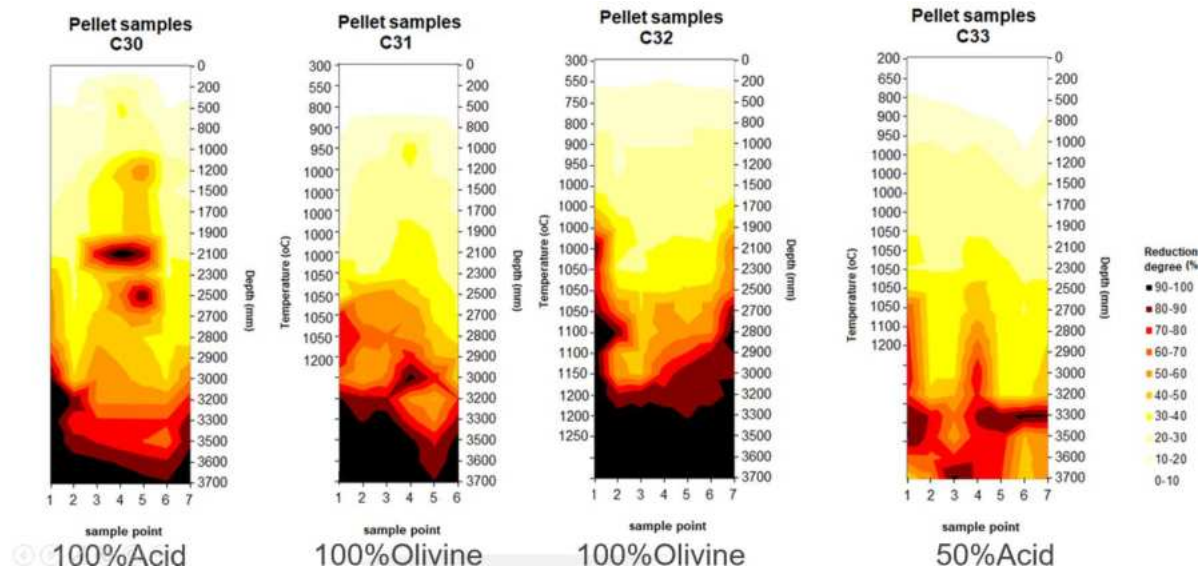


**Figure 116** Reduction degree of pellet layer samples positions 1-7 from EBF excavations C31-C33.

The reduction degree follows the same pattern as the alkali up-take. Reduction degree increase with the depth of the blast furnace and it is higher at the walls. In **Figure 117**, the reduction degree is compared with the alkali (potassium) up-take in pellets from all excavated pellet layers in EBF Campaign 32 and positions 1 to 7.

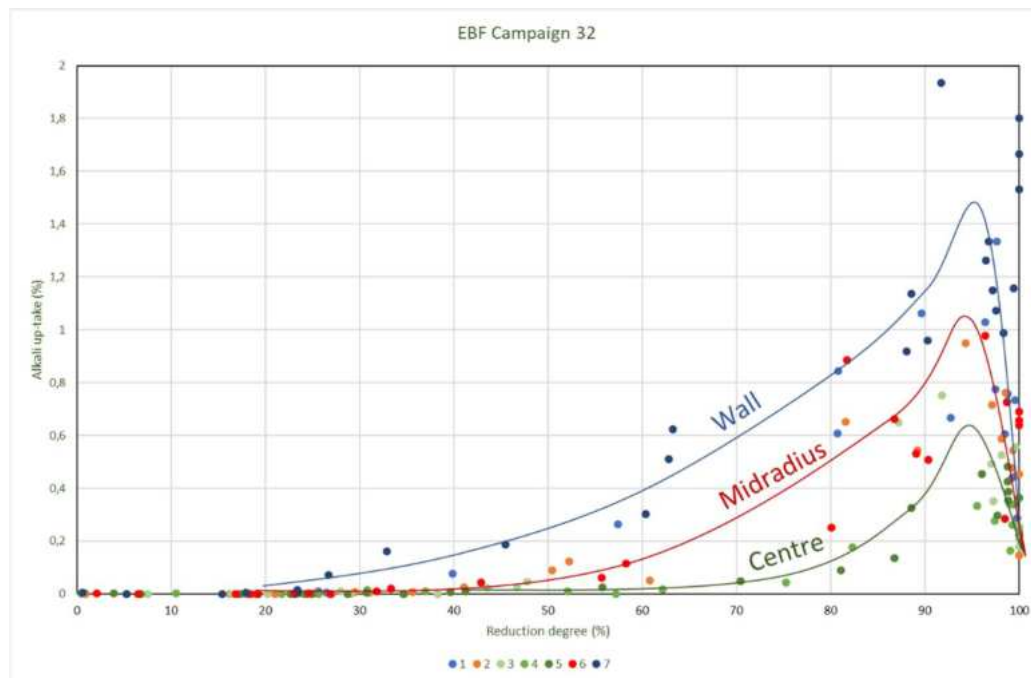


**Figure 117** Reduction degree versus alkali up-take in pellet layer samples positions 1-7 from EBF excavation C32.

It is seen in **Figure 117** that the alkali up-take increase with higher reduction degree. The alkali up-take in the pellets increase until the slag melts out and the alkali in the pellets decrease. At the same reduction degree the alkali up-take varies depending on position in the blast furnace cross section (centre, midradius or wall). Highest alkali up-take is at the wall and decrease towards the centre of the furnace.

In this project one week of sampling from the shaft probes have been investigated for alkali up-take. A total of eight material samples from upper shaft and eight from the lower shaft were collected. The upper shaft probe is 90 cm below the charging level and the lower shaft probe is situated 337 cm below the charging level. The probe material from each probe is divided into 2-6 bags, **Figure 118**, where the last bag is material from the wall. Typically between 3 and 4 bags are filled with material from a probe.

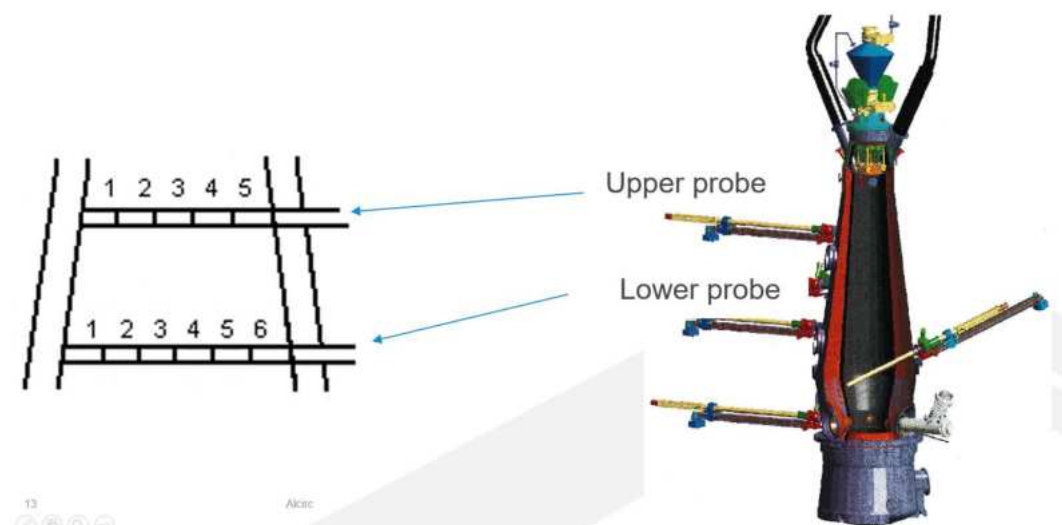


**Figure 118** Schematic view of material probes and maximum number of bags with material from each shaft probe.

Each bag from every probe measurement is sieved and sorted according to **Figure 119**.

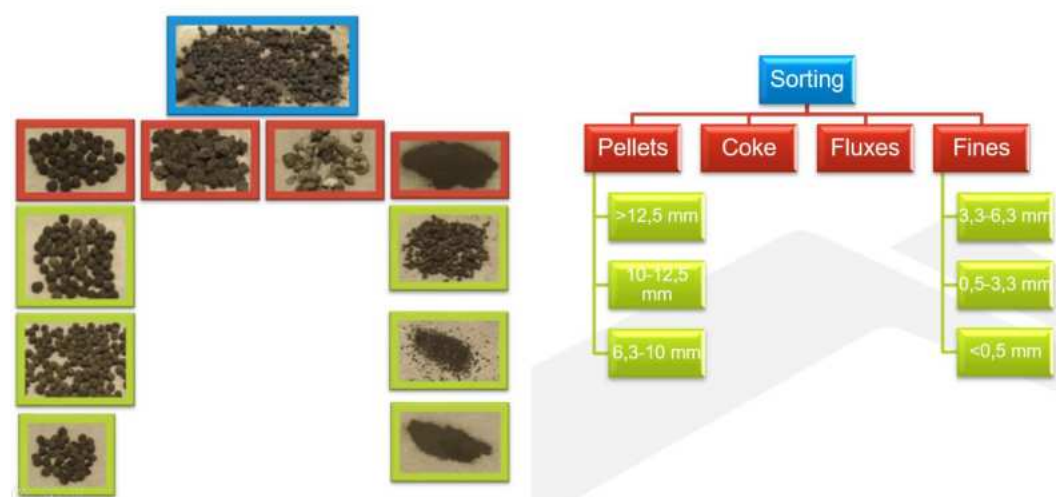


**Figure 119** Photos of each material and fraction investigated for alkali content.

Selected fractions from each bag (where there was enough material) were analysed with XRF for chemical analysis. The average K<sub>2</sub>O content at wall, midradius and centre of the EBF is summarized for the upper probe samples in **Table 18** and for lower probe samples in **Table 19** below. The fluxes and coke samples were analysed by SWERIM and the pellets and mixed fractions by LKAB.

**Table 18** Average K<sub>2</sub>O content(%) in upper probe samples.

Upper probe		Wall	Midradius	Centre	K <sub>2</sub> O (%)
Pellets	>12,5mm	0.12	0.048		<0.1
	10-12,5mm	0.049	0.025	0.096	0.1-0.5
	6,3-10mm				0.5-5
Mixed	3,3-6,3mm	0.038			5-15
	0,5-3,3mm				>15
	<0,5mm	0.54			
Fluxes		0.29	0.2	0.41	
Coke		0.28	0.18	0.17	

**Table 19** Average K<sub>2</sub>O content (%) in lower probe samples.

Lower probe		Wall	Midradius	Centre
Pellets	>12.5mm		0.64*	
	10-12.5mm	2.1	0.26	0.044
	6.3-10mm			
Mixed	3.3-6.3mm		0.54	0.099
	0.5-3.3mm	26.6	0.29	0.22
	<0.5mm	30.3	13.2*	
Fluxes		9.14	0.52	0.29
Coke		5.82	1.20	0.45

\* = Only one sample

The darker the colour is, the higher potassium content in the material for **Table 18** and **Table 19** above. In the upper probe materials the potassium content is not so high compared to the lower shaft probe. It is also seen that the average potassium content is higher at the wall position and it decreases towards the centre of the furnace. This could be expected from the excavated pellet layer samples in **Figure 118**. Highest average potassium content is found in the mixed materials for the fractions 0.5-3.3mm and <0.5mm from the lower shaft probe at the wall position. On the second and third place in potassium content are the fluxes and coke in the lower shaft probe measurements.

**Figure 120** compares the average potassium content with the carbon content for the analysed pellets and mixed fractions in the upper shaft probe.

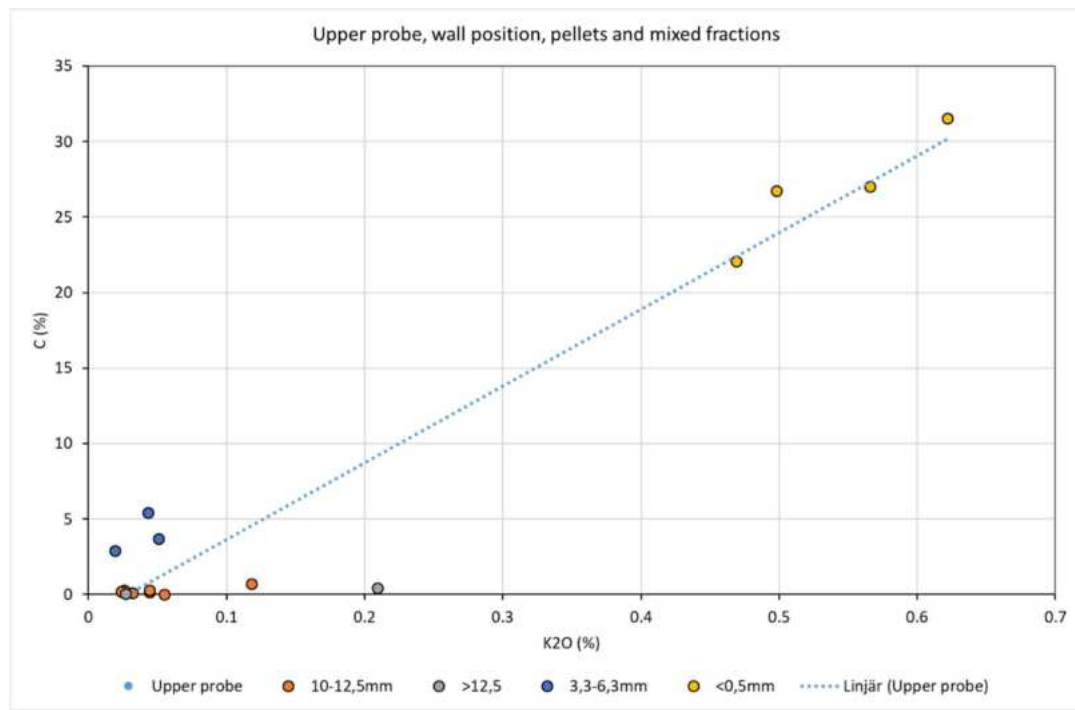


**Figure 120** Potassium and carbon content in pellets and mixed fractions from the upper shaft probe.

The carbon is found in the mixed fractions 3.3-6.3mm and <0.5mm with the highest potassium content. Coke has higher alkali content than the pellets when entering the blast furnace. Therefore, it is possible that the coke has disintegrated in the upper probe samples and hence are affecting the potassium content in the mixed fractions.

The average potassium content compared to carbon content in the lower shaft probe for the pellets and mixed fractions are visualized in **Figure 121** in the same way as for the upper shaft probe fractions.

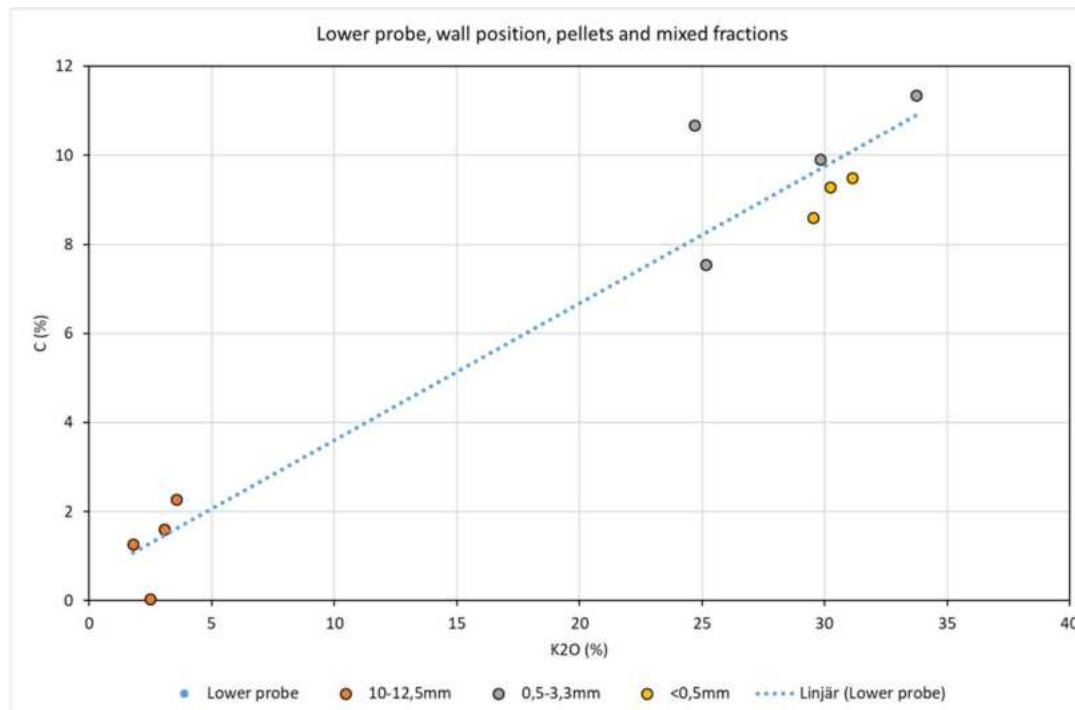


**Figure 121** Potassium and carbon content in pellets and mixed fractions from the lower shaft probe.

In the lower shaft probe the pellet fraction 10-12.5mm has started to pick up small amounts of carbon. The higher alkali content, the higher carbon content. Also here it is clear that most of the carbon and alkali (potassium) content is found in the mixed fractions (0.5-3.3mm and <0.5mm). The results from the shaft probe can be summarized as follows:

- More alkali in the lower shaft probes
- More alkali on the samples from the wall position
- More alkali in the mixed fractions with fines
- More C in the samples → More alkali too

Basket samples with fluxed potfurnace pellets have been studied for alkali up-take from EBF campaigns 31 and 32. Basket trials are performed prior to the quench of each EBF campaign. The baskets contain various types of burden materials such as pellets, lump, sinter, fluxes, coke or briquettes depending on the scope of interest. The baskets are then charged to the blast furnace prior to the quench on 24 pellet and 24 coke layers. When the last basket is charged to the EBF, the furnace is stopped and nitrogen gas is flushed through the furnace and out through the tap hole to cool down and stop the reactions in the burden materials. In these two investigations, pellets were placed in small baskets charged to every second pellet layer starting at pellet layer 1. Each basket was divided into small sections with 28 pellets/section/pellet type in order to obtain similar gas distribution for all materials, example in **Figure 122**.

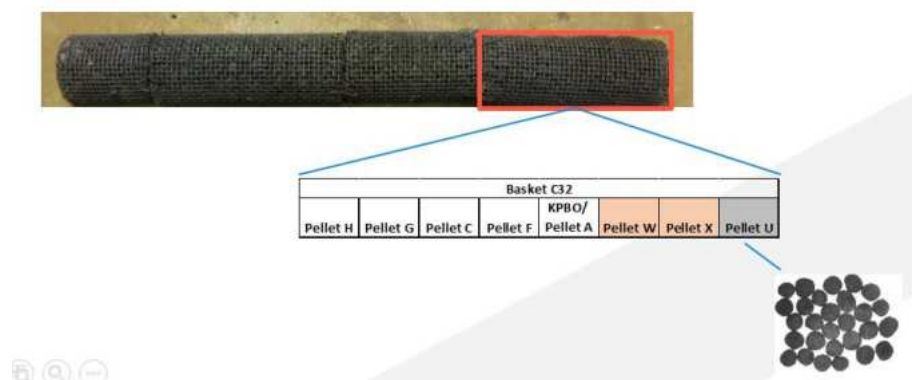


**Figure 122** Example of a basket divided into smaller sections with different pellet types in each compartment.

When the EBF is excavated, the baskets are recovered. Depth and placement of the baskets on the cross section of the furnace are documented, example **Figure 123**.

## EXCAVATED BASKETS C32

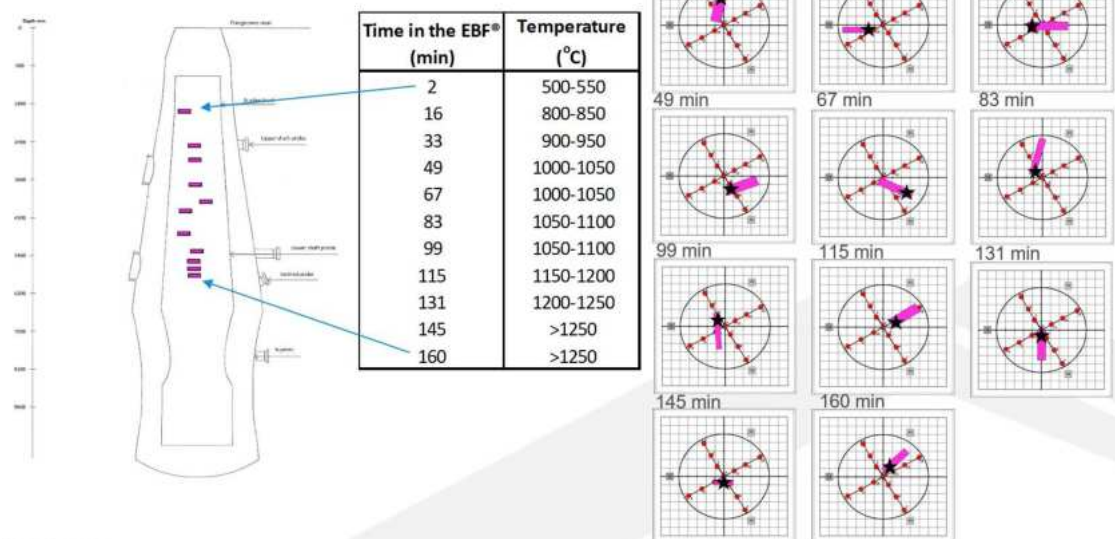


**Figure 123** Example of the excavated baskets from EBF campaign 32 with depth, time in the EBF before the stop, temperature from the vertical shaft probe for each basket and schematic views of placement on the cross section.

A Qemscan® was used to evaluate the alkali up-take for one pellet per material from each recovered basket together with an indurated pellet from each pellet type as reference. The mass% of alkali phases for the commercial pellet KPBO from baskets in the EBF C32 detected with the Qemscan is shown in **Figure 124**. The pink phases are with potassium and the blue phases has calcium too, and darker color means higher alkali content.

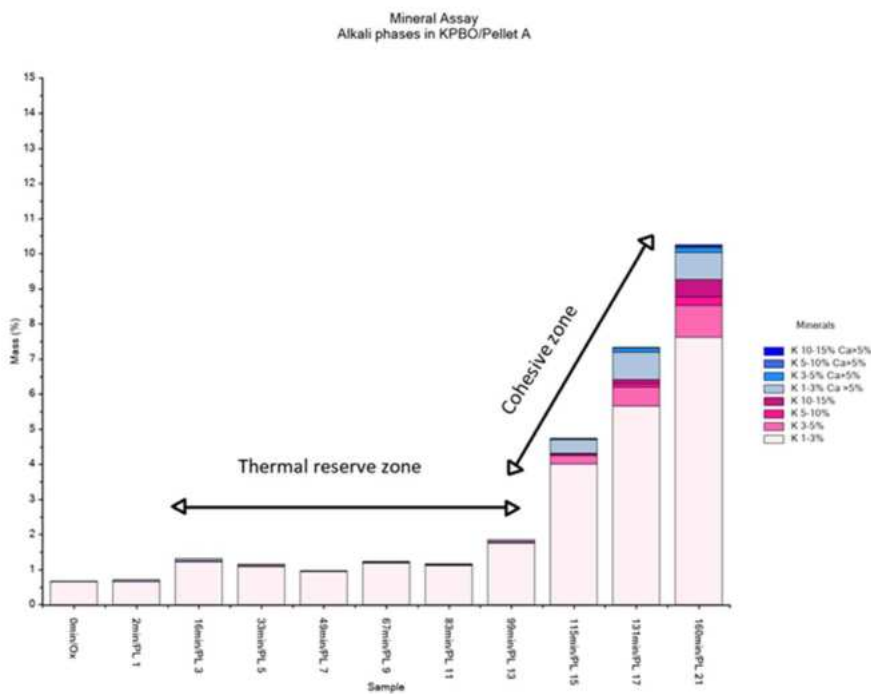


**Figure 124** Mass-% alkali containing phases in KPBO from baskets in EBF Campaign 32.

The alkali containing phases are almost constant from indurated pellet until the pellet reaches the cohesive zone. As the temperature rises in the beginning of the cohesive zone and the reduction degree increases, **Figure 125**, the higher mass% of alkali phases. Also, in the cohesive zone more

alkali rich phases occurs (the higher potassium content, the darker the colour).

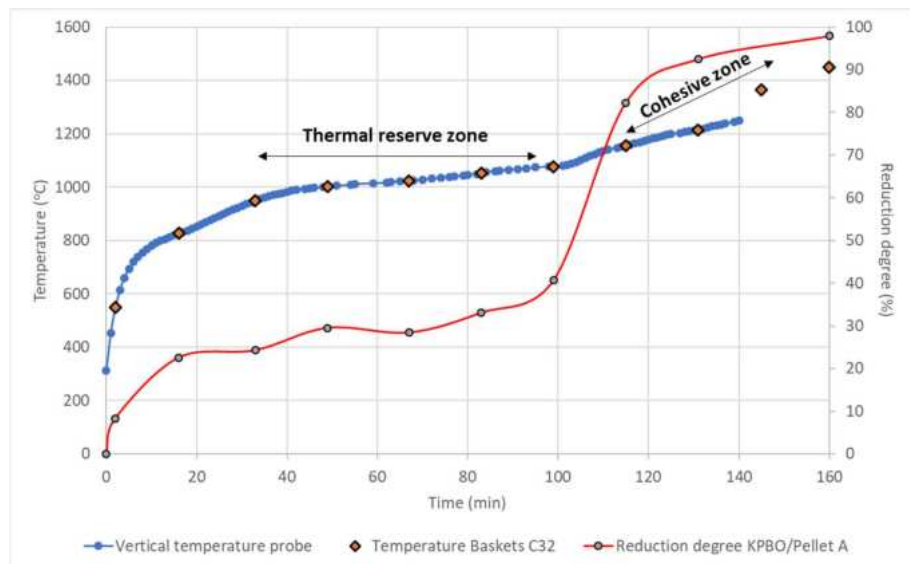
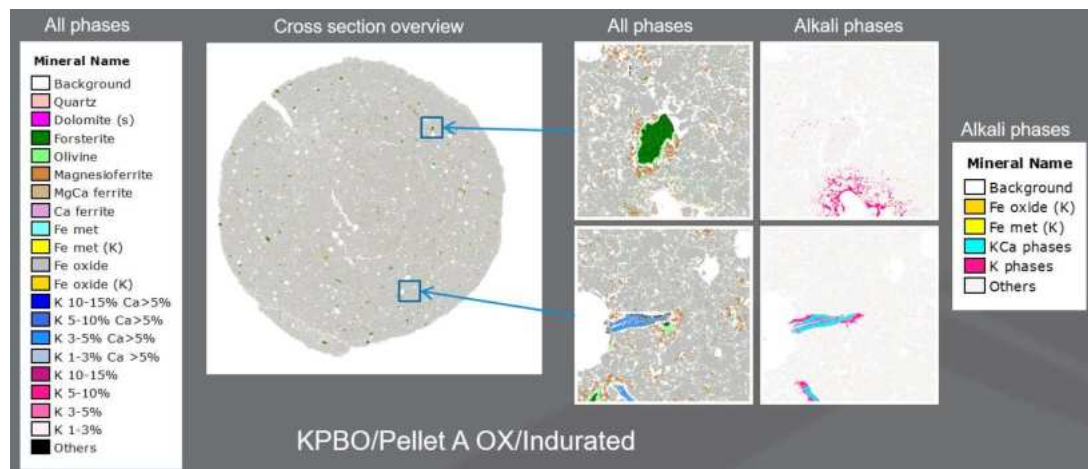
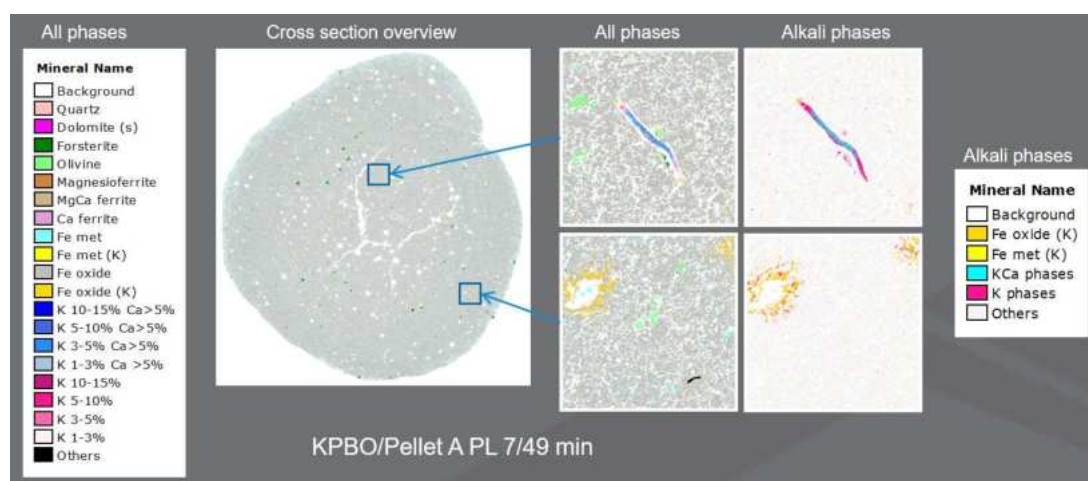


**Figure 125** Vertical temperature measurements and reduction degree of KPBO from baskets in EBF Campaign 31.

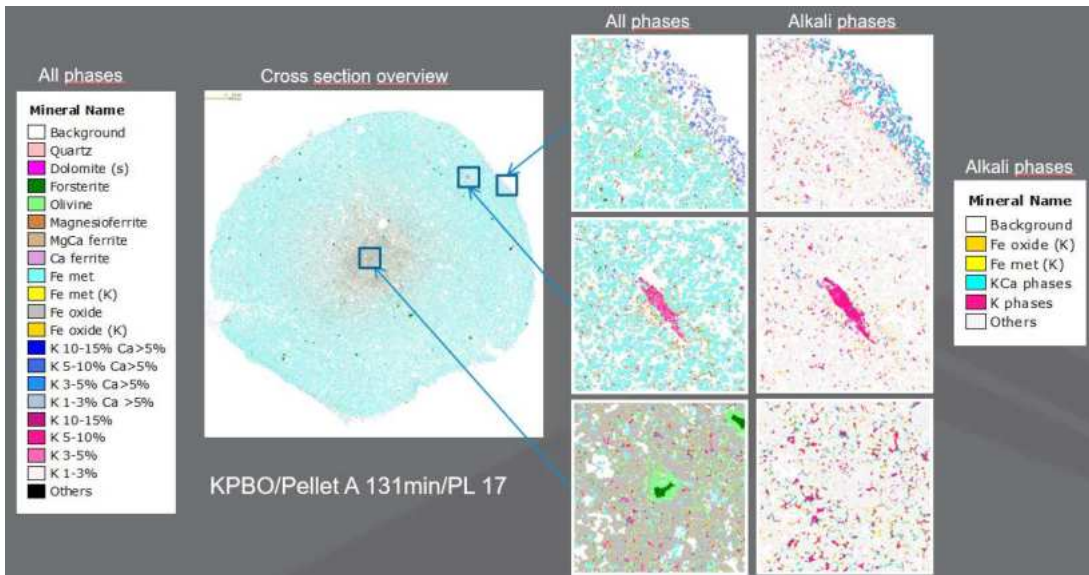
Investigation of alkali phases in the cross section of KPBO pellets after induration, from the thermal reserve zone and from the cohesive zone, **Figure 126**, were performed.



(a)



(b)



(c)

**Figure 126** Qemscan images of alkali phases in a) indurated pellet, b) pellet from the thermal reserve zone and c) pellet from the cohesive zone.

Alkali phases in KPBO are found in gangue minerals and in the iron oxide matrix around decomposed gangue minerals in the indurated pellets, **Figure 126 a**. The same applies to the the pellet from the thermal reserve zone, **Figure 126 b**. In the cohesive zone where most of the pellet is metallised (light blue in **Figure 126 c**) there is a build up of alkali phases around the pellet together with calcium. Alkali is found all over the pellet in silicate slags, but more pronounced in the centre where there is still some iron oxide left and in gangue minerals. Alkali up-take in the cohesive zone were studied for pellets with different basicity, B2, and different choise of additives. **Figure 127**, shows alkali phases for limestone/olivine pellets from campaign 31 with basicity between 0.2 and 1.3.

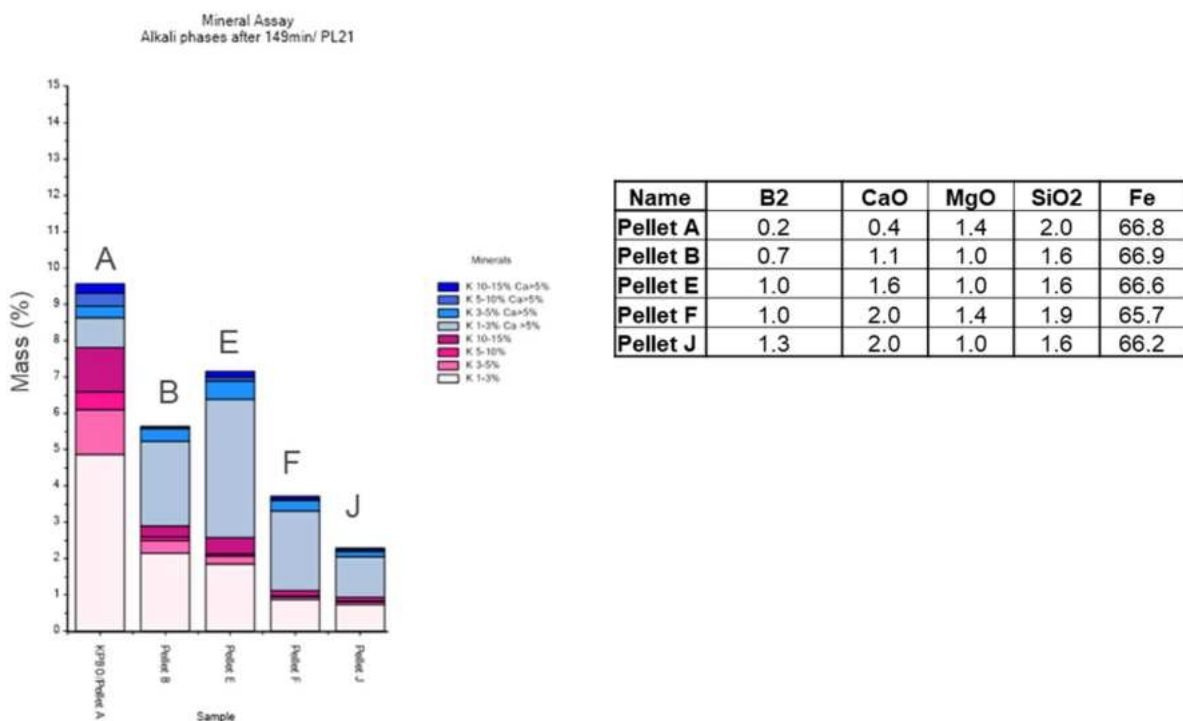
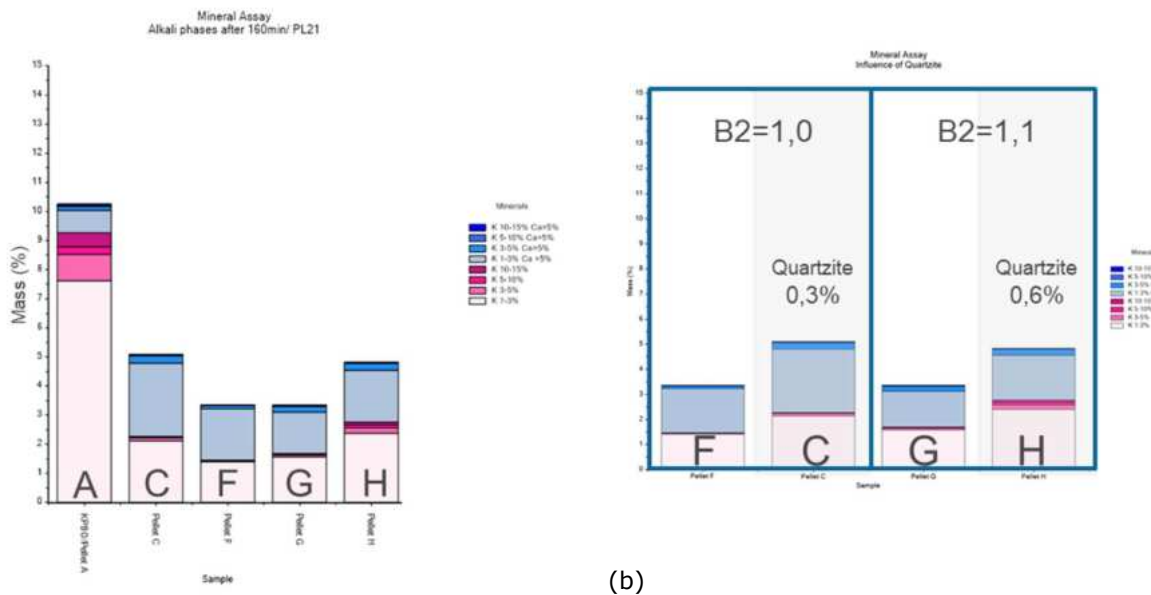


**Figure 127** Mass% of alkali phases in limestone/olivine pellets with increasing basicity from the cohesive zone in the EBF Campaign 31.

The trend is that with increasing basicity (pellet A/KPBO, B2=0.2→pellet J, B2=1.3), the alkali containing phases decreases. Pellet B was found on a slightly different location on the cross section, which might explain the lower amount of alkali phases.

In EBF campaign 32, KPBO (Pellet A) was used as reference pellet and limestone/olivine pellets with small addition of quartzite and basicity around 1.0 were investigated for alkali up-take, **Figure 128.**



(a)

Name	B2	CaO	MgO	SiO2	Fe
Pellet A	0.2	0.4	1.4	2.0	66.8
Pellet C	1.0	2.0	1.2	2.0	65.8
Pellet F	1.0	2.0	1.4	1.9	65.7
Pellet G	1.1	1.9	1.2	1.7	66.1
Pellet H	1.1	2.1	0.8	1.9	66.1

**Figure 128** Mass% of alkali phases in limestone/olivine pellets with increasing basicity from the cohesive zone in the EBF Campaign 31.

Compared with KPBO fluxed pellets with a basicity around 1 have again a lower alkali up-take. Pellet C and F and pellet G and H have the same basicity but different alkali up-take. Pellet C and pellet H also contain a small amount of quartzite which probably affects the higher alkali up-take for those pellets.

From the basket samples it can be concluded that:

- Alkali up-take take place in the cohesive zone
- In indurated pellets and pellet from the thermal reserve zone alkali is found in gangue and in the iron oxide matrix around decomposed gangue
- In the cohesive zone alkali is found in silicate slags and build ups around the pellets
- Alkali up-take is influenced by pellet basicity B2 and choice of additive
  - Increased basicity will decrease the alkali up-take
  - Addition of quartzite will increase the uptake (same basicity)

### 2.3.1.3.3 Coke reactivity tests in order to assess coke attack by alkali components (LTU)

Seven coke samples from LKAB EBF® after quenching and excavation in C31, were selected and collected by SWERIM for further reactivity tests using thermogravimetric analyser at LTU. **Figure 129** shows the location of the studied sample in the EBF. All samples subjected to reactivity test were located along the central line of the EBF.

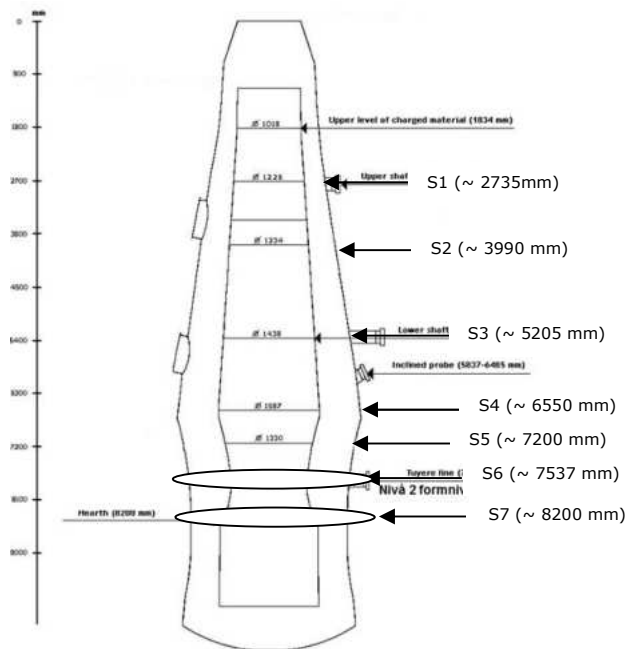


**Figure 129** Location of the studied sample in the EBF

**Figure 130** shows the received samples and the sample after preparation for reactivity tests, samples were crushed into 1-2 mm particles using a jaw crusher. A Netsch thermogravimetric analyser (TGA) coupled with a quadrupole mass spectroscopy (QMS) was used for reactivity tests. A schematic diagram of the instrument is given in **Figure 131**. **Figure 132** shows the applied thermal profile during the test. Samples were heated 20°C/min up to 600°C (where no reaction is expected to occur), this fast ramp is followed by a slow heating from 600°C till 1200°C at a heating rate 3 °C/min. A continuous flow of CO<sub>2</sub>, 300ml/min, was maintained through the whole thermal cycle.



**Figure 130** Received samples and samples after preparation for reactivity tests

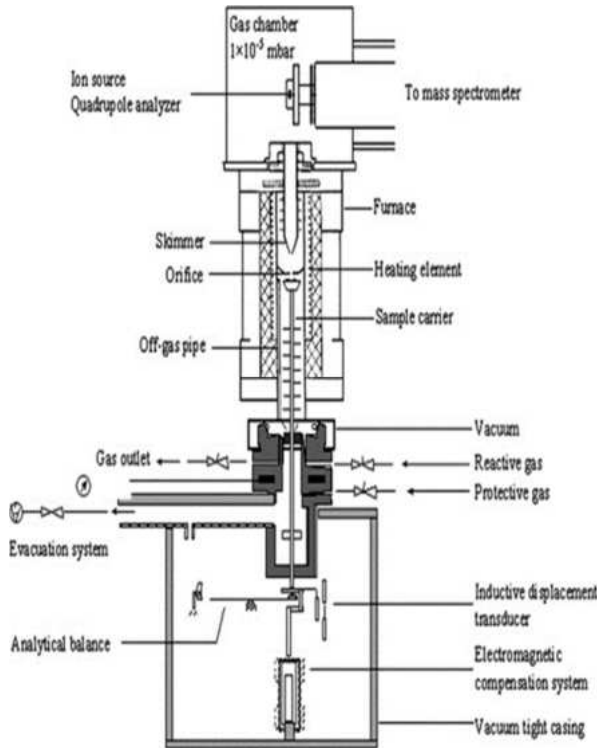


**Figure 131** Schematic diagram of the TGA/QMS.

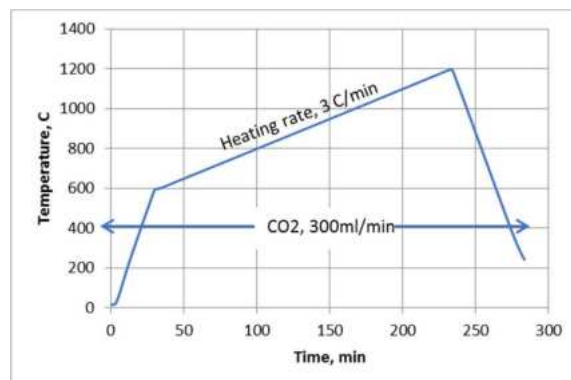


**Figure 132** Applied thermal profile during the test

The tested samples were analysed for their chemical composition and given in **Table 20**. In the table the alkali content ( $K_2O+Na_2O$ ) is highlighted.

**Table 20** Chemical composition of the tested samples

Sample	Fe	CaO	SiO <sub>2</sub>	MnO	S	Al <sub>2</sub> O <sub>3</sub>	MgO	Na <sub>2</sub> O	K <sub>2</sub> O	TiO <sub>2</sub>	Sum	SiO <sub>2</sub> /Al <sub>2</sub> O <sub>3</sub>	K <sub>2</sub> O+Na <sub>2</sub> O
S1	0.352	0.032	6.87	0.024	0.57	2.93	0.07	0.07	0.15	0.18	11.2	2.34	0.23
S2	0.330	0.036	7.34	0.028	0.58	3.13	0.08	0.07	0.18	0.18	11.8	2.34	0.25
S3	0.275	0.053	7.63	0.026	0.55	3.18	0.09	0.09	0.28	0.17	12.2	2.40	0.37
S4	0.246	0.010	7.17	0.084	0.52	3.04	0.10	0.33	1.18	0.16	12.7	2.35	1.51
S5	1.480	1.314	3.31	0.413	0.39	2.84	1.33	0.06	0.33	0.24	12.2	0.39	1.17
S6	0.259	0.024	6.87	0.201	0.54	3.01	0.13	0.51	1.58	0.16	13.1	2.08	2.28
S7	1.354	3.975	3.92	0.305	0.40	3.15	1.99	0.38	1.11	0.19	17.2		1.49

**Figure 133** shows the gasification of different tested coke (excavated samples) as a function of time and temperature. It was clear that no reaction has started before 830°C irrespective of the alkali content and the thermal history of the samples. However, it is very clear that coke reactivity increases as the alkali content increase and as the sample descend in the EBF, see **Figure 129** and **Table 21**.

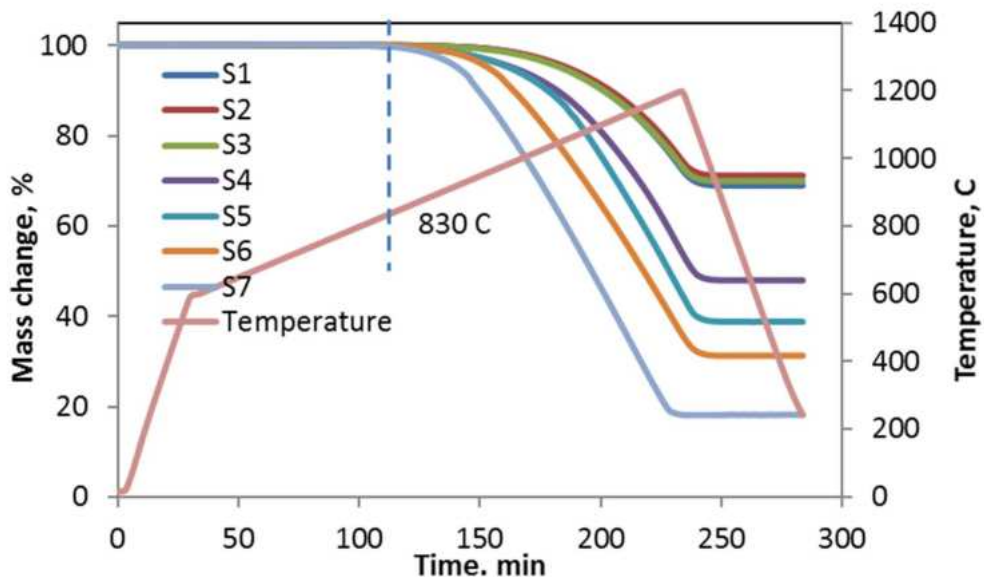


**Figure 133** Gasification of different tested cokes (excavated samples) as a function of time and temperature

**Figure 134** shows the detected carbon monoxide in the off-gas as a function of temperature and time. CO is the reaction product of the coke gasification and higher concentration of CO in the off-gas means higher reaction rate (keeping the experimental conditions identical). The earlier and the more carbon monoxide generated is an indication of earlier reaction between coke and  $\text{CO}_2$  (at lower temperature) and thus higher reactivity of the coke samples.

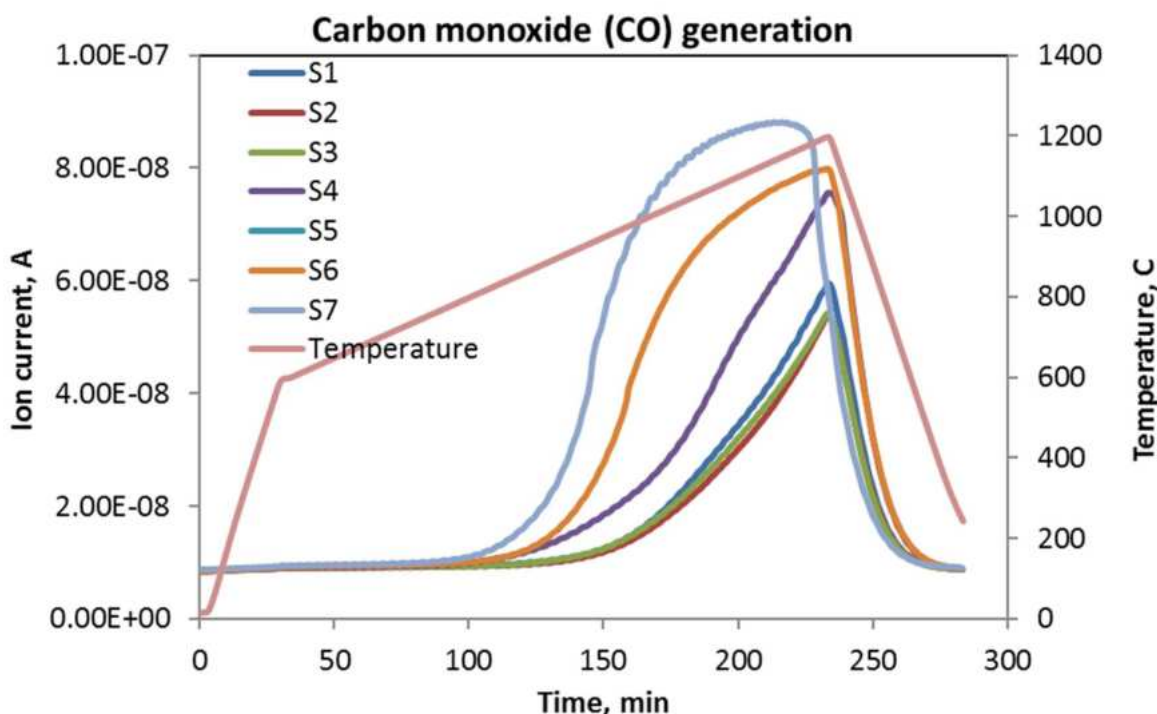


**Figure 134** Detected carbon monoxide in the off-gas as a function of temperature and time

The thermogravimetric curves in **Figure 133** were further evaluated and the corresponding reaction kinetic parameters, namely the activation energy were estimated according to Equations (4-7). The reaction kinetics were estimated based on Arrhenius kinetic model assuming a first order reaction. The non-isothermal curve is then discretised into infinite number of isothermal

segments. The apparent reaction rate

$$\frac{dw}{dt} = kw^n \quad (4)$$

$$k = A \exp\left(\frac{-E}{RT}\right) w^n \quad (5)$$

$$\frac{1}{w} = \left(\frac{dw}{dt}\right) = A \exp\left(\frac{-E}{RT}\right) \quad (6)$$

$$\ln k = \ln A - \frac{E}{RT} \quad (7)$$

for each isothermal segment was calculated using equation (6) Where,  $W$  is the reactive sample mass at time  $t$ ,  $A$  frequency factor,  $E$  activation energy,  $T$  absolute temperature,  $R$  gas constant,  $n$  the reaction order and  $k$  is the apparent reaction rate. The activation energy and the frequency factor values can be determined by plotting  $\ln k$  vs  $1/T$ , the slope of the resulting straight line is  $-E/R$  and the intercept is the frequency factor. **Figure 135** shows two examples for the Arrhenius plot for two of the studied samples.

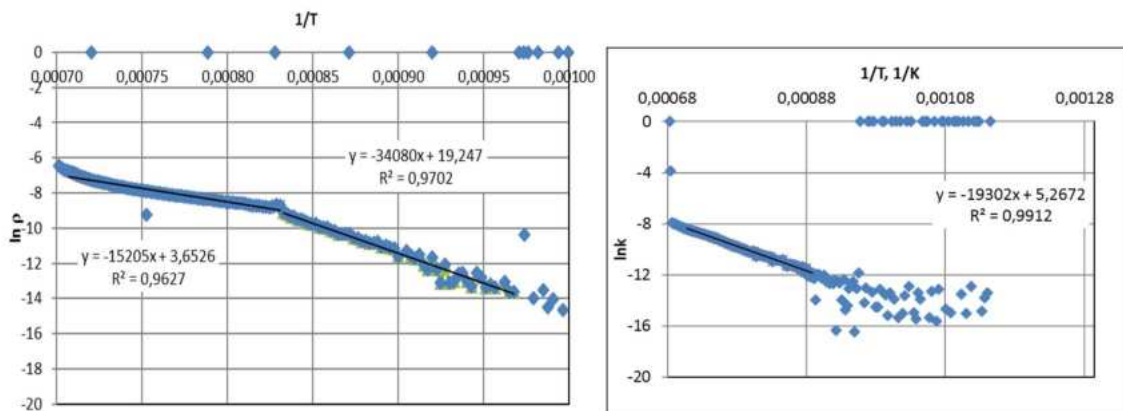


**Figure 135** Arrhenius plot of a studied sample

**Table 21** shows the estimated kinetic parameters and the corresponding temperature interval. Most of the sample showed one stage reaction specially the sample collected from the upper part of the EBF. The samples from the raceway showed two reactions steps associated with two activation energy values.

**Table 21** Estimated kinetic parameters and corresponding temperature interval

	Conversion	Temperature range, C	E <sub>a</sub> , kJ/mol	A, g/g.s	R <sup>2</sup>
S1	0-0.2	860-1140	197	26.4*10 <sup>2</sup>	0.98
S2	0-0.2	860-1140	196	20.9*10 <sup>2</sup>	0.96
S3	0-0.2	860-1140	184	795	0.97
S4	0-0.2	860-1140	160	193	0.99
S5	0-0.4	860-1140	182	18.5*10 <sup>2</sup>	0.99
S6	0-0.1	840-940	282	70.5*10 <sup>6</sup>	0.94
	0.1-0.5	960-1140	99	2	0.99
S7	0-0.1	760-930	283	22.8*10 <sup>7</sup>	0.96
	0.1-0.6	930-1140	126	38	0.97

A linear relation between the activation energy and the alkali content as well as the distance from the top of the EBF could be established (**Figure 136**). The activation energy was found to decrease with the increase in the alkali content. Accordingly, the activation energy was found to decrease as the samples descend in the EBF.

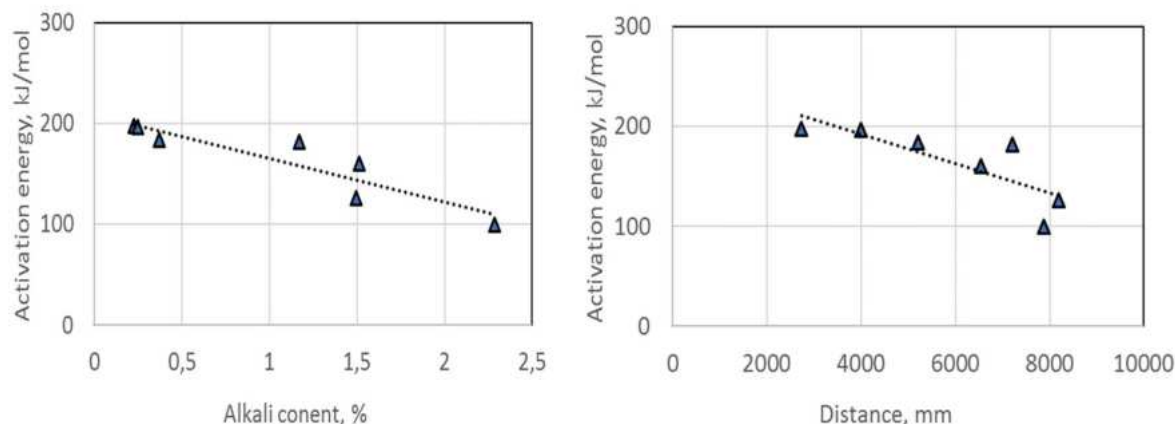


**Figure 136** Linear relation between the activation energy and the alkali content as well as the distance from the top of the EBF

It can be seen from the above results that the coke reactivity increases as its alkali content increases which can be attributed to the known catalytic effect of alkalis on gasification reaction. Moreover, some samples collected from the raceway showed highest reactivity although its alkali content is not highest. This can be attributed to their ash composition which is high iron, calcium and magnesium oxides, see **Table 20**. The effect of various ash components on gasification reaction is often expressed by alkali index [43, 44] the alkali index is calculated according to the following equation;

$$A = \text{Ash} \times \frac{Fe_2O_3 + Na_2O + K_2O + CaO + MgO}{Al_2O_3 + SiO_2}$$

### **2.3.1.3.4 Alkali impact on coke - Chemical and physical analyses of coke after retort tests (Dunafer)**

Based on what is specified in the research program of the project ISD Kokszoló Kft. carried out 12 Carbotest retort tests (**Figure 137**), 116 CRI, CSR tests and 6 granulometric composition specification. This activity was realized in the form of service activity.



**Figure 137** Carbotest equipment

Statements made during the tests in the laboratory of ISD Kokszoló Kft.:

- Na<sub>2</sub>O- and K<sub>2</sub>O-content do not change during coking (**Figure 138**).
- The increase in the ash content of coal makes coke properties worse (**Figure 139**).
- It became apparent by comparing coal and coke compositions that less volatile and thermally stable inorganic compounds transfer from coal into coke.
- Carbotest tests showed that ash content and alkalis significantly affect the quantity of by-products (**Figure 140**).

**Figure 141** presents ash analysis of samples broken into fractions by grain-size distribution. It shows that the composition of various grain sizes is very similar. Anomalies of alkali-balances demonstrated from ash content can in no way be justified by possible grain size distribution differences of samples.

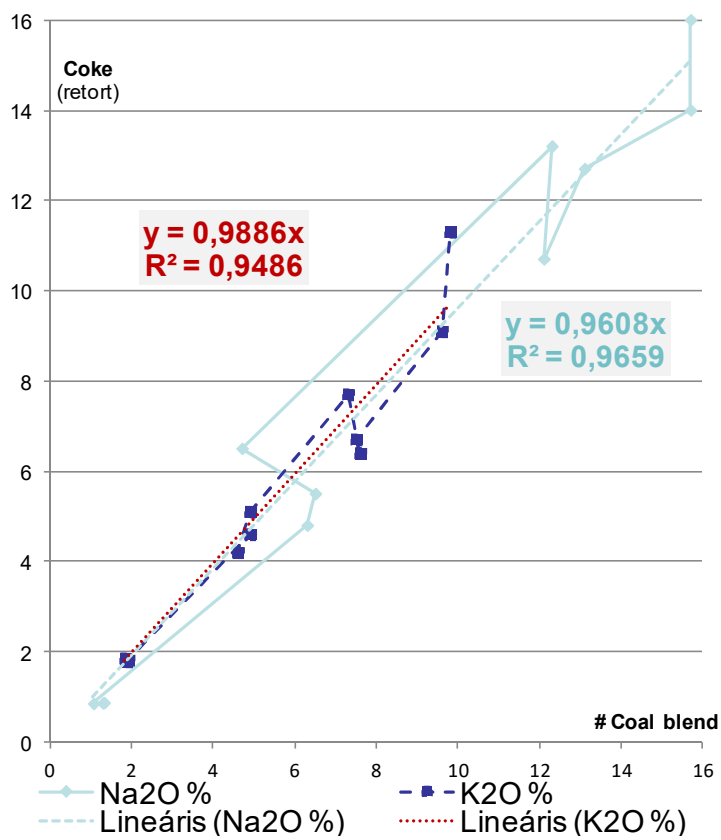


**Figure 138** Testing of the change in Na and K-content of coal and coke

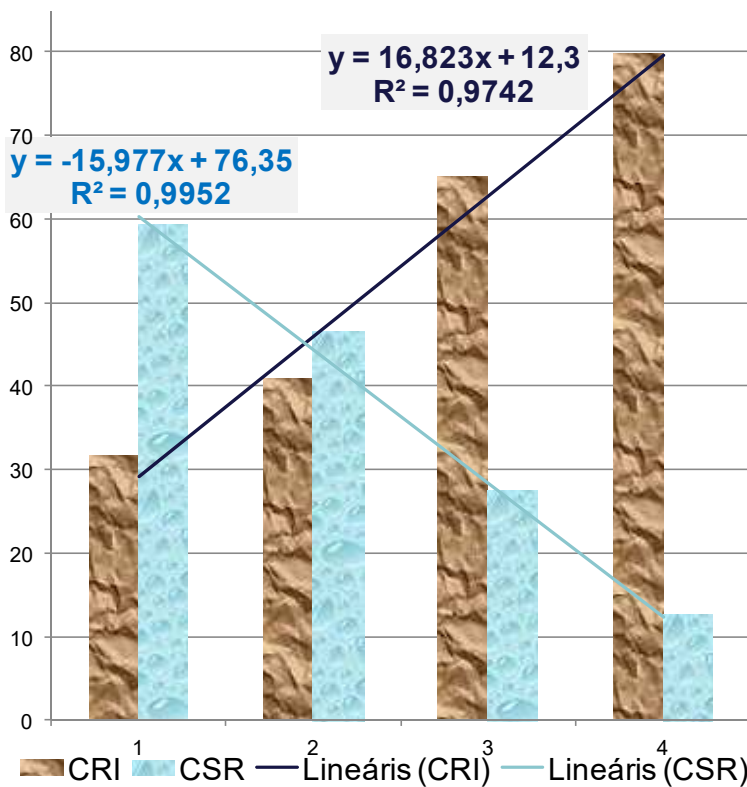


**Figure 139** Effect of ash content on coke quality

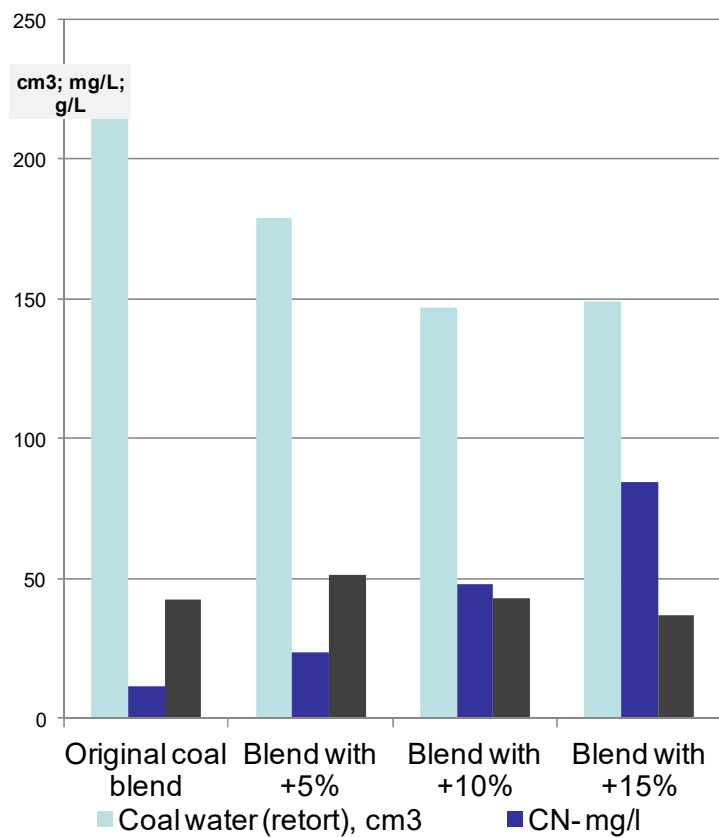


**Figure 140** Effect of the increase in alkalis on by-products

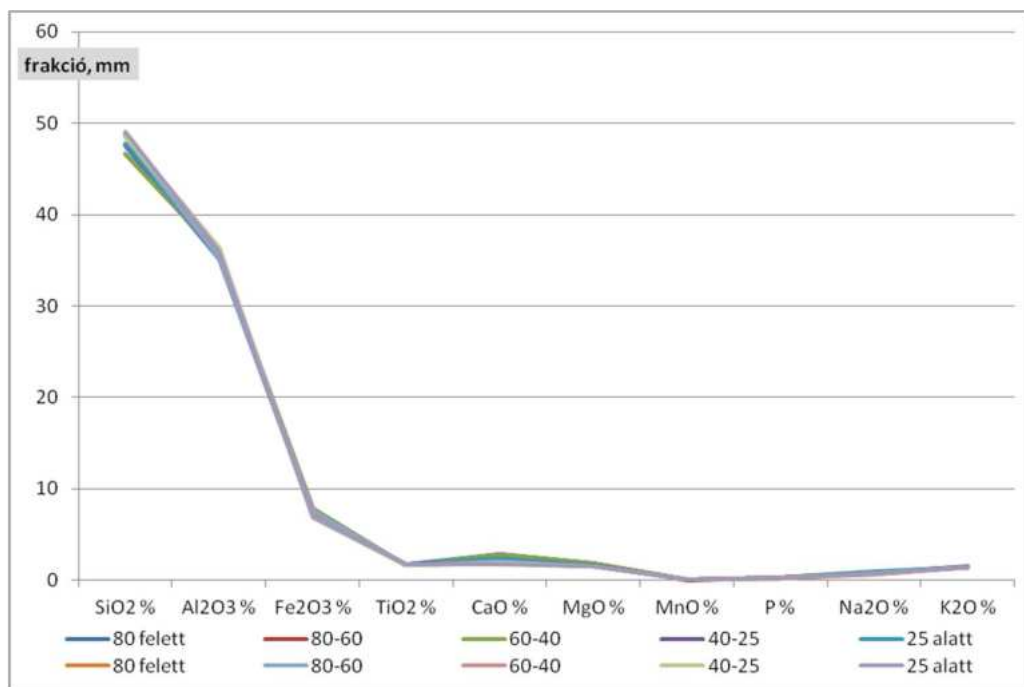


**Figure 141** Analysis of ash in cokes of various size fractions

### 2.3.1.3.5 Laboratory furnace trials with two-zone inductively heated reactor (BFI)

For investigation of the alkali impact especially on BF coke, laboratory scale trials with a two-zone coke bed reactor have been performed at BFI. Main part of the coke bed reactor is a vertical quartz glass reaction tube with 80 mm outer diameter, in which the coke bed is located and through which a predefined gas stream flows in upward direction.

The quartz glass reactor is built-up within a frame of aluminium profiles and consists of a gas-tight top container for charging and a discharge container with a moving bottom, in which the bulk material and coke is discharged after the trial. There are several gas inputs at the lower end of the reaction tube and at the discharge container, by which purge gas ( $N_2$ ) or the reaction gas ( $CO/CO_2/N_2/H_2$ ) is supplied. The product gas is taken from the top container for gas analysis. The heat energy is brought in by inductive heating of the carbonaceous material inside the quartz glass tube (e. g. coke pieces). The two-zone coke bed reactor provides two independent inductively heated temperature zones (two induction coils), simulating the evaporation of alkali compounds at the higher temperature zone (zone 1; lower part) and their condensation at the lower temperature zone (zone 2; upper part). In **Figure 142** a schematic view of the experimental set-up for the 2-zone coke bed reactor is presented. A photo of the experimental set-up for the two zone BFI coke bed reactor with the 25 kW HF-generator for zone 1 (left) and the quartz glass tube reactor with 10 kW HF-generator for zone 2 (right) is shown in **Figure 143**.

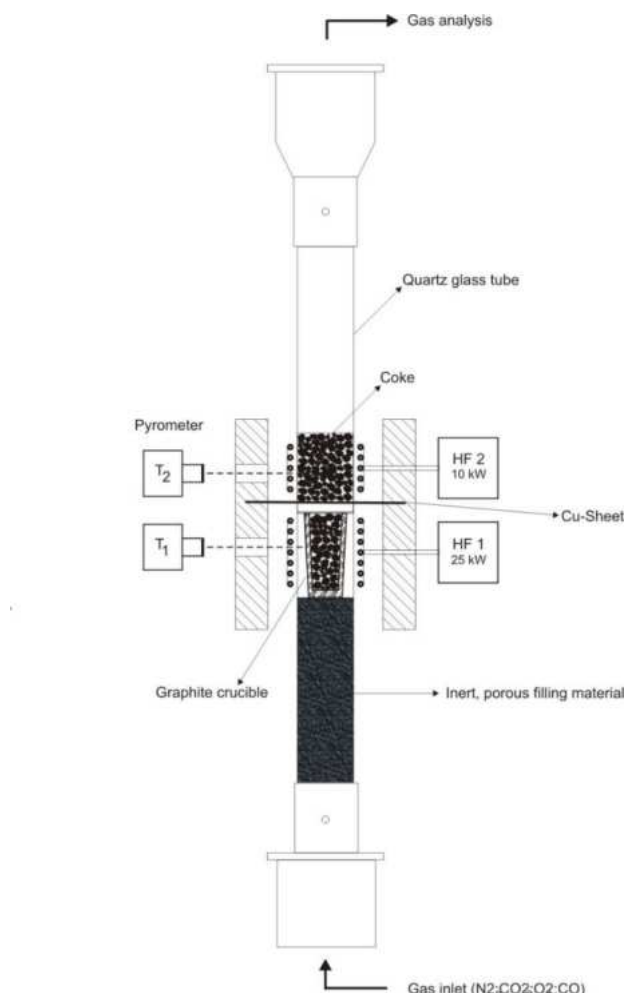


**Figure 142** Schematic view of the experimental set-up for the 2-zone coke bed reactor used for laboratory trials on the alkali impact on coke



**Figure 143** Experimental set-up for the two zone BFI coke bed reactor; left: quartz glass tube reactor with two induction coils; right: 25 kW HF-generator for zone 1

A new purchased a 25 kW high-frequency-(HF)-generator and inductor (120 mm diameter; and 120 mm height) was used for heating of the higher-temperature zone 1 (lower part of reactor). For heating of the lower-temperature zone 2 another HF-generator with 10 kW power was used combined with an inductor with 120 mm diameter and 60 mm height. For avoiding mutual disturbance of the HF-Generators, a shielding of the two induction coils with a 0.5 mm copper sheet and a sufficient distance (1-winding) between the induction coils is crucial. Both HF-Generators and the inductors are water cooled by a common cooler. They operate at a frequency of around 1000 kHz, which gives enough flexibility for inductive heating of a wide range of coke particle sizes down to 2 mm.

The temperature of the different coke bed zones in the reactor is controlled by dedicated high-temperature (HT) pyrometers (**Figure 144**), in connection with a controller. Each HF-generator (and each temperature zone) will be controlled by an own pyrometer, whose measurement beam leads through the middle of each induction coil (in between the copper windings) with the measurement spot being located at the coke (or graphite) surface within the quartz glass tube.



**Figure 144** HT-Pyrometer for temperature control

The lower end of the quartz glass tube is filled with an inert, porous filling material (burnt clay granules), which enables the gas flowing through the filling material. On this, a graphite crucible filled with a coke sample (and additives) is placed. The graphite crucible acts as a heating element to heat up the contained coke sample to the target temperature of 1300°C in the alkali evaporation zone (Zone 1). Here a small gap between the heated graphite crucible and the quartz glass tube assures sufficient thermal insulation and prevents damage to glass tube, whose operating temperature only is around 1200°C. Gas flow is forced through the graphite crucible by equally distributed drillings (8 mm) at the outer wall combined with a quartz cotton sealing of the gap between graphite crucible and quartz glass tube at the top end of the crucible.

**Figure 145** shows the two-zone reactor with inductive heating in operation. The heated graphite crucible filled with coke is located in the lower heating zone (Zone 1: alkali evaporation zone; 1300°C) and just coke is located in the upper heating zone (Zone 2: 800°C).



**Figure 145** Two-zone reactor with inductive heating in operation - Heated graphite crucible in the lower heating zone (Zone 1: alkali evaporation zone; 1300°C) and coke in upper heating zone (Zone 2: 800°C)

#### *Preparation of coke samples*

The aim is to prepare industrial coke samples in a way that potassium is added in amounts assumed to be present within the BF at the alkali cycling zone. In order to evaluate the influence of different alkali loads, even different amounts of potassium have been applied to the coke. For the coke, a metallurgical coke sample from VASD has been used, which was crushed and sieved to an average particle size of around 20 mm. The coke was dried at 105°C for > 12 h before further utilisation.

The potassium was applied to the coke by immersion into different potassium carbonate solutions

( $K_2CO_3$ ) for 30 minutes. Afterwards, the treated coke samples were dried at 105°C for > 12 h. After initial tests for determination of the specific amount of  $K_2CO_3$  pick-up, it was decided to use 3 different  $K_2CO_3$  solutions for the K pre-treatment, with the given target values of  $K_2O$ -load in the BF (**Table 22**).

**Table 22** Parameters for K pre-treatment of coke

Concentration of $K_2CO_3$ solution for coke pre-treatment in g/l	Target values of $K_2O$ -load in the BF in $K_2O/t$ HM (hot metal)	Target percentage of $K_2O$ in coke *	Target percentage of K in coke *
1014	24	2.4 %	2.0 %
338	8	0.8 %	0.7 %
169	4	0.4 %	0.3 %

\* assuming that all  $K_2O$  / K is found on coke; with 359 kg coke /t HM [45]

For the trials on inhibition of alkali circulation, an additional coke pre-treatment with kaolin slurry was applied (see description at Task 2.2).

#### *Performance of the trials with the two-zone reactor*

For the trials, the coke pieces (if applicable: with K pre-treatment) were placed in the graphite crucible (zone 1) together with an iron carrier, which was placed in the open space between the coke pieces. The iron carrier is used to simulate the presence of iron oxide(s) and metallic iron (after reduction) as in the industrial BF. In most of the trials hematite iron ore was used. Only for a series of four trials iron hydroxide was used with the intention to release the chemically bound  $H_2O$  and in this way to vary the  $H_2O$  concentration in the process gas. The rest of the coke was placed in the lower temperature zone (zone 2) above the graphite crucible directly within the quartz glass tube. The average input coke amount (for all trials) was 53 g within the graphite crucible (zone 1) and 225 g within the upper lower temperature zone (zone 2).

The input gas into the two-zone reactor was a simplified synthetic BF top gas (dry). The mixture was prepared by a gas mixing station from the pure components. The input gas composition is given in **Table 23**. The amount of the input gas flow in the reactor was 30 Ndm<sup>3</sup>/h.

**Table 23** Input gas composition for two-zone reactor trials (synthetic BF top gas)

Gas component	CO	$CO_2$	$H_2$	$N_2$
Amount in Vol.-%	24	26	3 / 5	Rest

Kaolin as coke additive has been applied for the trials on inhibition of alkali circulation (Task 2.2). In these cases, all the coke in both zones was coated with the same amount of kaolin. For some trials, further the input  $H_2$  concentration was varied starting from the base value of 3 Vol.-%  $H_2$  to 5 Vol.-%. The experimental parameters for all conducted trials in the 2-zone inductively heated fixed bed reactor are listed in **Table 24**. The table also includes the trials concerning Task 2.1 (Development of online-Tool for determination of alkali accumulation in BF) and Task 2.2 (Inhibition of alkali circulation), which are described in chapters 2.3.2.1.3 and 2.3.2.2.4.

**Table 24** Experimental parameters for trials in the 2-zone inductively heated fixed bed reactor

<b>Trial No.</b>	<b>Coke pretreatment with K<sub>2</sub>CO<sub>3</sub> solution [conc. of solution]</b>	<b>Corresponding target amount of K<sub>2</sub>O [kg K<sub>2</sub>O/t HM]</b>	<b>Coke additive</b>	<b>Additive (iron carrier) to graphite crucible</b>	<b>H<sub>2</sub> input in Vol.-%</b>	
V1	Without pretreatment	0	none	Hematite ore (ca. 50 g)	3 %	
V2	1014 g/l	24				
V3	338 g/l	8		Iron hydroxide (ca. 25 g)		
V4	169 g/l	4				
V5	Without pretreatment	0				
V6	1014 g/l	24				
V7	338 g/l	8				
V8	169 g/l	4				
V9	Without pretreatment	0		Kaolin (1x), ca. 1.5 %	Hematite ore (ca. 50 g)	
V10	1014 g/l	< 24		Kaolin (3x), ca. 5 %		
V11	Without pretreatment	0		Kaolin (3x), ca. 5 %		
V12	1014 g/l	< 24		Kaolin (1x), ca. 1.5 %		
V13	1014 g/l	24		None		
V14	1014 g/l	< 24		Kaolin (3x), ca. 5 %	5 %	
V16	Without pretreatment	0	none		3 %	
V17	Without pretreatment	0			5 %	

The temperature settings have been 1300°C at the (lower) alkali evaporation zone (zone 1) and 800°C at the (upper) zone (zone 2), where gasified alkali compounds are condensed again. The duration of one trial in the two-zone reactor is around 60 Minutes (Acquisition of one spectrum by the FTIR takes around 3 min).

During the trials, the process gas composition was constantly measured by a FTIR spectrometer for the main compounds CO, CO<sub>2</sub>, N<sub>2</sub> as well as for the minor compounds NH<sub>3</sub>, HCN and CH<sub>4</sub>. Especially NH<sub>3</sub> and HCN are investigated in this project as key components for assessment of the amount of circulating alkali components within the industrial BF.

After each trial, the coke both from zone 1 and zone 2 has been collected separately, weighed and analysed in terms of its K content.

#### *Assessment of coke properties exposed to different alkali loads at BF conditions*

The aim of the two-zone trials in the frame of task 1.3 is to assess the alkali impact on the coke properties at different alkali loads. Main coke property affected by alkali components and being able to be assessed even based on a small sample size is the coke reactivity. The reactivity was assessed by thermogravimetric analysis (TG analysis) of the coke from lower temperature zone 2. Here, a condensation of evaporated alkali compounds from the high temperature zone 2 as one step of an alkali cycle was expected.

For TG analysis, the sample coke was crushed to an average particle size of 1 mm. The sample mass used for TG analysis was around 500 mg. The parameters for TG analysis (heating rate and gas stream) have been similar to the procedure at LTU in order to ensure maximum comparability (refer to chapter 2.3.1.3.3). In **Figure 146** the TG equipment at BFI, as well as the applied heating programme and gas stream is presented.

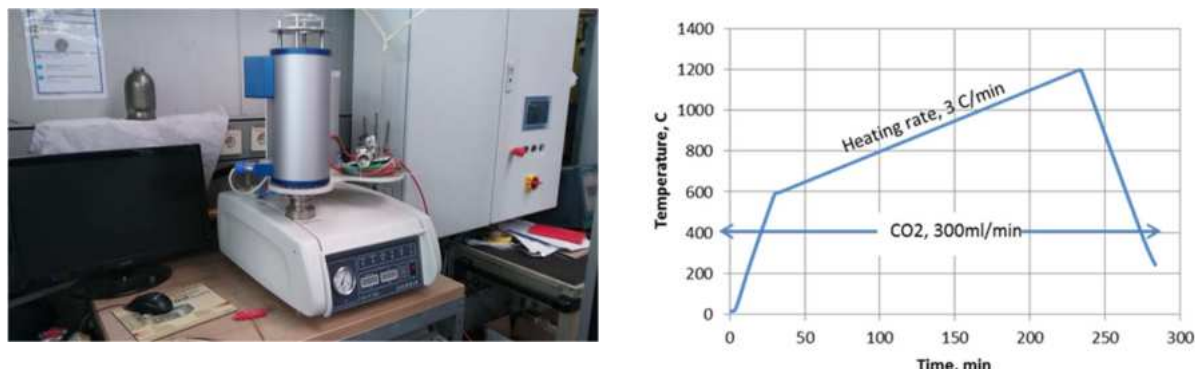


**Figure 146** Coke analysis by thermogravimetry. Left: TG equipment at BFI; Right: Applied heating programme and gas stream (similar to LTU procedure)

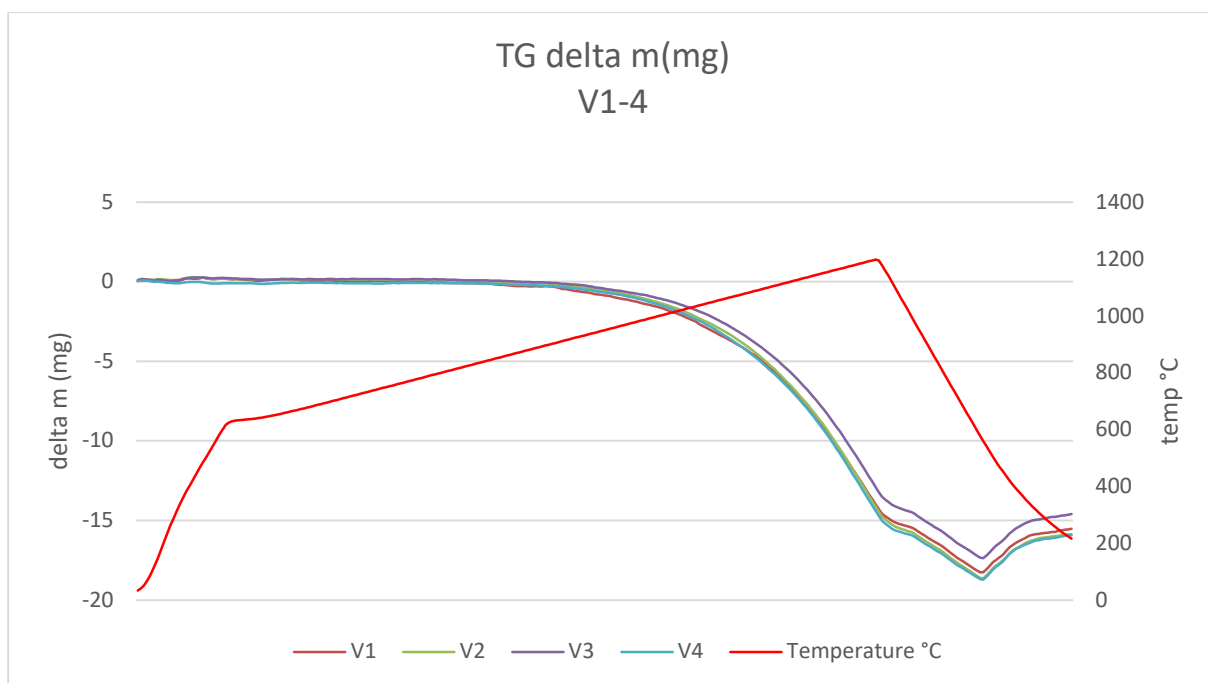


**Figure 147** Thermogravimetric measurement – Mass loss and temperature vs. time (V1-4)

A typical diagram of mass loss and temperature vs. time for trials V1-4 is presented in **Figure**

**147.** In spite of largely varying K load on the hot zone coke (zone 1), the variance between the different trials is low.

The coke reaction kinetics is assessed based on the determination of the activation energy  $E_a$  as described by LTU in chapter 2.3.1.3.3. A lower activation energy means a higher coke reactivity. The selected range considered for determination of the activation energy is between 880°C and 1150°C (**Figure 148**). The activation energy  $E_a$  finally is calculated as the slope of the double logarithmic plot of  $\ln k$  vs.  $1/T$ . This is exemplarily illustrated in **Figure 149**.

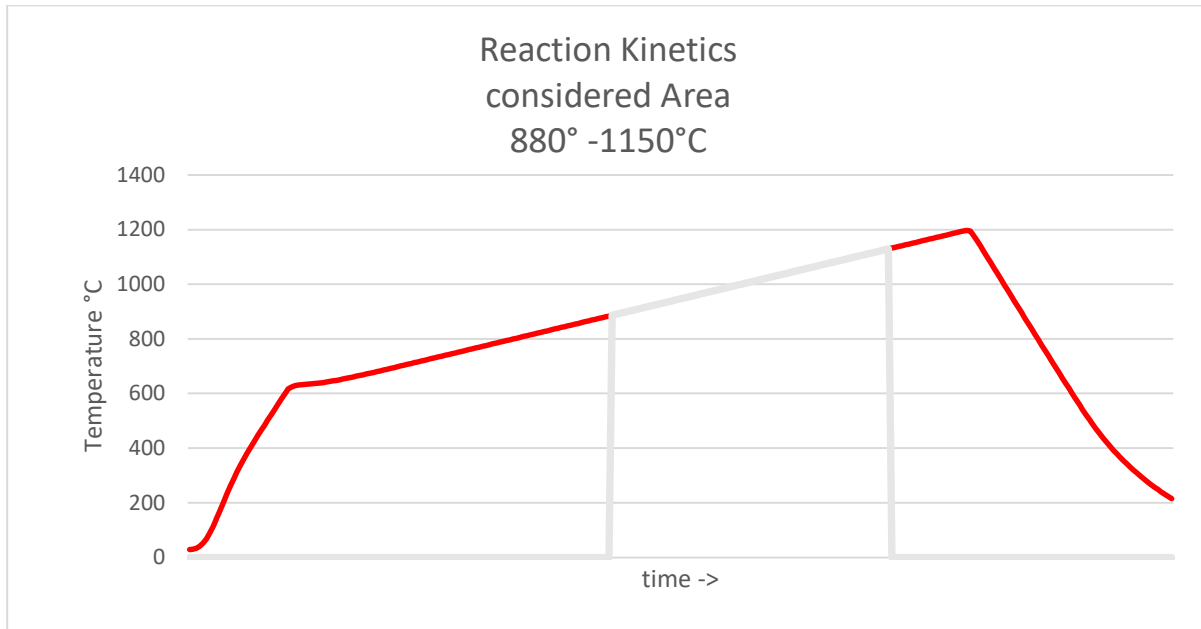


**Figure 148** Considered Range for determination of activation energy: 880° - 1150°C

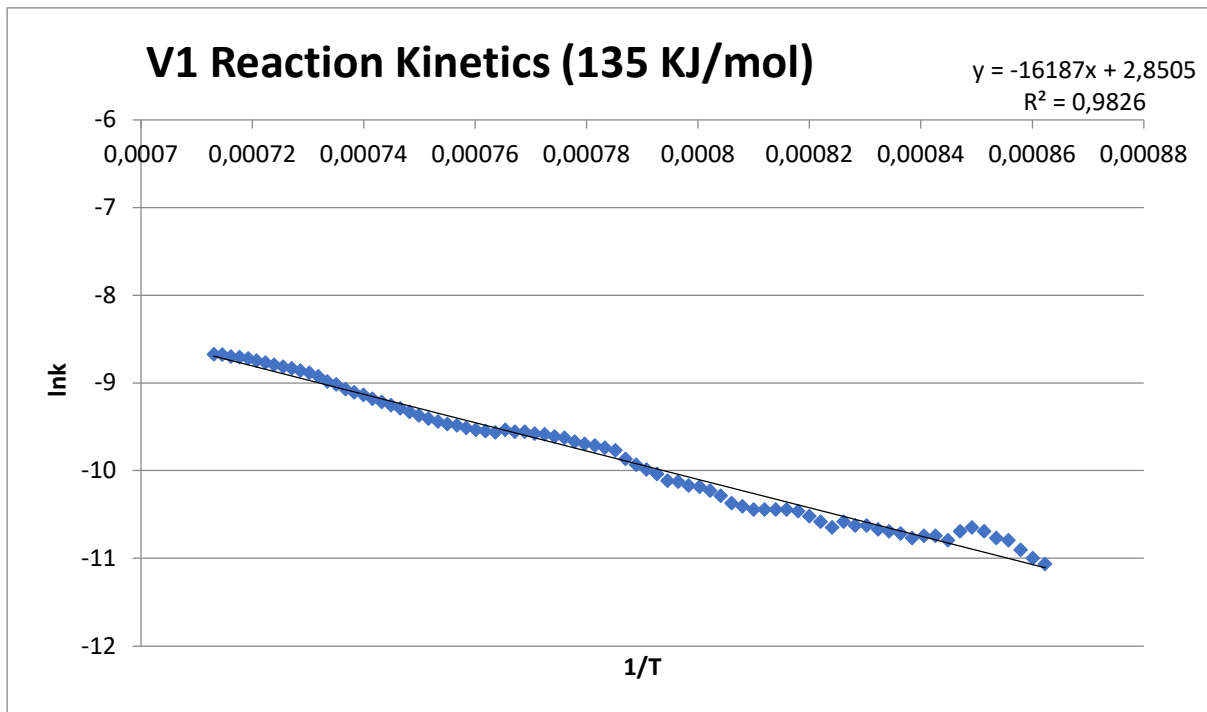


**Figure 149** Exemplary Arrhenius plot for determination of the activation energy  $E_a$  (V1)

The results of assessment of the activation energy are presented in **Table 25** and **Figure 150**. The calculated activation energies are quite scattered in a narrow range between 135 and 159 kJ/mol.

These values are in a comparable range with the results from coke samples excavated from the EBF (see chapter 2.3.1.3.3). But here in spite of the varying K load on the hot zone (zone 1) up to 2 % K, no significant increase and also no variation in K content at the lower temperature zone (zone 2) is observed. This means, only a low amount of evaporated K from zone 1 reaches the zone 2 within this experimental set-up. Reason for the negligible K carryover from zone 1 in the experimental reactor to zone 2 might be an insufficient gas stream between the two temperature zones or the insufficient condensation of the potassium compounds at the coke within zone 2, so that K may have been lost to other colder parts in the reactor.

The insufficient K condensation in zone 2 explains that no clear correlation is found between activation energy and the K content (load) of zone 1 (see **Figure 150**). Usually, with increasing K load a decreasing activation energy  $E_a$  would be expected, which is not observed here. The determined  $E_a$  values for V2-4 are located in a quite narrow range, which is just due to scattering caused by the evaluation procedure. The lower activation energy value of the V1 sample may be an outlier value.

To sum up the results, with the present experimental set-up no influence of different alkali loads in the "hot" zone 1 on the coke coke properties respectively the reactivity within zone 2 could be confirmed.

**Table 25** Assessment of coke reactivity - Overview on trial parameters and results

Trial Nr.	Kaolin pre-treatment	$K_2CO_3$ pretreatment of zone 1 coke; conc. of $K_2CO_3$ solution	K content of zone 1 coke in %	K content of zone 2 coke in %	Activation energy EA (in $KJ/mol^{-1}$ )
V1	none	none	0.17	0.16	135
V2	none	1014 g/l	1.96	0.17	150
V3	none	338 g/l	0.71	0.17	159
V4	none	169 g/l	0.54	0.17	155

# Alkali impact and Kaolin load on BF burden Material

## V1-4 Reaction Kinetics

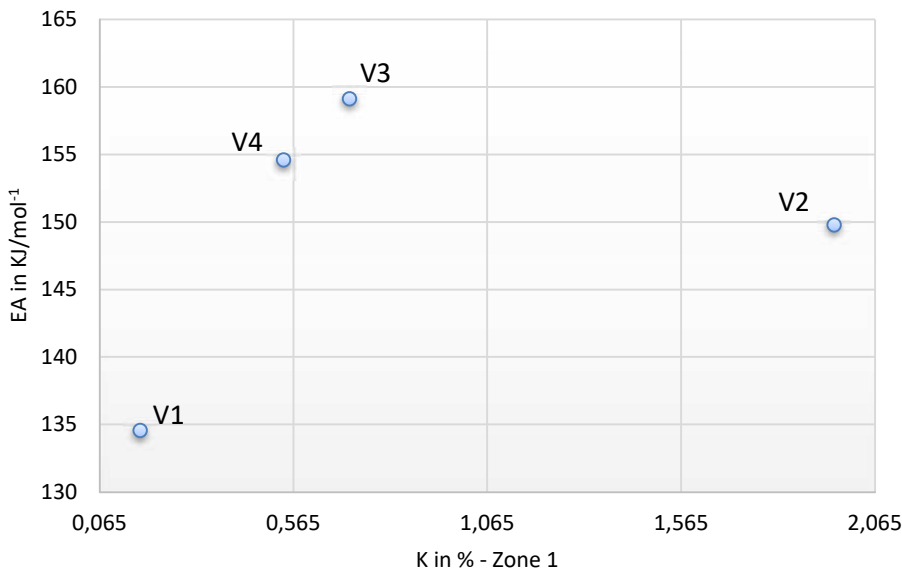


**Figure 150** Calculated activation energies Ea in correlation to K content of zone 1 coke

### 2.3.2 WP2 Methods for alkali control in the BF

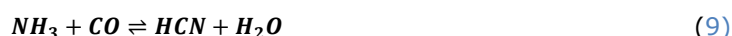
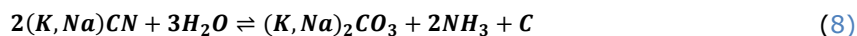
The main objectives with WP 2 are:

- Development of calculation /evaluation routine for the online top gas evaluation tool for determination of alkali accumulation in the different compared BF's based on NH<sub>3</sub> reaction efficiencies determined by laboratory trials
- Estimation of alkali accumulation within the BF and subsequently alkali load on coke during normal BF operation
- Development of novel methods for inhibition of BF alkali circulation by coke pre-treatment/coating using alkali absorbing additives or alkali absorbing mineral addition to the burden
- Investigation of the effect of BF slag composition on alkali removal capacity
- Development of a concept for improved adaption of BF operation with regard to improved alkali control in connection with the new developed online tool for determination of alkali accumulation

### 2.3.2.1 Task 2.1 Development on Online-Tool for determination of alkali-accumulation in BF

#### 2.3.2.1.1 Thermodynamic calculations concerning formation of NH<sub>3</sub> and HCN coupled to alkalis (SWERIM)

As gases move through the blast furnace (BF) their composition will change as they react and are exposed to different temperatures and the different burden materials. Therefore, the top gases in the BF should be dependent on the composition of material present in the BF. A theory is that the creation of NH<sub>3</sub> and HCN is directly connected to the alkali content in the BF through reaction (8) and (9) [48].



Thermodynamic calculations can show at what conditions NH<sub>3</sub> and HCN would be expected to form in the BF.

FactSage 7.2 was used by SWERIM to calculate if formation of NH<sub>3</sub> and HCN is thermodynamically favorable based on BF conditions and gas compositions from MS-measurements at SSAB in Oxelösund. The normal operation gas data from SSAB was given for dry gases so it had to be converted to wet gas using the H<sub>2</sub>O analysis from the MS measurements. The final input data is shown in **Table 26**.

**Table 26** Input data for calculations in FactSage.

	CO	CO <sub>2</sub>	N <sub>2</sub>	H <sub>2</sub>	H <sub>2</sub> O	NH <sub>3</sub>	H <sub>2</sub> S	C <sub>2</sub> H <sub>4</sub>	CH <sub>4</sub>	C <sub>3</sub> H <sub>6</sub>	C <sub>6</sub> H <sub>6</sub>	O <sub>2</sub>	SO <sub>2</sub>	SO <sub>3</sub>	HCN
mol/tHM	39259	46995	86711	5671	6663	2.7	1.1	594	7.1	6418	1885	177	0.01	177	3.9

Along the gas data, coke rate and top pressure was also used as input as shown in **Table 27**.

**Table 27** Input data for FactSage calculations.

Carbon per tHM	27517 mol/tHM
Top gas volume	194564 Nm <sup>3</sup> /h
Top pressure	1.069 atm

The calculations were performed for temperatures ranging from 50 to 2400°C to cover all the possible temperature conditions in the BF that usually varies from approximately 100°C in the top up to 2300°C in the raceway flame for a normal BF [4]. Addition of different levels of alkali (K<sub>2</sub>O(s)) and Na<sub>2</sub>O(s)) was done ranging from 1 kg alkali/tHM up to 7 kg alkali/tHM with different ratios of K<sub>2</sub>O/Na<sub>2</sub>O for certain calculations. The amounts used was taken from two previous studies on alkali input at BF [50], [51]. The results where recalculated to volume percentage from mole.

Calculations were first conducted for a system without alkalis. **Figure 151** show how the amount C(s) decreases as the temperature and gas volume in the system increases. The point where CO<sub>2</sub>(g) and C(s) start to decrease coincide with an increase of CO(g) at a temperature close to the point when the Boudouard reaction start [52]. The same gas distribution seen in the top gas at

91°C for CO(g) and CO<sub>2</sub>(g) was corresponding to 600°C and 660°C in the FactSage calculations. This is indicating that equilibrium has not time to form in the BF. Further, HCN(g) is only present at the highest temperatures considered for the calculations, indicating that HCN(g) may exist at the tuyere level/raceway of the BF but is not stable at the lower temperatures further up the BF.

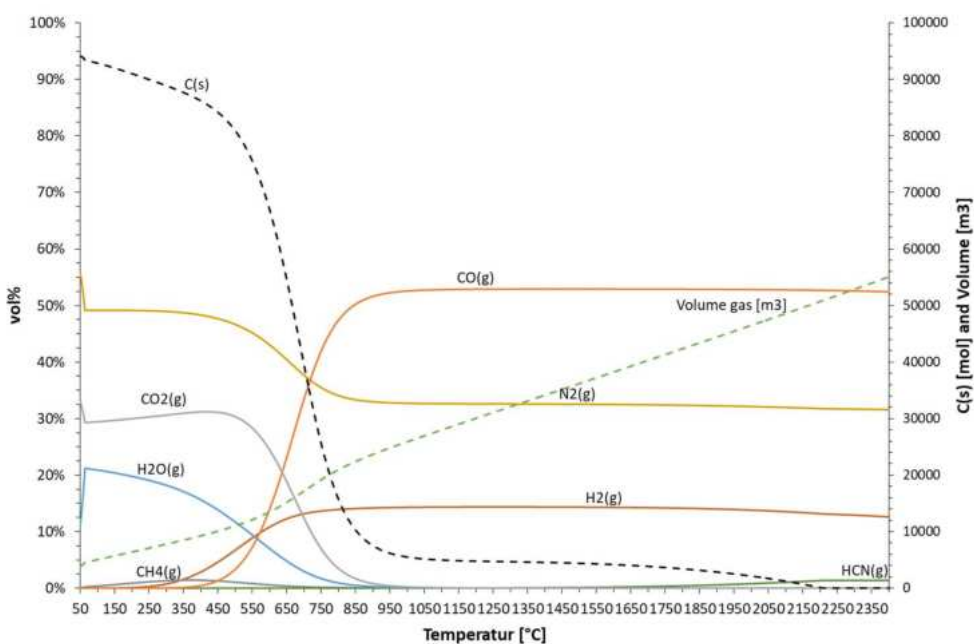


**Figure 151** Gases present over the temperature range, gas volume and mass C(s) for a system without alkalis.

Looking more closely at NH<sub>3</sub>(g) formation, **Figure 152** reveals that very little such gas is formed in the system with a maximum of 62 ppm at approximately 475°C. Measured concentrations of NH<sub>3</sub>(g) in top gas with MS at BF No. 4 was around 14 ppm at 91°C. The amount NH<sub>3</sub>(g) calculated by FactSage in the temperature range 600-660°C was around 35-40 ppm, which is higher than the measured concentrations but still in the same order of magnitude.

The amount HCN(g) measured in the top gas was 20 ppm at 91°C and compared to levels seen in **Figure 152**, the maximum HCN(g) formed was approximately 20 000 ppm at the highest temperature range. The amount HCN(g) is seen to decrease as temperature drops and is not stable at the top gas temperatures or in the 600-660°C range like NH<sub>3</sub>(g). The fact that HCN(g) was detected with the MS in the top gas at BF No. 4 in Oxelösund indicates that the gas flow is fast in the BF and that equilibrium is not achieved before the gas reaches the top. This is in contrast to the measurements at the EBF as no HCN was detected, only NH<sub>3</sub>. Thus, the gas composition with respect to NH<sub>3</sub> and HCN can be closer to equilibrium here than in an industrial furnace. Moreover, the calculations implies that the presence of HCN(g) was independent from the presence of NH<sub>3</sub>(g) which is in contrast to equation (9). No potassium source was included in the first calculations as input data was from top gases and the inclusion of potassium could possibly lead to the formation of KCN(g).

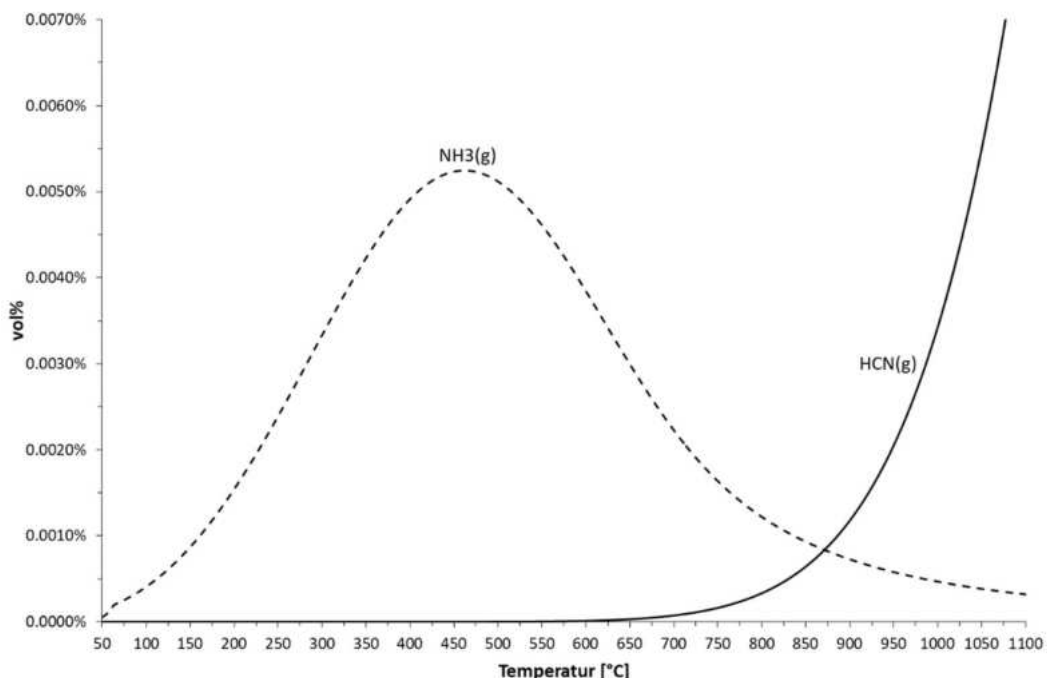


**Figure 152**  $\text{NH}_3(\text{g})$  and  $\text{HCN}(\text{g})$  present in the system at lower temperature.

The addition of alkali to the calculations lead to the formation of several alkali species e.g.  $\text{KCN}(\text{g})$  or  $\text{Na}_2\text{CO}_3(\text{s})$ . It did not affect the equilibrium amount of  $\text{NH}_3(\text{g})$  or  $\text{HCN}(\text{g})$  for any calculation at lower temperatures nor did it affect the major gases in any visible way. **Figure 153** shows that at lower temperature, the levels of  $\text{NH}_3(\text{g})$  and  $\text{HCN}(\text{g})$  did not change but alkali gas was now also formed in the process compared to **Figure 152**. The amount of alkali gases depended on the input of alkali to the system.

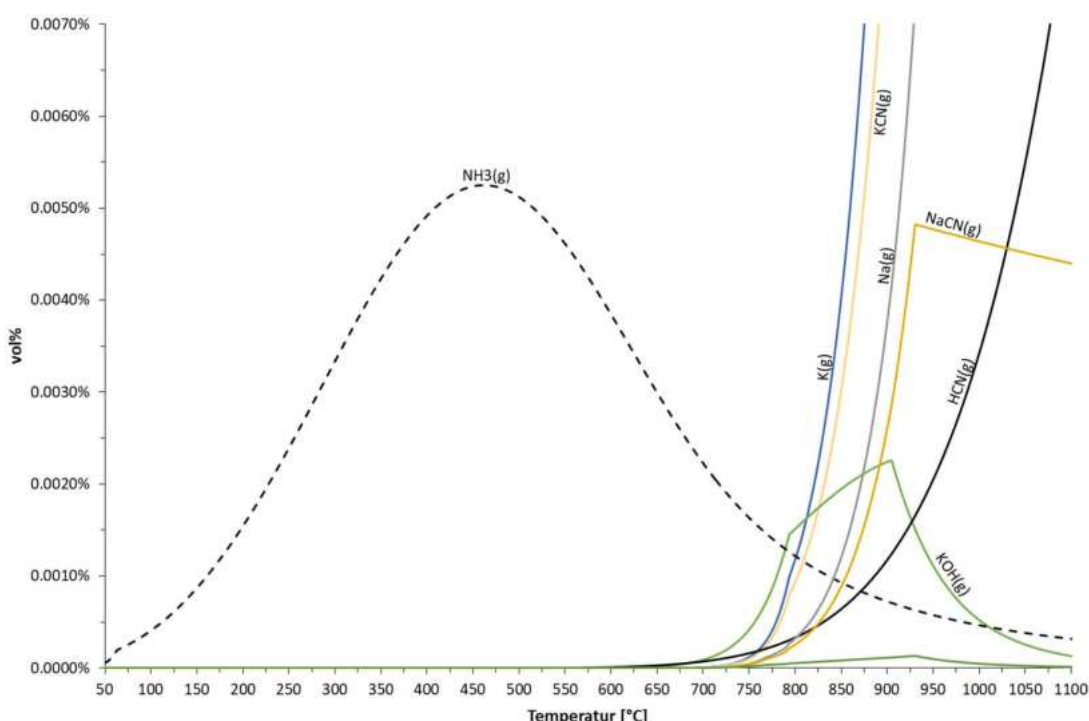


**Figure 153**  $\text{NH}_3(\text{g})$  and  $\text{HCN}(\text{g})$  formed when 3 kg  $\text{K}_2\text{O}/\text{tHM}$  and 1 kg  $\text{Na}_2\text{O}/\text{tHM}$  was added.

Looking closer at the formation of  $\text{HCN}(\text{g})$  and how it varies with different alkali loads (**Figure 154**) reveals that a dependence is only seen at temperatures above 2200°C. For temperatures below 2200°C, the curves merge and become one line. The formation of  $\text{HCN}$  seem to be negative-

ly correlated to the alkali load, indicating that the alkali added to the system gave less HCN(g) at higher temperatures as small amounts of KCN(g) or NaCN(g) formed instead.

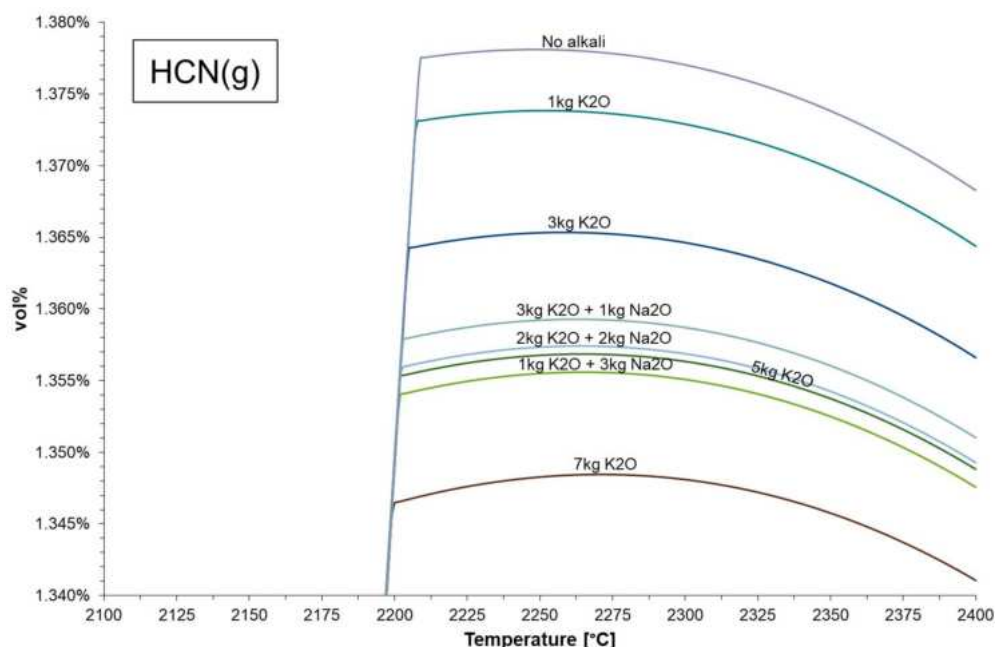


**Figure 154** HCN(g) formed in all calculations.

Concluded from the thermodynamic calculations on NH<sub>3</sub> and HCN formation in BF is that the presence of alkali in the system did not affect the formation of NH<sub>3</sub>(g) but lowered the formation of HCN(g) at temperatures above 2200°C. Nevertheless, alkalis did not affect the equilibrium amount of HCN(g) below that temperature. Moreover, the presence of HCN and NH<sub>3</sub> at top gas conditions is not thermodynamically favored which implies that equilibrium is not reached as both NH<sub>3</sub> and HCN in ppm levels were measured at BF No.4 in Oxelösund.

### 2.3.2.1.2 Thermodynamic calculations on NH<sub>3</sub> and HCN formation (BFI)

Initially BFI has performed thermodynamic calculations with the Software FactSage concerning the formation of ammonia (NH<sub>3</sub>) and hydrogen cyanide (HCN) in conjunction with alkali components in the BF.

These calculations were performed in order to reveal the possible influence of relevant side parameters on NH<sub>3</sub> or HCN formation. For this purpose, calculations of the thermodynamic equilibrium of a typical blast furnace top gas composition have been performed. The molar gas composition taken into consideration is given in **Table 28**.

**Table 28** BF top gas composition taken into consideration for thermodynamic equilibrium calculations

Component	CO	CO <sub>2</sub>	H <sub>2</sub> O	CH <sub>4</sub>	NO <sub>2</sub>	NO	H <sub>2</sub> S	C <sub>2</sub> H <sub>2</sub>	HCl	N <sub>2</sub>
Amount in mol	23	24	5	1	0.01	0.01	0.01	0.01	0.01	47

Even in the above mentioned top gas without the presence of alkali components the thermodynamic equilibrium calculations indicate the formation/presence of NH<sub>3</sub> and HCN. The most relevant side parameters have been varied, like the temperature, the amount of H<sub>2</sub>O in top

gas/furnace gas, and the partial pressure of hydrogen ( $H_2$ ). The most pronounced influence on the amount of formed  $NH_3$  and  $HCN$  are attributed to the temperature and the hydrogen activity. In **Figure 155** respectively **Figure 156** the calculated amount of  $NH_3$  and  $HCN$  (mole, log scale) are presented in dependency on the temperature respectively the hydrogen activity ( $pH_2$ ; log scale). In the temperature range of 100 to 200°C the amount of  $NH_3$  decreases strongly with rising temperature, while  $HCN$  increases up to a maximum at 600°C and then decreases again (**Figure 155**). Both, the  $NH_3$  and the  $HCN$  amount increase strongly with rising hydrogen activity, while the slope of the  $HCN$  amount is significantly lower than that of the  $NH_3$  amount (**Figure 156**). These results indicate the importance also to consider temperature values at the relevant reaction zones and (measured) hydrogen values in the evaluation of the BF top gas analysis for quantification of accumulated alkali components in the BF.

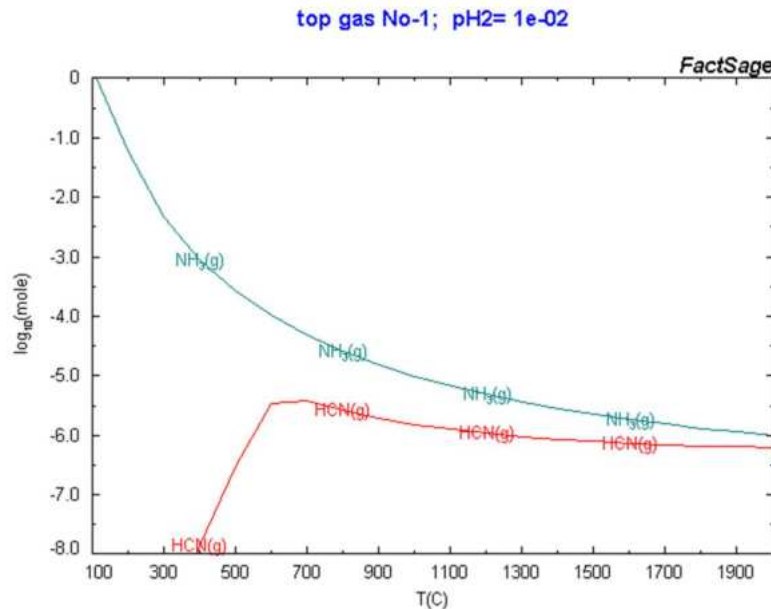


**Figure 155** Calculated amount of  $NH_3$  and  $HCN$  (mole, log scale) in dependency on the temperature

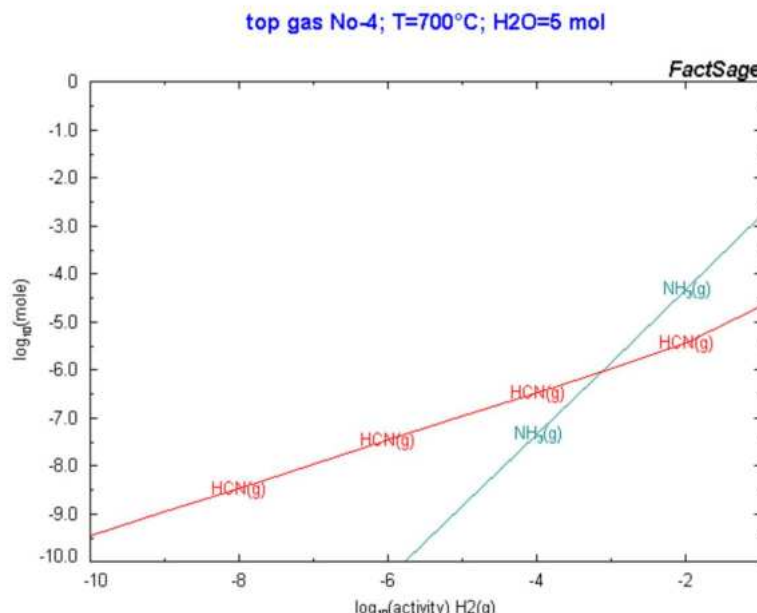


**Figure 156** Calculated amount of  $NH_3$  and  $HCN$  (mole, log scale) in dependency on the hydrogen activity (log scale)

Afterwards, the influence of alkali components on the formation of NH<sub>3</sub> and HCN in the blast furnace has been assessed by thermodynamic calculations. KCN was selected as alkali component. At relatively low temperature of 700°C (where previously the maximum of HCN was calculated), and an assumed hydrogen partial pressure of 1e-02 bar, the amount of KCN was varied. The result of these calculations is presented in **Figure 157**, where the amount of HCN and NH<sub>3</sub> in the BF top gas (y-axis: logarithmic, mole) is correlated to the amount of KCN (x-axis: Alpha = mol KCN).

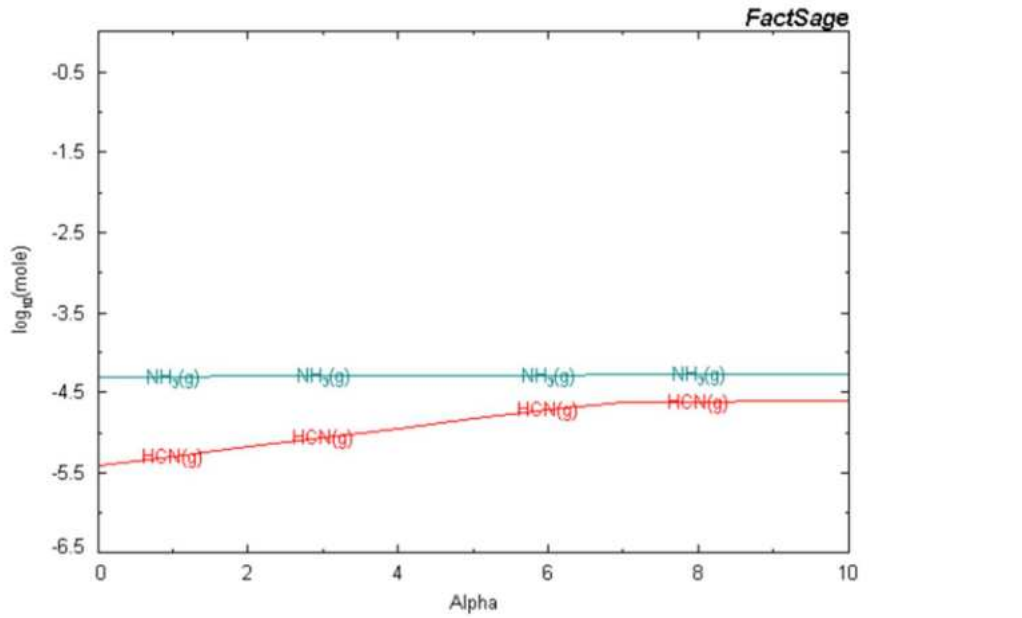


**Figure 157** Calculated amount of HCN and NH<sub>3</sub> in BF top gas in correlation to the amount of KCN (Alpha = mol KCN)

The thermodynamic equilibrium calculations indicate that the amount of formed HCN(g) slightly increases with rising content of KCN (up to 6 mol KCN), while the amount of formed NH<sub>3</sub>(g) only increases to a very low extent at the same conditions. This leads to the assumption, that HCN(g) measured within the BF top gas might be more important as indicator component for circulating alkali components than NH<sub>3</sub>(g). This initial assumption is clarified by further thermodynamic calculations.

#### *Deepened thermochemical calculations for quantification of NH<sub>3</sub> and HCN*

Afterwards deepened thermodynamic equilibrium calculations on the correlation between NH<sub>3</sub> (and HCN) and alkali components in the blast furnace have been performed by BFI. The aim is a better quantification of the formed NH<sub>3</sub> or HCN in connection with the assumed alkali load in form of KCN, and in this way to contribute to the development of a calculation routine for determination of the amount of accumulated /circulating alkali components derived from the BF top gas analysis. The impact of sodium compounds has not been calculated here due to the lower amount and hence the expected lower contribution to the NH<sub>3</sub> and HCN formation.

The base data used for the calculations are as follows:

- Top gas composition – main aspects (based on [45])
  - HC's: 250 mg/Nm<sup>3</sup> -> are calculated as CH<sub>4</sub> -> 0.04 % (rounded)
  - CO/CO<sub>2</sub> ratio in final top gas (ca. 200°C): Calculated based on CO<sub>2</sub> / (CO + CO<sub>2</sub>) = 0.4 (since a higher stability of the trace compounds NH<sub>3</sub> and HCN is expected at more

- reducing conditions, here a lower gas utilisation is assumed compared to most modern BF's)
- Hydrogen: 1 to 3 Vol.-%
  - Amount of top gas: 1500 Nm<sup>3</sup>/t hot metal (comparable to VASD BF's)
  - Alkali load: up to 8 kg K<sub>2</sub>O/t hot metal

The equilibrium calculations were performed with the Software FactSage® separately for seven hypothetic temperature zones in the blast furnace from 1800°C near the raceway to 200°C in the final top gas. For simplification, no gas transfer between the different zones was taken into account. The gas composition within the different temperature zones was assumed for the main components CO and CO<sub>2</sub> based on a typical course of the gas utilisation with temperature as presented in **Figure 158**.

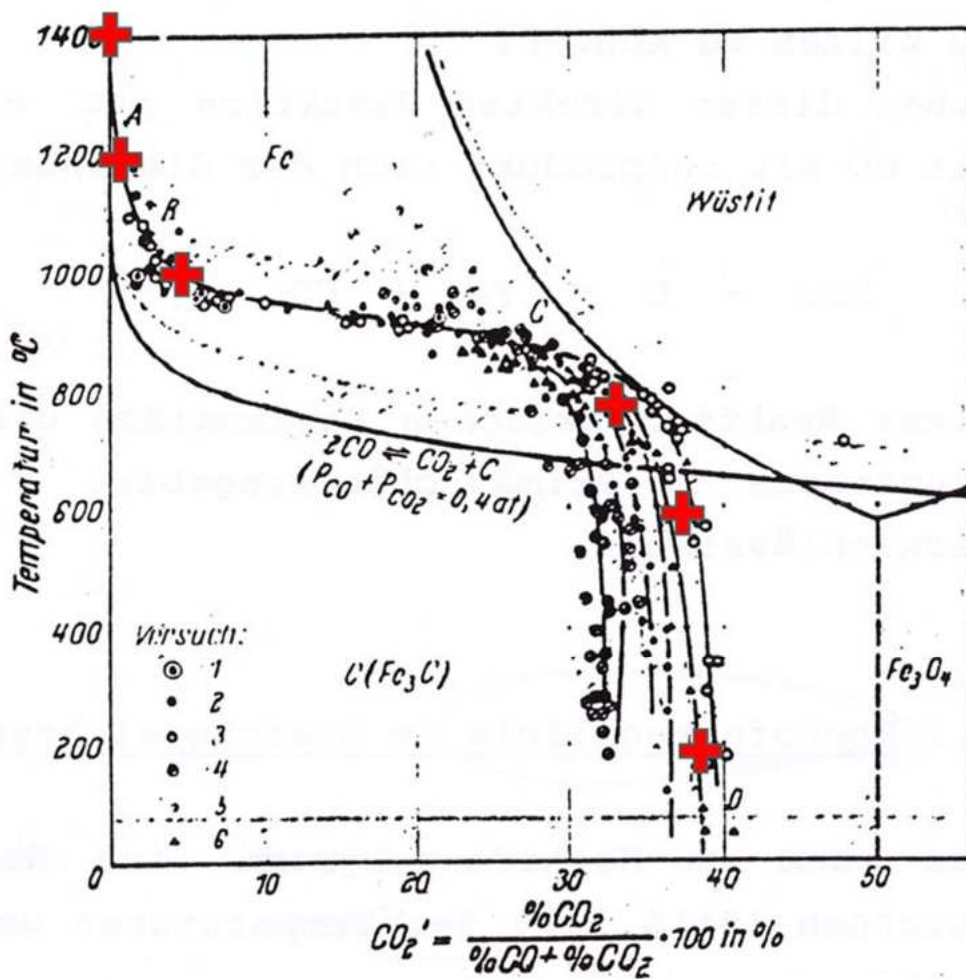


**Figure 158** Change of gas utilisation in the BF with temperature (in Baur-Glaessner diagram) [42]  
- red: selected BF zones

Following from this, in **Table 29** the input data for the thermodynamic calculations in terms of gas composition (equivalent to Vol-%) and pressure are listed for the different BF zones. An increasing pressure was taken into account from the top of the BF (Zone No. 1) to the zone near the raceway (Zone No. 7).

In order to assess the quantity of the formed gas components, the values from **Table 29** were converted to the reference basis on 1 t of hot metal (HM), which means 1500 Nm<sup>3</sup> top gas per t HM for the example of a BF with comparable size like VASD. These gas composition input data at different BF zones are listed in **Table 30**. The calculation pattern for the thermodynamic

equilibrium calculations with the varied parameters is presented in **Table 31**. For each temperature zone, 15 calculations were done including three “blocks” with varied (increasing) hydrogen concentration. Each “block” of calculations includes 5 varied (decreasing) KCN input amounts.

**Table 29** Gas composition input data at different BF zones (in mole; Basis: 100 mole of main components N<sub>2</sub>, CO, CO<sub>2</sub>)

BF zone No.	1	2	3	4	5	6	7
Temperature in °C	200	600	800	1000	1200	1400	1800
Final P (atm)	1	1.5	1.5	2	2	2	2.5
N <sub>2</sub>	55	55	55	55	55	55	55
CO	28	28	31	43	44.6	45	45
CO <sub>2</sub>	17	17	14	2	0.5	0	0
H <sub>2</sub> O	0	0	0	0	0	0	0
H <sub>2</sub>	variable						
CH <sub>4</sub>	0.04	0.04	0.04	0.04	0.04	0.04	0.04
NO <sub>2</sub>	0.005	0.005	0.005	0.005	0.005	0.005	0.005
NO	0.005	0.005	0.005	0.005	0.005	0.005	0.005
H <sub>2</sub> S	0.01	0.01	0.01	0.01	0.01	0.01	0.01
HCl	0.005	0.005	0.005	0.005	0.005	0.005	0.005
HF	0.0005	0.0005	0.0005	0.0005	0.0005	0.0005	0.0005
KCN	variable						

**Table 30** Gas composition input data at different BF zones (in mole;  
Basis: 1 t of hot metal -> 1500 Nm<sup>3</sup> top gas / t HM)

BF zone No.	1	2	3	4	5	6	7
Temperature in °C	200	600	800	1000	1200	1400	1800
Final P (atm)	1	1.5	1.5	2	2	2	2.5
N <sub>2</sub>	36830	36830	36830	36830	36830	36830	36830
CO	18683	18683	20491	28929	29833	30134	30134
CO <sub>2</sub>	11451	11451	9643	1205	301	0	0
H <sub>2</sub> O	0	0	0	0	0	0	0
H <sub>2</sub>	variable						
CH <sub>4</sub>	27	27	27	27	27	27	27
NO <sub>2</sub>	3	3	3	3	3	3	3
NO	3	3	3	3	3	3	3
H <sub>2</sub> S	7	7	7	7	7	7	7
HCl	3	3	3	3	3	3	3
HF	0.3	0.3	0.3	0.3	0.3	0.3	0.3
KCN	variable						

**Table 31** Calculation pattern with varied parameters for the thermodynamic equilibrium calculations (each for all 7 BF zones)

Calculation No.	H <sub>2</sub> in Vol.-%	H <sub>2</sub> in mole/t hot metal	KCN equivalent to kg K <sub>2</sub> O/t HM	KCN in mole/t hot metal
No-01	1	670	8	170
No-02			6	127.5
No-03			4	85
No-04			2	42.5
No-05			0	0
No-06	2	1339	8	170
No-07			6	127.5
No-08			4	85
No-09			2	42.5
No-10			0	0
No-11	3	2009	8	170
No-12			6	127.5
No-13			4	85
No-14			2	42.5
No-15			0	0

As follows, the results of the thermodynamic equilibrium calculations are presented and discussed.

**Figure 159** shows the calculated amount of formed NH<sub>3</sub> for each BF reaction zone and the different input amount of H<sub>2</sub> and KCN. In the following **Figure 160** and **Figure 161**, the same facts are presented for HCN at different scales. In Figure 160, the scale of the vertical axis (Amount of HCN) is much larger than that for NH<sub>3</sub> (**Figure 159**), while **Figure 161** for comparison with NH<sub>3</sub> has the same scale.

The highest amount of ammonia (NH<sub>3</sub>) was calculated for BF zone 2 (600°C). Afterwards the amount strongly decreases to around 1/4 of the zone 2 value at zone 4 (1000°C) (see **Figure 159**). For HCN, only a negligible amount is calculated for lower temperature than BF zone 4 (1000°C), but the calculated HCN amount strongly increases with further increasing temperature. In **Figure 160** the scale of the vertical axis (Amount of HCN) allows to display the maximum HCN amount at zone 7 (1800°C), which is > 400x higher compared to that of zone 4 (1000°C) (see **Figure 161**). At lower temperature up to 800°C (zone 1 to 3), the calculated amount of NH<sub>3</sub> is higher compared to that of HCN. But beginning with 1000°C (zone 4) HCN becomes the much more dominant component compared to NH<sub>3</sub>.

**Figure 159** to **Figure 161** already give a good overview on the sensitivity of the calculated NH<sub>3</sub> respectively HCN amount either on the hydrogen content (which is the difference in height of the "5-column-blocks") or on the KCN (alkali) content (which is the increase of the calculated gas amount within one "5-column-block"). In any case, the influence of hydrogen content on the calculated amount of gas components is higher than the influence of a varied KCN content. This spread is even much larger for the calculated NH<sub>3</sub> amount compared to the HCN amount.

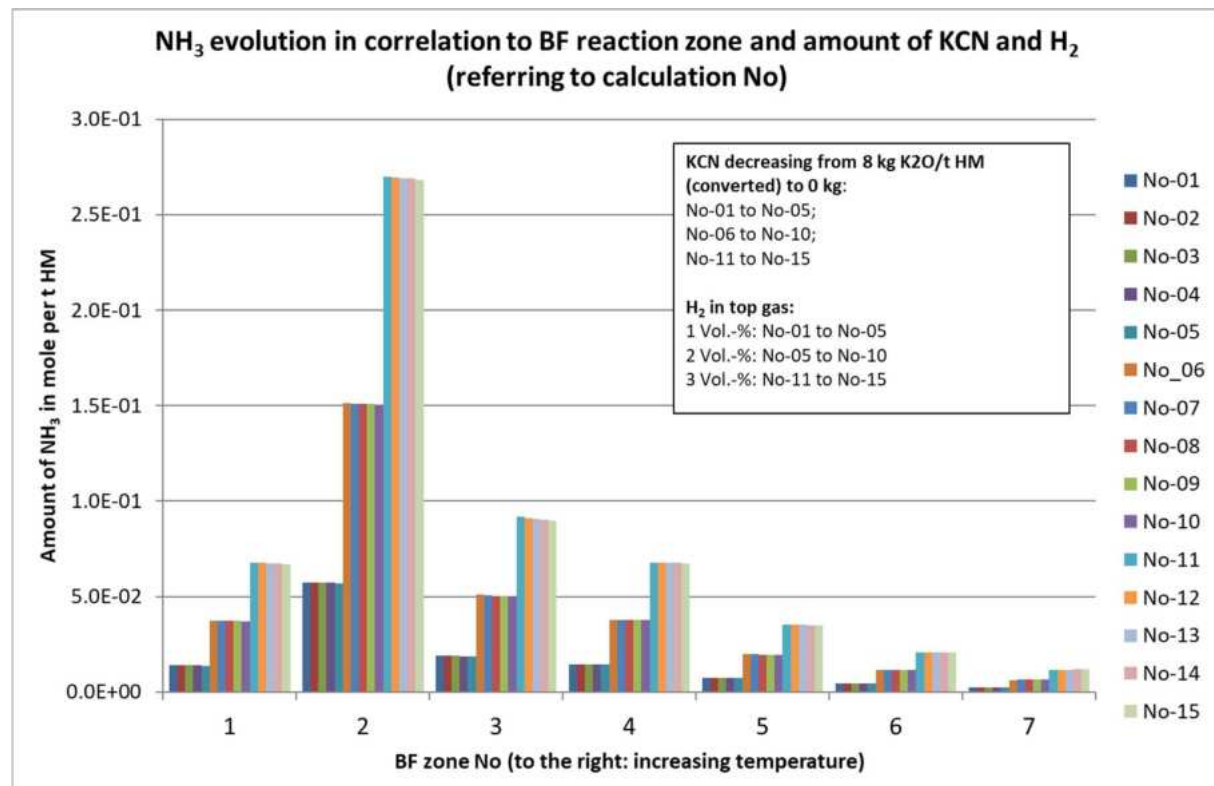


**Figure 159** Calculated amount of formed NH<sub>3</sub> for each BF reaction zone and the different input amount of H<sub>2</sub> and KCN.

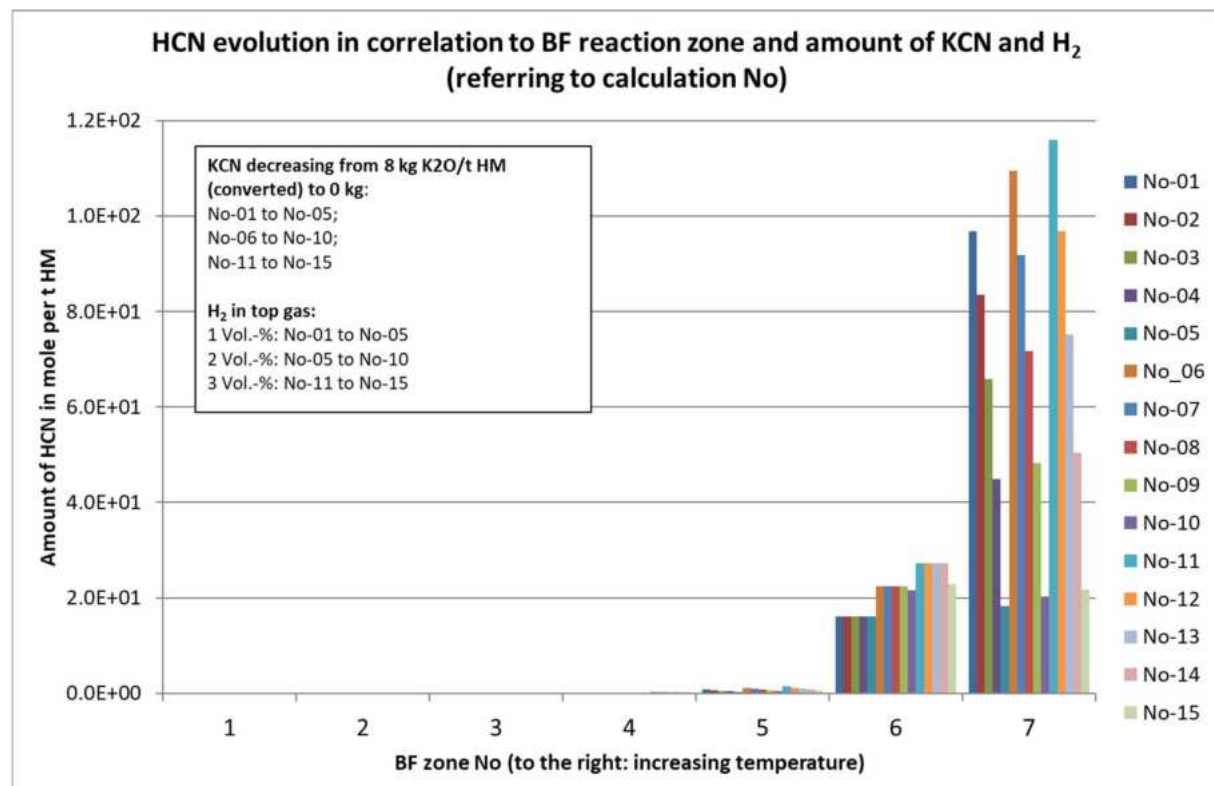


**Figure 160** Calculated amount of formed HCN for each BF reaction zone and the different input amount of H<sub>2</sub> and KCN.

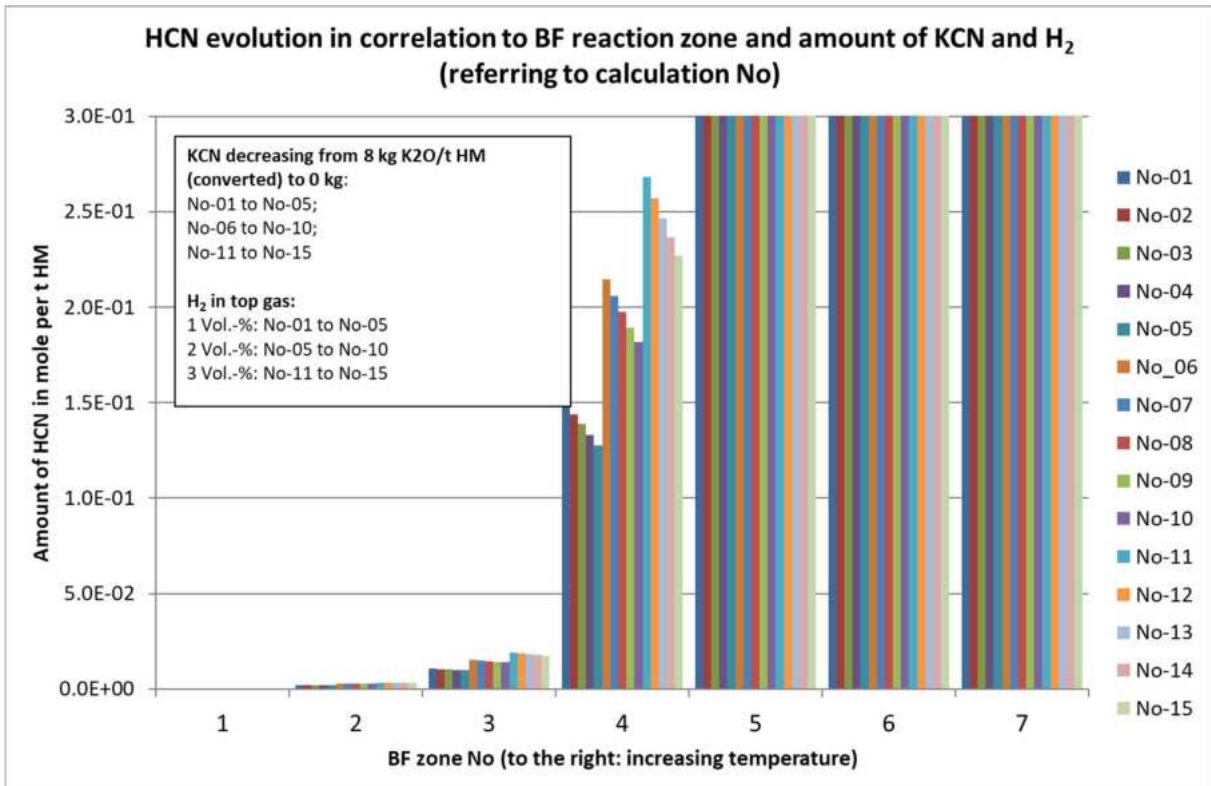


**Figure 161** Calculated amount of formed HCN for each BF reaction zone and the different input amount of H<sub>2</sub> and KCN (Same scale as for NH<sub>3</sub>; **Figure 159**)

In the following figures, correlations of the calculated gas components to the content of alkali components (KCN) and to the hydrogen content are calculated as linear regressions for selected BF temperature zones.

In **Figure 162**, the correlation of calculated NH<sub>3</sub> to the amount of K compounds (KCN, expressed as K<sub>2</sub>O) is presented for BF zone 2 (600°C), in which the maximum NH<sub>3</sub> values are found. The same correlation is presented in **Figure 163** for BF zone 4 (1000°C), in which the alkali cycle within the BF is assumed. **Figure 164** shows the correlation of calculated NH<sub>3</sub> to the amount of H<sub>2</sub> for BF zone 2 and 4 (600; 1000°C). Here only data points without any KCN content are included.

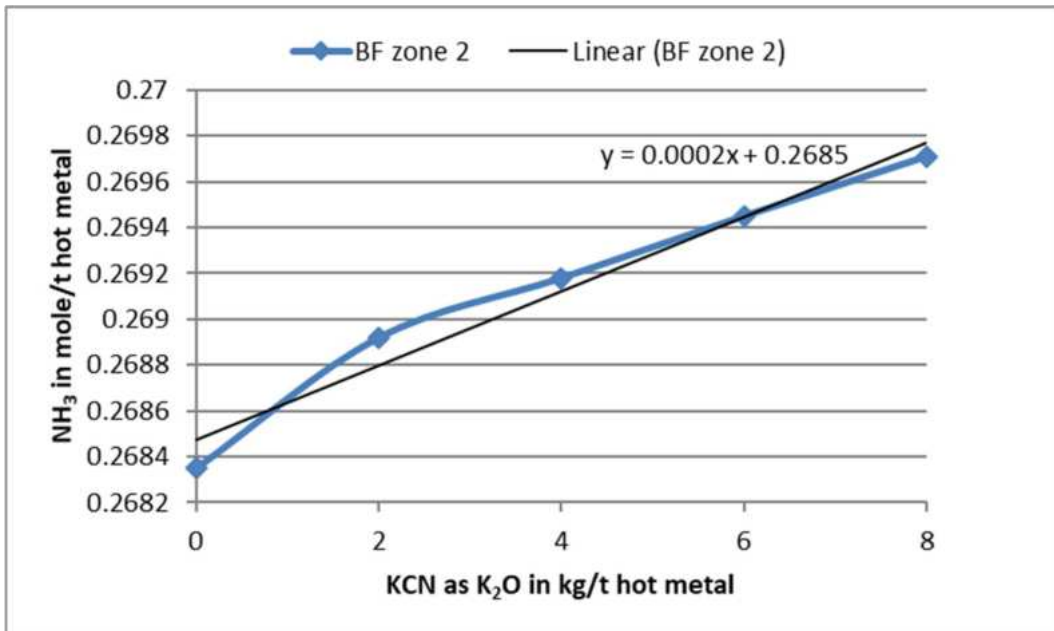


**Figure 162** Correlation of calculated  $\text{NH}_3$  to the amount of K compounds (KCN, expressed as  $\text{K}_2\text{O}$ ), BF zone 2 ( $600^\circ\text{C}$ )

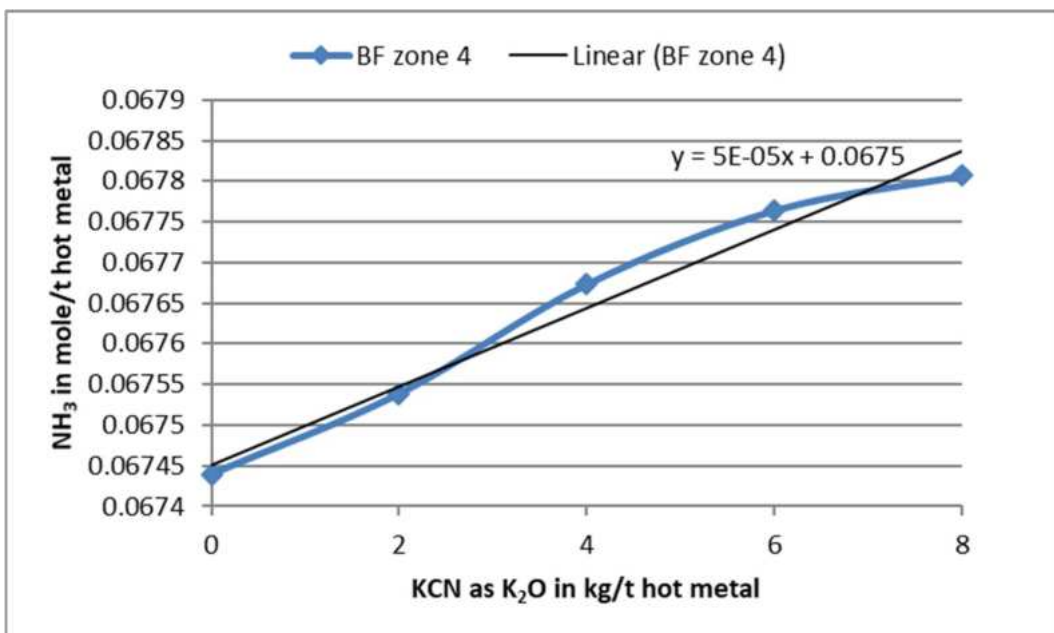


**Figure 163** Correlation of calculated  $\text{NH}_3$  to amount of the K compounds (KCN, expressed as  $\text{K}_2\text{O}$ ), BF zone 4 ( $1000^\circ\text{C}$ )

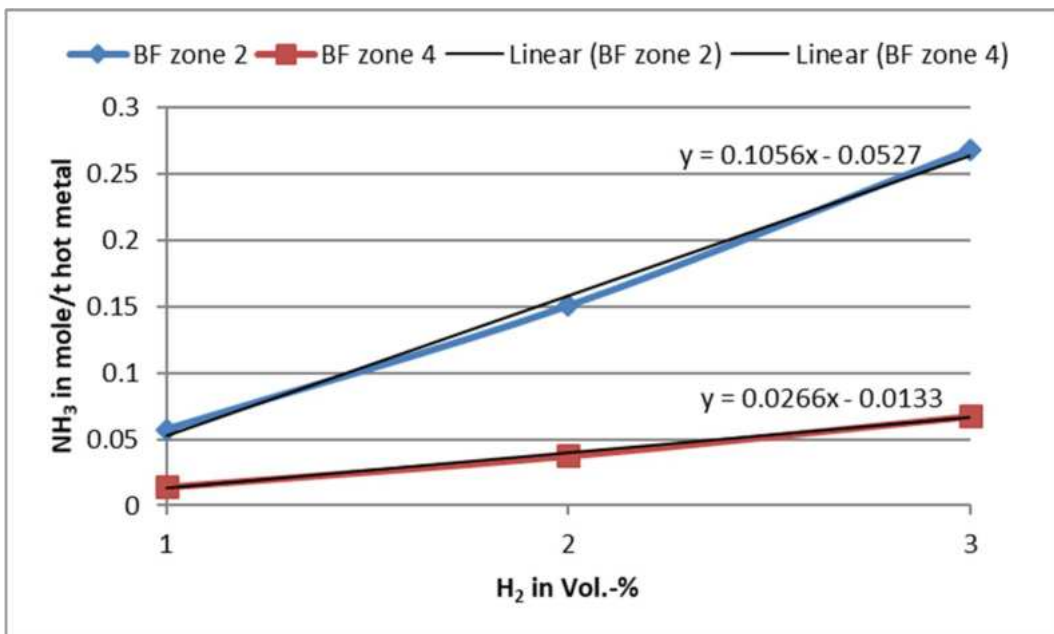


**Figure 164** Correlation of calculated NH<sub>3</sub> to the amount of H<sub>2</sub> – BF zone 2 and 4 (600; 1000°C), no KCN

In **Figure 165**, the correlation of calculated HCN to the amount of K compounds (KCN, expressed as K<sub>2</sub>O) is presented for BF zone 4 (1000°C), while the same correlation is presented in **Figure 166** for BF zone 7 (1800°C), in which the maximum HCN amount was calculated. **Figure 167** shows the correlation of calculated HCN to the amount of H<sub>2</sub> for BF zone 4 (1000°C), while in **Figure 168** the same correlation is compared for BF zone 4 and 7 (1800°C). In both cases only data points without any KCN content are included.

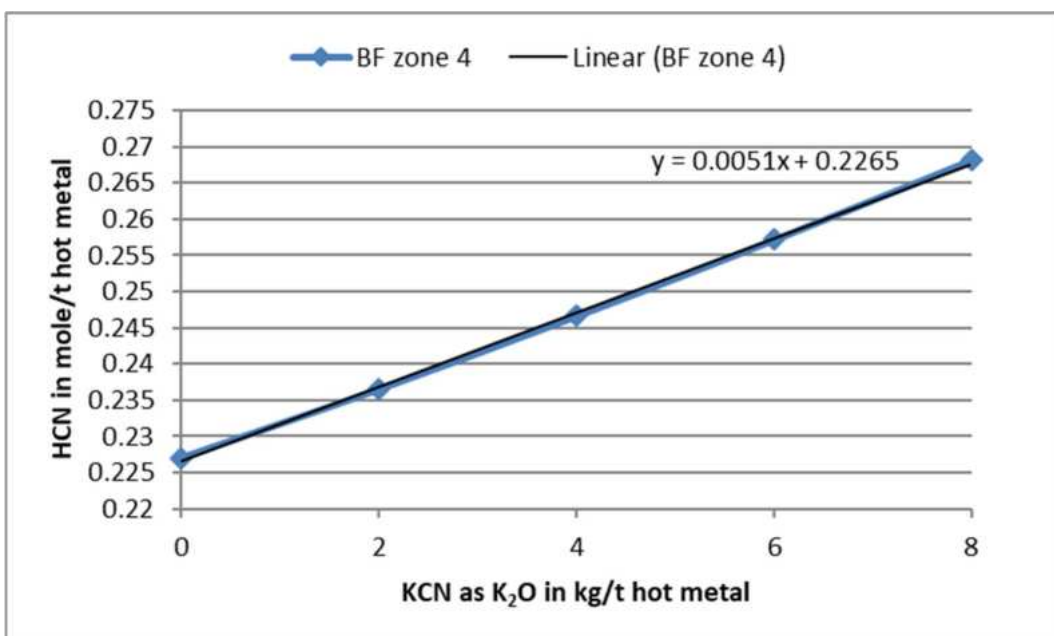


**Figure 165** Correlation of calculated HCN to the amount of K compounds (KCN, expressed as K<sub>2</sub>O), BF zone 4 (1000°C)

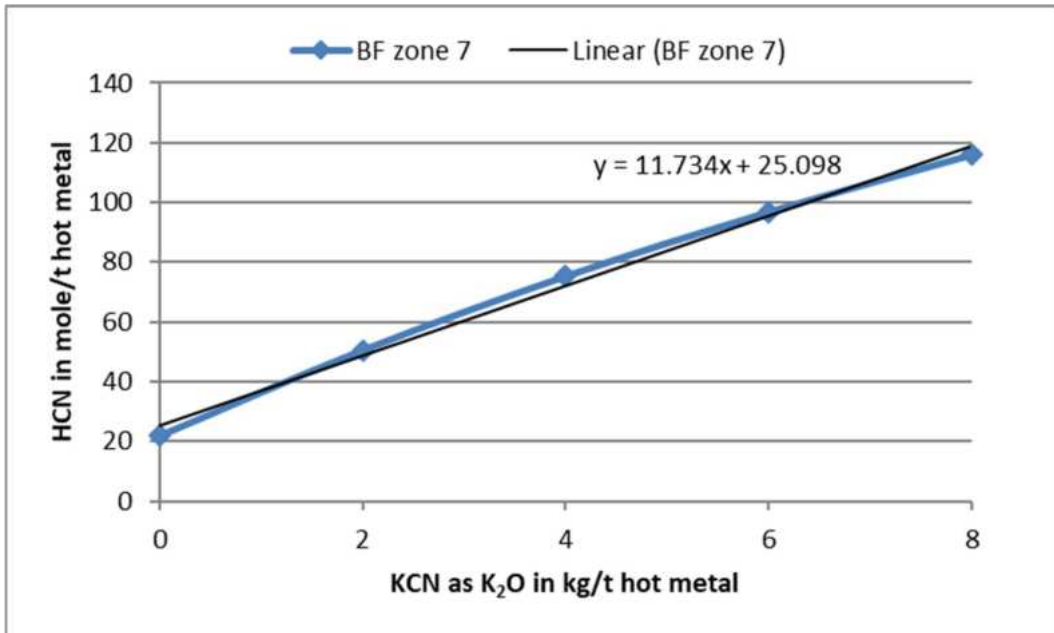


**Figure 166** Correlation of calculated HCN to the amount of K compounds (KCN, expressed as  $\text{K}_2\text{O}$ ), BF zone 7 ( $1800^\circ\text{C}$ )

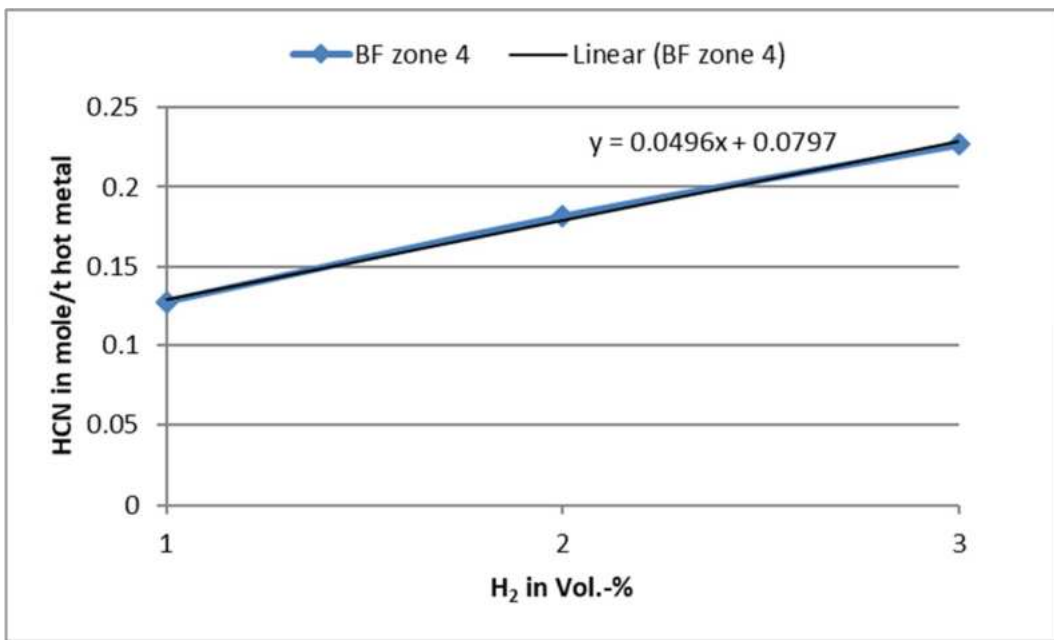


**Figure 167** Correlation of calculated HCN to the amount of  $\text{H}_2$  – BF zone 4 ( $1000^\circ\text{C}$ ), no KCN

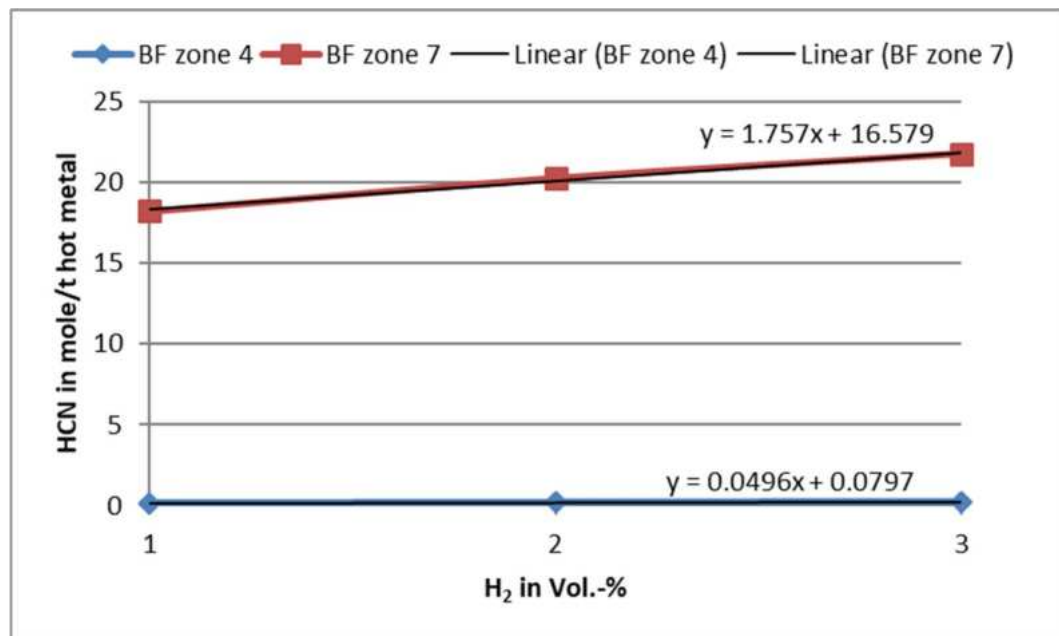


**Figure 168** Correlation of calculated HCN to the amount of H<sub>2</sub> – BF zone 4 and 7 (1000; 1800°C), no KCN

The results of the thermodynamic equilibrium calculations are summarized as follows:

For NH<sub>3</sub> there is only a low influence of the alkali (KCN) amount. This applies for BF zone 2 (600°C; **Figure 162**) and with even lower influence for BF zone 4 (1000°C; **Figure 163**). In contrast to this, the influence of H<sub>2</sub> on NH<sub>3</sub> is significantly higher in both aforementioned BF zones (**Figure 164**).

For HCN, the influence of the alkali amount already at BF zone 4 (1000°C) is much higher than those for NH<sub>3</sub> even in BF zone 2 (highest NH<sub>3</sub>) (**Figure 165**). At BF zone 7 (1800°C), a very high influence of the alkali (KCN) amount on HCN was calculated (**Figure 166**). But also for HCN, the influence of H<sub>2</sub> on the calculated HCN amount is still higher than the influence of alkali compounds (KCN) (**Figure 167**, **Figure 168**).

Based on these results, the formation of NH<sub>3</sub> was quantified exemplarily based on BF zone 2 (600°C), where the highest NH<sub>3</sub> values have been calculated. An **increase of 1 kg K<sub>2</sub>O/t HM** (as KCN) would result in an increased NH<sub>3</sub> amount by 0.0002 mol. This would mean an **increased NH<sub>3</sub> concentration in the BF top gas by 3e-09 -> 0.003 ppm** (total top gas: 68348 mole/t HM; at 2 Vol.-% H<sub>2</sub>), which will only hardly be measurable.

In contrast to this, the effect of a variation in H<sub>2</sub> content on the NH<sub>3</sub> concentration is much higher. An **increase of 1 Vol.-% H<sub>2</sub>** in the BF top gas in this case would result in an **increased NH<sub>3</sub> concentration by 1.6 ppm**, which is still low but measurable.

The same calculations for BF zone 4 (1000°C) result in an increased **HCN concentration** in the BF top gas by **0.075 ppm** for an increase of 1 kg K<sub>2</sub>O/t HM (as KCN), which might be hard to measure. The influence of H<sub>2</sub> on the HCN concentration is higher with an increase of **0.73 ppm HCN** with an increased H<sub>2</sub> concentration by 1 Vol.-%.

For BF zone 7 (1800°C) the influence of the alkali content (K<sub>2</sub>O) on the HCN concentration in the BF gas is much higher compared to zone 4 (increased **HCN concentration** in the BF top gas by **540 ppm** for an increase of 1 kg K<sub>2</sub>O/t HM (as KCN)). An **increase of 1 Vol.-% H<sub>2</sub>** in the BF top gas at BF zone 7 would result in an **increased HCN concentration by 268 ppm**. These values would clearly be measurable.

The thermodynamic calculations lead to the following final conclusions regarding the feasibility of the top gas measurements as a basis for the online tool for determination of alkali accumulation in the BF:

- NH<sub>3</sub> seems to be unsuitable as an indicator for the amount of accumulated alkali components in the BF, since the calculated increase in concentration would be too low to be measured. Further, the influence of (variations in) the H<sub>2</sub> concentration strongly overwhelms the influence of alkali compounds on NH<sub>3</sub> formation.
- HCN seems to be better suited as an indicator for the amount of accumulated alkali components, since the calculated concentration is already higher than that of the NH<sub>3</sub> at the assumed alkali circulation zone (ca. 1000°C). Especially at high temperature (1800°C), the amount of the formed HCN is high (>> 100 ppm) with a very clear positive correlation to the alkali content. In an operational BF, a part of the formed HCN from the high temperature zone would be expected to "survive" within the final top gas, even if it would not be thermodynamically stable at these conditions. But also for HCN formation, the amount of H<sub>2</sub> must be taken into account.

### **2.3.2.1.3** Lab tests with the inductively heated two-zone coke bed reactor for determination of NH<sub>3</sub> and HCN formation in conjunction with alkali components (BFI)

The results of the thermodynamic calculations suggest a low, but possible influence of the alkali load in the BF on the amount or concentration of HCN or - with even more uncertainty - NH<sub>3</sub>, which could be used as tracer compound(s) within the BF top gas to provide online information on the alkali accumulation in the BF (-> Online-Tool). In order to examine the suitability of the HCN or NH<sub>3</sub> measurement within the top gas for determination of the alkali accumulation, and to contribute to the development of a possible calculation routine on this correlation, gas analyses of these components have been carried out during laboratory trials with the two-zone reactor. The experimental set-up and procedure is described in detail for Task 1.3 (see chapter 2.3.1.3.5). The process gas from the two-zone reactor passes through a filter for dust removal. Then it is transferred via a heated pipe to a FTIR gas analyser.

For the trials, coke samples prepared with different alkali loads in the hot zone of the reactor (zone 1) have been used. Since the hydrogen partial pressure was found to play an important role for NH<sub>3</sub> and HCN formation, also the variation of the hydrogen input concentration within the synthetic BF gas has been investigated as important parameter.

In **Table 32** the main process parameters and results of process gas analyses are presented. For a more detailed overview on the process parameters, see **Table 24**. The trials V1-V4 respectively V5-V8 each represent a series of varied K content on the coke (zone 1), all with an input H<sub>2</sub> concentration of 3 %. The only difference of V5 to V8 to the series before, is the use of iron hydroxide as iron carrier (instead of hematite iron ore) within the graphite crucible. Iron hydroxide releases H<sub>2</sub>O when heated, so it was intended to use this as another process variant. But the gas analyses did not reveal significant differences in H<sub>2</sub>O concentration between these two series (average H<sub>2</sub>O < 1 Vol.-%), so the evaluation of NH<sub>3</sub> and HCN in connection with H<sub>2</sub>O was not useful. Within V13 and V17, a higher input H<sub>2</sub> concentration of 5 % was applied in contrast to the other trials, where H<sub>2</sub> concentration is 3 %.

A typical behaviour of the CO and CO<sub>2</sub> gas composition of the process gas with time is presented exemplarily for V1-V4 within **Figure 169**. At begin of the trials, CO<sub>2</sub> increasingly reacts to CO, so

the concentration of these main compounds constantly changes. The CO and CO<sub>2</sub> concentrations only reach a steady state at begin of the second half of the trials (starting from spectrum No. 9; around 30 min). For this reason, only the averages of the NH<sub>3</sub> and HCN measurement values during constant gas composition (the second half of the trial) were taken for all further evaluations. These results are reported within **Table 32**.

From this procedure follows, that the analysed percentage of K within the zone 1 coke after the trial is the most useful value determining the state of K load during the second half of the trial. Hence, this value was used for evaluation of all correlations with the K content / load.

**Figure 170** shows an exemplary plot for the measurement of the HCN concentration vs. time (No. of spectra -> 3 min per spectrum). The measured values scatter significantly between the different spectra, which underlines that the use of the average value (from the second half of the trial) is crucial for further evaluation.

**Table 32** Main process parameters and results of process gas analyses – Average values (V1-8, 13, 16, 17)

	Main process parameters			Process gas analyses - Average values *	
Trial No.	Zone 1 coke pre-treatment with K <sub>2</sub> CO <sub>3</sub> solution; conc. of solution	K in % - zone 1 **	H <sub>2</sub> input in Vol.-%	NH <sub>3</sub> in ppm	HCN in ppm
V1	none	0.17	3 %	6	3
V2	1014 g/l	1.96	3 %	1	14
V3	338 g/l	0.71	3 %	15	6
V4	169 g/l	0.54	3 %	12	12
V5	none	0.16	3 %	4 ***	13
V6	1014 g/l	1.16	3 %	6 ***	8
V7	338 g/l	0.5	3 %	0 ***	8
V8	169 g/l	0.37	3 %	1 ***	9
V13	1014 g/l	1.45	5 %	0	14
V16	none	0.15	3 %	0	5
V17	none	0.15	5 %	0	7

\* during constant gas composition

\*\* after trial

\*\*\* not reliable

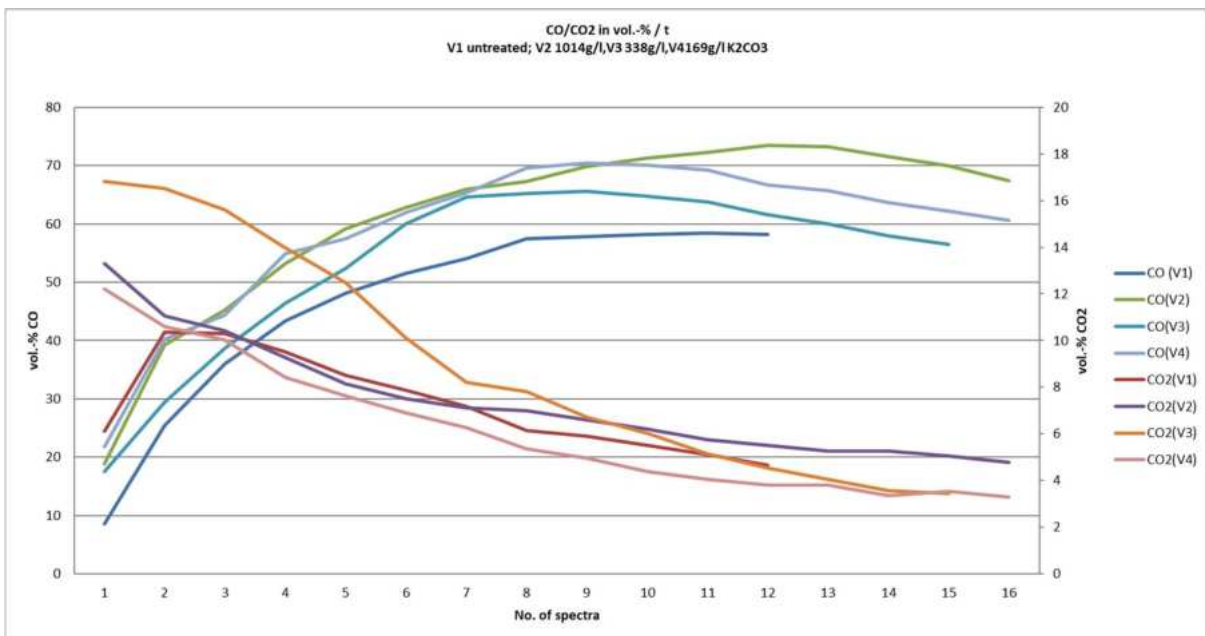


**Figure 169** Typical CO and CO<sub>2</sub> content of product gas vs. time (no. of spectra) - V 1-4

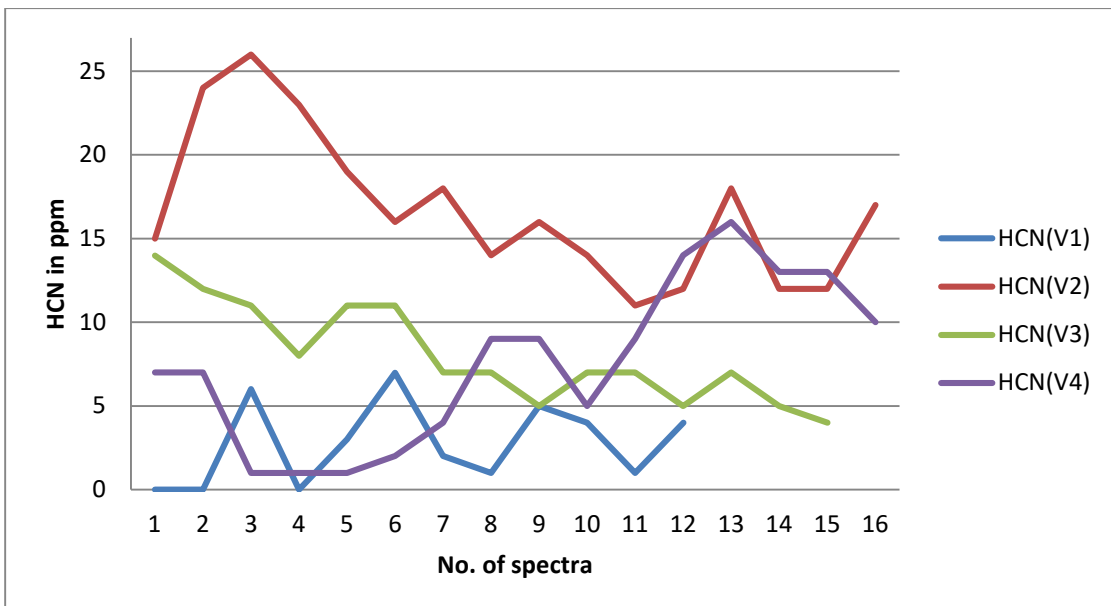


**Figure 170** Exemplary plot for HCN measurements vs. time (No. of spectra) - V1-4

As follows, the results of the gas analyses are evaluated in terms of the correlation with the potassium load / accumulation in the highest temperature zone (Zone 1). Further, the influence of the input hydrogen concentration is assessed.

#### NH<sub>3</sub> Formation

The measurement of NH<sub>3</sub> throughout the trials in the two-zone reactor only performed fairly satisfactory for the first four trials (V1-V4). For all the following trials, the measured NH<sub>3</sub> values were either not reliable any more due to an extreme scattering during the trial (V5-V8) or no NH<sub>3</sub> was detected any more. The reason might be the formation of solid precipitations from NH<sub>3</sub> (e. g. NH<sub>4</sub>Cl) within the reactor or the pipes, which may be formed in combination with accumulated volatile trace compounds (e. g. chlorides).

For (V1-4), **Figure 171** shows the average NH<sub>3</sub> concentration in correlation to the K content in

zone 1 coke. By evaluation of all data points, the regression line suggests a decreasing  $\text{NH}_3$  concentration with increasing K content, which is the opposite behaviour as expected. If V2 would be removed from the evaluation as an outlier value, the expected positive correlation of the  $\text{NH}_3$  concentration with the K content in coke would be resulting.

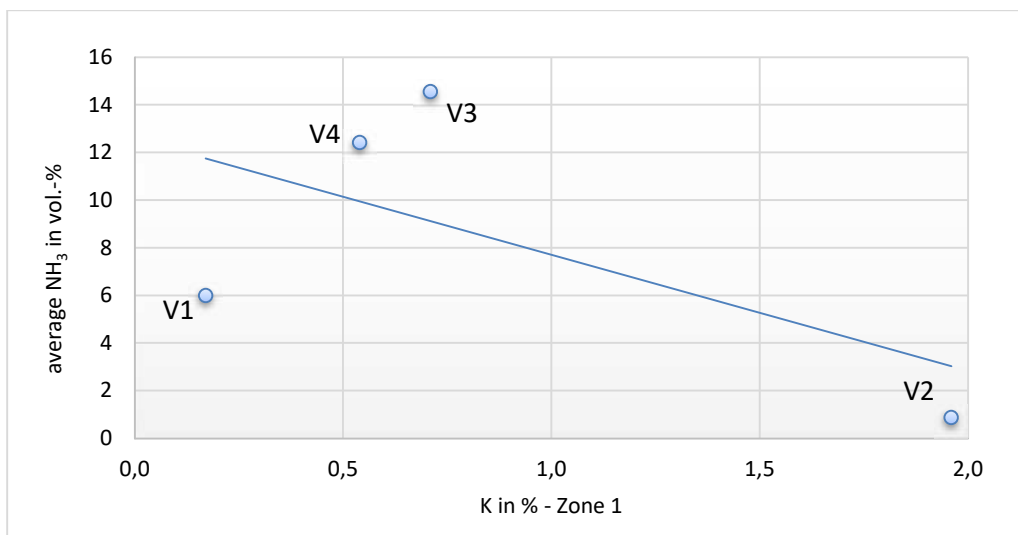


**Figure 171** Average  $\text{NH}_3$  concentration in correlation to K content in zone 1 (V1-4)

#### *HCN Formation*

In contrast to the measurement of  $\text{NH}_3$ , the measurement of HCN has proven to be much more reliable, so that the HCN concentrations could be determined for all trials.

For V1-V4 (all 3 %  $\text{H}_2$ , hematite iron ore), the measured average HCN concentration positively correlates with the K content of the coke in zone 1 (**Figure 172**). But the coefficient of determination with  $R^2=0.6$  is not very large due to the scattered values.

The same evaluation for V5-V8 (all 3 %  $\text{H}_2$ , iron hydroxide) shows a slightly negative correlation of the average HCN concentration with the K content of the coke in zone 1 (**Figure 173**).

In **Figure 174** the average HCN concentration is shown in correlation to the K content of coke in zone 1 for a (high)  $\text{H}_2$  input concentration of 5 % (V13 and 17). Here, the expected positive correlation is observed.

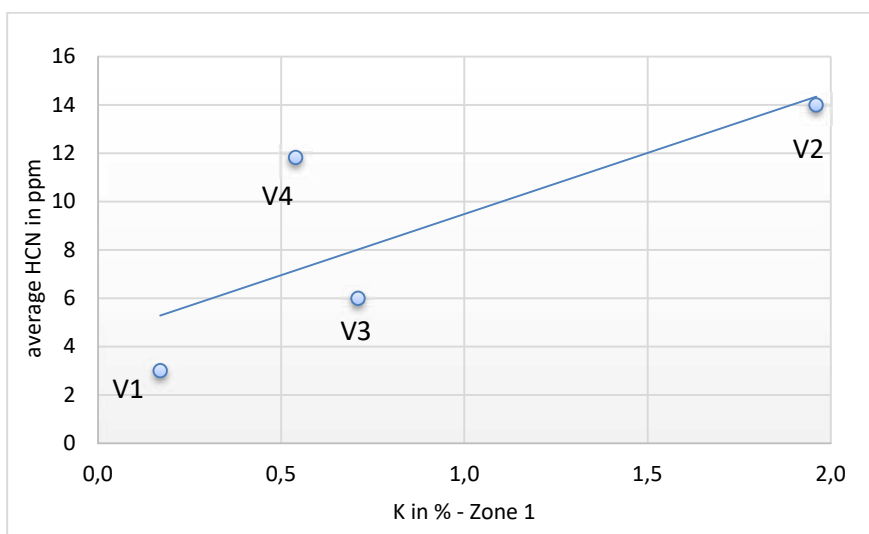


**Figure 172** Average HCN concentration in correlation to K content in zone 1 (V1-4; all 3 %  $\text{H}_2$ )

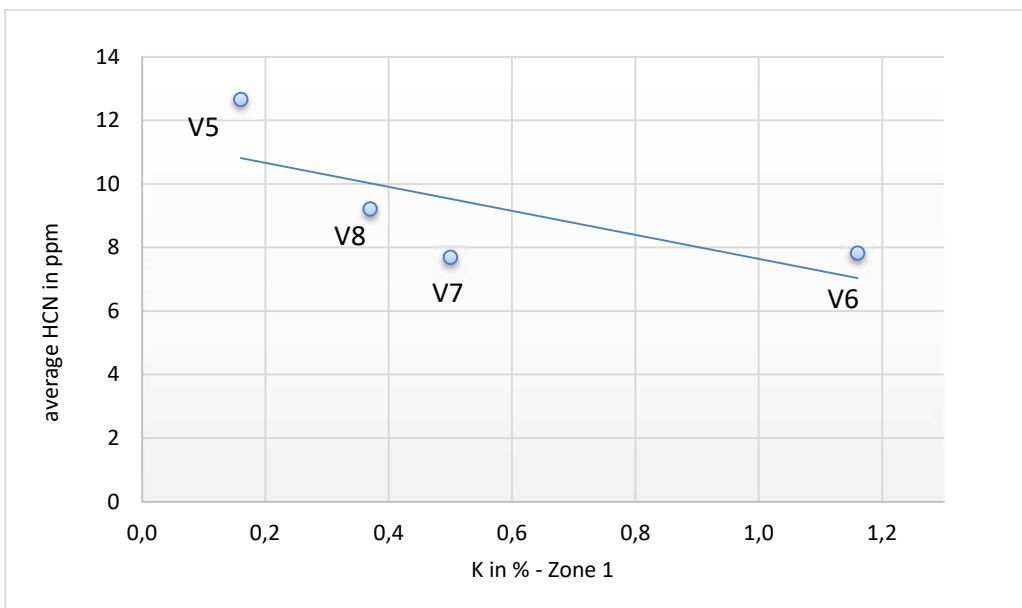


**Figure 173** Average HCN concentration in correlation to K content in zone 1 (V5-8, all 3 % H<sub>2</sub>)

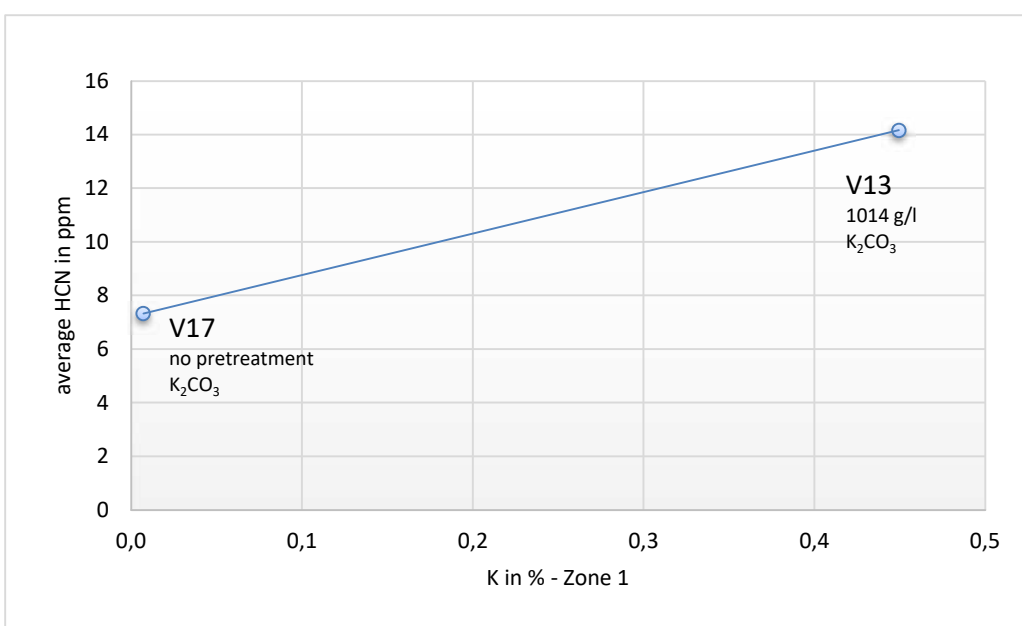


**Figure 174** Average HCN concentration in correlation to K content in zone 1 (V13 and 17, both 5 % H<sub>2</sub>)

As follows, the influence of the input H<sub>2</sub> concentration on the HCN concentration in the process gas is evaluated.

In **Figure 175** the average HCN concentration together with the K content of coke in zone 1 is illustrated for 3 % and 5 % H<sub>2</sub> (V1, V16 and V17). Here only the coke without K pre-treatment is compared. The figure suggests, that with increased H<sub>2</sub> input (V17), a significantly higher HCN concentration is observed (2.4x compared to V1; 1.6x compared to V16).

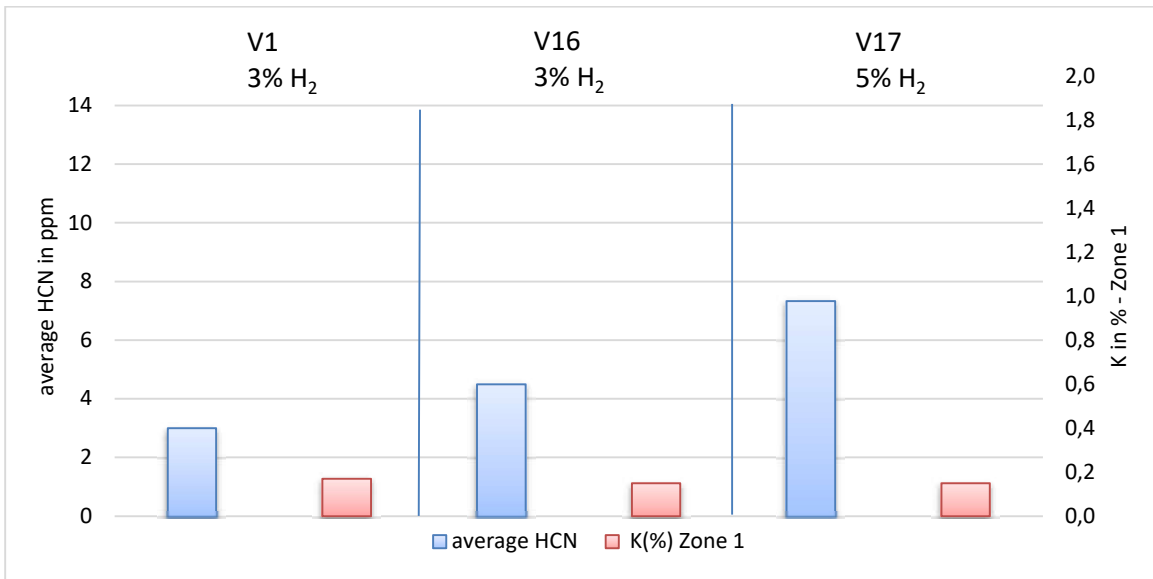


**Figure 175** Average HCN concentration compared to K content in zone 1 - coke without K pre-treatment – 3 % and 5 % H<sub>2</sub> (V1, V16 and V17)

In **Figure 176** the average HCN concentration together with the K content of coke in zone 1 is illustrated for 3 % and 5 % H<sub>2</sub> (V2, V13). Here only the coke with high K pre-treatment is compared. Even if the measured HCN values for both trials with around 14 ppm are comparable, for the higher H<sub>2</sub> input concentration (V13) this HCN value is reached with around 25 % less K content within the zone 1 coke. This suggests a positive influence of H<sub>2</sub> on the measured HCN concentration, which is also supported by **Figure 177**, where the average HCN concentration together with the K content of coke in zone 1 is illustrated for 3 % and 5 % H<sub>2</sub> and additional 5 % kaolin pre-treatment of the coke (refer to Task 2.2; V2, V13). Here, at comparable K load a higher HCN concentration is measured for the higher H<sub>2</sub> input.

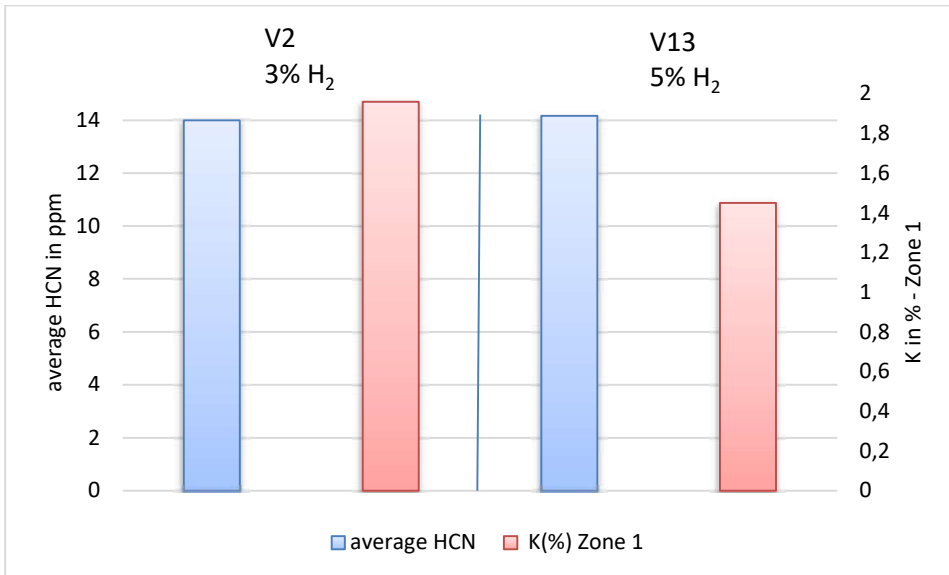


**Figure 176** Average HCN concentration compared to K content in zone 1 - coke with high K pre-treatment – 3 % and 5 % H<sub>2</sub> (V2, V13)

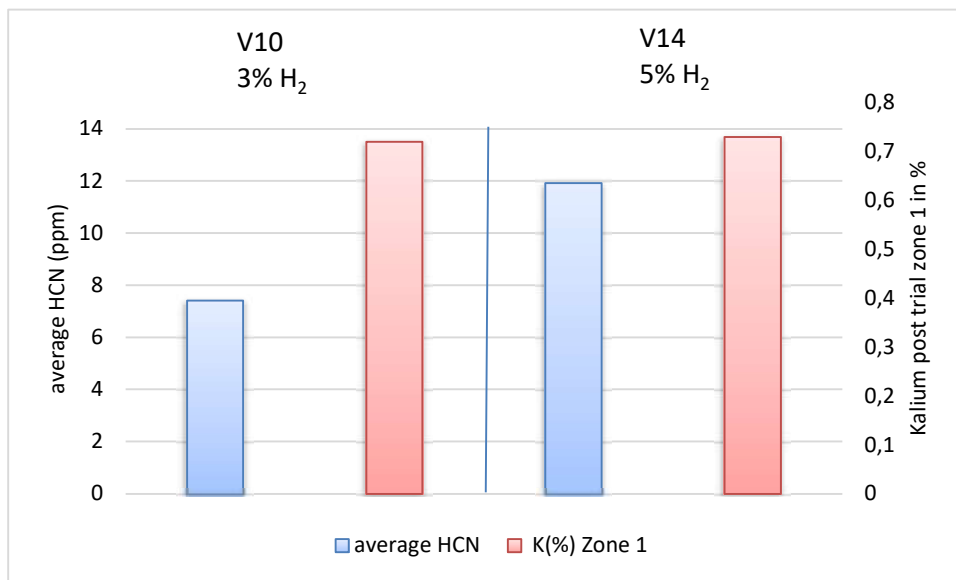


**Figure 177** Average HCN concentration compared to K content in zone 1 - coke with high K pre-treatment and 5 % Kaolin pre-treatment – 3 % and 5 % H<sub>2</sub> (V10, V14)

#### Conclusions on HCN formation

Based on the results of all gas analyses from the two-zone reactor trials at BFI (including the trials with kaolin pre-treatment of coke), a linear regression has been calculated for the average measured HCN concentration in correlation to the K content in zone 1 (**Figure 178**).

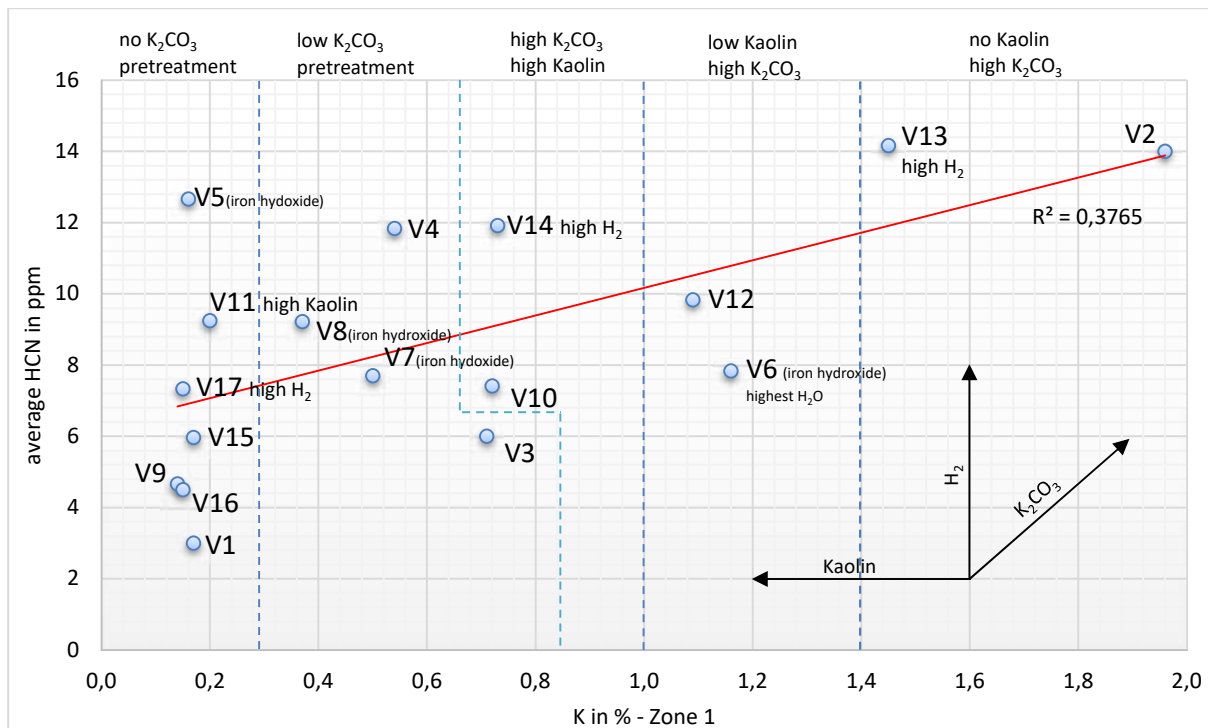


**Figure 178** Overview - Average HCN concentration in correlation to K content for all two-zone reactor trials at BFI (including kaolin pre-treatment)

The result is a clearly positive correlation between the measured HCN and the K content in the coke, but the coefficient of determination with  $R^2=0.38$  is not very high, which reflects the highly scattered values. Also other standard methods for regression have been tested, but did not result in a better coefficient of determination than the linear regression.

Especially the trials with the highest input hydrogen concentration (V13, 14, 17) show significantly higher HCN values than other trials with comparable K content. A clear influence of the kaolin pre-treatment (see Task 2.2) on the measured HCN concentration was not observed.

As a final conclusion, the BFI lab tests for determination of NH<sub>3</sub> and HCN formation in conjunction with alkali components at BF conditions give a clear indication, that the measurement of HCN in the BF top gas might be a promising method to deliver useful information on the actual alkali accumulation within a blast furnace. But it must be noted, that other parameters like the H<sub>2</sub> concentration may have an even larger influence on the formation of HCN than K components have (as thermodynamic calculations show).

Compared to HCN, the measurement of NH<sub>3</sub> in the top gas seems to be more difficult and hence not reliable, which makes it unsuitable for the intended measurement of alkali accumulation within the BF.

Based on the set of data investigated within this project, it was not possible to develop a simple calculation routine suitable for determination of the amount of circulating alkali components in the BF, even though some correlations with the HCN content have been found.

### **2.3.2.2 Task 2.2 Inhibition of alkali circulation**

#### **2.3.2.2.1** Preparation of test coke (modified ash composition) to be used in laboratory tests, as basket samples and for CRI/CSR (SWERIM, LTU, LKAB)

Test coke with modified ash composition was prepared in a small scale coking test retort at DMT GmbH & Co. KG in Germany. The recipes for preparation of test coke were designed based on a standard coal blend used by SSAB where the ash composition has been modified by additions of kaolin (Al-silicate), bauxite (Al<sub>2</sub>O<sub>3</sub>) and silica (SiO<sub>2</sub>) in the form of silversand. Minerals added to the test coke were fined grained and the chemical composition can be seen in **Table 33**. Kaolin added in test coke contains the clay mineral kaolinite Al<sub>2</sub>Si<sub>2</sub>O<sub>5</sub>(OH)<sub>4</sub>. During carbonization tests, the hydroxyl group is probably lost and the mineral is converted to metakaolin (Al<sub>2</sub>Si<sub>2</sub>O<sub>7</sub>) or spinel (Si<sub>3</sub>Al<sub>4</sub>O<sub>12</sub>).

**Table 33** Chemical analysis of kaolin, silversand and bauxite added in test coke.

	Kaolin	Silversand	Bauxite
CaO %	0.05		
MgO %	0.17		
SiO <sub>2</sub> %	57.1	99.2	5.34
Al <sub>2</sub> O <sub>3</sub> %	38.5	0.17	90.5
MnO %	<0.01		
TiO <sub>2</sub> %	0.09		3.0
K <sub>2</sub> O %	3.15		
P <sub>2</sub> O <sub>5</sub> %	0.14		
SO <sub>3</sub> %	0.01		
Fe <sub>2</sub> O <sub>3</sub> %	0.79	0.054	1.07
LOI %	12.3	0.1	0.14

A total of 10 different carbonization tests were conducted, three of these were reference cokes in where one was corresponding to the standard coal mix and the other two tests were containing the standard blend with additions of 5% pet coke, see **Table 34**. Tests with number 4-10 specified in the table contained different amounts of added minerals to the reference coal blend with 5% pet coke. Carbonization tests were conducted to have similar conditions as during coke production at SSAB with regard to particle size distribution, moisture content and bulk density of coal blend. Also similar conditions during coking were used with 4 hours coking time and an oven temperature of 1030°C.

**Table 34** Carbonization tests in small scale coking retort at DMT in Germany.

Nr	Coal blend	LV coal %	MV coal %	HV coal %	Pet coke %	Kaolin %	Silversand %	Bauxite %
1R	2% kaolin	40	28	25	5	2		
2R	Base blend	40	32	28				
3R	0.5% kaolin	40	29.5	25	5	0.5		
4R	Base blend + pet coke	40	30	25	5			
5R	Base blend + pet coke	40	30	25	5			
6R	1% kaolin	40	29	25	5	1		
7R	1% silversand	40	29	25	5		1	
8R	2% silversand	40	28	25	5		2	
9R	1%bauxite	40	29	25	5			1
10R	2% bauxite	40	28	25	5			2

In **Table 35**, results from carbonization tests are shown. Coke yield is lowest for base blend (2R), which is expected as presence of pet coke in the other coal blends will contribute to both lower volatile- and ash content and thus, increase the fixed carbon content. The ash content of the different minerals is reflected in the resulting coke yields as the value is increasing with added amount of mineral. Highest coke yield can be found for blends containing 2% silversand (8R) and bauxite respectively (10R). The corresponding blend containing 2% kaolin (1R) have a bit lower coke yield value, probably because kaolin contains around 12% volatile matter.

**Table 35** Results from carbonization tests.

Nr	Coal blend	Coke yield	Max. internal gas pressure (measured)	Max. internal gas pressure (estimated)	Max. wall load (estimated)	CRI	CSR
		%	mbar	mbar	mbar	%	%
1R	2% kaolin	79.6	27	7	5	19.1	69.5
2R	Base blend	78.2	53	28	12	17.2	71.2
3R	0.5% kaolin	79.0	40	13	8	19.7	69.5
4R	Base blend + pet coke	79.1	52	17	10	19.8	70.1
5R	Base blend + pet coke	79.4	60	19	11	20.5	69.5
6R	1% kaolin	79.5	48	12	7	19.5	70.6
7R	1% silversand	79.7	66	15	7	19.2	67.8
8R	2% silversand	80.0	42	14	5	18.9	67.5
9R	1%bauxite	79.6	77	19	5	19.7	68.9
10R	2% bauxite	79.9	54	17	4	19.0	68.1

When comparing the CSR/CRI results for test coke corresponding to 2R to test 4R-5R (**Table 35**) it can be seen that the CRI is increased from 17.2% to 19.8-20.5% while the CSR is decreased from 71.2% to 70.1-69.5% when adding 5% pet coke to the standard coal blend. The influence of mineral additions to the coal blend with pet coke seems to lower the reactivity slightly and also contribute to a decreased strength. This are in accordance with the expected behaviour as mineral additions increases the ash content and thus, decrease the amount of carbon with coking- and reactive properties.

### 2.3.2.2.2 Kinetic studies on coke with modified ash (LTU)

The gasification of coke with modified ash composition has been studied by *LTU* with the same thermogravimetric analyser and method as described in Task 1.3 (**Figure 131**, **Figure 132**). The purpose was to study the effect of added materials on the alkali uptake and its effect on coke properties while descending in the BF.

**Table 34** shows the studied coal blends. The prepared coke samples were investigated for their reactivity using thermogravimetric analyzer by *LTU* under the same conditions as stated previously in Task 1.3 and the generated CO was also identified. **Figure 179** and **Figure 180** show the mass loss curves and the generated CO of the samples during gasification. It was obvious from the mass loss curves and the CO peaks that ash composition modification has a marginal effect on the coke gasification reaction.

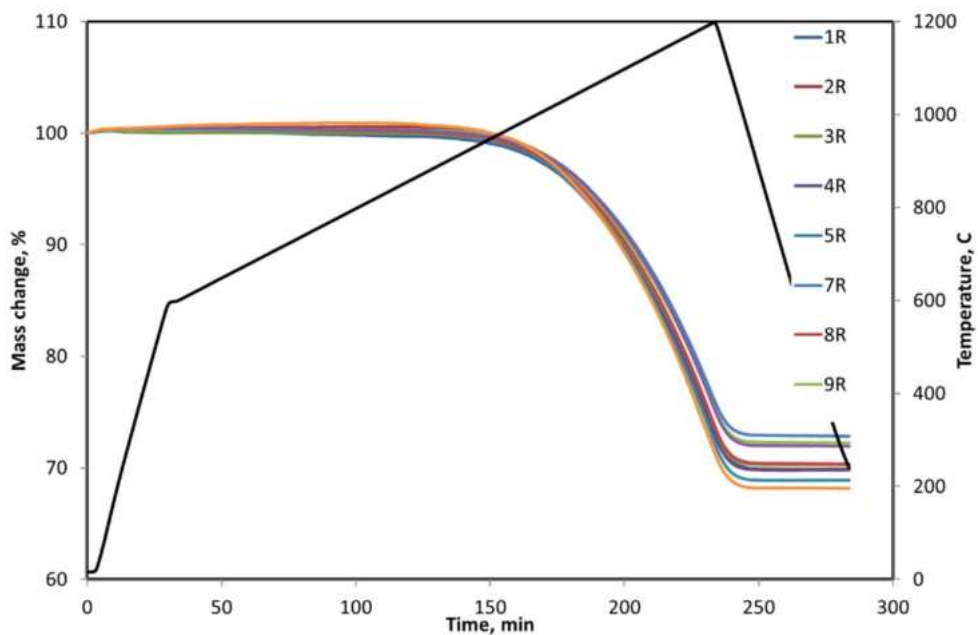


**Figure 179** Mass loss curves of the samples during gasification

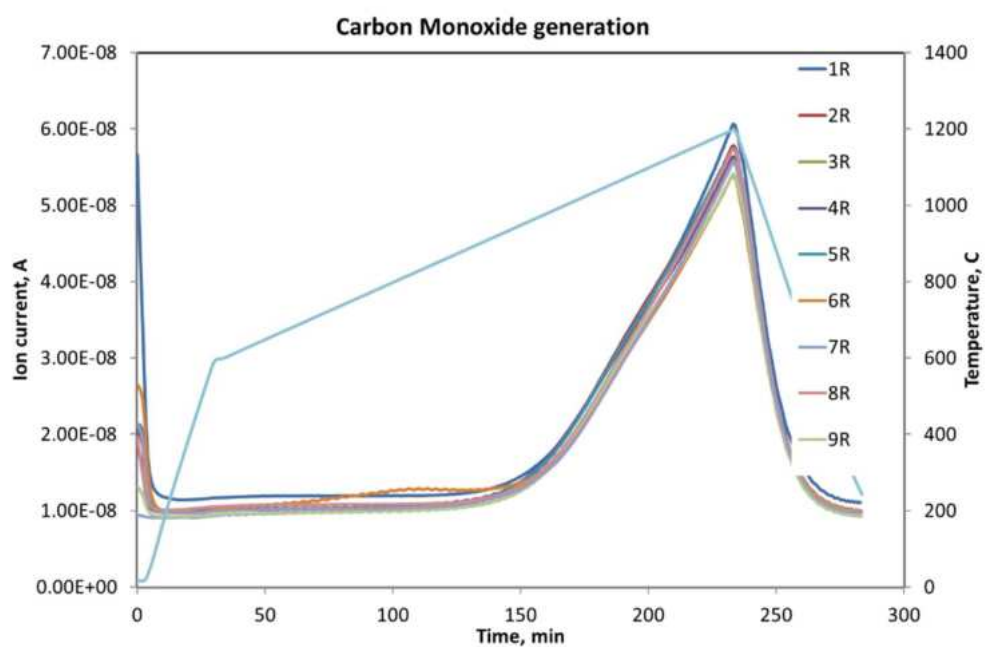


**Figure 180** Generated CO of the samples during gasification

The gasification kinetic parameters for modified ash coke were further estimated using similar approach to the previously mentioned method in Task 1.3 and given in **Table 36**.

**Table 36** Estimated activation energy values (Ea), frequency factor (A) and regression coefficient (R2)

	Coal blend	Ea, kJ/mol	A, g/g.s	R2
1 R	2% kaolin	186	938	0.97
2 R	Base blend	164	143	0.96
3 R	0.5% kaolin	184	795	0.97
4 R	Base blend + pet coke	161	109	0.96
5 R	Base blend + pet coke	161	143	0.98
6 R	1% kaolin	185	995	0.96
7 R	1% silversand	171	230	0.97
8 R	2% silversand	168	185	0.97
9 R	1% bauxite	160	85	0.97
10 R	2% bauxite	166	154	0.98

The activation energy values of all blends lies in a narrow range with an average value of 168 kJ/mol. However, blends with added kaolin showed highest activation energy (blends R1, 3 and 6). Blends with added silversand showed a bit higher activation energy (R7 and 8) compared to blends with added Bauxite (R9 and 10).

### 2.3.2.2.3 Investigation on basket samples in LKAB EBF® (SWERIM, LKAB)

The test coke has been further investigated by basket samples in LKAB EBF during campaign 32 and 33 in 2016 and 2017 respectively where the baskets have been charged to the EBF to descent with the burden until process is stopped and quenched by injected nitrogen gas from the top. The results in the following text are presented concisely based on results in [46] and [47]. The aim was to examine the possibility to bind alkali in compounds eliminating the catalytic effect by alkali on coke gasification and enhance the alkali output via slag by producing coke with modified ash composition. For campaign 32, selected test coke charged to the EBF in baskets contained 1% kaolin (R1), 1% silversand (R2) and 1% bauxite (R3) as well as a base coke (BC). Note that new abbreviations of the test cokes are used compared to list of carbonization tests in **Table 34**, e.g R1 with 1% kaolin was denoted as 6R earlier. The base coke (BC) was the reference coke (BC) containing standard coal blend with additions of 5% pet coke (4R and 5R in **Table 34**). The selected test cokes for the basket samples in C32 are summarized in **Table 37**. In addition to the reference coke produced at DMT in Germany, test cokes containing minerals has also been compared to SSABs standard coke (SC) that was put in neighbouring baskets.

**Table 37** Test coke in basket samples to LKABs EBF in campaign C32.

	Coal blend	LV [%]	MV [%]	HV [%]	Pet coke [%]	Kaolin [%]	Silversand [%]	Bauxite [%]
BC	Base coke + pet coke	40	30	25	5			
R1	1% kaolin	40	29	25	5	1		
R2	1% silversand	40	29	25	5		1	
R3	1% bauxite	40	29	25	5			1

BC was loaded in all baskets, separated from the test coke by a wall made of wire-mesh. The influence of alkali on the test coke was examined by characterising the samples with XRF, XRD, SEM/EDS and TGA. This was done to confirm any difference between the test cokes and the base coke in terms of chemical composition, phases in the coke ash, degree of graphitisation and reactivity. The charging schedule of baskets is shown in **Figure 181** below. Baskets were charged in 6 different coke layers in where baskets numbered as 1-3 and 5-6 respectively were tied together in a row. All baskets charged containing R1 (kaolin) and BC1 were found during the excavation. Basket 3 containing R2 ( $\text{SiO}_2$ ) and BC2 in BL 25 and 29 as well as basket 6 containing R3 ( $\text{Al}_2\text{O}_3$ ) and BC3 in BL level 29 and 31 were not found during the excavation of the EBF. None retrieved baskets are marked with grey in **Figure 181**.

BL	Basket 1	Basket 2	Basket 3	Basket 5	Basket 6	Basket 7
17	R1	BC1		R2	BC2	
21	R1	BC1		R2	BC2	
25	R1	BC1		R2	BC2	
29	R1	BC1		R2	BC2	
31	R1	BC1		R2	BC2	
33	R1	BC1		R2	BC2	

**Figure 181** Charging schedule of baskets with test coke and base coke in C32.

The levels from which the baskets were excavated and the total time in the EBF while running are shown in **Figure 182**. Basket 1 and 3 from BL 33 containing R1 (kaolin) and R2 ( $\text{SiO}_2$ ) were found at the lowest level in the EBF at a depth of 4570 mm below the charging level and 1.2 meters above the raceway. The basket containing R3 ( $\text{Al}_2\text{O}_3$ ) from BL 33 was found at a depth of 4512 mm below the charging level. All baskets also contained the corresponding base coke (BC1, BC2 and BC3).

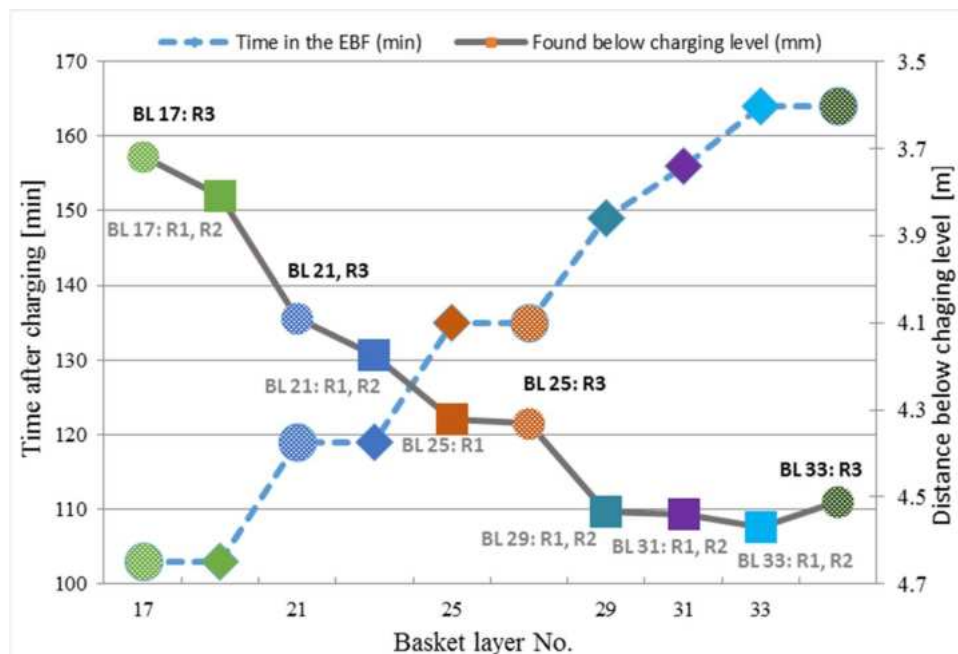


**Figure 182** Depth of the excavated baskets from the EBF in C32, and total time after charging.

The horizontal position of the basket samples in the EBF varied, see **Figure 183**. All baskets had different horizontal position.

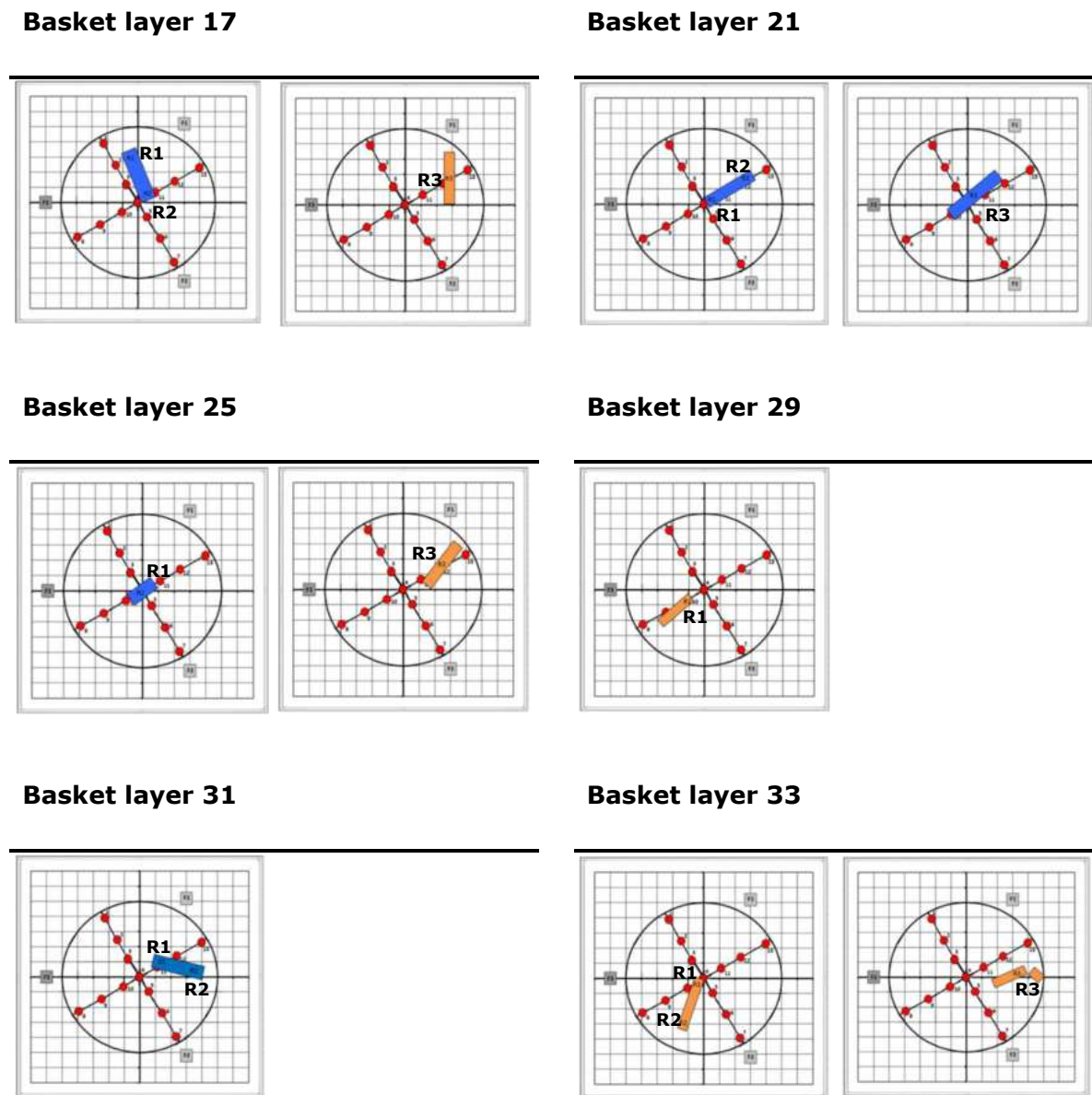


**Figure 183** Horizontal position of the baskets in the EBF during C32.

The sum of potassium oxide ( $K_2O$ ) and sodium oxide ( $Na_2O$ ) at each level for R1, R2 and corresponding reference cokes in the EBF is shown in **Figure 184**. It can be seen that the amount of alkali in coke ash increase with increasing distance below the charging level in general. The alkali content ( $K_2O+Na_2O$ ) was higher in R1 (kaolin) compared to BC1 in BL 17 (-3.8 m), 29 (-4.5 m) and 31 (-4.5m). The content of alkali was about 10 times higher in the coke from BL 29 (-4.5 m) than in the feed coke. The concentration of alkali is higher in BC2 compared to R2 at all levels. The highest level of alkali in BC2 is at -4.45 m and at level -4.5 m for R3.

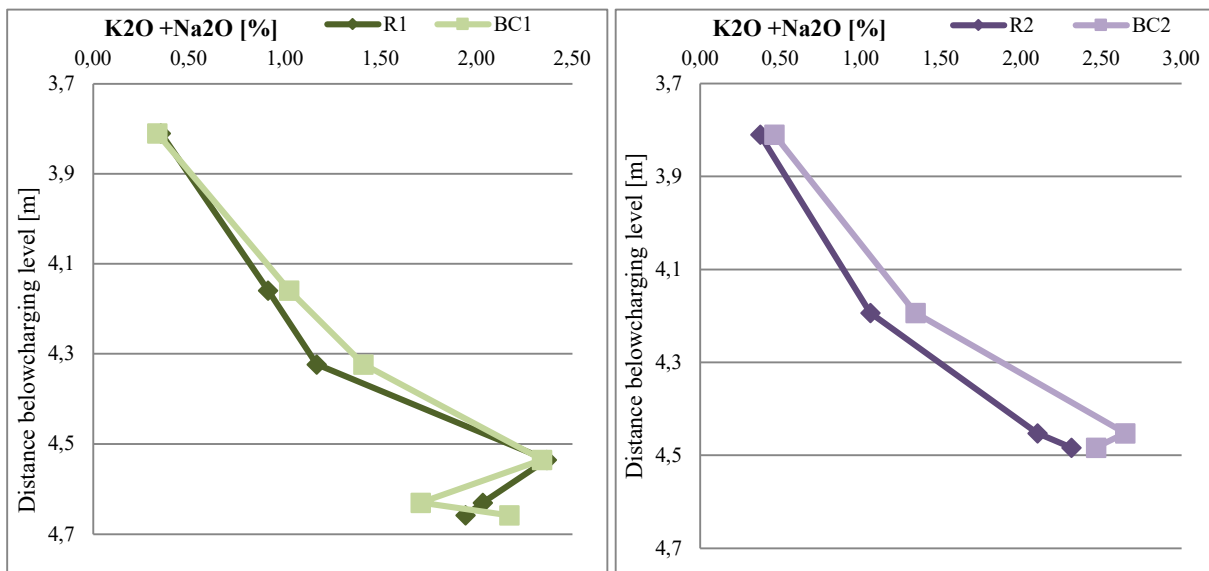


**Figure 184** Alkali concentration plotted against the EBF height from the top in C32. R1 (kaolin) and BC1 is in the left-hand image and R2 ( $\text{SiO}_2$ ) and BC2 is in the right-hand image.

The Alkali concentration of R3 ( $\text{Al}_2\text{O}_3$ ) and BC3 is shown in **Figure 185**. The concentration of alkali increases with the height from the charging level in the EBF, besides in R3 and BC3 at BL 21 (-4.1m). The alkali content in R3 was higher than in BC3, at all levels besides at BL 33 (-4.5m). The coke ash content was generally higher in R3 compared with the BC3.

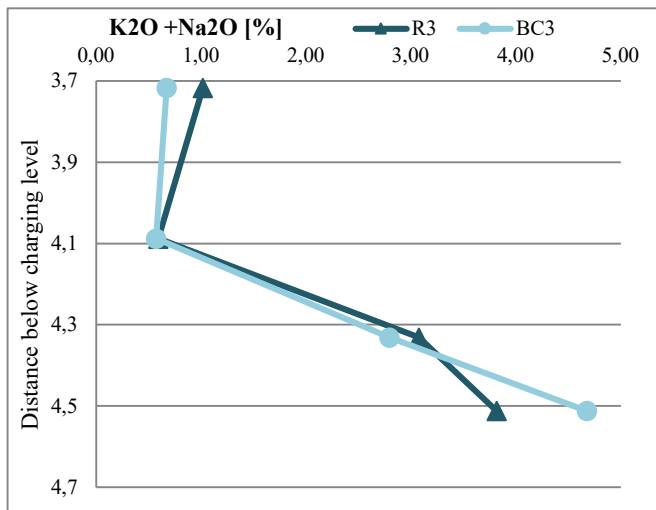


**Figure 185** Alkali concentration plotted against the EBF height from the top for R3 ( $\text{Al}_2\text{O}_3$ ) and BC3 in C32.

**Table 38** shows a summary of the mineral phases identified in XRD for R1, R2, R3 and SC (SSAB Standard Coke) from basket level 33. Graphite, carbon and quartz were found in all coke types in BL 33. The alkali bearing mineral leucite and the aluminosilicate mullite were found in R1, R2 and SC. Kalsilite was found in R1, R2, R3, BC3 and SC with the highest relative peak in SC and R3. Corundum ( $\text{Al}_2\text{O}_3$ ) was found in R3 and was also the mineral phase added to the coal blend R3.

**Table 38** Summary of the mineral phases found in R1 (kaolin), R2 (SiO<sub>2</sub>), R3 (Al<sub>2</sub>O<sub>3</sub>) and SC from BL 33 in C32.

Sample	Graphite C	Carbon C	Quartz SiO <sub>2</sub>	Leucite KAISi <sub>2</sub> O <sub>6</sub>	Mullite Al <sub>4</sub> Si <sub>2</sub> O <sub>8</sub>	Kalsilite KAISiO <sub>4</sub>	Corundum Al <sub>2</sub> O <sub>3</sub>	Iron carbide Fe <sub>3</sub> C
BC3_33	X	X	X			X		
R1_33	X	X	X	X	X	X		
R2_33	X	X	X	X	X	X		
R3_33	X	X	X			X	X	X
SC	X	X	X	X	X	X		

Microscopic examination in SEM of green samples as well as surface- and core samples pro-cured in EBF was conducted. The most common mineral phase that was identified with SEM/EDS in the green coke was the aluminosilicate meta kaolinite. A few particles containing alkali, including both potassium and sodium, were identified with the EDS. The particles containing alkali were aluminosilicates, which were found both at surface and in the core of the coke pieces.

A summary of identified phases by SEM in pro-cured samples are seen in **Table 39** and the corresponding SEM images for R1, R2 and R3 are seen in **Figure 186-Figure 188**. As for the green samples, the mineral phases were distributed throughout the whole coke piece in varying size and shape, fine divided particles in clusters, single particles in varying size and as a fibrous structure in the coke matrix. Alkali, mainly potassium, bearing minerals was widely detected with SEM/EDS in all analysed coke pieces from BL 33. The content of potassium, silica and aluminium varied within the different phases. Potassium was also detected in the coke matrix, throughout the whole pieces. Alkali bearing aluminosilicates were the most frequently detected phases, the two most common phases were kalsilite and leucite. SiO<sub>2</sub> particles with a higher content of potassium were detected in all samples beside in R3 (Al<sub>2</sub>O<sub>3</sub>).

**Table 39** Phases detected with SEM/EDS. The number to the left corresponds to the markers in Figure 186-Figure 188 in C32.

Nr.	Phase	Coke samples				
		BC3_33	R1_33	R2_33	R3_33	SC_33
1	Quartz SiO <sub>2</sub>	X	X	X	X	X
2	Corundum Al <sub>2</sub> O <sub>3</sub>				X	
3	Wustite FeO		X	X	X	X
4	Feldspar Ca <sub>2</sub> AlSiO <sub>5</sub>	X	X			
5	K-feldspar K <sub>2</sub> Si <sub>4</sub> O <sub>9</sub>				X	
6	Leucite KAISi <sub>2</sub> O <sub>6</sub>	X	X	X	X	X
7	Sanidine (K,NA)AlSi <sub>3</sub> O <sub>8</sub>		X			X
8	Kalsilite KAISiO <sub>4</sub>	X	X	X	X	X
9	(K,NA) <sub>3</sub> Al <sub>10</sub> Si <sub>10</sub> O <sub>38</sub>	X	X			
10	(K,Na) <sub>2</sub> OAl <sub>4</sub> Si <sub>4</sub> O <sub>15</sub>	X	X	X	X	X

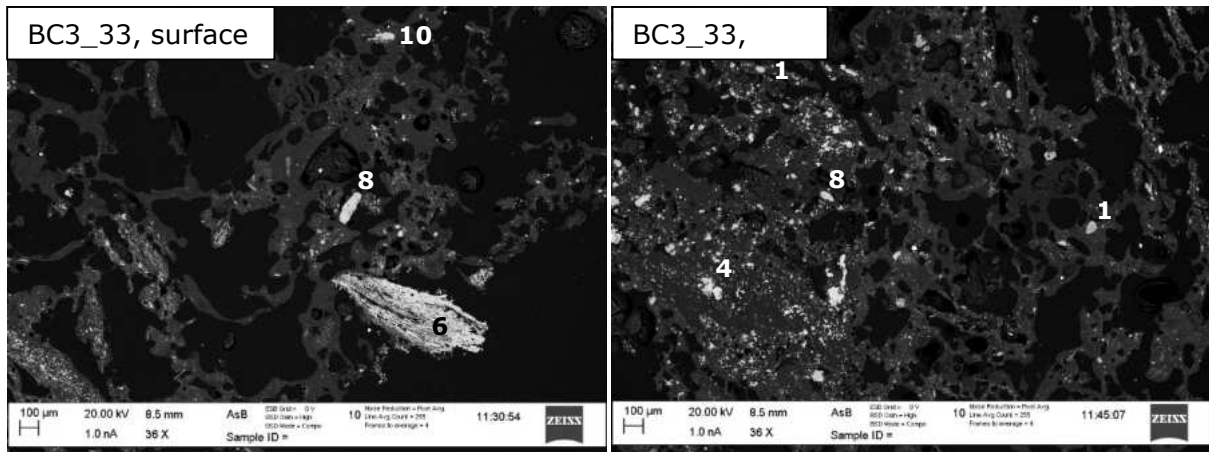


**Figure 186** SEM images of the surface and core of BC3 from BL 3 (C32).

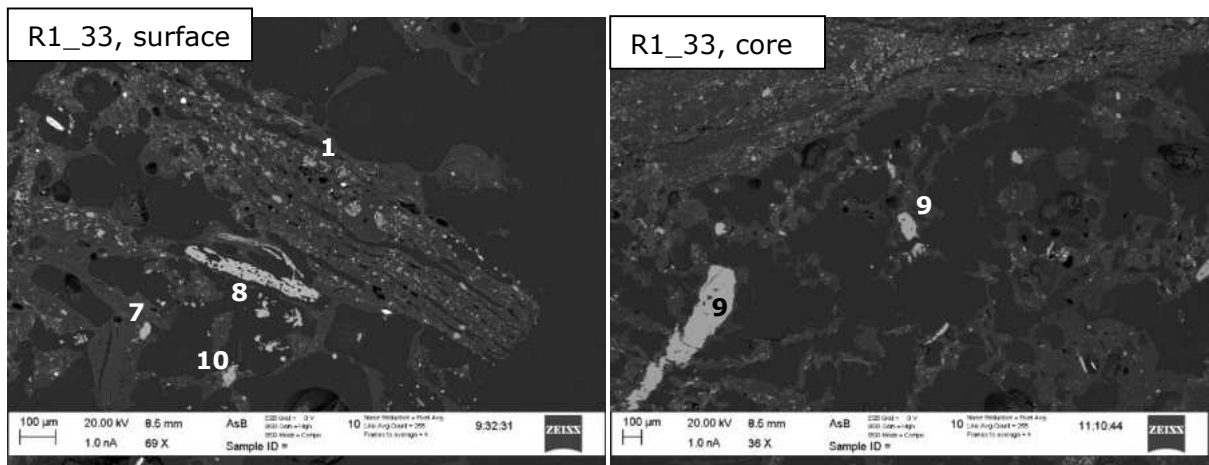


**Figure 187** SEM images of the surface and core of R1 from BL 33 (C32).

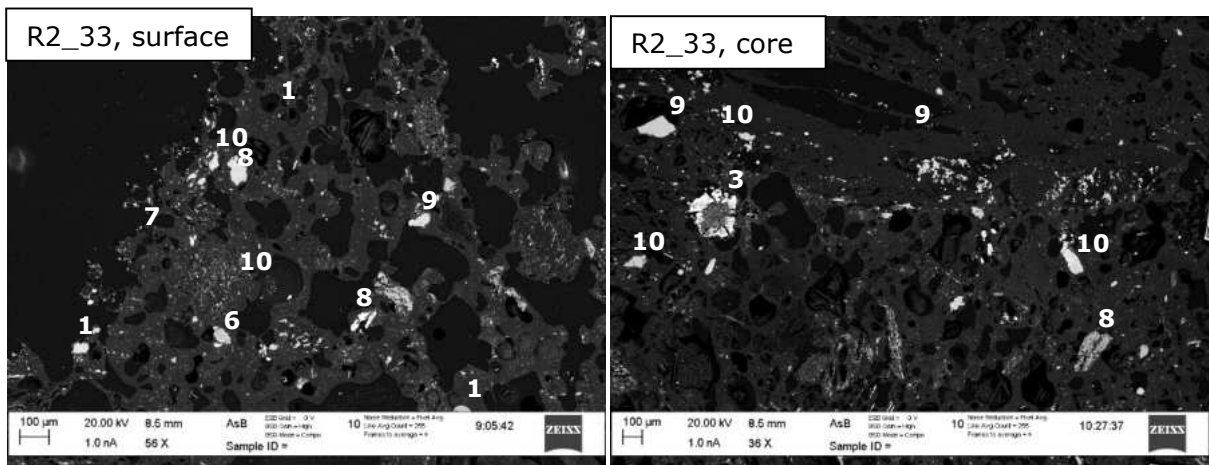


**Figure 188** SEM images of the surface and the core of R2 from BL 33 (C32).

As coke descent through a blast furnace, it is exposed to extreme reacting conditions and high temperatures leading to increased degree of coke graphitization. Coke graphitization means that the ordering of the carbon structure has increased, i.e. a more crystal structure which contributes to reduced coke reactivity. The degree of graphitization is represented by the  $L_c$  values, method is described in [47].  $L_c$  values of samples are seen in **Table 40** and in **Figure 189**, the  $L_c$  values are

plotted against the vertical position of the excavated baskets. A general trend seen is that the  $L_c$  values were increasing with increasing distance from the charging level and thus the temperature. The  $L_c$  values of R3 ( $\text{Al}_2\text{O}_3$ ) and BC3 were lower than the other test cokes located at similar vertical position in the EBF. The values were also significantly lower at the largest distance from the charging level, at BL 33. R2 from BL 31 has almost the same horizontal position in the EBF as BC3 and R3 in layer 33 and the difference between the vertical positions of the baskets were only 29 mm. These baskets can thus directly be compared with each other, besides that R3/BC3 had been in the EBF 4 minutes longer. For R2 (L31), the  $L_c$  value was 26.7 Å whereas the corresponding value for R3 (L33) was 21.8.

**Table 40**  $L_c$  values and the vertical position in the EBF, BC=base coke, R1=1% kaolin, R2=1%  $\text{SiO}_2$ , R3=1%  $\text{Al}_2\text{O}_3$ .

BL	Position [m]	$L_c$		Position [m]	$L_c$		Position [m]	$L_c$	
		BC1 [Å]	R1 [Å]		BC2 [Å]	R2 [Å]		BC3 [Å]	R3 [Å]
17	3.81	22.1	19.0	3.81	20.9	20.2	3.72	18.0	19.0
21	4.16	21.6	19.5	4.19	19.0	20.3	4.09	20.5	20.5
25	4.32	24.2	25.3	-	-	-	4.33	23.6	20.1
29	4.54	27.5	30.9	-	-	-	-	-	-
31	4.63	26.1	28.4	4.45	24.1	26.7	-	-	-
33	4.66	27.24	29.8	4.48	29.0	23.3	4.51	20.6	21.8

Of all samples, BC3 and R3 have the two highest concentrations of alkali and also the lowest  $L_c$  values at BL 33. The  $L_c$  values are plotted against the alkali concentration in the coke pieces in **Figure 189**. BC1, R1, BC2 and R2 follows a clear trend in where the  $L_c$  value is increasing with the alkali content and thus also the distance from the charging level. Meanwhile the  $L_c$  value of BC3 was first increased until BL 25, the value was then decreased at BL 33 where the alkali content was highest. The  $L_c$  values of R3 were almost constant at all levels in the EBF, independent of alkali content. The coke samples with the 5 highest alkali contents, exceeding 2.5 % has a lower degree of graphitization.

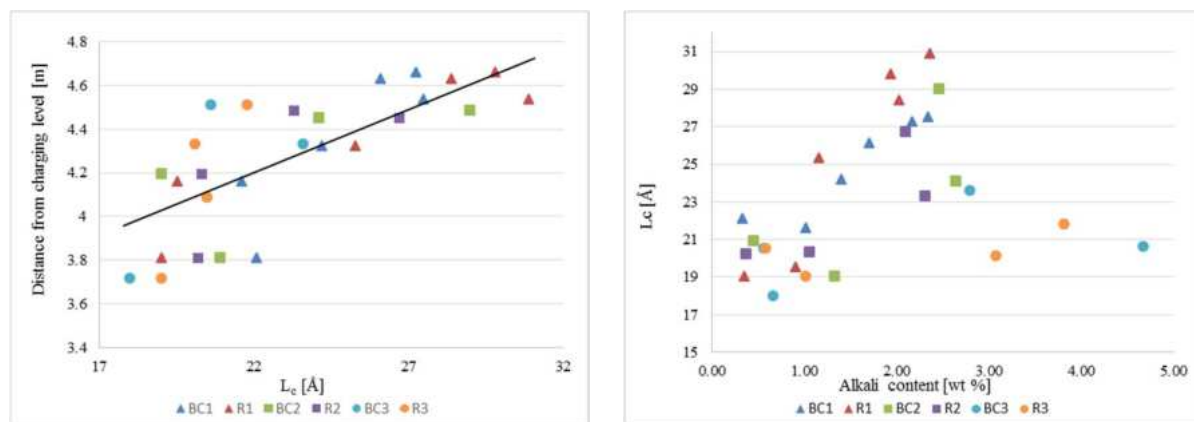


**Figure 189**  $L_c$  values plotted against the position in the EBF.

The reactivity of the different coke samples have been studied by Thermogravimetric Analysis (TGA). Among the original coke samples, as expected, no significant difference in reactivity could be seen. The starting temperature of the solution loss reaction was plotted against the alkali

content for all procured samples analysed with TG, see **Figure 190**. The trend shows that the temperature at which the reaction start decreases with increasing alkali content.

The carbon conversion in all coke samples from BL 33, R3 and BC3 from BL 25 and R1 and BC1 from BL31, at 1150°C and 950°C is plotted against the alkali content, see right-hand image in **Figure 190**. Same trend can be seen at both temperatures. The carbon conversion was increasing with increasing alkali content in the coke independent if it was base coke or some of the test cokes. The highest conversion was for BC3 from BL 33 of 17.3% at 950 °C and 71.6% at 1150 °C. BC1 from BL 33 had the lowest conversion of 4.6% at 950°C, it was a small difference between the samples with an alkali content below 2.5%. BC1 from BL 31 had the lowest conversion of 35.1% at 1150°C. The final temperature was set to 1150°C to avoid the influence of available carbon in the samples.

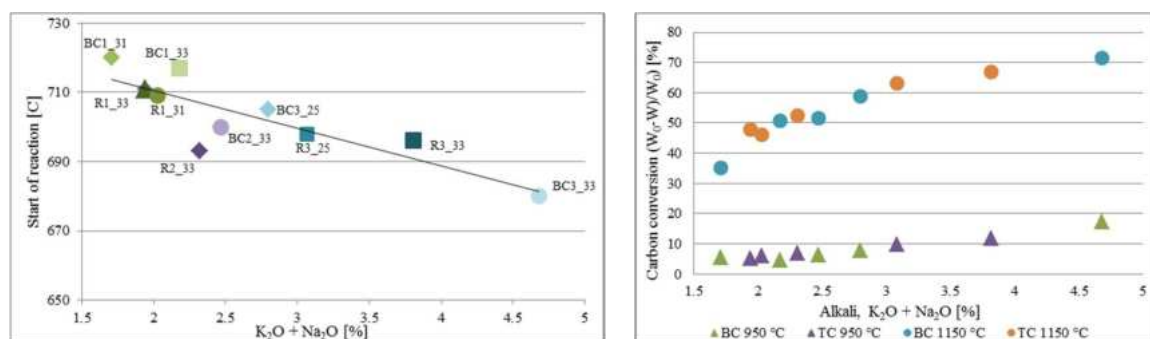


**Figure 190** Start of reaction and carbon conversion plotted against alkali content.

The activation energy plotted against the alkali content is shown in left-hand image of **Figure 191**. The activation energy was decreasing with increasing alkali content in the coke independent of which coke type it was. The test coke R3 (Al<sub>2</sub>O<sub>3</sub> addition) has the highest alkali value of 3.8% and the base coke has the highest alkali content of 4.9%.

The apparent reaction rate (gg<sup>-1</sup>s<sup>-1</sup>) at 800 and 850°C is shown in **Figure 191**. The apparent reaction rate is increasing with increasing alkali content. The apparent reaction rate was highest for BC3 at both temperatures, BC3 also has the highest content of catalysing components, R3 (Al<sub>2</sub>O<sub>3</sub> addition) had the second highest at both temperatures. R1 (Kaolin addition) has a higher apparent reaction rate and a lower alkali content than BC1, the same trend can be seen for R2 (SiO<sub>2</sub> addition) and BC2 at 850°C.

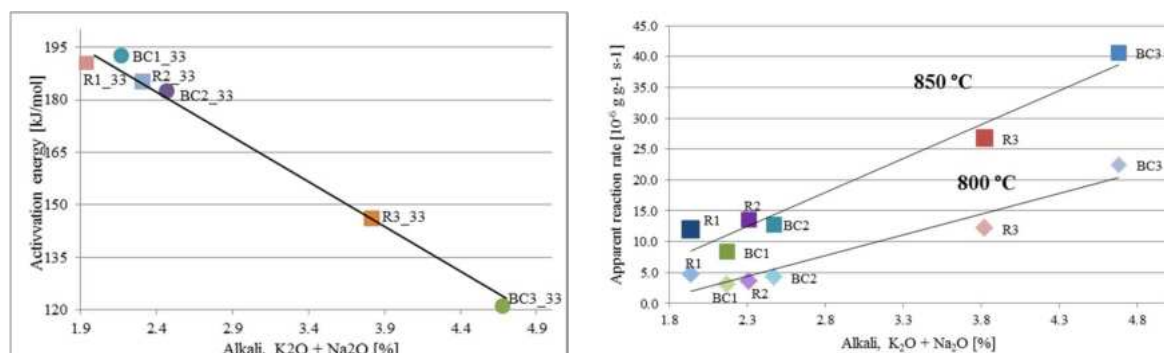


**Figure 191** Alkali content plotted against activation energy (left). Apparent reaction rate plotted against alkali content in coke samples (right).

The main conclusions from the evaluation of basket samples containing test coke with modified ash

composition from C32 was that the alkali content in coke was increasing with distance from charging level and dependent on the horizontal position in the furnace. The extent of alkali uptake was more influenced by the conditions at each position, which the mineral addition could not overcome. From XRD and SEM examination of the samples, all aluminosilicates identified contained alkali, the main alkali containing phases found was Kalsilite and Leucite and alkali was distributed throughout the whole coke piece. The results also showed that the base coke in most cases had a higher alkali content except for the test coke with addition of bauxite where the relation was opposite in most cases. During the SEM/EDS analysis of R3, unreacted grains with bauxite were found, which was also confirmed in the XRD. This indicates that bauxite was inactive in the absorption of alkali. Unreacted grains with quartz were found in all samples and also some grains with alkali in.

Study of the graphitisation degree of pro-cured samples revealed that the graphitisation increased with distance from charging level, except when the alkali content exceeded 2.3%. This indicates that alkali destroys the graphite structure in the coke. Furthermore, by TGA results it could be confirmed that the reactivity of coke increased with alkali content. The carbon conversion and thus the reactivity increased with the alkali content in both the test coke and the base coke. The reactivity of the test coke was thus not decreased due to the mineral addition.

In EBF campaign C33 2017, 16 new basket samples were charged prior quenching and excavation that contained test coke with addition of 2% kaolin in the coal blend, which is corresponding to carbonization test 1R in **Table 34**, test coke coated with kaolin and a reference coke (4R and 5R in **Table 34**). Coke coated with kaolin was prepared by immersing coke (4R and 5R) in a slurry containing 33% kaolin for 1 minute. The charging schedule of baskets in K33 is shown in **Figure 192** below. RC is the reference coke, TC is corresponding to test coke with 2% kaolin in coal blend, CC1 is coke coated with the 23% kaolin slurry and CC2 is the coke coated with 33% kaolin slurry. A more detailed description of methods and results can be found in [46].

<b>Layer</b>	<b>Basket 1</b>		<b>Basket 2</b>			<b>Basket 5</b>		<b>Basket 6</b>	
<b>20</b>	RC	TC	RC	CC1		RC	TC	RC	CC2
<b>24</b>	RC	TC	RC	CC1		RC	TC	RC	CC2
<b>28</b>	RC	TC	RC	CC1		RC	TC	RC	CC2
<b>32</b>	RC	TC	RC	CC1		RC	TC	RC	CC2

**Figure 192** Charging schedule of baskets containing reference coke, test coke with 2% kaolin and coated coke in C33. Retrieved samples at excavation are highlighted in red text.

Of all 16 baskets charged to the EBF, only 3 ½ baskets were retrieved. These baskets had been charged in burden level 20 and 28 and are highlighted by red text in charging schedule in **Figure 192**. According to the schedule, none of the baskets containing coated cokes could be found. The depth and horizontal position of retrieved baskets are shown in **Figure 193**.

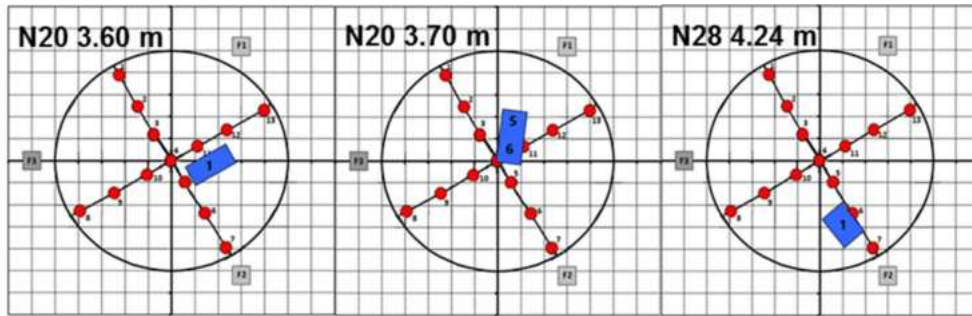


**Figure 193** Horizontal position of baskets retrieved from C33 in EBF after excavation.

The alkali content in basket samples after being in the EBF is plotted against depth below charging level in **Figure 194**. Based on this, no correlation between alkali content and depth from charging level can be seen, neither in the test coke (TC) with 2% kaolin or the reference coke (RC). The TC samples in basket N28K1 had an alkali level in between the two other TC samples that was found further up the EBF. Two TC samples also had similar alkali levels despite being found at different depths. Basket sample N20K6 RC found closest to the middle of the EBF had the highest total alkali content. By comparing TC and RC within the same basket it is seen that the alkali content is always higher in coke containing kaolin. N28K1 and N20K5 had similar alkali contents even though they were found on different levels in the EBF. This is indicating that horizontal positioning mattered more than vertical i.e. the temperature exposure and gas composition of the EBF mattered more than position. The temperature probes indicated that the heat profile had been central above the height where the samples were found and the melting of basket N20K6 found in the middle indicated that the highest gas flow was at the center of the EBF. During the previous campaign 32 the temperature profile in the EBF had been flatter, as revealed by the alkali distribution described in Task 1.3.

The graphitization degree of coke in basket samples from C32 and C33 are compared in **Figure 194**. TC from C32 is corresponding to test coke containing 1% kaolin. In general, higher  $L_c$  values are found for coke from C33 despite being found higher up in the shaft. This is supported by the distribution of coke and pellets in burden layers shown in **Table 17**, with more pellets distributed towards the walls in C33 compared to C32 causing a more centralized gas flow. Moreover, the alkali content in coke from C33 was also lower in general, which indicated that the circulating alkali load could have been lower compared to C32. This could be attributed to the more pronounced central gas flow, which is a known counteraction to increase alkali outputs via the top.

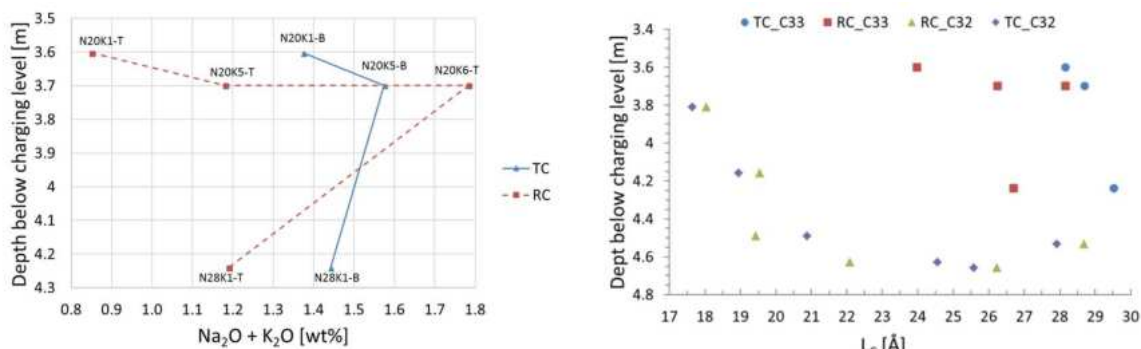


**Figure 194** Alkali content in coke from retrieved baskets after C33 (left) and graphitization degree of coke from baskets in C32 and C33 (right) as function of distance from charging level.

The effect of wt-% K<sub>2</sub>O on start of reaction temperature and activation energy in coke with 0, 1 and 2% kaolin in coke ash is shown in **Figure 195**. The general trend is that the start temperature and activation energy for the coke gasification reaction are both reduced with increasing potassium content. Among the different coke types studied, the kaolin addition seems to have no or a very small impact on the start of reaction temperature based on the high goodness of fit (94%) of the trendline. A larger spread in the data is shown when plotting the activation energy versus K<sub>2</sub>O. The coke containing 2% kaolin seem to have lower activation energy in proportion to the K<sub>2</sub>O content compared to both reference coke and coke with 1% kaolin.

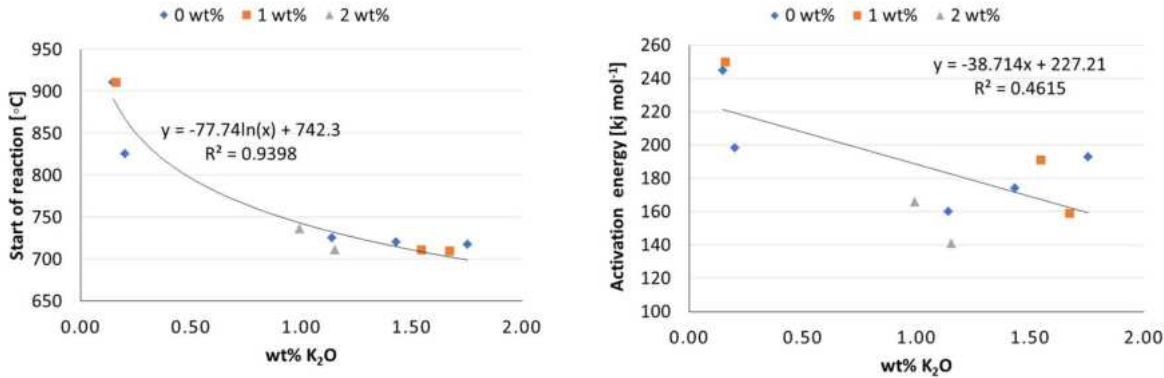


**Figure 195** Start of reaction (left) and activation energy (right) of coke with 0%, 1% and 2% kaolin as a function of K<sub>2</sub>O wt-%.

Reaction rate for the samples increases in general with increased K<sub>2</sub>O content as seen in **Figure 196**. The increase was similar for all samples and showed that the kaolin addition did not change the reaction rate and that it was alkali that was the main reason behind the increase. The increased reaction rate could be fitted to an exponential curve well with a R<sup>2</sup> of 80%. The SSAB coke was excavated from the coke layers and is corresponding to an industrially produced coke with significantly lower reaction rate in proportion to the alkali content compared to the reference- and test cokes produced in laboratory scale.

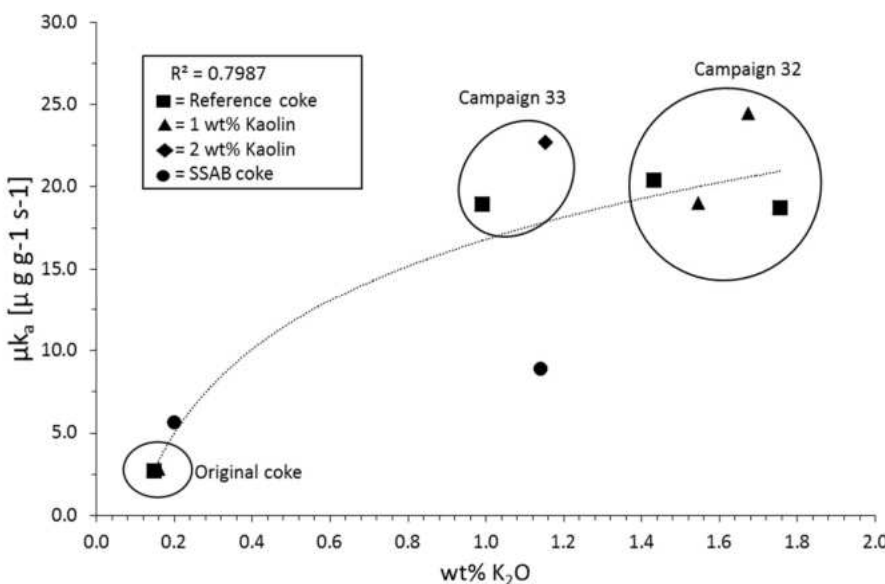


**Figure 196** Reaction rate as a function of wt-% K<sub>2</sub>O in coke at 900°C.

To further examine the effect of mineral additions to coke ash with respect to alkali, laboratory investigations on coke with kaolin additions (2%, 4% and 8%) to coke ash and a kaolin coated

coke was conducted. The coated coke was prepared from the reference coke (RC\_DMT) according to the same procedure as described earlier. For the trials, coke in the size range 3-4 mm was used. The different coke types were first treated for uptake of alkali vapour in a laboratory furnace (Tamman) by reducing  $K_2CO_3$  with activated carbon in the bottom of a graphite crucible forming gaseous K. The gas could ascend and come in contact with the above coke through a perforated graphite spacer, see outline in **Figure 197**. The trials were conducted in inert atmosphere (Ar) and the heating rate was 10°C/min up to 1150°C and the furnace was thereafter kept at that temperature for 4 hours before cooling. The K/coke ratio was for each trial 4% based on stoichiometric formation of K from  $K_2CO_3$ . Activated carbon was added in excess to ensure complete reduction of  $K_2CO_3$ .

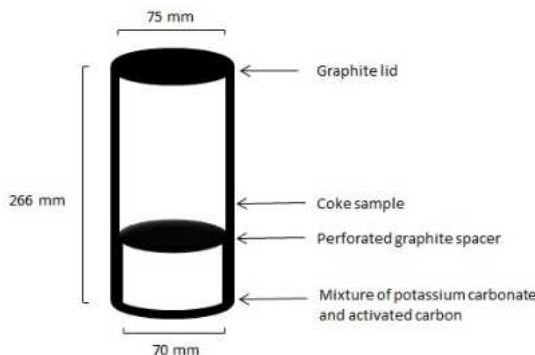


**Figure 197** Graphite crucible for alkali vapour generation and uptake in coke.

The different treatments of coke with alkalis are summarized in **Table 41**. Coke types named RC and TC\_2% are the similar coke as studied in basket samples from EBF C33 whereas the other cokes were specially produced for these trials at LTU, see recipes in **Table 42**.

**Table 41** Summary of alkali impregnation trials.

Trial	Coke type	Abbreviation
1	Reference coke produced at DMT in Germany, 4R+5R	RC_DMT
2	Reference coke produced at LTU, same recipe as RC	RC_LTU
3	Test coke with 2% kaolin, produced at DMT	TC_2%DMT
4	Test coke with 4% kaolin, produced at LTU	TC_4%LTU
5	Test coke with 8% kaolin, produced at LTU	TC_8%LTU
6	Kaolin coated reference DMT coke	TC_coatedDMT

**Table 42** Recipes of cokes produced at LTU.

	<b>RC_LTU</b>	<b>TC_4%</b>	<b>TC_8%</b>
LV coal %	40	38.4	36.8
MV coal %	30	28.8	27.6
HV coal %	25	24	23
Pet coke %	5	4.8	4.6
Kaolin %	0	4	8

The total content of potassium, here assumed to be in the form of  $K_2O$ , before and after treatment of coke for  $K_2O$  uptake is shown in **Figure 198**. Highest  $K_2O$  content was found in the coke with

8% kaolin and lowest in the coated coke, even though the coated coke had the highest initial content of K<sub>2</sub>O. Moreover, the coated coke was the only sample that had lost weight after the trial. This might be due to loss e.g. chemically bound water from the kaolin clay. The coated coke was dried in 105°C before the treatment with alkali vapour. Both reference cokes and the coke containing 2% kaolin had similar K<sub>2</sub>O uptake of 2%. Moreover, balances of in- and outgoing oxides that should be stable and not react during these conditions such as Al<sub>2</sub>O<sub>3</sub> and CaO indicated that the accuracy of the analyses is too low for comparison in the hundredths-range of percentages. Thus, the potassium content after the alkali uptake trials for both RC and the TC-2% can be regarded as similar. Complete analyses of cokes can be found in **Appendix Table A4**.



**Figure 198** Potassium content (wt.-%) in coke before and after trials for uptake of potassium and the total weight change of coke.

As the coated coke was made from RC\_DMT, similar uptake of potassium or even higher was expected as the capacity of binding alkali in the coke ash should not have been changed after coating. However, the potassium uptake was 10% lower in the coated coke compared to RC\_DMT which might be explained by the coating working as a protection shield against alkali penetration. The difference might also be explained by analytical errors as already discussed.

To study the impact of alkali uptake on coke reactivity and if the usage of kaolin incorporated in coke ash or as coating is shown to reduce the negative effects of alkali on coke, trials in a vertical tube furnace was conducted for study of gasification (with CO<sub>2</sub>). A sample of 20 grams of coke was placed in an Al<sub>2</sub>O<sub>3</sub> crucible. At the bottom of the crucible there were holes smaller than the particle size of the coke. The filled crucible was heated up to 800°C with a rate of 0.8°C/min and a flowrate of argon at 100ml/min. When the sample reached 800°C the argon was switched to CO<sub>2</sub> with the same flowrate as the argon and the heating rate switched to 2°C/min. When the furnace temperature reached 1150°C the sample was kept at that temperature for four hours and the flowrate of CO<sub>2</sub> was kept as previously at 100 ml/min. After four hours when the furnace was cooling down, the CO<sub>2</sub> was replaced with argon with a rate of 100 ml/min. A scale was connected to the test to measure the weight change during the course of the trial. A summary of all conducted trials in tube furnace is found in **Table 43**. The abbreviation for coke after potassium

uptake trials is PUP (potassium uptake).

**Table 43** Summary of conducted gasification trials in tube furnace.

Trial	Coke type	Abbreviation
1	Reference coke produced at DMT in Germany	RC_DMT
2	RC_DMT in Tamman furnace after potassium uptake	RC_DMT_PUP
3	Test coke with 2% kaolin, produced at DMT after potassium uptake	TC_2%DMT_PUP
4	Reference coke produced at LTU after potassium uptake	RC_LTU_PUP
5	Test coke with 4% kaolin produced at LTU after potassium uptake	TC_4%LTU_PUP
6	Test coke with 8% kaolin produced at LTU	TC_8%LTU
7	Test coke with 8% kaolin produced at LTU after potassium uptake	TC_8%LTU_PUP
8	Kaolin coated coke produced at LTU after potassium uptake	TC_coated_DMT_PUP

In **Figure 199**, weight loss- and temperature curves from two trials (No. 2 and 7) are shown. The weight loss started between 875-1000°C in all trials except for TC\_8%LTU\_PUP (no. 7) and RC\_LTU\_PUP (no.4). As the gas had to be switched manually from Ar to CO<sub>2</sub> it is suspected that this was not done for TC\_8%LTU\_PUP (no. 7) and RC\_LTU\_PUP (no.4) until the temperature reached the isothermal at 1150°C (1130 was the sample temperature). The total weight loss for these samples was also significantly lower, with more than 10% difference from the other samples. Hence, these trials cannot be compared to the other trials with respect to the reactivity properties for temperatures below 1130°C.

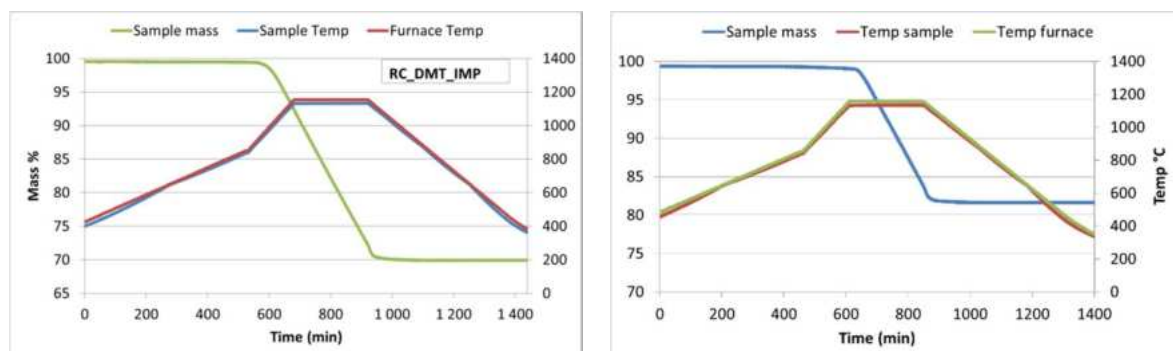


**Figure 199** Sample weight and temperature as a function of time for RC\_DMT\_PUP (Left) and TC\_8%LTU\_PUP (right) in tube furnace.

The start of reaction temperatures were manually read from the weight loss curves and are summarized in **Table 44**. As seen for trial no. 4 and no. 7, the start of reaction temperature is for both cases 1130°C, which is not likely without keeping an inert atmosphere. For the trials with green coke i.e. no alkali (No. 1 and No. 6), the solution loss reaction started earlier for the reference coke compared to the coke containing 8% kaolin, despite higher alkali content in the latter. This is in accordance with the CRI results presented in

**Table 35**, where kaolin containing coke had lower CRI values than the reference coke (4R and 5R). For cokes produced at DMT and exposed to alkali vapour (RC\_DMT\_PUP, TC\_2%DMT\_PUP), the coke containing 2% kaolin had nearly 20°C higher start of reaction temperature but the alkali content was also slightly lower in this coke. Apart from the two trials with late switching to CO<sub>2</sub> atmosphere, the coated coke had the highest start of reaction temperature but also lowest alkali content among the cokes exposed to alkali vapour. Compared to both green cokes after reaction in tube furnace, the coated coke had a significantly higher start of reaction temperature than these, despite containing more alkali.

**Table 44** Start of reaction for TC and RC cokes.

Trial	Abbreviation	Start of reaction	K <sub>2</sub> O + Na <sub>2</sub> O %	Tot. weight loss %
1	RC_DMT	927°C	0.20	17.7
2	RC_DMT_PUP	875°C	2.11	30.0
3	TC_2%DMT_PUP	894°C	2.07	28.6
4	RC_LTU_PUP	NA	2.11	19.0
5	TC_4%LTU_PUP	928°C	1.96	26.1
6	TC_8%LTU	949°C	0.36	15.6
7	TC_8%LTU_PUP	NA	2.29	18.3
8	TC_coated_DMT_PUP	976°C	1.94	19.2

The apparent reaction rate and carbon conversion at 950-1000°C, 1050-1100°C and 1130°C as a function of alkali content for the cokes with alkali uptake (PUP) is shown in **Figure 200**. Both reaction rate and carbon conversion increases with alkali content for all temperatures in general. The highest reaction rate is found for RC\_DMT\_PUP at 1130°C with a carbon conversion of 12%, followed by TC\_2%DMT\_PUP at the same temperature. The difference in reaction rate for these two cokes are also comparable at the temperature interval 950-1000°C but not at the temperature interval 1050-1100°C. If the small difference in alkali content between the different cokes is due to analytical errors which thereby can be neglected, then the reactivity of cokes seem to decline with increasing incorporation of kaolin in coke ash for all temperature intervals and lowest reactivity can be reached by coating the coke with kaolin. However, the difference in reaction rate between coke containing 4% and 8% respectively is small at 1130°C. The apparent reaction rates and carbon conversions from all trials are summarized in **Table A5 in Appendix**.

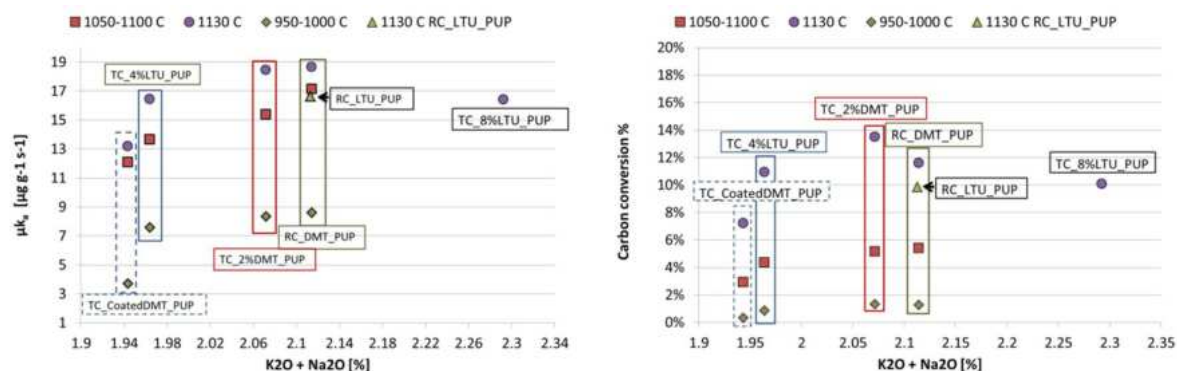


**Figure 200** Apparent Reaction rate as a function of alkali content for the coke types exposed to alkali vapour.

A comparison of the coated coke to the green cokes with respect to apparent reaction rates at 950–1000°C, 1050–1100°C and 1130°C is seen in **Figure 201**. The apparent reaction rate at 950–1000°C and 1130°C is only slightly higher for TC\_CoatedDMT\_PUP than the reference coke even though the alkali content is significantly higher. The extent of carbon conversion is lowest for the coated coke at 1130°C compared to the green coke with 8% kaolin.

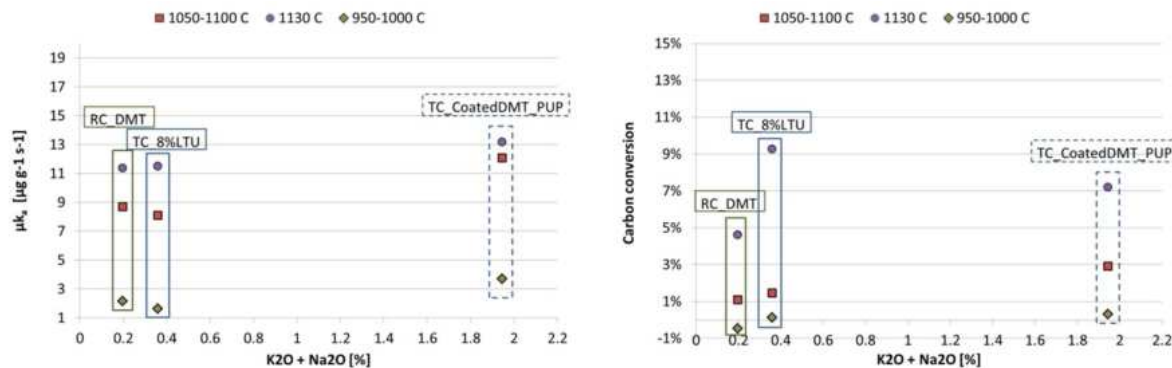


**Figure 201** Apparent Reaction rate as a function of alkali content for the different coke types.

The XRD diffractograms of green coke, alkali treated (PUP) and reacted (R) test coke containing 2% kaolin and the corresponding reference coke is shown in **Figure 202**. For the green coke found furthest down in the diagrams, alkali associated mineral phases could hardly be detected, only small intensity peaks of Leucite could be identified. The green reference coke produced at DMT was also tested in the tube furnace (RC\_DMT\_R) and the XRD results reveals that the same type of mineral phases are present as before but now with higher relative intensities. This can be explained by higher ash content in the sample after the reactivity test having an amplifying effect. For the samples with potassium uptake after Tamman furnace, no Kalsilite could be found with XRD even though both samples had an ash content of 13–14% and the total alkali content was above 2% in both. Instead, the Kalsilite peaks appear first after the cokes had been in the tube furnace with highest relative intensities found for the test coke (TC\_2%\_DMT\_PUP+R). This could indicate that the kaolin addition in TC\_2%DMT has contributed to the alkali capturing and that more alkali was present as free alkali in the coke matrix within the reference coke.

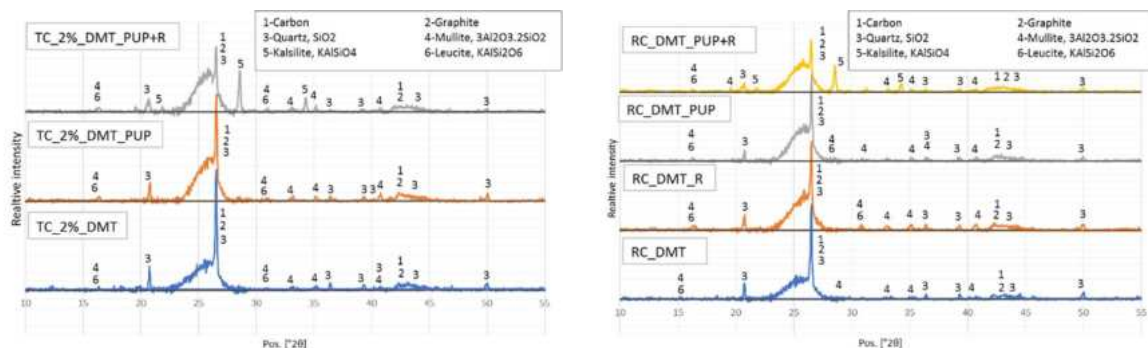


**Figure 202** XRD diffractograms of test coke with 2% kaolin and reference coke.

The XRD diffractograms of green coke, alkali treated and reacted test coke for coke containing 4% kaolin and the coated coke respectively are shown in **Figure 203**. Also for these, alkali associated phases are hardly detected for the green samples and no Kalsilite can be found in the coke samples before these were treated in the tube furnace. The peak corresponding to Kalsilite in test coke with 4% kaolin is relatively the coke peak at 26° not as high compared to the previous diffractogram of

TC\_2%. However, the relative intensity of Kalsilite is comparable to the reference coke RC\_DMT seen in previous figure. For the coated coke, the intensity peak of Kalsilite is small and comparable to Leucite. Both TC\_4%LTU and TC\_CoatedDMT had the lowest alkali uptake according to the chemical analysis which might explain the rather low relative intensities for alkali associated phases.

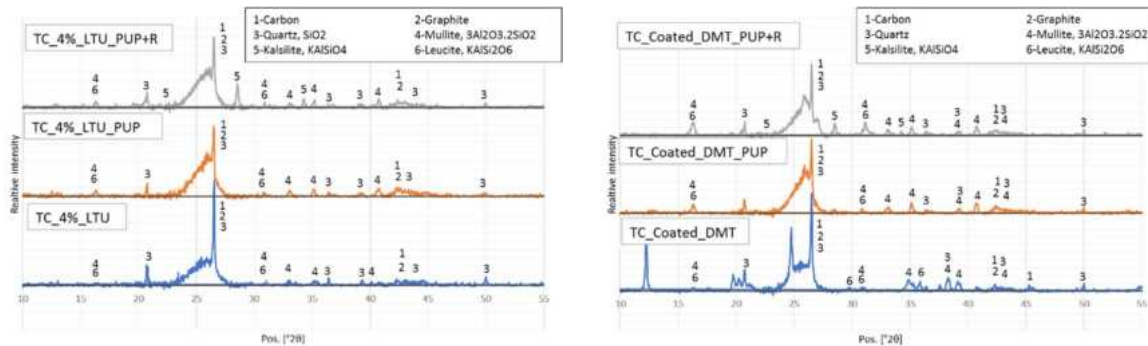


**Figure 203** XRD diffractograms of test coke with 4% kaolin and coated coke.

In **Figure 204** the XRD diffractograms of coke containing 8% kaolin and the corresponding reference coke produced at LTU is shown. Relative the other peaks, the intensity of the peak corresponding to Kalsilite is higher in the TC\_8% coke after alkali treatment and reaction in tube furnace. As for the other samples, the Kalsilite peak appears first after the being in the tube furnace in both TC\_8% and RC\_LTU.

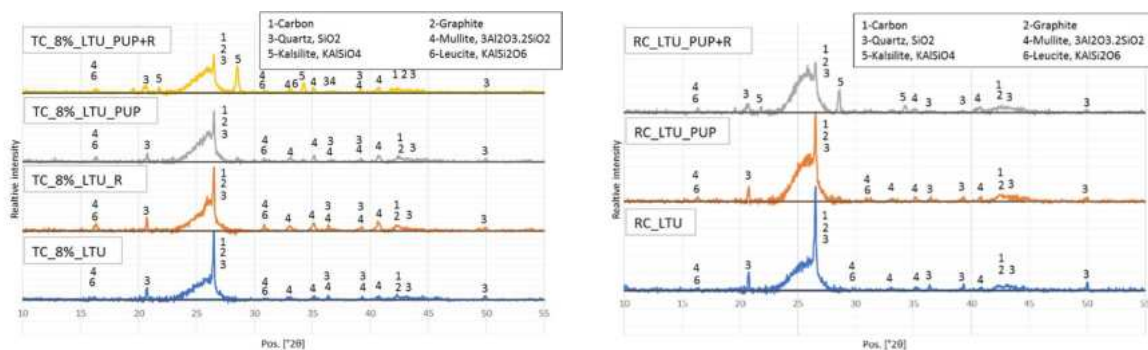


**Figure 204** XRD diffractograms of test coke with 8% kaolin and reference coke from LTU.

The graphitisation degrees of all coke have been calculated based on the same method as described in (1) and (2) and is plotted as a function of alkali content in **Figure 205**. Unlike investigations of basket samples, these cokes have been exposed to same temperatures and gas atmospheres which allows for a direct comparison between the different coke types. Alkalies are believed to have a negative impact on the coke structure and thereby also the graphitisation degree. After alkali treatment trials, highest graphitization degree is corresponding to the coated coke while the lowest value is found for the RC\_LTU coke. The coke type with highest alkali content in relation to the  $L_c$  value is TC\_8% whereas the lowest alkali content in relation to  $L_c$  is TC\_4%. Still, the TC\_2%DMT coke shows on a higher graphitization degree than the corresponding reference coke RC\_DMT and both are containing the same alkali content. According to the XRD-results, higher relative intensities of Kalsilite were found in TC\_2%DMT which could be attributed to the kaolin addition. The modified ash could thereby help in reducing the negative effect of alkali on coke reactivity and structure by formation of potassium containing aluminosilicates. The coated coke had a lower alkali uptake after impregnation compared to the other cokes, which could be explained by the coating working as a protection shield against alkali penetration. Moreover, the reactivity properties were comparable to cokes without alkali uptake and the graphitization degree

was significantly higher than in these, see **Table A6 in Appendix**. Thus, the results indicated in overall that the kaolin addition to coke ash or as coating seems to be beneficial for prevention of alkalis negative effects on coke. All cokes treated with potassium in the Tamman furnace had K<sub>2</sub>O content of similar level, roughly 2%. Further, all cokes prepared at DMT with kaolin, both added before cokemaking and as coating, showed lower reaction rates with CO<sub>2</sub> at all temperature intervals studied compared to the reference coke.

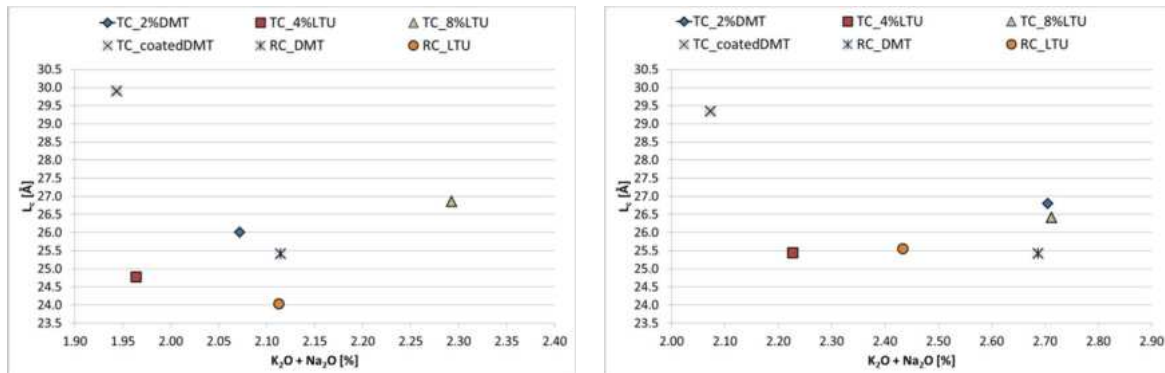


**Figure 205** Graphitisation degrees of alkali treated cokes (left) and after reactivity trials (right).

### 2.3.2.2.4 Lab-scale trials for determination of alkali inhibiting effect by coke pre-treatment with alkali absorbing additives (BFI)

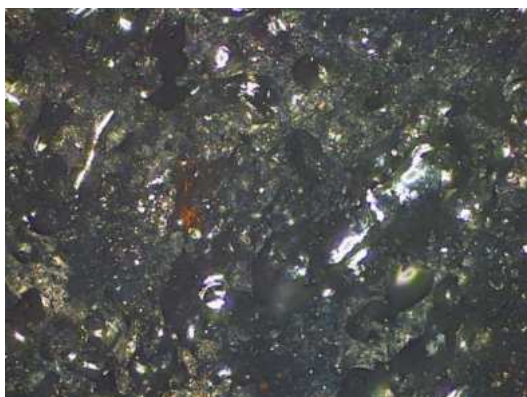
Based on previous results with reactivity tests on coke with modified ash and coated coke samples at the LKAB EBF (chapter 2.3.2.2), and supported by results of thermodynamic calculations, BFI also selected kaolin as the most promising coke additive aiming in capturing the alkali components into high-melting K compounds like kalsilite (KAISiO<sub>4</sub>), so that they can be discharged from the alkali cycle in the blast furnace.

In contrast to the previously described trials by SWERIM and LKAB, which were using kaolin mostly as additive for cokemaking, here the *coating* of near-industrial scale coke pieces with kaolin was investigated by lab trials with the inductively heated two-zone reactor (see chapter 2.3.1.3.5, Task 1.3). Industrial coke samples from VASD (crushed to 20 mm coke pieces) were used. Alkali components were only applied to the coke of the high-temperature zone (alkali evaporating zone) using K<sub>2</sub>CO<sub>3</sub> solution (see description in chapter 2.3.1.3.5). The applied alkali amount with a target of 2 % K (for preparation in 1014 g/l K<sub>2</sub>CO<sub>3</sub> solution) corresponds to the alkali load expected to be present within the alkali circulation zone of industrials BF's.

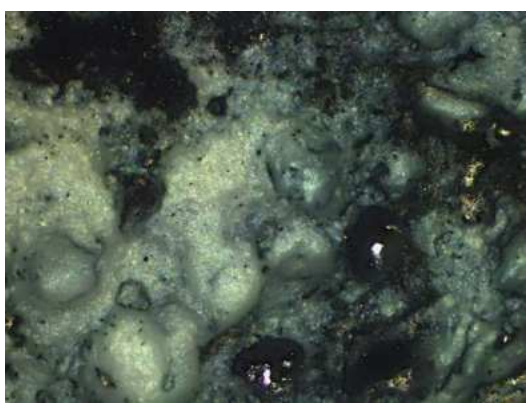
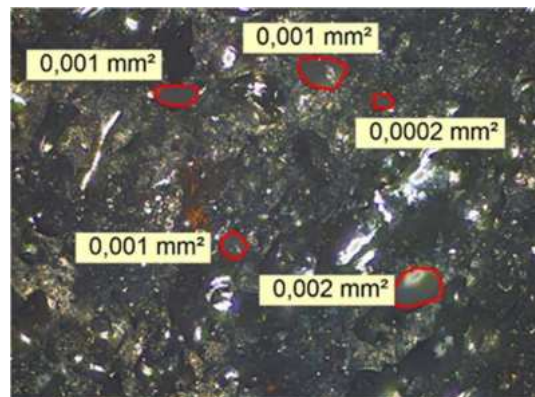
For coating the coke samples with the kaolin, a slurry of 14 % kaolin in water has been prepared. A kaolin addition of around 1.5 % (of the total weight) was obtained by 1x immersion in the slurry and drying afterwards. With 3x immersion into the slurry (and intermediate drying after each immersion), a kaolin content of around 5 % was obtained. If K pre-treated coke (for zone 1) is used, this pre-treatment is applied prior to the kaolin coating. In order to minimise K loss by dissolution of K<sub>2</sub>CO<sub>3</sub> when using coke samples with K pre-treatment, the immersion in the kaolin slurry was only kept short for all kaolin coated samples. For all trials with kaolin coated coke, the same coating is applied for the coke in both temperature zones of the two-zone reactor (zone 1 and zone 2), while only the coke in zone 1 is pre-treated with potassium carbonate.

Gas analyses for HCN were performed during the trials in the two-zone reactor (for description of procedure, see chapter 2.3.1.3.5, Task 1.3). After the trial, only the coated coke from the lower-

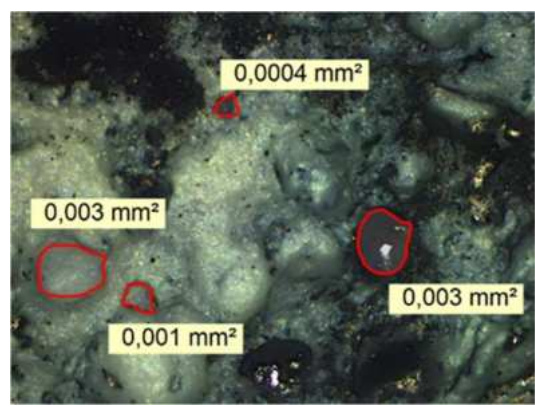
temperature zone (zone 2) of the two-zone reactor, which is exposed to condensing alkali components, was investigated for coke reactivity.



Coke untreated



Coke + kaolin 1x



Coke + kaolin 3x

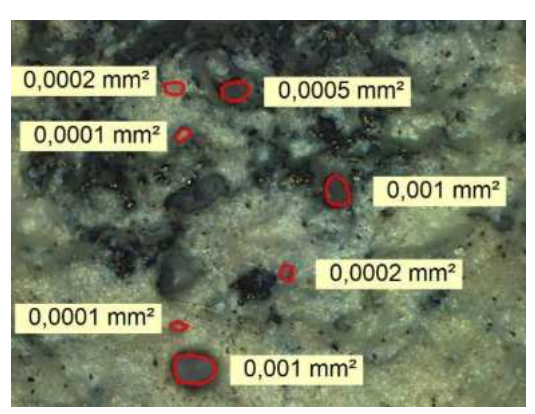


**Figure 206** Microscopic images - Comparison of surfaces (left) and pore diameters (right) of untreated coke (1<sup>st</sup> row) with a coke after kaolin pre-treatment (1x and 3x; 2<sup>nd</sup> and 3<sup>rd</sup> row)

In **Figure 206** the microscopic images of the coke surfaces with and without kaolin coating are presented. Surfaces (left) and pore diameters (right) of untreated coke (1<sup>st</sup> row) are compared with two cokes after kaolin pre-treatment (1x and 3x; 2<sup>nd</sup> and 3<sup>rd</sup> row). It is clearly shown, that the pores are increasingly sealed with repeated immersion in the kaolin slurry (pore diameters decrease from 1x to 3x kaolin).

#### Gas analyses – HCN

The intended absorption of alkali compounds by the kaolin coating is expected to result in lower potassium evaporation from the hot zone (zone 1), and in this way in lower HCN concentration within the process gas (cf. Task 2.1). This behaviour was investigated by HCN gas analyses with the FTIR spectrometer as described for Task 2.1.

Within **Table 45** the process parameters, the K content of coke samples and the results of the process gas analyses are presented. All trials with kaolin coating and the comparative trials without additive or pre-treatment are listed (V9-17). Here, it is shown that the analysed K content in the coke of zone 2 after the trials virtually is the same for all trials, independently from the K content in zone 1 and from the kaolin coating. So, it becomes obvious that the expected alkali carry-over from the high-temperature zone to the lower-temperature zone does not take place. This might be explained by insufficient gas stream between the two temperature zones or by condensation of evaporated alkali compounds at other parts of the reactor.

**Table 45** Process parameters, K content of coke samples and results of process gas analyses – trials with kaolin and comparative trials without additive or pre-treatment – Average values (V9-17)

	Process parameters			Coke sample		Process gas analyses - Average values **
Trial No.	Coke pretreatment with $K_2CO_3$ solution; conc. of solution	Coke additive	$H_2$ input in Vol.-%	K in % Zone 1*	K in % Zone 2*	HCN in ppm
V1	none	none	3 %	0.17	0.16	3
V2	1014 g/l	none	3 %	1.96	0.17	14
V9	none	Kaolin (1x), ca. 1.5 %	3 %	0.14	0.16	5
V10	1014 g/l	Kaolin (3x), ca. 5 %	3 %	0.72	0.16	7
V11	none	Kaolin (3x), ca. 5 %	3 %	0.20	0.16	9
V12	1014 g/l	Kaolin (1x), ca. 1.5 %	3 %	1.09	0.16	10
V13	1014 g/l	None	5 %	1.45	0.15	14
V14	1014 g/l	Kaolin (3x), ca. 5 %	5 %	0.73	0.18	12
V16	none	none	3 %	0.15	0.15	5
V17	none		5 %	0.15	0.17	7

\* after trial; \*\* during second half of trial

In **Figure 207** the average HCN concentration compared to the K content in zone 1 is presented for a coke without K pre-treatment (0 – 5 % kaolin, V9, V11 and V16), while **Figure 208** presents the same issue for a coke with high K pre-treatment (0 – 5 % kaolin, V2, V10 and V12). In both figures, the hydrogen input content is 3 Vol.-%. For a higher H<sub>2</sub> content of 5 Vol.-%, the average HCN concentration compared to the K content in zone 1 is shown in **Figure 209** for coke with high K pre-treatment (0 and 5 % kaolin, V13, V14). In the mentioned figures, the measured HCN concentrations in the process gas are quite in line with the K content of the coke in zone 1. An inhibiting effect on the HCN formation just due to the kaolin coating was not observed.

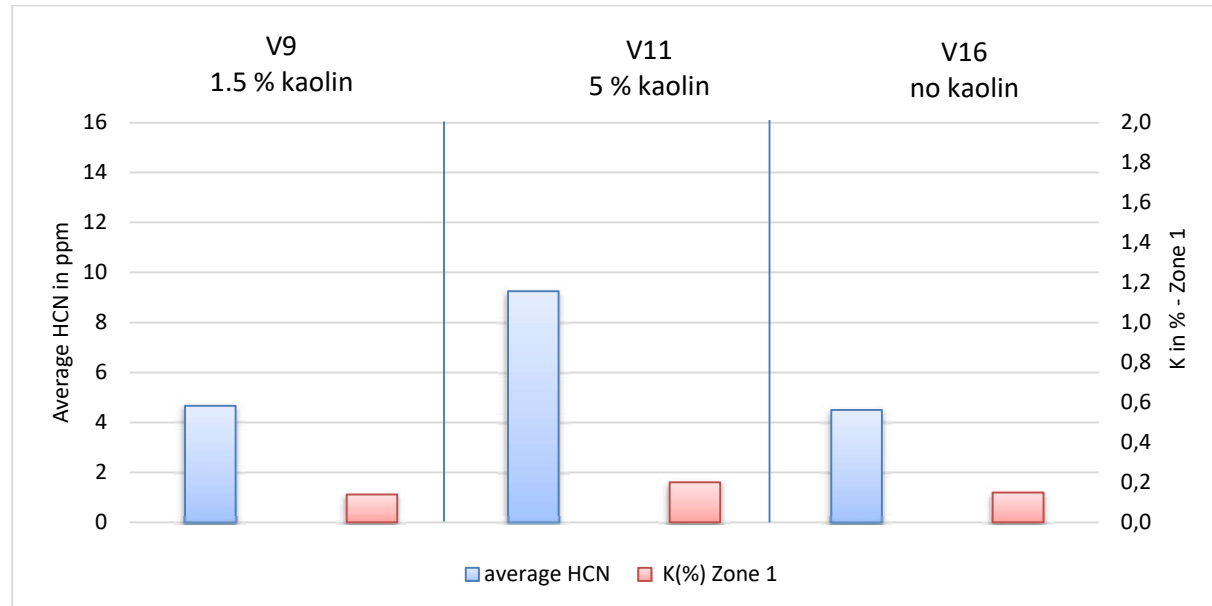


**Figure 207** Average HCN concentration compared to K content in zone 1 - coke without K pre-treatment (0 – 5 % kaolin, all 3 % H<sub>2</sub>; V9, V11 and V16)

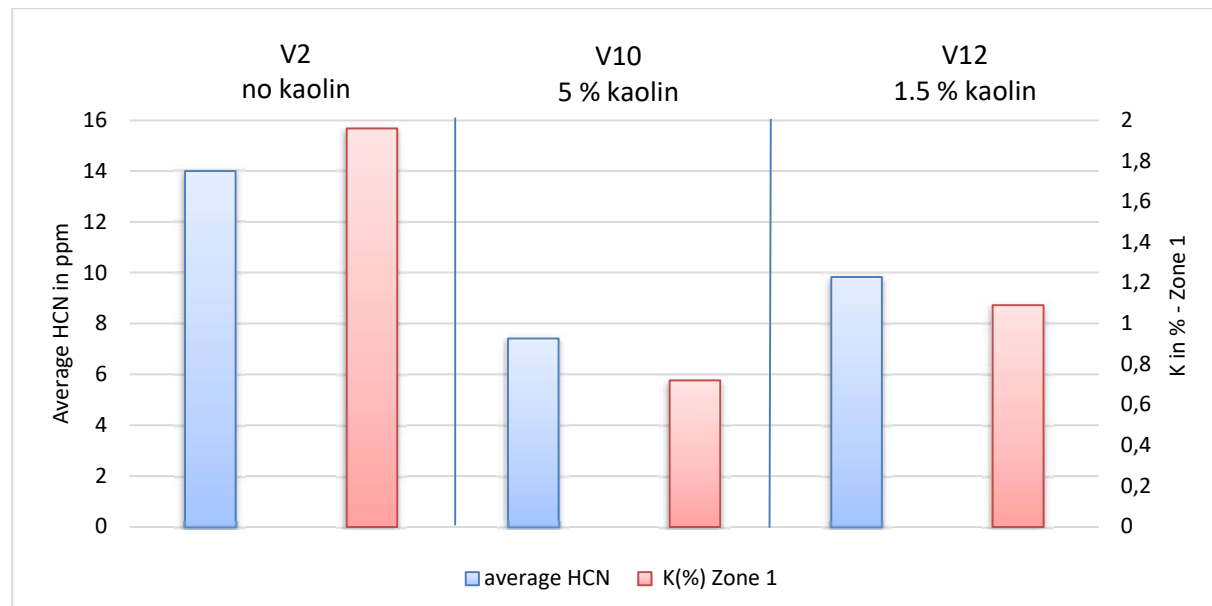


**Figure 208** Average HCN concentration compared to K content in zone 1 - coke with high K pre-treatment (0 – 5 % kaolin, all 3 % H<sub>2</sub>; V2, V10 and V12)

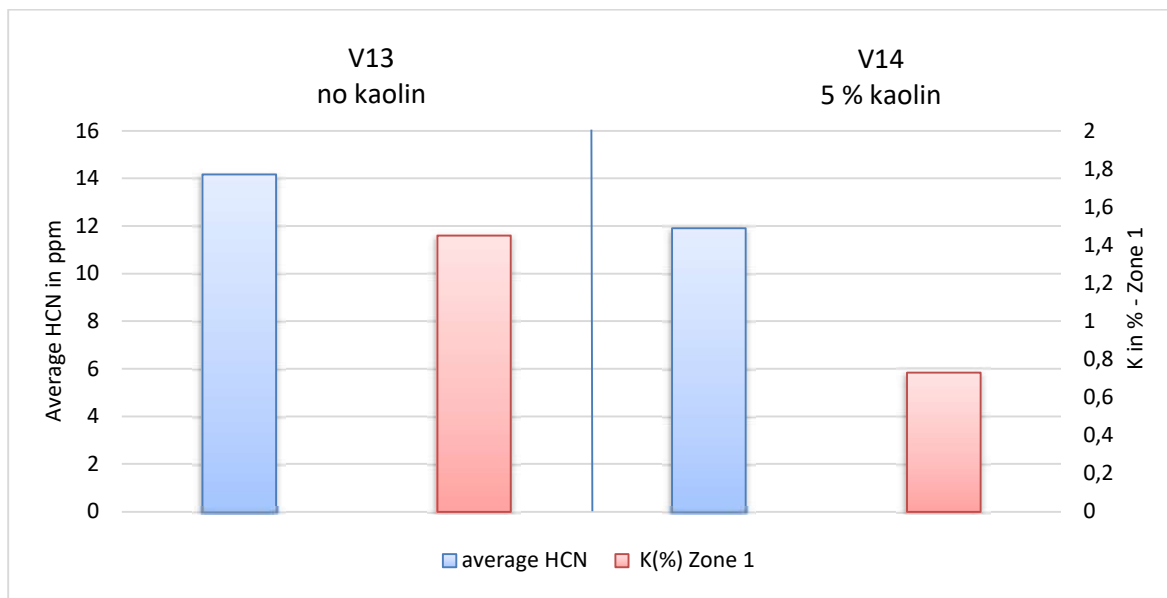


**Figure 209** Average HCN concentration compared to K content in zone 1 - coke with high K pre-treatment (0 and 5 % kaolin, all 5 % H<sub>2</sub>; V13, V14)

#### Influence of kaolin coating on coke reactivity in zone 2

In the same way as described for the BFI trials within Task 1.3, thermogravimetric analysis (TG analysis) of the kaolin coated coke from lower temperature zone 2 have been made in order to assess the coke reactivity (respectively the activation energy Ea) in dependency on the K load and on the amount of kaolin coating.

In **Figure 210** the determined activation energies Ea are presented in correlation with kaolin pre-treatment (no K pre-treatment; high K pre-treatment). As expected, due to the missing variation of the K content in all coke samples from zone 2, also no clear correlation of the kaolin content with the Ea values is observed either for a high K pre-treatment (right part of figure) or coke samples without K pre-treatment (left part of figure). For the trials without K pre-treatment, the Ea values are more scattered than those with K pre-treatment, but in average, they are in the same range. The scattering may be due to random variations in the coke surface (like pore diameters).

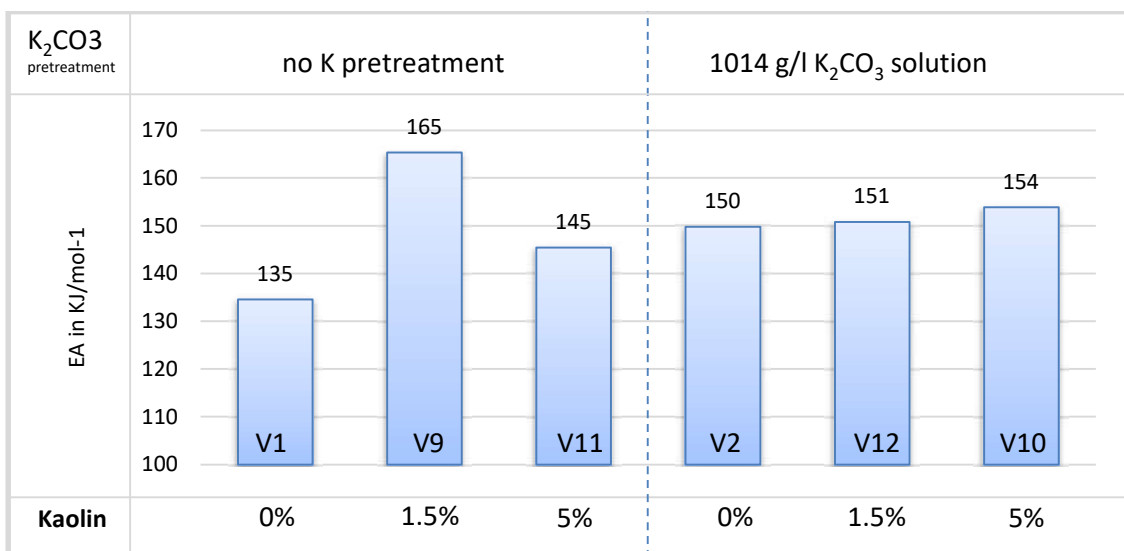


**Figure 210** Activation energy Ea in correlation with kaolin pre-treatment (no K pre-treatment; high K pre-treatment)

Finally, considering all the results, it was found that with the present experimental set-up a positive influence of kaolin coating on the capture of alkali components and thus the inhibition of alkali circulation could not be confirmed. This might be explained by problems with the experimental set-up like insufficient gas stream between the two temperature zones or by condensation of evaporated alkali compounds at other parts of the reactor.

### 2.3.2.2.5 Alkali adsorbing mineral addition in basket samples (SWERIM, LKAB)

The alkali uptake during descent in LKAB EBF® has been compared between lumpy olivine and briquettes made of fine-grained olivine and lime. The higher porosity and surface area of briquettes was believed to be more advantageous for alkali adsorption. The samples were charged as basket samples in EBF during C32 in 4 different pellet layers before the process was stopped. The charging schedule of baskets is shown in **Figure 211** where briquettes are labelled as "B" and lumps as "L". The empty space in baskets containing briquettes were filled up with iron ore pellets to fixate the briquette position.

Layer	Basket 1	Basket 2
22	B	L
26	L	B
30	B	L
34	L	B



**Figure 211** Charging schedule of olivine briquettes and lumps (left). A filled basket containing olivine briquette and iron ore pellets (right).

Baskets in layers 22-30 were all found below the lower shaft probe during excavation but baskets in layer 34 were missing, see approximate vertical position in **Figure 212**. According to the latest temperature measurements with the lower probe, all samples should have been exposed to temperatures higher than 820-900°C.

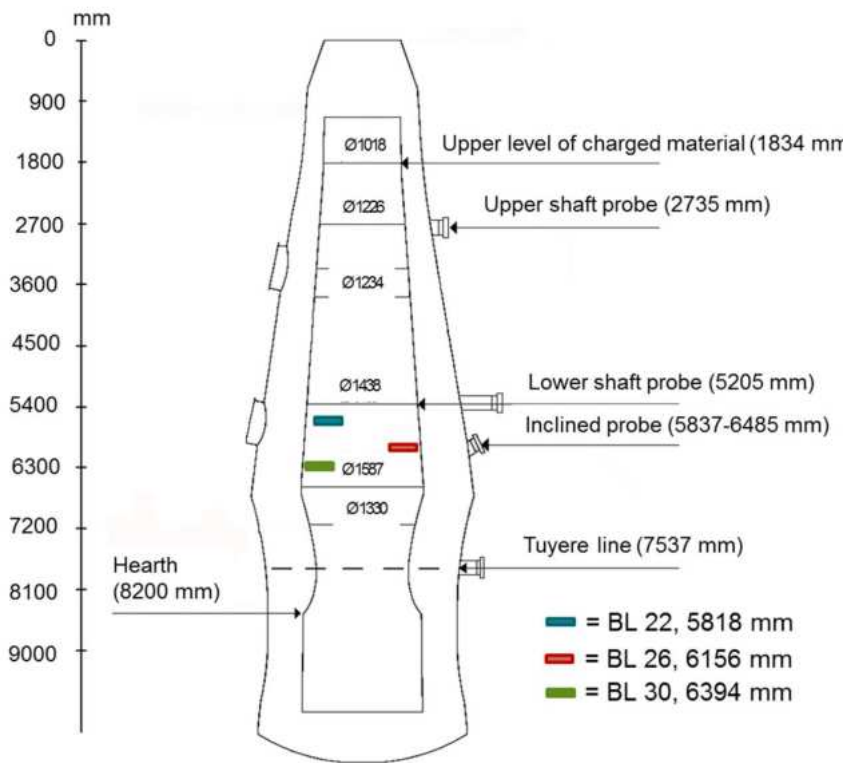


**Figure 212** Vertical positions of retrieved basket samples containing olivine briquettes and lumps.

Analyses of the alkali content showed that the adsorption was highest in samples in baskets found furthest down in the EBF but unexpectedly most pronounced in the lumpy olivine. However, compared to the green analysis, the adsorption capacity of alkali is modest in all samples with less than 0.3% uptake.

**Table 46** Chemical analysis of green samples and samples pro-cured in LKAB EBF.

BL	Basket	Sample	CaO [%]	MgO [%]	SiO <sub>2</sub> [%]	Al <sub>2</sub> O <sub>3</sub> [%]	MnO [%]	Cr <sub>2</sub> O <sub>3</sub> [%]	NiO [%]	K <sub>2</sub> O [%]	Fe <sub>2</sub> O <sub>3</sub> [%]	Na <sub>2</sub> O [%]	Tot [%]
green	B	B	20.8	36.4	31.9	1.48	0.15	0.44	0.45	0.06	8.13	<0.01	99.8
green	L	L	0.14	50.3	42.4	0.52	0.09	0.14	0.32	0.04	5.94	<0.01	99.9
22	1	B	15.6	40.7	34	1.44	0.1	0.33	0.37	0.11	6.99	0.03	99.7
22	2	L	0.2	50	42.1	0.87	0.09	0.3	0.29	0.1	6.01	<0.01	100.0
26	1	L	0.08	50.6	41.7	0.74	0.09	0.22	0.32	0.19	6.05	<0.01	100.0
26	2	B	18.8	39.7	32.1	1.44	0.1	0.32	0.34	0.12	6.72		99.6
30	1	B	15.2	41.4	34.9	1.14	0.1	0.33	0.29	0.26	5.86	<0.01	99.5
30	2	L	0.41	48.7	42.4	1.29	0.08	0.26	0.26	0.33	6.13	<0.01	99.9

According to the SEM characterization of briquette sample from BL-30, alkali was found in Si-phases with no or very little CaO, see **Figure 213**. This could be related to the fact that Ca<sup>2+</sup> and K<sup>+</sup> are competing about the same interstitial positions in the Si-network of a slag. Some alkali could be found inside the pores of olivine grains, but the highest concentrations appeared to be in phases situated in mixed regions of olivine and binder. As the binder phase is surrounding the olivine grains, reaction of alkali with minerals in olivine might be hindered. Thus, CaO as binder might have a negative effect on the alkali uptake capacity, which is supported by the lower alkali uptake in briquettes than lumps.

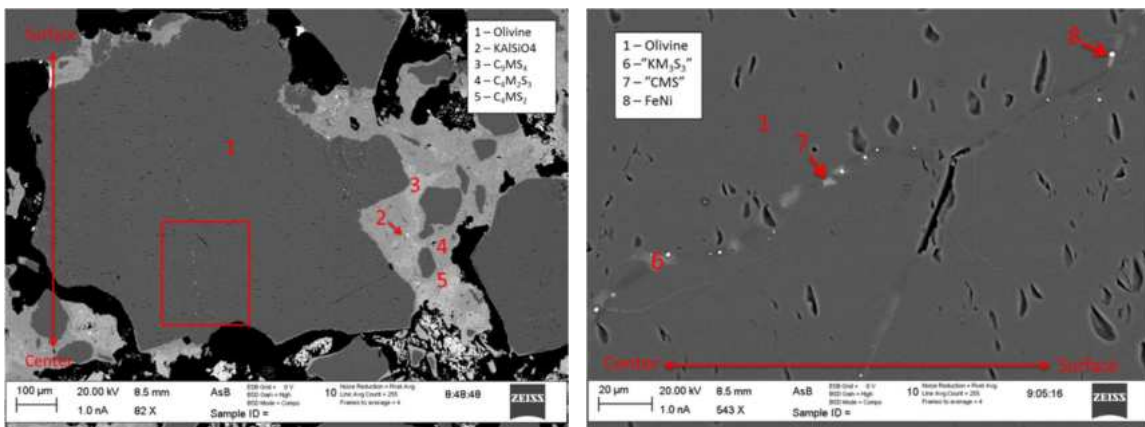


**Figure 213** SEM microphotograph of surface piece from olivine briquette BB. Right-hand image is corresponding to highlighted area to the left.

### 2.3.2.3 Task 2.3 Impact from slag compositions

#### 2.3.2.3.1 Alkali gasification from slag (LTU)

##### Thermodynamic calculations on the alkali capacity of BF slag (LTU)

The thermodynamic calculations on the alkali capacity of BF slag were carried out utilizing the Equilib module of FactSage 7.2. The databases employed in the calculations were FactPS and FTox-id. The equilibrium potassium content of the BF slag was calculated at 1500°C and a total gas pressure of 2 atmospheres (if not otherwise noted). In the calculations, 100 g of slag was chosen to be in equilibrium with 56.5 g of N<sub>2</sub>. The ratio between slag and gas was based on the slag rate, blast volume and nitrogen in the blast in BF No.3 at SSAB Luleå. In principle, the ratio can be chosen arbitrarily as the purpose of the calculations was to investigate which changes in conditions that creates a thermodynamic driving force for changes in alkali capacity in the slag. In addition to the slag phase and gas phase, a solid carbon phase in the form of graphite was introduced in the calculations to represent coke. The slag compositions utilized in the calculations are presented in **Figure 214**. In addition to the oxides presented in **Figure 214**, TiO<sub>2</sub> was kept constant at 0.5 wt.% and sulphur at 1.0 wt.% in all calculations. The potassium input in the calculations was 3 wt.% K<sub>2</sub>O in the slag.

**Table 47** Calculation cases used to determine parameters exerting a thermodynamic driving force on the potassium capacity of BF slag. % $M_{x}O$  given in wt. %.

Studied parameter	Range of the parameter	%CaO	%SiO <sub>2</sub>	%Al <sub>2</sub> O <sub>3</sub>	%MgO	%Na <sub>2</sub> O	%MnO
B2 (%CaO/%SiO <sub>2</sub> )	0.8-1.3	Variable	Variable	12	10	1	0.5
%MgO at const. B2	5-15	Variable	Variable	12	Variable	1	0.5
%MgO at const. B3	5-15	Variable	35.65	12	Variable	1	0.5
%Al <sub>2</sub> O <sub>3</sub> at B2=0.8	9-14	Variable	Variable	Variable	10	1	0.5
%Al <sub>2</sub> O <sub>3</sub> at B2=1.0	9-14	Variable	Variable	Variable	10	1	0.5
%Al <sub>2</sub> O <sub>3</sub> at B2=1.2	9-14	Variable	Variable	Variable	10	1	0.5
%MnO at const. B2	0.4-2.4	Variable	Variable	12	10	1	Variable
%Na <sub>2</sub> O at const. B2	0-2	Variable	Variable	12	10	Variable	0.5
Temp. (°C)	1400-1650	36	36	12	10	1	0.5
Tot. pressure (atm.)	1-3	36	36	12	10	1	0.5

#### Laboratory-scale experiments on evaporation of potassium

The impact of BF slag compositions and hearth temperature on the kinetics of potassium evaporation and the final potassium content of the slag was studied using synthetic BF slag compositions. The experiments were conducted utilizing a two-level full factorial design with three variables: B2 basicity, wt.% MgO and temperature. The experimental matrix is shown in **Figure 214**. The basicity was chosen to be varied between 0.8 and 1.1 to cover a wide range of operational conditions. The range of the %MgO was designed to represent the high MgO contents of the Swedish BFs. The temperature was varied to see the effect of changed hearth heat levels. The three centre points was utilized to evaluate the reproducibility of the experiments.

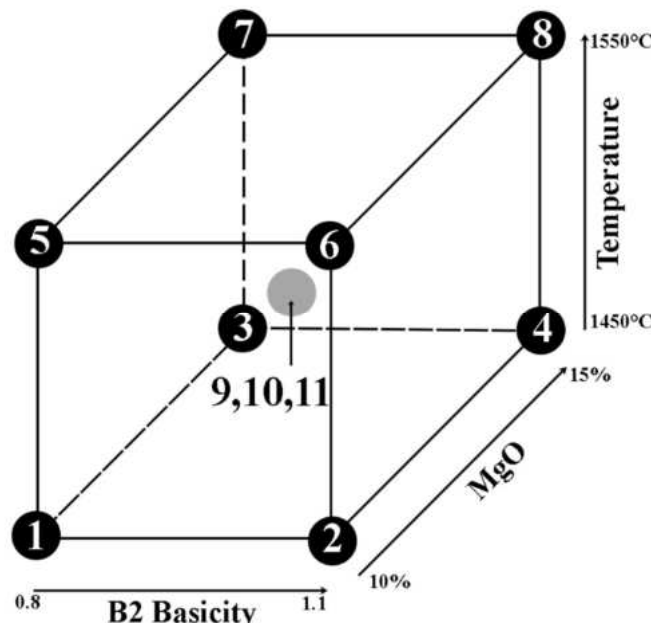


**Figure 214** Experimental matrix of the two-level full factorial design with three variables

To account for all experiments in the experimental matrix, five synthetic slags were created. The compositions of the slags are presented in **Table 48**. The melting points of each slag was determined utilizing the equilibrium module in FactSage 7.1 with the FactPS and FToxid databases. The synthesis was accomplished in graphite crucibles placed in a chamber furnace set for a temperature exceeding the melting temperature of all slags. After the synthesis, the slags had some larger grains formed during the cooling; therefore, each slag was crushed and ground individually. Representative samples of the ground slags were used in the subsequent experiments.

**Table 48** Slag compositions for the full factorial design.

Slag Nr.	B2	%CaO	%SiO <sub>2</sub>	%Al <sub>2</sub> O <sub>3</sub>	%MgO
1	0.80	34.7	43.3	12.0	10.0
2	1.10	40.9	37.1	12.0	10.0
3	0.80	32.4	40.6	12.0	15.0
4	1.10	38.2	34.8	12.0	15.0
5	0.95	36.8	38.7	12.0	12.5

Three different systems were recognized to be of interest to study: i) slag/coke/hot metal, ii) slag/coke and iii) slag/hot metal. The third system had to be ruled out as graphite crucibles were required to maintain the slag composition during the actual experiments. The full factorial design was made on the slag/coke system with the graphite crucible and small graphite cylinders representing the coke, **Figure 215 a)**. Actual coke was omitted to avoid the coke ash from influencing the slag composition. The first system, slag/coke/hot metal, was studied for three additional experiments to study if the results were any different. The eleven experiments for the slag/coke system are presented in **Table 49**. The three experiments of the slag/coke/hot metal system were chosen as experiment N5, N6 and N7 to allow changes in both B2 basicity and %MgO.

**Table 49** Experiments for the two-level full factorial design are denoted N1-N11 and the three additional experiments of the slag/coke/hot metal system are labeled H5-H7

Experiment's name	Slag Nr.	B2	MgO (wt.%)	Temperature (°C)
N1	1	0.8	10	1450
N2	2	1.1	10	1450
N3	3	0.8	15	1450
N4	4	1.1	15	1450
N5	1	0.8	10	1550
N6	2	1.1	10	1550
N7	3	0.8	15	1550
N8	4	1.1	15	1550
N9	5	0.95	12.5	1500
N10	5	0.95	12.5	1500
N11	5	0.95	12.5	1500
H5	1	0.8	10	1550
H6	2	1.1	10	1550
H7	3	0.8	15	1550

The addition of  $K_2CO_3$  up to a level representing 3wt.%  $K_2O$  was made prior to the actual evaporation experiments. 3wt.% was chosen based on similar experiments in a previous project. The crushed and ground synthetic slag was mixed thoroughly with the  $K_2CO_3$  and the graphite cylinders. In order to measure the temperature as close to the melt as possible the thermocouple was placed in the slag, enclosed by graphite to avoid the alumina tube surrounding the thermocouple to dissolve in the slag, **Figure 215 b)**. The experiments were conducted in a TAMMAN furnace. **Figure 215 c)** shows the crucible with the thermocouple going through the lid to the left and the alumina tube passing  $N_2$  gas at a rate of 2 l/min (STP) in the centre. In addition to the nitrogen added by the top-blowing, nitrogen to shield the furnace was added in 8 l/min (STP) through the bottom, below the crucible. The rightmost hole of **Figure 215 c)** is the sampling point where slag samples were taken using a copper rod. The first slag sample was taken when the slag reached the desired experimental temperature. A total of seven samples were taken for each experiment, one after the temperature was reached and then after 5, 10, 20, 40, 80 and 120 minutes.

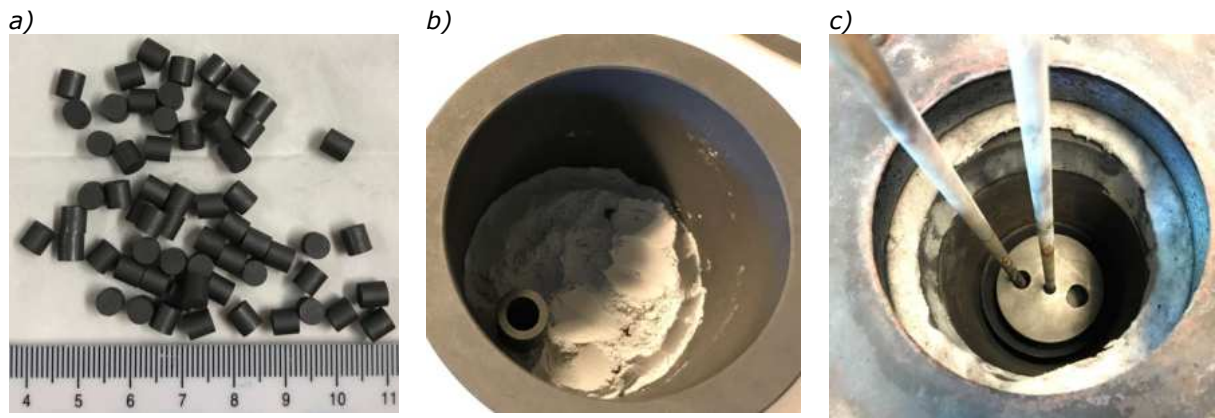


**Figure 215** Experimental setup with a) graphite cylinders representing coke, b) crucible prepared with synthetic slag and graphite enclosure for the thermocouple and c) TAMMAN furnace prepared for experiment.

The experimental setup for the three experiments conducted for the slag/coke/hot metal system was somewhat different. The slag and iron was separated during the heating period by placing the iron in an inner graphite tube, **Figure 216 a)**. The inner graphite tube was removed prior to the first sample at the experiment temperature, **Figure 216 b)**. The setup did not allow the thermocouple to be placed inside the crucible; instead, the thermocouple was placed on the outside, right next to the crucible.

The slag samples were analysed for potassium using ICP-OES after digestion in aqua regia at 100°C.

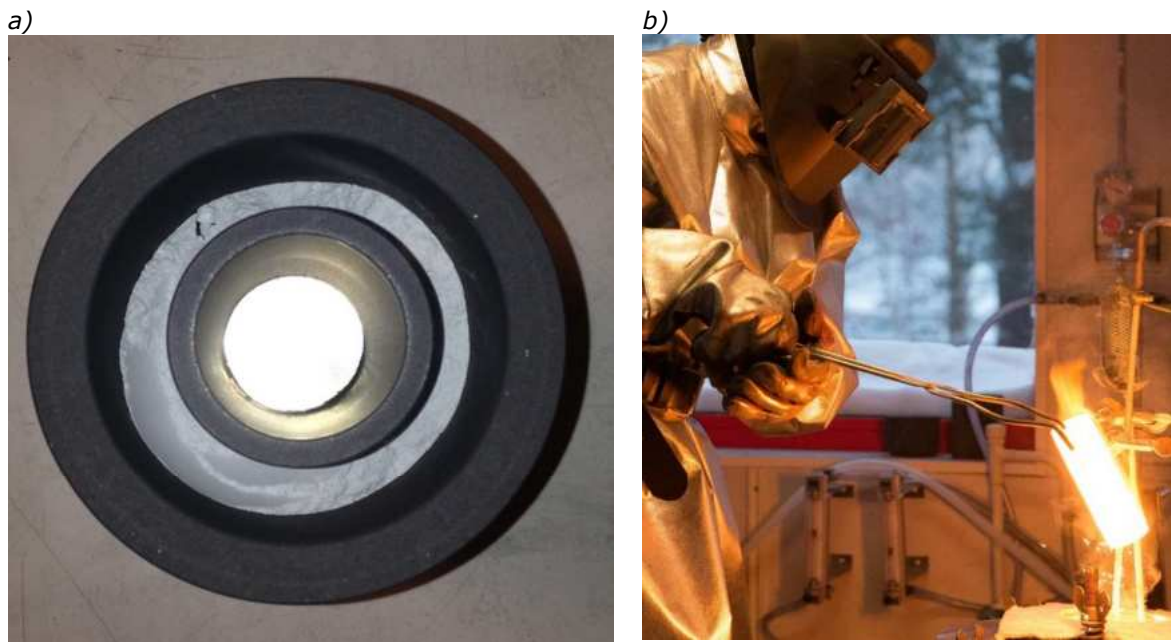


**Figure 216** a) Inner graphite tube separating the slag from the iron. b) removing the inner graphite tube.

#### *Laboratory-scale experiments on BF slags from the industry*

The same experimental setup as the slag/coke system was used to study the potassium evaporation from industrial slag samples. A total of six slag samples were provided, two from VoestAlpine (VASD) and four from Dunaferr. **Table 50** presents the chemical composition of the samples.

**Table 50** Composition (wt.%) of industrial slag samples

Element	VoestAlpine 1	VoestAlpine 2	Dunaferr 1	Dunaferr 2	Dunaferr 3	Dunaferr 4
<b>CaO</b>	31.16	31.85	31.87	38.47	40.10	43.28
<b>MgO</b>	10.42	10.32	13.45	9.61	9.59	9.72
<b>SiO<sub>2</sub></b>	37.53	38.77	38.45	38.42	35.56	34.41
<b>Al<sub>2</sub>O<sub>3</sub></b>	11.92	11.75	11.98	9.24	11.31	9.94
<b>Fe</b>	3.52	0.68	0.23	0.25	0.29	0.16
<b>K<sub>2</sub>O</b>	1.89	2.29	1.04	1.26	0.57	0.29
<b>Na<sub>2</sub>O</b>	0.49	0.56	0.61	0.54	0.36	0.25
<b>S</b>	0.65	0.59	1.05	1.09	1.52	1.30
<b>TiO<sub>2</sub></b>	0.50	0.54	0.34	0.34	0.25	0.23
<b>P</b>	0.01	0.01	0.00	0.00	0.00	0.00
<b>MnO</b>	1.91	2.64	0.87	0.73	0.38	0.34
<b>Pb</b>	0.00	0.00	0.00	0.00	0.00	0.00
<b>Zn</b>	0.00	0.00	0.00	0.00	0.00	0.00
<b>Ba</b>	0.00	0.00	0.09	0.07	0.07	0.07

Four slag samples were chosen for the experiments. The choice was based on the compositional range of the design of experiments, **Figure 217**. I.e., the industrial slags with compositions within (or close to) the rectangle in **Figure 217** was chosen. Therefore, the experiments were made us-

ing VoestAlpine 1, Dunafer 1, Dunafer 2 and Dunafer 3. VoestAlpine 2 was not chosen as the composition of VoestAlpine 1 was similar in terms of the %MgO and B2 basicity.

Prior to the experiments, the slags were crushed and ground. Representative samples were taken, and the potassium content was increased to 3 wt.% by additions of  $K_2CO_3$ . The experiments, sampling and analyses were conducted in the same manner as for the synthetic slags.

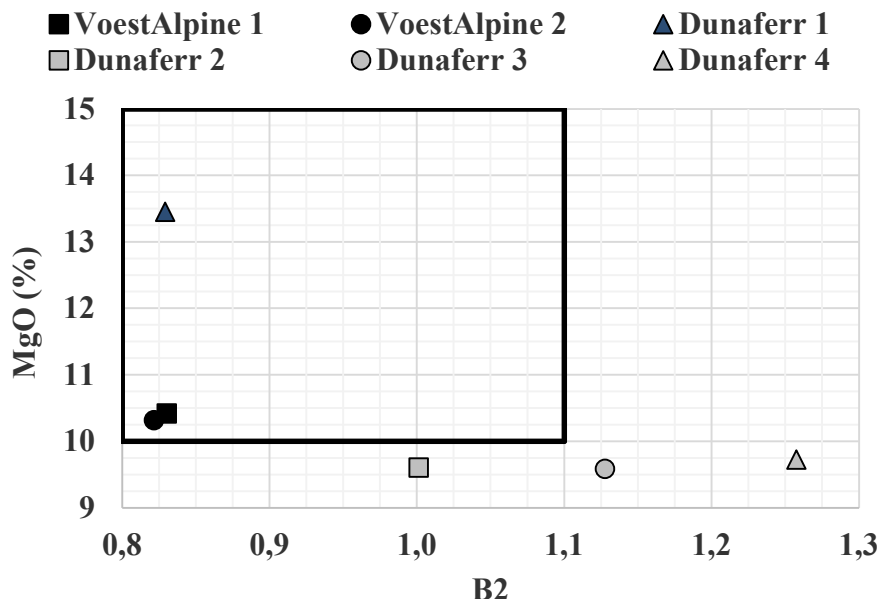


**Figure 217** Placement of the industrial slag samples within the compositional range of the design of experiments (outlined rectangle).

#### *Thermodynamic calculations on rate of evaporation*

The Equilib module of FactSage 7.2 was used to calculate the rate of potassium evaporation from the synthetic and industrial slags. The databases employed in the calculations were the FToxic and FactPS databases. In the laboratory-scale experiments, the crucible dimensions and top-gas additions were known. Therefore, the rate of refreshing the gas below the lid was estimated and the calculations were performed as an open system. This means that the nitrogen gas was added and the equilibrium between the gas phase and slag phase was reached. The gas phase was removed, and the new composition of the slag phase was allowed to reach equilibrium with a new mass of nitrogen gas. Based on the estimated rate of refreshing the nitrogen gas under the lid, this procedure was repeated until reaching 120 min, which was the end of the laboratory-scale experiments.

In the calculations, the slag compositions of **Table 48** and **Table 50** were utilized. However, as the temperature in the calculations were the experimental temperatures, the starting potassium content was chosen as the potassium content of the slag sample at 0 min in the experiments. In the calculations, graphite was included to represent the graphite cylinders and crucible.

## **Results and discussion**

### *Preliminary results on alkali capacity in synthetic BF slag*

The equilibrium alkali capacities of BF slag at the conditions specified earlier are presented in **Figure 218**. The compositional parameters with significant effect on the potassium capacity were determined to be the B2 basicity and the MgO content, **Figure 218 a-b**). Both the rise in B2 basicity and increasing MgO contents are accompanied by higher concentrations of basic oxides. As  $K_2O$

is one of the most basic oxides (electronegativity of 0.8 compared to 1.0 of CaO), the activity coefficient of potassium increases as well. Therefore, the equilibrium content of potassium decreases in the slag. Interestingly, the thermodynamic driving force for potassium evaporation increases at constant B3 basicity with increasing replacement of CaO with MgO despite CaO being more basic than MgO.

Parameters of less significance were the Al<sub>2</sub>O<sub>3</sub>, MnO and Na<sub>2</sub>O content, **Figure 218 c-d**). The two latter were only studied in a short compositional interval relevant for the BF slag. The Al<sub>2</sub>O<sub>3</sub>, being an amphoteric oxide, appears to have low effect on the equilibrium potassium content at low, medium and high B2 basicities.

As the potassium evaporates to the gas phase, both the temperature and the total pressure greatly affect the equilibrium content of potassium in the slag, **Figure 218 e-f**). Considering the results presented in **Figure 218**, the thermodynamic driving force for evaporation of potassium is the lowest at low B2 basicity, low MgO, low temperature and high total pressure.

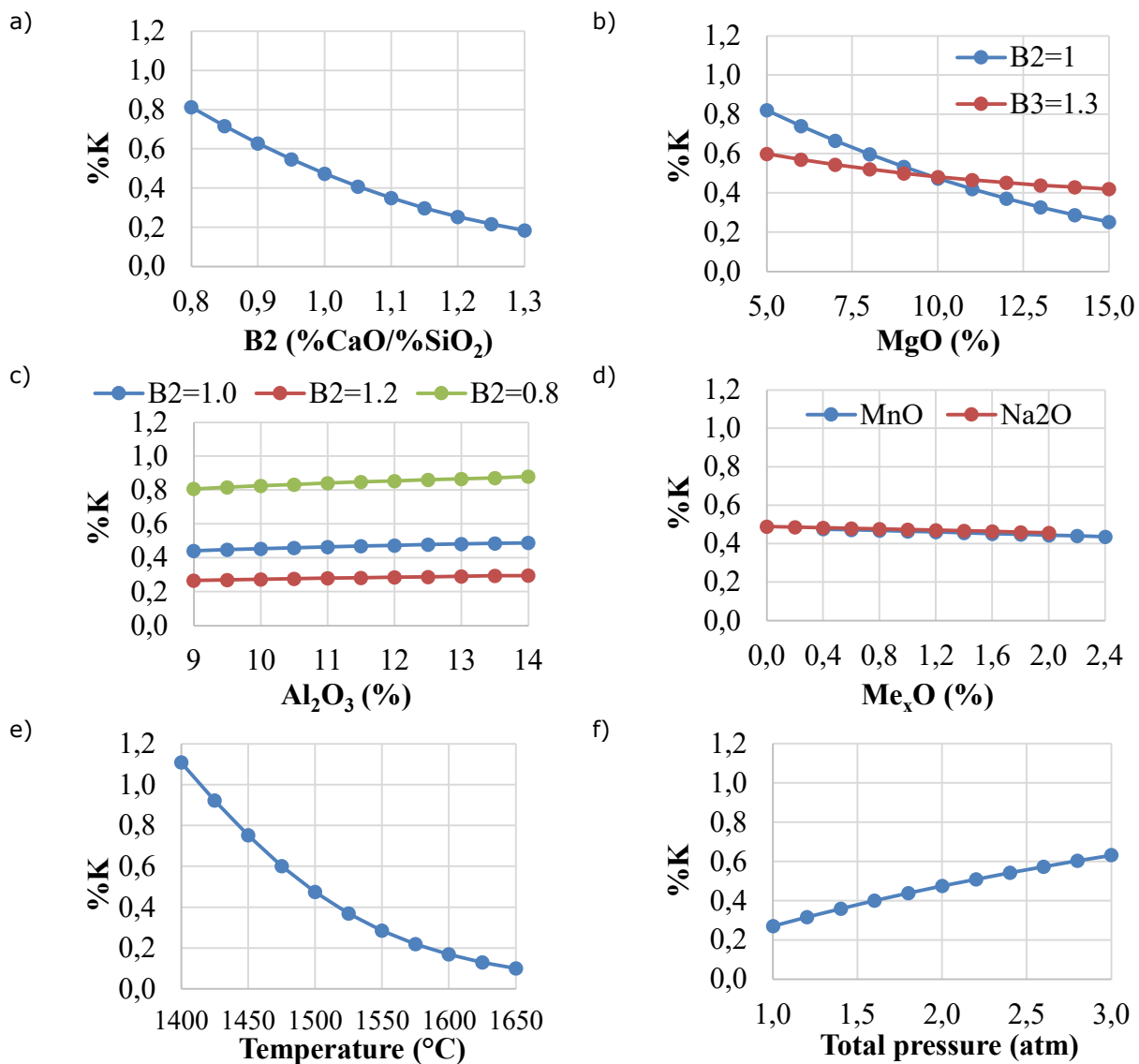


**Figure 218** Thermodynamic potassium content of BF final slag depending on a) B2 basicity b) MgO content at constant B2 and B3 basicity c) Al<sub>2</sub>O<sub>3</sub> d) MnO and Na<sub>2</sub>O content e) temperature and f) total pressure.

**Table 51** gives an idea of the alkali capacity of the synthetic BF slag when starting from 3 wt.% of potassium at room temperature and heating up to 1450°C or 1550°C, holding this temperature for 40 and 120 minutes. Considering the results, the temperature and basicity are the two tested factors of greatest importance on the alkali capacity. The effect of the MgO content is ambiguous. At 1450°C and B2 of 0.8, N1 and N2, the effect of the MgO content was of less significance. However, comparing N3-N6, increasing MgO contents resulted in lower alkali capacities. The alkali capacities presented in Table 51 are generally lower than those presented in the thermodynamic calculations, **Figure 218**. This difference can be attributed to the removal of the gas phase in the experiments, which drives the evaporation further. Nonetheless, both the experiments and calculations suggest that the B2 basicity is of great importance to consider when designing slags of high alkali capacity. The literature reports studies where BF slag was allowed to form equilibrium with a surrounding gas phase containing gaseous potassium [53-56]. In these experiments, the increasing B2 [53, 54] and B3 [54, 55] basicities were clearly linked to lower alkali capacities of the BF slag. These results are in line with both the thermodynamic calculations and laboratory-scale experiments of the present study. Wang et al. [53] reported that incremental increases in MgO contents, from 6 to 16 wt.%, consistently improved the alkali capacity of the BF slag at constant B2 basicity. However, the results presented by Kärsrud [54] suggested that incremental additions of MgO to the BF slag at constant B2 basicities successively decreased the alkali capacity of the slag. Considering the present study, the thermodynamic calculations agree with the results of Kärsrud [54] and contradict those of Wang et al. [53]. However, as previously stated the effect of MgO was inconclusive in the laboratory-scale experiments of the present study but the results lean more towards the conclusions of Kärsrud [54] considering experiments N3-N6, **Table 51**.

Although the effect of MgO appears to be negative at constant B2 basicities, increasing MgO contents at a constant B3 basicity was shown to improve the alkali capacity [53, 54] suggesting that replacing CaO with MgO favours the retention of potassium in the slag. These results contradicts the thermodynamic calculations, **Figure 218 b)**.

In the study of Lan et al. [56], a different approach was selected. Instead of maximizing the alkali retention, the alkali and sulphur capacity was simultaneously considered, which resulted in conditions of ideal alkali capacity with maintained sulphur capacity. Lan et al. [56] concluded that the comprehensive, or combined, alkali and sulphur capacity increased with increasing B2 basicities, reaching a maximum at a basicity of 1, and there after decreasing. Furthermore, at constant B2 basicities, increasing MgO contents initially improved the comprehensive alkali and sulphur capacity, reaching a maximum at 10.6 wt.% and then decreasing again. Although the results of Wang et al. [53] and Kärsrud [54] are promising in terms of improved alkali capacity when keeping the B3 constant and increasing the MgO content, the results of Lan et al. [56] suggests that the comprehensive alkali and sulphur capacity decreases with this alteration in slag composition. In addition to changing the basicity and MgO content, Lan et al. [56] studied changes in the Al<sub>2</sub>O<sub>3</sub> content finding that the comprehensive alkali and sulphur capacity reached a maximum at 15.1 wt.%.

**Table 51** Alkali capacity at 1450°C

Label	Temperature (°C)	B2	%MgO	%K at 40 min	%K at 120 min
N1	1450	0.8	10	1.78	0.84
N2	1450	0.8	15	1.75	0.93
N3	1450	1.1	10	0.90	0.22
N4	1450	1.1	15	0.62	0.05
N5	1550	0.8	10	1.23	0.16
N6	1550	0.8	15	0.61	0.04
N7	1550	1.1	10	0.10	0.02
N8	1550	1.1	15	0.16	0.02

In the present study, the alkali capacity was studied in slag samples representing the final slag composition of the BF slag. In the study made by Ivanov et al. [57], slag samples designed to represent both the primary slag and final slag was subjected to similar experiments as presented here. In their study, Ivanov et al. [57] concluded that the role of the primary slag is to absorb as much alkalis as possible since the evaporation of potassium from this type of slag was virtually non-existent depending on the composition. On the other hand, they concluded that the role of the final slag was to discharge as much of the absorbed alkalis as possible. Therefore, the rate of evaporation of potassium is of importance to study.

#### *Rate of evaporation of potassium from synthetic BF slags*

The evaporation curves for the three replicates, N9-N11, are presented in **Figure 219**. As seen in **Figure 219 a)**, some potassium evaporated during the heating up to the actual experimental temperature. Experiment N11 had a slightly lower initial potassium content but the evaporation curve follows the same trend. In **Figure 219 b)**, the potassium content was normalized with respect to the potassium content analysed for the first sample at zero minutes. Both plots in **Figure 219** shows that the reproducibility of the experiments is good.

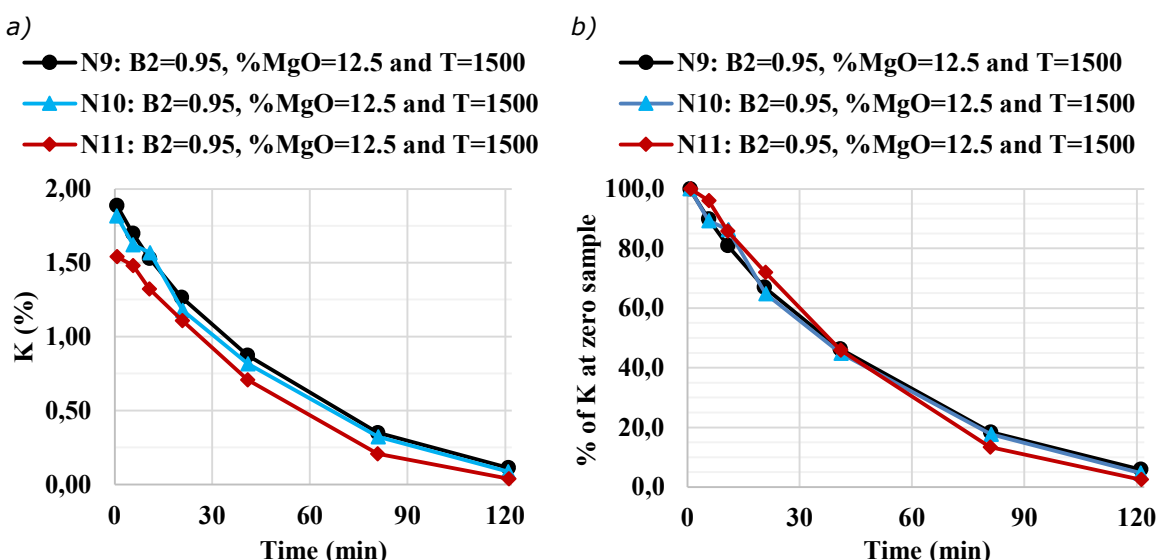


**Figure 219** Triplicate with a) %K on the y-axis and b) % of initial potassium analyzed at zero minutes on the y-axis.

The experiments at 1450°C and 1550°C are presented in **Figure 220 a)** and **Figure 220 b)**, respectively. In Figure 220 a), the effect of MgO on the evaporation rate appears to be less at a B2 basicity of 0.8. However, at the higher basicity, the higher value of MgO exhibits a faster evaporation rate of potassium. At 1550°C, **Figure 220 b)**, the opposite is observed; i.e., higher MgO is accompanied by a higher evaporation rate at the lower basicity but not at the higher one. Apart from the effect of MgO, the results of increasing the basicity and temperature on the rate of evaporation is in line with the thermodynamic calculations.

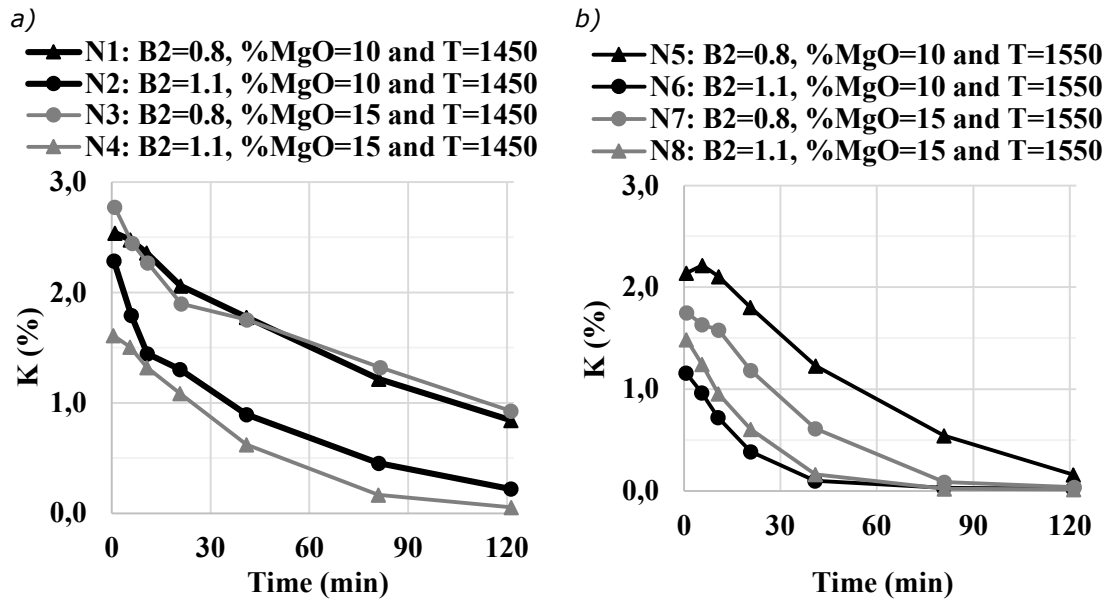


**Figure 220** Comparison of temperature pairs a) N1/N5, b) N3/N7, c) N2/N6 and d) N4/N8.

In a thorough study performed by Forsberg [58], the evaporation of potassium from synthetic BF slags was shown to follow first order kinetics. Therefore, in order to quantify the evaporation rates, each experiment of the present study was evaluated based on the kinetics of the first order reaction, **Equation (10)**, i.e. evaporation with mass transfer being the limiting parameter. Integrating **Equation (10)**, using the initial potassium content at t=0min of %K<sub>start</sub>, gives **Equation (11)**.

$$-\frac{d(\%K)}{dt} = k'(\%K) \quad (10)$$

$$-\ln (\%K/\%K_{start}) = k't \quad (11)$$

where k' is the apparent rate constant and t is the time. Utilizing **Equation (11)**, the results were plotted and the apparent rate constant was determined as the slope of the curve, **Figure 221**.

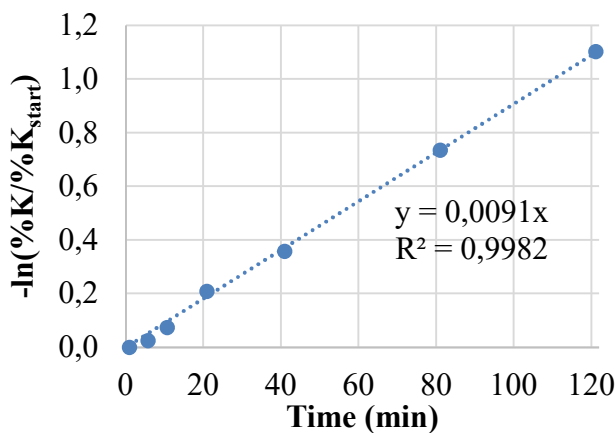


**Figure 221** Relationship between  $-\ln(\%K/\%K_{\text{start}})$  and time measured for experiment N1:  $B_2=0.8$ ,  $\text{MgO}=10\%$  and  $T=1450^\circ\text{C}$ .

The apparent rate constant and the coefficient of determination,  $R^2$ , for each experiment are presented in **Table 52**. The apparent rate constant was used as response parameter in the evaluation using multiple linear regression.

**Table 52** Apparent rate constant and coefficient of determination for the different experiments.

Label	B2	MgO (%)	T (°C)	k' ( $\text{min}^{-1}$ )	R2
N1	0.80	10.0	1450	0.0091	1.00
N2	1.10	10.0	1450	0.0200	0.97
N3	0.80	15.0	1450	0.0095	0.94
N4	1.10	15.0	1450	0.0275	0.99
N5	0.80	10.0	1550	0.0192	0.95
N6	1.10	10.0	1550	0.0484	0.97
N7	0.80	15.0	1550	0.0324	0.97
N8	1.10	15.0	1550	0.0524	0.99
N9	0.95	12.5	1500	0.0222	0.99
N10	0.95	12.5	1500	0.0236	0.98
N11	0.95	12.5	1500	0.0276	0.97

#### *Multiple linear regression of evaporation of potassium*

The experimental design utilizing the two-level full factorial design allows each variable to be studied independently. Furthermore, interactions between variables can be studied. The results of experiment N1-N11, **Table 49**, was fitted by multiple linear regression to the expression presented in **Equation (12)**.

$$y = \beta_0 + \beta_1 B_2 + \beta_2 (\%MgO) + \beta_3 T + \beta_{12} B_2 (\%MgO) + \beta_{13} B_2 T + \beta_{23} (\%MgO) T + \varepsilon \quad (12)$$

where  $y$  is the response parameter chosen as  $k'$ , the  $B_2$ ,  $\%MgO$  and  $T$  (temperature) are the three variables,  $\beta_0$  a constant term, the other  $\beta$ s the model parameters and  $\varepsilon$  the residual response variation not explained by the model. Fitting the experimental results of **Table 52** to the expression in **Equation (12)** provided a poor model. Although the  $R^2$ , model validity and model reproducibility

showed good values, the predictability ( $Q^2$ ) was only 0.19. The main features of the model that showed potential of improvement were skewness of the distribution of the response parameter and removal of statistically insignificant parameters. By transforming the  $k'$  value by log-transformation, the skewness was minimized. The insignificant parameters of least importance to the model were removed one by one. These parameters were the interaction terms  $\beta_{12}$  and  $\beta_{23}$ . The final model had an  $R^2$ ,  $Q^2$ , model validity and reproducibility of 0.92, 0.84, 0.78 and 0.96, respectively, **Figure 222 a)**. The coefficients of the model showed that increasing B2, %MgO and temperature increases the apparent rate constant and therefore evaporation rate of potassium, **Figure 222 b)**. These parameters were significant on the 95% confidence level. The interaction between B2 and temperature was not significant on this confidence level, **Figure 222 b)**. However, it was kept in the model as the residuals attained a curvature form if the interaction term was removed. All experiments showed residuals within four standard deviations, **Figure 222 c)**, which suggests no outliers. Experiment N5 deviated slightly from the straight line of the residuals of the remaining experiments suggesting that N5 was not fully explained by the model. **Figure 222 d)** shows the observed values vs. the predicted ones, illustrating that the model predicts the evaporation rate well.

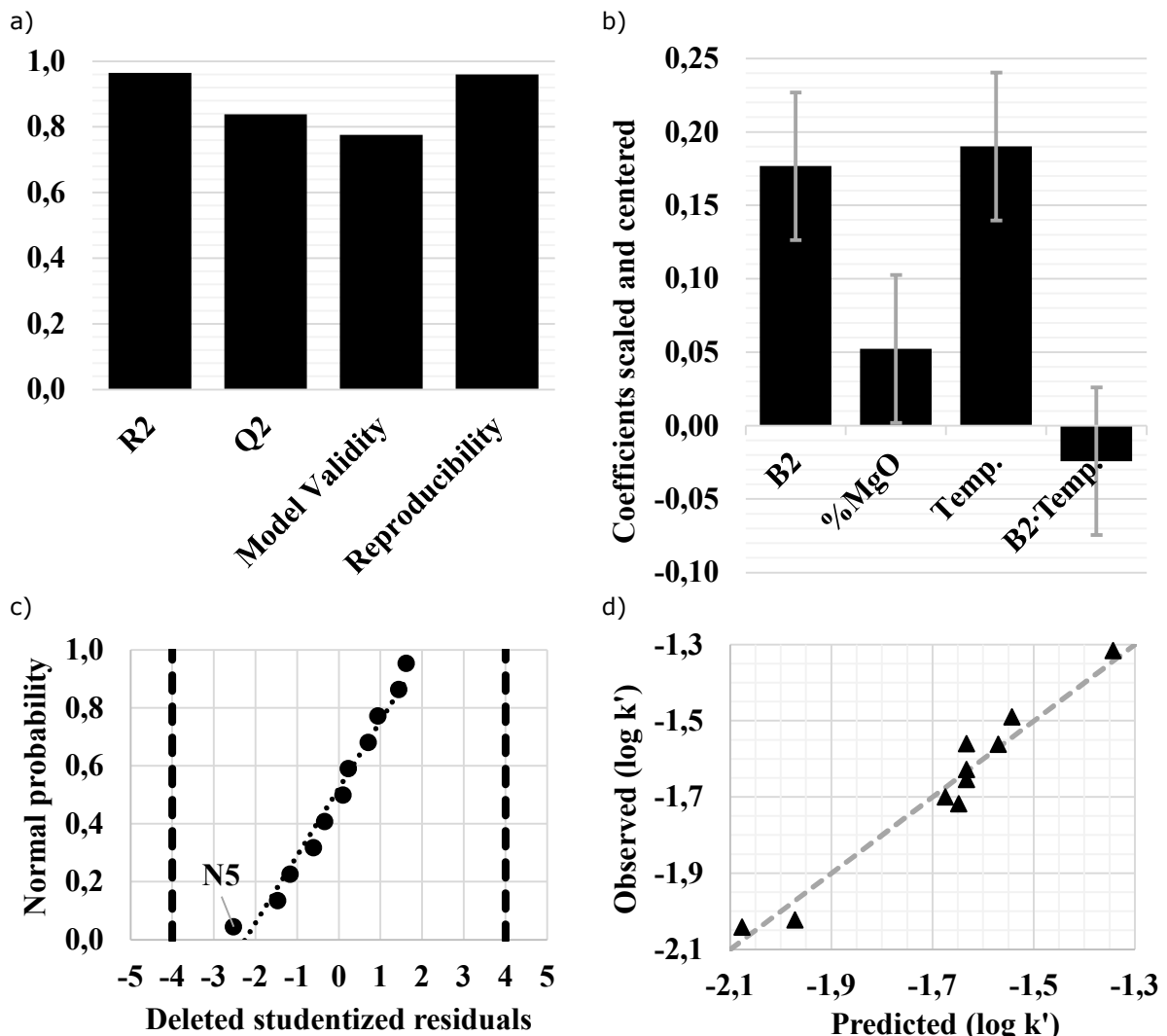


**Figure 222 a)** Summary of model fit **b)** Scaled and centred coefficients **c)** residuals plot **d)** observed vs. predicted.

The final expression of the model is presented in **Equation (13)**. Based on this equation the contour plot presented in **Figure 223** was produced. The plot illustrates the effect of changing temperature, B2 basicity and MgO content on the apparent reaction rate,  $k'$ .

$$\log k' = -13.31 + 6.01 * B2 + 0.021 * (\%MgO) + 0.0069 * T - 0.0032 * B2 * T \quad (13)$$

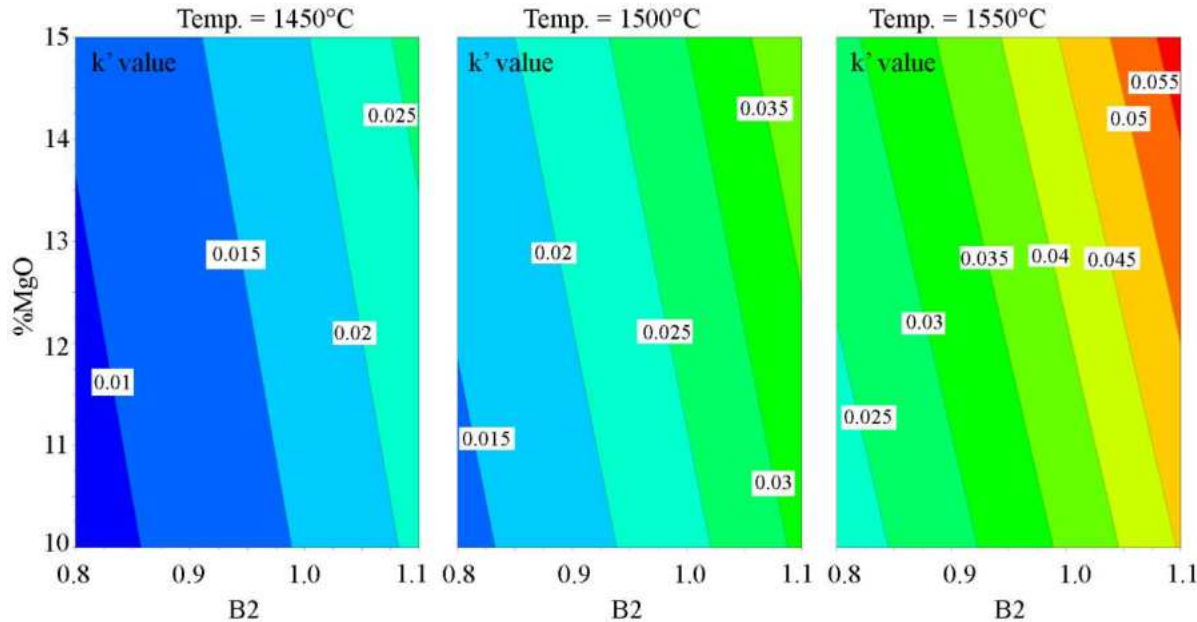


**Figure 223** Contour plot based on Equation (13).

The evaporation of potassium from BF slags have been studied in previous publications [55, 57-59]. The rate constant has been shown to increase with increasing B2 [57, 59] and B3 [55, 58] basicities. This is in line with the results of the present study. Furthermore, Forsberg [58] also found that substituting CaO by MgO did not affect the evaporation rate of potassium. These results contradicted that of Amatatsu et al. [55] who found that increasing MgO contents at constant B3 basicities lowered the evaporation rate. In the study performed by Ivanov et al. [57], the effect of MgO at constant B2 basicities was insignificant between 7.5 and 9.5 %MgO. However, increasing the MgO content to 10 wt.% clearly increased the rate of potassium evaporation [57]. In terms of MgO, the present study suggested that the effect of increasing additions of MgO is statistically significant. However, the evaporation curves of experiment N1 and N3 presented in **Figure 220 a)** shows that the effect can be low in certain conditions. Nonetheless, the full factorial design showed that there was not a statistically significant interaction effect between the MgO content and B2 basicity.

Amatatsu et al. [55] showed that iron oxide can increase the rate constant. Furthermore,  $\text{Al}_2\text{O}_3$  and  $\text{TiO}_2$ -additions inhibits the evaporation of potassium [55, 59]. These results concerning  $\text{Al}_2\text{O}_3$  are consistent with those of Ivanov et al. [57] who showed that increasing  $\text{Al}_2\text{O}_3$  contents at constant B2 basicity decreased the evaporation rate of potassium. In addition, increasing temperatures significantly increase the evaporation rate of potassium [55, 57, 59]. The results concerning temperature is in line with the present study. Furthermore, Amatatsu et al. [55] found that the positive effect on the evaporation rate provided by lower basicities was removed at higher temperatures (1500°C). Although the parameter describing the interaction between B2 and temperature was

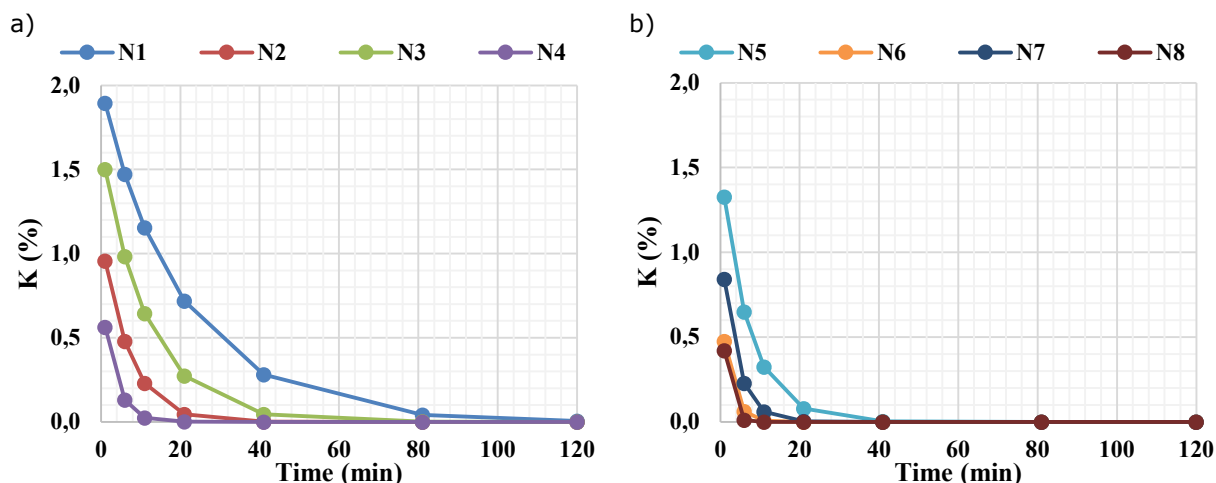
included in the regression model of **Equation (13)** in the present study, the effect is of lesser importance. Had it been as significant as found by Amatatsu et al. [55], the fields separating different values for  $k'$  of the rightmost figure in **Figure 223** would be horizontal.

Forsberg [58] showed that the reaction rate is not influenced by the gas flow rate over the melt. Considering that changes in slag composition strongly effects the evaporation rate and that the process is a first order reaction, Forsberg [58] concluded that diffusion within the slag phase is likely to be the limiting factor. In liquid slag phases, the diffusion depends on the mobility of the ions, in this case the  $K^+$ ,  $O^{2-}$  and possibly the counterdiffusion of other ions. When consulting studies of glass melts, Forsberg [58] found that the diffusion of  $O^{2-}$  or complex silicate anions possibly is the rate-limiting step. This explains why the basicity has a large effect on the evaporation of potassium. When the basicity is lowered, the silica will form three-dimensional networks, which has to diffuse in conjunction with the potassium cation. Therefore, fulfilling the role of the final BF slag (presented by Ivanov et al. [57]) in terms of minimizing alkali evaporation and maximizing alkali discharge from the BF, the main parameter to control is indeed the basicity. The results of the regression model offers a way to estimate the changes in rate of evaporation based on changes in slag composition and temperature. The model does not account for changes in  $FeO$ ,  $Al_2O_3$  and  $TiO_2$ , which have been shown to have some effect on the evaporation of potassium.

Designing experimental plans using a full factorial design including a large number of parameters (e.g. B2 basicity,  $MgO$ , temperature,  $Al_2O_3$ ,  $TiO_2$  and  $FeO$ ) requires a considerable amount of experiments to be performed (six parameters requires 67 experiments). The idea of modelling the experimental setup with FactSage 7.2 was to investigate if effects coming from these elements could be accounted for.

#### *Thermodynamic modelling of evaporation of potassium*

The results of the calculations on the evaporation of potassium from BF slag corresponding to the conditions of the laboratory-scale experiments are presented in **Figure 224**. Both the results from 1450°C (**Figure 224 a)**) and 1550°C (**Figure 224 b)**) were evaluated using the first order kinetics utilizing **Equation (11)**. The plots of **Figure 224 c-d)** suggests that the first order kinetics could be estimated by calculating on thermodynamic equilibrium in an open system where the equilibrated gas phase is removed and continually replaced.



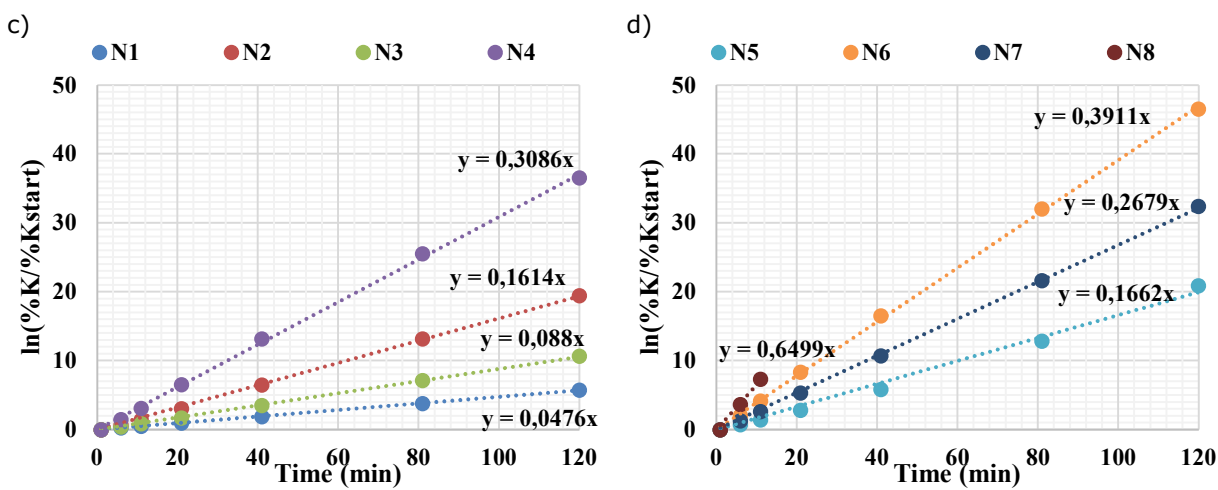


**Figure 224** Thermodynamic calculations in an open system representing the laboratory-scale experiments at a) 1450°C and b) 1550°C. c-d) Transformations in accordance to the first order kinetics.

The apparent rate constants determined by the thermodynamic calculations were considerably larger than those determined experimentally. However, the magnitude to which the calculations overestimated the evaporation rate of potassium could be estimated by a linear relationship, **Figure 225**. This suggests that changes in evaporation rate of potassium attributed to the B2 basicity, MgO content and temperature can be accounted for by thermodynamic calculations and a linear relation determined for the present experimental setup.

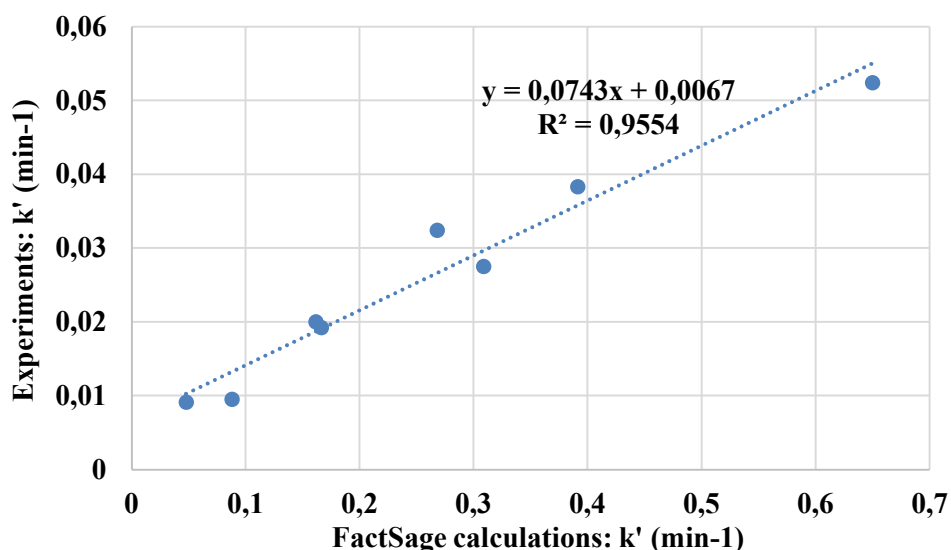


**Figure 225** Linear relationship between the apparent rate constant determined in the laboratory-scale experiments and FactSage calculations.

#### *Industrial slag samples and application of models*

The results of the potassium evaporation of the industrial slag samples in the laboratory-scale experiments are presented as the blue lines in **Figure 226**. Based on the B2 basicity, MgO content and experimental temperature, the regression model presented in **Equation (13)** was used to estimate the evaporation rate of potassium (red lines). In addition, the slag compositions were used as input in FactSage calculations to determine the apparent rate constant. This constant was transformed using the equation of **Figure 225** to account for the overestimation of the evaporation

rate. The results of this FactSage route is presented as the green lines in **Figure 226**. The calculations agree fairly well for all slag compositions except for Dunaferr 3, the experiment farthest away from the experimental matrix. Altogether, the results suggest that the regression model and FactSage calculations can be used to estimate changes in the evaporation rate of potassium and thus aid in the design of slags with adequate alkali retention facilitating the output of potassium from the BF.

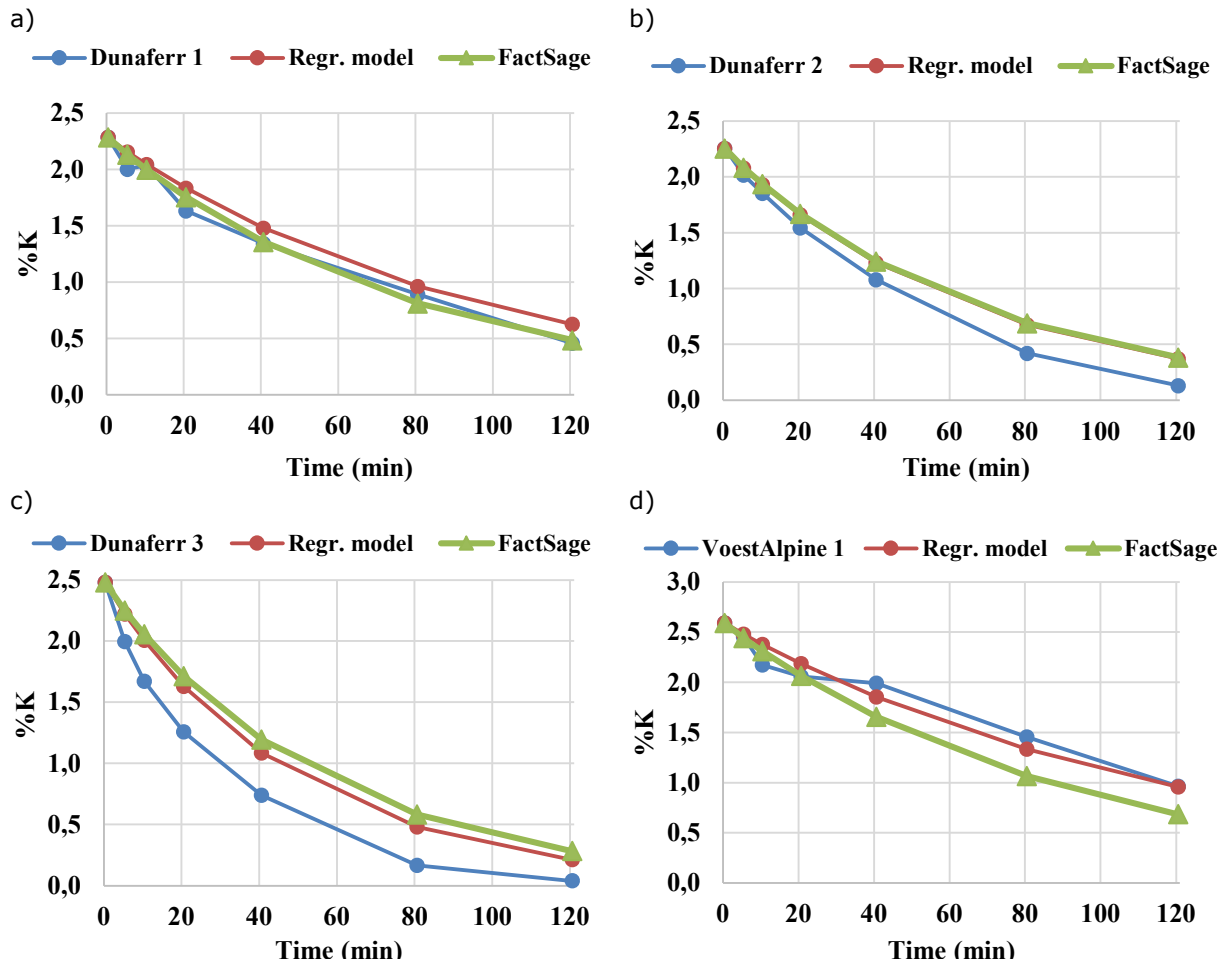


**Figure 226** Potassium evaporation determined experimentally, by the regression model and by FactSage calculations of the industrial slag samples a) Dunaferr 1 b) Dunaferr 2 c) Dunaferr 3 and d) VoestAlpine 1.

*Changed system: slag/coke/hot metal*

**Figure 227 a)** illustrates the evaporation curves of the experiments of the slag/coke/hot metal system and the corresponding experiments of the slag/coke system. The curves illustrate a clear difference in evaporation rate. The apparent reaction rate was calculated according to the slopes of the trend lines in **Figure 227 b)**. In experiment N6 and N7, a faster evaporation was recorded than the corresponding experiments of H6 and H7, respectively. As the thermocouple couldn't be placed in the same position in the slag/coke/hot metal experiments as in the slag/coke experiments the actual temperature may differ between the experiments. In fact, the thermocouple was dipped in the slag after the final experiment in the slag/coke/hot metal setup showing a 26°C lower temperature than measured right outside the crucible, i.e. 1524°C. Thus, the faster evaporation rate in the slag/coke system is likely to stem from a higher temperature. The difference in the N5/H5 pair did not follow this trend. As the temperature was found to be one of the key parame-

ters affecting the evaporation rate, the comparison between the two systems was inconclusive. However, the comparison within the three experiments in the new system could be made. Increasing the B2 basicity between the H5 and H6 experiments proved to increase the evaporation rate of potassium. The increase in MgO from 10 to 15 wt.% between H5 and H7 contradicted the previous experiments as the higher MgO content lowered the rate of potassium evaporation. In the experiments by Forsberg [58], the contact with carbon-saturated iron was shown to have no effect on the apparent rate constant of potassium evaporation from slag. Considering these previous findings and the fact that the experimental results of experiment H5 in **Figure 227 b)** was somewhat scattered as compared to previous experiments, the effect of the MgO content cannot be stated to be different when the slag is in contact with the hot metal.

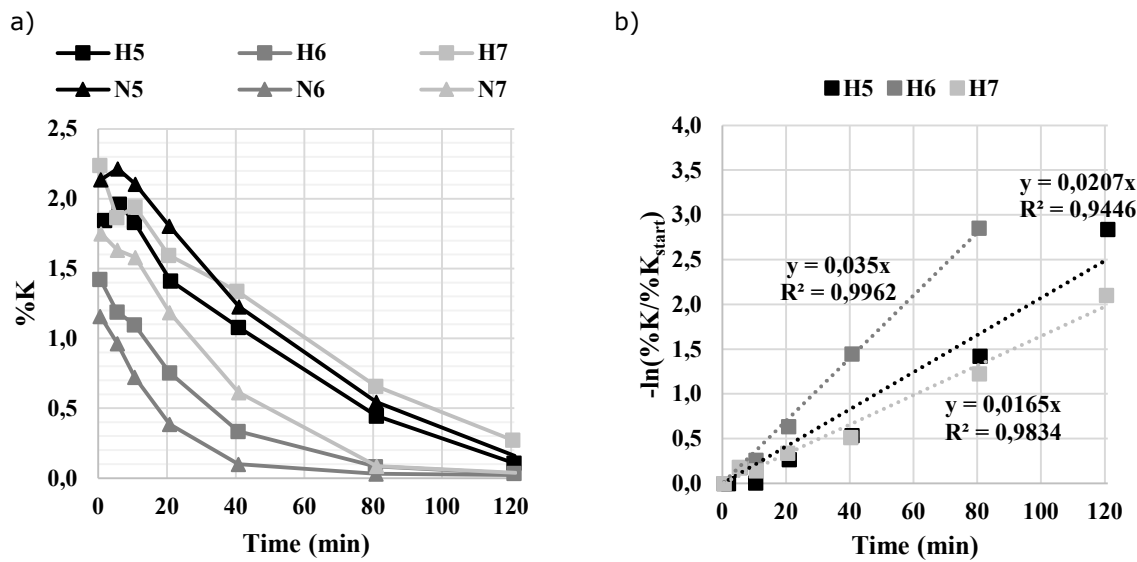


**Figure 227** Comparison of evaporation from slag/coke/hot metal and slag/coke system. b) First order kinetics evaluation of slag/coke/hot metal experiments.

### 2.3.2.3.2 Alkali evaporation from coke (SWERIM)

Some additional trials have been conducted to study if the kaolin addition in coke could contribute to formation of stable alkali compounds that can be brought to the BF-slag without being reduced and vaporized. The kinetics behind the evaporation of alkali from coke could differ depending on e.g. composition or ash modification in different coke samples. The samples of interest are ones that have been through the EBF and now contains different levels of alkali. Coke was sampled from campaign 32 and 33 with a total of 3 different type of cokes used. **Table 53** shows the three samples used along their alkali content and depth below charging level. Samples #1-#2 was SSAB industrially produced coke and sample #3 is corresponding to test coke from basket sample containing 2% kaolin.

**Table 53** Samples used in the vertical furnace experiment.

Test name	Original name	wt%	Depth below charging [m]
		K <sub>2</sub> O+Na <sub>2</sub> O	
Coke #1	K32 PL7:2	1.45	4.04
Coke #2	K32 PL6:2	0.30	3.45
Coke #3	N28K1-B 2wt% kaolin	1.44	4.24

The samples chosen came from a similar horizontal position in the EBF marked with the blue square in **Figure 228**. Depth below charging differed between the samples with coke #2 being the coke found at the lowest depth.

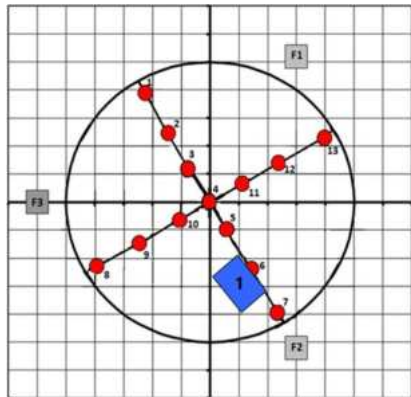


**Figure 228** Approximate position of coke samples in the EBF.

All three samples have been examined previously with respect to the reactivity properties in TGA. The results have been compiled in **Figure 229** and it is showing that samples #1-#2 started to react at higher temperatures than coke #3. The figure shows the 10 percent average of the data points which helps with showing the general trends for the data better. Start of reaction was determined as the point when the curve reaches above  $7 \mu k_a$  which gave the start of the reaction for coke #1 at  $892^\circ\text{C}$ . Coke #2 first went above the limit at  $924^\circ\text{C}$  and then went down again. The curve went above  $7 \mu k_a$  continuously first at  $951^\circ\text{C}$ . The start of the reaction was considered to be at the first temperature as **Figure 229** shows that the coke's reaction rate was at a plateau and then increased after  $951^\circ\text{C}$ . Coke #3 started to react at approximately  $815\text{-}820^\circ\text{C}$ .

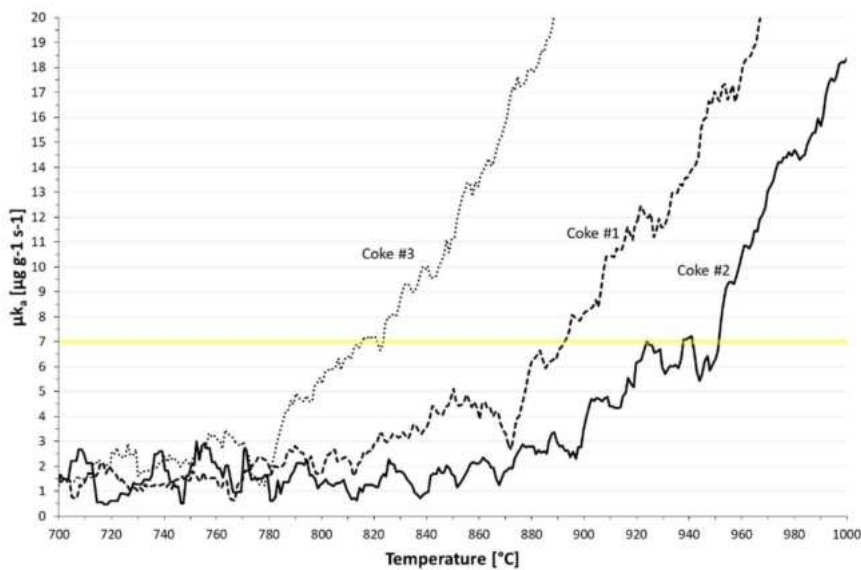


**Figure 229** Apparent reaction rate of the coke samples after the EBF.

Interesting with the result was that Coke #1 and Coke #3 had very similar alkali levels (1.45 and 1.44 respectively) and very different start of reaction. The difference could be explained by how the different cokes were produced. Coke #3 (2% kaolin) was made in a smaller experimental setup after SSAB's recipe and coke #1-2 was made in SSAB Luleå's full size coke production plant, which could lead to slight difference in the coke quality. The lowest reaction rate was for Coke #2 and it

had also the lowest alkali content. Differences in reactivity between industrially produced coke to coke made in lab- or pilot scale have been seen earlier, see **Figure 196**.

For the evaporation studies, the samples were crushed manually and a fraction between 2.8 mm to 4 mm was sieved out so that the results could more easily be compared to other experiments going on at the time. Approximately 30 g of coke was placed in a graphite crucible with holes drilled through the bottom to allow for a better gas flow through it. The crucible was hung in the furnace from molybdenum wires and the wires were attached to a scale. Thus, allowing the weight of the sample to be measured continuously during the experiment. A schematic figure of the furnace can be seen in **Figure 230**.

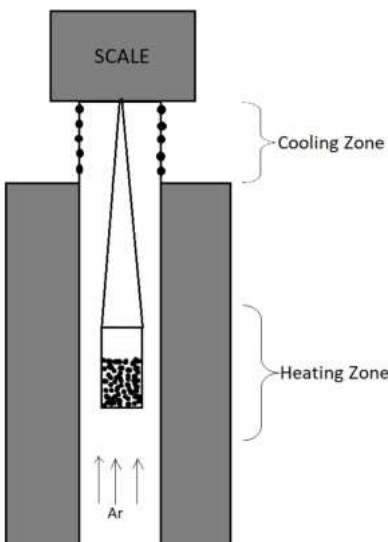


**Figure 230** Schematic view of the vertical furnace used.

The sample was heated up to the target temperature with a heating rate of  $2.5^{\circ}\text{C}/\text{min}$  which was the maximum of the furnace used. Chosen target temperature was  $1600^{\circ}\text{C}$  with a target cooling rate of  $2.5^{\circ}\text{C}/\text{min}$ .

Coke #1 and coke #2 did not start to react until approximately  $1250^{\circ}\text{C}$  whereas Coke #3 started to react at approximately  $1300^{\circ}\text{C}$ , see **Figure 231**. Highest weight loss was recorded for Coke #3 with around 12% lost followed by Coke #1 and Coke #2 with 10 and 9% weight loss respectively.

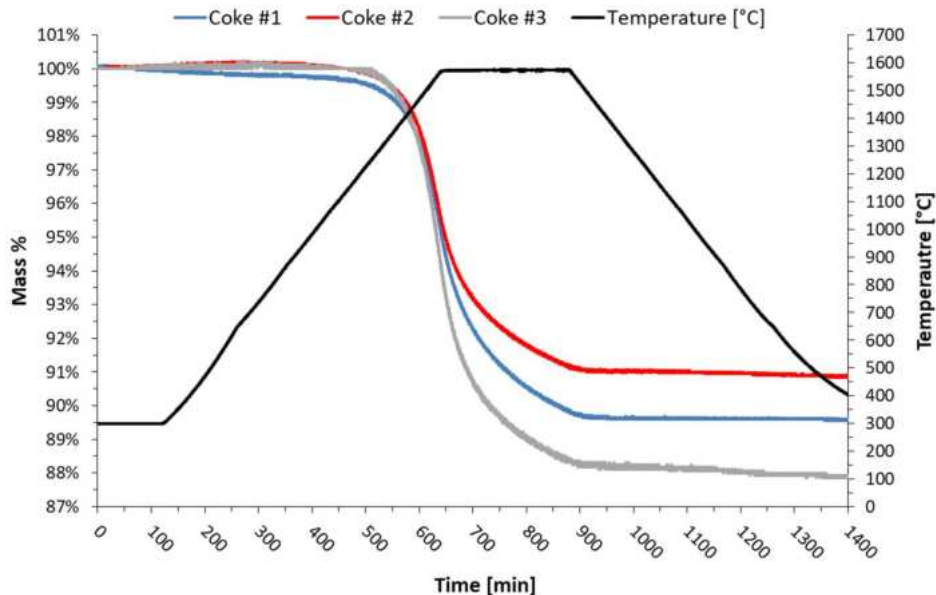


**Figure 231** Mass change in percent for the different coke types used.

No visible change could be seen on coke #1 and coke #2 after the furnace. The top of coke #3 in the crucible was covered in a white light fluff and the coke did not come out as easy from the crucible like the other sample did, see **Figure 232**. There were also signs that the crucible had taken damage in the bottom side wall, something that could indicate that the graphite had reduced some component in the coke sample.



**Figure 232** Coke #3 sample covered in a white fluff after the furnace. Inner diameter of the crucible was 40 mm.

To clearly see the start of the reaction the derivative of the mass was plotted in **Figure 233**. The figure shows that the reactions started at 1200-1250°C and was a bit later for coke #3 compared to the other two. The largest mass change per second occurred for coke #3 which also resulted in the largest mass drop in the end. The instability of the curve makes it hard to define an exact start of reaction.

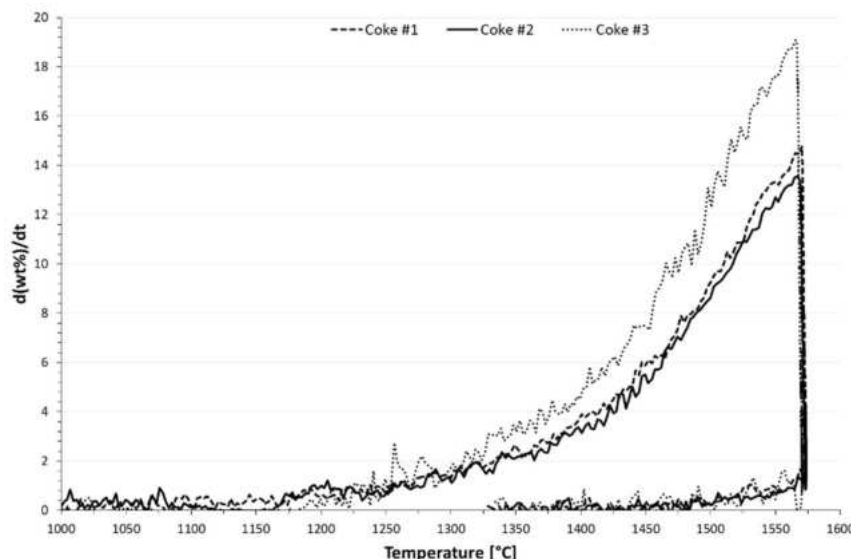


**Figure 233** Mass change per minute in the furnace for the three coke samples.

The results from the XRF in **Table 54** show that alkali decreased in all samples with K<sub>2</sub>O decreasing most in coke #1 and #3. The percentage drop of total alkali was 76% for coke #1, 37% for coke #2 and 82% for coke #3. The amount of SiO<sub>2</sub> and Al<sub>2</sub>O<sub>3</sub> increased after the furnace, the ratio SiO<sub>2</sub>/Al<sub>2</sub>O<sub>3</sub> increased slightly for all samples with a percentage increase in the range of 2 to 3.9%. The similar decrease in alkali between coke #1 and #3 indicates that the 2wt% addition of kaolin did not bind the alkali in a more stable phase in coke #3. However, no kalsilite could either be detected in this sample during examination by XRD (1). The white material seen on coke #3 after the furnace could be a silicate composition while the SiO<sub>2</sub> content in the sample was 0.5% unit higher according to XRF so no significant difference was seen in the analysis to indicate anything. XRD or SEM would have been needed to differentiate the composition better between the samples.

**Table 54** Chemical analysis from XRF for the coke samples before and after the furnace.

Before furnace												
Coke	Fe	CaO	SiO <sub>2</sub>	MnO	P <sub>2</sub> O <sub>5</sub>	S	Al <sub>2</sub> O <sub>3</sub>	MgO	Na <sub>2</sub> O	K <sub>2</sub> O	TiO <sub>2</sub>	Sum
#1	0.32%	0.08%	7.19%	0.03%	0.04%	0.56%	3.32%	0.10%	0.31%	1.14%	0.16%	13.12%
#2	0.39%	0.11%	6.50%	0.04%	0.05%	0.56%	2.99%	0.09%	0.10%	0.20%	0.17%	11.08%
#3	0.24%	0.03%	7.39%	0.18%	0.02%	0.65%	3.83%	0.12%	0.29%	1.15%	0.16%	13.82%

After furnace												
Coke	Fe	CaO	SiO <sub>2</sub>	MnO	P <sub>2</sub> O <sub>5</sub>	S	Al <sub>2</sub> O <sub>3</sub>	MgO	Na <sub>2</sub> O	K <sub>2</sub> O	TiO <sub>2</sub>	Sum
#1	0.39%	0.12%	9.45%	0.04%	0.03%	0.45%	4.29%	0.08%	0.01%	0.37%	0.20%	15.37%
#2	0.38%	0.10%	9.58%	0.03%	0.03%	0.45%	4.24%	0.08%	0.02%	0.19%	0.19%	15.24%
#3	0.35%	0.03%	10.18%	0.11%	0.01%	0.56%	5.14%	0.06%	0.01%	0.28%	0.20%	16.80%

The LECO analysis before and after the furnace (**Table 55**) shows that carbon increased in the

samples, which is indicating that mostly the more volatile ash components had been removed in the furnace. The total weight loss in % of C from samples revealed that coke#3 lost around 7% compared to 3% in the others. Thus, more C has been consumed in this sample for reduction of ash components.

**Table 55** LECO analysis showing carbon content in the coke samples before and after the furnace.

Coke	C Before Furnace	C After Furnace	C loss
#1	84.5%	91.0%	3.04%
#2	83.9%	90.2%	2.33%
#3	83.9%	88.8%	6.84%

To summarize the evaporation trials, the evaporation kinetics and the total alkali lost was highest in the coke containing kaolin, even though the initial alkali content was comparable to one of the reference cokes. However, the cokes were from different EBF campaigns and the test coke was a laboratory produced coke whereas the reference cokes had been produced in industrial scale. To make conclusions about the effect of kaolin addition to the coke, studies on alkali evaporation from coke should be conducted on coke with same origin and alkali content. Moreover, XRD examination of the test coke (1) could not identify the potassium bearing aluminosilicate kalsilite despite the rather high alkali content. In test coke from a previous campaign (2) with similar alkali contents, kalsilite could be detected. Thus, further characterization by XRD and SEM are needed to confirm the presence of alkali in the different cokes, if it is bound in the mineral phases or as free alkalis. Studies on which conditions that are favorable for formation of i.e. kalsilite could also clarify why no kalsilite could be identified in coke by XRD examination after alkali impregnation trials.

#### 2.3.2.4 Task 2.4 Concept for improved adaption of BF operation

Based on results from on-line measurements (Task 1.2), thermodynamic calculations on HCN and NH<sub>3</sub> formation (Task 2.1) and lab tests for correlation of HCN and NH<sub>3</sub> content to an alkali load it could be seen that HCN was most suitable as indicator for the accumulated load of alkalis in the BF. However, the thermodynamic calculations also indicated that HCN is not stable at BF top conditions and the content of HCN is also affected by other parameters such as moisture content, oxygen potential, H<sub>2</sub> etc. For the online measurements at SSAB BF No.4 in Oxelösund, the HCN content in top gas have been plotted against the estimated circulating load of K<sub>2</sub>O (**Figure 234**) and according to this, no clear correlation is seen. In the right-hand image, the relative intensity of alkali emission in raceway has been plotted against the accumulated K<sub>2</sub>O and now a positive correlation is indicated when comparing the relative change of the curves. Thus, although HCN is formed by the reactions of alkalis, the content seems affected by other parameters that make it difficult to use for direct indication on the circulating alkali load. Moreover, the formation of HCN was most pronounced at higher temperatures (above 1800°C) according to the thermodynamic calculations which means that most of the HCN detected in the top might origin from the lower part of the BF and the content in the gas have probably changed during ascending. This is supported by the strong correlation observed between HCN and relative intensities of alkali emissions in raceway in the statistical analysis of the measurements coupled to process data. In the EBF, the NH<sub>3</sub> content was shown to follow the alkali content in dust and sludge. Thus, measurements of HCN in

top gas could also be indicative for the amount of alkali output via the top but this requires further studies on dust and sludge composition in relation to HCN. Based on this, top gas measurements of NH<sub>3</sub> and HCN could be more suitable for indications on alkali output via the top whereas measurements of the relative intensity of alkali emissions in raceway is more promising for indications on the total circulating load of alkalis. A possible on-line evaluation tool could thereby include measurements of HCN in top gas combined with raceway measurements at several tuyeres for indications on the recirculating load of alkalis.

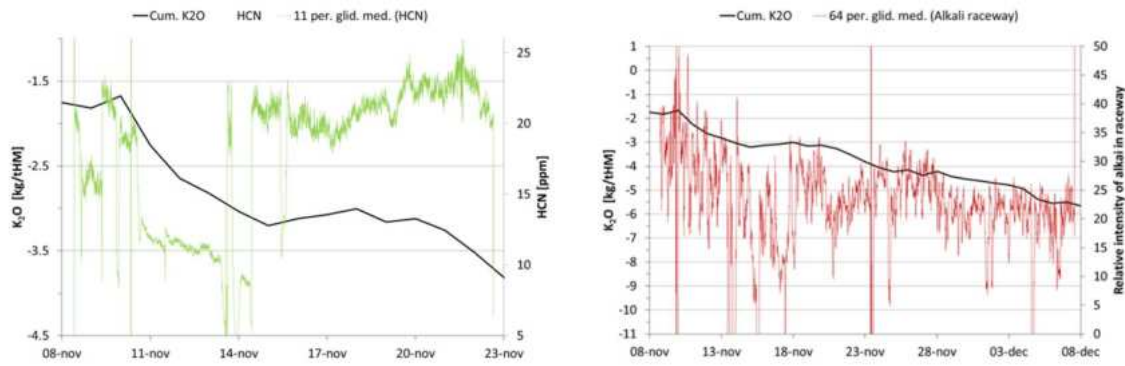


**Figure 234** Accumulated K<sub>2</sub>O versus HCN content in top gas (left) and relative intensity of alkali in raceway (right) for SSAB BF No. 4.

Study of alkali uptake in burden materials in Task 1.3 revealed that the distribution of alkalis can be controlled by the gas profile. With a more centralized gas profile, less alkali uptake in coke and pellets were seen compared to when the EBF was more wall-working. Also higher alkali uptakes in the centre samples were seen when operating with a more centralized gas profile. Operating with an acid pellet had alkali uptakes higher up in the shaft compared to olivine pellets, which confirms the importance of basicity on alkali uptake. Thermodynamical calculations and laboratory tests for study on alkali evaporation from slag confirmed that the basicity should be kept low to avoid alkali evaporation. Thermodynamic calculations in Task 1.3 showed that slag has a key role in the alkali removal and that passage via raceway or at the vicinity of the raceway for an alkali containing slag should be avoided for high alkali removal.

The thermodynamical calculations on energy consumption by alkali recirculation in the BF indicated that the assumed reactions associated with the recirculation of 15 kg K/tHM contribute to an energy consumption of 14.7 kWh, which is corresponding to a coke consumption of 1.3 kg/tHM. In addition to this, the coke consumption by the detrimental effect on coke by alkalis referring to the catalytic effect on gasification reaction has been estimated based on the laboratory trials conducted in Task 2.1. The final carbon conversion (**Table A5 in Appendix A**) for reference coke from DMT (RC\_DMT) after the gasification test was 19%, which can be compared to 34% carbon conversion for the same coke but with 2% K<sub>2</sub>O after alkali treatment (RC\_DMT\_PUP). Thus, the coke containing 2% K<sub>2</sub>O had 15% higher C-consumption compared to the original coke. Kaolin was incorporated in coke ash or used as coating on the coke to study if presence of kaolin could reduce the detrimental effects of alkalis on coke. From the same trials, coke containing 2% kaolin (TC\_2%DMT\_PUP) and a kaolin coated coke (TC\_coatedDMT\_PUP), both with 2% K<sub>2</sub>O, showed on carbon conversions of 33% and 25% respectively. Both are indicating that the C-consumption becomes lower when kaolin is used, which might be explained by formation of alkali bearing phases that prevents the catalytic effects by alkalis on coke gasification.

To summarize, important parameters for control of the alkali circulating load and reduced detrimental effects by alkali on coke in BF are:

- Low slag basicity
- Central gas profile
- Minimum amount of slag containing alkali, that pass in the high temperature zone in raceway or in the vicinity of the raceway
- Indications on the accumulated alkali load by raceway measurements on relative intensities of alkali emissions combined with top gas measurements of HCN.
- Coke with modified ash or coating by kaolin.

### **2.3.3 WP3 Validation of new developed alkali control methods at operational BF**

The main objectives of WP 3 are as follows:

- Validation of long term industrial application of the new developed online top gas evaluation tool for determination of the alkali cycle amount in the BF
- Proof of industrial applicability of alkali control concept developed in Task 2.4
- Development of an overall concept for improved BF alkali control with special emphasis on the different operational conditions and raw material input at the compared BF's

#### **2.3.3.1 Task 3.1 Industrial trials**

The aim of the industrial trials was the validation of the new developed online top gas evaluation tool in order to determine the actual amount of the alkali cycle in the BF. Even if many efforts have been made within the previous work packages to determine correlations between the envisaged top gas components NH<sub>3</sub> and HCN, and the alkali amount in the BF, the situation was too complex to develop a simple calculation routine for quantification of the actual alkali amount in the BF. Many other parameters have been found also to have a significant influence on formation of these gas compounds.

Nevertheless, the results of the previous work packages show, that the measured amount of HCN and (with weaker correlation) NH<sub>3</sub> could however be an option to get some qualitative information on the alkali accumulation in the BF by comparision of the measured concentration in the top gas during a longer periods with otherwise comparable operating conditions. Due to this reason, industrial top gas measuring campaigns with attention on NH<sub>3</sub> and HCN have been performed at VASD within this task. Further, a deepened evaluation of the industrial measurements at the SSAB BF and the EBF® within WP 1 and 2 was performed.

##### **2.3.3.1.1 Industrial top gas measuring campaigns with attention on NH<sub>3</sub> and HCN at VASD**

Based on the results delivered by the different measuring campaigns alkali behaviour has been analysed with attention on NH<sub>3</sub> and HCN. During the measurement trial with the mass spectroscopy it has been able to collect 14 days of valid data. The values for HCN from mass spectroscopy and NH<sub>3</sub> from TDLS have been compared with several process data. The top gas conditions are shown in **Figure 235** with respect to NH<sub>3</sub> and HCN.

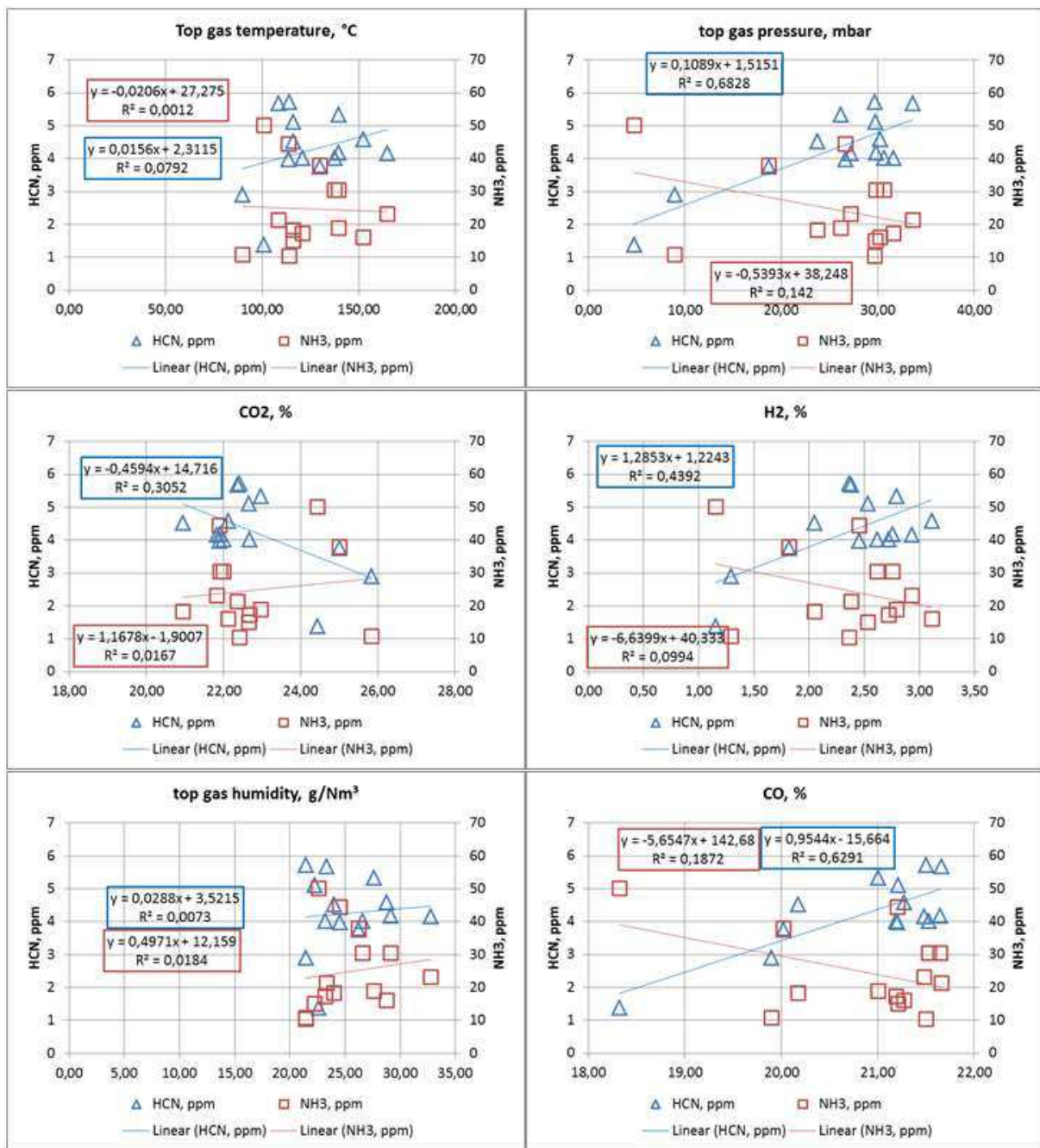


**Figure 235** Influence of top gas conditions on NH<sub>3</sub> and HCN

The results are indicating that the influence of top gas condition on HCN is stronger than on NH<sub>3</sub>. While top gas temperature and humidity doesn't show any influence, top gas pressure, CO, CO<sub>2</sub> and H<sub>2</sub> does on HCN but not or only little on NH<sub>3</sub>. After analysing the alkali balance neither HCN nor NH<sub>3</sub> is showing any close connection. During this trial HCN and NH<sub>3</sub> behave contrary, see **Figure 236**. This trend between NH<sub>3</sub> and HCN was also observed when evaluating top gas measurements at SSAB in Oxelösund.

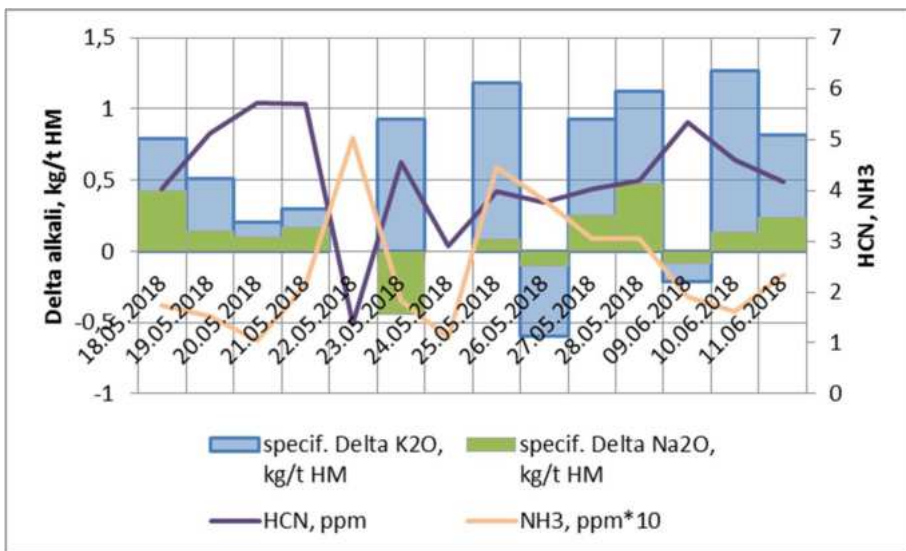


**Figure 236** HCN and NH<sub>3</sub> compared to alkali balance during trial (delta = input minus output)

In **Figure 237** the days before the BF1 blow down are shown as every minute average. At the beginning NH<sub>3</sub> varies by height up to 200 ppm and average NH<sub>3</sub> value is about 47 ppm. Up next the burden charging has been changed to a centre working furnace. Now NH<sub>3</sub> gets lower at about 25 ppm in average. Nevertheless there are several very high peaks which are coincident with high top gas temperature. After this period the burden charging has been changed again in order to prepare for blow-down. Coal injection has been stopped and distribution of coke has been more evenly across the burden level. Now NH<sub>3</sub> gets very low and is about 14 ppm in average. NH<sub>3</sub> value increases to a significant higher level as the burden level is very low. At the same time the top gas temperature keeps its level. The reason for the increase in NH<sub>3</sub> is not clear, but a positive correlation between NH<sub>3</sub> and lower burden level was also observed at SSAB BF No.4 in Oxelösund. At the same time the gas temperature at the wall and above the burden set point is decreasing for a couple of minutes and is recovering again (see **Figure 238**). NH<sub>3</sub> gets higher after that and the average content is about the order of the first day. The highest values doesn't exceed 150 ppm till a sharp increase in the top gas temperature due to a rather big decrease in the burden level.

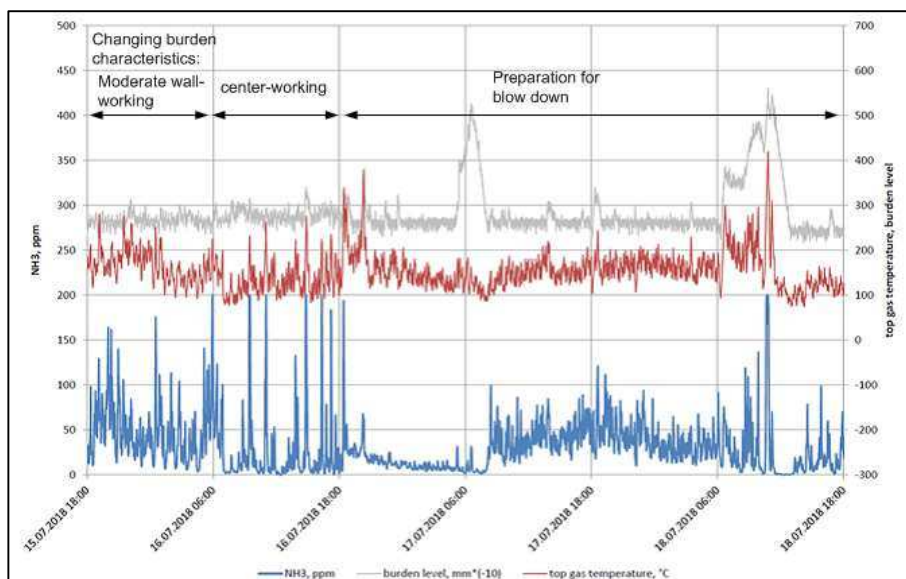


**Figure 237** NH<sub>3</sub> and top gas temperature for a selected period

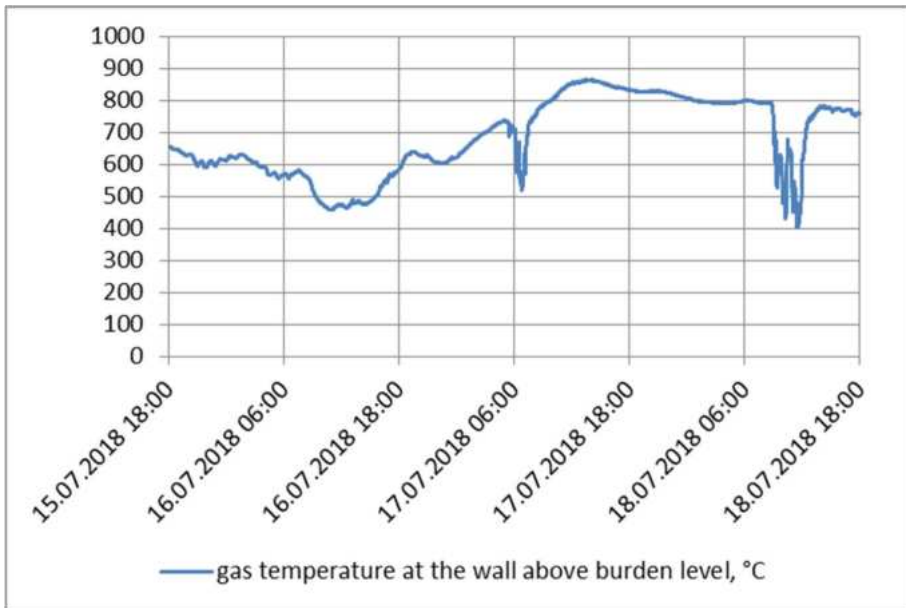


**Figure 238** gas temperature at the wall and above burden level

While looking at these results a correlation between top gas temperature and  $\text{NH}_3$  can be expected. In **Figure 239** the correlations for two periods are shown. In general an increase in top gas temperature leads to an increase in  $\text{NH}_3$ . The strength of the correlation is different and is only valid during rather stable BF conditions. In times with changing demand on production accompanied with a lot of short BF stops correlations between  $\text{NH}_3$  in top gas and process conditions are not identifiable. In **Figure 240** the behaviour of  $\text{NH}_3$  and the top gas temperature is shown. Additionally two values for the burden level are plotted. Due to some issues with the charging system the burden level decreases and the top gas temperature increases. At the same time  $\text{NH}_3$  increases and has a similar trend as the temperature. The peaks in the  $\text{NH}_3$  trend can be referred to charging. Fresh and cold material let the temperature and  $\text{NH}_3$  decrease and after heating up again  $\text{NH}_3$  increases too. Since the measuring system is temperature compensated there shouldn't be an interfering influence from temperature. If the  $\text{NH}_3$  concentration in the top gas is really changing with the top gas temperatures or if there are any other hidden effects appearing cannot be established. Maybe the position of the probe as shown in **Figure 99** has not been suitable because underneath the probe there has been the chance and room for an accumulation of top gas dust. This dust may release  $\text{NH}_3$  in case of changing top gas temperatures and is therefore responsible for the variations in the measured  $\text{NH}_3$  concentrations.

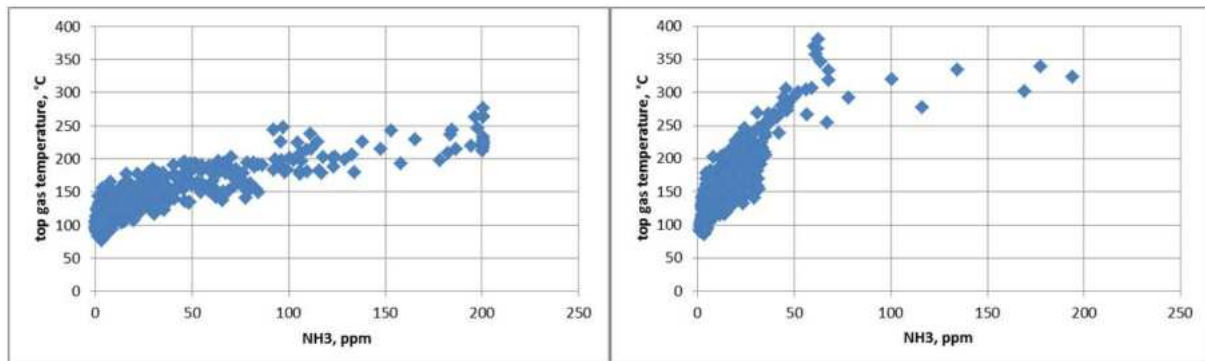


**Figure 239** Correlation between top gas temperature and  $\text{NH}_3$  for two periods, left: period during centre working charging, right: blow down preparation period till 17th July 8:00

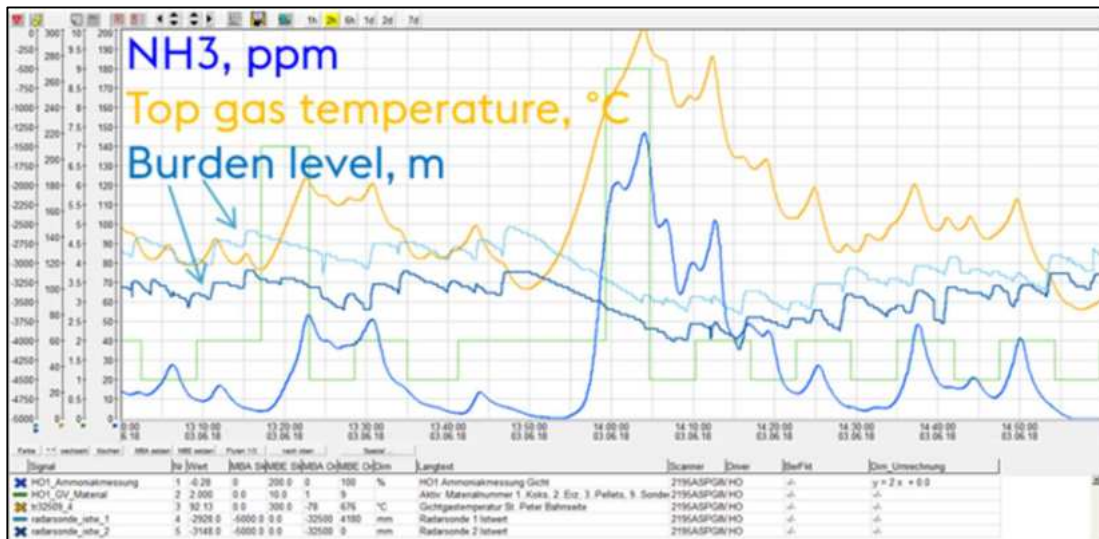


**Figure 240** Behaviour of NH<sub>3</sub> and top gas temperature for a period of two hours

Regarding the correlation between NH<sub>3</sub> in top gas and the alkali circulation a balance of alkalis has been done. Since it has not been possible to quantify the circulation of alkalis in the BF the difference between in- and outflow of K<sub>2</sub>O and Na<sub>2</sub>O has been taken for deeper analysis. The results are shown in **Figure 241** with values on a daily basis. NH<sub>3</sub> does not show any clear trend regarding alkali balance: High values of NH<sub>3</sub> are coincident with low and high difference in the specific alkali balance. A correlation between NH<sub>3</sub> in the top gas and the alkali balance does not exist during this period - no matter if you look at the specific or absolute values. At the end it seems that the determination of the alkali circulation via NH<sub>3</sub> measurement is not possible with the above described approach.

However, the measurement of HCN within the top gas might be better suited for a qualitative long-term monitoring of the alkali state in the BF (see **Figure 236**), but the data set is yet too small to clearly confirm the feasibility of this measurement/evaluation method.

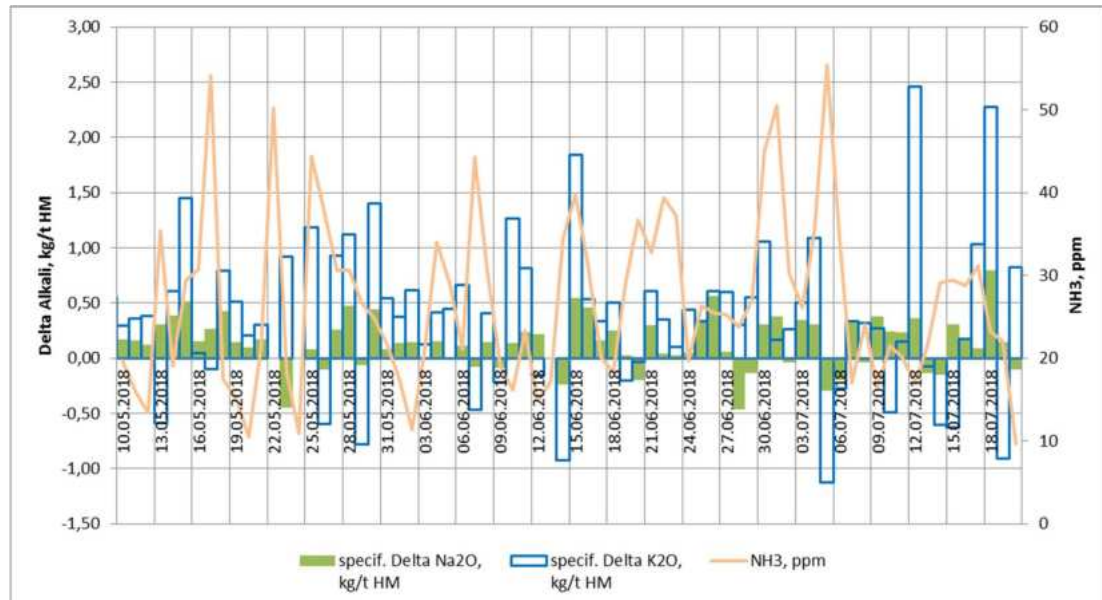


**Figure 241** Daily average of NH<sub>3</sub> and specific Alkali balance (input minus output per ton of HM)

### **2.3.3.1.2** Deepened evaluation of industrial measurements at the SSAB BF and the EBF® aiming in validation of the found correlations between NH<sub>3</sub> and HCN in top gas and alkali amount (SWERIM, SSAB, LKAB, LTU)

The main results of the industrial measurements at SSAB BF and at the EBF® regarding the correlations between NH<sub>3</sub> and HCN in top gas and alkali amount are summarized as follows:

- The HCN content in top gas was shown to be positively correlated to flame temperature according to multivariate analysis, meaning that the HCN content increases with increased flame temperature (Task 1.2). This is supported by the thermodynamic calculations in Task 2.1, showing that the HCN content increases with temperature and is highest at raceway temperatures. The calculations also showed that the presence of HCN and NH<sub>3</sub> at top gas conditions is not thermodynamically favourable which implies that equilibrium composition in top gas was not reached at LKAB EBF® and SSAB BF No.4 for the time periods studied as HCN and/or NH<sub>3</sub> could be detected at ppm levels. This could be coupled to the positive correlations observed with multivariate analyses between NH<sub>3</sub> and HCN contents in top gas to conditions in the lower part of the BF, such as cooling effects, flame temperature and relative intensities of alkali emissions in raceway, implying that NH<sub>3</sub> and HCN are formed from reactions occurring at higher temperatures than present in the top of the BF. Thus, a significant part of the HCN detected in top gas could have been formed in raceway. As no or very small contents of HCN was measured at the LKAB EBF®, the top gas compositions could be closer to equilibrium than at the industrial furnace with more of the formed HCN already reacted before the gas reaches the top.
- According to the thermodynamic calculations on formation of HCN and NH<sub>3</sub> by SWERIM, alkalis in the form of K<sub>2</sub>O will affect the formation of HCN only for temperatures higher than 2200°C, the amount of HCN formed will decrease when the alkali load increases. This is contradictory to the calculations performed by BFI showing that alkalis in the form of KCN have a positive effect on the formation of HCN. The calculations performed by SWERIM were based on alkalis in the form of K<sub>2</sub>O instead of KCN, which might explain why the results deviate. In contrast, the formation of NH<sub>3</sub> was shown to be unaffected by the presence of alkalis in the system and also by HCN according to the calculations. BFI calculations showed that the NH<sub>3</sub> was only affected by KCN to a small extent. Thus, the results from calculations by BFI and SWERIM on NH<sub>3</sub> formation are supporting each other.
- Multivariate analysis of process data combined with the on-line measurement data from BF No. 4 in Oxelösund revealed that the HCN content measured in the top gas and alkali emissions in raceway are positively correlated. As laboratory trials showed that the relative intensity of potassium adsorption was linearly proportional to the potassium vapour, the alkali emissions in raceway measured could thereby be coupled quantitatively to the relative amount of alkalis passing raceway. In addition, the relative change of estimated circulating alkali load and relative intensity of alkali emissions was shown to be positively correlated (**Figure 78**), which also confirms the correlation. Based on this, the HCN content in top gas could be coupled to the relative intensity of alkali emissions in raceway, which in turn could be related to the relative amount of alkalis. However, the statistical model for correlating the measured alkali emissions to the process in the industrial furnace was weak, which can be explained by that the measurement was limited to only one tuyere out of 20.
- NH<sub>3</sub> content measured in top gas at the LKAB EBF® could be linked to the alkali content in dust and sludge but the correlation to alkali output via the slag and the estimated circulat-

ing load was weak. The on-line top gas measurements on NH<sub>3</sub> by MS could thereby only be indicative for the alkali output via the top. However, as the thermodynamical calculations on NH<sub>3</sub> formation conducted by BFI and SWERIM respectively showed that the alkali load had no or only weak impact on the amount of NH<sub>3</sub> formed, the alkali content in dust and sludge is perhaps only correlated indirectly to the NH<sub>3</sub> content in top gas.

- The total light intensity dropped by unknown reasons for the alkali emission measurement in raceway at the LKAB EBF®. This could be due to the process, damage of the equipment or a combination. The reason for this needs to be clarified to enable validation of the method.
- Alkali balancing for estimation of the circulating load requires accurate analyses of raw materials and outgoing materials, as seen by the sensitivity analysis conducted in Task 1.1 where the results were showing that small analytical errors will have large impact on the alkali balance. Thus, the results of the on-line measurements on top gas and in raceway in Task 1.2 could not be evaluated quantitatively against the circulating alkali load due to the difficulties in closing up the alkali balance.
- The impact of basicity on alkali uptake in slag was verified within this project by the alkali balancing performed in Task 1.1, statistical models on data from LKAB EBF and SSAB BF No. 4 in Task 1.2 as well as laboratory trials on alkali evaporation from slag in Task 2.3. Thermodynamical modelling showed the totally dominating role of the slag phase for the removal of alkalis as well as the importance that a minimum amount of the alkali containing slag is passing through the high-temperature regions of the blast furnace, i.e. raceway and vicinity of raceway. The modelling also shows that the carbonate and cyanide cycles claimed by several authors, probably have low importance for the circulating load of alkalis in a blast furnace.
- The study of alkali uptake in burden materials from the LKAB EBF® revealed that coke had in general a higher alkali uptake than pellets but the alkali distribution with respect to depth and horizontal positions showed on similar trends for both materials with generally higher alkali contents at the walls and at higher depths. The influence of gas profile on the alkali distribution and uptake in pellets and coke could also be seen. For a more central gas flow, higher alkali contents could be found in the materials in the centre and the overall alkali load seemed lower compared to a campaign with more gas distributed towards the walls. Thus, this is an indication on that operating with a more central gas profile is advantageous for higher alkali outputs via the top.
- Coke with modified ash by additions of kaolin and a kaolin coated coke were shown to have lower reactivity compared to the reference coke with same alkali content based on trials performed in laboratory. Based on XRD results, the relative intensity of kalsilite peaks was higher in coke treated with kaolin compared to reference cokes, implying that the kaolin addition favours the formation of alkali bearing phases in coke ash.

Finally, also these results indicate that NH<sub>3</sub> measurement in the top gas seems not to be feasible for obtaining reliable information on the alkali accumulation inside the BF, while HCN measurements in the top gas are better suited for a qualitative long-term monitoring of alkalis. Also the measurement of alkali emissions in the raceway is a promising method for monitoring of the alkali state in the BF.

### **2.3.3.2 Task 3.2 Development of an overall concept for improved alkali control at the BF**

The proposed overall concept for improved alkali control at the BF involves the measures for control of the alkali circulating load and reduced detrimental effects by alkali on coke in BF as described for Task 2.4 (chapter 2.3.2.4):

- Low slag basicity
- Central gas profile
- Minimum amount of slag containing alkali, that pass in the high temperature zone in raceway or in the vicinity of the raceway
- Coke with modified ash or coating by kaolin.

Part of this concept would be a continuous qualitative measurement of the alkali load in the BF either by HCN measurement in the top gas and/or by spectrometric measurement of K or Na in the raceway. When an increased alkali load would be detected by the mentioned on-line measurements, one of the measures for alkali control in the blast furnace as described above would be triggered. For both types of measurement, the HCN measurement in the top gas (by mass spectrometer) and for the spectrometric measurement of K or Na in the raceway, the feasibility of a long-term measurement at an industrial blast furnace has been proven. The spectrometric measurement in the raceway could be improved if the measurements would be done on several tuyeres for a better overview of the alkalis passing the raceway. Then the correlation of the measured amount of K and Na to the overall alkali load would be improved as well. But here, a long-term data evaluation for a specific blast furnace will be necessary to obtain usable results for reliable qualitative determination of the alkali state.

### **2.3.4 WP4 Project coordination, documentation and reporting**

The project coordination, documentation and reporting was an ongoing task throughout the whole duration of the project. The following coordination meetings and TGS meetings have been carried out including presentations from all partners:

- Kick-Off-Meeting at BFI in Düsseldorf (Germany), 13.08.2015
- 2<sup>nd</sup> meeting at VASD in Leoben (Austria), 10.12.2015
- TGS 1 meeting, 20.05.2016 in Liège (Belgium); presentation of 1st annual report
- 3<sup>rd</sup> meeting at Mefos in Luleå (Sweden), 08.09.2016
- 4<sup>th</sup> meeting at Dunafer in Dunaújváros (Hungary), 27.01.2017
- TGS 1 meeting in Avilès (Spain), 17.05.2017, presentation of mid-term report
- 5th meeting at LKAB in Kiruna (Sweden), 06.-07.09.2017
- 6<sup>th</sup> meeting at SSAB in Oxelösund (Sweden), 23.-24.01.2018
- Working meeting at LTU in Luleå (Sweden), 07.-08.06.2018, for discussion of alkali control concept
- Telco on Actual results, 24.10.2018
- Final consortium meeting in Düsseldorf, 28-29.11.2018

Further, the following reports on the ALCIRC project have been prepared for the European Commission:

- 1<sup>st</sup> Annual report 2015
- Mid-term-report (end of 2016)
- 2<sup>nd</sup> annual report 2017

## **2.4 Conclusions**

### *Alkali balancing, distribution and impact on burden materials (WP1)*

Estimation of the alkali circulating load at SSAB BF No.4 and the LKAB EBF based on analyses and weights of in- and outgoing materials indicated that alkalis were drained from the BF in the first case and accumulated in the second. The average K<sub>2</sub>O input was up to 1.5 kg/tHM, while the Na<sub>2</sub>O input was 0.9 kg/tHM. A sensitivity analysis on K<sub>2</sub>O content in slag and slag amount revealed that even small analytical errors in the 0.05% range will have significant impact on the balance. Thus, correct alkali balances is difficult to achieve with available data and existing sampling procedures. A detailed alkali balancing has been done at VASD with the analysis of all relevant materials. The total Na<sub>2</sub>O input was between 1.5 and 2 kg/tHM, while the K<sub>2</sub>O input was between 7 and 8 kg/tHM. During the campaign the sum of the Na<sub>2</sub>O output has been higher than the sum of the input. K<sub>2</sub>O behaves different: At the end the K<sub>2</sub>O input was significantly higher (up to 15%) than the output. Dunafer has determined the alkali balances at its blast furnace in three test periods and worked out correlations associated with alkali content in slag respectively alkali removal via slag. The average K<sub>2</sub>O input was up to 1.5 kg/tHM, while the average Na<sub>2</sub>O input amounted to maximum 1.9 kg/t HM. Balance deficits in alkali balance have been significant: The deficits of Na<sub>2</sub>O- and K<sub>2</sub>O-balances have reverse signs in each period (in-out: positive value for Na<sub>2</sub>O; negative for K<sub>2</sub>O). The main influencing parameters on the alkali content in slags at the investigated BF's are the slag temperature and the basicity. An increase in the hot metal temperature, which simultaneously means an increase in slag temperature, has led to lower potassium content in the slag. The same behaviour has been found for the basicity.

Detailed modelling of the reactions occurring between an alkali rich gas and the various condensed materials within a BF were made by LTU using FACTSAGE. The results showed that the slag phase is essential for alkali removal and also the importance of having a minimum amount of alkali containing slag passing through the high temperature regions of the blast furnace i.e. raceway and vicinity of raceway. The modelling also shows that the carbonate and cyanide cycles claimed by several authors, probably have low importance for the circulating load of alkalis in the BF.

The calculated energy impact of alkali compounds in the blast furnace ions resulted in an energy consumption of 29 MJ/tHM (8 kWh/tHM) for a circulating K load of 15 kg/tHM (SWERIM). This is corresponding to the energy consumption 0.44 kWh/tHM for a circulating load of 1 kg K<sub>2</sub>O, which has also roughly been confirmed by BFI calculations. In these calculations it is assumed, that the energy from the exothermic reactions occurring above the cohesive zone contributes to the concerned chemical reactions in these zones. However, if it is assumed that the energy from the exothermic reactions above the cohesive zone is considered as lost and will only contribute to an increased top gas temperature, the energy consumed will correspond to 53 MJ/tHM (14.7 kWh),

which is equivalent to an additional coke consumption of 1.3 kg/tHM (1.36 kg coal per kg coke; energy value: 8.6 kWh/kg coal).

Investigations on alkali uptake in burden materials based on samples from several campaigns showed that the alkali uptake was highest in coke compared to pellets and that the alkali uptake increased with depth from charging level in general for all materials. The alkali uptake in pellets was seen to be highest in the cohesive zone with alkali present in silicate slags and build ups around the pellets. In indurated pellets and pellets from the thermal reserve zone, alkali was found in gangue and in the iron oxide matrix around the decomposed gangue. Increased basicity will decrease the alkali uptake in pellets whereas additions of quartzite will increase it. By comparing two campaigns operating with different gas profiles, one being more central working and the other more wall working, the alkali uptake in coke and pellets was higher towards the walls in the latter case. The overall alkali circulating load was also indicated to be lower in the campaign with a more central gas profile. Moreover, evaluation of coke in TGA revealed that alkali increase coke reactivity.

#### *On-line measurements and thermodynamic calculations (WP1 and WP2)*

The NH<sub>3</sub> content in top gas measured at the LKAB EBF and SSAB BF No.4 in Oxelösund was shown to increase with increasing moisture content in the top gas and decrease with increasing eta CO. At the EBF, high NH<sub>3</sub> contents was also observed at high skinflow temperatures and low burden levels. The correlations to skinflow could be linked to the gas distribution and more favorable conditions for NH<sub>3</sub> contents in top gas when the BF is wall working. This was also supported by measurements at BF1 VASD with higher NH<sub>3</sub> content in top gas when the BF was wall working and when the burden level dropped. For the alkali balancing, no correlation between alkali load and NH<sub>3</sub> could be seen at the industrial BF's or the LKAB EBF. However, the alkali content in dust and sludge was shown to be positively correlated to NH<sub>3</sub> at the EBF, implying that measurement of the NH<sub>3</sub> content in top gas can be indicative for alkali outputs via the top but not the total alkali circulating load. Moreover, thermodynamical calculations by SWERIM and BFI showed that the formation of NH<sub>3</sub> is not or only to a very small extent affected by presence of alkalis. The conclusion is thereby that NH<sub>3</sub> content in top gas is not suitable as an indicator for the total alkali recirculating load.

HCN was only detected in a very low amount in the top gas at the LKAB EBF whereas the concentration in top gas at BF No.4 in Oxelösund was higher than that of NH<sub>3</sub> and the compounds seemed negatively correlated to each other. The same trend was observed at the MS measurements at VASD BF1 with higher concentrations of HCN compared to NH<sub>3</sub> and also with an indicated negative correlation. By the statistical modelling of process data combined with the on-line measurements of top gas and alkali emissions in raceway, the HCN content in top gas was shown to be positively correlated to the relative alkali emissions in raceway and flame temperature. Thermodynamic calculations on HCN formation by BFI indicated that the amount of HCN increased with alkali load but the presence of HCN is not thermodynamically stable at top gas temperatures, implying that equilibrium is not reached and that HCN measured in top gas was formed in the lower part of the BF. Lab tests conducted by BFI for determination of NH<sub>3</sub> and HCN formation in the presence of alkalis revealed that the content of HCN correlates positively with the alkali content and therefore could be used as an indication on alkali accumulation in the BF. Moreover, the relative intensity of alkali emissions measured in raceway was shown to be positively

correlated to the relative change of estimated alkali circulating load at BF No. 4 and laboratory trials verified that the relative intensities of potassium adsorption is indirectly proportional to the potassium concentration in the gas phase. Thus, the raceway measurements on alkali emissions by a lance with optical fibre connected to a spectrometer can be used for indications on when larger amounts of alkalis are passing. However, the alkali emissions was only measured in one tuyere at BF No.4 out of twenty which also can explain the weak statistical model obtained for prediction of intensity of alkali emission by process- and tap data. The HCN content in top gas could not be coupled quantitatively to the circulating load of alkalis due to the difficulties to close up the balances by available data concluded in Task 1.1. No clear correlation was even seen when comparing the relative changes of HCN and the estimated circulating load of alkalis. In addition, the results from thermodynamic calculations and statistical analyses of process data and top gas measurements implied that the formation of HCN takes place in the high temperature zone and is proportional to the alkali load. However, as the gas ascends, other parameters will have impact on the HCN content and the final concentration measured in top gas will not directly be readable for the circulating alkali load in the BF.

#### *Inhibition of alkali circulation and impact from slag composition*

Coke with modified ash composition was studied by basket samples in the LKAB EBF and in additional laboratory trials with purpose to study if the detrimental effects by alkali on coke could be limited. Reactivity studies on untreated coke showed that the mineral additions in coke ash had only marginal effects on coke reactivity and reaction kinetics. For basket samples, no conclusions could be drawn regarding if the mineral additions had been beneficial or not due to the varying conditions each basket had been exposed to. However, kaolin was shown to be the only mineral that had been active in alkali adsorption and further studies in laboratory was therefore focusing on coke with kaolin incorporated in coke ash or as coating. Based on these trials, kaolin in coke as or as coating was indicated to be beneficial for prevention of alkalis negative effects on coke as these showed on lower reaction rates with CO<sub>2</sub> at all temperature intervals studied compared to the reference coke. Also, the relative intensities of peaks corresponding to the alkali bearing phase kalsilite was higher for coke with kaolin compared to the corresponding reference coke, which implies that the kaolin additions favour formation of alkali bearing phases in coke ash.

The alkali capacity of BF slags was studied using thermodynamic calculations and laboratory scale experiments (LTU). The thermodynamic calculations suggested that the driving force for evaporation of potassium is lowest at low basicities and low MgO contents. These were the two compositional parameters of greatest importance. The laboratory-scale experiments confirmed the effect of basicity whereas the effect of MgO was ambiguous.

#### *Overall concept for improved alkali control at the BF*

Part of the concept for improved alkali control at the BF is a continuous qualitative measurement of the alkali load in the BF either by HCN measurement in the top gas and/or by spectrometric measurement of K or Na in the raceway. When an increased alkali load would be detected, the previously described measures for alkali control in the blast furnace like decreased slag basicity would be triggered.

For both types of measurement, the HCN measurement in the top gas (by mass spectrometer) and

for the spectrometric measurement of K or Na in the raceway, the feasibility of a long-term measurement at an industrial blast furnace has been proven. The spectrometric measurement in the raceway could be improved if the measurements would be done on several tuyeres for a better overview of the alkalis passing the raceway. Then the correlation of the measured amount of K and Na to the overall alkali load would be improved as well. But here, a long-term data evaluation for a specific blast furnace will be necessary to obtain usable results for reliable qualitative determination of the alkali state.

#### *Recommendations for industrial implementation of online measurements*

For (semi-quantitative) online measurement/evaluation of alkali accumulation within the blast furnace, two technical options for industrial implementation are usable:

- Measurement of alkali compounds directly in the raceway by using a lance with optical fibre connected to a spectrometer. This technique was proven to be applicable at the tuyeres of an industrial blast furnace.
- Measurement of HCN in the top gas as an indirect indication on alkali accumulation in the BF. - For this task, a mass spectrometer worked reliably in industrial conditions, while a FTIR gas analyser delivered ambiguous results. While at Dunafer a FTIR system generally worked, at VASD the measurement was not reliable due to the formation of Ni containing deposits on the gas cell mirrors. Even if the origin of the disturbing Ni compounds at VASD could finally not be clarified within this research project, this cannot be regarded as a general obstacle for use of a FTIR analyser at BF top gas. However, for avoiding FTIR measurement problems with Ni compounds it is recommended to design the BF gas sampling system without using any Ni containing (e. g. stainless steel) gas tubes.

Further, the measurement of the NH<sub>3</sub> content in the top gas was shown to be indicative for alkali outputs via the top. For this measurement, TDLS gas analysers (tunable diode laser spectroscopy) have proven the industrial applicability. The big advantage of the TDLS is that it is an in-situ measuring system and therefore a gas sampling and preparation is not necessary. Two configurations for laser spectroscopy are available, one as a cross-over system with laser source and receiver opposite to each other and one with a (single) gas diffusion probe. The TDLS systems should be installed in a way to prevent dust accumulation or water condensation before the optical windows (cross-over system) respectively the sensor head (diffusion probe), which would disturb the measurement.

#### *Recommendations for future R&D work*

Based on the outcome of this research project, the following future R&D work is recommended:

- Deeper investigation of the complex correlations between operational BF parameters, the alkali accumulation and the content of trace compounds within the top gas (e. g. HCN concentration) for further development of the online measurements for determination of alkali accumulation.
- Starting from promising initial results within this research project, more intensive investigations of different means for protecting coke from alkali attack are recommended (e. g. use of further additives and procedures).

## **2.5 Publications and patents**

Conference papers:

- Alkali in the Blast Furnace –Influence of modified ash composition in coke and charging practice, A. Gullberg et.al, ICSTI 2018, contribution ID 189.

Master thesis:

- J. Carlsson, "Alkali Circulation in the Blast Furnace - Process Correlations and Counter Measures," Luleå University of Technology, 2018.
- J. Olofsson, Alkali Control in the Blast Furnace – Influence of Modified Ash Composition and Charging Practice. Master, Luleå University of Technology, 2017.

## List of Tables

- Table 1 Comparison of main technical data of operational BF's at Dunafer, SSAB and VASD
- Table 2 Alkali balance for run with 20% acid pellets (period 1) and 100% olivine pellets (period 2)  
at SSAB in Oxelösund
- Table 3 share of material flow in % of total mass per day
- Table 4 Test periods for BF alkali balancing at Dunafer
- Table 5 Results of alkali balances at Dunafer during four test periods
- Table 6 Alkali balances at industrial BF's – Summary of results
- Table 7 Blast amount and composition as well as composition of injection coal
- Table 8 Raw material data used in the calculations
- Table 9 Assumed hot metal composition at temperatures above the temperature of the cohesive zone. In wt%.
- Table 10 Main assumptions and parameters for the thermodynamic calculations
- Table 11 Main alkali components to be taken into account in the thermochemical calculations
- Table 12 Energy consumption due to K input and -cycle
- Table 13 Energy consumption due to Na input and -cycle
- Table 14 Summary of variable influence (+/-) on MS-NH<sub>3</sub> for day-models.
- Table 15 Samples of interest from the EBF in the Alcirc project.
- Table 16 Process conditions prior to the quench of the EBF campaigns 30-33.
- Table 17 Charging sequence in the EBF prior to the quench. W→C wall to centre and C→W centre to wall.
- Table 18 Average K2O content(%) in upper probe samples.
- Table 19 Average K2O content (%) in lower probe samples.
- Table 20 Chemical composition of the tested samples
- Table 21 Estimated kinetic parameters and corresponding temperature interval
- Table 22 Parameters for K pre-treatment of coke
- Table 23 Input gas composition for two-zone reactor trials (synthetic BF top gas)
- Table 24 Experimental parameters for trials in the 2-zone inductively heated fixed bed reactor
- Table 25 Assessment of coke reactivity - Overview on trial parameters and results
- Table 26 Input data for calculations in FactSage.
- Table 27 Input data for FactSage calculations.
- Table 28 BF top gas composition taken into consideration for thermodynamic equilibrium  
calculations
- Table 29 Gas composition input data at different BF zones (in mole; Basis: 100 mole of main  
components N<sub>2</sub>, CO, CO<sub>2</sub>)
- Table 30 Gas composition input data at different BF zones (in mole; Basis: 1 t of hot metal ->  
1500 Nm<sup>3</sup> top gas / t HM)
- Table 31 Calculation pattern with varied parameters for the thermodynamic equilibrium calculations  
(each for all 7 BF zones)
- Table 32 Main process parameters and results of process gas analyses – Average values (V1-8, 13,  
16, 17)
- Table 33 Chemical analysis of kaolin, silversand and bauxite added in test coke.
- Table 34 Carbonization tests in small scale coking retort at DMT in Germany.
- Table 35 Results from carbonization tests.

Table 36 Estimated activation energy values (E<sub>a</sub>), frequency factor (A) and regression coefficient (R<sup>2</sup>)

Table 37 Test coke in basket samples to LKABs EBF in campaign C32.

Table 38 Summary of the mineral phases found in R1 (kaolin), R2 (SiO<sub>2</sub>), R3 (Al<sub>2</sub>O<sub>3</sub>) and SC from BL 33 in C32.

Table 39 Phases detected with SEM/EDS. The number to the left corresponds to the markers in Figure 186-Figure 188 in C32.

Table 40 Lc values and the vertical position in the EBF, BC=base coke, R1=1% kaolin, R2=1% SiO<sub>2</sub>, R3=1% Al<sub>2</sub>O<sub>3</sub>.

Table 41 Summary of alkali impregnation trials.

Table 42 Recipes of cokes produced at LTU.

Table 43 Summary of conducted gasification trials in tube furnace.

Table 44 Start of reaction for TC and RC cokes.

Table 45 Process parameters, K content of coke samples and results of process gas analyses – trials with kaolin and comparative trials without additive or pre-treatment – Average values (V9-17)

Table 46 Chemical analysis of green samples and samples pro-cured in LKAB EBF.

Table 47 Calculation cases used to determine parameters exerting a thermodynamic driving force on the potassium capacity of BF slag. %M<sub>x</sub>O given in wt. %.

Table 48 Slag compositions for the full factorial design.

Table 49 Experiments for the two-level full factorial design are denoted N1-N11 and the three additional experiments of the slag/coke/hot metal system are labeled H5-H7

Table 50 Composition (wt.%) of industrial slag samples

Table 51 Alkali capacity at 1450°C

Table 52 Apparent rate constant and coefficient of determination for the different experiments.

Table 53 Samples used in the vertical furnace experiment.

Table 54 Chemical analysis from XRF for the coke samples before and after the furnace.

Table 55 LECO analysis showing carbon content in the coke samples before and after the furnace.

## List of Figures

- Figure 1: Simplified alkali cycle mechanism (only K) in the BF and option for draining alkalis via the slag
- Figure 2 Alkali output (K<sub>2</sub>O) in BF at SSAB in Oxelösund June-October 2016.
- Figure 3 Slag volume in relation to the K<sub>2</sub>O content in slag June-October 2016.
- Figure 4 K<sub>2</sub>O output and basicity from autumn 2017 at BF No.4 SSAB in Oxelösund.
- Figure 5 Sensitivity analysis of K<sub>2</sub>O balance with respect to K<sub>2</sub>O content in slag and the slag amount.
- Figure 6 Overview of campaign 32 LKAB EBF 2016
- Figure 7 Preliminary potassium balance - Campaign 32 LKAB EBF
- Figure 8 Preliminary Sodium balance - Campaign 32 LKAB EBF
- Figure 9 Rough relative K<sub>2</sub>O balance for BF1 at VASD
- Figure 10 Rough relative Na<sub>2</sub>O balance for BF1 at VASD
- Figure 11 Evolution of relative amount of hot metal and slag
- Figure 12 Specific Na<sub>2</sub>O and K<sub>2</sub>O input
- Figure 13 Contribution of alkali output flow
- Figure 14 Absolute alkali in- and output in t/day and cumulated data in tons and relative HM and slag amount
- Figure 15 Change of the mean temperature of sub-stock level temperature and increase in burden slipping
- Figure 16 Alkali balance for one month considering only variation in slag and sinter analysis
- Figure 17 Alkali content in slag depending on HM temperature and basicity
- Figure 18 In-depth analysis of slag samples (same symbols belong to same taps)
- Figure 19 Variation of the content in Na<sub>2</sub>O (left) and K<sub>2</sub>O (right) compared to the regular slag analysis
- Figure 20 Recalculation of K<sub>2</sub>O balance with corrected K<sub>2</sub>O content of the slag
- Figure 21 Distribution of K<sub>2</sub>O content in the slag (left) and basicity B2 (right)
- Figure 22 Distribution of K<sub>2</sub>O after data selection (left) and HM temperature for the defined groups (right)
- Figure 23 Flame temperature (left) and top gas temperature (right)
- Figure 24 share of pulverized coal in reducing rate (left) and MgO content of slag (right)
- Figure 25 Al<sub>2</sub>O<sub>3</sub> (left) and Mn (right) in slag
- Figure 26 permeability (left) and heat flow in the belly and lower stack (right)
- Figure 27 specific K<sub>2</sub>O flow and its cumulated mass
- Figure 28 Automatic coke sampler on the belt conveyor system
- Figure 29 Automatic dynamic railway weighing machine for blast furnace slag
- Figure 30 Frequency distribution of coke ash percentage (battery I and III; pink: phase I, green: phase II, blue: phase III, purple: Phase IV)
- Figure 31 Frequency distribution of coke S percentage (battery I and III; pink: phase I, green: phase II, blue: phase III, purple: Phase IV)
- Figure 32 Frequency distribution of coke K<sub>2</sub>O percentage (battery I and III, pink: phase I, green: phase II, blue: phase III, purple: Phase IV)
- Figure 33 Frequency distribution of coke Na<sub>2</sub>O percentage (battery I and III, pink: phase I, green: phase II, blue: phase III, purple: Phase IV)

Figure 34 Statistical tests to determine correlations of alkali removal, jointly for data of all three test periods – Part 1: slag basicity, hot metal temperature vs slag K<sub>2</sub>O, Na<sub>2</sub>O and slag S content (pink: phase I, green: phase II, blue: phase III, purple: Phase IV)

Figure 35 Statistical tests to determine correlations of alkali removal, jointly for data of all three test periods – Part 2: Frequency distributions of hot metal temperature, slag basicity, slag K<sub>2</sub>O, slag Na<sub>2</sub>O, slag MgO, slag Al<sub>2</sub>O<sub>3</sub> and slag S content (pink: phase I, green: phase II, blue: phase III, purple: Phase IV)

Figure 36 K<sub>2</sub>O inputs and outputs (kg; proportion) during Phase III

Figure 37 Na<sub>2</sub>O inputs and outputs (kg; proportion) during Phase III

Figure 38 a) Cumulative difference (inputs-outputs) K<sub>2</sub>O and Na<sub>2</sub>O; b) Time trend of Na<sub>2</sub>O and K<sub>2</sub>O percentage in BF slag (Phase III)

Figure 39 Statistical evaluations to determine correlations concerning K<sub>2</sub>O and Na<sub>2</sub>O content of slag (Phase III)

Figure 40 Schematic illustration of calculation steps.

Figure 41 Potassium containing compounds formed upon cooling of the gas coming from raceway.

Figure 42 Potassium containing compounds formed upon cooling of the gas coming from raceway while interacting with coke.

Figure 43 Potassium containing compounds formed upon further cooling of the gas interacting with slag formers at 1300°C.

Figure 44 Schematic description of the assumed potassium cycle (left) and reactions (right).

Figure 45 Characteristic chemical reactions and reaction mechanism for potassium compounds in the blast furnace [42]

Figure 46 Scheme of alkali balance calculation model with reaction units and material streams (given numbers: temperatures in °C)

Figure 47 Calculation result for 1 kg K<sub>2</sub>O input (as KAlSiO<sub>4</sub>) - Amount of material streams in kg

Figure 48 Calculation result for 1 kg K<sub>2</sub>O input (as KAlSiO<sub>4</sub>): Elemental distribution of K within the different streams (in kg)

Figure 49 Calculation result for 1 kg Na<sub>2</sub>O input (as NaAlSiO<sub>4</sub>): Amount of materials streams in kg

Figure 50 Calculation result for 1 kg Na<sub>2</sub>O input (as NaAlSiO<sub>4</sub>): Elemental distribution of Na within the different streams (in kg)

Figure 51 K balance at VASD blast furnace

Figure 52 Process view of LKAB EBF

Figure 53 Principle sketch of MS outline.

Figure 54 Position of tuyeres T1-T3 in EBF.

Figure 55 Optical fibre was mounted as the PC injection lance (left). Typical spectrum from raceway (right).

Figure 56 Temperature and relative intensities of Na, K and in raceway measured with a spectrometer on light guided from the raceway by optical fibre during C32 in EBF.

Figure 57 Heat losses from shell, tuyeres, skinflow temperatures, burden level and alkali in raceway and slag.

Figure 58 MS analysis of NH<sub>3</sub>, H<sub>2</sub>O, HCN shown together with other top gas parameters.

Figure 59 Overview of some process parameters, alkali in slag together with MS and raceway measurements during EBF campaign C32.

Figure 60 Alkali in BF dust and sludge together with average MS-NH<sub>3</sub> during sampling time.

Figure 61 Alkalies in BF-slag together with MS-H<sub>2</sub>O and MS-NH<sub>3</sub>.

Figure 62 Alkalies in slag together with mean values for alkali intensity in raceway.

- Figure 63 MS-NH<sub>3</sub> vs. eta CO
- Figure 64 MS-H<sub>2</sub>O vs. eta CO
- Figure 65 MS-NH<sub>3</sub> vs. top gas temperature
- Figure 66 MS-H<sub>2</sub>O vs. top gas temperature
- Figure 67 Total cooling losses tuyeres (left) and skin flow temperature (right) as a function of NH<sub>3</sub> in top gas.
- Figure 68 Score scatter plot (left) and DmodX line plot (right) for M1 with Y=NH<sub>3</sub>.
- Figure 69 VIP plot of M1 showing the most important variables to explain NH<sub>3</sub>.
- Figure 70 Coefficient plot of M1 showing the influence (+/-) of variables on NH<sub>3</sub>.
- Figure 71 Score scatter plot (left) and DModX line plot of M2 with alkali in raceway=Y.
- Figure 72 VIP plot of M2 showing the variables with highest impact on Y=alkali in raceway.
- Figure 73 Coefficient plot of M2 showing the influence (+/-) of variables on Y=alkali in raceway.
- Figure 74 VIP plot of M3
- Figure 75 Coefficient plot of M3 showing the influence (+/-) of variables on alkali emission in raceway.
- Figure 76 Concentrations of HCN, NH<sub>3</sub> and H<sub>2</sub>O measured by MS and blast flow for the period.
- Figure 77 Cooling losses, flame temperature, relative intensity of emissions related to alkali in raceway, burden level, K<sub>2</sub>O in slag, blast flow and brick temperature for the period with raceway measurements at BF No.4 in Oxelösund.
- Figure 78 Cumulative amount of K<sub>2</sub>O and relative intensity of emissions related to alkali in raceway.
- Figure 79 Alkali measurements in the raceway compared to the K<sub>2</sub>O in slag.
- Figure 80 MS-NH<sub>3</sub> and MS-HCN concentrations together with alkali content in dust and sludge samples. Dashed vertical lines are highlighting occasions with decreased burden level.
- Figure 81 (Left) Score plot over the PCA model MSP. (Right) Loading plot for the same PCA model.
- Figure 82 VIP plot for the OPLS model where Y=HCN, NH<sub>3</sub>.
- Figure 83 Coefficient plot for the OPLS model where Y=HCN, NH<sub>3</sub> showing the influence (+/-) of variables on NH<sub>3</sub>.
- Figure 84 Coefficient plot for the OPLS model where Y=HCN, NH<sub>3</sub> showing the influence (+/-) of variables on HCN.
- Figure 85 VIP plot for the OPLS model with Y=Alkali raceway.
- Figure 86 Coefficient plot for the OPLS model with Y=alkali raceway.
- Figure 87 Principle of the tub furnace prepared with scale (left) and spectroscopic (right) measurements. The sample was placed in a crucible and heated.
- Figure 88 Spectra recorded at experimental time 56.7 and 62.8%.
- Figure 89 Spectra recorded at experimental times 72.3 to 88.2%.
- Figure 90 The weight loss of the sample and light intensity absorbed by reduced and degassed Potassium in the tub furnace.
- Figure 91 The weight loss of Potassium as a function of the light intensity absorbed in the tub furnace.
- Figure 92 BF top gas measurement scheme at VASD
- Figure 93 Position of gas sampling at BF1 at VASD
- Figure 94 Results during activation of the FTIR and after a couple of hours (blue: CO, red: NH<sub>3</sub>)
- Figure 95 FTIR spectra for stable conditions (left) and implausible conditions (right) of measurement
- Figure 96 Mirror of the gas cell with depositions

- Figure 97 Depositions in the sampling system
- Figure 98 Configuration of cross over TDLS (upper part: transmitter, lower part: receiver)
- Figure 99 configuration of the TDLS with the gas diffusion probe (analysing unit within the blue box, probe within the green box)
- Figure 100 Cross over results during the start-up (NH<sub>3</sub> is shown in % of 400 ppm)
- Figure 101 Area in front of the receiver filled with dust particles (left) and condensation (right)
- Figure 102 Daily average of NH<sub>3</sub> in top gas in ppm from 14th of May till 20th of July
- Figure 103 O<sub>2</sub> (%) content in the top gas measured with the MS
- Figure 104 Reliable measuring data of HCN and NH<sub>3</sub> in top gas during MS campaign
- Figure 105 Comparison of NH<sub>3</sub> measured with MS (red line) and TDLS (green line)
- Figure 106 Measured H<sub>2</sub>O percentage and frequency distribution (pink: phase I, green: phase II, blue: phase III, purple: phase IV)
- Figure 107 Measured HCN percentage and frequency distribution (pink: phase I, green: phase II, blue: phase III, purple: phase IV)
- Figure 108 Measured NH<sub>3</sub> percentage and frequency distribution (pink: phase I, green: phase II, blue: phase III, purple: phase IV)
- Figure 109 Measured NO<sub>2</sub> percentage and frequency distribution (pink: phase I, green: phase II, blue: phase III, purple: phase IV)
- Figure 110 a)-d) Examples of statistical tests performed to search correlations for the FTIR top gas measurements
- Figure 111 Material sampling positions during operation (a) and excavation (b).
- Figure 112 Potassium up-take in excavated pellets from the last four campaigns in the EBF.
- Figure 113 Radial positions of coke samples from shaft
- Figure 114 Alkali (potassium) up-take in coke and pellet samples from Campaigns 31 and 32 and temperature measurement with the vertical probe.
- Figure 115 Crushing strength of non-sintered pellets from EBF Campaigns 30-33.
- Figure 116 Reduction degree of pellet layer samples positions 1-7 from EBF excavations C31-C33.
- Figure 117 Reduction degree versus alkali up-take in pellet layer samples positions 1-7 from EBF excavation C32.
- Figure 118 Schematic view of material probes and maximum number of bags with material from each shaft probe.
- Figure 119 Photos of each material and fraction investigated for alkali content.
- Figure 120 Potassium and carbon content in pellets and mixed fractions from the upper shaft probe.
- Figure 121 Potassium and carbon content in pellets and mixed fractions from the lower shaft probe.
- Figure 122 Example of a basket divided into smaller sections with different pellet types in each compartment.
- Figure 123 Example of the excavated baskets from EBF campaign 32 with depth, time in the EBF before the stop, temperature from the vertical shaft probe for each basket and schematic views of placement on the cross section.
- Figure 124 Mass-% alkali containing phases in KPBO from baskets in EBF Campaign 32.
- Figure 125 Vertical temperature measurements and reduction degree of KPBO from baskets in EBF Campaign 31.
- Figure 126 Qemscan images of alkali phases in a) indurated pellet, b) pellet from the thermal reserve zone and c) pellet from the cohesive zone.

- Figure 127 Mass% of alkali phases in limestone/olivine pellets with increasing basicity from the cohesive zone in the EBF Campaign 31.
- Figure 128 Mass% of alkali phases in limestone/olivine pellets with increasing basicity from the cohesive zone in the EBF Campaign 31.
- Figure 129 Location of the studied sample in the EBF
- Figure 130 Received samples and samples after preparation for reactivity tests
- Figure 131 Schematic diagram of the TGA/QMS.
- Figure 132 Applied thermal profile during the test
- Figure 133 Gasification of different tested cokes (excavated samples) as a function of time and temperature
- Figure 134 Detected carbon monoxide in the off-gas as a function of temperature and time
- Figure 135 Arrhenius plot of a studied sample
- Figure 136 Linear relation between the activation energy and the alkali content as well as the distance from the top of the EBF
- Figure 137 Carbotest equipment
- Figure 138 Testing of the change in Na and K-content of coal and coke
- Figure 139 Effect of ash content on coke quality
- Figure 140 Effect of the increase in alkalis on by-products
- Figure 141 Analysis of ash in cokes of various size fractions
- Figure 142 Schematic view of the experimental set-up for the 2-zone coke bed reactor used for laboratory trials on the alkali impact on coke
- Figure 143 Experimental set-up for the two zone BFI coke bed reactor; left: quartz glass tube reactor with two induction coils; right: 25 kW HF-generator for zone 1
- Figure 144 HT-Pyrometer for temperature control
- Figure 145 Two-zone reactor with inductive heating in operation - Heated graphite crucible in the lower heating zone (Zone 1: alkali evaporation zone; 1300°C) and coke in upper heating zone (Zone 2: 800°C)
- Figure 146 Coke analysis by thermogravimetry. Left: TG equipment at BFI; Right: Applied heating programme and gas stream (similar to LTU procedure)
- Figure 147 Thermogravimetric measurement – Mass loss and temperature vs. time (V1-4)
- Figure 148 Considered Range for determination of activation energy: 880° -1150°C
- Figure 149 Exemplary Arrhenius plot for determination of the activation energy Ea (V1)
- Figure 150 Calculated activation energies Ea in correlation to K content of zone 1 coke
- Figure 151 Gases present over the temperature range, gas volume and mass C(s) for a system without alkalis.
- Figure 152 NH<sub>3</sub>(g) and HCN(g) present in the system at lower temperature.
- Figure 153 NH<sub>3</sub>(g) and HCN(g) formed when 3 kg K<sub>2</sub>O/tHM and 1 kg Na<sub>2</sub>O/tHM was added.
- Figure 154 HCN(g) formed in all calculations.
- Figure 155 Calculated amount of NH<sub>3</sub> and HCN (mole, log scale) in dependency on the temperature
- Figure 156 Calculated amount of NH<sub>3</sub> and HCN (mole, log scale) in dependency on the hydrogen activity (log scale)
- Figure 157 Calculated amount of HCN and NH<sub>3</sub> in BF top gas in correlation to the amount of KCN (Alpha = mol KCN)
- Figure 158 Change of gas utilisation in the BF with temperature (in Baur-Glaessner diagram) [42] - red: selected BF zones

- Figure 159 Calculated amount of formed NH<sub>3</sub> for each BF reaction zone and the different input amount of H<sub>2</sub> and KCN.
- Figure 160 Calculated amount of formed HCN for each BF reaction zone and the different input amount of H<sub>2</sub> and KCN.
- Figure 161 Calculated amount of formed HCN for each BF reaction zone and the different input amount of H<sub>2</sub> and KCN (Same scale as for NH<sub>3</sub>; Figure 159)
- Figure 162 Correlation of calculated NH<sub>3</sub> to the amount of K compounds (KCN, expressed as K<sub>2</sub>O), BF zone 2 (600°C)
- Figure 163 Correlation of calculated NH<sub>3</sub> to amount of the K compounds (KCN, expressed as K<sub>2</sub>O), BF zone 4 (1000°C)
- Figure 164 Correlation of calculated NH<sub>3</sub> to the amount of H<sub>2</sub> – BF zone 2 and 4 (600; 1000°C), no KCN
- Figure 165 Correlation of calculated HCN to the amount of K compounds (KCN, expressed as K<sub>2</sub>O), BF zone 4 (1000°C)
- Figure 166 Correlation of calculated HCN to the amount of K compounds (KCN, expressed as K<sub>2</sub>O), BF zone 7 (1800°C)
- Figure 167 Correlation of calculated HCN to the amount of H<sub>2</sub> – BF zone 4 (1000°C), no KCN
- Figure 168 Correlation of calculated HCN to the amount of H<sub>2</sub> – BF zone 4 and 7 (1000; 1800°C), no KCN
- Figure 169 Typical CO and CO<sub>2</sub> content of product gas vs. time (no. of spectra) - V 1-4
- Figure 170 Exemplary plot for HCN measurements vs. time (No. of spectra) - V1-4
- Figure 171 Average NH<sub>3</sub> concentration in correlation to K content in zone 1 (V1-4)
- Figure 172 Average HCN concentration in correlation to K content in zone 1 (V1-4; all 3 % H<sub>2</sub>)
- Figure 173 Average HCN concentration in correlation to K content in zone 1 (V5-8, all 3 % H<sub>2</sub>)
- Figure 174 Average HCN concentration in correlation to K content in zone 1 (V13 and 17, both 5 % H<sub>2</sub>)
- Figure 175 Average HCN concentration compared to K content in zone 1 - coke without K pre-treatment – 3 % and 5 % H<sub>2</sub> (V1, V16 and V17)
- Figure 176 Average HCN concentration compared to K content in zone 1 - coke with high K pre-treatment – 3 % and 5 % H<sub>2</sub> (V2, V13)
- Figure 177 Average HCN concentration compared to K content in zone 1 - coke with high K pre-treatment and 5 % Kaolin pre-treatment – 3 % and 5 % H<sub>2</sub> (V10, V14)
- Figure 178 Overview - Average HCN concentration in correlation to K content for all two-zone reactor trials at BFI (including kaolin pre-treatment)
- Figure 179 Mass loss curves of the samples during gasification
- Figure 180 Generated CO of the samples during gasification
- Figure 181 Charging schedule of baskets with test coke and base coke in C32.
- Figure 182 Depth of the excavated baskets from the EBF in C32, and total time after charging.
- Figure 183 Horizontal position of the baskets in the EBF during C32.
- Figure 184 Alkali concentration plotted against the EBF height from the top in C32. R1 (kaolin) and BC1 is in the left-hand image and R2 (SiO<sub>2</sub>) and BC2 is in the right-hand image.
- Figure 185 Alkali concentration plotted against the EBF height from the top for R3 (Al<sub>2</sub>O<sub>3</sub>) and BC3 in C32.
- Figure 186 SEM images of the surface and core of BC3 from BL 3 (C32).
- Figure 187 SEM images of the surface and core of R1 from BL 33 (C32).
- Figure 188 SEM images of the surface and the core of R2 from BL 33 (C32).

- Figure 189 Lc values plotted against the position in the EBF.
- Figure 190 Start of reaction and carbon conversion plotted against alkali content.
- Figure 191 Alkali content plotted against activation energy (left). Apparent reaction rate plotted against alkali content in coke samples (right).
- Figure 192 Charging schedule of baskets containing reference coke, test coke with 2% kaolin and coated coke in C33. Retrieved samples at excavation are highlighted in red text.
- Figure 193 Horizontal position of baskets retrieved from C33 in EBF after excavation.
- Figure 194 Alkali content in coke from retrieved baskets after C33 (left) and graphitization degree of coke from baskets in C32 and C33 (right) as function of distance from charging level.
- Figure 195 Start of reaction (left) and activation energy (right) of coke with 0%, 1% and 2% kaolin as a function of K<sub>2</sub>O wt-%.
- Figure 196 Reaction rate as a function of wt-% K<sub>2</sub>O in coke at 900°C.
- Figure 197 Graphite crucible for alkali vapour generation and uptake in coke.
- Figure 198 Potassium content (wt.-%) in coke before and after trials for uptake of potassium and the total weight change of coke.
- Figure 199 Sample weight and temperature as a function of time for RC\_DMT\_PUP (Left) and TC\_8%LTU\_PUP (right) in tube furnace.
- Figure 200 Apparent Reaction rate as a function of alkali content for the coke types exposed to alkali vapour.
- Figure 201 Apparent Reaction rate as a function of alkali content for the different coke types.
- Figure 202 XRD diffractograms of test coke with 2% kaolin and reference coke.
- Figure 203 XRD diffractograms of test coke with 4% kaolin and coated coke.
- Figure 204 XRD diffractograms of test coke with 8% kaolin and reference coke from LTU.
- Figure 205 Graphitisation degrees of alkali treated cokes (left) and after reactivity trials (right).
- Figure 206 Microscopic images - Comparison of surfaces (left) and pore diameters (right) of untreated coke (1st row) with a coke after kaolin pre-treatment (1x and 3x; 2nd and 3rd row)
- Figure 207 Average HCN concentration compared to K content in zone 1 - coke without K pre-treatment (0 – 5 % kaolin, all 3 % H<sub>2</sub>; V9, V11 and V16)
- Figure 208 Average HCN concentration compared to K content in zone 1 - coke with high K pre-treatment (0 – 5 % kaolin, all 3 % H<sub>2</sub>; V2, V10 and V12)
- Figure 209 Average HCN concentration compared to K content in zone 1 - coke with high K pre-treatment (0 and 5 % kaolin, all 5 % H<sub>2</sub>; V13, V14)
- Figure 210 Activation energy Ea in correlation with kaolin pre-treatment (no K pre-treatment; high K pre-treatment)
- Figure 211 Charging schedule of olivine briquettes and lumps (left). A filled basket containing olivine briquette and iron ore pellets (right).
- Figure 212 Vertical positions of retrieved basket samples containing olivine briquettes and lumps.
- Figure 213 SEM microphotograph of surface piece from olivine briquette BB. Right-hand image is corresponding to highlighted area to the left.
- Figure 214 Experimental matrix of the two-level full factorial design with three variables
- Figure 215 Experimental setup with a) graphite cylinders representing coke, b) crucible prepared with synthetic slag and graphite enclosure for the thermocouple and c) TAMMAN furnace prepared for experiment.
- Figure 216 a) Inner graphite tube separating the slag from the iron. b) removing the inner graphite tube.

Figure 217 Placement of the industrial slag samples within the compositional range of the design of experiments (outlined rectangle).

Figure 218 Thermodynamic potassium content of BF final slag depending on a) B2 basicity b) MgO content at constant B2 and B3 basicity c) Al<sub>2</sub>O<sub>3</sub> d) MnO and Na<sub>2</sub>O content e) temperature and f) total pressure.

Figure 219 Triplicate with a) %K on the y-axis and b) % of initial potassium analyzed at zero minutes on the y-axis.

Figure 220 Comparison of temperature pairs a) N1/N5, b) N3/N7, c) N2/N6 and d) N4/N8.

Figure 221 Relationship between -ln(%K/%Kstart) and time measured for experiment N1: B2=0.8, MgO=10% and T=1450°C.

Figure 222 a) Summary of model fit b) Scaled and centred coefficients c) residuals plot d) observed vs. predicted.

Figure 223 Contour plot based on Equation (13).

Figure 224 Thermodynamic calculations in an open system representing the laboratory-scale experiments at a) 1450°C and b) 1550°C. c-d) Transformations in accordance to the first order kinetics.

Figure 225 Linear relationship between the apparent rate constant determined in the laboratory-scale experiments and FactSage calculations.

Figure 226 Potassium evaporation determined experimentally, by the regression model and by FactSage calculations of the industrial slag samples a) Dunafer 1 b) Dunafer 2 c) Dunafer 3 and d) VoestAlpine 1.

Figure 227 Comparison of evaporation from slag/coke/hot metal and slag/coke system. b) First order kinetics evaluation of slag/coke/hot metal experiments.

Figure 228 Approximate position of coke samples in the EBF.

Figure 229 Apparent reaction rate of the coke samples after the EBF.

Figure 230 Schematic view of the vertical furnace used.

Figure 231 Mass change in percent for the different coke types used.

Figure 232 Coke #3 sample covered in a white fluff after the furnace. Inner diameter of the crucible was 40 mm.

Figure 233 Mass change per minute in the furnace for the three coke samples.

Figure 234 Accumulated K<sub>2</sub>O versus HCN content in top gas (left) and relative intensity of alkali in raceway (right) for SSAB BF No. 4.

Figure 235 Influence of top gas conditions on NH<sub>3</sub> and HCN

Figure 236 HCN and NH<sub>3</sub> compared to alkali balance during trial (delta = input minus output)

Figure 237 NH<sub>3</sub> and top gas temperature for a selected period

Figure 238 gas temperature at the wall and above burden level

Figure 239 Correlation between top gas temperature and NH<sub>3</sub> for two periods, left: period during centre working charging, right: blow down preparation period till 17th July 8:00

Figure 240 Behaviour of NH<sub>3</sub> and top gas temperature for a period of two hours

Figure 241 Daily average of NH<sub>3</sub> and specific Alkali balance (input minus output per ton of HM)

## **List of Symbols, Indices, Acronyms and Abbreviations**

### ***Symbols***

### ***Indices***

<i>B2</i>	<i>basicity of slag B2 = (CaO)/(SiO<sub>2</sub>)</i>
<i>B4</i>	<i>basicity of slag B4 = (CaO+MgO)/(SiO<sub>2</sub>+Al<sub>2</sub>O<sub>3</sub>)</i>

### ***Abbreviations***

<i>BF</i>	<i>Blast furnace</i>
<i>EBF®</i>	<i>Experimental blast furnace</i>
<i>EDX</i>	<i>Energy Dispersive X-Ray Analysis</i>
<i>HM</i>	<i>Hot metal</i>
<i>FTIR</i>	<i>Fourier-transform-infrared spectroscopy</i>
<i>MS</i>	<i>mass spectroscopy</i>
<i>RAFT</i>	<i>raceway adiabatic flame temperature</i>
<i>TDLS</i>	<i>tunable diode laser spectroscopy</i>

## List of References

- [1] R. Lin, U. Janhsen, S. Widner: Investigations of chlorine and alkali behaviour in the blast furnace and optimisation of blast furnace slag with respect to alkali retention capacity. Final report, EUR 20586 EN, 2003
- [2] B.K.C. Chan, I.A.S. Edwards, H. Marsh: Fundamental studies of the formation, structure and reactivity of metallurgical cokes as related to blast furnace operation. Final report, EUR 14294 EN, 1992
- [3] DEVELOPMENT OF AN ALKALI-RESISTANT COKE. Final report, EUR 12652 EN, 1990
- [4] Development of alkali metal compounds removal systems for use with hot particulate removal. Final report, EUR 14935 EN, 1995
- [5] R. Klima, O. Höfer, U. Chiarotti: Investigation of accretion formation in a blast furnace shaft. Final report, 2005
- [6] U. Janhsen, A. Günbati, C. Sautner: Changes in the microstructure of coke while passing the blast furnace with respect to the quality of the charged coke and the behaviour of nut coke in the blast furnace. Final report, EUR 22439 EN, 2007
- [7] U. Janhsen, L. Di Sante, J. M. Steiler: Coke quality for blast furnace operation with high levels of coal/oil injection. Final report, EUR 20105 EN, 2002
- [8] Altpeter, W.; Beppler, E.; Gerstenberg, B.; Kannappel, M.: Auswirkungen von Alkalien im Hochofen. stahl und eisen 108 (1988), Nr. 17
- [9] Lu, W-K; Holditch, J. E.: Alkali control – A canadian experience. Ironmaking Proceedings, Vol. 41, Pittsburgh, 1982.
- [10] Kurunov, I.; Titov, V.; Arsamascev, A.; Basov, V; Tikhonov, D.: Analysis of alkali removal influenced by blast furnace operating conditions. Proceedings, METEC InSteelCon, Düsseldorf, 27 June-1 July 2011
- [11] Taguchi, S; Koitabashi, T.; Tsuchiya, N.; Takahashi, H.: Behavior of alkalis and zinc in blast furnace and their influences on the furnace operation. Tetsu to Hagane 68 (1982) Nr. 15 p. 2346/53
- [12] Steiler, J.M.; Nicolle, R.; Wanin, M.; Thirion, C.; Flamion, D.: Investigation on potassium build-up in the blast furnace. Proc. AIME-ISS Ironmaking Conf.43 (1984) p. 427/37
- [13] Lowthian Bell, I.: Chemical Phenomena of iron smelting. George Rutledge & sons, London, (1872) Section XXVI On the presence of alkaline cyanides in the blast furnace p. 134/43
- [14] Lowthian Bell, I.: The manufacture of iron and steel. George Rutledge & sons, London, (1884) Section IX. On the chemical changes as they take place in the blast furnace p. 176/233
- [15] Kinney, S.P.; Guernsey, E.W.: The occurrence of alkali cyanides in the iron blast furnace. Ind. Eng. Chem. 17 (1925) Nr. 7 p. 670/74
- [16] Davies, J.; Moon, J.T.; Traice, F.B.: Alkalies in the blast furnace. Ironmaking and Steelmaking 5 (1978) Nr. 4 p. 151/61
- [17] Lilius, K.: On the nature of circulating alkali load in the blast furnace. Scand. J. Metallurgy 9 (1980) p. 139/47
- [18] B. Björkman, Properties of Blast Furnace Slags with high MgO Content. Proc., The 5th Japan-Nordic Countries Joint Symposium on Science and Technology of Process Metallurgy, Sep. 1992, Helsinki, Finland. Published by Jernkontoret.
- [19] Hilding, T. S.: Investigation of Accretion formation in Blast furnace Shaft. Master's thesis, Lulea Technical University, 2001

- [20] J. Kaczorowski; T. Lindstad: THE EFFECT OF POTASSIUM IMPREGNATION ON THE BOUDOUARD REACTIVITY OF SELECTED SINGLE-SOURCE AND COMMERCIAL COKES, Proc. INFACON XI, 2007
- [21] Alam, M.; Debroy, T.: KCN as a catalytic precursor in coke CO<sub>2</sub> reaction. Ironmaking Steelmaking 12 (1985) Nr. 5 p. 203/08
- [22] Lundgren, M.: Development of Coke Properties during the Descent in the Blast Furnace. Doctoral Thesis, Lulea University of Technology, 2013
- [23] Turkdogan, E.T.; Josephic, P.H.: Ammonia and hydrogen cyanide in blast furnace stack. Ironmaking and steelmaking 11 (1984) Nr. 4 p. 192/201
- [24] Bale, CW, Bélisle, E, Chartrand, P, Decterov, SA, Eriksson, G, Hack, K, Jung, IH, Kang, YB, Melancon, J, Pelton, AD, Robelin, C, Petersen, S, FactSage thermochemical software and databases - recent developments, Calphad, 33, 2009, 295-311.
- [25] Shimomura, Y, Nishikawa, K, Arino, S, Katayama, T, Hida, Y, Isoyama, T, On the internal state of the lumpy zone of blast furnace, ISIJ Int., 17, 1977, 381.
- [26] Sasaki, K, Nakatani, F, Hatano, M, Watanabe, M, Shimoda, T, Yokotani, K, Ito, T, Yokoi, T, Investigation of quenched No 2 blast furnace at Kokura Works, Trans. ISIJ, 17, 1977, 252.
- [27] Kanbara, K, Shigemi, A, Blast furnace dissection, Nippon Steel Technical Report Overseas, 10, 1977, 47.
- [28] Kurunov, I, Titov, V, Arsamascev, A, Basov, V, Tikhonov, D, Analysis of alkali removal influenced by blast furnace operating conditions, Proc., METEC InSteelCon, Düsseldorf, June, 2011.
- [29] Hooey, PL, Zarins, K, Dahlstedt, A, Annersten, H, Behaviour of kaolinite coated olivine pellets in blast furnace, Ironmaking and Steelmaking, 31, 2004, 333-41.
- [30] Eliasson, E, Hooey, PL, Annersten, H, Lindblom, B, Formation of potassium slag in olivine fluxed blast furnace pellets, Ironmaking and Steelmaking, 34, 2007, 422-430.
- [31] Ryösä, E, Wikström, J, Lindblom, B, Rutqvist, E, Benedictus, A, Butcher, A, Investigation of Minerals and Iron Oxide Alterations in Olivine Pellets Excavated from the LKAB Experimental Blast Furnace, Proc., In: Ninth Int. Congress for Applied Mineralogy, Brisbane, Queensland, September 2008, pp. 545-55.
- [32] Lundgren, M, Sundqvist Ökvist, L, Björkman, B, Coke reactivity under blast furnace conditions and in the CSR/CRI test, Steel Res. Int., 80, 2009, 396-401.
- [33] Lundgren, M, Sundqvist Ökvist, L, Hyllander, G, Jansson, B, Björkman, B, High temperature coke characteristics in the blast furnace - evaluation of coke properties in the raceway area, Proc., In SCANMET IV, Vol. 2, June 2012, Luleå, Sweden, pp. 157-68.
- [34] Lin, R et al. Investigation of chlorine and alkali behaviour in the blast furnace and optimization of blast furnace slag with respect to alkali retention capacity, European Comission, Final report, EU20586EN, Contract no 7210-PR/068, 2003, pp. 338, ISBN 92-894-4766-4.
- [35] Ezezobor, DE, Balogun, SA, Zinc accumulation during recycling of iron oxide wastes in the blast furnace, Ironmaking and Steelmaking, 33, 2006, 419-25.
- [36] van der Velde, MTP, van der Steel, J, Boon, LA, Molenaar, R, Experience of Alkalies and Zinc on the Blast Furnaces at Hoogovens IJmuiden, Presentation at European Blast Furnace Committee, Port Talbot, October, 1998.
- [37] Lu, WK, Holditch, JE, Alkali control in the blast furnace: Theory and Practice, Proc., In: Conf. on the operation of the blast furnace, Theory and Practice, Arles, France, June 1980,

Vol 3, pp. 1-18.

- [38] Lilius, K, On the nature of the circulating alkali load in blast furnaces, *Scand. J Metall.*, 9, 1980, 139-47.
- [39] Abraham, KP, Staffansson, L-I, The alkali problem in the blast furnace, *Scand. J Metall.*, 4, 1975, 193-204.
- [40] Averin, VV, Khodak, LZ, Physicochemical Conditions of the Formation and Decomposition of Cyanides in a Blast Furnace, *Russian Metallurgy (Metally)*, 2001, No 1, 17.
- [41] Leimalm, U, Lundgren, M, Sundqvist Ökvist, L, Björkman, B, Off-gas dust in an Experimental Blast Furnace, Part 1: Characterization of Flue Dust, Sludge and Shaft Fines, *ISIJ Int.*, 2010, 50, 1560-1569.
- [42] H.W. Gudenau et. al. , *Vom Erz zum Stahl. Materialsammlung Praktikum Eisenhüttenmännische Verfahrenstechnik*, RWTH Aachen, Institut für Eisenhüttenkunde, 1990
- [43] Lahijani P, Zainal ZA, Mohamed AR. Catalytic effect of iron species on CO 2 gasification reactivity of oil palm shell char. *Thermochimica Acta*. 2012;546:24-31
- [44] Huo W, Zhou Z, Chen X, Dai Z, Yu G. Study on CO<sub>2</sub> gasification reactivity and physical characteristics of biomass, petroleum coke and coal chars. *Bioresour Technol*. 2014;159:143-149.
- [45] Best Available Techniques (BAT) Reference Document for Iron and Steel Production; Industrial Emissions Directive 2010/75/EU (Integrated Pollution Prevention and Control); European Commission, 2012
- [46] J. Carlsson, "Alkali Circulation in the Blast Furnace - Process Correlations and Counter Measures," Luleå University of Technology, 2018.
- [47] J. Olofsson, Alkali Control in the Blast Furnace – Influence of Modified Ash Composition and Charging Practice. Master, Luleå University of Technology, 2017.
- [48] E. T. Turkdogan and P. H. Josephic, "Ammonia and Hydrogen Cyanide Formation in Blast Furnace Stack," *Ironmaking and Steelmaking*, vol. 11, no. 4. pp. 192–201, 1984.
- [49] M. Geerde, R. Chaigneau, I. Kurunov, O. Lingardi, and J. Ricketts, *Modern Blast Furnace Ironmaking: An Introduction*, Third. Amsterdam: IOS Press BV, 2015.
- [50] I. F. Kurunov, V. N. Titov, V. L. Emel'yanov, S. A. Lysenko, and A. N. Arzamastsev, "Analysis of the behavior of alkalis in a blast furnace," *Metallurgist*, vol. 53, no. 9–10, pp. 533–542, Sep. 2009.
- [51] V. P. Gridasov, G. N. Logachev, S. N. Pishnograev, A. V. Pavlov, V. A. Gostenin, and A. V. Chevychelov, "Behavior of Alkalies in Blast Furnaces," *Metallurgist*, vol. 59, no. 9–10, pp. 761–765, Jan. 2016.
- [52] T. Hilding, "Evolution of coke properties while descending through a blast furnace," Luleå tekniska universitet, 2005
- [53] Wang C-, Lu Q, Ma M-, Liu S-, Hou D-. Potassium capacity of BF slag. *Kang T'ieh*. 2006;41(12):15-18.
- [54] Karsrud K. ALKALI CAPACITIES OF SYNTHETIC BLAST FURNACE SLAGS AT 1500 degree C. *Scand J Metall.* 1984;13(2):98-106.
- [55] AMATATSU M, STUTS V, GUDENAU HW. Evaporation-and absorption-rate of potassium through blast-furnace slag. *Transactions of the Iron and Steel Institute of Japan*. 1985;25(9):949-952.
- [56] Lan C, Lyu Q, Liu X, Jiang M, Zhang S, Li F. Comprehensive desulfurization and

dealkalization capacity of blast furnace slag. Transactions of the Indian Institute of Metals. 2018:1-7.

- [57] Ivanov O, Savov L, Janke D. Experimental studies of the alkali behaviour in blast furnace type slags. Steel Res Int. 2004;75(7):442-448.
- [58] Forsberg S. Volatilization of potassium from synthetic slags of blast furnace type. 1987;TRITA-MEL 075.
- [59] Friedrichs HA, Gudenau H, Stutz V. Zur verflüchtigung von kalium aus Schlacken. Archiv für das Eisenhüttenwesen. 1984;55(4):137-142.

## **Appendices**

**Appendix 1 Thermodynamic calculations - LTU – Task 1.1**

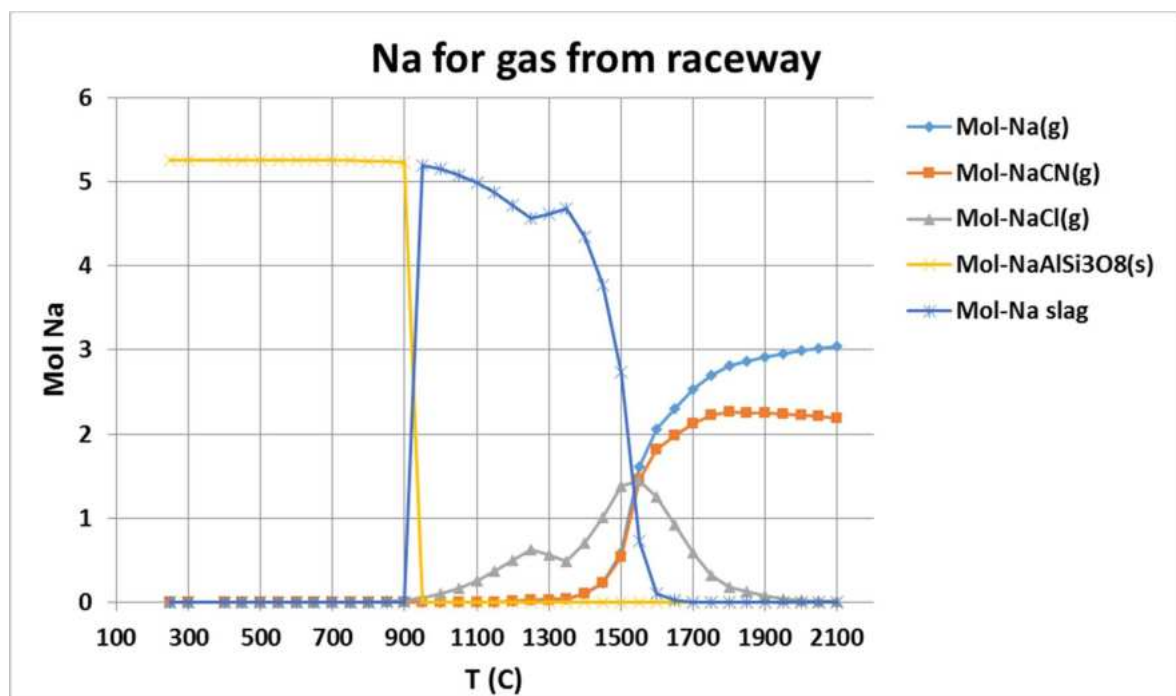
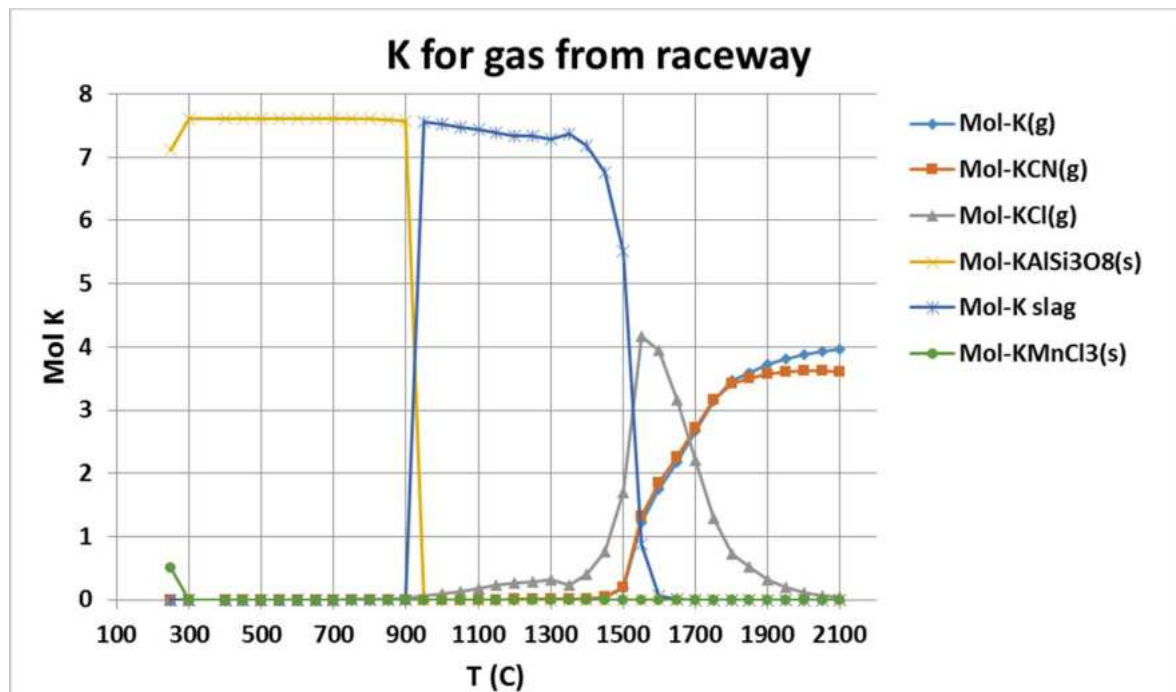
**Appendix A SWERIM – Tasks 1.1, 1.2, 2.2.**

## Appendices

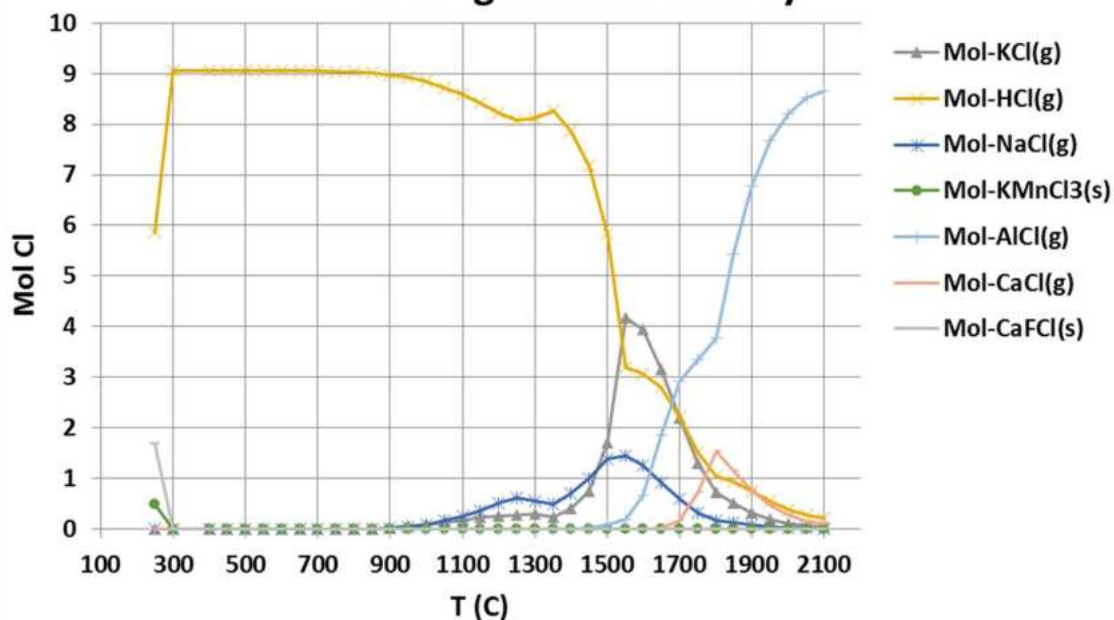
### **Appendix 1 (LTU, Task 1.1)**

#### **Appendix 1.1**

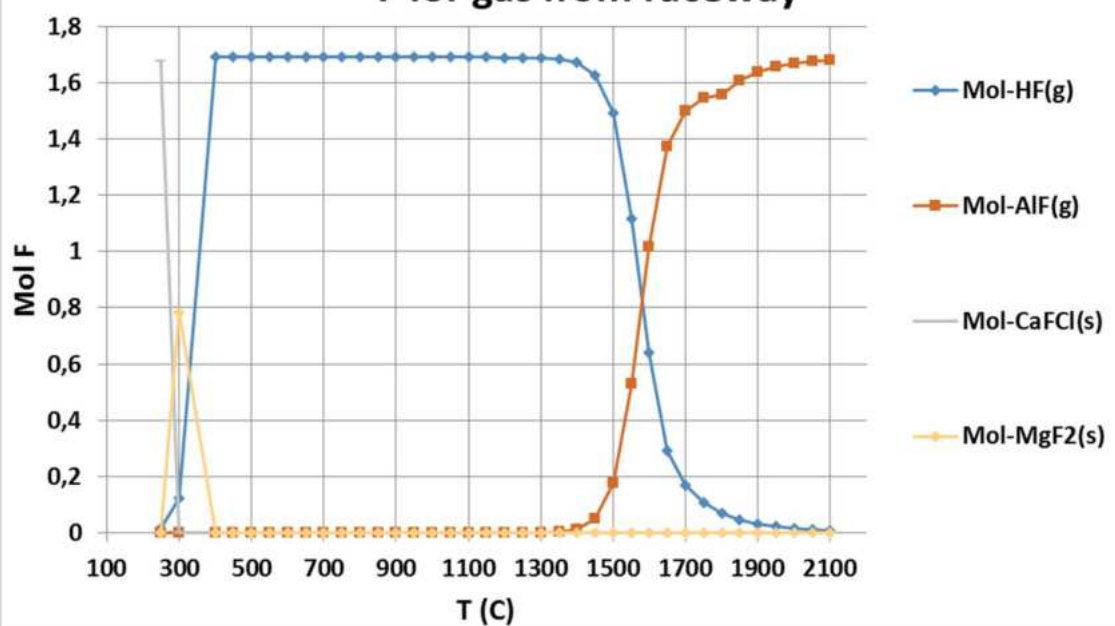
Calculated equilibrium amounts for a gas from raceway cooling down without any interaction with condensed phases. Jump in the plots at 1350°C corresponds to the assumed change in total pressure from 2.6 atm to 2 atm at the assumed cohesive zone. Plots contain compounds formed in unneglectable amount containing K, Na, Cl and F.



### Cl for gas from raceway

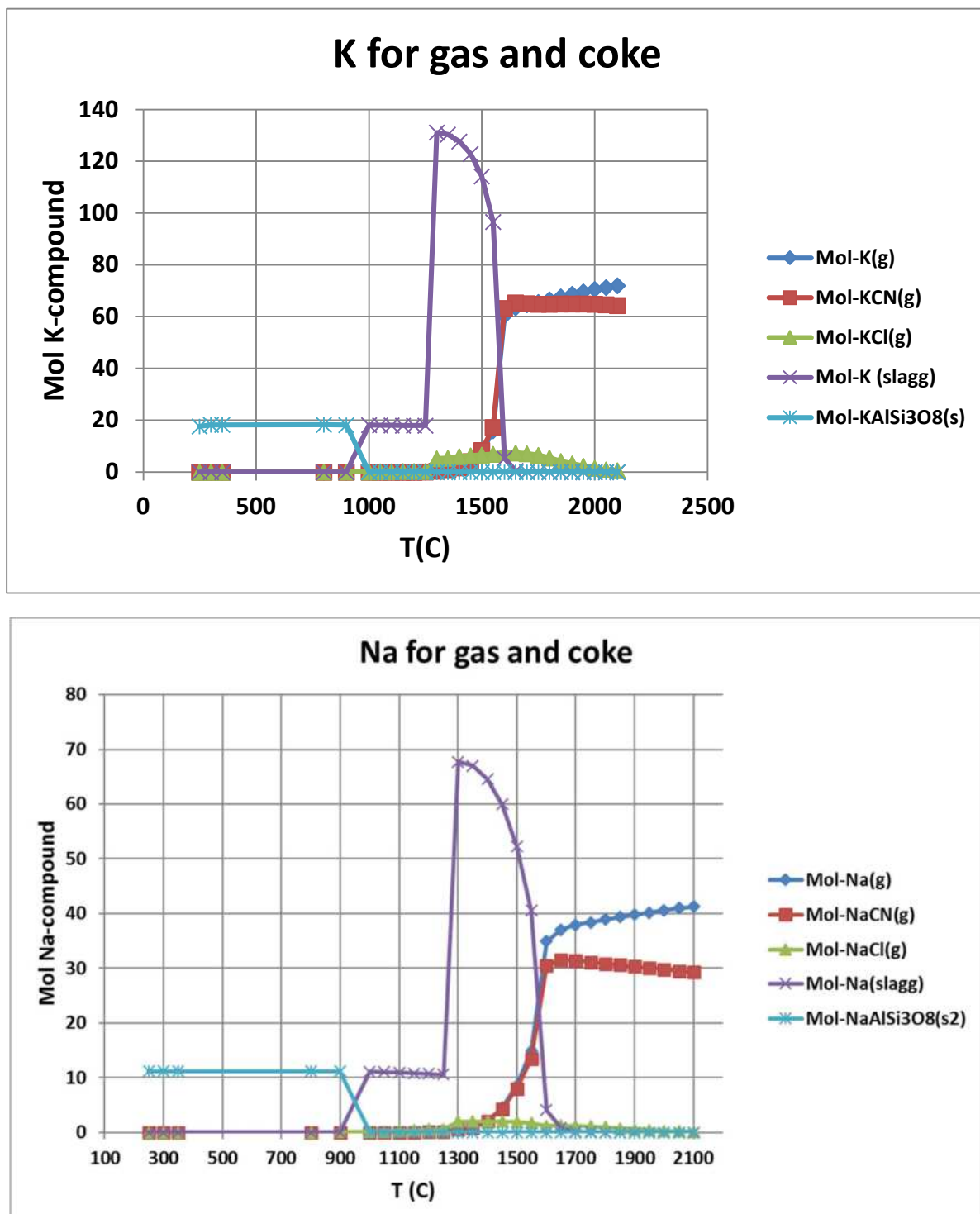


### F for gas from raceway

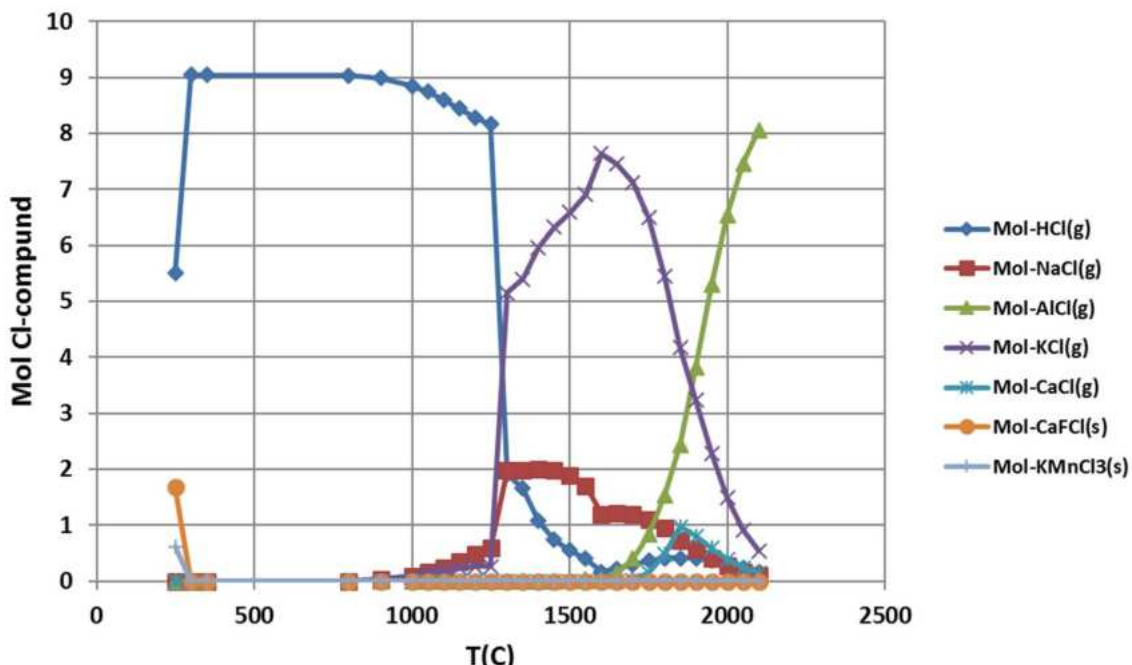


## Appendix 1.2

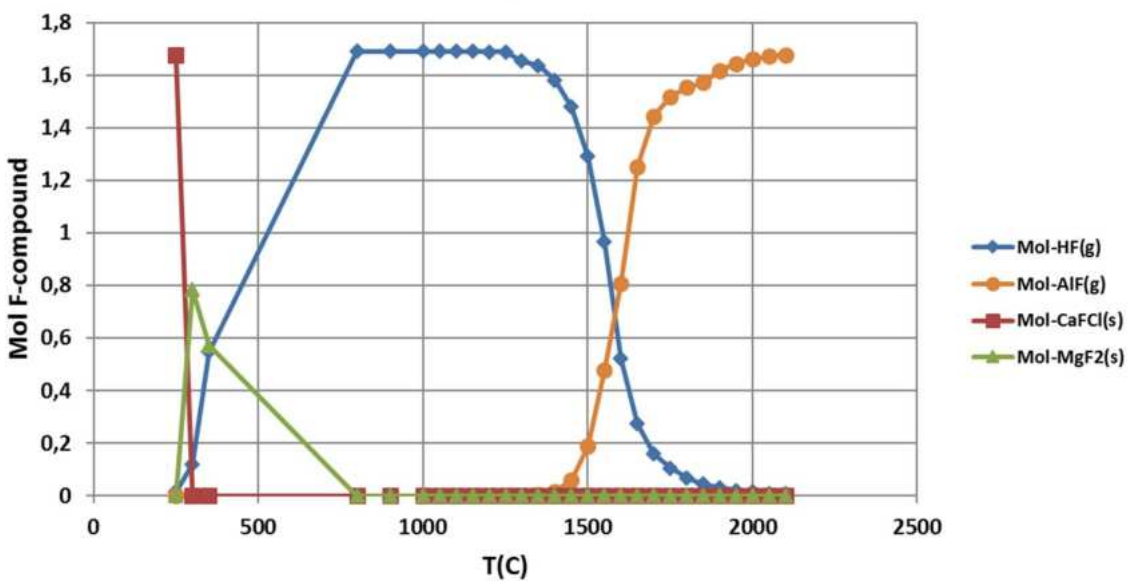
Calculated equilibrium amounts for a gas from raceway cooling down while interacting with coke. At temperatures above 1250°C the coke is enriched in alkaline as described in text whereas at lower temperatures the coke composition is considered as the original one. At 1350°C the total pressure is changed from 2.6 atm to 2 atm at the assumed cohesive zone. Plots contain compounds formed in unneglectable amount containing K, Na, Cl and F.



### Cl from gas and coke

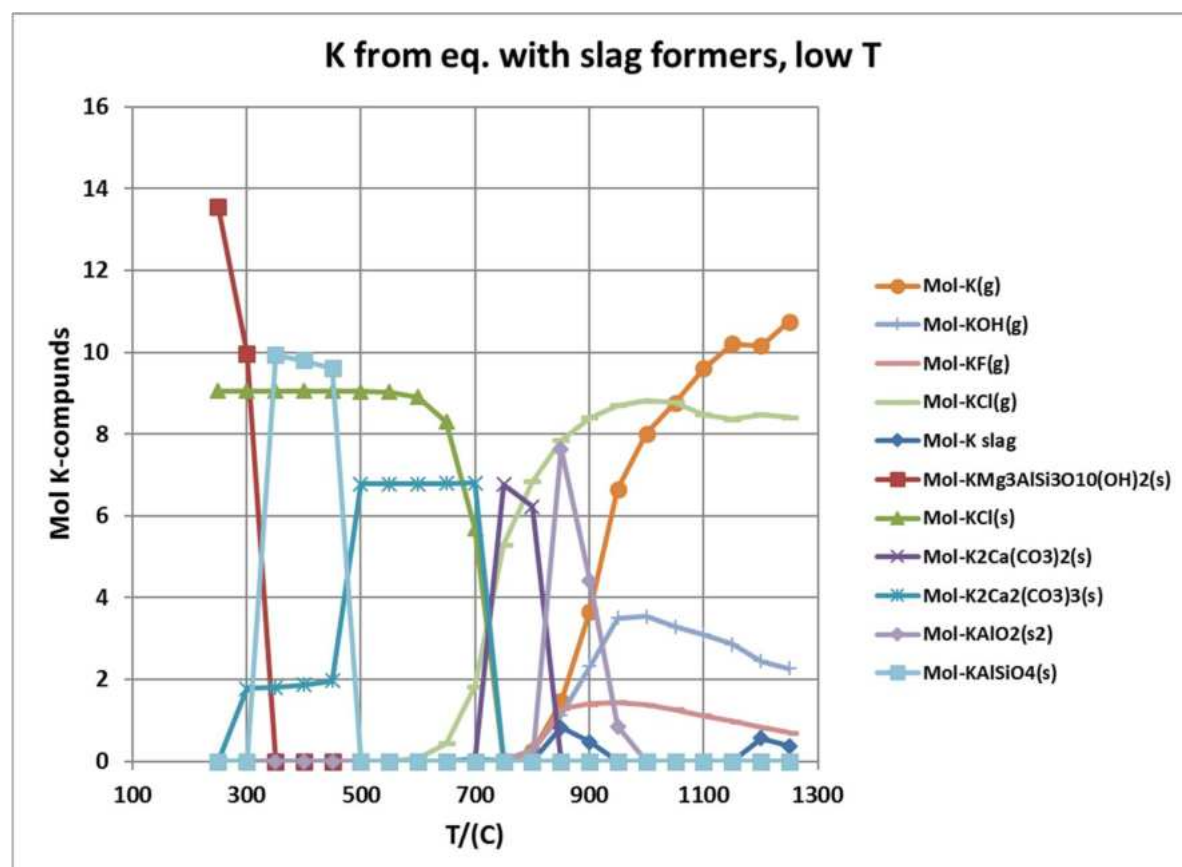
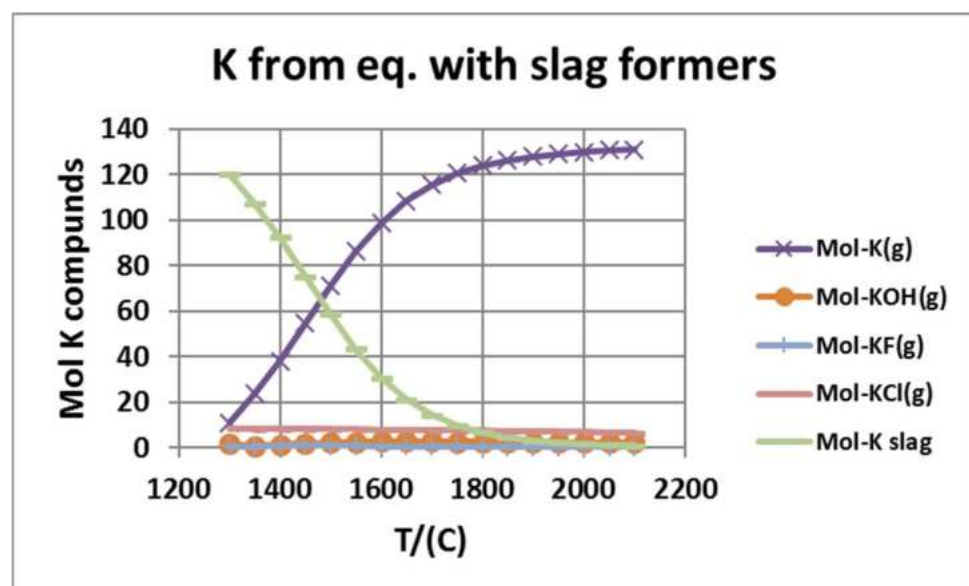


### F from gas and coke

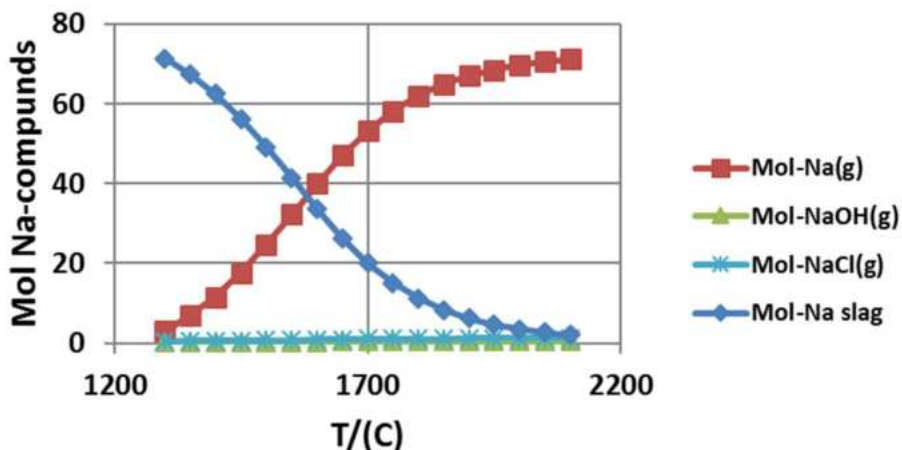


### Appendix 1.3

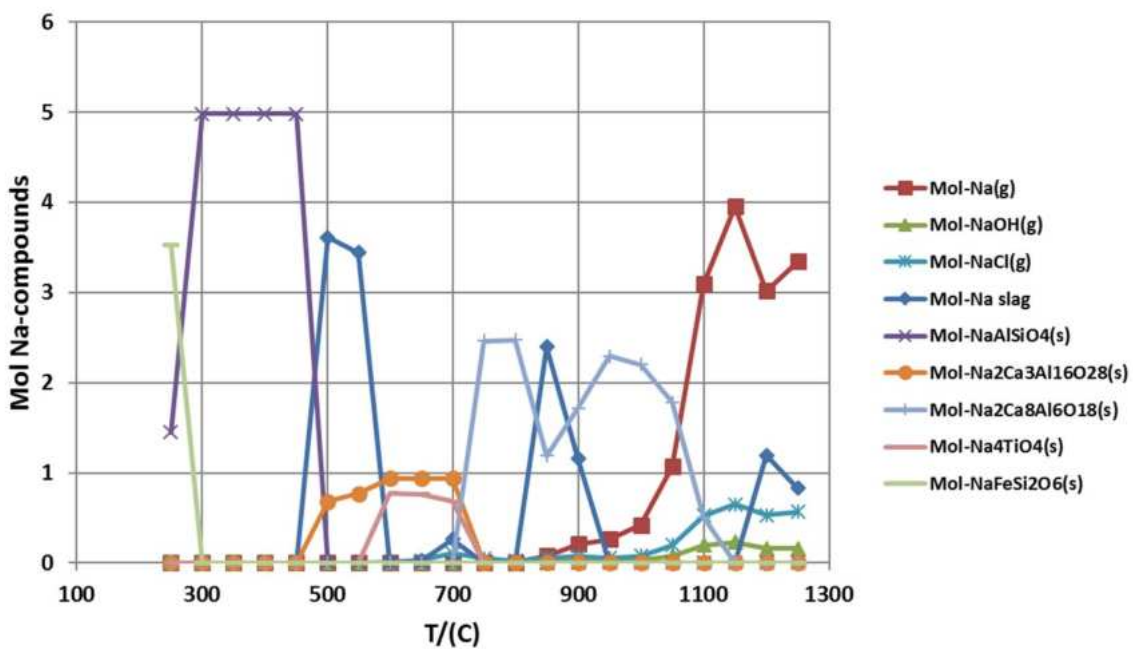
Calculated equilibrium amounts for a gas from raceway cooling down while interacting with slag formers. At 1350°C the total pressure is changed from 2.6 atm to 2 atm at the assumed cohesive zone. Plots contain compounds formed in unnegelectable amount containing K, Na, Cl, F and Zn.

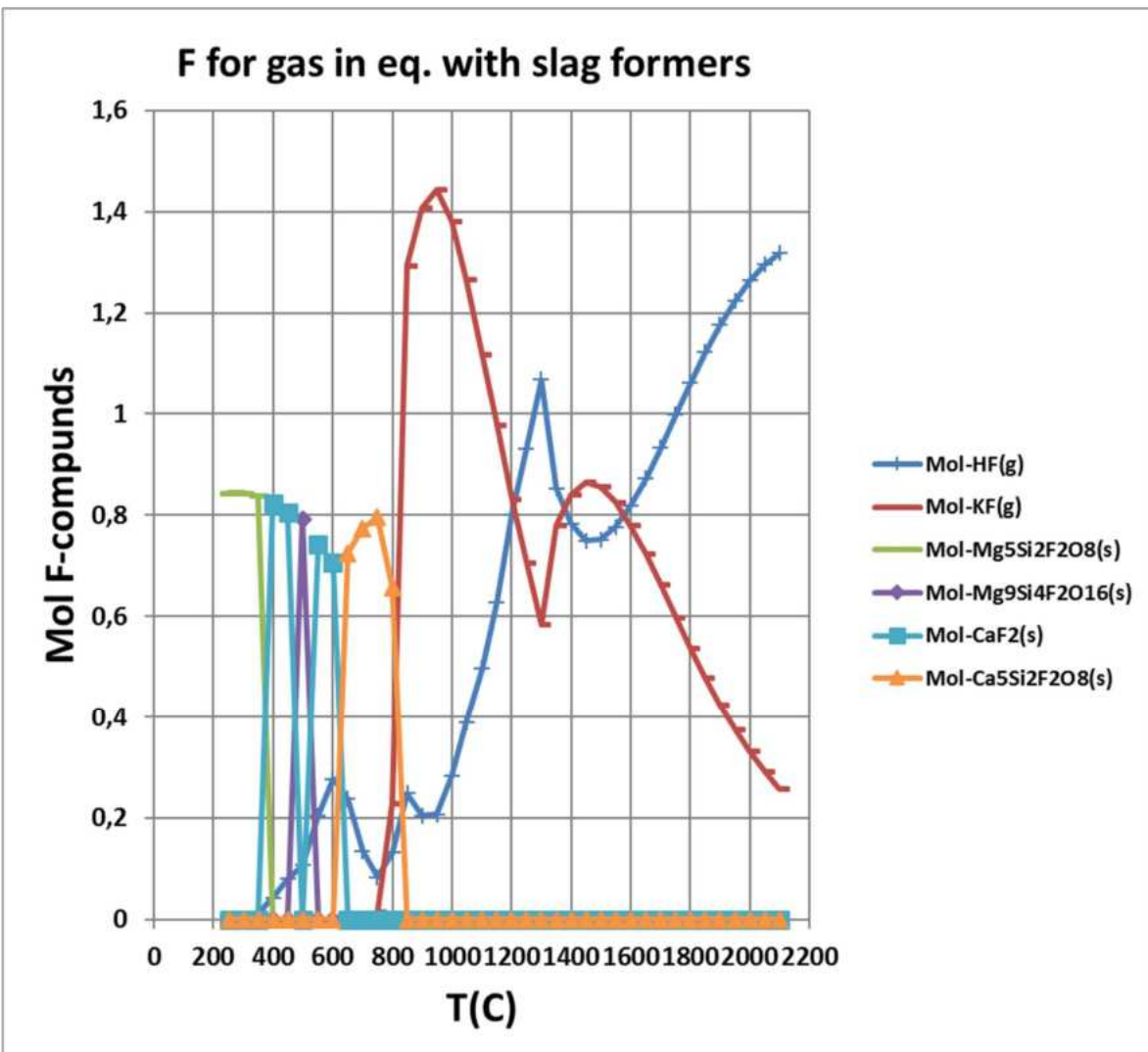
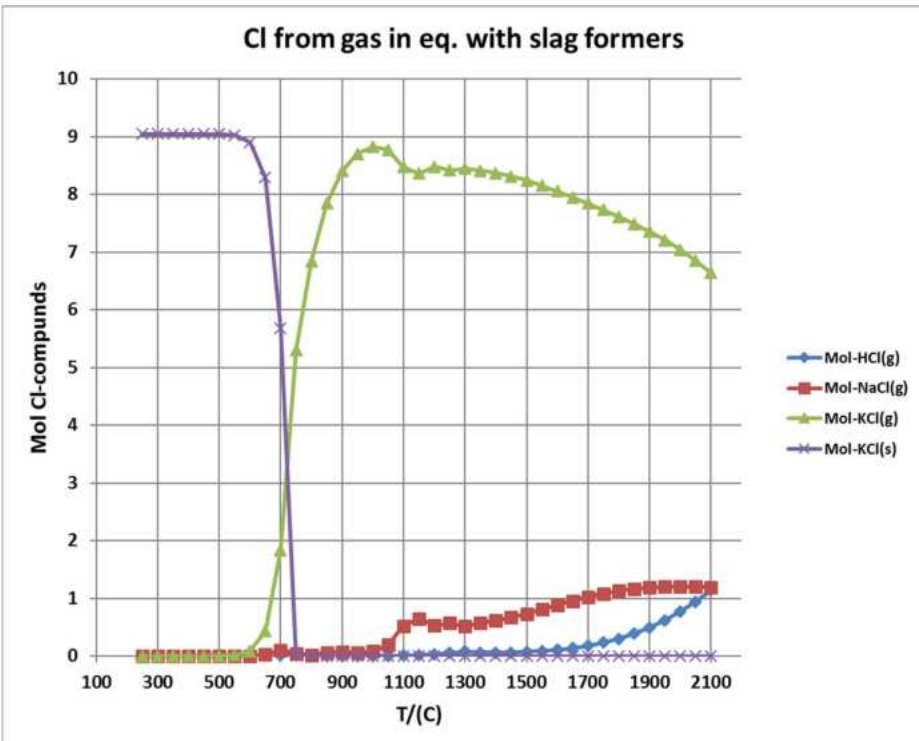


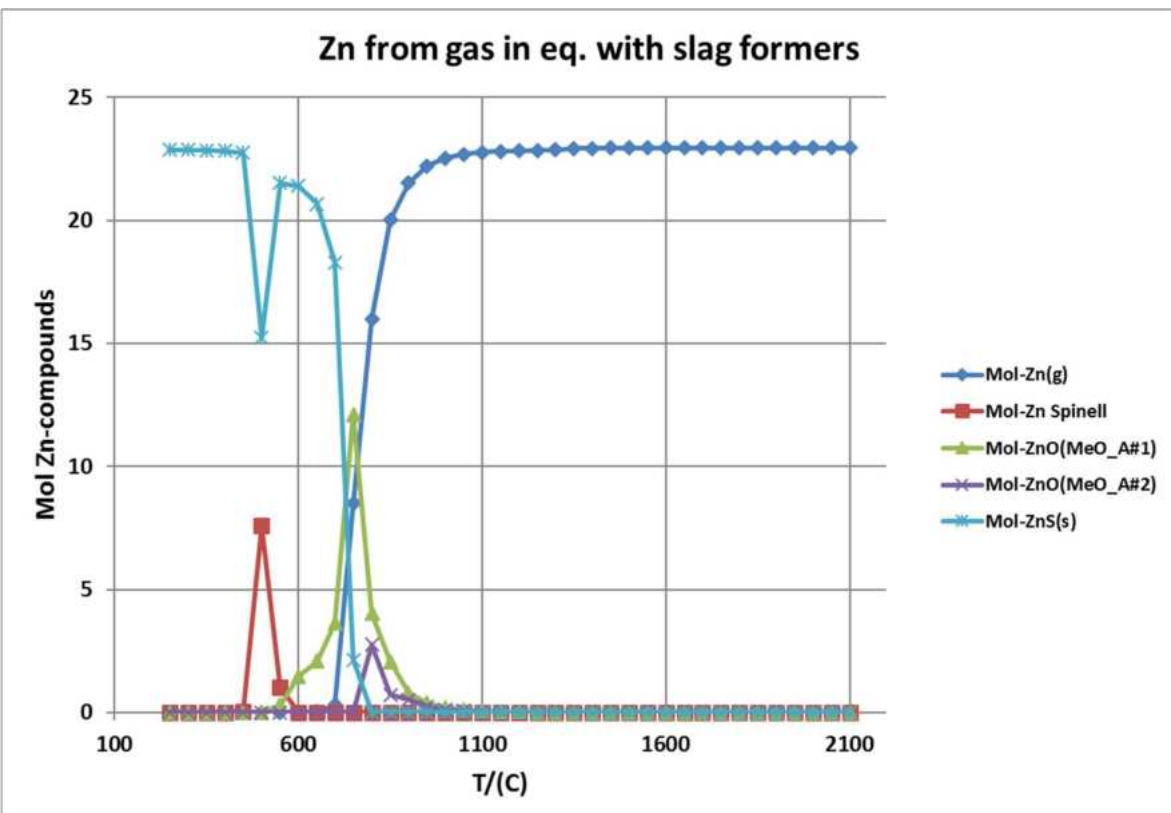
### Na from eq. with slag formers



### Na from eq. with slag formers, low T

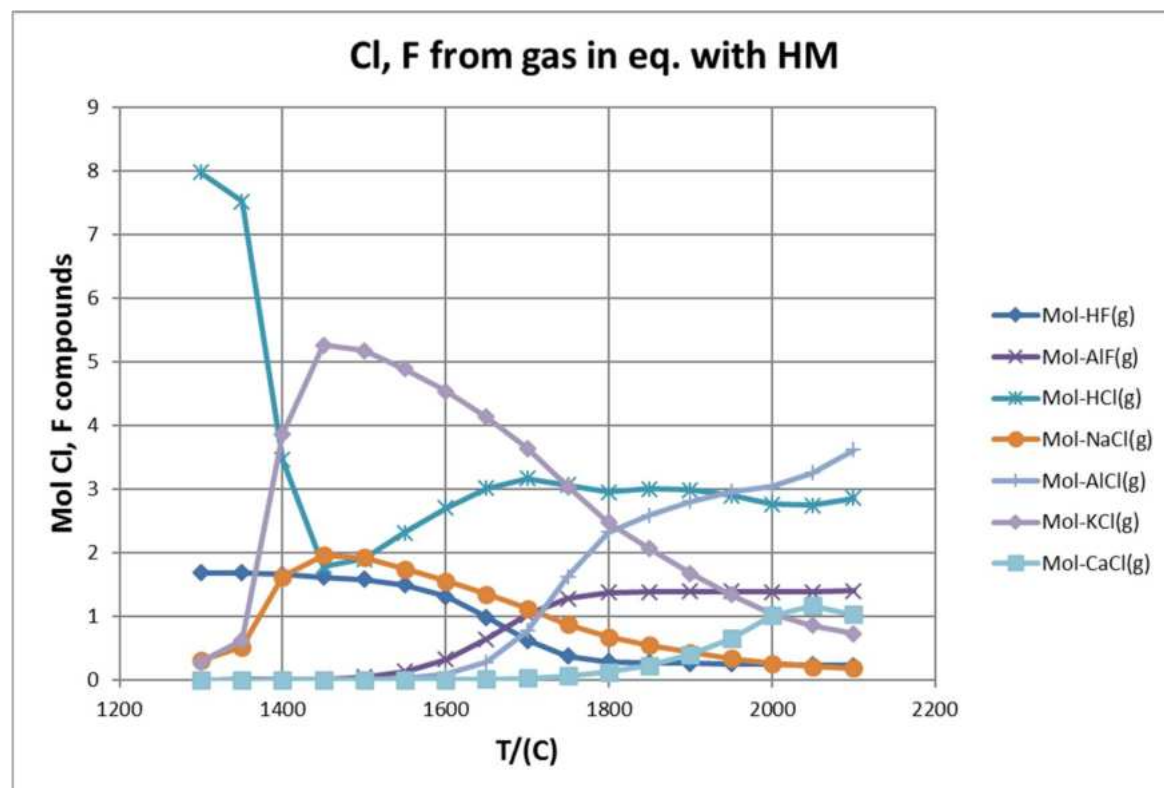
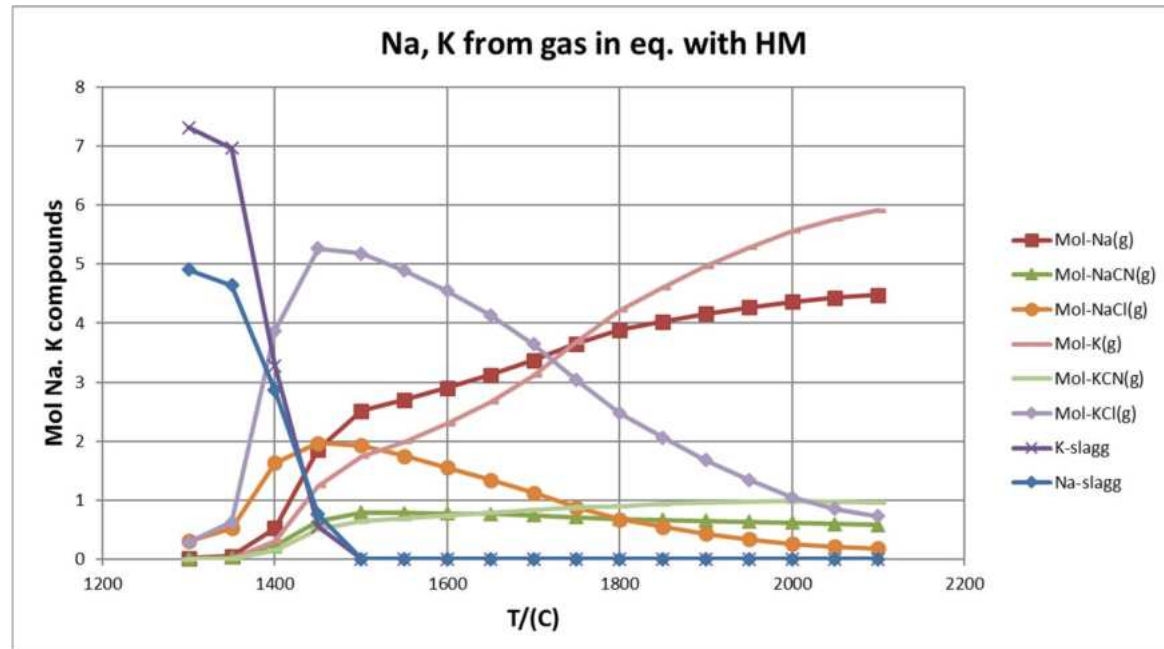






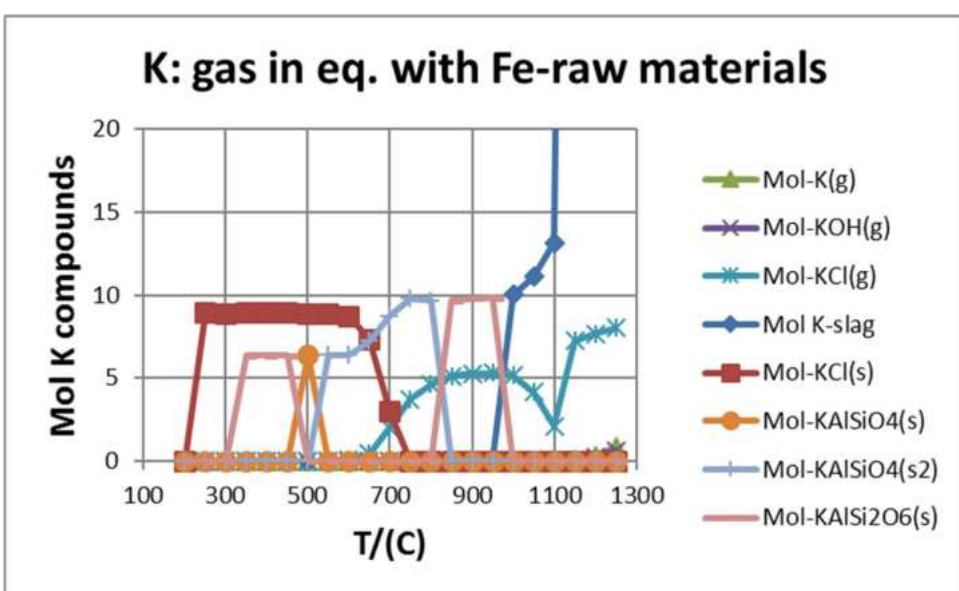
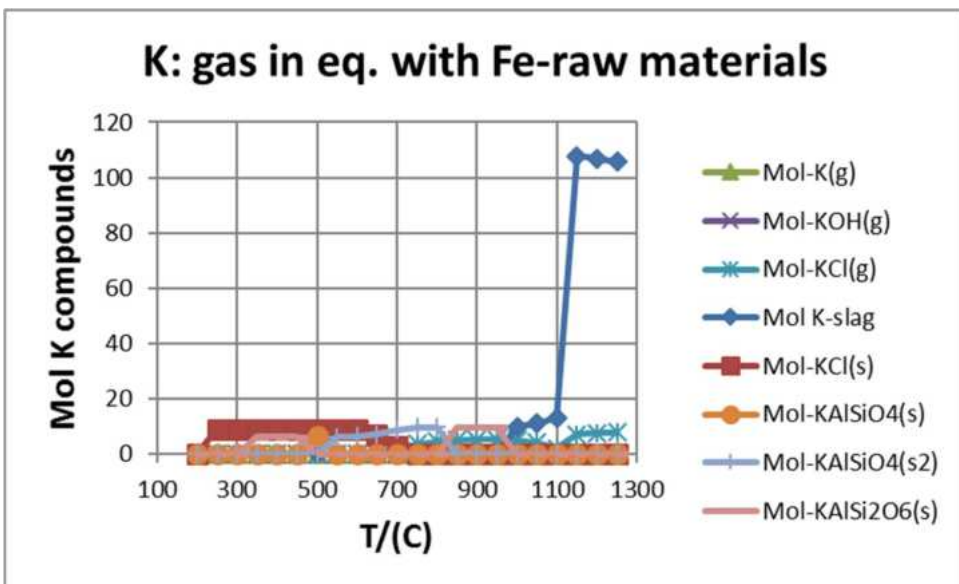
#### Appendix 1.4

Calculated equilibrium amounts for a gas from raceway cooling down while interacting with hot metal. At 1350°C the total pressure is changed from 2.6 atm to 2 atm at the assumed cohesive zone. Plots contain compounds formed in unneglectable amount containing K, Na, Cl, F and Zn.

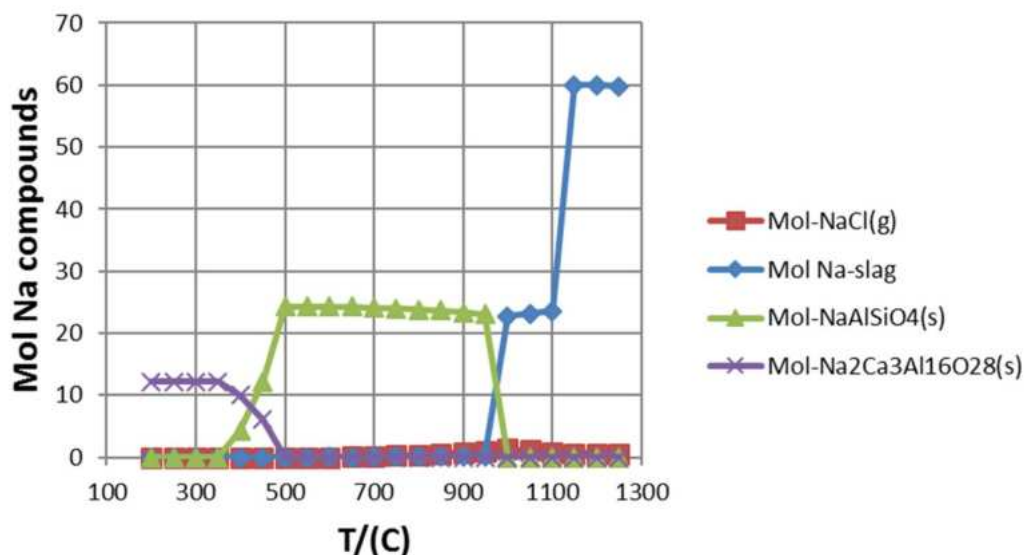


## Appendix 1.5

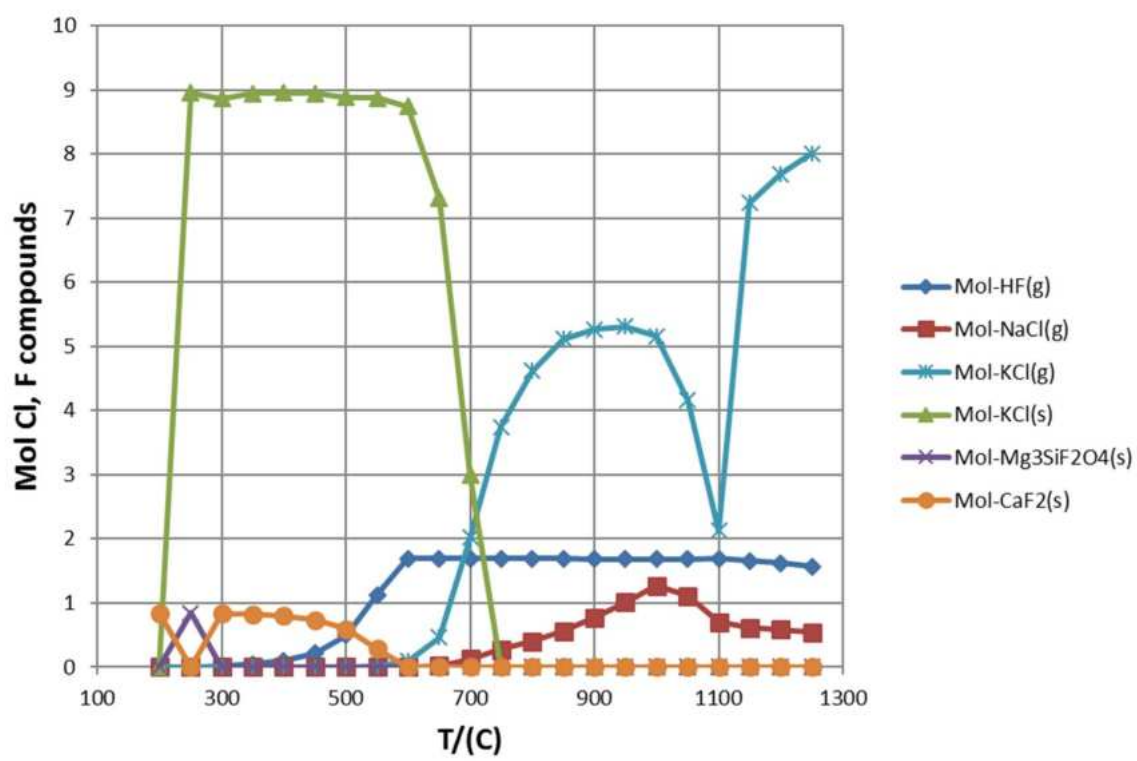
Calculated equilibrium amounts for a gas from raceway cooling down while interacting with iron oxide bearing material. From 1200°C and below, no accumulation of alkalis is assumed in the charged solid materials. Plots contain compounds formed in unneglectable amount containing K, Na, Cl, F and Zn.



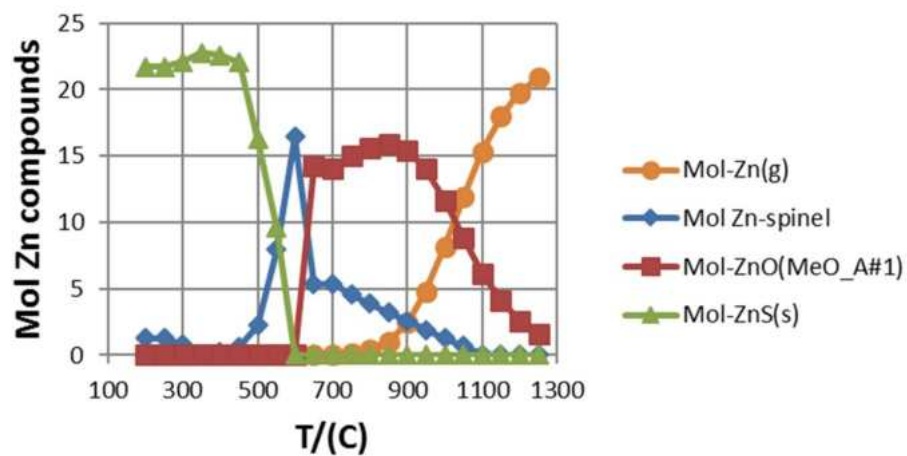
### Na: gas in eq. with Fe-raw materials



### Cl, F: gas in eq. with Fe-raw materials



## Zn: gas in eq. with Fe-raw materials



***Appendix A (SWERIM)***

**Table A1** Reaction and reaction enthalpies for calculations on energy consumption of alkali cycle in Task 1.1.

Nr	Reaction	Temp products	Fraction	n K	Temp reactants	delta H, J	delta G, J	location
1)	K2O + C --> 2K(g) + CO (g)	1650	3/4 of circ.load	288.5	1650	47725166.6	-39734990	Hearth
3)	K2SiO3 + 3C --> 2K + Si (HM) + 3CO (g)	1650	1/4 of circ.load	96.2	1650	65114669.5	-158156.5	Hearth
5)	K (g) + 0.5N2 + C --> KCN (g)	2100	1/2 of circ.load	192.3	1650	-30914796.5	-8.06E+03	Raceway
6a)	K(g) --> K(g)	1200	3/8 of circ.load	144.0	1650	-1350481.5	12722506.2	Cohesive zone
6)	2K (g,l) + CO (g)--> K2O (l) + C(s)	1200	3/8 of circ.load	144.0	1200	-25614171.9	9411906.1	Cohesive zone
7a)	KCN (g) --> KCN (g,l)	1200	3/8 of circ.load	144.0	2100	-31097462.9	41366655.3	Cohesive zone
7)	2KCN (g,l) + CO(g) --> K2O (l) + N2 (g) + 3C	1200	3/8 of circ.load	144.0	1200	-1071847.1	14300896.8	Cohesive zone
					<b>Total</b>	<b>22.8</b>		
8a)	K (g) --> K(g)	950	1/8 of circ.load	48	1650	-699937.6	6539545.1	Lumpy zone
8)	2K(g) + CO2 (g) + SiO2 (l) --> K2SiO3 (s,l) + CO	950	1/8 of circ.load	48	950	-12564697.9	-6689170.1	Lumpy zone
9a)	KCN (g) --> KCN (l)	950	1/8 of circ.load	48	2100	-11269565	16763224.3	Lumpy zone
9)	2KCN (g,l) + 3CO2 (g) + SiO2 (l) --> K2SiO3 (s) + N2 + 5CO	950	1/8 of circ.load	48	950	3864396.9	-6010551.1	Lumpy zone
10)	K2SiO3 --> k2SiO3	1650	1/4 of circ.load	96	950	12681018.3	-27062219	Hearth
11)	K2O (l) --> K2O(l)	1650	3/4 of circ.load	288	1200	13867200.1	-37056144.9	Hearth
					Totalt	28.7	MJ/trj (15 kg/tHM K)	
						8.0	kWh/trj	

**Excluding**

**8a-9a**

**53.2**

MJ/trj (15 kg/tHM K)

**Table A2** Variable list and statistics of EBF variables for Multivariate analysis

<b>Variable</b>	<b>Unit</b>	<b>Mean</b>	<b>STD</b>
Blast flow	Nm <sup>3</sup> /h	1546.9	31.7
Blast temperature	°C	1198.8	9.0
Mv toppgas-temp	°C	156.2	46.3
Heat loss tuyeres	kW	94.8	7.2
Heat loss double shell	kW	40.7	8.8
Tot heat losses by water cooling	kW	172.0	12.8
Heat loss from shell	kW	72.8	1.6
Eta CO	-	47.5	2.4
Direct reduction degree	-	34.6	3.0
Carbon solution loss per kg HM	kgC/tHM	109.2	9.6
CO in top gas	%	23.9	1.0
CO <sub>2</sub> in top gas	%	21.8	1.2
H <sub>2</sub> in top gas	%	3.7	0.2
Mv lower skinflow	°C	876.5	41.7
Mv upper skinflow	°C	785.6	30.8
MS_NH <sub>3</sub>	ppm	9.9	2.5
MS_H <sub>2</sub> O	ppm	12.8	4.6
Raceway alkali	-	8631.6	7385.3
Raceway temp	°C	1885.8	106.8
Skin-flow temp refr 30° 16.80m	°C	859.6	50.5
Skin-flow temp refr 90° 16.80m	°C	893.9	46.4
Skin-flow temp refr 150° 16.80m	°C	904.7	38.5
Skin-flow temp refr 210° 16.80m	°C	889.8	46.0
Skin-flow temp refr 270° 16.80m	°C	881.8	56.4
Skin-flow temp refr 330° 16.80m	°C	846.0	41.0
Skin-flow temp refr 30° 17.41m	°C	760.0	37.7
Skin-flow temp refr 90° 17.41m	°C	812.2	39.9
Skin-flow temp refr 150° 17.41m	°C	822.4	39.2
Skin-flow temp refr 210° 17.41m	°C	799.6	38.5
Skin-flow temp refr 270° 17.41m	°C	792.7	49.7
Skin-flow temp refr 330° 17.41m	°C	751.5	66.2
RAFT	°C	2239.0	43.4
SI_Fe	%	0.6	0.8
SI_CaO	%	29.7	2.0
SI_SiO <sub>2</sub>	%	33.5	3.1
SI_MnO	%	0.2	0.1
SI_S	%	1.3	0.2
SI_Al <sub>2</sub> O <sub>3</sub>	%	14.4	0.9
SI_MgO	%	14.5	0.9
SI_Na <sub>2</sub> O	%	0.5	0.1
SI_K <sub>2</sub> O	%	0.7	0.2
SI_V <sub>2</sub> O <sub>5</sub>	%	0.1	0.1
SI_TiO <sub>2</sub>	%	1.3	0.8
SI_Bas	%	0.9	0.1
SI_P <sub>2</sub> O <sub>5</sub>	%	0.008	0.004
Ox degree		1.0	0.0
HM_C	%	4.3	0.2
HM_Si	%	1.5	0.3
HM_Mn	%	0.2	0.0
HM_P	%	0.03	0.00
HM_S	%	0.05	0.03
HM_Ni	%	0.03	0.001
HM_V	%	0.3	0.02
HM_Ti	%	0.2	0.05
HM_Cr	%	0.0	0.001
HM_Cu	%	0.0	0.001
burden level	cm	67.8	3.3

**Table A3** Variable list and statistics for Multivariate Analysis of SSAB data in Task 1.2.

<b>Variable</b>	<b>Explanation</b>	<b>Unit</b>	<b>Mean</b>	<b>STD</b>
O2_PCT_AV_BLASTER	O2 enrichment of blast	%	3.7	0.003
PCT_H2_I_TOOPPGAS	H2 in top gas	%	3.0	0.14
BLASTERFLODE_KNM3PH	Blast flow	kNm3/h	117.8	1.35
eta_CO	etaCO	-	54.9	1.07
SYRGASMANGD	Sum of blast and lance addition of O2	kNm3/h	4.3	0.05
BLASTERFUKT_GPNM3	Blast moisture	g/Nm3	12.6	4.70
FLAMTEMPERATUR_C	Flame temp.	°C	2177.2	32.6
BLASTERTEMPERATUR_C	Blast temp.	°C	1024.1	20.3
SYRGAS_VIA_BLASTER_KNM3PH	Oxygen through blast	kNm3/h	1.7	0.07
SYRGAS_VIA_LANS_KNM3PH	Oxygen through lance	kNm3/h	2.6	0.06
TOPPGASTEMP_C	Top gas temp.	°C	97.3	23.7
PCT_CO_I_TOOPPGAS	CO in top gas	%	20.8	0.41
PCT_CO2_I_TOOPPGAS	CO2 in top gas	%	25.1	0.50
SOND_MEDEL_DM	Burden level	dm	-27.3	262.2
ETA_CO_2	etaCO2	-	54.7	0.92
TOPPTRYCK_MBAR	Gauge pressure top	mbar	80.2	2.38
KYLEFFEKT_TOT	Total cooling effect	MJ/h	31196.8	2428.8
NH3 [ppm]	Top gas content	ppm	7.6	4.66
H2O [ppm]	Top gas content	ppm	26346.6	8157.6
H2S [ppm]	Top gas content	ppm	5.1	1.07
C2H4 [ppm]	Top gas content	ppm	2737.1	329.8
CH4 [ppm]	Top gas content	ppm	33.9	4.71
C3H6 [ppm]	Top gas content	ppm	26718.5	6082.1
Bensen [ppm]	Top gas content	ppm	9263.3	1342.7
O2 [%]	Top gas content	%	0.1	0.03
SO2 [ppm]	Top gas content	ppm	0.1	0.10
SO3 [ppm]	Top gas content	ppm	571.5	244.2
HCN [ppm]	Top gas content	ppm	21.2	1.35
Alkali Raceway	Alkali raceway	-	0.1	0.05

**Table A4** Chemical analyses of green coke, after trials for alkali uptake and after reactivity tests in task 2.1. PUP=potassium uptake, R=reactivity tests.

Coke type	Fe	CaO	SiO2	MnO	P2O5	S	Al2O3	MgO	Na2O	K2O	TiO2	V2O5	Sum
RC_DMT	0.50	0.07	6.43	0.09	0.03	0.71	3.05	0.06	0.05	0.14	0.18	0.00	11.33
RC_DMT_PUP	0.40	0.04	6.40	0.08	0.03	0.71	3.09	0.07	0.05	2.06	0.15	0.00	13.08
RC_DMT_PUP+R	0.25	0.00	8.78	0.06	0.03	0.69	4.32	0.13	0.08	2.60	0.16	0.00	17.10
RC_DMT_R	0.32	0.00	7.53	0.15	0.04	0.76	3.59	0.10	0.07	0.26	0.20	0.00	13.02
RC_LTU	0.43	0.09	6.00	0.03	0.05	0.72	3.09	0.06	0.05	0.17	0.18	0.00	10.88
RC_LTU_PUP	0.28	0.02	5.90	0.01	0.04	0.68	2.92	0.06	0.05	2.06	0.15	0.00	12.18
RC_LTU_PUP+R	0.22	0.03	7.19	0.35	0.06	0.71	3.78	0.11	0.07	2.36	0.16	0.00	15.04
TC_2%DMT	0.32	0.00	7.85	0.03	0.03	0.68	4.03	0.08	0.06	0.21	0.17	0.00	13.46
TC_2%DMT_PUP	0.24	0.00	7.33	0.02	0.02	0.64	3.57	0.07	0.05	2.02	0.13	0.00	14.10
TC_2%DMT_PUP+R	0.23	0.00	9.62	0.04	0.03	0.65	5.16	0.14	0.08	2.62	0.15	0.00	18.73
TC_4%LTU	0.51	0.04	8.23	0.05	0.05	0.61	4.56	0.11	0.06	0.29	0.16	0.00	14.67
TC_4%LTU_PUP	0.24	0.00	7.87	0.01	0.04	0.62	4.50	0.10	0.06	1.91	0.13	0.00	15.48
TC_4%LTU_PUP+R	0.28	0.03	10.73	0.03	0.06	0.62	6.19	0.20	0.10	2.13	0.16	0.00	20.53
TC_8%LTU	0.36	0.01	9.37	0.02	0.05	0.54	5.71	0.14	0.06	0.30	0.13	0.00	16.69
TC_8%LTU_PUP	0.22	0.00	8.54	0.01	0.04	0.49	5.20	0.12	0.05	2.24	0.11	0.00	17.01
TC_8%LTU_PUP+R	0.19	0.00	10.88	0.02	0.05	0.53	6.75	0.19	0.08	2.63	0.11	0.00	21.44
TC_8%LTU_R	0.34	0.01	11.06	0.04	0.06	0.60	6.86	0.23	0.08	0.36	0.14	0.00	19.79
TC_coatedDMT	0.24	0.00	11.32	0.02	0.04	0.34	6.66	0.17	0.06	0.32	0.11	0.00	19.27
TC_coatedDMT_PUP	0.20	0.00	11.77	0.01	0.04	0.37	7.39	0.21	0.08	1.87	0.10	0.00	22.02
TC_coatedDMT_PUP+R	0.22	0.17	13.1	0.03	0.04	0.38	7.95	0.55	0.09	1.98	0.11	0	24.60

**Table A5** Reaction rates and carbon conversions for reactivity tests in Task 2.1.

Coke type	Reaction rate ( $\mu\text{ka}$ )			Carbon conversion (%)		
	950-1000	1050-1100	1130	950-1000	1050-1100	1130
RC_DMT	2.158	8.707	11.386	-0.45%	1.09%	4.63%
RC_DMT_PUP	8.600	17.142	18.646	1.25%	5.39%	11.59%
TC_2%DMT_PUP	8.356663305	15.38687494	18.4424689	0.013132	5.15%	13.48%
RC_LTU_PUP	none	none	16.648	none	none	9.87%
TC_4%LTU_PUP	7.591	13.669	16.435	0.85%	4.34%	10.93%
TC_8%LTU	1.646	8.104	11.505	0.13%	1.46%	9.28%
TC_8%LTU_PUP	none	none	16.420	none	none	10.07%
TC_coated_DMT_PUP	3.705	12.089	13.179	0.32%	2.92%	7.21%

**Table A6** Calculated graphitization degrees in Task 2.1

Coke types	Mean Lc-	FWHM - Lc-	Gaussian Lc-	Temperature	SiO <sub>2</sub>	Al <sub>2</sub> O <sub>3</sub>	Alkali
	Value	Value	Value	[°C]	[wt%]	[wt%]	[wt%]
<b>2% kaolin DMT (PUP)</b>	26.0	23.6	27.7	1227	7.33	3.57	2.07
<b>4% kaolin LTU (PUP)</b>	24.8	22.6	26.6	1190	7.87	4.50	1.96
<b>8% kaolin LTU (PUP)</b>	26.9	23.6	26.7	1251	8.54	5.20	2.29
<b>Coated (PUP)</b>	29.9	27.7	30.5	1324	11.77	7.39	1.94
<b>Ref. DMT (PUP)</b>	25.4	23.3	27.7	1210	6.40	3.09	2.11
<b>Ref. LTU (PUP)</b>	24.0	21.9	26.8	1166	5.90	2.92	2.11
<b>2% kaolin DMT (PUP+R)</b>	26.8	24.2	29.1	1249	9.62	5.16	2.70
<b>4% kaolin LTU (PUP+R)</b>	25.4	23.3	27.2	1210	10.73	6.19	2.23
<b>8% kaolin LTU (PUP+R)</b>	26.4	23.8	27.0	1239	10.88	6.75	2.71
<b>Coated (PUP+R)</b>	29.4	27.9	32.1	1312	13.08	7.95	2.07
<b>Ref DMT (PUP+R)</b>	25.4	23.4	28.2	1210	8.78	4.32	2.69
<b>Ref LTU (PUP+R)</b>	25.5	23.4	27.8	1214	7.19	3.78	2.43
<b>2% kaolin DMT</b>	19.0	16.5	20.8	938	7.85	4.03	0.27
<b>4% kaolin LTU</b>	18.7	16.5	20.6	916	8.23	4.56	0.35
<b>8% kaolin LTU</b>	19.9	17.5	21.3	988	9.37	5.71	0.36
<b>Coated</b>	22.2	21.2	22.5	1100	11.32	6.66	0.37
<b>Ref DMT</b>	17.9	16.2	20.7	860	6.43	3.05	0.20
<b>Ref LTU</b>	18.8	16.6	21.0	921	6.00	3.09	0.22

**Technical Annex I**

**FORMS B2**

Research & Innovation  
Research Fund for Coal and Steel

Annex I

**TECHNICAL ANNEX**

<b>Project acronym:</b>	AlCirc
<b>Project title:</b>	Assessing and control of alkaline circulation in BF operation
<b>Grant Agreement N°:</b>	RFSR-6-2016-00002.

**B2-1 PROJECT OBJECTIVES**

The overall research project objective is improved blast furnace (BF) process stability and energy efficiency with increasing flexibility in raw material selection, taking into account deteriorating raw material qualities in terms of alkali content.

This is achieved by developing and establishing new methods for online alkali control in the BF, based on a novel *online top gas evaluation tool* for determination of the alkali accumulation in the operational blast furnace. This tool consists of the *top gas measurement equipment* (FTIR or MS) and the *evaluation routine* for determination of the alkali accumulation / cycle.

The new online tool will be applied for monitoring of the alkali cycle amount at selected representative BF's with elevated alkali input and with differences in the source of alkali components. The selected BF's differ in operational modes. Monitoring of the alkali cycle amount enables the premature detection of operational states with elevated alkali load. In this way, countermeasures for alkali control may be triggered at an early stage in order to prevent operational disturbances at the BF.

For BF alkali control some promising novel measures are developed within the research project, like coke pre-treatment/coating with alkali absorbing minerals as well as a more optimised adjustment of BF slag composition.

Finally, concepts will be worked out for improved BF alkali control by combined application of the online top gas evaluation tool with selected methods for inhibition of the alkali circulation. The concepts will consider the special restraints at the different operational BF's. Finally the concepts will be validated by operational trials at the different BF's in comparison with normal operational data.

**FORMS B2**

**B2-2 WORK PACKAGE DESCRIPTION**

<b>WP No</b>	<b>1</b>
--------------	----------

<b>Work package Title</b>	Characterization of alkali re-circulation in the BF	<b>Number of man hours</b>
<b>WP Leader</b> (full name & acronym)	VASD	
<b>Beneficiary (s)</b> (full name & acronym)	VDEH-BETRIEBSFORSCHUNGSIINSTITUT GMBH (BFI)	910
	SWEREA MEFOS AB (MEFOS)	3104
	VOESTALPINE STAHL DONAWITZ GMBH (VASD)	950
	ISD DUNAFERR DUNAI VASMU ZARTKORUEN MUKODO RESZVENYTARSASAG (Dunafer)	2250
	SSAB EMEA AB (SSAB)	130
	LUOSSAVAARA-KIIRUNAVAARA AB (LKAB)	720
	LULEA TEKNiska UNIVERSitet (LTU)	340
<b>Total</b>		<b>8404</b>

**1 – Objectives**

*(Objectives clearly stated in a concise manner using bullet points (½ page)).*

- Definition of reference state concerning alkali behaviour / balance in different industrial BF and one Experimental BF and their correlation to operational parameters of the BF
- Performance of continuous NH<sub>3</sub> concentration measurements at the BF top gas during different defined normal operational conditions. NH<sub>3</sub> is an indicator for the amount of the BF alkali cycle
- Estimation of alkali circulation and alkali load on coke during normal BF operation
- Definition of reference state concerning alkali impact on BF burden materials like coke, fluxes and ferrous materials (with special emphasis on the different input materials and operational conditions at the compared BF's)

30/2/14

## FORMS B2

### 2 - Work programme and distribution of tasks with indication of participating beneficiaries

(Specify the beneficiary's responsibilities within each task).

#### 1.1 Alkali behaviour / balance in different industrial BF (BFI, Dunafer, LKAB, MEFOS, SSAB, VASD)

- Determination of BF process data and alkali balance during normal operation at Dunafer, SSAB, VASD and LKAB (Experimental BF)
- Determination of correlation between operational parameters and alkali balance at Dunafer, SSAB, VASD and LKAB (Experimental BF)
  - Thermodynamic calculations for identification of mechanisms concerning enrichment/depletion of alkalis depending on BF process parameters (BFI) based on operational set-ups and burden materials. LTU will study the mechanisms of alkali circulation through thermodynamic (FACTSAGE) modelling with emphasis on conditions and chemistry in the Swedish blast furnaces (SSAB), including LKAB's Experimental BF.
  - Impact of alkali balance on energy consumption - analysed in heat an mass balance calculation using operational data from the BFs (BFI, MEFOS, LKAB, SSAB)

#### 1.2 New on-line measurements (BFI, Dunafer, LKAB, MEFOS, SSAB, VASD).

- NH<sub>3</sub> analysis of BF top gas via FTIR Spectrometer. This analysis is an approach to quantify the BF alkali cycle (BFI, Dunafer, VASD).
  - An FTIR spectrometer will be installed at the top gas pipe the operational blast furnaces (BF) of:
    - Dunafer -> Installation and measurement by Dunafer
    - VASD -> Installation and measurement by BFI
  - BFI and Dunafer will perform continuous NH<sub>3</sub> concentration measurements at the BF top gas during different defined normal operational conditions
- NH<sub>3</sub> analysis of BF top gas via mass spectrometer. This analysis is an approach to quantify the BF alkali cycle (MEFOS, LKAB, SSAB).
  - MEFOS will install a mass spectrometer at the operational blast furnaces at SSAB and the LKAB Experimental BF for performance of continuous NH<sub>3</sub> concentration measurements at the BF top gas during different defined normal operational conditions
- Vertical/horizontal analysis of in-furnace gas collected at
  - Upper and lower shaft probe in the LKAB Experimental BF (LKAB, MEFOS)
  - Trough vertical probe in the LKAB Experimental BF allowing descending with the burden (LKAB, MEFOS)
- Alkali emission in raceway guided with an optical fibre and analyses with spectrometer using Plank's radiation law in the LKAB Experimental BF and in one of SSAB industrial BF (MEFOS, LKAB, SSAB)
- Comparison of the feasibility and advantages of each method, FTIR and mass spectrometer measurements. Assessment of suitability for continuous on-line measurements (BFI, MEFOS, LKAB, SSAB)
- Estimation of alkali circulation and alkali load on coke during normal operation at Dunafer, SSAB, VASD and LKAB Experimental BF based on the online-measurements and results of Task 2.1 (BFI, MEFOS)

#### 1.3: Alkali impact on BF burden materials (BFI, Dunafer, VASD, MEFOS, LKAB, LTU, SSAB)

- Coke attack by alkali components in the BF

## FORMS B2

- Definition of standard coke properties (such as CRI/CSR, ash composition, reactivity etc.) at the different operational BF's (Dunafer, SSAB, VASD)
- Assessment of coke properties exposed to different alkali loads at BF conditions.
  - Thermodynamic calculations are conducted to identify role of coke ash and slag chemistry on alkali impact on coke and draining alkalies (BFI, MEFOS)
  - Preparation of small quantities of test coke (modified alkali load) to be used in laboratory tests or by CRI/CSR (Dunafer)
  - Laboratory furnace trials with 2-zone inductively heated fixed bed reactor (FBR), which is capable for simulation of alkali evaporation (zone 1) and condensation (zone 2) on the coke samples – Application of different alkali loads (BFI)
  - Coke testing procedures: e. g. surface properties, mineral phases, reactivity, CRI/CSR, etc. (BFI, MEFOS). LTU will determine the reactivity for untreated coke samples using a previous used method employing sophisticated TG/DTA/QMS equipment
- Investigation of alkali uptake in fluxes and ferrous materials (coke, fluxes and ferrous material) and impact on their properties are investigated by analyses of collected shaft samples pro-cured in LKAB Experimental BF trough probe samples and after quenching and excavation
  - Analysis of coke samples from the LKAB experimental BF (MEFOS)
  - Analysis of ferrous material samples from the LKAB Experimental BF (LKAB)
  - Analysis of slag formers (fluxes) from the LKAB Experimental BF (MEFOS)
- LTU will model the reactions between alkali containing coke ash, coke minerals and slag using FACTSAGE for conditions and chemistry in the Swedish blast furnaces.

### 3 - Interrelation with other work packages (please give WP No)

(Briefly describe the interrelation with the other WPs).

- **Tasks 1.1 and 1.2** deliver base data for each investigated operational BF concerning the operational data, alkali state and –balance, top gas- and in-furnace gas composition. These base data will be used in **Tasks 2.1, 2.2 and 2.3**.
- **Task 1.3** initially delivers base data concerning input coke properties and alkali uptake in fluxes and ferrous materials at different BF's. Further, **Task 1.3** receives data on the amount of alkali cycle from **Task 2.1**. The alkali loads on coke determined here, are the basis for laboratory furnace trials for testing the alkali attack on coke at simulated BF conditions.

### 4 - Deliverables and milestones

(Define the deliverables and milestones, give the foreseen date of production and assign them to a responsible partner).

- D 1.1 Alkali balance, mass balance and operational data on the investigated industrial operational BF's (Dunafer, SSAB, VASD, MEFOS)
- D 1.2 Determination of correlation between operational parameters and alkali balance during normal operation at the BF's of Dunafer, SSAB and VASD (BFI, Dunafer, LKAB, MEFOS, SSAB, VASD)
- D 1.3 Determination of ammonia concentration in BF top gas at normal operational conditions (BFI, Dunafer, MEFOS, SSAB, VASD, LKAB)
- D 1.4 Determination of in-furnace gas composition at LKAB Experimental BF (MEFOS, LKAB)
- D 1.5 Determination of standard coke properties (e. g. CRI/CSR) for input cokes as well as especially prepared cokes with altered ash composition (Dunafer, SSAB, VASD)

Bo 4/14

**FORMS B2**

D 1.6 Determination of reference state concerning coke alkali attack within the alkali cycle zone (lab trials) - to be compared with standard coke properties (BFI)

D 1.7 Description of alkali distribution for burden materials in the Experimental BF (MEFOS, LKAB)

D 1.8 Results from thermodynamic modelling showing the impact from selected components on alkali gasification (LTU)

## FORMS B2

## B2-2 WORK PACKAGE DESCRIPTION

WP No 2

Work package Title	Methods for alkali control in the BF	Number of man hours
<b>WP Leader</b> (full name & acronym)	BFI	
<b>Beneficiary (s)</b> (full name & acronym)	VDEH-BETRIEBSFORSCHUNGSIINSTITUT GMBH (BFI)	2020
	SWEREA MEFOS AB (MEFOS)	1690
	VOESTALPINE STAHL DONAWITZ GMBH (VASD)	350
	ISD DUNAFERR DUNAI VASMU ZARTKORUEN MUKODO RESZVENYTARSASAG (Dunafer)	900
	SSAB EMEA AB (SSAB)	120
	LUOSSAVAARA-KIIRUNAVAARA AB (LKAB)	360
	LULEA TEKNiska UNIVERSITET (LTU)	2060
<b>Total</b>		<b>7500</b>

**1 – Objectives**

(Objectives clearly stated in a concise manner using bullet points (½ page)).

- Development of calculation /evaluation routine for the online top gas evaluation tool for determination of alkali accumulation in the different compared BF's based on NH<sub>3</sub> reaction efficiencies determined by laboratory trials
- Estimation of alkali accumulation within the BF and subsequently alkali load on coke during normal BF operation
- Development of novel methods for inhibition of BF alkali circulation by coke pre-treatment/coating using alkali absorbing additives or alkali absorbing mineral addition to the burden
- Investigation of the effect of BF slag composition on alkali removal capacity with sustained S removal
- Development of a concept for improved adaption of BF operation with regard to improved alkali control in connection with the new developed online tool for determination of alkali accumulation

BD 6/14

PAGE 6 / 14

## FORMS B2

### **2 - Work programme and distribution of tasks with indication of participating beneficiaries**

*(Specify the beneficiary's responsibilities within each task).*

#### 2.1 Development of Online-Tool for determination of alkali accumulation in BF (BFI, Dunafer, VASD, LKAB, MEFOS)

- Development of online-evaluation routine based on results of Task 1.2 (BFI)
  - Thermodynamic calculations concerning the formation of NH<sub>3</sub> (and HCN) in conjunction with alkali components in the BF
  - Lab tests for determination of the NH<sub>3</sub>-formation in conjunction with alkali components at BF conditions. Here, coke with different alkali loads will be heated in a 2-zone inductively heated fixed bed reactor (FBR), which is capable for simulation of alkali evaporation (zone 1) and condensation (zone 2) within the BF alkali cycle.
  - Based on the determined NH<sub>3</sub> reaction efficiencies, a calculation routine will be developed for determination of the amount of circulating alkalis derived from the measured NH<sub>3</sub> concentration in top gas
- Determination of alkali cycle at different industrial BF at varying operational conditions (BFI, Dunafer, SSAB, VASD, LKAB, MEFOS)
  - The amount of the alkali cycle at the compared BF's will be determined by use of the measured NH<sub>3</sub> concentration data in the top gas and the new developed online-evaluation routine (BFI)
  - The measured NH<sub>3</sub> concentration data in the BF top gas of Dunafer and SSAB will be provided by these industrial partners (Dunafer, SSAB)
  - BFI in coop. with VASD will provide the measured NH<sub>3</sub> concentration data in the BF top gas of VASD (BFI, VASD)

#### 2.2 Inhibition of alkali circulation (BFI, Dunafer, VASD, MEFOS, LKAB, LTU)

- Development of coke pre-treatment/coating procedure using alkali absorbing additives
  - Selection of suitable pre-treatment / coating agents by thermodynamic calculations (e. g. kaolinite, secondary raw materials; BFI)
  - Development of suitable pre-treatment / coating procedures (BFI...)
  - Lab scale trials for determination of alkali inhibiting effect on coke resulting from selected pre-treatment/coating procedures (BFI)
    - Thermal treatment of coke test batches at BF conditions in 2-zone FBR and subsequent evaluation of coke properties (e. g. surface properties, mineral phases in coating, reactivity, CRI/CSR)
    - Evaluation of slag properties resulting from coke pre-treatment (e. g. mineral phases in liquid and solid slag)
    - Identification of most effective coke pre-treatment/coating procedure resulting in minimised coke attack by alkali components
- Preparation of small quantities of test coke (modified ash composition) to be used in laboratory tests, as basket samples or by CRI/CSR (MEFOS)
  - Kinetic studies on gasification of pre-treated coke and laboratory produced coke with altered ash composition. (LTU)
  - Investigation on basket samples in the LKAB Experimental BF (MEFOS, LKAB)
- Alkali absorbing mineral addition in basket samples (LKAB, MEFOS, LKAB) LTU will characterize samples with XRD, SEM/EDS and study gasification and alkali evaporation.

## FORMS B2

### 2.3 Impact from slag compositions (LTU, MEFOS, SSAB)

- Studies on the kinetics of alkali gasification from slag and in-burden materials relative their composition
  - Impact of changing slag compositions on the alkali capacity of the slag and on the kinetics of alkali evaporation from the slag. Evaporation mechanisms for alkali from a blast furnace slag formed in different locations in the blast furnace and evaporation kinetics of alkali from blast furnace slag in contact with hot metal. Both tests in TG/DTA/QMS equipment as well as sampling from large scale lab studies will be carried out. Comparison with synthetic slags and with model calculations using FACTSAGE
  - Possibility to design slag with high alkali binding ability and sufficient S dissolution, requirement on slag volume
  - Alkali gasification from in-furnace material as coke, ferrous material and slag formers of different type collected during operation as well as from the burden and in basket samples during excavation
  - Transfer of results to practical BF Operation

### 2.4 Concept for improved adaption of BF operation (BFI, Dunafer, VASD, LKAB, SSAB)

- Development of a concept for improved alkali control in the BF to be used in WP3. Connected application with Task 2.1, 2.2 and 2.3.
- Evaluation of suitable operational means for controlling the alkali output at the BF in connection with the new developed Online-Tool for determination of alkali accumulation
  - Possible operational means for alkali control in the BF: Adjustment of slag composition, increased slag amount, decreased flame temperature, coke and burden pre-treatment.
  - Assessment of different specific operational scenarios for periodic and/or continuous alkali control at the 3 compared BF's based on top gas measurements. Specific constraints at each BF will be considered.

### 3 - Interrelation with other work packages (please give WP No)

(Briefly describe the interrelation with the other WPs).

- **Task 2.1** (new online evaluation tool) delivers quantitative data on the amount of alkali cycle and consequently the alkali load on coke and burden within the different BF's. These data will be used in **Task 2.2** and **2.3** in order to develop methods for inhibition of the alkali circulation (**Task 2.2**) as well as new methods for improvement of slag composition in terms of alkali removal (**Task 2.3**), based on the determined alkali load.
- **Task 2.4**, the development of a concept for improved adaption of BF operation includes the results of **Tasks 2.1, 2.2, and 2.3** and delivers results to **Task 3.1**.

### 4 - Deliverables and milestones

(Define the deliverables and milestones, give the foreseen date of production and assign them to a responsible partner).

D 2.1 Evaluation routine for determination of alkali accumulation within the BF based on online top gas composition data (e. g. ammonia), thermodynamic calculations and laboratory trials (BFI)

D 2.2 Determination of BF alkali accumulation at varying operational conditions (BFI, Dunafer, SSAB, VASD, MEFOS)

D 2.3 Selection of a suitable coke pre-treatment/coating procedure (in terms of coating agents and coating procedure) for best inhibition of alkali attack on coke in the BF (BFI)

BD 8/14

**FORMS B2**

- D 2.4 Comparative evaluation of basket samples for advice on innovative burden design (BFI, MEFOS)
- D 2.5 Comparative results for impact of alkali on coke gasification with and without modified ash composition or coating (MEFOS)
- D 2.6 Preliminary results on laboratory studies on alkali capacity of slag (LTU, MEFOS)
- D 2.7 Result for the impact of slag composition on alkali gasification and advice on slag design for the BF (LTU, MEFOS)
- D 2.8 Concept for improved adaption of BF operation based on application of the online top gas evaluation tool and new means for alkali control (All)

**FORMS B2**

**B2-2 WORK PACKAGE DESCRIPTION**

WP No 3

Work package Title	Validation of new developed alkali control methods at operational BF	Number of man hours
<b>WP Leader</b> (full name & acronym)	MEFOS	
<b>Beneficiary (s)</b> (full name & acronym)	VDEH-BETRIEBSFORSCHUNGSIINSTITUT GMBH (BFI)	1120
	SWEREA MEFOS AB (MEFOS)	800
	VOESTALPINE STAHL DONAWITZ GMBH (VASD)	500
	ISD DUNAFERR DUNAI VASMU ZARTKORUEN MUKODO RESZVENYTARSASAG (Dunafer)	1450
	SSAB EMEA AB (SSAB)	260
	LUOSSAVAARA-KIIRUNAVAARA AB (LKAB)	350
	LULEA TEKNiska UNIVERSITET (LTU)	0
<b>Total</b>		<b>4480</b>

**1 – Objectives**

*(Objectives clearly stated in a concise manner using bullet points (½ page)).*

- Validation of long term industrial application of the new developed online top gas evaluation tool for determination of the alkali cycle amount in the BF
- Proof of industrial applicability of alkali control concept developed in Task 2.4
- Development of an overall concept for improved BF alkali control with special emphasis on the different operational conditions and raw material input at the compared BF's

**2 - Work programme and distribution of tasks with indication of participating beneficiaries**

*(Specify the beneficiary's responsibilities within each task).*

**3.1 Industrial trials (BFI, Dunafer, VASD, SSAB, MEFOS)**

- Validation of new online top gas evaluation tool combined with adjusted adaption of BF operational parameters
- Long term application of the alkali control concept in Task 2.4 at the 3 different operational BF's in order to prove its industrial applicability
  - Application of top gas measurements and online top gas evaluation tool at the operational BF at Dunafer, SSAB and VASD
  - Variation of identified BF parameters for alkali control at the operational BF at Dunafer, SSAB and VASD. Assessment of alkali control efficiency.

**3.2 Development of an overall concept for improved alkali control at the BF (All)**

- Based on the results of Task 2.4 and 3.1 an overall concept for improved BF alkali control at European level will be developed with special emphasis on deteriorating raw material qualities and increased use of recycling materials

BD 10/14

**FORMS B2**

**3 - Interrelation with other work packages (please give WP No)**

*(Briefly describe the interrelation with the other WPs).*

**Task 3.1** comprises industrial trials for validation of the new developed alkali control methods, which have been developed specifically for the different BF's within **Task 2.4**. **Task 3.1** finally delivers results to the development of an overall concept for improved alkali control at the BF (**Task 3.2**).

**4 - Deliverables and milestones**

*(Define the deliverables and milestones, give the foreseen date of production and assign them to a responsible partner).*

D 3.1 Demonstration of feasibility of the online top gas evaluation tool at industrial BF's (BFI, MEFOS, Dunafer, SSAB and VASD)

D 3.2 Provision of an overall alkali control concept for European BF emphasizing deteriorating raw material qualities and increased use of recycling materials (All)

## FORMS B2

## B2-2 WORK PACKAGE DESCRIPTION

WP No 4

Work package Title	Project coordination, documentation and reporting	Number of man hours
<b>WP Leader</b> (full name & acronym)	BFI	
<b>Beneficiary (s)</b> (full name & acronym)	VDEH-BETRIEBSFORSCHUNGSIINSTITUT GMBH (BFI)	450
	SWEREA MEFOS AB (MEFOS)	300
	VOESTALPINE STAHL DONAWITZ GMBH (VASD)	220
	ISD DUNAFERR DUNAI VASMU ZARTKORUEN MUKODO RESZVENYTARSASAG (Dunafer)	250
	SSAB EMEA AB (SSAB)	200
	LUOSSAVAARA-KIIRUNAVAARA AB (LKAB)	200
	LULEA TEKNiska UNIVERSitet (LTU)	250
<b>Total</b>		<b>1870</b>

**1 – Objectives**

- Co-ordination of the partners work; Internal documentation of progress and results within consortium
- Performance of joint meetings for discussion of methods and results
- Preparation of RFCS written reports on the achieved results (Progress reports, Mid-term report, final report)
- Presentation of work progress as well as presentation of written reports at the TGS meetings

**2 - Work programme and distribution of tasks with indication of participating beneficiaries***(Specify the beneficiary's responsibilities within each task).*

- Reporting and discussion (All)
  - Performance of coordination meetings, TGS meetings
  - Presentations for the meetings
  - Discussion of results and work carried out
- Preparation of mid-term and final report (All)

**3 - Interrelation with other work packages (please give WP No)***(Briefly describe the interrelation with the other WPs).*

- All WP's

**4 - Deliverables and milestones***(Define the deliverables and milestones, give the foreseen date of production and assign them to a responsible partner).*

D 4.1 Written reports: Progress reports, Midterm report and Final report (All)

D 4.2 Presentations for coordination meetings and TGS meetings (All)

30/10/14

## FORMS B2

**B2-3 PROGRAMME BAR CHART (TASK, PARTNER, DELIVERABLES, MILESTONES)**  
**Please use dark colours for better readability**

Work package	Work package title	Deliverables	Hours on project/ Beneficiary							1 <sup>st</sup> year	2 <sup>nd</sup> year	3 <sup>rd</sup> year	4 <sup>th</sup> year
			BFI	MEFOS	VASD	Duna.	SSAB	LKAB	LTU				
WP 1	Characterization of alkali re-circulation in the BF	910	3104	950	2250	130	720	340					
Task 1.1	Alkali behavior/balance in different BFs	D 1.1, D 1.2	120	440	300	800	20	80	120				
Task 1.2	New on-line measurements	D 1.3, D 1.4	450	2244	600	1200	90	240	0				
Task 1.3	Alkali impact on BF burden materials	D 1.5 – 1.8	340	420	50	250	20	400	220				
WP 2	Methods for alkali control in the BF	2020	1690	350	900	120	360	2060					
Task 2.1	Development of Online-Tool for determination of alkali accumulation in BF	D 2.1, D 2.2	900	600	150	400	20	200	0				
Task 2.2	Inhibition of alkali circulation	D 2.3 – 2.5	900	390	0	300	0	80	790				
Task 2.3	Impact from slag compositions	D 2.6, D 2.7	0	700	0	0	20		1270				
Task 2.4	Concept for improved adaptation of BF operation	D 2.8	220	0	200	200	80	80	0				
WP 3	Validation of new developed alkali control methods at operational BF		1120	800	500	1450	260	350	0				

BD/B/4

**FORMS B2**

<b>Task 3.1</b>	Industrial trials	D 3.1	900	600	250	1200	180	0	0
<b>Task 3.2</b>	Development of an overall concept for improved alkali control at the BF	D 3.2	220	200	250	80	350	0	
<b>WP 4</b>	Project coordination, documentation and reporting	D 4.1, D 4.2	450	300	220	250	200	200	250
<b>Total Hours on project</b>			4500	5894	2020	4850	7101	1630	2650

## Getting in touch with the EU

### In person

All over the European Union there are hundreds of Europe Direct information centres. You can find the address of the centre nearest you at:  
[https://europa.eu/european-union/contact\\_en](https://europa.eu/european-union/contact_en)

### On the phone or by email

Europe Direct is a service that answers your questions about the European Union. You can contact this service:

- by freephone: 00 800 6 7 8 9 10 11 (certain operators may charge for these calls),
- at the following standard number: +32 22999696 or
- by email via: [https://europa.eu/european-union/contact\\_en](https://europa.eu/european-union/contact_en)

## Finding information about the EU

### Online

Information about the European Union in all the official languages of the EU is available on the Europa website at: [https://europa.eu/european-union/index\\_en](https://europa.eu/european-union/index_en)

### EU publications

You can download or order free and priced EU publications at: <https://publications.europa.eu/en/publications>. Multiple copies of free publications may be obtained by contacting Europe Direct or your local information centre (see [https://europa.eu/european-union/contact\\_en](https://europa.eu/european-union/contact_en)).

### EU law and related documents

For access to legal information from the EU, including all EU law since 1951 in all the official language versions, go to EUR-Lex at: <https://eur-lex.europa.eu>

### Open data from the EU

The EU Open Data Portal (<https://data.europa.eu/euodp/en/home>) provides access to datasets from the EU. Data can be downloaded and reused for free, for both commercial and non-commercial purposes.

The objective of the research project is to achieve improved blast furnace (BF) process stability and energy efficiency with increasing raw material flexibility by assessment and control of alkalines.

By determination of alkali balances at different industrial BF's in combination with extensive thermodynamic calculations, a deep understanding of the alkali behaviour and associated energy consumption in the BF was achieved. Further, new methods for on-line determination of alkali accumulation in the blast furnace were tested and validated by industrial measurements and thermodynamic calculations: BF top gas measurements by FTIR gas analyser (NH<sub>3</sub> and HCN), mass spectrometer, TDLS device, as well as the spectrometric measurement of K or Na in the raceway.

Especially, the HCN measurement in top gas and the spectrometric measurement in the raceway have been confirmed to be promising for monitoring of variations in BF alkali load, enabling the premature detection of operational states with elevated alkali load.

Promising measures for BF alkali control, respectively enhanced removal of alkalies are the application of a low slag basicity, a central gas profile and the minimisation of alkali containing slag passing the high temperature zone in vicinity of the raceway. By use of coke with modified ash or kaolin coating, promising results were obtained in protecting coke from alkali attack.

The final concept for alkali control involves a continuous qualitative measurement of the alkali load in the BF either by HCN measurement in the top gas and/or by spectrometric measurement of K or Na in the raceway in combination with the investigated methods for inhibition of the alkali circulation.

